JAERI-M
84-135

RECIRCULATION PUMP SUCTION LINE200% BREAK INTEGRAL TEST AT ROSA-III WITH TWO LPCI FAILURES, RUN 983

August 1984

Mitsuhiro SUZUKI, Yoshinari ANODA, Kanji TASAKA,
Hiroshige KUMAMARU, Hideo NAKAMURA,
Taisuke YONOMOTO, Hideo MURATA and
Masayoshi SHIBA

日本原子力研究所
Japan Atomic Energy Research Institute

JAERI-M レポートは，日本原子力研究所が不定期に公刊している研究報告書です。

入手の問合わせは，日本原子力研究所技術情報部情報資料課（〒319—11 茨城県那珂郡東海村）あて，お申しこしください。なお，このほかに財団法人原子力弘済会資料センター（〒319—11 茨城県那珂郡東海村日本原子力研究所内）で複写による実費頒布をおこなっております。

JAERI-M reports are issued irregularly.

Inquiries about availability of the reports should be addressed to Information Section, Division of Technical Information, Japan Atomic Energy Research Institute, Tokai-mura, Naka-gun, Ibaraki-ken 319—11, Japan.

編集兼発行　日本原子力研究所
印　　刷　日立高速印刷株式会社

JAERI-M 84-135

RECIRCULATION PUMP SUCTION LINE 200% BREAK INTEGRAL TEST AT ROSA-III WITH TWO LPCI FAILURES, RUN 983

Mitsuhiro SUZUKI, Yoshinari ANODA, Kanji TASAKA,
Hiroshige KUMAMARU, Hideo NAKAMURA, Taisuke YONOMOTO,
Hideo MURATA and Masayoshi SHIBA

Department of Nuclear Safety Research,
Tokai Research Establishment, JAERI
(received July 2 , 1984)

This report presents the experimental data of the 200% suction line break test RUN 983 at ROSA-III, which was conducted as one of counterpart tests to a FIST program test sponsored by GE, EPRI and USNRC. The similarity study between the ROSA-III and FIST tests is on the way. The report also presents the information on the ROSA-III test facility, experiment conditions, experiment results and the effects of the power generation rate, feedwater temperature and the MSIV trip level comparing with another 200% break test, RUN 902.

Major conclusions obtained are as follows.

(1) Change of the MSIV trip level from L2 to L1 gives little change in pressure response and mass inventory in the large recirculation line break test.

(2) Feedwater flashing results in reduction of depressurization and delay in the LPCS and LPCI actuations, which cause higher PCT.

(3) The lower PCT in RUN 983 is the results of lower heat flux and larger mass inventory compared with that of RUN 902.

Keywords: BWR, LOCA, ECCS, Integral Test, ROSA-III Program, Large Break, Recirculation Loop Suction Line Break, FIST, Counterpart Test

ＬＰＣＩ２系統故障を仮定したＲＯＳＡ－Ⅲ再循環ポンプ吸込側200％破断総合試験，ＲＵＮ 983

日本原子力研究所東海研究所安全工学部
鈴木　光弘・安濃田良成・田坂　完二・熊丸　博滋
中村　秀夫・与能本泰介・村田　秀夫・斯波　正誼

（１９８４年７月２日受理）

本報はＲＯＳＡ－Ⅲにおける再循環ループ吸込側配管200％破断実験，ＲＵＮ 983の実験結果をまとめたものである。この実験は，米国のＧＥ，ＥＰＲＩ，ＮＲＣによるＦＩＳＴ計画との対応実験の１つとして実施されたものであり，ＲＯＳＡ－ⅢとＦＩＳＴ両装置の相似性の検討は別途進められている。

本報は，上記の実験結果の他に，ＲＯＳＡ－Ⅲ試験装置と実験条件に関する情報を記し，更に他の標準的実験条件のＲＵＮ 902の実験結果と比較することにより炉心出力や給水系温度，主蒸気隔離弁（ＭＳＩＶ）閉信号の相違が及ぼす大口径破断実験への影響をまとめた。

主な結論は以下の通りである。

(1) ＭＳＩＶ閉信号がＬ２からＬ１水位に変化しても系圧力変化と冷却水インベントリに及ぼす影響は小さい。

(2) 給水系フラッシングは，減圧速度の低下をもたらし，ＬＰＣＳ及びＬＰＣＩ作動をおくらせ，ＰＣＴを高くする。

(3) ＲＵＮ983のＰＣＴが，ＲＵＮ 902に比べて低くなったのは，ヒーターロッドの熱流束が低いこととシュラウド内の冷却水インベントリーが多かったことによるものである。

Contents

目　　次

List of Tables

List of Figures

1. Introduction

The Rig of Safety Assessment (ROSA)-III program[1] was initiated in 1976 to study the thermal-hydraulic behavior of a Boiling Water Reactor (BWR) during a posturated Loss of Coolant Accident (LOCA) with the Emergency Core Cooling System (ECCS) actuation and to provide the data base to evaluate the predictability of computer codes developed for reactor safety analysis. The ROSA-III test facility[2] was fabricated in 1978 and consisted of the volumetrically scaled (1/424) primary system of a 3800 MW BWR/6(251-848)[3] with the electrically heated core, the break simulator and the scaled ECCS. Special emphasis of the ROSA-III test program is made on the following objectives, as

(1) To study the fundamental thermal hydraulic behavior of a BWR during a LOCA.

(2) To provide the system data required to improve and evaluate the analytical codes currently used to predict the LOCA response of large BWRs. The performance of the Engineered Safety Features (ESFs), with particular emphasis on ECCSs, are of primary interest.

(3) To identify and investigate any unexpected event(s) or threshold(s) in the response of the plant and develop analytical techniques that adequately describe and account for such unexpected behavior.

To meet these objectives various kinds of ROSA-III tests have been performed and their results have been descrived and published[4]-[25].

Up to the present time, similar experimental studies on the BWR/LOCA phenomena have been performed in the world, such as TLTA[26] and FIST.[27] The FIST facility has two active recirculation loops and a full-height electrically heated core. Major differences between the ROSA-III facility and FIST facility are the number of fuel bundles, height of core, maximum core heat flux and volumetric scaling ratio to the reference BWR (The FIST simulates a BWR/6 218-624 system by a scaling factor of 1/624). It is an urgent interest to study the effect of individual specification of each test facility on the transient thermal hydraulic phenomena simulating a BWR/LOCA.

RUN 983, conducted on Feb. 24, 1983 simulates a 200% double-ended break at the recirculation pump suction line with the assumption of single failure on one LPCI diesel generator and is conducted as a counter part test for the FIST 200% large break test with the similar test conditions. The major objective of the ROSA-III test RUN 983 is to investigate the similarity of test facilities between ROSA-III and FIST by comparing the test results.

The similarity study between the ROSA-III and FIST facilities, however, is now under preparation and will be presented in the near future. On the other hand, the effect of key test parameter such as power generation rate and MSIV trip level can be investigated by comparing the test results of RUN 983 with the other ROSA-III large break test RUN 902.

The report presents experiment data of the ROSA-III test RUN 983 and findings as to the effects of different test conditions. Descriptions of the ROSA-III test facility, instrumentations and test conditions and procedures are briefly presented in Chapters 2, 3 and 4, respectively. Chapter 5 describes the measured experiment data and processed data such as average fluid density and break flow rate in RUN 983. Chapter 6 describes the effects of different test parameters shown above between RUN 983 and RUN 902 on the large break LOCA phenomena.

2. ROSA-III Test Facility

The ROSA-III test facility is a volumetrically scaled (1/424) BWR system with an electrically heated core designed to study the response of the primary system, the core and the ECCS during the postulated LOCA. The test facility is instrumented such that various thermal-hydraulic parameters are measured and recorded during the test. Details of the test facility can be refered to the reference (2).

The test facility consists of four subsystems. These subsystems are : (a) the pressure vessel, (b) the steam line and the feedwater line, (c) the recirculation loops and (d) the ECCS. Figures 2.1, 2.2 and 2.3 illustrate configuration of the test facility, the pressure vessel internals and the piping schematics, respectively. Table 2.1 compares the major dimensions of the ROSA-III test facility to the corresponding dimensions of the reference BWR system.

The ROSA-III pressure vessel includes various components in it simulating the internal structures of the reactor vessel in the BWR system as shown in Fig. 2.4. The interior of the vessel is divided into the core, the lower plenum, the upper plenum, the downcomer annulus, the steam separator, the steam dome and the steam dryer. The core is consisted of four simulated fuel assemblies of half length and a control rod simulator. Each fuel assembly contains 62 heater rods (Fig. 2.5) and 2 water rods spaced in a 8 x 8 square array and supported by spacers and upper and lower tie plates. The heater rod is heated electrically with upper and lower tie plates. The heater rod is heated electrically with chopped cosine power distribution along the axis as shown in Fig. 2.6. The effective heated length is 1880 mm, one half of the active length of a BWR fuel rod. The electric power supplied to each fuel assembly "A", "B", "C" or "D" is controlled samely in RUN 983 in order to obtain the flat radial power profile. The heater rods in each assembly are divided into three groups with respect to heat generation rate as shown in Fig. 2.7. The local peaking factor in each group is 1.1, 1.0 and 0.875. In RUN 983, the initial core power was limitted as 3.614 MW. The orifice plate with 44 mm I.D. in one assembly is inserted at at each core inlet to control the core inlet flow.

The steam line is connected to the steam dome of the pressure vessel. A control valve is installed in the steam line to control the steam dome pressure in steady state before the initiation of the test. The steam line has a branch in which the Automatic Depressurization System (ADS) is

installed. The operation of valves in the steam line is described in Chap.4. The feedwater is supplied from the feedwater tank (FWT) through the feedwater line (Fig. 2.8) and the feedwater sparger (Fig.2.9) below the steam separator.

Figure 2.10 shows the recirculation lines consisted of two loops. Each loop is furnished with a recirculation pump and two jet pumps. The jet pumps are installed outside the pressure vessel to simulte the relative volume and the relative height to the core. Two break simulators and a Quick Shut-off Valves (QSV) are installed in the broken loop. The break simulator consists of an orifice or a nozzle to determine the break size and a Quick Opening Blowdown Valve (QOBV) to initiate the test. The break mode (double-ended or split), the break size and the break location can be changed as test parameters. In RUN 983, a break nozzle with inner diameter of 26.2 mm was installed at the PV side of break simulating scaled BWR recirculation piping flow area and an orifice with inner diameter of 10.1 mm was installed at the MRP side of break simulating the scaled BWR jet pump drive nozzle flow areas. Figure 2.10 shows the QOBV, a QSV and flow orifice installed upstream of the QOBV.

The ROSA-III test facility is furnished with all kinds of the ECCS available in the BWR system, i.e., the High Pressure Core Spray (HPCS), the Low Pressure Core Spray (LPCS), the Low Pressure Coolant Injection (LPCI), and the Automatic Depressurization System (ADS). The HPCS and the LPCS spray the cooling water on the top of the core. The LPCI injects the cooling water into the core bypass. Each ECCS consists of a pump, a tank, piping, and a control system. In RUN 983, a single failure of one LPCI diesel generator was assumed and therefore HPCS, LPCS, 1 LPCI and ADS were available.

The water level in the upper downcomer, which has influencial contribution in the small break LOCA test, is measured and used for trip signals of MSIV closure and ECCS actuation as follows.

MSIV Closure = L1 + 3s
HPCS Actuation = 27 s
LPCS Actuation = (L1 + 40s) + (P less than 1.86 MPa)
LPCI Actuation = (L1 + 40s) + (P less than 1.57 MPa)
ADS Actuation = L1 + 120s
Scram Level = L3 (Initial Level)

where, L1 and L3 are the water level trip points in the upper downcomer as shown in Table 4.1.

Table 2.1 Primary chracteristics of ROSA-III and BWR/6

	BWR-6	ROSA-III	BWR/ROSA
No. of Recirc. Loops	2	2	1
No. of Jet Pumps	24	4	6
No. of Separators	251	1	251
No. of Fuel Assemblies	848	4	212
Active Fuel Length (m)	3.76	1.88	2
Total Volume (m^3)	621	1.42	437
Power (MW)	3800	4.40	864
Pressure (MPa)	7.23	7.23	1
Core Flow (kg/s)	1.54×10^4	36.4	424
Recirculation Flow (l/s)	2970	7.01	424
Feedwater Flow (kg/s)	2060	4.86	424
Feedwater Temp (K)	489	489	1

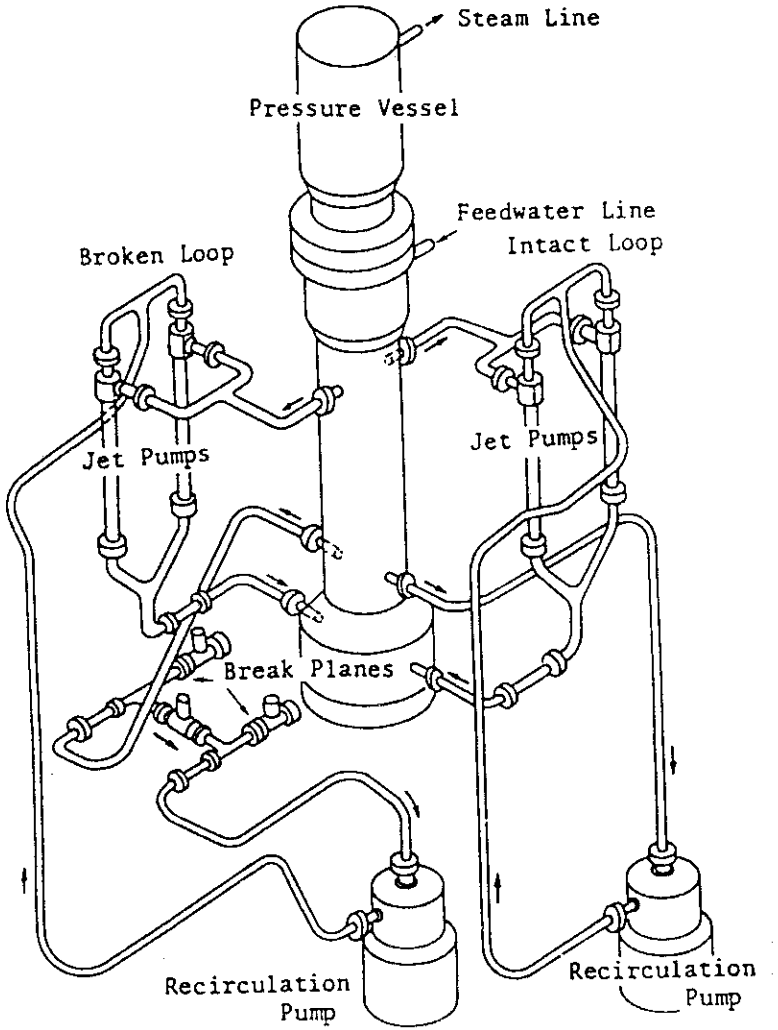

Fig. 2.1 Schematic diagram of ROSA-III test facility

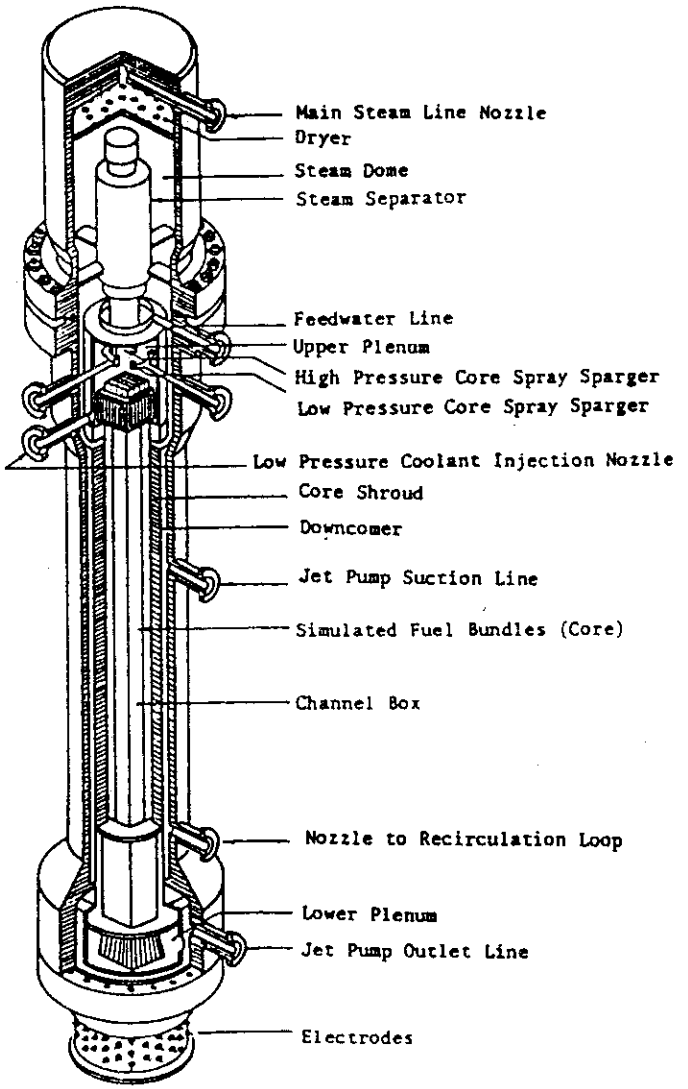

Fig. 2.2 Internal structure of pressure vessel of ROSA-III

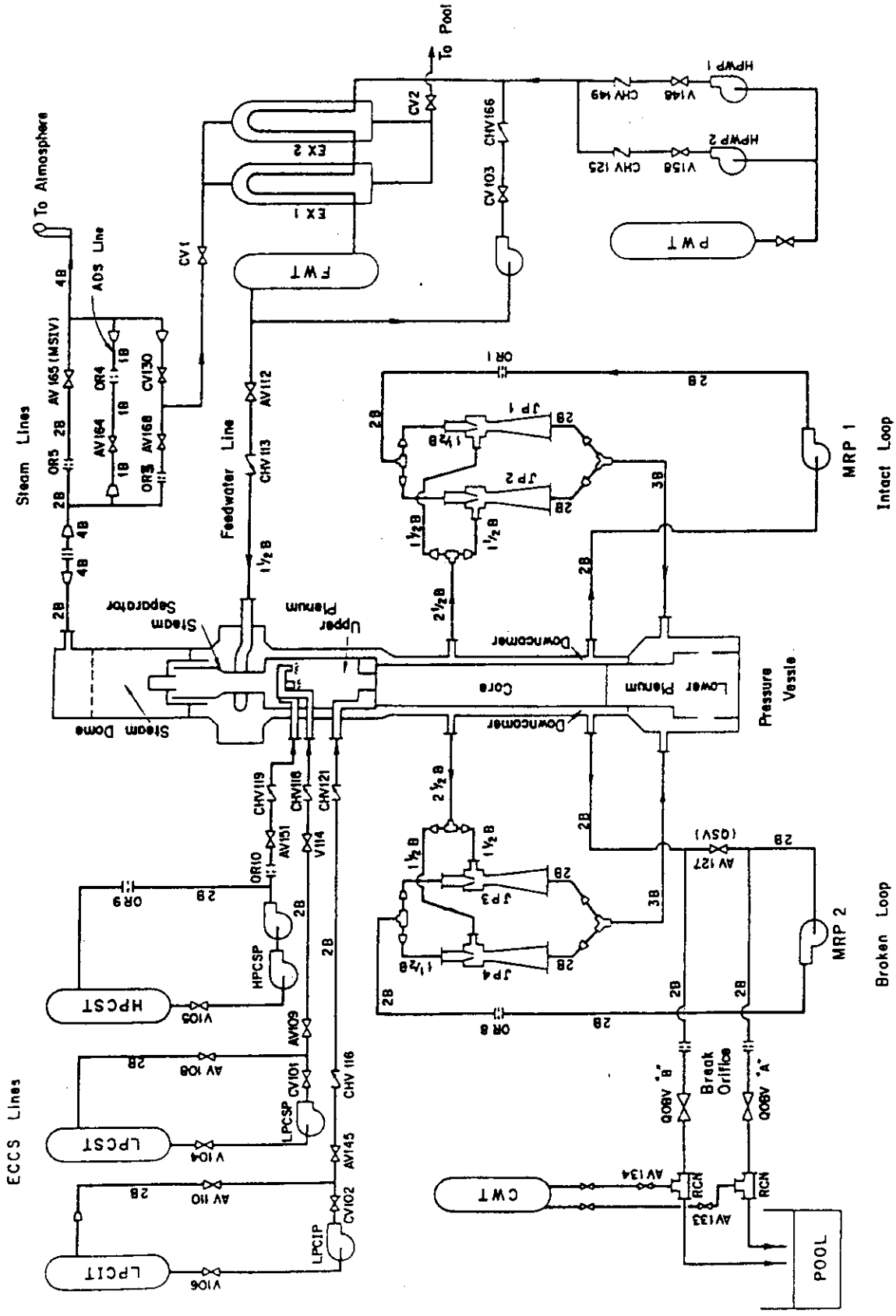

Fig. 2.3 ROSA-III piping schematic

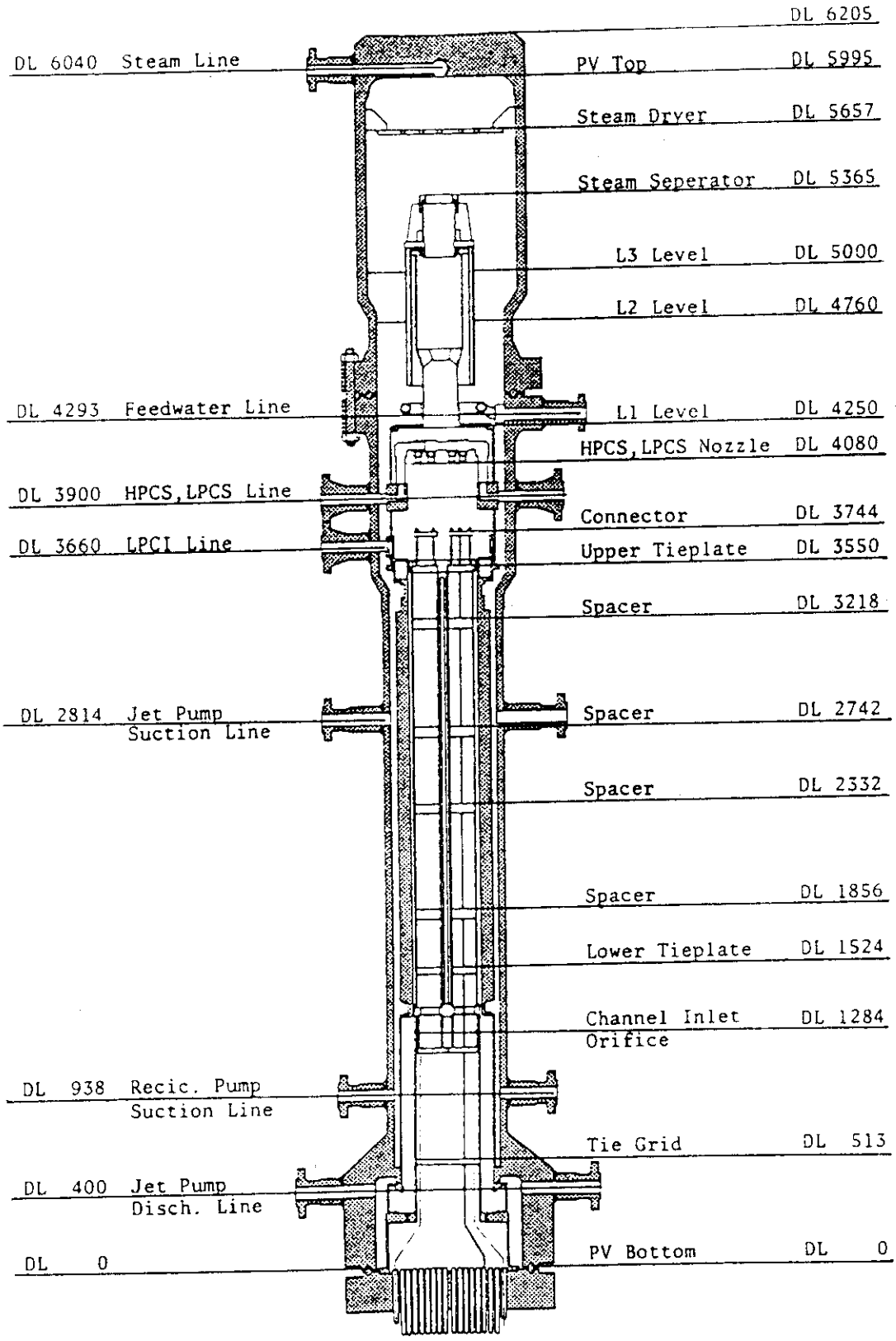

Fig. 2.4 Pressure vessel internals arrangement

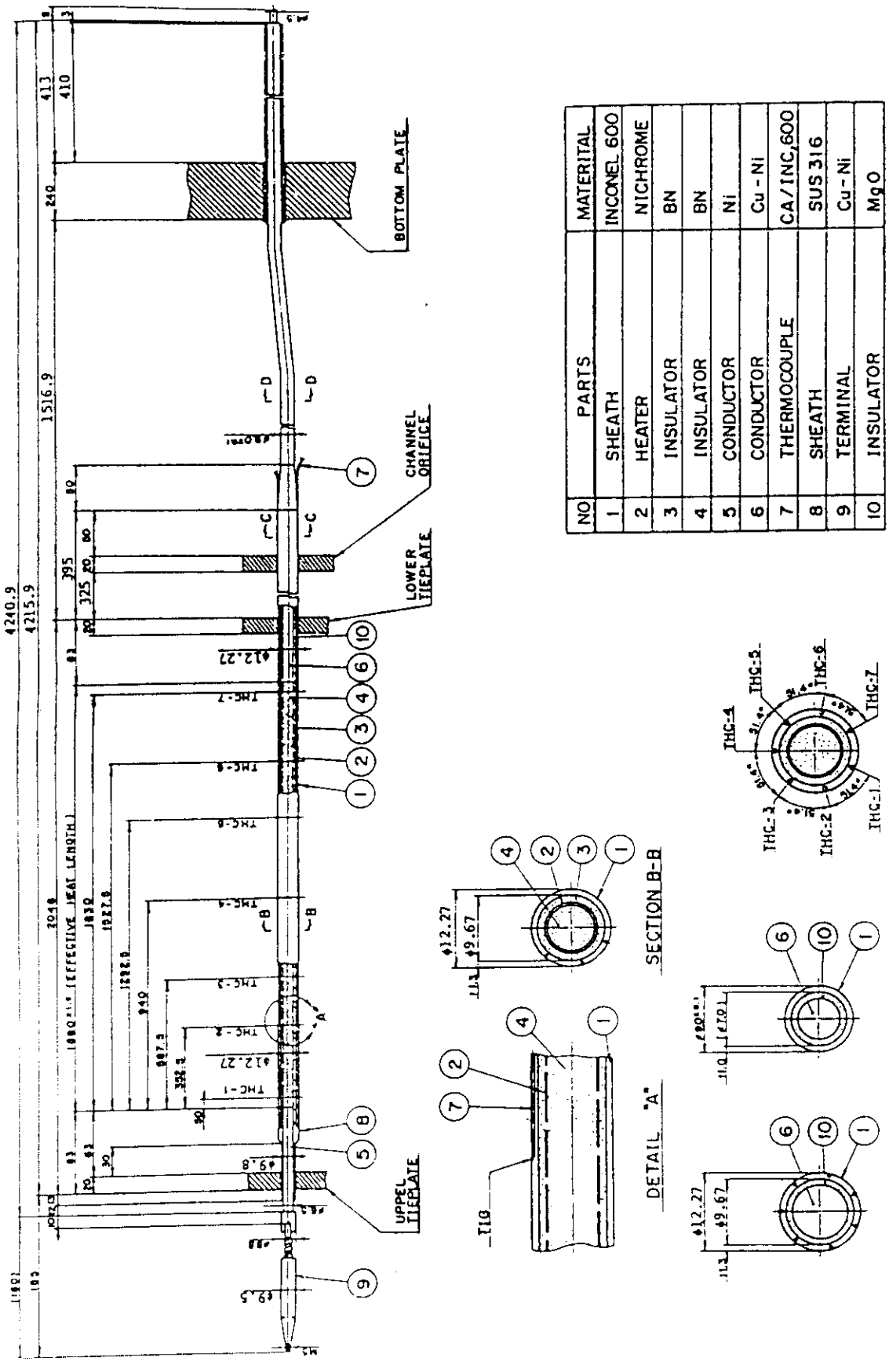

NO	PARTS	MATERITAL
1	SHEATH	INCONEL 600
2	HEATER	NICHROME
3	INSULATOR	BN
4	INSULATOR	BN
5	CONDUCTOR	Ni
6	CONDUCTOR	Cu - Ni
7	THERMOCOUPLE	CA/INC,600
8	SHEATH	SUS 316
9	TERMINAL	Cu - Ni
10	INSULATOR	MgO

Fig. 2.5 Simulated fuel rod of ROSA-III

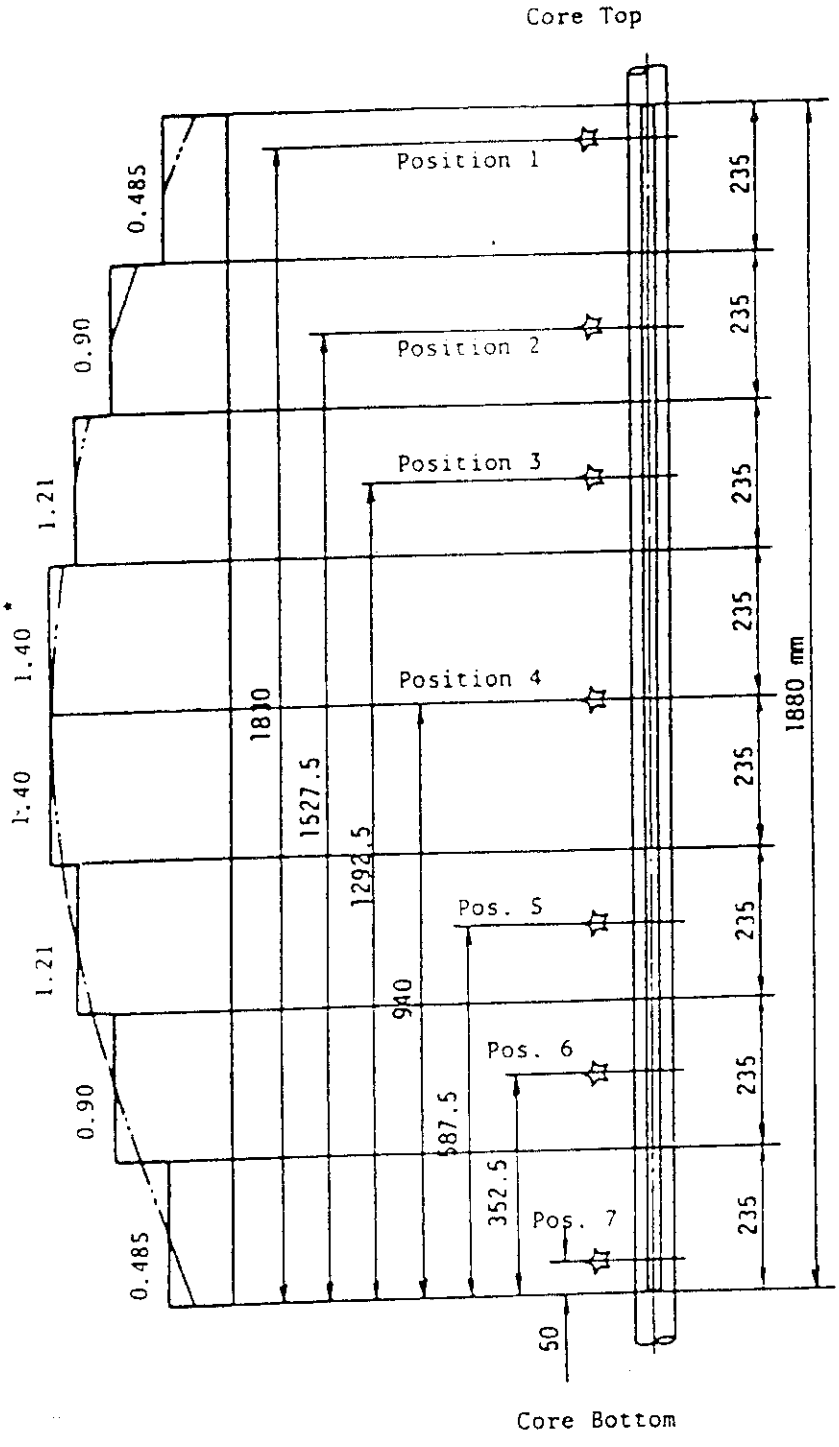

Fig. 2.6 Axial power distribution of heater rod

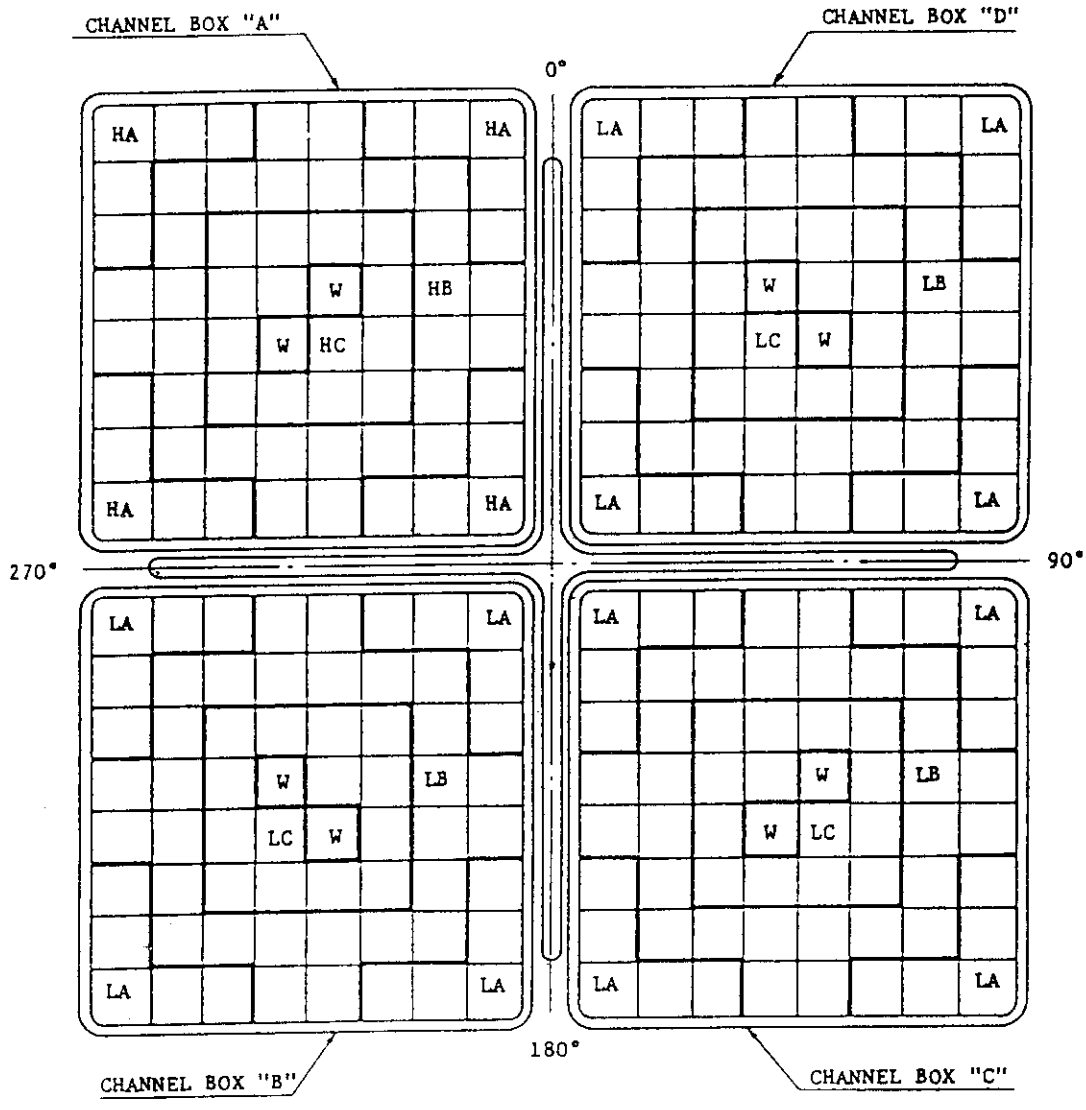

Region	Bundle A			Bundles B,C and D			Water Rods
	HA	HB	HC	LA	LB	LC	W
Linear Heat Rate (kW/m)	11.92	10.84	9.49	11.92	10.84	9.49	0.0
Local Peaking Factor	1.1	1.0	0.875	1.1	1.0	0.875	0.0
Number of Rods	20	28	14	60	84	42	8

Fig. 2.7 Radial power distribution of core

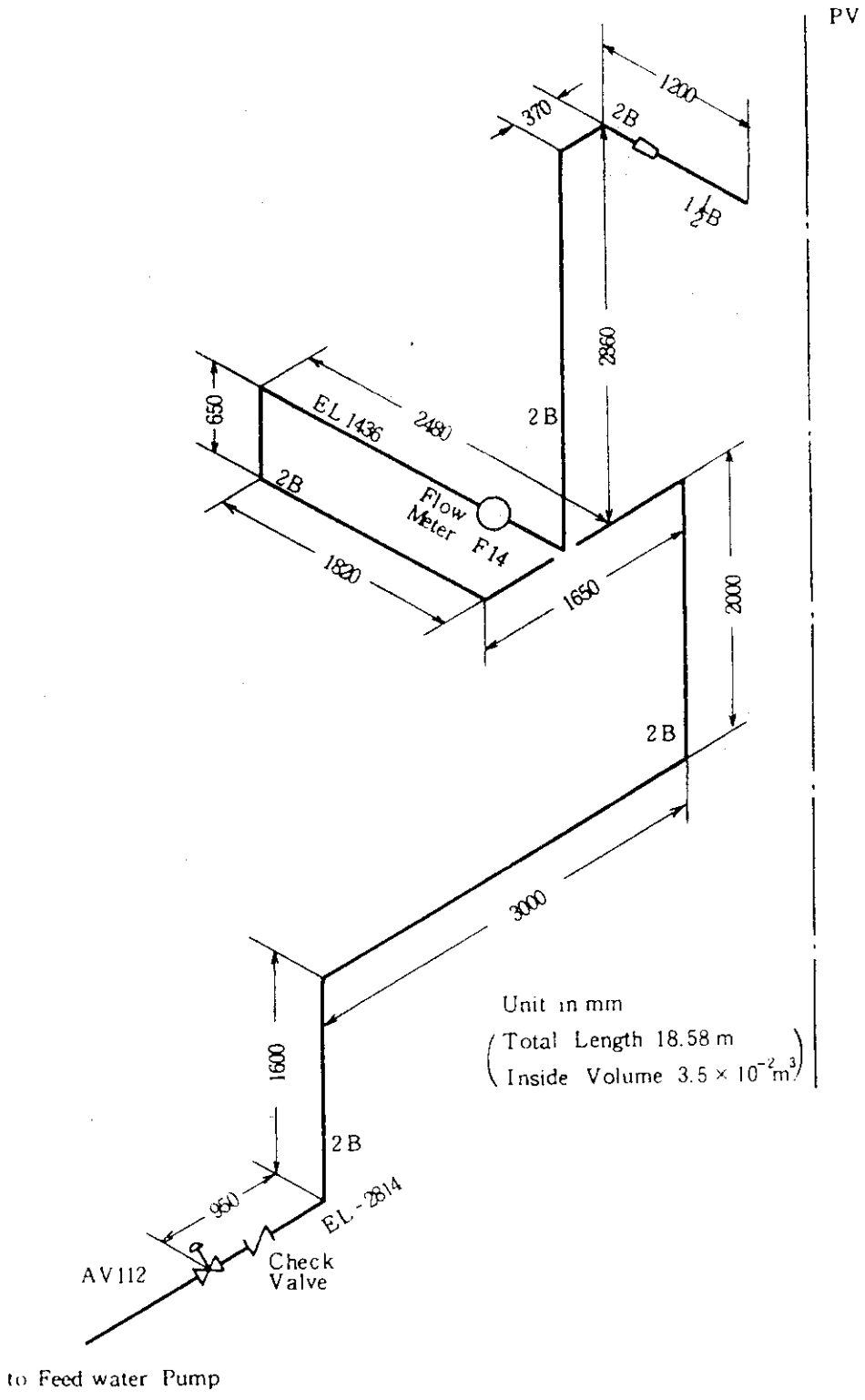

Fig. 2.8 Feedwater line between PV and AV-112

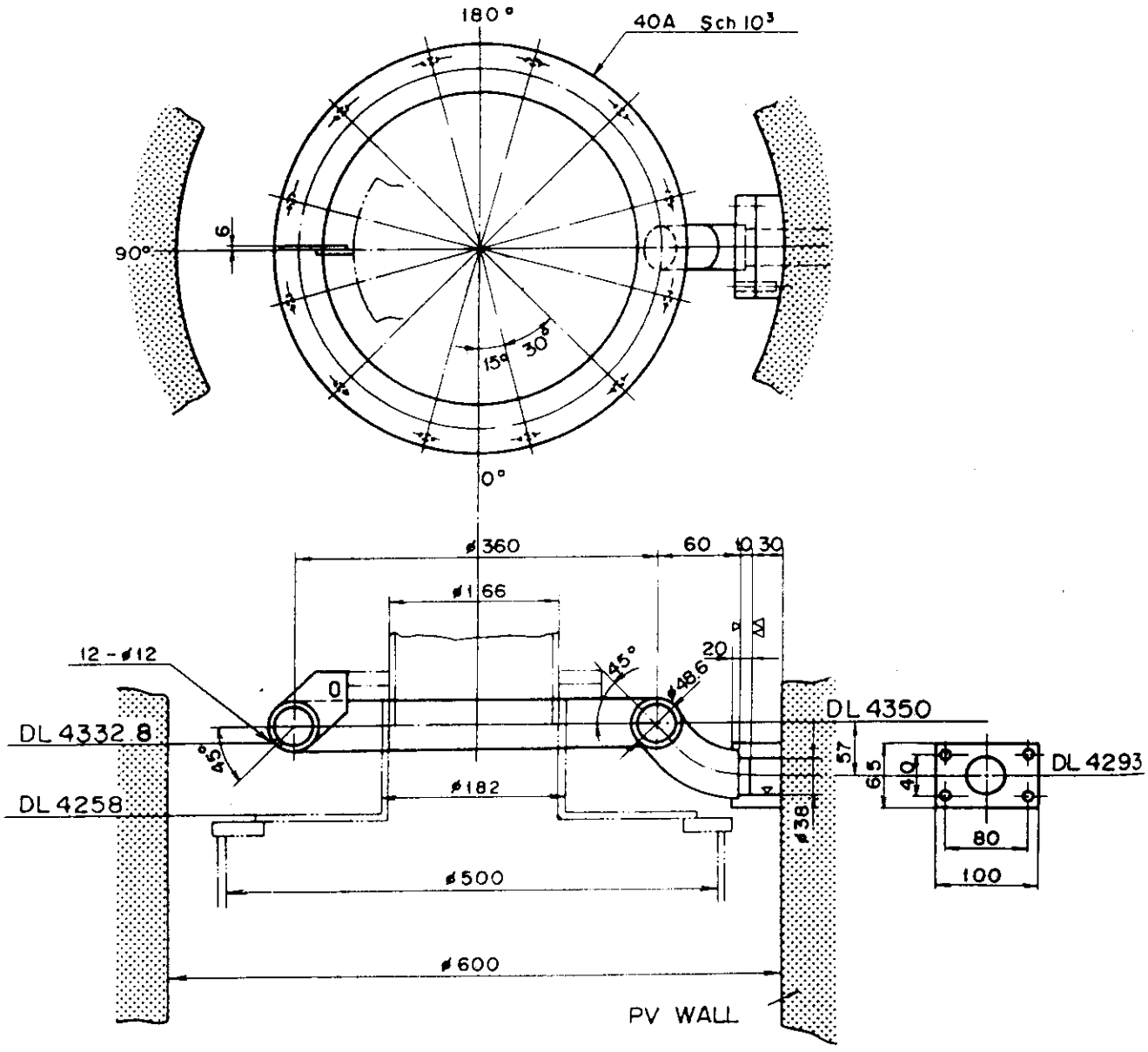

Fig. 2.9 Feedwater sparger configuration

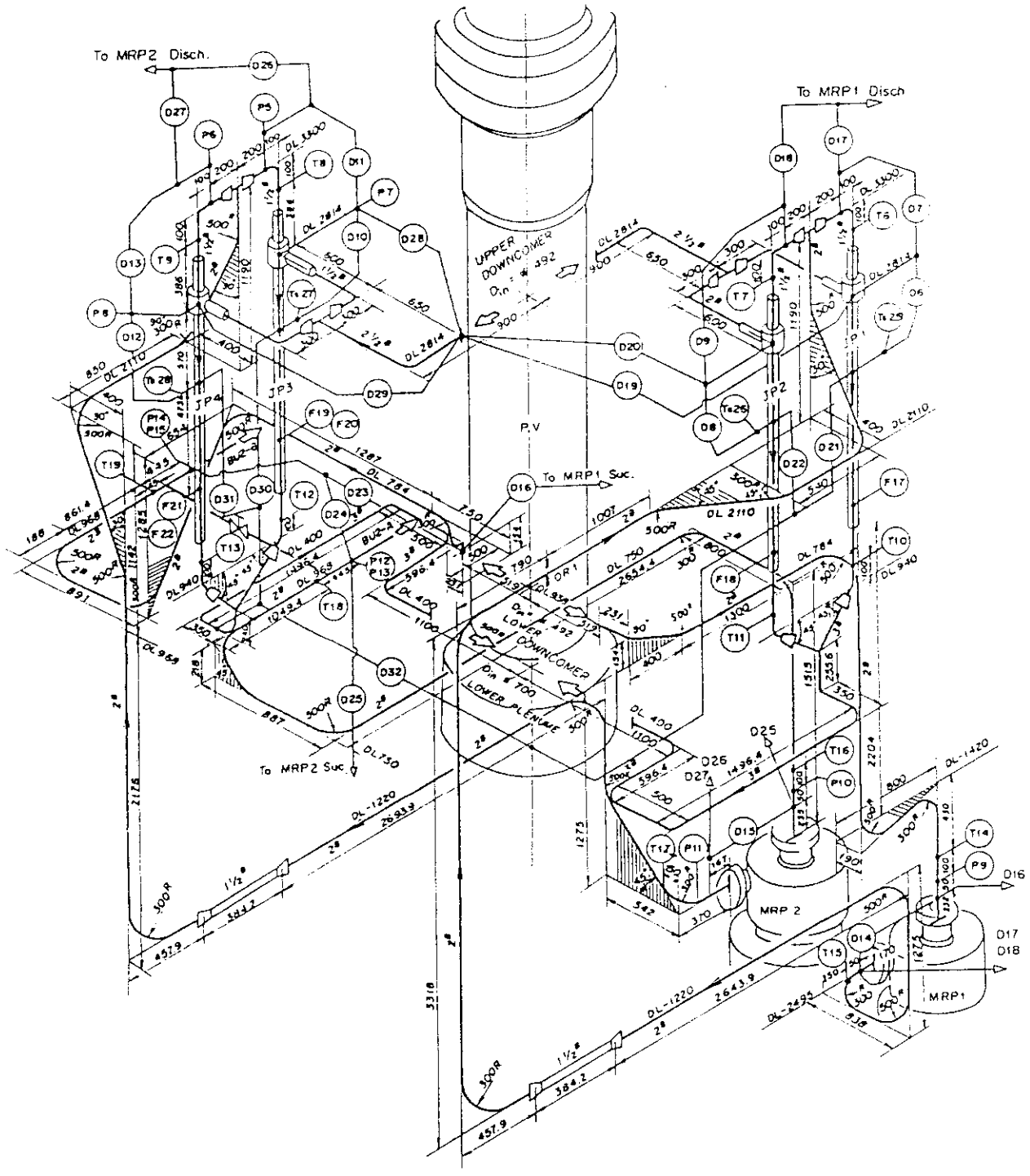

Fig. 2.10 Piping layout of recirculation loops and jet pumps

3. Instrumentation

The instrumentation of the ROSA-III is designed to obtain thermal-hydraulic data during the simulated BWR LOCA. The data obtained from the experiments will contribute to assess the analytical computer codes for LOCA analyses and to investigate the transient fluid and fuel responses during the simulated LOCA. Table 3.1 summarizes the No.4 instrumentation list used in RUN 984.

Tables 3.2 and 3.3 show the measurement list of RUN 984 and the core instrumentation list, respectively. Instrumentation locations are shown in Fig. 3.1 through Fig. 3.6.

Typical measured parameters in the ROSA-III are pressure, differential pressure, flow rate, electric power, pump speed, fluid and metal temperatures, collapsed liquid level, two-phase mixture level, fluid density, trip signals and so on.

Pressure and differential pressure transducers are two-wire, direct-current type which convert diaphragm displacement to electric capacitance. The pressure lead pipes are either the standard single, cylindrical pipes used in conjunction with condensate pots, or dual concentric cylinders capable of the circulation of cooling water to prevent flashing of the fluid.

The flow rate is measured by four types of instrumentations, i.e., turbine flow meter, orifice type flow meter, Venturi type flow meter and momentum flux measurement equipment depending on the fluid condition and measuring location. The turbine flow meter is used for subcooled water flow such as ECCS injection flow and feedwater flow. The orifice type flow meter is used for both flows, one is steam line flow including ADS flow and another one is jet pump discharge flow in the intact loop. The Venturi flow meters used for recirculation flows in both loops and jet pump discharge flow in the intact loop. The momentum flux measurement using drag-disk is shown later.

The temperatures of the fluid, structural material and fuel rod cladding are measured with chromel-alumel thermocouples (CA T/C) of 1.6 or 1.0 mmφ. The thermocouples for fuel rod cladding temperatures are imbedded at the surface of the cladding as shown in Fig. 2.5. There are seven (max.) thermocouples for one fuel rod along the axial direction and total measuring points of rod cladding temperatures for A, B, C and D channels are 72, 29, 42 and 18, respectively.

Liquid levels are measured by either differential pressure transducers, described above or needle type electrical conductivity probes (CP) developed in the ROSA-III program. The probes are distributed along the vessel height to detect the existence of water or vapor at different levels.

The electric power supplied to the simulated fuel rods is controlled to follow the predetermined power curve with function of time and measured by a fast response electric power meter.

Pump speed is measured by a pulse generator integral of the pump. Trip signals such as selected valve positions, decay heat and pump coastdown simulation initiations and so on are detected in order to record the exact actuation times of trip signals.

Fluid density in the pipe is measured by means of gamma densitometers. Preliminary studies indicate that a three-beam densitometer should be used to determine the flow regime. Figure 3.7 shows the beam directions of the two-beam and three-beam gamma densitometers. The gamma-ray source is ^{137}Cs and the detector is a water cooled NaI(Tl) scintillation counter.

Momentum flux is measured by a drag disk as shown in Fig. 3.8. The combination of signals from a drag disk and a gamma densitometer is used to determine the two-phase flow rate as shown in Fig. 3.9.

The data acquisition system (DATAC 2000B, Iwasaki Tsushinki Co.) scans all of signals with the frequency up to 30 Hz. The data recorded on magnetic tape are processed by the FACOM M200 system computer at JAERI by off-line control. After evaluation, for example by comparing the initial and final pressure values with standard values, the data is reprocessed using the correct conversion factors as determined from the consistency examination.

More detailed information on the data processing procedure are available in reference (28).

Table 3.1 ROSA-III instrumentation summary list in RUN 983

TYPE	SENSOR	NUMBER	NOTE	
PRESSURE	PRESSURE TRANSDUCER	20		
DIFFERENTIAL PRESSURE	DP CELL	60	PV AND LOOP	44
			LEVEL MEASUREMENT	5
			FLOW METER	11
FLUID TEMPERATURE	CA THERMOCOUPLE	85	PRIMARY LOOP	35
			DTT	4
			TIE ROD	14
			UPPER PLENUM	10
			LOWER PLENUM	10
			TIE PLATE	12
			BY PASS	0
FUEL ROD TEMPERATURE	CA THERMOCOUPLE	133		
SLAB SURFACE TEMPERATURE	CA THERMOCOUPLE	7	CORE BARREL	0
			PRESSURE VESSEL	0
			CHANNEL BOX	7
			SHROUD SUPPORT	0
SLAB INNER TEMPERATURE	CA THERMOCOUPLE	0	JP DIFFUSER	0
			PV WALL	0
VOLUMETRIC FLOW RATE	TURBINE METER	3	ECCS LOOP	3
	VENTURI METER	4	PRIMARY LOOP	10
	ORIFICE METER	6		
MASS FLOW RATE	TURBINE METER	4	RECIC. LOOP	4
	ORIFICE METER	3	STEAM LINE	3
LIQUID LEVEL	CONDUCTIVITY PROBE	56		
	CAPACITANCE PROBE	0		
DENSITY	GAMMA DENSITOMETER	10	2 BEAM GD	2
			3 BEAM GD	2
MOMENTUMR FLUX	DRAG DISK	7		
SIGNAL	ON/OFF SWITCH	14		
PUMP SPEED	REVOLUTION COUNTER	2		
ELECTRIC POWER	VA METER	2		
TOTAL		416		

Table 3.2 Measurement list for RUN 983

1Ch.- 50Ch.

Ch.	Item	Symbol	ID.		Location	Fig.No.	Range			Unit	Accuracy
1	Press.	P- 1	PA	1	Lower Plenum	Fig.5. 1	0.100	-	10.0	MPa	1.08%FS
2	Press.	P- 2	PA	2	Upper Plenum	Fig.5. 1	0.100	-	10.0	MPa	1.08%FS
3	Press.	P- 3	PA	3	Steam Dome	Fig.5. 1	0.100	-	10.0	MPa	1.08%FS
4	Press.	P- 4	PA	4	Downcomer Bottom	Fig.5. 1	0.100	-	10.0	MPa	1.08%FS
5	Press.	P- 5	PA	5	JP-3 Drive	Fig.5. 2	0.100	-	10.0	MPa	1.08%FS
6	Press.	P- 6	PA	6	JP-4 Drive	Fig.5. 2	0.100	-	10.0	MPa	1.08%FS
7	Press.	P- 7	PA	7	JP-3 Suction	Fig.5. 2	0.100	-	10.0	MPa	1.08%FS
8	Press.	P- 8	PA	8	JP-4 Suction	Fig.5. 2	0.100	-	10.0	MPa	1.08%FS
9	Press.	P- 9	PA	9	MRP-1 Suction	Fig.5. 3	0.100	-	10.0	MPa	1.08%FS
10	Press.	P-10	PA	10	MRP-2 Suction	Fig.5. 3	0.100	-	10.0	MPa	1.08%FS
11	Press.	P-11	PA	11	MRP-2 Delivery	Fig.5. 3	0.100	-	10.0	MPa	1.08%FS
12	Press.	P-12	PA	12	Break A Upstream	Fig.5. 4	0.100	-	10.0	MPa	1.08%FS
13	Press.	P-13	PA	13	Break A Downstream	Fig.5. 4	0.100	-	10.0	MPa	1.08%FS
14	Press.	P-14	PA	14	Break B Upstream	Fig.5. 5	0.100	-	10.0	MPa	1.08%FS
15	Press.	P-15	PA	15	Break B Downstream	Fig.5. 5	0.100	-	10.0	MPa	1.08%FS
16	Press.	P-16	PA	16	Steam Line	Fig.5. 6	0.100	-	10.0	MPa	1.08%FS
17	Press.	P-17	PA	17	JP-1,2 Outlet Spool	Fig.5. 7	0.100	-	10.0	MPa	1.08%FS
18	Press.	P-18	PA	18	JP-3,4 Outlet Spool	Fig.5. 7	0.100	-	10.0	MPa	1.08%FS
19	Press.	P-19	PA	19	Break A Spool Piece	Fig.5. 4	0.100	-	10.0	MPa	1.08%FS
20	Press.	P-30	PA	20	Break B Spool Piece		0.100	-	10.0	MPa	1.08%FS
21	Diff.P.	D- 1	PD	21	Lower Pl.-Upper Pl.	Fig.5. 8	-50.0	-	350.	kPa	0.63%FS
22	Diff.P.	D- 2	PD	22	Upper Pl.-Steam Dome	Fig.5. 9	-10.0	-	90.0	kPa	0.63%FS
23	Diff.P	D- 3	PD	23	Lower Plenum Head	Not Measured					
24	Diff.P.	D- 4	PD	24	Downcomer Head	Fig.5.10	0.0	-	100.	kPa	0.63%FS
25	Diff.P.	D- 5	PD	25	PV Bottom-Top	Fig.5.11	-100.	-	900.	kPa	0.63%FS
26	Diff.P.	D- 6	PD	26	JP-1 Disch.-Suction	Fig.5.12	-100.	-	300.	kPa	0.63%FS
27	Diff.P.	D- 7	PD	27	JP-1 Drive -Suction	Fig.5.13	0.0	-	2.50	MPa	0.63%FS
28	Diff.P.	D- 8	PD	28	JP-2 Disch.-Suction	Fig.5.12	-100.	-	300.	kPa	0.63%FS
29	Diff.P.	D- 9	PD	29	JP-2 Drive -Suction	Fig.5.13	0.0	-	2.50	MPa	0.63%FS
30	Diff.P.	D-10	PD	30	JP-3 Disch.-Suction	Fig.5.14	-100.	-	300.	kPa	0.63%FS
31	Diff.P.	D-11	PD	31	JP-3 Drive -Suction	Fig.5.15	-4.00	-	2.00	MPa	0.63%FS
32	Diff.P.	D-12	PD	32	JP-4 Disch.-Suction	Fig.5.14	-100.	-	300.	kPa	0.63%FS
33	Diff.P.	D-13	PD	33	JP-4 Drive -Suction	Fig.5.15	-4.00	-	2.00	MPa	0.63%FS
34	Diff.P.	D-14	PD	34	MRP-1 Deliv.-Suction	Fig.5.16	-0.100	-	2.50	MPa	0.63%FS
35	Diff.P.	D-15	PD	35	MRP-2 Deliv.-Suction	Fig.5.16	-0.100	-	2.50	MPa	0.63%FS
36	Diff.P.	D-16	PD	36	DC Bottom- MRP-1 Suc.	Fig.5.17	-50.0	-	50.0	kPa	0.63%FS
37	Diff.P.	D-17	PD	37	MRP1 Deliv.-JP1 Drive	Fig.5.18	0.0	-	250.	kPa	0.63%FS
38	Diff.P.	D-18	PD	38	MRP1 Deliv.-JP2 Drive	Fig.5.18	0.0	-	250.	kPa	0.63%FS
39	Diff.P.	D-19	PD	39	DC Middle-JP1 Suction	Fig.5.19	0.0	-	250.	kPa	0.63%FS
40	Diff.P.	D-20	PD	40	DC Middle-JP2 Suction	Fig.5.19	0.0	-	250.	kPa	0.63%FS
41	Diff.P.	D-21	PD	41	JP1 Disch.-Lower Pl.	Fig.5.20	-100.	-	100.	kPa	0.63%FS
42	Diff.P.	D-22	PD	42	JP2 Disch.-Lower Pl.	Fig.5.20	-100.	-	100.	kPa	0.63%FS
43	Diff.P.	D-23	PD	43	DC Bottom- Break B	Failure	-60.0	-	540.	kPa	0.63%FS
44	Diff.P.	D-24	PD	44	Break B- Break A	Fig.5.21	0.0	-	100.	kPa	0.63%FS
45	Diff.P.	D-25	PD	45	Break A- MRP2 Suction	Fig.5.22	-500.	-	100.	kPa	0.63%FS
46	Diff.P.	D-26	PD	46	MRP2 Deliv.-JP3 Drive	Fig.5.23	-500.	-	500.	kPa	0.63%FS
47	Diff.P.	D-27	PD	47	MRP2 Deliv.-JP4 Drive	Fig.5.23	-500.	-	500.	kPa	0.63%FS
48	Diff.P.	D-28	PD	48	DC Middle-JP3 Suction	Fig.5.24	-250.	-	250.	kPa	0.63%FS
49	Diff.P.	D-29	PD	49	DC Middle-JP4 Suction	Fig.5.24	-250.	-	250.	kPa	0.63%FS
50	Diff.P.	D-30	PD	50	JP3 Disch.-Confluence	Fig.5.25	-100.	-	100.	kPa	0.63%FS

Table 3.2 Measurement List for RUN 983 (Continued)

51Ch.- 100Ch.

Ch.	Item	Symbol	ID.		Location	Fig.No.	Range			Unit	Accuracy
51	Diff.P.	D-31	PD	51	JP4 Disch.-Confluence	Fig.5.25	-100.	-	100.	kPa	0.63%FS
52	Diff.P.	D-32	PD	52	Confluence -Lower Pl.	Fig.5.26	-50.0	-	50.0	kPa	0.63%FS
53	Diff.P.	D-33	PD	53	Lower Pl.-DC Middle	Fig.5.27	-250.	-	250.	kPa	0.63%FS
54	Diff.P.	D-34	PD	54	Lower Pl.-DC Bottom	Fig.5.28	-250.	-	250.	kPa	0.63%FS
55	Diff.P.	D-35	PD	55	DC Bottom-DC Middle	Fig.5.29	-50.0	-	50.0	kPa	0.63%FS
56	Diff.P.	D-36	PD	56	DC Middle-Steam Dome	Fig.5.30	-50.0	-	50.0	kPa	0.63%FS
57	Diff.P.	D-37	PD	57	Lower Pl.Mid-Upper PL	Not Measured					
58	Diff.P.	D-38	PD	58	Lower Pl.Bottom-Mid.	Fig.5.31	0.0	-	50.0	kPa	0.63%FS
59	Diff.P.	D-39	PD	59	Upper Pl.-DC High	Fig.5.32	-20.0	-	100.	kPa	0.63%FS
60	Diff.P.	D-40	PD	60	Channel Orifice A	Fig.5.33	-50.0	-	50.0	kPa	0.63%FS
61	Diff.P.	D-41	PD	61	Channel Orifice B	Fig.5.34	-50.0	-	50.0	kPa	0.63%FS
62	Diff.P.	D-42	PD	62	Channel Orifice C	Fig.5.35	-25.0	-	75.0	kPa	0.63%FS
63	Diff.P.	D-43	PD	63	Channel Orifice D	Fig.5.36	-50.0	-	50.0	kPa	0.63%FS
64	Diff.P.	D-44	PD	64	Lower Plenum Head	Fig.5.37	-100.	-	100.	kPa	0.63%FS
65	Level	WL- 1	LM	65	HPCS Tank	Fig.5.37	0.0	-	2.30	m	1.00%FS
66	Level	WL- 2	LM	66	LPCS Tank	Fig.5.38	0.0	-	2.30	m	1.00%FS
67	Level	WL- 3	LM	67	LPCI Tank	Fig.5.38	0.0	-	4.25	m	1.00%FS
68	Level	WL- 4	LM	68	Upper Downcomer	Fig.5.39	3.90	-	6.04	m	1.00%FS
69	Level	WL- 5	LM	69	Lower Downcomer	Fig.5.39	0.938	-	3.90	m	1.00%FS
70	Mass.F.	F- 1	FM	70	Steam Line (Low Range)	Fig.5.40	0.0	-	1.13	kg/s	0.92%FS
71	Mass.F.	F- 2	FM	71	Steam Line(High Range)	Fig.5.40	0.0	-	3.00	kg/s	0.92%FS
72	Mass.F.	F- 3	FM	72	Steam Line (Mid Range)	Fig.5.40	0.0	-	1.94	kg/s	1.40%FS
73	Vol.F.	F- 7	FV	73	HPCS (Upper Plenum)	Fig.5.41	0.0	-	0.250E-02	m3/s	0.79%FS
74	Vol.F.	F- 9	FV	74	LPCS (Upper Plenum)	Fig.5.41	0.0	-	0.250E-02	m3/s	0.79%FS
75	Vol.F.	F-11	FV	75	LPCI (Core Bypass)	Fig.5.41	0.0	-	0.830E-02	m3/s	0.79%FS
76	Vol.F.	F-15	FV	76	Feedwater	Fig.5.42	0.0	-	0.100E-01	m3/s	0.79%FS
77	Vol.F.	F-16	FV	77	PWT Flow	Not Measured	0.0	-	0.420E-02	m3/s	0.79%FS
78	Vol.F.	F-17	FV	78	JP1 Discharge	Fig.5.43	0.0	-	0.170E-01	m3/s	0.88%FS
79	Vol.F.	F-18	FV	79	JP2 Discharge	Fig.5.43	0.0	-	0.170E-01	m3/s	0.88%FS
80	Vol.F.	F-19	FV	80	JP3 Disch. Positive	Fig.5.44	0.0	-	0.170E-01	m3/s	0.92%FS
81	Vol.F.	F-20	FV	81	JP3 Disch. Negative	Fig.5.45	0.0	-	0.500E-02	m3/s	0.92%FS
82	Vol.F.	F-21	FV	82	JP4 Disch. Positive	Fig.5.44	0.0	-	0.170E-01	m3/s	0.92%FS
83	Vol.F.	F-22	FV	83	JP4 Disch. Negative	Fig.5.45	0.0	-	0.500E-02	m3/s	0.92%FS
84	Mass.F.	F-23	FM	84	JP1,2 Outlet Spool	Not Measured	0.0	-	30.0	kg/s	1.40%FS
85	Mass.F.	F-24	FM	85	JP3,4 Outlet Spool	Not Measured	0.0	-	30.0	kg/s	1.40%FS
86	Mass.F.	F-25	FM	86	Break A Spool Piece	Not Measured	0.0	-	30.0	kg/s	1.40%FS
87	Mass.F.	F-26	FM	87	Break B Spool Piece	Not Measured	0.0	-	30.0	kg/s	1.40%FS
88	Vol.F.	F-27	FV	88	MRP-1	Fig.5.46	0.0	-	0.120E-01	m3/s	0.88%FS
89	Vol.F.	F-28	FV	89	MRP-2	Fig.5.46	0.0	-	0.120E-01	m3/s	0.63%FS
90	Diff.P.	D-F1	PD	90	F1 Orifice	Fig.5.47	0.0	-	4.90	kPa	0.63%FS
91	Diff.P.	D-F2	PD	91	F2 Orifice	Fig.5.48	0.0	-	34.9	kPa	0.63%FS
92	Diff.P.	D-F3	PD	92	F3 Orifice	Fig.5.49	0.0	-	14.6	kPa	0.63%FS
93	Diff.P.	D-F17	PD	93	F17 Venturi	Fig.5.50	0.0	-	98.1	kPa	0.63%FS
94	Diff.P.	D-F18	PD	94	F18 Venturi	Fig.5.51	0.0	-	98.1	kPa	0.63%FS
95	Diff.P.	D-F19	PD	95	F19 Orifice	Fig.5.52	0.0	-	147.	kPa	0.63%FS
96	Diff.P.	D-F20	PD	96	F20 Orifice	Fig.5.53	0.0	-	13.2	kPa	0.63%FS
97	Diff.P.	D-F21	PD	97	F21 Orifice	Fig.5.54	0.0	-	147.	kPa	0.63%FS
98	Diff.P.	D-F22	PD	98	F22 Orifice	Fig.5.55	0.0	-	13.2	kPa	0.63%FS
99	Diff.P.	D-F27	PD	99	F27 Venturi	Fig.5.56	0.0	-	200.	kPa	0.63%FS
100	Diff.P.	D-F28	PD	100	F28 Venturi	Fig.5.57	0.0	-	200.	kPa	0.63%FS

Table 3.2 Measurement List for RUN 983 (Continued)

101Ch.- 150Ch.

Ch.	Item	Symbol	ID.		Location	Fig.No.	Range			Unit	Accuracy
101	Power	W- 1	WE	101	2100 kW Power Supplier	Fig.5.58	0.0	-	0.210E+04	kW	1.00%FS
102	Power	W- 2	WE	102	3150 kW Power Supplier	Fig.5.58	0.0	-	0.315E+04	kW	1.00%FS
103											
104	Rev.	N- 1	SR	104	MRP-1 Revolution	Fig.5.59	0.0	-	0.500E+04	RPM	1.08%FS
105	Rev.	N- 2	SR	105	MRP-2 Revolution	Fig.5.59	0.0	-	0.500E+04	RPM	1.08%FS
106	Signal	S- 1	EV	106	Break Signal A	Fig.5.60					
107	Signal	S- 2	EV	107	Break Signal B	Fig.5.60					
108	Signal	S- 3	EV	108	QSV Signal	Fig.5.60					
109	Signal	S- 6	EV	109	HPCS Valve	Fig.5.61					
110	Signal	S- 7	EV	110	LPCS Valve	Fig.5.61					
111	Signal	S- 8	EV	111	LPCI Valve	Fig.5.61					
112	Signal	S- 9	EV	112	Feedwater Control	Fig.5.60					
113	Signal	S-10	EV	113	MSIV Signal	Fig.5.60					
114	Signal	S-11	EV	114	Steam Line Valve	Fig.5.60					
115	Signal	S-12	EV	115	ADS Valve	Fig.5.61					
116	Signal	S-13	EV	116	MRP-1 Power OFF	Fig.5.62					
117	Signal	S-14	EV	117	MRP-2 Power OFF	Fig.5.62					
118	Signal	RD- 1	EV	118	MRP-1 Rev. Direction	Failure					
119	Signal	RD- 2	EV	119	MRP-2 Rev. Direction	Failure					
120	Density	DF- 1	DE	120	JP1,2 Outlet Beam A	Not Measured	0.0	-	0.100E+04	kg/m3	1.00%FS
121	Density	DF- 2	DE	121	JP1,2 Outlet Beam B	Not Measured	0.0	-	0.100E+04	kg/m3	1.00%FS
122	Density	DF- 3	DE	122	JP1,2 Outlet Beam C	Not Measured	0.0	-	0.100E+04	kg/m3	1.00%FS
123	Density	DF- 4	DE	123	JP3,4 Outlet Beam A	Fig.5.63	0.0	-	0.100E+04	kg/m3	1.00%FS
124	Density	DF- 5	DE	124	JP3,4 Outlet Beam B	Fig.5.64	0.0	-	0.100E+04	kg/m3	1.00%FS
125	Density	DF- 6	DE	125	JP3,4 Outlet Beam C	Fig.5.65	0.0	-	0.100E+04	kg/m3	1.00%FS
126	Density	DF- 7	DE	126	Break A Beam A	Fig.5.66	0.0	-	0.100E+04	kg/m3	1.00%FS
127	Density	DF- 8	DE	127	Break A Beam B	Fig.5.67	0.0	-	0.100E+04	kg/m3	1.00%FS
128	Density	DF- 9	DE	128	Break B Beam A	Fig.5.68	0.0	-	0.100E+04	kg/m3	1.00%FS
129	Density	DF-10	DE	129	Break B Beam B	Fig.5.69	0.0	-	0.100E+04	kg/m3	1.00%FS
130	Mo.Flux	M- 1	MF	130	JP1,2 Outlet Spool		0.0	-	0.220E+05	kg/ms2	1.00%FS
131	Mo.Flux	M- 2	MF	131	JP3,4 Outlet Spool		0.0	-	0.220E+05	kg/ms2	1.00%FS
132	Mo.Flux	M- 3	MF	132	Break A (Low Range)	Fig.5.70	0.0	-	0.220E+05	kg/ms2	1.00%FS
133	Mo.Flux	M- 4	MF	133	Break B (Low Range)	Fig.5.71	0.0	-	0.220E+05	kg/ms2	1.00%FS
134	Mo.Flux	M- 5	MF	134	Break A (High Range)	Fig.5.72	0.0	-	0.220E+06	kg/ms2	1.00%FS
135	Mo.Flux	M- 6	MF	135	Break B (High Range)	Fig.5.73	0.0	-	0.220E+06	kg/ms2	1.00%FS
136	Mo.Flux	M- 7	MF	136	Break Orifice	Not Measured	0.0	-	0.220E+05	kg/ms2	1.00%FS
137											
138	Fluid T.	T- 1	TE	138	Lower Plenum	Fig.5.74	273.	-	673.	K	0.64%FS
139	Fluid T.	T- 2	TE	139	Upper Plenum	Fig.5.74	273.	-	673.	K	0.64%FS
140	Fluid T.	T- 3	TE	140	Steam Dome	Fig.5.75	273.	-	673.	K	0.64%FS
141	Fluid T.	T- 4	TE	141	Upper Downcomer	Fig.5.76	273.	-	673.	K	0.64%FS
142	Fluid T.	T- 5	TE	142	Lower Downcomer	Fig.5.76	273.	-	673.	K	0.64%FS
143	Fluid T.	T- 6	TE	143	JP-1 Drive	Fig.5.77	273.	-	673.	K	0.64%FS
144	Fluid T.	T- 7	TE	144	JP-2 Drive	Fig.5.77	273.	-	673.	K	0.64%FS
145	Fluid T.	T- 8	TE	145	JP-3 Drive	Fig.5.78	273.	-	673.	K	0.64%FS
146	Fluid T.	T- 9	TE	146	JP-4 Drive	Fig.5.78	273.	-	673.	K	0.64%FS
147	Fluid T.	T-10	TE	147	JP-1 Discharge	Fig.5.79	273.	-	673.	K	0.64%FS
148	Fluid T.	T-11	TE	148	JP-2 Discharge	Fig.5.79	273.	-	673.	K	0.64%FS
149	Fluid T.	T-12	TE	149	JP-3 Discharge	Fig.5.80	273.	-	673.	K	0.64%FS
150	Fluid T.	T-13	TE	150	JP-4 Discharge	Fig.5.80	273.	-	673.	K	0.64%FS

Table 3.2 Measurement List for RUN 983 (Continued)

151Ch.- 200Ch.

Ch.	Item	Symbol	ID.		Location	Fig.No.	Range			Unit	Accuracy
151	Fluid T.	T-14	TE	151	MRP-1 Suction	Fig.5.77	273.	-	673.	K	0.64%FS
152	Fluid T.	T-15	TE	152	MRP-1 Delivery	Fig.5.77	273.	-	673.	K	0.64%FS
153	Fluid T.	T-16	TE	153	MRP-2 Suction	Fig.5.78	273.	-	673.	K	0.64%FS
154	Fluid T.	T-17	TE	154	MRP-2 Delivery	Fig.5.78	273.	-	673.	K	0.64%FS
155	Fluid T.	T-18	TE	155	Break A Upstream	Fig.5.81	273.	-	673.	K	0.64%FS
156	Fluid T.	T-19	TE	156	Break B Upstream	Fig.5.81	273.	-	673.	K	0.64%FS
157	Fluid T.	T-20	TE	157	RCN A Condenced Water	Not Used	273.	-	698.	K	0.64%FS
158	Fluid T.	T-21	TE	158	RCN B Condenced Water	Not Used	273.	-	698.	K	0.64%FS
159	Fluid T.	T-22	TE	159	Discharged Steam	Fig.5.75	273.	-	673.	K	0.64%FS
160	Fluid T.	T-24	TE	160	JP-1,2 Outlet Spool	Fig.5.79	273.	-	763.	K	0.64%FS
161	Fluid T.	T-25	TE	161	JP-3,4 Outlet Spool	Fig.5.80	273.	-	763.	K	0.64%FS
162	Fluid T.	T-26	TE	162	Break A Spool Piece	Fig.5.81	273.	-	763.	K	0.64%FS
163	Fluid T.	T-27	TE	163	Break B Spool Piece	Fig.5.81	273.	-	763.	K	0.64%FS
164	Fluid T.	T-28	TE	164	Feedwater	Fig.5.82	273.	-	673.	K	0.64%FS
165	Fluid T.	T-29	TE	165	Break Orifice 1	Not Measured	273.	-	673.	K	0.64%FS
166	Fluid T.	T-30	TE	166	Break Orifice 2	Not Measured	273.	-	673.	K	0.64%FS
167	Fluid T.	T-31	TE	167	Break A Down DD(Low)	Not Measured	273.	-	673.	K	0.64%FS
168	Fluid T.	T-32	TE	168	Break B Down DD(Low)	Not Measured	273.	-	673.	K	0.64%FS
169	Fluid T.	T-33	TE	169	Break A Up. DD(High)		273.	-	673.	K	0.64%FS
170	Fluid T.	T-34	TE	170	Break B Up. DD(High)		273.	-	673.	K	0.64%FS
171	Fluid T.	T-F17	TE	171	JP1 Fluid D. Correc.		273.	-	673.	K	0.64%FS
172	Fluid T.	T-F18	TE	172	JP2 Fluid D. Correc.		273.	-	673.	K	0.64%FS
173	Fluid T.	T-F19	TE	173	JP3 Fluid D. Correc.		273.	-	673.	K	0.64%FS
174	Fluid T.	T-F21	TE	174	JP4 Fluid D. Correc.		273.	-	673.	K	0.64%FS
175	Fluid T.	T-35	TE	175	Feedwater Temperature		273.	-	673.	K	0.64%FS
176	Fluid T.		TE	176	Steam L. (F-110-3)		273.	-	673.	K	0.64%FS
177	Slab T.	TS-13	TE	177	Filler Block C Pos.1	Not Measured	273.	-	673.	K	0.64%FS
178	Slab T.	TS-14	TE	178	Filler Block C Pos.2	Not Measured	273.	-	673.	K	0.64%FS
179	Slab T.	TS-15	TE	179	Filler Block C Pos.3		273.	-	673.	K	0.64%FS
180	Slab T.	TS-16	TE	180	Filler Block C Pos.4	Not Measured	273.	-	673.	K	0.64%FS
181	Slab T.	TS-17	TE	181	Filler Block C Pos.5	Not Measured	273.	-	673.	K	0.64%FS
182	Slab T.	TS-18	TE	182	Filler Block C Pos.6		273.	-	673.	K	0.64%FS
183	Slab T.	TS-19	TE	183	Filler Block A Pos.1	Not Measured	273.	-	673.	K	0.64%FS
184	Slab T.	TS-20	TE	184	Filler Block A Pos.2	Not Measured	273.	-	673.	K	0.64%FS
185	Slab T.	TS-21	TE	185	Filler Block A Pos.3	Not Measured	273.	-	673.	K	0.64%FS
186	Slab T.	TS-22	TE	186	Filler Block A Pos.4	Not Measured	273.	-	673.	K	0.64%FS
187	Slab T.	TS-23	TE	187	Filler Block A Pos.5	Not Measured	273.	-	673.	K	0.64%FS
188	Slab T.	TS-24	TE	188	Filler Block A Pos.6	Not Measured	273.	-	673.	K	0.64%FS
189	Slab T.	TS-25	TE	189	JP-1 Diffuser Wall	Not Measured	273.	-	673.	K	0.64%FS
190	Slab T.	TS-26	TE	190	JP-2 Diffuser Wall	Not Measured	273.	-	673.	K	0.64%FS
191	Slab T.	TS-27	TE	191	JP-3 Diffuser Wall	Not Measured	273.	-	673.	K	0.64%FS
192	Slab T.	TS-28	TE	192	JP-4 Diffuser Wall	Not Measured	273.	-	673.	K	0.64%FS
193	Slab T.	TS-29	TE	193	PV Wall Inside 1-1		273.	-	673.	K	0.64%FS
194	Slab T.	TS-30	TE	194	PV Inner Surface 1-2	Not Measured	273.	-	673.	K	0.64%FS
195	Slab T.	TS-31	TE	195	PV Inner Surface 1-3		273.	-	673.	K	0.64%FS
196	Slab T.	TS-32	TE	196	PV Wall Inside 2		273.	-	673.	K	0.64%FS
197	Slab T.	TS-33	TE	197	PV Wall Inside 3		273.	-	673.	K	0.64%FS
198	Slab T.	TS-34	TE	198	PV Wall Inside 4		273.	-	673.	K	0.64%FS
199	Slab T.	TS-35	TE	199	L.P. Inner Surface	Not Measured	273.	-	673.	K	0.64%FS
200	Slab T.	TS-36	TE	200	L.P. Wall Inside		273.	-	673.	K	0.64%FS

Table 3.2 Measurement List for RUN 983 (Continued)

201Ch.- 250Ch.

Ch.	Item	Symbol	ID.	Location	Fig.No.	Range	Unit	Accuracy
201	Temp.	TF- 1	TE 201	A11 Fuel Rod Pos.1	Fig.5.83, 114	273. - 0.147E+04	K	0.64%FS
202	Temp.	TF- 2	TE 202	A11 Fuel Rod Pos.2	Fig.5.83, 115	273. - 0.147E+04	K	0.64%FS
203	Temp.	TF- 3	TE 203	A11 Fuel Rod Pos.3	Fig.5.83, 116	273. - 0.147E+04	K	0.64%FS
204	Temp.	TF- 4	TE 204	A11 Fuel Rod Pos.4	Fig.5.83, 117	273. - 0.147E+04	K	0.64%FS
205	Temp.	TF- 5	TE 205	A11 Fuel Rod Pos.5	Fig.5.83, 118	273. - 0.147E+04	K	0.64%FS
206	Temp.	TF- 6	TE 206	A11 Fuel Rod Pos.6	Fig.5.83, 119	273. - 0.147E+04	K	0.64%FS
207	Temp.	TF- 7	TE 207	A11 Fuel Rod Pos.7	Fig.5.83, 120	273. - 0.147E+04	K	0.64%FS
208	Temp.	TF- 8	TE 208	A12 Fuel Rod Pos.1	Fig.5.84, 114	273. - 0.147E+04	K	0.64%FS
209	Temp.	TF- 9	TE 209	A12 Fuel Rod Pos.2	Fig.5.84, 115	273. - 0.147E+04	K	0.64%FS
210	Temp.	TF- 10	TE 210	A12 Fuel Rod Pos.3	Fig.5.84, 116	273. - 0.147E+04	K	0.64%FS
211	Temp.	TF- 11	TE 211	A12 Fuel Rod Pos.4	Fig.5.84, 117	273. - 0.147E+04	K	0.64%FS
212	Temp.	TF- 12	TE 212	A12 Fuel Rod Pos.5	Fig.5.84, 118	273. - 0.147E+04	K	0.64%FS
213	Temp.	TF- 13	TE 213	A12 Fuel Rod Pos.6	Fig.5.84, 119	273. - 0.147E+04	K	0.64%FS
214	Temp.	TF- 14	TE 214	A12 Fuel Rod Pos.7	Fig.5.84, 120	273. - 0.147E+04	K	0.64%FS
215	Temp.	TF- 15	TE 215	A13 Fuel Rod Pos.1	Fig.5.85, 114	273. - 0.147E+04	K	0.64%FS
216	Temp.	TF- 16	TE 216	A13 Fuel Rod Pos.2	Fig.5.85, 115	273. - 0.147E+04	K	0.64%FS
217	Temp.	TF- 17	TE 217	A13 Fuel Rod Pos.3	Fig.5.85, 116	273. - 0.147E+04	K	0.64%FS
218	Temp.	TF- 18	TE 218	A13 Fuel Rod Pos.4	Fig.5.85, 117	273. - 0.147E+04	K	0.64%FS
219	Temp.	TF- 19	TE 219	A13 Fuel Rod Pos.5	Fig.5.85, 118	273. - 0.147E+04	K	0.64%FS
220	Temp.	TF- 20	TE 220	A13 Fuel Rod Pos.6	Fig.5.85, 119	273. - 0.147E+04	K	0.64%FS
221	Temp.	TF- 21	TE 221	A13 Fuel Rod Pos.7	Fig.5.85, 120	273. - 0.147E+04	K	0.64%FS
222	Temp.	TF- 22	TE 222	A14 Fuel Rod Pos.1	Not Measured	273. - 0.147E+04	K	0.64%FS
223	Temp.	TF- 23	TE 223	A14 Fuel Rod Pos.2	Not Measured	273. - 0.147E+04	K	0.64%FS
224	Temp.	TF- 24	TE 224	A14 Fuel Rod Pos.3	Not Measured	273. - 0.147E+04	K	0.64%FS
225	Temp.	TF- 25	TE 225	A14 Fuel Rod Pos.4	Not Measured	273. - 0.147E+04	K	0.64%FS
226	Temp.	TF- 26	TE 226	A14 Fuel Rod Pos.5	Not Measured	273. - 0.147E+04	K	0.64%FS
227	Temp.	TF- 27	TE 227	A14 Fuel Rod Pos.6	Not Measured	273. - 0.147E+04	K	0.64%FS
228	Temp.	TF- 28	TE 228	A14 Fuel Rod Pos.7	Not Measured	273. - 0.147E+04	K	0.64%FS
229	Temp.	TF- 29	TE 229	A15 Fuel Rod Pos.1	Not Measured	273. - 0.147E+04	K	0.64%FS
230	Temp.	TF- 30	TE 230	A15 Fuel Rod Pos.4	Not Measured	273. - 0.147E+04	K	0.64%FS
231	Temp.	TF- 31	TE 231	A17 Fuel Rod Pos.1	Not Measured	273. - 0.147E+04	K	0.64%FS
232	Temp.	TF- 32	TE 232	A17 Fuel Rod Pos.4	Fig.5.103	273. - 0.147E+04	K	0.64%FS
233	Temp.	TF- 33	TE 233	A22 Fuel Rod Pos.1	Fig.5.86, 121	273. - 0.147E+04	K	0.64%FS
234	Temp.	TF- 34	TE 234	A22 Fuel Rod Pos.2	Fig.5.86, 122	273. - 0.147E+04	K	0.64%FS
235	Temp.	TF- 35	TE 235	A22 Fuel Rod Pos.3	Fig.5.86, 123	273. - 0.147E+04	K	0.64%FS
236	Temp.	TF- 36	TE 236	A22 Fuel Rod Pos.4	Fig.5.86, 124	273. - 0.125E+04	K	0.64%FS
237	Temp.	TF- 37	TE 237	A22 Fuel Rod Pos.5	Fig.5.86, 125	273. - 0.125E+04	K	0.64%FS
238	Temp.	TF- 38	TE 238	A22 Fuel Rod Pos.6	Fig.5.86, 126	273. - 0.125E+04	K	0.64%FS
239	Temp.	TF- 39	TE 239	A22 Fuel Rod Pos.7	Fig.5.86, 127	273. - 0.125E+04	K	0.64%FS
240	Temp.	TF- 40	TE 240	A24 Fuel Rod Pos.1	Not Measured	273. - 0.125E+04	K	0.64%FS
241	Temp.	TF- 41	TE 241	A24 Fuel Rod Pos.2	Not Measured	273. - 0.125E+04	K	0.64%FS
242	Temp.	TF- 42	TE 242	A24 Fuel Rod Pos.3	Not Measured	273. - 0.125E+04	K	0.64%FS
243	Temp.	TF- 43	TE 243	A24 Fuel Rod Pos.4	Not Measured	273. - 0.125E+04	K	0.64%FS
244	Temp.	TF- 44	TE 244	A24 Fuel Rod Pos.5	Not Measured	273. - 0.125E+04	K	0.64%FS
245	Temp.	TF- 45	TE 245	A24 Fuel Rod Pos.6	Not Measured	273. - 0.125E+04	K	0.64%FS
246	Temp.	TF- 46	TE 246	A24 Fuel Rod Pos.7	Not Measured	273. - 0.125E+04	K	0.64%FS
247	Temp.	TF- 47	TE 247	A26 Fuel Rod Pos.1	Not Measured	273. - 0.125E+04	K	0.64%FS
248	Temp.	TF- 48	TE 248	A26 Fuel Rod Pos.2	Not Measured	273. - 0.125E+04	K	0.64%FS
249	Temp.	TF- 49	TE 249	A28 Fuel Rod Pos.1	Not Measured	273. - 0.125E+04	K	0.64%FS
250	Temp.	TF- 50	TE 250	A28 Fuel Rod Pos.4	Fig.5.104	273. - 0.125E+04	K	0.64%FS

Table 3.2 Measurement List for RUN 983 (Continued)

251Ch.- 300Ch.

Ch.	Item	Symbol	ID.	Location	Fig.No.	Range	Unit	Accuracy
251	Temp.	TF- 51	TE 251	A31 Fuel Rod Pos.1	Not Measured	273. - 0.125E+04	K	0.64%FS
252	Temp.	TF- 52	TE 252	A31 Fuel Rod Pos.4	Fig.5.105	273. - 0.125E+04	K	0.64%FS
253	Temp.	TF- 53	TE 253	A33 Fuel Rod Pos.1	Fig.5.87	273. - 0.125E+04	K	0.64%FS
254	Temp.	TF- 54	TE 254	A33 Fuel Rod Pos.2	Fig.5.87	273. - 0.125E+04	K	0.64%FS
255	Temp.	TF- 55	TE 255	A33 Fuel Rod Pos.3	Fig.5.87	273. - 0.125E+04	K	0.64%FS
256	Temp.	TF- 56	TE 256	A33 Fuel Rod Pos.4	Fig.5.87	273. - 0.125E+04	K	0.64%FS
257	Temp.	TF- 57	TE 257	A33 Fuel Rod Pos.5	Fig.5.87	273. - 0.125E+04	K	0.64%FS
258	Temp.	TF- 58	TE 258	A33 Fuel Rod Pos.6	Fig.5.87	273. - 0.125E+04	K	0.64%FS
259	Temp.	TF- 59	TE 259	A33 Fuel Rod Pos.7	Fig.5.87	273. - 0.125E+04	K	0.64%FS
260	Temp.	TF- 60	TE 260	A34 Fuel Rod Pos.1	Not Measured	273. - 0.125E+04	K	0.64%FS
261	Temp.	TF- 61	TE 261	A34 Fuel Rod Pos.2	Not Measured	273. - 0.125E+04	K	0.64%FS
262	Temp.	TF- 62	TE 262	A34 Fuel Rod Pos.3	Not Measured	273. - 0.125E+04	K	0.64%FS
263	Temp.	TF- 63	TE 263	A34 Fuel Rod Pos.4	Not Measured	273. - 0.125E+04	K	0.64%FS
264	Temp.	TF- 64	TE 264	A34 Fuel Rod Pos.5	Not Measured	273. - 0.125E+04	K	0.64%FS
265	Temp.	TF- 65	TE 265	A34 Fuel Rod Pos.6	Not Measured	273. - 0.125E+04	K	0.64%FS
266	Temp.	TF- 66	TE 266	A34 Fuel Rod Pos.7	Not Measured	273. - 0.125E+04	K	0.64%FS
267	Temp.	TF- 67	TE 267	A37 Fuel Rod Pos.1	Not Measured	273. - 0.125E+04	K	0.64%FS
268	Temp.	TF- 68	TE 268	A37 Fuel Rod Pos.4	Not Measured	273. - 0.125E+04	K	0.64%FS
269	Temp.	TF- 69	TE 269	A42 Fuel Rod Pos.1	Not Measured	273. - 0.125E+04	K	0.64%FS
270	Temp.	TF- 70	TE 270	A42 Fuel Rod Pos.4	Not Measured	273. - 0.125E+04	K	0.64%FS
271	Temp.	TF- 71	TE 271	A44 Fuel Rod Pos.1	Not Measured	273. - 0.125E+04	K	0.64%FS
272	Temp.	TF- 72	TE 272	A44 Fuel Rod Pos.2	Not Measured	273. - 0.125E+04	K	0.64%FS
273	Temp.	TF- 73	TE 273	A44 Fuel Rod Pos.3	Not Measured	273. - 0.125E+04	K	0.64%FS
274	Temp.	TF- 74	TE 274	A44 Fuel Rod Pos.4	Not Measured	273. - 0.125E+04	K	0.64%FS
275	Temp.	TF- 75	TE 275	A44 Fuel Rod Pos.5	Not Measured	273. - 0.125E+04	K	0.64%FS
276	Temp.	TF- 76	TE 276	A44 Fuel Rod Pos.6	Not Measured	273. - 0.125E+04	K	0.64%FS
277	Temp.	TF- 77	TE 277	A44 Fuel Rod Pos.7	Not Measured	273. - 0.125E+04	K	0.64%FS
278	Temp.	TF- 78	TE 278	A48 Fuel Rod Pos.1	Not Measured	273. - 0.125E+04	K	0.64%FS
279	Temp.	TF- 79	TE 279	A48 Fuel Rod Pos.4	Not Measured	273. - 0.125E+04	K	0.64%FS
280	Temp.	TF- 80	TE 280	A51 Fuel Rod Pos.1	Not Measured	273. - 0.125E+04	K	0.64%FS
281	Temp.	TF- 81	TE 281	A51 Fuel Rod Pos.4	Not Measured	273. - 0.125E+04	K	0.64%FS
282	Temp.	TF- 82	TE 282	A53 Fuel Rod Pos.1	Not Measured	273. - 0.125E+04	K	0.64%FS
283	Temp.	TF- 83	TE 283	A53 Fuel Rod Pos.4	Not Measured	273. - 0.125E+04	K	0.64%FS
284	Temp.	TF- 84	TE 284	A57 Fuel Rod Pos.1	Not Measured	273. - 0.125E+04	K	0.64%FS
285	Temp.	TF- 85	TE 285	A57 Fuel Rod Pos.4	Fig.5.106	273. - 0.125E+04	K	0.64%FS
286	Temp.	TF- 86	TE 286	A62 Fuel Rod Pos.1	Not Measured	273. - 0.125E+04	K	0.64%FS
287	Temp.	TF- 87	TE 287	A62 Fuel Rod Pos.4	Not Measured	273. - 0.125E+04	K	0.64%FS
288	Temp.	TF- 88	TE 288	A66 Fuel Rod Pos.1	Not Measured	273. - 0.125E+04	K	0.64%FS
289	Temp.	TF- 89	TE 289	A66 Fuel Rod Pos.4	Not Measured	273. - 0.125E+04	K	0.64%FS
290	Temp.	TF- 90	TE 290	A68 Fuel Rod Pos.1	Not Measured	273. - 0.125E+04	K	0.64%FS
291	Temp.	TF- 91	TE 291	A68 Fuel Rod Pos.4	Fig.5.107	273. - 0.125E+04	K	0.64%FS
292	Temp.	TF- 92	TE 292	A71 Fuel Rod Pos.1	Not Measured	273. - 0.125E+04	K	0.64%FS
293	Temp.	TF- 93	TE 293	A71 Fuel Rod Pos.4	Fig.5.108	273. - 0.125E+04	K	0.64%FS
294	Temp.	TF- 94	TE 294	A73 Fuel Rod Pos.1	Not Measured	273. - 0.125E+04	K	0.64%FS
295	Temp.	TF- 95	TE 295	A73 Fuel Rod Pos.4	Fig.5.109	273. - 0.125E+04	K	0.64%FS
296	Temp.	TF- 96	TE 296	A75 Fuel Rod Pos.1	Not Measured	273. - 0.125E+04	K	0.64%FS
297	Temp.	TF- 97	TE 297	A75 Fuel Rod Pos.4	Not Measured	273. - 0.125E+04	K	0.64%FS
298	Temp.	TF- 98	TE 298	A77 Fuel Rod Pos.1	Fig.5.88, 128	273. - 0.125E+04	K	0.64%FS
299	Temp.	TF- 99	TE 299	A77 Fuel Rod Pos.2	Fig.5.88, 129	273. - 0.125E+04	K	0.64%FS
300	Temp.	TF-100	TE 300	A77 Fuel Rod Pos.3	Fig.5.88, 130	273. - 0.125E+04	K	0.64%FS

Table 3.2 Measurement List for RUN 983 (Continued)

301Ch.- 350Ch.

Ch.	Item	Symbol	ID.	Location	Fig.No.	Range	Unit	Accuracy
301	Temp.	TF-101	TE 301	A77 Fuel Rod Pos.4	Fig.5.88, 131	273. - 0.125E+04	K	0.64%FS
302	Temp.	TF-102	TE 302	A77 Fuel Rod Pos.5	Fig.5.88, 132	273. - 0.125E+04	K	0.64%FS
303	Temp.	TF-103	TE 303	A77 Fuel Rod Pos.6	Fig.5.88, 133	273. - 0.125E+04	K	0.64%FS
304	Temp.	TF-104	TE 304	A77 Fuel Rod Pos.7	Failure	273. - 0.125E+04	K	0.64%FS
305	Temp.	TF-105	TE 305	A82 Fuel Rod Pos.1	Not Measured	273. - 0.125E+04	K	0.64%FS
306	Temp.	TF-106	TE 306	A82 Fuel Rod Pos.4	Not Measured	273. - 0.125E+04	K	0.64%FS
307	Temp.	TF-107	TE 307	A84 Fuel Rod Pos.1	Not Measured	273. - 0.125E+04	K	0.64%FS
308	Temp.	TF-108	TE 308	A84 Fuel Rod Pos.4	Fig.5.110	273. - 0.125E+04	K	0.64%FS
309	Temp.	TF-109	TE 309	A85 Fuel Rod Pos.1	Not Measured	273. - 0.125E+04	K	0.64%FS
310	Temp.	TF-110	TE 310	A85 Fuel Rod Pos.2	Not Measured	273. - 0.125E+04	K	0.64%FS
311	Temp.	TF-111	TE 311	A85 Fuel Rod Pos.3	Not Measured	273. - 0.125E+04	K	0.64%FS
312	Temp.	TF-112	TE 312	A85 Fuel Rod Pos.4	Not Measured	273. - 0.125E+04	K	0.64%FS
313	Temp.	TF-113	TE 313	A85 Fuel Rod Pos.5	Not Measured	273. - 0.125E+04	K	0.64%FS
314	Temp.	TF-114	TE 314	A85 Fuel Rod Pos.6	Not Measured	273. - 0.125E+04	K	0.64%FS
315	Temp.	TF-115	TE 315	A85 Fuel Rod Pos.7	Not Measured	273. - 0.125E+04	K	0.64%FS
316	Temp.	TF-116	TE 316	A87 Fuel Rod Pos.1	Fig.5.89	273. - 0.125E+04	K	0.64%FS
317	Temp.	TF-117	TE 317	A87 Fuel Rod Pos.2	Fig.5.89	273. - 0.125E+04	K	0.64%FS
318	Temp.	TF-118	TE 318	A87 Fuel Rod Pos.3	Fig.5.89	273. - 0.125E+04	K	0.64%FS
319	Temp.	TF-119	TE 319	A87 Fuel Rod Pos.4	Fig.5.89	273. - 0.125E+04	K	0.64%FS
320	Temp.	TF-120	TE 320	A87 Fuel Rod Pos.5	Fig.5.89	273. - 0.125E+04	K	0.64%FS
321	Temp.	TF-121	TE 321	A87 Fuel Rod Pos.6	Fig.5.89	273. - 0.125E+04	K	0.64%FS
322	Temp.	TF-122	TE 322	A87 Fuel Rod Pos.7	Fig.5.89	273. - 0.125E+04	K	0.64%FS
323	Temp.	TF-123	TE 323	A88 Fuel Rod Pos.1	Fig.5.90	273. - 0.125E+04	K	0.64%FS
324	Temp.	TF-124	TE 324	A88 Fuel Rod Pos.2	Fig.5.90	273. - 0.125E+04	K	0.64%FS
325	Temp.	TF-125	TE 325	A88 Fuel Rod Pos.3	Fig.5.90	273. - 0.125E+04	K	0.64%FS
326	Temp.	TF-126	TE 326	A88 Fuel Rod Pos.4	Fig.5.90	273. - 0.125E+04	K	0.64%FS
327	Temp.	TF-127	TE 327	A88 Fuel Rod Pos.5	Fig.5.90	273. - 0.125E+04	K	0.64%FS
328	Temp.	TF-128	TE 328	A88 Fuel Rod Pos.6	Fig.5.90	273. - 0.125E+04	K	0.64%FS
329	Temp.	TF-129	TE 329	A88 Fuel Rod Pos.7	Fig.5.90	273. - 0.125E+04	K	0.64%FS
330	Temp.	TF-130	TE 330	B11 Fuel Rod Pos.1	Fig.5.91	273. - 0.125E+04	K	0.64%FS
331	Temp.	TF-131	TE 331	B11 Fuel Rod Pos.2	Fig.5.91	273. - 0.125E+04	K	0.64%FS
332	Temp.	TF-132	TE 332	B11 Fuel Rod Pos.3	Fig.5.91	273. - 0.125E+04	K	0.64%FS
333	Temp.	TF-133	TE 333	B11 Fuel Rod Pos.4	Fig.5.91	273. - 0.125E+04	K	0.64%FS
334	Temp.	TF-134	TE 334	B11 Fuel Rod Pos.5	Fig.5.91	273. - 0.125E+04	K	0.64%FS
335	Temp.	TF-135	TE 335	B11 Fuel Rod Pos.6	Fig.5.91	273. - 0.125E+04	K	0.64%FS
336	Temp.	TF-136	TE 336	B11 Fuel Rod Pos.7	Failure	273. - 0.125E+04	K	0.64%FS
337	Temp.	TF-137	TE 337	B13 Fuel Rod Pos.4	Fig.5.111	273. - 0.125E+04	K	0.64%FS
338	Temp.	TF-138	TE 338	B22 Fuel Rod Pos.1	Fig.5.92, 121	273. - 0.125E+04	K	0.64%FS
339	Temp.	TF-139	TE 339	B22 Fuel Rod Pos.2	Fig.5.92, 122	273. - 0.125E+04	K	0.64%FS
340	Temp.	TF-140	TE 340	B22 Fuel Rod Pos.3	Fig.5.92, 123	273. - 0.125E+04	K	0.64%FS
341	Temp.	TF-141	TE 341	B22 Fuel Rod Pos.4	Fig.5.92, 124	273. - 0.125E+04	K	0.64%FS
342	Temp.	TF-142	TE 342	B22 Fuel Rod Pos.5	Fig.5.92, 125	273. - 0.125E+04	K	0.64%FS
343	Temp.	TF-143	TE 343	B22 Fuel Rod Pos.6	Fig.5.92, 126	273. - 0.125E+04	K	0.64%FS
344	Temp.	TF-144	TE 344	B22 Fuel Rod Pos.7	Fig.5.92, 127	273. - 0.125E+04	K	0.64%FS
345	Temp.	TF-145	TE 345	B31 Fuel Rod Pos.4	Not Measured	273. - 0.125E+04	K	0.64%FS
346	Temp.	TF-146	TE 346	B33 Fuel Rod Pos.4	Not Measured	273. - 0.125E+04	K	0.64%FS
347	Temp.	TF-147	TE 347	B51 Fuel Rod Pos.4	Not Measured	273. - 0.125E+04	K	0.64%FS
348	Temp.	TF-148	TE 348	B53 Fuel Rod Pos.4	Not Measured	273. - 0.125E+04	K	0.64%FS
349	Temp.	TF-149	TE 349	B66 Fuel Rod Pos.4	Not Measured	273. - 0.125E+04	K	0.64%FS
350	Temp.	TF-150	TE 350	B77 Fuel Rod Pos.1	Fig.5.93, 128	273. - 0.125E+04	K	0.64%FS

Table 3.2 Measurement List for RUN 983 (Continued)

351Ch.- 400Ch.

Ch.	Item	Symbol	ID.		Location	Fig.No.	Range		Unit	Accuracy
351	Temp.	TF-151	TE	351	B77 Fuel Rod Pos.2	Fig.5.93, 129	273.	-	0.125E+04 K	0.64%FS
352	Temp.	TF-152	TE	352	B77 Fuel Rod Pos.3	Fig.5.93, 130	273.	-	0.125E+04 K	0.64%FS
353	Temp.	TF-153	TE	353	B77 Fuel Rod Pos.4	Fig.5.93, 131	273.	-	0.125E+04 K	0.64%FS
354	Temp.	TF-154	TE	354	B77 Fuel Rod Pos.5	Fig.5.93, 132	273.	-	0.125E+04 K	0.64%FS
355	Temp.	TF-155	TE	355	B77 Fuel Rod Pos.6	Fig.5.93, 133	273.	-	0.125E+04 K	0.64%FS
356	Temp.	TF-156	TE	356	B77 Fuel Rod Pos.7	Fig.5.93, 134	273.	-	0.125E+04 K	0.64%FS
357	Temp.	TF-157	TE	357	B86 Fuel Rod Pos.4	Not Measured	273.	-	0.125E+04 K	0.64%FS
358	Temp.	TF-158	TE	358	C11 Fuel Rod Pos.1	Fig.5.94	273.	-	0.125E+04 K	0.64%FS
359	Temp.	TF-159	TE	359	C11 Fuel Rod Pos.2	Fig.5.94	273.	-	0.125E+04 K	0.64%FS
360	Temp.	TF-160	TE	360	C11 Fuel Rod Pos.3	Fig.5.94	273.	-	0.125E+04 K	0.64%FS
361	Temp.	TF-161	TE	361	C11 Fuel Rod Pos.4	Fig.5.94	273.	-	0.125E+04 K	0.64%FS
362	Temp.	TF-162	TE	362	C11 Fuel Rod Pos.5	Fig.5.94	273.	-	0.125E+04 K	0.64%FS
363	Temp.	TF-163	TE	363	C11 Fuel Rod Pos.6	Fig.5.94	273.	-	0.125E+04 K	0.64%FS
364	Temp.	TF-164	TE	364	C11 Fuel Rod Pos.7	Fig.5.94	273.	-	0.125E+04 K	0.64%FS
365	Temp.	TF-165	TE	365	C13 Fuel Rod Pos.1	Fig.5.95	273.	-	0.125E+04 K	0.64%FS
366	Temp.	TF-166	TE	366	C13 Fuel Rod Pos.2	Fig.5.95	273.	-	0.125E+04 K	0.64%FS
367	Temp.	TF-167	TE	367	C13 Fuel Rod Pos.3	Fig.5.95	273.	-	0.125E+04 K	0.64%FS
368	Temp.	TF-168	TE	368	C13 Fuel Rod Pos.4	Fig.5.95	273.	-	0.125E+04 K	0.64%FS
369	Temp.	TF-169	TE	369	C13 Fuel Rod Pos.5	Fig.5.95	273.	-	0.125E+04 K	0.64%FS
370	Temp.	TF-170	TE	370	C13 Fuel Rod Pos.6	Fig.5.95	273.	-	0.125E+04 K	0.64%FS
371	Temp.	TF-171	TE	371	C13 Fuel Rod Pos.7	Fig.5.95	273.	-	0.125E+04 K	0.64%FS
372	Temp.	TF-172	TE	372	C15 Fuel Rod Pos.4	Not Measured	273.	-	0.125E+04 K	0.64%FS
373	Temp.	TF-173	TE	373	C22 Fuel Rod Pos.1	Fig.5.96, 121	273.	-	0.125E+04 K	0.64%FS
374	Temp.	TF-174	TE	374	C22 Fuel Rod Pos.2	Fig.5.96, 122	273.	-	0.125E+04 K	0.64%FS
375	Temp.	TF-175	TE	375	C22 Fuel Rod Pos.3	Fig.5.96, 123	273.	-	0.125E+04 K	0.64%FS
376	Temp.	TF-176	TE	376	C22 Fuel Rod Pos.4	Fig.5.96, 124	273.	-	0.125E+04 K	0.64%FS
377	Temp.	TF-177	TE	377	C22 Fuel Rod Pos.5	Fig.5.96, 125	273.	-	0.125E+04 K	0.64%FS
378	Temp.	TF-178	TE	378	C22 Fuel Rod Pos.6	Fig.5.96, 126	273.	-	0.125E+04 K	0.64%FS
379	Temp.	TF-179	TE	379	C22 Fuel Rod Pos.7	Fig.5.96, 127	273.	-	0.125E+04 K	0.64%FS
380	Temp.	TF-180	TE	380	C31 Fuel Rod Pos.4	Not Measured	273.	-	0.125E+04 K	0.64%FS
381	Temp.	TF-181	TE	381	C33 Fuel Rod Pos.1	Fig.5.97	273.	-	0.125E+04 K	0.64%FS
382	Temp.	TF-182	TE	382	C33 Fuel Rod Pos.2	Fig.5.97	273.	-	0.125E+04 K	0.64%FS
383	Temp.	TF-183	TE	383	C33 Fuel Rod Pos.3	Fig.5.97	273.	-	0.125E+04 K	0.64%FS
384	Temp.	TF-184	TE	384	C33 Fuel Rod Pos.4	Fig.5.97	273.	-	0.125E+04 K	0.64%FS
385	Temp.	TF-185	TE	385	C33 Fuel Rod Pos.5	Fig.5.97	273.	-	0.125E+04 K	0.64%FS
386	Temp.	TF-186	TE	386	C33 Fuel Rod Pos.6	Fig.5.97	273.	-	0.125E+04 K	0.64%FS
387	Temp.	TF-187	TE	387	C33 Fuel Rod Pos.7	Fig.5.97	273.	-	0.125E+04 K	0.64%FS
388	Temp.	TF-188	TE	388	C35 Fuel Rod Pos.4	Not Measured	273.	-	0.125E+04 K	0.64%FS
389	Temp.	TF-189	TE	389	C66 Fuel Rod Pos.4	Not Measured	273.	-	0.125E+04 K	0.64%FS
390	Temp.	TF-190	TE	390	C68 Fuel Rod Pos.4	Not Measured	273.	-	0.125E+04 K	0.64%FS
391	Temp.	TF-191	TE	391	C77 Fuel Rod Pos.1	Fig.5.98, 128	273.	-	0.125E+04 K	0.64%FS
392	Temp.	TF-192	TE	392	C77 Fuel Rod Pos.2	Fig.5.98, 129	273.	-	0.125E+04 K	0.64%FS
393	Temp.	TF-193	TE	393	C77 Fuel Rod Pos.3	Fig.5.98, 130	273.	-	0.125E+04 K	0.64%FS
394	Temp.	TF-194	TE	394	C77 Fuel Rod Pos.4	Fig.5.98, 131	273.	-	0.125E+04 K	0.64%FS
395	Temp.	TF-195	TE	395	C77 Fuel Rod Pos.5	Fig.5.98, 132	273.	-	0.125E+04 K	0.64%FS
396	Temp.	TF-196	TE	396	C77 Fuel Rod Pos.6	Fig.5.98, 133	273.	-	0.125E+04 K	0.64%FS
397	Temp.	TF-197	TE	397	C77 Fuel Rod Pos.7	Fig.5.98, 134	273.	-	0.125E+04 K	0.64%FS
398	Temp.	TF-198	TE	398	D11 Fuel Rod Pos.4	Fig.5.113	273.	-	0.125E+04 K	0.64%FS
399	Temp.	TF-199	TE	399	D13 Fuel Rod Pos.4	Fig.5.113	273.	-	0.125E+04 K	0.64%FS
400	Temp.	TF-200	TE	400	D22 Fuel Rod Pos.1	Fig.5.99, 121	273.	-	0.125E+04 K	0.64%FS

Table 3.2 Measurement List for RUN 983 (Continued)

401Ch.- 450Ch.

Ch.	Item	Symbol	ID.	Location	Fig.No.	Range	Unit	Accuracy
401	Temp.	TF-201	TE 401	D22 Fuel Rod Pos.2	Fig.5.99, 122	273. - 0.125E+04	K	0.64%FS
402	Temp.	TF-202	TE 402	D22 Fuel Rod Pos.3	Fig.5.99, 123	273. - 0.125E+04	K	0.64%FS
403	Temp.	TF-203	TE 403	D22 Fuel Rod Pos.4	Fig.5.99, 124	273. - 0.125E+04	K	0.64%FS
404	Temp.	TF-204	TE 404	D22 Fuel Rod Pos.5	Fig.5.99, 125	273. - 0.125E+04	K	0.64%FS
405	Temp.	TF-205	TE 405	D22 Fuel Rod Pos.6	Fig.5.99, 126	273. - 0.125E+04	K	0.64%FS
406	Temp.	TF-206	TE 406	D22 Fuel Rod Pos.7	Fig.5.99, 127	273. - 0.125E+04	K	0.64%FS
407	Temp.	TF-207	TE 407	D31 Fuel Rod Pos.4	Not Measured	273. - 0.125E+04	K	0.64%FS
408	Temp.	TF-208	TE 408	D33 Fuel Rod Pos.4	Not Measured	273. - 0.125E+04	K	0.64%FS
409	Temp.	TF-209	TE 409	D51 Fuel Rod Pos.4	Not Measured	273. - 0.125E+04	K	0.64%FS
410	Temp.	TF-210	TE 410	D53 Fuel Rod Pos.4	Not Measured	273. - 0.125E+04	K	0.64%FS
411	Temp.	TF-211	TE 411	D66 Fuel Rod Pos.4	Not Measured	273. - 0.125E+04	K	0.64%FS
412	Temp.	TF-212	TE 412	D77 Fuel Rod Pos.4	Fig.5.112	273. - 0.125E+04	K	0.64%FS
413	Temp.	TF-213	TE 413	D86 Fuel Rod Pos.4	Not Measured	273. - 0.125E+04	K	0.64%FS
414	Fluid T.	TW- 1	TE 414	A45 Tie Rod Pos.1	Fig.5.100	273. - 0.125E+04	K	0.64%FS
415	Fluid T.	TW- 2	TE 415	A45 Tie Rod Pos.2	Fig.5.100	273. - 0.125E+04	K	0.64%FS
416	Fluid T.	TW- 3	TE 416	A45 Tie Rod Pos.3	Fig.5.100	273. - 0.125E+04	K	0.64%FS
417	Fluid T.	TW- 4	TE 417	A45 Tie Rod Pos.4	Fig.5.100	273. - 0.125E+04	K	0.64%FS
418	Fluid T.	TW- 5	TE 418	A45 Tie Rod Pos.5	Fig.5.100	273. - 0.125E+04	K	0.64%FS
419	Fluid T.	TW- 6	TE 419	A45 Tie Rod Pos.6	Fig.5.100	273. - 0.125E+04	K	0.64%FS
420	Fluid T.	TW- 7	TE 420	A45 Tie Rod Pos.7	Fig.5.100	273. - 0.125E+04	K	0.64%FS
421	Fluid T.	TW- 8	TE 421	B45 Tie Rod Pos.1	Not Measured	273. - 0.125E+04	K	0.64%FS
422	Fluid T.	TW- 9	TE 422	B45 Tie Rod Pos.2	Not Measured	273. - 0.125E+04	K	0.64%FS
423	Fluid T.	TW-10	TE 423	B45 Tie Rod Pos.3	Not Measured	273. - 0.125E+04	K	0.64%FS
424	Fluid T.	TW-11	TE 424	B45 Tie Rod Pos.4	Not Measured	273. - 0.125E+04	K	0.64%FS
425	Fluid T.	TW-12	TE 425	B45 Tie Rod Pos.5	Not Measured	273. - 0.125E+04	K	0.64%FS
426	Fluid T.	TW-13	TE 426	B45 Tie Rod Pos.6	Not Measured	273. - 0.125E+04	K	0.64%FS
427	Fluid T.	TW-14	TE 427	B45 Tie Rod Pos.7	Not Measured	273. - 0.125E+04	K	0.64%FS
428	Fluid T.	TW-15	TE 428	C45 Tie Rod Pos.1	Fig.5.101	273. - 0.125E+04	K	0.64%FS
429	Fluid T.	TW-16	TE 429	C45 Tie Rod Pos.2	Fig.5.101	273. - 0.125E+04	K	0.64%FS
430	Fluid T.	TW-17	TE 430	C45 Tie Rod Pos.3	Fig.5.101	273. - 0.125E+04	K	0.64%FS
431	Fluid T.	TW-18	TE 431	C45 Tie Rod Pos.4	Fig.5.101	273. - 0.125E+04	K	0.64%FS
432	Fluid T.	TW-19	TE 432	C45 Tie Rod Pos.5	Fig.5.101	273. - 0.125E+04	K	0.64%FS
433	Fluid T.	TW-20	TE 433	C45 Tie Rod Pos.6	Fig.5.101	273. - 0.125E+04	K	0.64%FS
434	Fluid T.	TW-21	TE 434	C45 Tie Rod Pos.7	Fig.5.101	273. - 0.125E+04	K	0.64%FS
435	Fluid T.	TW-22	TE 435	D45 Tie Rod Pos.1	Not Measured	273. - 0.125E+04	K	0.64%FS
436	Fluid T.	TW-23	TE 436	D45 Tie Rod Pos.2	Not Measured	273. - 0.125E+04	K	0.64%FS
437	Fluid T.	TW-24	TE 437	D45 Tie Rod Pos.3	Not Measured	273. - 0.125E+04	K	0.64%FS
438	Fluid T.	TW-25	TE 438	D45 Tie Rod Pos.4	Not Measured	273. - 0.125E+04	K	0.64%FS
439	Fluid T.	TW-26	TE 439	D45 Tie Rod Pos.5	Not Measured	273. - 0.125E+04	K	0.64%FS
440	Fluid T.	TW-27	TE 440	D45 Tie Rod Pos.6	Not Measured	273. - 0.125E+04	K	0.64%FS
441	Fluid T.	TW-28	TE 441	D45 Tie Rod Pos.7	Not Measured	273. - 0.125E+04	K	0.64%FS
442	Fluid T.	TC- 1	TE 442	Channel Box A Inlet	Fig.5.135	273. - 0.125E+04	K	0.64%FS
443	Fluid T.	TC- 2	TE 443	Channel Box B Inlet	Fig.5.135	273. - 0.125E+04	K	0.64%FS
444	Fluid T.	TC- 3	TE 444	Channel Box C Inlet	Fig.5.135	273. - 0.125E+04	K	0.64%FS
445	Fluid T.	TC- 4	TE 445	Channel Box D Inlet	Fig.5.135	273. - 0.125E+04	K	0.64%FS
446	Fluid T.	TC- 5	TE 446	Channel Box Outlet A-1	Fig.5.136	273. - 0.125E+04	K	0.64%FS
447	Fluid T.	TC- 6	TE 447	Channel Box Outlet A-2	Fig.5.136	273. - 0.125E+04	K	0.64%FS
448	Fluid T.	TC- 7	TE 448	Channel Box Outlet A-3	Fig.5.136	273. - 0.125E+04	K	0.64%FS
449	Fluid T.	TC- 8	TE 449	Channel Box Outlet A-4	Fig.5.136	273. - 0.125E+04	K	0.64%FS
450	Fluid T.	TC- 9	TE 450	Channel Box Outlet A-6	Fig.5.136	273. - 0.125E+04	K	0.64%FS

Table 3.2 Measurement List for RUN 983 (Continued)

451Ch.- 500Ch.

Ch.	Item	Symbol	ID.	Location	Fig.No.	Range			Unit	Accuracy
451	Fluid T.	TC-10	TE 451	Channel Box Outlet C-1	Fig.5.137	273.	-	0.125E+04	K	0.64%FS
452	Fluid T.	TC-11	TE 452	Channel Box Outlet C-2	Fig.5.137	273.	-	0.125E+04	K	0.64%FS
453	Fluid T.	TC-12	TE 453	Channel Box Outlet C-3	Fig.5.137	273.	-	0.125E+04	K	0.64%FS
454	Fluid T.	TC-13	TE 454	Channel Box Outlet C-4	Fig.5.137	273.	-	0.125E+04	K	0.64%FS
455	Fluid T.	TC-14	TE 455	Channel Box Outlet C-6	Fig.5.137	273.	-	0.125E+04	K	0.64%FS
456	Fluid T.	TG- 1	TE 456	Upper Tieplate A Up.1	Fig.5.138, 140	273.	-	0.125E+04	K	0.64%FS
457	Fluid T.	TG- 2	TE 457	Upper Tieplate A Up.2	Not Measured	273.	-	0.125E+04	K	0.64%FS
458	Fluid T.	TG- 3	TE 458	Upper Tieplate A Up.3	Not Measured	273.	-	0.125E+04	K	0.64%FS
459	Fluid T.	TG- 4	TE 459	Upper Tieplate A Up.4	Fig.5.138, 141	273.	-	0.125E+04	K	0.64%FS
460	Fluid T.	TG- 5	TE 460	Upper Tieplate A Up.5	Not Measured	273.	-	0.125E+04	K	0.64%FS
461	Fluid T.	TG- 6	TE 461	Upper Tieplate A Up.6	Not Measured	273.	-	0.125E+04	K	0.64%FS
462	Fluid T.	TG- 7	TE 462	Upper Tieplate A Up.7	Not Measured	273.	-	0.125E+04	K	0.64%FS
463	Fluid T.	TG- 8	TE 463	Upper Tieplate A Up.8	Not Measured	273.	-	0.125E+04	K	0.64%FS
464	Fluid T.	TG- 9	TE 464	Upper Tieplate A Up.9	Not Measured	273.	-	0.125E+04	K	0.64%FS
465	Fluid T.	TG-10	TE 465	Upper Tieplate A Up.10	Fig.5.138, 142	273.	-	0.125E+04	K	0.64%FS
466	Fluid T.	TG-11	TE 466	Upper Tieplate A Lo.1	Fig.5.139, 140	273.	-	0.125E+04	K	0.64%FS
467	Fluid T.	TG-12	TE 467	Upper Tieplate A Lo.2	Not Measured	273.	-	0.125E+04	K	0.64%FS
468	Fluid T.	TG-13	TE 468	Upper Tieplate A Lo.3	Not Measured	273.	-	0.125E+04	K	0.64%FS
469	Fluid T.	TG-14	TE 469	Upper Tieplate A Lo.4	Fig.5.139, 141	273.	-	0.125E+04	K	0.64%FS
470	Fluid T.	TG-15	TE 470	Upper Tieplate A Lo.5	Not Measured	273.	-	0.125E+04	K	0.64%FS
471	Fluid T.	TG-16	TE 471	Upper Tieplate A Lo.6	Not Measured	273.	-	0.125E+04	K	0.64%FS
472	Fluid T.	TG-17	TE 472	Upper Tieplate A Lo.7	Not Measured	273.	-	0.125E+04	K	0.64%FS
473	Fluid T.	TG-18	TE 473	Upper Tieplate A Lo.8	Not Measuted	273.	-	0.125E+04	K	0.64%FS
474	Fluid T.	TG-19	TE 474	Upper Tieplate A Lo.9	Not Measured	273.	-	0.125E+04	K	0.64%FS
475	Fluid T.	TG-20	TE 475	Upper Tieplate A Lo.10	Fig.5.139, 142	273.	-	0.125E+04	K	0.64%FS
476	Fluid T.	TG-21	TE 476	Upper Tieplate C Up.1	Fig.5.143, 145	273.	-	0.125E+04	K	0.64%FS
477	Fluid T.	TG-22	TE 477	Upper Tieplate C Up.2	Not Measured	273.	-	0.125E+04	K	0.64%FS
478	Fluid T.	TG-23	TE 478	Upper Tieplate C Up.3	Not Measured	273.	-	0.125E+04	K	0.64%FS
479	Fluid T.	TG-24	TE 479	Upper Tieplate C Up.4	Fig.5.143, 146	273.	-	0.125E+04	K	0.64%FS
480	Fluid T.	TG-25	TE 480	Upper Tieplate C Up.5	Not Measured	273.	-	0.125E+04	K	0.64%FS
481	Fluid T.	TG-26	TE 481	Upper Tieplate C Up.6	Not Measured	273.	-	0.125E+04	K	0.64%FS
482	Fluid T.	TG-27	TE 482	Upper Tieplate C Up.7	Not Measured	273.	-	0.125E+04	K	0.64%FS
483	Fluid T.	TG-28	TE 483	Upper Tieplate C Up.8	Not Measured	273.	-	0.125E+04	K	0.64%FS
484	Fluid T.	TG-29	TE 484	Upper Tieplate C Up.9	Not Measured	273.	-	0.125E+04	K	0.64%FS
485	Fluid T.	TG-30	TE 485	Upper Tieplate C Up.10	Fig.5.143, 147	273.	-	0.125E+04	K	0.64%FS
486	Fluid T.	TG-31	TE 486	Upper Tieplate C Lo.1	Fig.5.144, 145	273.	-	0.125E+04	K	0.64%FS
487	Fluid T.	TG-32	TE 487	Upper Tieplate C Lo.2	Not Measured	273.	-	0.125E+04	K	0.64%FS
488	Fluid T.	TG-33	TE 488	Upper Tieplate C Lo.3	Not Measured	273.	-	0.125E+04	K	0.64%FS
489	Fluid T.	TG-34	TE 489	Upper Tieplate C Lo.4	Fig.5.144, 146	273.	-	0.125E+04	K	0.64%FS
490	Fluid T.	TG-35	TE 490	Upper Tieplate C Lo.5	Not Measured	273.	-	0.125E+04	K	0.64%FS
491	Fluid T.	TG-36	TE 491	Upper Tieplate C Lo.6	Not Measured	273.	-	0.125E+04	K	0.64%FS
492	Fluid T.	TG-37	TE 492	Upper Tieplate C Lo.7	Not Measured	273.	-	0.125E+04	K	0.64%FS
493	Fluid T.	TG-38	TE 493	Upper Tieplate C Lo.8	Not Measured	273.	-	0.125E+04	K	0.64%FS
494	Fluid T.	TG-39	TE 494	Upper Tieplate C Lo.9	Not Measured	273.	-	0.125E+04	K	0.64%FS
495	Fluid T.	TG-40	TE 495	Upper Tieplate C Lo.10	Fig.5.144, 147	273.	-	0.125E+04	K	0.64%FS
496	Slab T.	TB- 1	TE 496	C.B. A1 Inner ,Pos.1	Not Measured	273.	-	0.125E+04	K	0.64%FS
497	Slab T.	TB- 2	TE 497	C.B. A1 Inner ,Pos.2	Not Measured	273.	-	0.125E+04	K	0.64%FS
498	Slab T.	TB- 3	TE 498	C.B. A1 Inner ,Pos.3	Not Measured	273.	-	0.125E+04	K	0.64%FS
499	Slab T.	TB- 4	TE 499	C.B. A1 Inner ,Pos.4	Not Measured	273.	-	0.125E+04	K	0.64%FS
500	Slab T.	TB- 5	TE 500	C.B. A1 Inner ,Pos.5	Not Measured	273.	-	0.125E+04	K	0.64%FS

Table 3.2 Measurement List for RUN 983 (Continued)

501Ch.- 550Ch.

Ch.	Item	Symbol	ID.	Location	Fig.No.	Range	Unit	Accuracy
501	Slab T.	TB- 6	TE 501	C.B. A1 Inner ,Pos.6	Not Measured	273. - 0.125E+04	K	0.64%FS
502	Slab T.	TB- 7	TE 502	C.B. A1 Inner ,Pos.7	Not Measured	273. - 0.125E+04	K	0.64%FS
503	Slab T.	TB- 8	TE 503	C.B. A2 Inner ,Pos.1	Not Measured	273. - 0.125E+04	K	0.64%FS
504	Slab T.	TB- 9	TE 504	C.B. A2 Inner ,Pos.2	Not Measured	273. - 0.125E+04	K	0.64%FS
505	Slab T.	TB-10	TE 505	C.B. A2 Inner ,Pos.3	Not Measured	273. - 0.125E+04	K	0.64%FS
506	Slab T.	TB-11	TE 506	C.B. A2 Inner ,Pos.4	Not Measured	273. - 0.125E+04	K	0.64%FS
507	Slab T.	TB-12	TE 507	C.B. A2 Inner ,Pos.5	Not Measured	273. - 0.125E+04	K	0.64%FS
508	Slab T.	TB-13	TE 508	C.B. A2 Inner ,Pos.6	Not Measured	273. - 0.125E+04	K	0.64%FS
509	Slab T.	TB-14	TE 509	C.B. A2 Inner ,Pos.7	Not Measured	273. - 0.125E+04	K	0.64%FS
510	Slab T.	TB-15	TE 510	C.B. B Inner ,Pos.1	Not Measured	273. - 0.125E+04	K	0.64%FS
511	Slab T.	TB-16	TE 511	C.B. B Inner ,Pos.2	Not Measured	273. - 0.125E+04	K	0.64%FS
512	Slab T.	TB-17	TE 512	C.B. B Inner ,Pos.3	Not Measured	273. - 0.125E+04	K	0.64%FS
513	Slab T.	TB-18	TE 513	C.B. B Inner ,Pos.4	Not Measured	273. - 0.125E+04	K	0.64%FS
514	Slab T.	TB-19	TE 514	C.B. B Inner ,Pos.5	Not Measured	273. - 0.125E+04	K	0.64%FS
515	Slab T.	TB-20	TE 515	C.B. B Inner ,Pos.6	Not Measured	273. - 0.125E+04	K	0.64%FS
516	Slab T.	TB-21	TE 516	C.B. B Inner ,Pos.7	Not Measured	273. - 0.125E+04	K	0.64%FS
517	Slab T.	TB-22	TE 517	C.B. C Inner ,Pos.1	Not Measured	273. - 0.125E+04	K	0.64%FS
518	Slab T.	TB-23	TE 518	C.B. C Inner ,Pos.2	Not Measured	273. - 0.125E+04	K	0.64%FS
519	Slab T.	TB-24	TE 519	C.B. C Inner ,Pos.3	Not Measured	273. - 0.125E+04	K	0.64%FS
520	Slab T.	TB-25	TE 520	C.B. C Inner ,Pos.4	Not Measured	273. - 0.125E+04	K	0.64%FS
521	Slab T.	TB-26	TE 521	C.B. C Inner ,Pos.5	Not Measured	273. - 0.125E+04	K	0.64%FS
522	Slab T.	TB-27	TE 522	C.B. C Inner ,Pos.6	Not Measured	273. - 0.125E+04	K	0.64%FS
523	Slab T.	TB-28	TE 523	C.B. C Inner ,Pos.7	Not Measured	273. - 0.125E+04	K	0.64%FS
524	Slab T.	TB-29	TE 524	C.B. D Inner ,Pos.1	Not Measured	273. - 0.125E+04	K	0.64%FS
525	Slab T.	TB-30	TE 525	C.B. D Inner ,Pos.2	Not Measured	273. - 0.125E+04	K	0.64%FS
526	Slab T.	TB-31	TE 526	C.B. D Inner ,Pos.3	Not Measured	273. - 0.125E+04	K	0.64%FS
527	Slab T.	TB-32	TE 527	C.B. D Inner ,Pos.4	Not Measured	273. - 0.125E+04	K	0.64%FS
528	Slab T.	TB-33	TE 528	C.B. D Inner ,Pos.5	Not Measured	273. - 0.125E+04	K	0.64%FS
529	Slab T.	TB-34	TE 529	C.B. D Inner ,Pos.6	Not Measured	273. - 0.125E+04	K	0.64%FS
530	Slab T.	TB-35	TE 530	C.B. D Inner ,Pos.7	Not Measured	273. - 0.125E+04	K	0.64%FS
531	Fluid T.	TB-36	TE 531	C.B. A Outer ,Pos.1	Fig.5.102,148	273. - 0.125E+04	K	0.64%FS
532	Fluid T.	TB-37	TE 532	C.B. A Outer ,Pos.2	Fig.5.102,148	273. - 0.125E+04	K	0.64%FS
533	Fluid T.	TB-38	TE 533	C.B. A Outer ,Pos.3	Fig.5.102,148	273. - 0.125E+04	K	0.64%FS
534	Fluid T.	TB-39	TE 534	C.B. A Outer ,Pos.4	Fig.5.102,148	273. - 0.125E+04	K	0.64%FS
535	Fluid T.	TB-40	TE 535	C.B. A Outer ,Pos.5	Fig.5.102,148	273. - 0.125E+04	K	0.64%FS
536	Fluid T.	TB-41	TE 536	C.B. A Outer ,Pos.6	Fig.5.102,148	273. - 0.125E+04	K	0.64%FS
537	Fluid T.	TB-42	TE 537	C.B. A Outer ,Pos.7	Fig.5.102,148	273. - 0.125E+04	K	0.64%FS
538	Fluid T.	TB-43	TE 538	C.B. C Outer ,Pos.1	Not Measured	273. - 0.125E+04	K	0.64%FS
539	Fluid T.	TB-44	TE 539	C.B. C Outer ,Pos.2	Not Measured	273. - 0.125E+04	K	0.64%FS
540	Fluid T.	TB-45	TE 540	C.B. C Outer ,Pos.3	Not Measured	273. - 0.125E+04	K	0.64%FS
541	Fluid T.	TB-46	TE 541	C.B. C Outer ,Pos.4	Not Measured	273. - 0.125E+04	K	0.64%FS
542	Fluid T.	TB-47	TE 542	C.B. C Outer ,Pos.5	Not Measured	273. - 0.125E+04	K	0.64%FS
543	Fluid T.	TB-48	TE 543	C.B. C Outer ,Pos.6	Not Measured	273. - 0.125E+04	K	0.64%FS
544	Fluid T.	TB-49	TE 544	C.B. C Outer ,Pos.7	Not Measured	273. - 0.125E+04	K	0.64%FS
545	Fluid T.	TP- 1	TE 545	Lower Pl. Center 1	Fig.5.149	273. - 0.125E+04	K	0.64%FS
546	Fluid T.	TP- 2	TE 546	Lower Pl. Center 2	Fig.5.149	273. - 0.125E+04	K	0.64%FS
547	Fluid T.	TP- 3	TE 547	Lower Pl. Center 3	Fig.5.149	273. - 0.125E+04	K	0.64%FS
548	Fluid T.	TP- 4	TE 548	Lower Pl. Center 4	Fig.5.149	273. - 0.125E+04	K	0.64%FS
549	Fluid T.	TP- 5	TE 549	Lower Pl. Center 5	Fig.5.149	273. - 0.125E+04	K	0.64%FS
550	Fluid T.	TP- 6	TE 550	Lower Pl. Center 7	Fig.5.149	273. - 0.125E+04	K	0.64%FS

Table 3.2 Measurement List for RUN 983 (Continued)

551Ch.- 600Ch.

Ch.	Item	Symbol	ID.		Location	Fig.No.	Range			Unit	Accuracy
551	Slab T.	TP- 7	TE	551	Lower Pl. North 1	Not Measured	273.	-	0.125E+04	K	0.64%FS
552	Slab T.	TP- 8	TE	552	Lower Pl. North 2	Not Measured	273.	-	673.	K	0.64%FS
553	Slab T.	TP- 9	TE	553	Lower Pl. North 4	Not Measured	273.	-	673.	K	0.64%FS
554	Slab T.	TP-10	TE	554	Lower Pl. North 6	Not Measured	273.	-	673.	K	0.64%FS
555	Slab T.	TP-11	TE	555	Lower Pl. South 1	Not Measured	273.	-	673.	K	0.64%FS
556	Slab T.	TP-12	TE	556	Lower Pl. South 2	Not Measured	273.	-	673.	K	0.64%FS
557	Slab T.	TP-13	TE	557	Lower Pl. South 4	Not Measured	273.	-	673.	K	0.64%FS
558	Slab T.	TP-14	TE	558	Lower Pl. South 6	Not Measured	273.	-	673.	K	0.64%FS
559	Level	LB- 1	LM	559	C.B.Liquid Level A1-1	Not Measured					
560	Level	LB- 2	LM	560	C.B.Liquid Level A1-2	Not Measured					
561	Level	LB- 3	LM	561	C.B.Liquid Level A1-3	Not Measured					
562	Level	LB- 4	LM	562	C.B.Liquid Level A1-4	Not Measured					
563	Level	LB- 5	LM	563	C.B.Liquid Level A1-5	Not Measured					
564	Level	LB- 6	LM	564	C.B.Liquid Level A1-6	Not Measured					
565	Level	LB- 7	LM	565	C.B.Liquid Level A1-7	Not Measured					
566	Level	LB- 8	LM	566	C.B.Liquid Level A2-1	Fig.5.150					
567	Level	LB- 9	LM	567	C.B.Liquid Level A2-2	Fig.5.150					
568	Level	LB-10	LM	568	C.B.Liquid Level A2-3	Fig.5.150					
569	Level	LB-11	LM	569	C.B.Liquid Level A2-4	Fig.5.150					
570	Level	LB-12	LM	570	C.B.Liquid Level A2-5	Fig.5.150					
571	Level	LB-13	LM	571	C.B.Liquid Level A2-6	Fig.5.150					
572	Level	LB-14	LM	572	C.B.Liquid Level A2-7	Fig.5.150					
573	Level	LB-15	LM	573	C.B.Liquid Level B-1	Fig.5.151					
574	Level	LB-16	LM	574	C.B.Liquid Level B-2	Fig.5.151					
575	Level	LB-17	LM	575	C.B.Liquid Level B-3	Fig.5.151					
576	Level	LB-18	LM	576	C.B.Liquid Level B-4	Fig.5.151					
577	Level	LB-19	LM	577	C.B.Liquid Level B-5	Fig.5.151					
578	Level	LB-20	LM	578	C.B.Liquid Level B-6	Failure					
579	Level	LB-21	LM	579	C.B.Liquid Level B-7	Failure					
580	Level	LB-22	LM	580	C.B.Liquid Level C-1	Failure					
581	Level	LB-23	LM	581	C.B.Liquid Level C-2	Fig.5.152					
582	Level	LB-24	LM	582	C.B.Liquid Level C-3	Fig.5.152					
583	Level	LB-25	LM	583	C.B.Liquid Level C-4	Failure					
584	Level	LB-26	LM	584	C.B.Liquid Level C-5	Fig.5.152					
585	Level	LB-27	LM	585	C.B.Liquid Level C-6	Failure					
586	Level	LB-28	LM	586	C.B.Liquid Level C-7	Fig.5.152					
587	Level	LB-29	LM	587	C.B.Liquid Level D-1	Not Measured					
588	Level	LB-30	LM	588	C.B.Liquid Level D-2	Not Measured					
589	Level	LB-31	LM	589	C.B.Liquid Level D-3	Not Measured					
590	Level	LB-32	LM	590	C.B.Liquid Level D-4	Not Measured					
591	Level	LB-33	LM	591	C.B.Liquid Level D-5	Not Measured					
592	Level	LB-34	LM	592	C.B.Liquid Level D-6	Not Measured					
593	Level	LB-35	LM	593	C.B.Liquid Level D-7	Not Measured					
594	Level	LL- 1	LM	594	Ch.Box Outlet A1-5	Not Measured					
595	Level	LL- 2	LM	595	Ch.Box Outlet A1-6	Not Measured					
596	Level	LL- 3	LM	596	Ch.Box Outlet A1-7	Not Measured					
597	Level	LL- 4	LM	597	Ch.Box Outlet A2-5	Failure					
598	Level	LL- 5	LM	598	Ch.Box Outlet A2-6	Fig.5.153					
599	Level	LL- 6	LM	599	Ch.Box Outlet A2-7	Fig.5.153					
600	Level	LL- 7	LM	600	Ch.Box Outlet A-1	Fig.5.154					

Table 3.2 Measurement List for RUN 983 (Continued)

601Ch.- 650Ch.

Ch.	Item	Symbol	ID.		Location	Fig.No.	Range	Unit	Accuracy
601	Level	LL- 8	LM	601	Ch.Box Outlet A-2	Failure			
602	Level	LL- 9	LM	602	Ch.Box Outlet A-3	Fig.5.154			
603	Level	LL-10	LM	603	Ch.Box Outlet A-4	Fig.5.154			
604	Level	LL-11	LM	604	Ch.Box Outlet A-6	Failure			
605	Level	LL-12	LM	605	Ch.Box Outlet C1-5	Fig.5.155			
606	Level	LL-13	LM	606	Ch.Box Outlet C1-6	Failure			
607	Level	LL-14	LM	607	Ch.Box Outlet C1-7	Fig.5.155			
608	Level	LL-15	LM	608	Ch.Box Outlet C2-5	Not Measured			
609	Level	LL-16	LM	609	Ch.Box Outlet C2-6	Not Measured			
610	Level	LL-17	LM	610	Ch.Box Outlet C2-7	Not Measured			
611	Level	LL-18	LM	611	Ch.Box Outlet C-1	Fig.5.156			
612	Level	LL-19	LM	612	Ch.Box Outlet C-2	Fig.5.156			
613	Level	LL-20	LM	613	Ch.Box Outlet C-3	Fig.5.156			
614	Level	LL-21	LM	614	Ch.Box Outlet C-4	Fig.5.156			
615	Level	LL-22	LM	615	Ch.Box Outlet C-6	Fig.5.156			
616	Level	LL-23	LM	616	Ch.Box Inlet A-1	Fig.5.157			
617	Level	LL-24	LM	617	Ch.Box Inlet A-2	Fig.5.157			
618	Level	LL-25	LM	618	Ch.Box Inlet B-1	Not Measured			
619	Level	LL-26	LM	619	Ch.Box Inlet B-2	Not Measured			
620	Level	LL-27	LM	620	Ch.Box Inlet C-1	Fig.5.158			
621	Level	LL-28	LM	621	Ch.Box Inlet C-2	Fig.5.158			
622	Level	LL-29	LM	622	Ch.Box Inlet D-1	Not Measured			
623	Level	LL-30	LM	623	Ch.Box Inlet D-2	Not Measured			
624	Level	LL-31	LM	624	Lower Pl. North 1	Fig.5.161			
625	Level	LL-32	LM	625	Lower Pl. North 2	Fig.5.161			
626	Level	LL-33	LM	626	Lower Pl. North 3	Failure			
627	Level	LL-34	LM	627	Lower Pl. North 4	Failure			
628	Level	LL-35	LM	628	Lower Pl. North 5	Failure			
629	Level	LL-36	LM	629	Lower Pl. North 6	Failure			
630	Level	LL-37	LM	630	Lower Pl. South 1	Not Measured			
631	Level	LL-38	LM	631	Lower Pl. South 2	Not Measured			
632	Level	LL-39	LM	632	Lower Pl. South 3	Not Measured			
633	Level	LL-40	LM	633	Lower Pl. South 4	Not Measured			
634	Level	LL-41	LM	634	Lower Pl. South 5	Not Measured			
635	Level	LL-42	LM	635	Lower Pl. South 6	Not Measured			
636	Level	LL-43	LM	636	Guide Tube North 0	Fig.5.160			
637	Level	LL-44	LM	637	Guide Tube North 1	Fig.5.160			
638	Level	LL-45	LM	638	Guide Tube North 3	Fig.5.160			
639	Level	LL-46	LM	639	Guide Tube North 6	Fig.5.160			
640	Level	LL-47	LM	640	Guide Tube South 0	Not Measured			
641	Level	LL-48	LM	641	Guide Tube South 1	Not Measured			
642	Level	LL-49	LM	642	Guide Tube South 3	Not Measured			
643	Level	LL-50	LM	643	Guide Tube South 6	Not Measured			
644	Level	L- 1	LM	644	Downcomer D-Side 1	Fig.5.161			
645	Level	L- 2	LM	645	Downcomer D-Side 2	Fig.5.161			
646	Level	L- 3	LM	646	Downcomer D-Side 3	Fig.5.161			
647	Level	L- 4	LM	647	Downcomer D-Side 4	Fig.5.161			
648	Level	L- 5	LM	648	Downcomer D-Side 5	Fig.5.161			
649	Level	L- 6	LM	649	Downcomer B-Side 1	Not Measured			
650	Level	L- 7	LM	650	Downcomer B-Side 2	Not Measured			

Table 3.2 Measurement List for RUN 983 (Continued)

651Ch.- 700Ch.

Ch.	Item	Symbol	ID.		Location	Fig.No.	Range			Unit	Accuracy
651	Level	L- 8	LM	651	Downcomer B-Side 3	Not Measured					
652	Level	L- 9	LM	652	Downcomer B-Side 4	Not Measured					
653	Level	L-10	LM	653	Downcomer B-Side 5	Not Measured					
654	Void	VF- 1	VD	654	A54 Tie Rod Pos.1	Not Measured	0.0	-	1.00		
655	Void	VF- 2	VD	655	A54 Tie Rod Pos.2	Not Measured	0.0	-	1.00		
656	Void	VF- 3	VD	656	A54 Tie Rod Pos.3	Not Measured	0.0	-	1.00		
657	Void	VF- 4	VD	657	A54 Tie Rod Pos.4	Not Measured	0.0	-	1.00		
658	Void	VF- 5	VD	658	A54 Tie Rod Pos.5	Not Measured	0.0	-	1.00		
659	Void	VF- 6	VD	659	A54 Tie Rod Pos.6	Not Measured	0.0	-	1.00		
660	Void	VF- 7	VD	660	A54 Tie Rod Pos.7	Not Measured	0.0	-	1.00		
661	Void	VF- 8	VD	661	B54 Tie Rod Pos.1	Not Measured	0.0	-	1.00		
662	Void	VF- 9	VD	662	B54 Tie Rod Pos.2	Not Measured	0.0	-	1.00		
663	Void	VF-10	VD	663	B54 Tie Rod Pos.3	Not Measured	0.0	-	1.00		
664	Void	VF-11	VD	664	B54 Tie Rod Pos.4	Not Measured	0.0	-	1.00		
665	Void	VF-12	VD	665	B54 Tie Rod Pos.5	Not Measured	0.0	-	1.00		
666	Void	VF-13	VD	666	B54 Tie Rod Pos.6	Not Measured	0.0	-	1.00		
667	Void	VF-14	VD	667	B54 Tie Rod Pos.7	Not Measured	0.0	-	1.00		
668	Void	VF-15	VD	668	C54 Tie Rod Pos.1	Not Measured	0.0	-	1.00		
669	Void	VF-16	VD	669	C54 Tie Rod Pos.2	Not Measured	0.0	-	1.00		
670	Void	VF-17	VD	670	C54 Tie Rod Pos.3	Not Measured	0.0	-	1.00		
671	Void	VF-18	VD	671	C54 Tie Rod Pos.4	Not Measured	0.0	-	1.00		
672	Void	VF-19	VD	672	C54 Tie Rod Pos.5	Not Measured	0.0	-	1.00		
673	Void	VF-20	VD	673	C54 Tie Rod Pos.6	Not Measured	0.0	-	1.00		
674	Void	VF-21	VD	674	C54 Tie Rod Pos.7	Not Measured	0.0	-	1.00		
675	Void	VF-22	VD	675	D54 Tie Rod Pos.7	Not Measured	0.0	-	1.00		
676	Void	VF-23	VD	676	D54 Tie Rod Pos.7	Not Measured	0.0	-	1.00		
677	Void	VF-24	VD	677	D54 Tie Rod Pos.7	Not Measured	0.0	-	1.00		
678	Void	VF-25	VD	678	D54 Tie Rod Pos.7	Not Measured	0.0	-	1.00		
679	Void	VF-26	VD	679	D54 Tie Rod Pos.7	Not Measured	0.0	-	1.00		
680	Void	VF-27	VD	680	D54 Tie Rod Pos.7	Not Measured	0.0	-	1.00		
681	Void	VF-28	VD	681	D54 Tie Rod Pos.7	Not Measured	0.0	-	1.00		
682	Void	VE- 1	VD	682	Channel A Outlet 1	Not Measured	0.0	-	1.00		
683	Void	VE- 2	VD	683	Channel A Outlet 2	Not Measured	0.0	-	1.00		
684	Void	VE- 3	VD	684	Channel A Outlet 3	Not Measured	0.0	-	1.00		
685	Void	VE- 4	VD	685	Channel B Outlet 1	Not Measured	0.0	-	1.00		
686	Void	VE- 5	VD	686	Channel B Outlet 2	Not Measured	0.0	-	1.00		
687	Void	VE- 6	VD	687	Channel B Outlet 3	Not Measured	0.0	-	1.00		
688	Void	VE- 7	VD	688	Channel C Outlet 1	Not Measured	0.0	-	1.00		
689	Void	VE- 8	VD	689	Channel C Outlet 2	Not Measured	0.0	-	1.00		
690	Void	VE- 9	VD	690	Channel C Outlet 3	Not Measured	0.0	-	1.00		
691	Void	VE-10	VD	691	Channel D Outlet 1	Not Measured	0.0	-	1.00		
692	Void	VE-11	VD	692	Channel D Outlet 2	Not Measured	0.0	-	1.00		
693	Void	VE-12	VD	693	Channel D Outlet 3	Not Measured	0.0	-	1.00		
694	Void	VE-13	VD	694	Lower Plenum Bottom 1	Not Measured	0.0	-	1.00		
695	Void	VE-14	VD	695	Lower Plenum Bottom 2	Not Measured	0.0	-	1.00		
696	Void	VE-15	VD	696	Lower Plenum Bottom 3	Not Measured	0.0	-	1.00		
697	Void	VP- 1	VD	697	Lower Plenum Inlet	Not Measured	0.0	-	1.00		
698	Void	VP- 2	VD	698	Lower Plenum Inlet	Not Measured	0.0	-	1.00		

Table 3.3 Core instrumentation map

Item	Pos. / DL / Rod NO.	Core Outlet	Pos.1	Pos.2	Pos.3	Pos.4	Pos.5	Pos.6	Pos.7	Core Inlet
		3660	3417	3114.5	2879.5	2527	2174.5	1939.5	1637	1454
Surface Temp.	A11		TF 1	TF 2	TF 3	TF 4	TF 5	TF 6	TF 7	
	A12		TF 8	TF 9	TF 10	TF 11	TF 12	TF 13	TF 14	
	A13		TF 15	TF 16	TF 17	TF 18	TF 19	TF 20	TF 21	
	A14		TF 22	TF 23	TF 24	TF 25	TF 26	TF 27	TF 28	
	A15		TF 29			TF 30				
	A17		TF 31			TF 32				
	A22		TF 33	TF 34	TF 35	TF 36	TF 37	TF 38	TF 39	
	A23		TF 40	TF 41	TF 42	TF 43	TF 44	TF 45	TF 46	
	A24		TF 47	TF 48	TF 49	TF 50	TF.51	TF 52	TF 53	
	A26		TF 54			TF 55				
	A28		TF 56			TF 57				
	A31		TF 58			TF 59				
	A33		TF 60	TF 61	TF 62	TF 63	TF 64	TF 65	TF 66	
	A34		TF 67	TF 68	TF 69	TF 70	TF 71	TF 72	TF 73	
	A35		TF 74			TF 75				
	A37		TF 76			TF 77				
	A42		TF 78			TF 79				
Fluid Temp.	A44	TC 1	TF180	TF181	TF182	TF183	TF184	TF185	TF186	TC 2
Surface Temp.	A45		TF 80			TF 81				
	A46		TF 82			TF 83				
	A48		TF 84			TF 85				
	A51		TF 86			TF 87				
	A53		TF 88			TF 89				
	A54		TF 90							
	A57		TF 91			TF 92				
	A62		TF 93			TF 94				
	A64		TF 95			TF 96				
	A66		TF 97			TF 98				
	A68		TF 99			TF100				
	A71		TF101			TF102				
	A73		TF103			TF104				
	A75		TF105			TF106				
	A77		TF107			TF108				

Table 3.3 Core instrumentation map (Continued)

Item	Pos. / Rod NO. / DL	Core Outlet	Pos.1	Pos.2	Pos.3	Pos.4	Pos.5	Pos.6	Pos.7	Core Inlet
		3660	3417	3114.5	2879.5	2527	2174.5	1939.5	1637	1454
Surface Temp.	A82		TF109			TF110				
	A84		TF111			TF112				
	A86		TF113			TF114				
	A88		TF115			TF116				
	B11					TF117				
	B13					TF118				
	B15		TF119	TF120	TF121	TF122	TF123	TF124	TF125	
	B31					TF126				
	B33					TF127				
	B35					TF128				
Fluid Temp.	B44	TC 3	TF187	TF188	TF189	TF190	TF191	TF192	TF193	TC 4
Surface Temp.	B51					TF129				
	B53					TF130				
	B85		TF131	TF132	TF133	TF134	TF135	TF136	TF137	
	C11					TF138				
	C13					TF139				
	C15					TF140				
	C31					TF141				
	C33		TF142	TF143	TF144	TF145	TF146	TF147	TF148	
	C35					TF149				
Fluid Temp.	C44	TC 5	TF194	TF195	TF196	TF197	TF198	TF199	TF200	TC 6
Surface Temp.	C51					TF150				
	C53					TF151				
	C77		TF152	TF153	TF154	TF155	TF156	TF157	TF158	
	D11					TF159				
	D13					TF160				
	D27		TF161	TF162	TF163	TF164	TF165	TF166	TF167	
	D31					TF168				
	D33					TF169				
	D35					TF170				
Fluid Temp.	D44	TC 7	TF201	TF202	TF203	TF204	TF205	TF206	TF207	TC 8
Surface Temp.	D51					TF171				
	D53					TF172				
	D88		TF173	TF174	TF175	TF176	TF177	TF178	TF179	

Table 3.3 Core instrumentation map (Continued)

Item	Pos. / Rod NO. / DL	Core Outlet	Pos.1	Pos.2	Pos.3	Pos.4	Pos.5	Pos.6	Pos.7	Core Inlet
		3660	3417	3114.5	2879.5	2527	2174.5	1939.5	1673	1454
Void	A55		VF 1	VF 2	VF 3	VF 4	VF 5	VF 6	VF 7	
	B55		VF 8	VF 9	VF 10	VF 11	VF 12	VF 13	VF 14	
	C55		VF 15	VF 16	VF 17	VF 18	VF 19	VF 20	VF 21	
	D55		VF 22	VF 23	VF 24	VF 25	VF 26	VF 27	VF 28	
Channel Box Surface Temp.	A1*		TB 1	TB 2	TB 3	TB 4	TB 5	TB 6	TB 7	
	A2*		TB 8	TB 9	TB 10	TB 11	TB 12	TB 13	TB 14	
	B*		TB 15	TB 16	TB 17	TB 18	TB 19	TB 20	TB 21	
	C*		TB 22	TB 23	TB 24	TB 25	TB 26	TB 27	TB 28	
	D*		TB 29	TB 30	TB 31	TB 32	TB 33	TB 34	TB 35	
Liquid Level in the Channel Box	A1*		LB 1	LB 2	LB 3	LB 4	LB 5	LB 6	LB 7	
	A2*		LB 8	LB 9	LB 10	LB 11	LB 12	LB 13	LB 14	
	B*		LB 15	LB 16	LB 17	LB 18	LB 19	LB 20	LB 21	
	C*		LB 22	LB 23	LB 24	LB 25	LB 26	LB 27	LB 28	
	D*		LB 29	LB 30	LB 31	LB 32	LB 33	LB 34	LB 35	

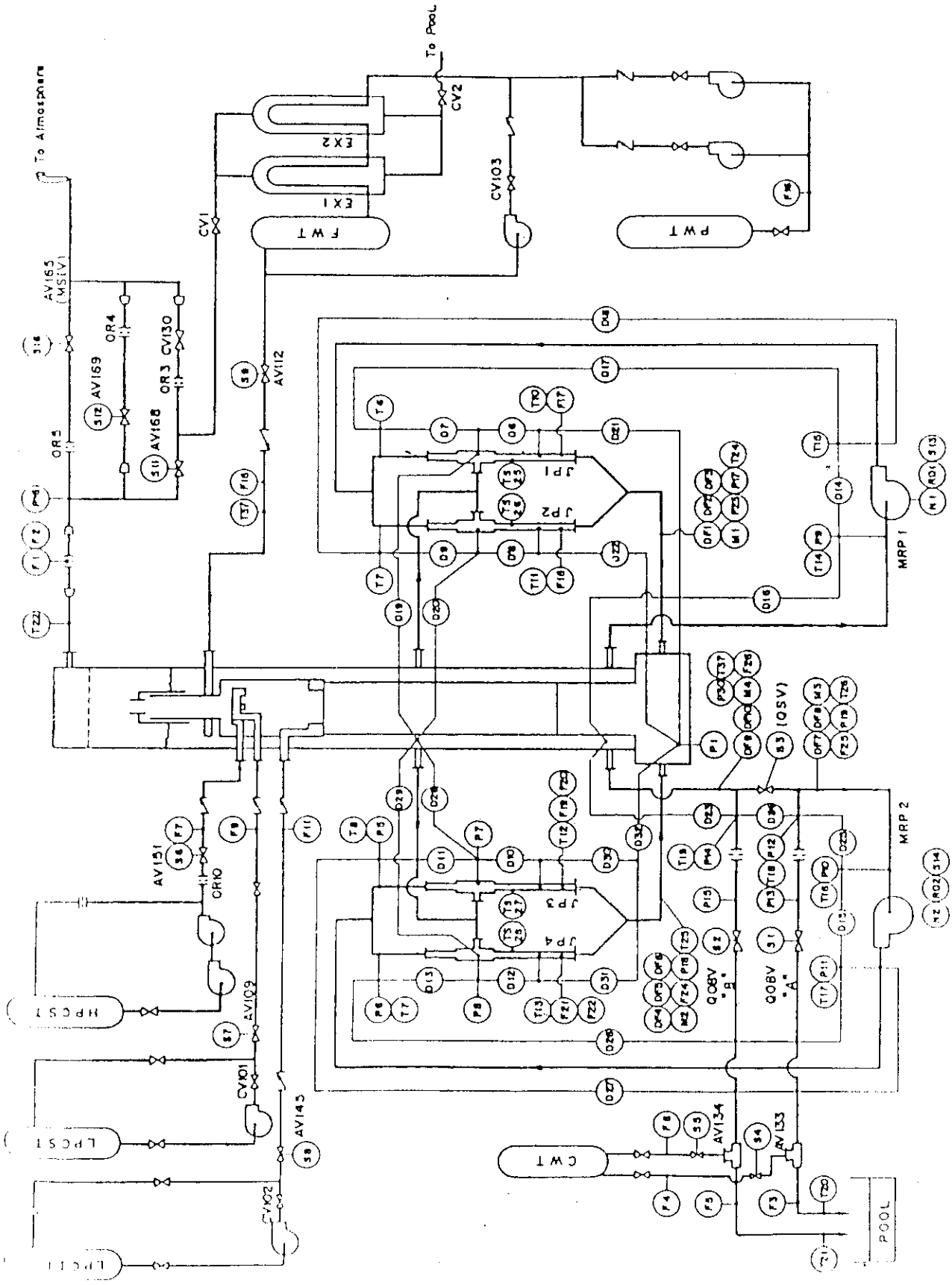

Fig. 3.1 Instrumentation location of ROSA-III test facility

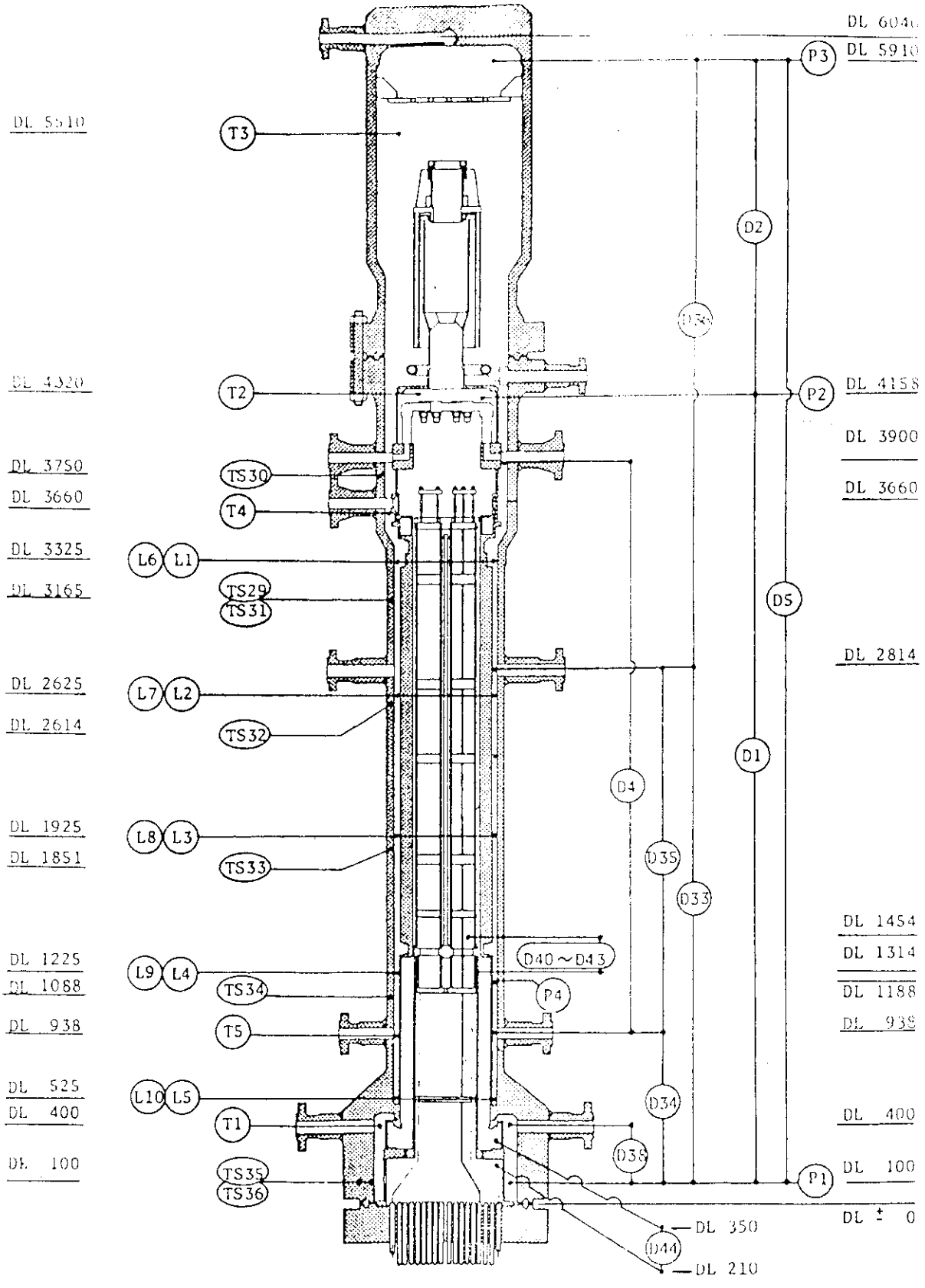

Fig. 3.2 Instrumentation location in pressure vessel

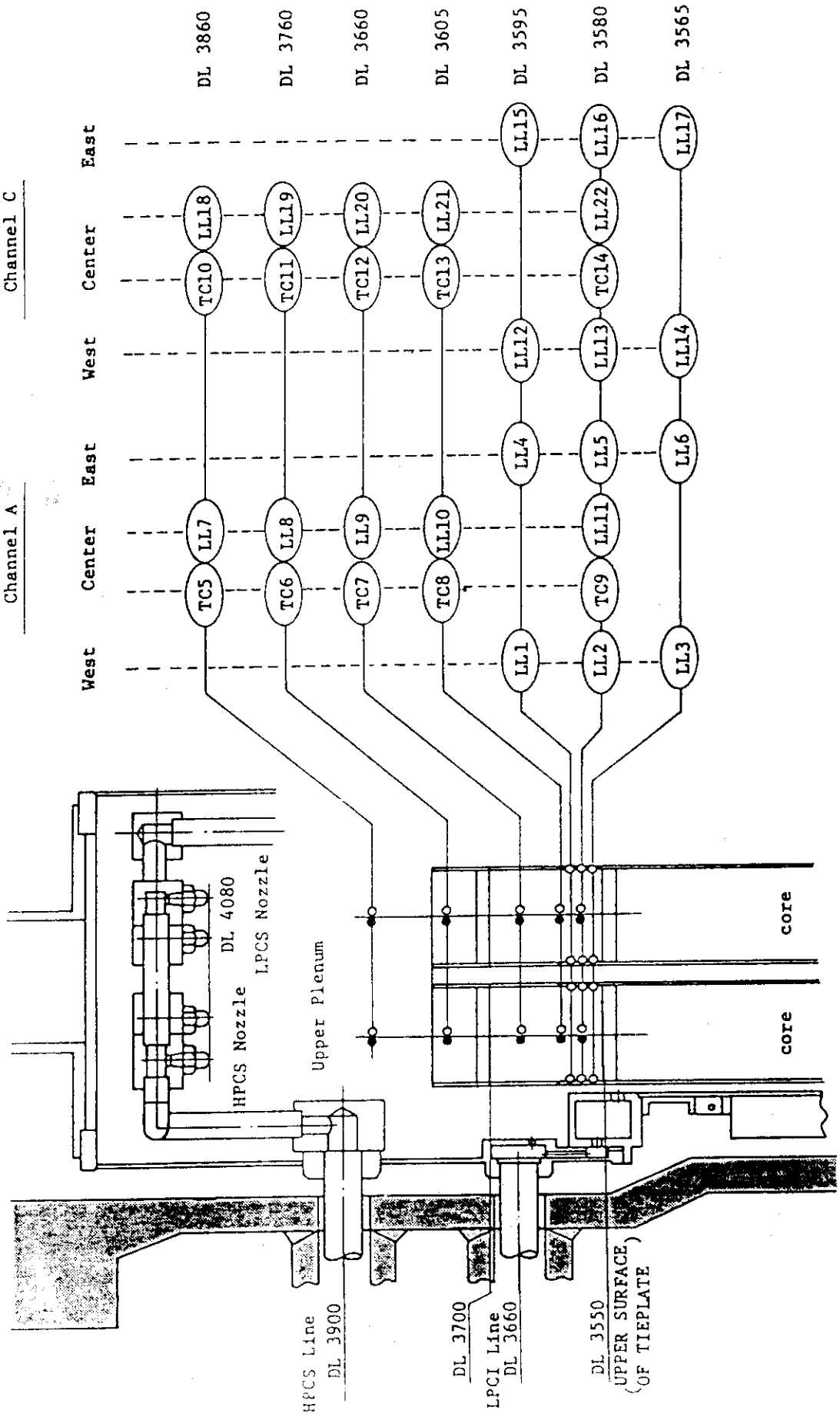

Fig. 3.3 Upper plenum instrumentation

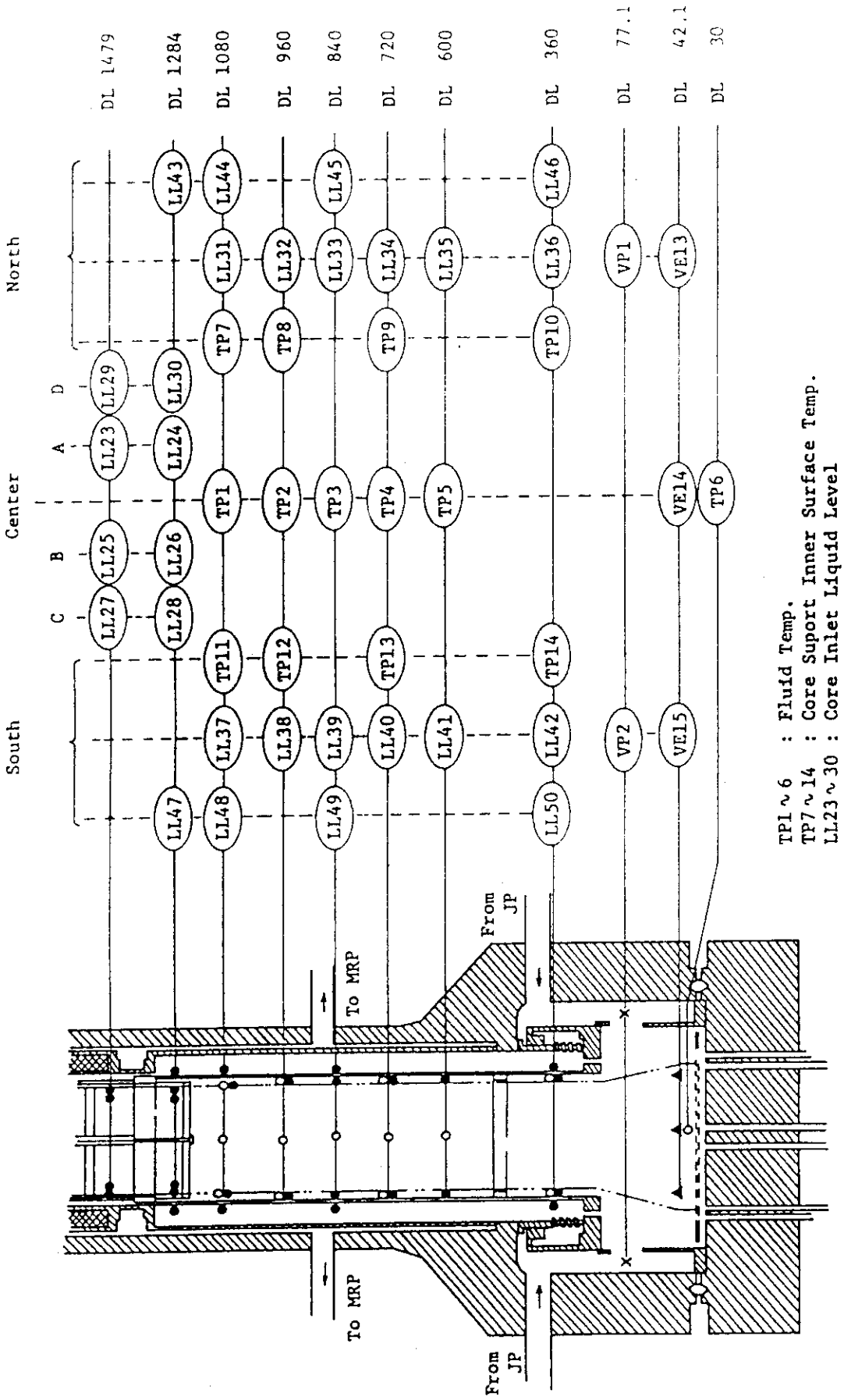

Fig. 3.4 Lower plenum instrumentation

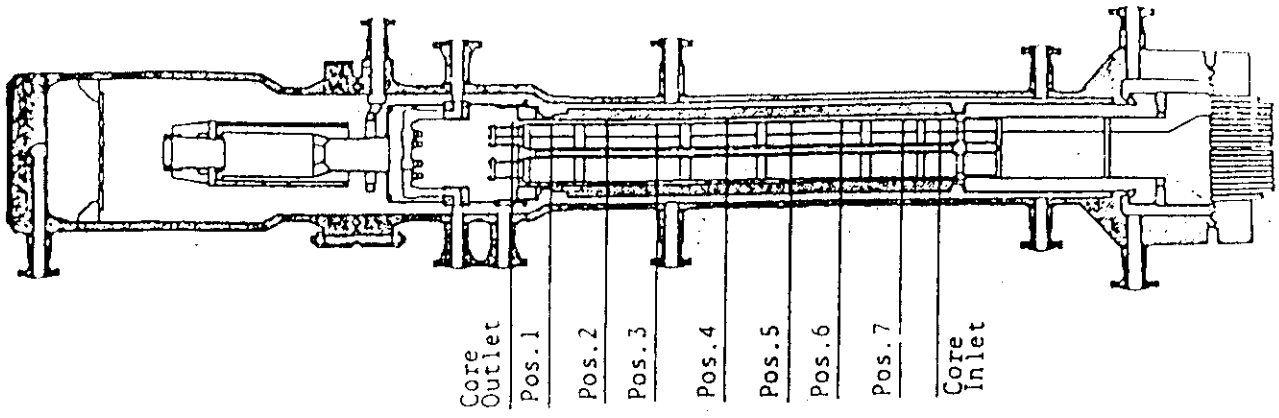

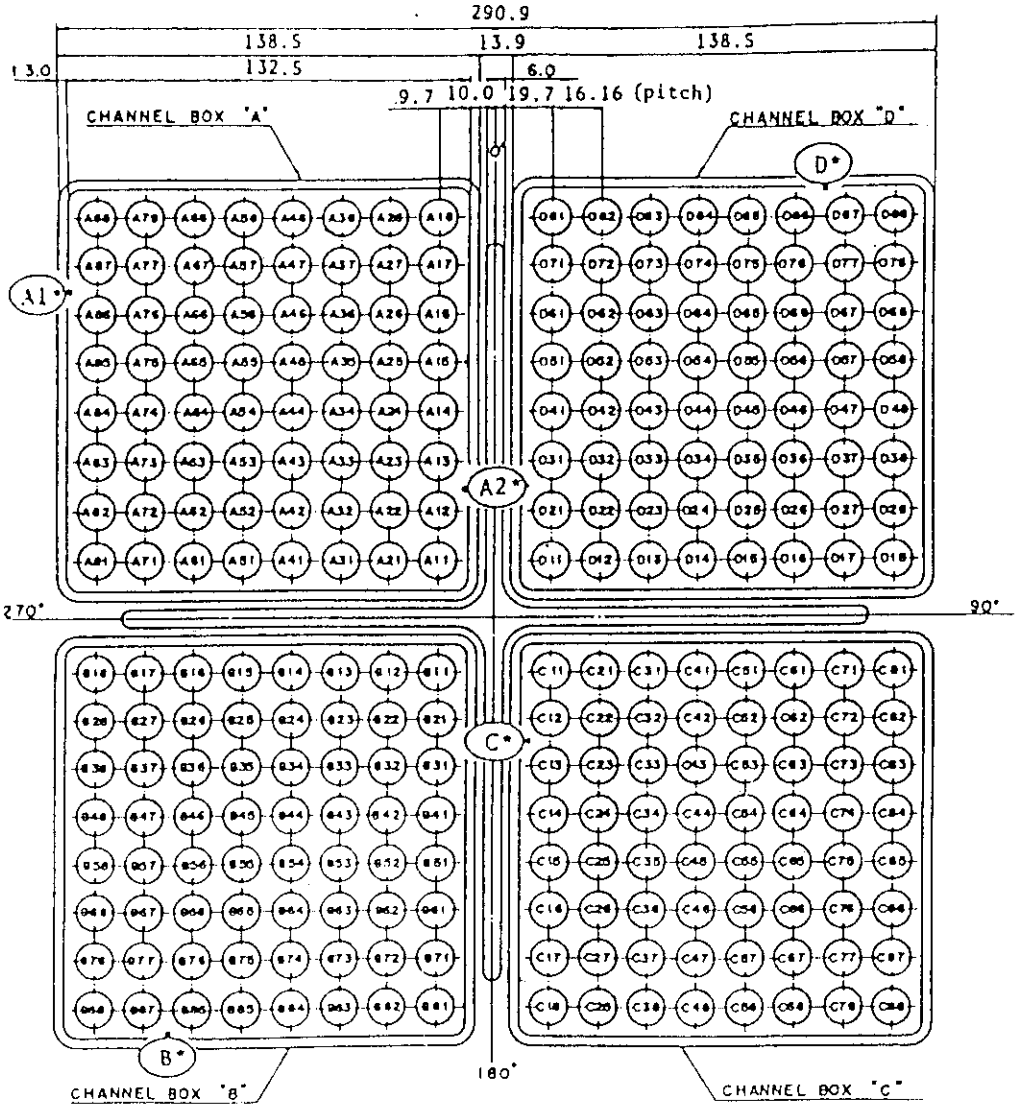

Heater rod O.D. is 12.27mm

A54, B54, C54 and D54 are water rod simulators with void probes, O.D. = 15.01mm

A45, B45, C45 and D45 are water rod simulators with thermocouples, O.D. = 15.01mm

Fig. 3.5 Core instrumentation (cf. Table 3.3)

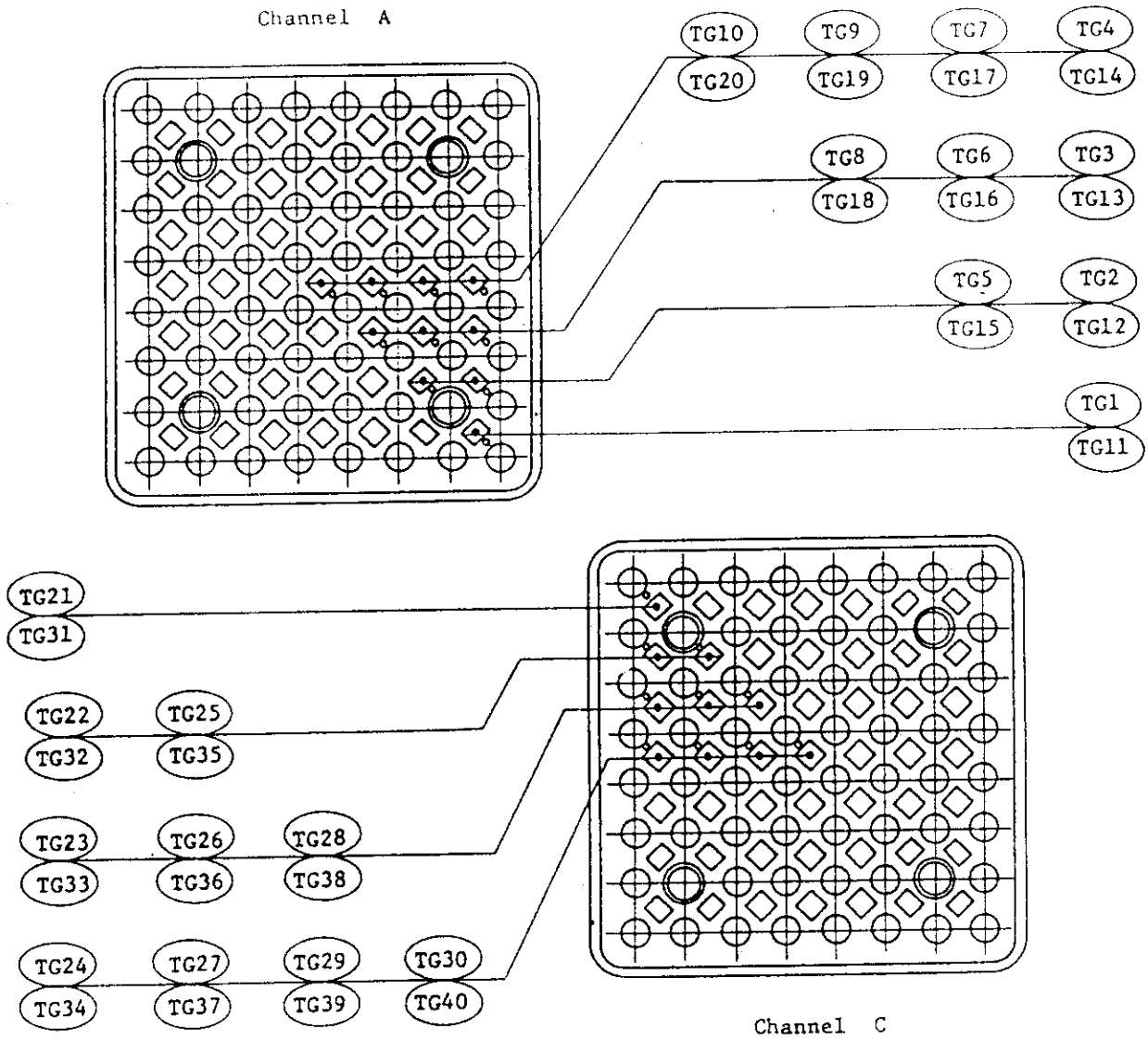

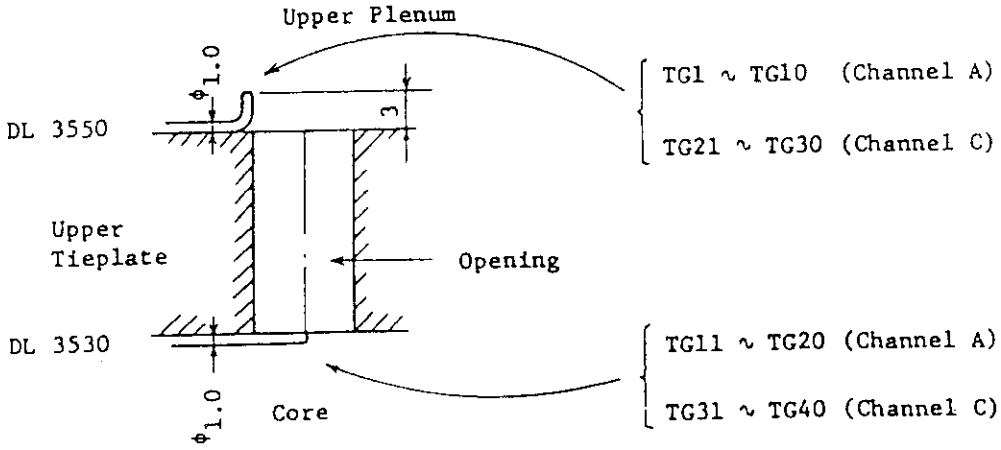

Fig. 3.6 Upper tieplate instrumentations

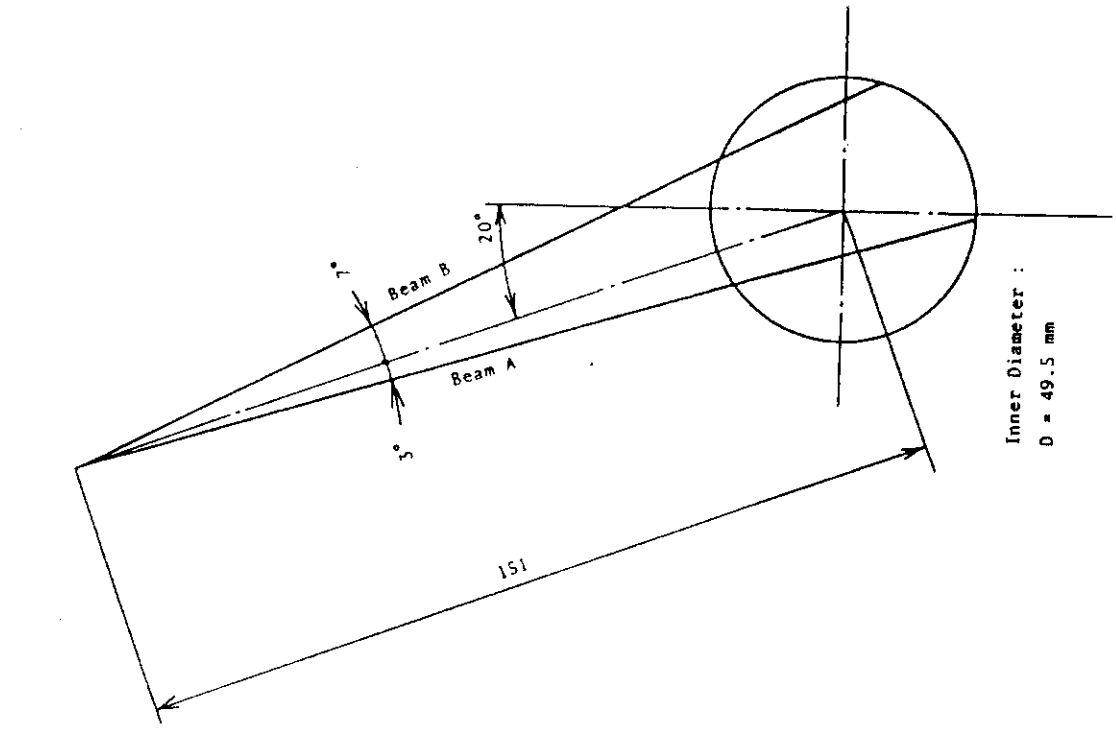

Fig. 3.8 Beam directions of two-beam gamma densitometer

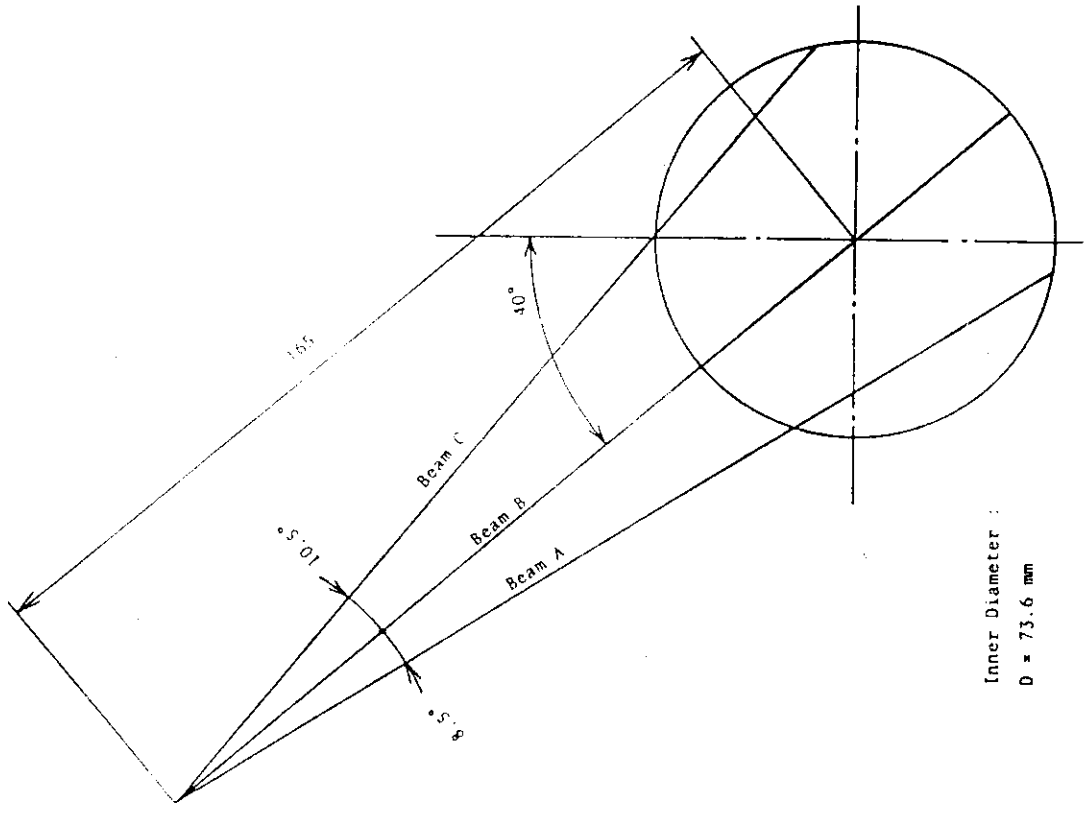

Fig. 3.7 Beam directions of three-beam gamma densitometer

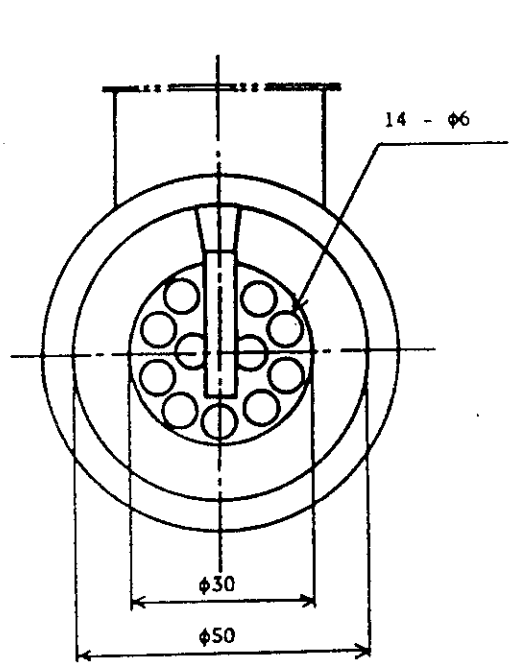

(a) High Range Drag Disc

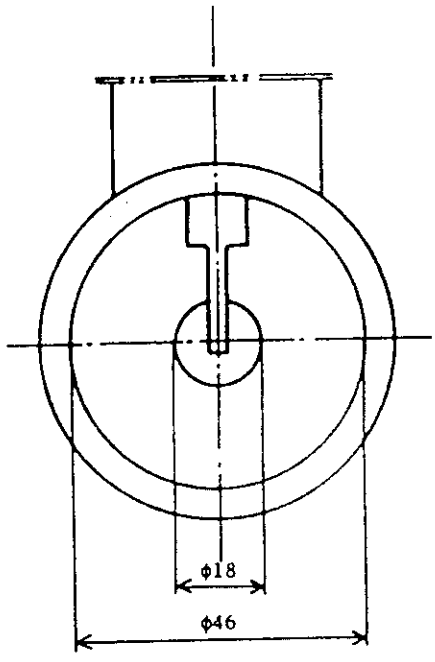

(b) Low Range Drag Disc

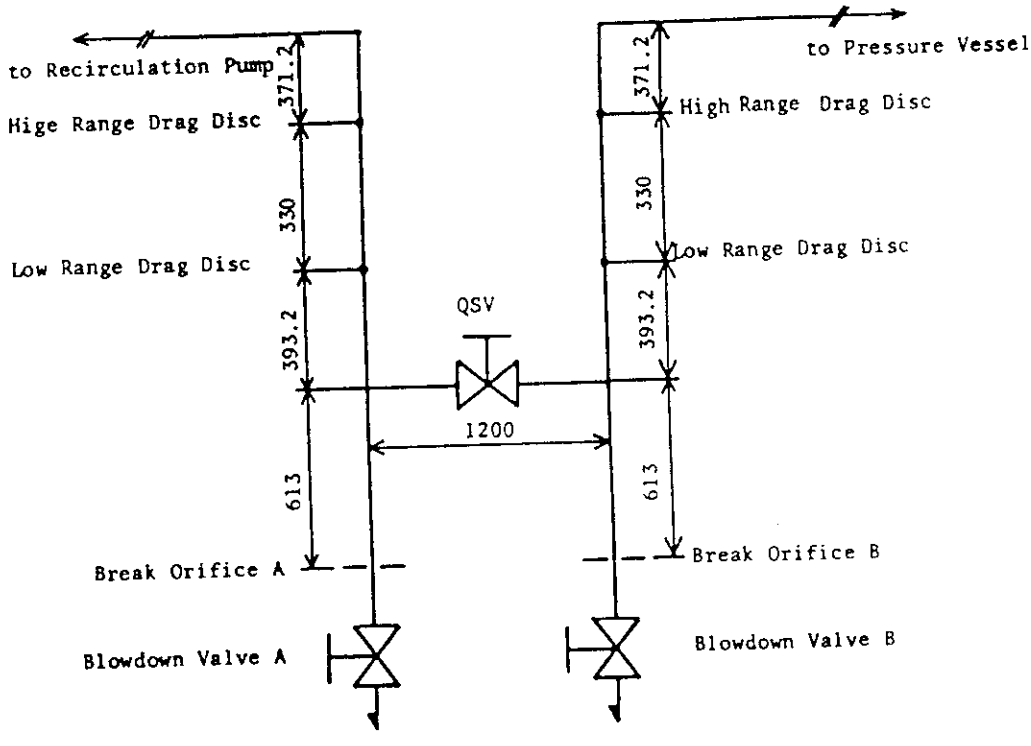

(c) Location of Drag Discs

Fig. 3.9 Configuration and location of drag disks

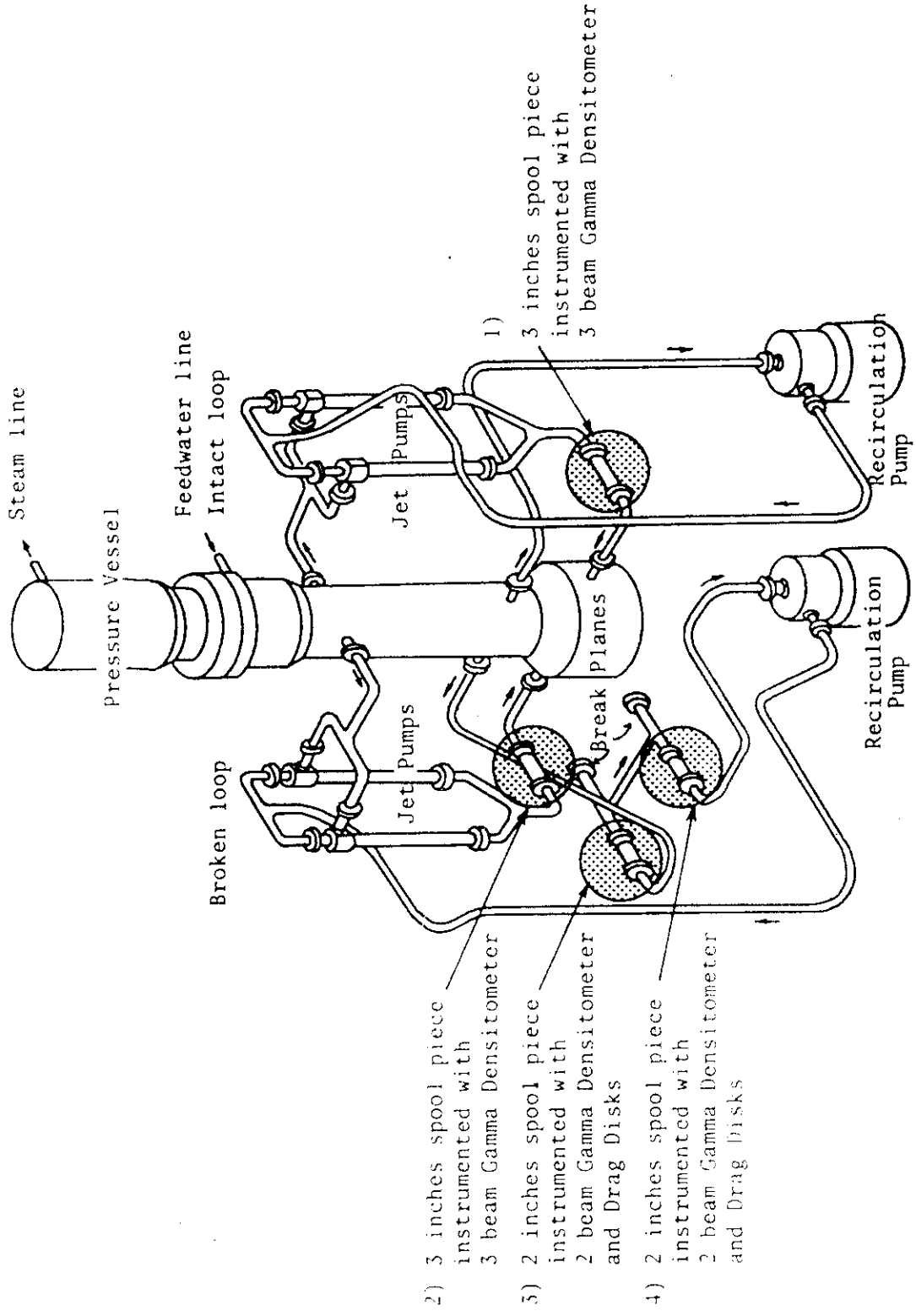

Fig. 3.10 Location of two-phase flow measurement spool pieces

4. Test Conditions and Procedure

RUN 983 is a 200% break test at the recirculation pump (MRP2) suction line in the broken recirculation loop. The initial and transient test conditions of RUN 983 shown below are determined to simulate those of the corresponding FIST test. The FIST test simulating design basis accident in a BWR/6 (218-624) has the 1/624 scaled break flow areas of 0.348 ft^2 and 1.878 ft^2 for the break flow areas at the jet pump side and recirculation side, respectively. The former area corresponds to total jet pump drive nozzle flow area in the broken loop and the latter area to the pipe flow area in the recirculation loop of the reference BWR. The flow areas of break orifice and nozzle of the ROSA-III test RUN 983 correspond to these FIST break areas. Blowdown is initiated by opening two QOBVs and closing the QSV placed between the two break simulators. The initial conditions of the test are established after heat-up process; the steam dome pressure is 7.22 MPa, the lower plenum temperature is 551.5 K giving the subcooling of 11.6 K, the core inlet flow rate is 35.9 kg/s, the core heat generating rate is 3.614 MW. The estimated average quality in the upper plenum is 3.4%. The initial water level in the upper downcomer is 4.83 m. The detailed conditions are summarized in Table 4.1.

To conduct the test, makeup water (pure water) is pumped into the primary system of the test facility and electric power is supplied to the core to heat the water in the system and to achieve the expected condition in the upper portion of the pressure vessel. The core power, 3.614 MW, corresponds to 40% of the volumetrically scaled rated power of one bundle, 8.96 MW of the reference BWR. The core power[29] is controlled after the break initiation as shown in Fig. 4.2. The power is kept constant for the first 8 seconds and reduced along the curve shown in the figure which simulates the surface heat flux of high power nuclear rod of BWR. The maximum linear heat rate of the peak power rod is 11.92 kw/m before the break initiation.

The schematic of the main steam line are shown in Fig. 4.3. The main steam line of the ROSA-III has three branches for (1) steady flow, (2) ADS and (3) transient line, but the third one is not used in RUN 983. Before the break initiation, CV-130 in the steady flow branch controls the steam flow to maintain the steam dome pressure constant and CV-1 and CV-2 are opened to provide steam to the heat exchanger to heat the feedwater. At the break initiation, the steam flow control is terminated and thereafter the

steam flow is limitted at the OR-3 with 18.0 mm I.D.. At the system pressure of 6.7 MPa, the pressure control system is actuated again by controlling CV-130. The MSIV closure is actuated by L1 level signal (3.62 m from bottom of PV; estimated as 10 s after break from the previously performed test). CV-1 and CV-2 are closed simaltaneously after break initiation. Tables 4.2 and 4.3 show the characteristics and the control sequence of steam discharge line valves in the present test, respectively. The feedwater supply is terminated between 2 and 4 s after the break by closing AV-112 in the feedwater line (see Fig.2.8). The coolant recirculation pumps are tripped to start coasting down at the break initiation.

The HPCS starts to inject water 27 s after break. The LPCS and LPCI can inject cooling water after the primary system pressure is reduced below 1.87 MPa and 1.57 MPa, respectively by receiving the L1 level signal with time delay of 40s. The injection flow rates of HPCS, LPCS and LPCI and ADS orifice flow area in RUN 983 are changed from the standard ROSA-III tests as shown in Table 4.1 in order to simulate the FIST test conditions. Specified system pressures for actuating LPCS and LPCI were also simulated by the FIST condition. The test was terminated after all the core is quenched at 978 s after the break initiation.

Table 4.1 Test conditions of RUN 983

Parameters			Specified Value	Measured Value
Break Conditions				
Location			Suction Line	Suction Line
Type			Orifice/Nozzle	Orifice/Nozzle
Break Orifice Diameter			10.1/26.2	10.1/26.2
Initial Test Conditions				
Steam Dome Pressure (MPa)			7.19	7.19
Lower Plenum Temperature (K)			552	551.5
Lower Plenum Subcooling (K)			11.0	11.6
Core Inlet Flow Rate(*1) (kg/s)			32.0	35.9
Core Outlet Quality(*2) (%)			-	3.4
Power Supplied to Core (kJ/s)			3600(2700+900)	3614(2710+904)
Max. Linear Heat Rate (kJ/m.s)				
Channel A	P.F.=	1.1	11.89	11.92
		1.0	10.81	10.84
		0.875	9.46	9.49
Channel B.C.D.	P.F.=	1.1	11.89	11.92
		1.0	10.81	10.81
		0.875	9.46	9.49
Power Curve			Fig.4.2	Fig.5.58
Fuel Assembly Number			4	4
Water Level in PV (m)			5.0	4.8
Feed Water Conditions				
Temperature		(K)	296	296
Flow Rate		(kg/s)	-	1.25(Fig.5.42)
Valve Closure Time (s)			2	2-4

(*1) Flow rate includes the core bypass flow rate

(*2) Average quality in the upper plenum

Table 4.1 (Cont'd)

Items		Specified Value	Measured Value
Steam Line Conditions			
Steady State Flow Rate	(kg/s)	-	1.29
Transient Flow Rate	(kg/s)	-	Fig.5.40
MSIV Closure	(s)		13
Safety Relief Valve Set Point	(MPa)	8.13	not opened
ECCS Conditions			
HPCS			
Injection Location		Upper Plenum	Upper Plenum
Initiation Time	t (t)	27	27
Initiation Pressure	p (MPa)	-	5.57
Coolant Temperature	(K)	322 (49°C)	322 (49°C)
Injection Flow Rate	(m^3/s)	-	Fig.5.41
LPCS			
Injection Location		Upper Plenum	Upper Plenum
Initiation Time	t (t)	$L1^{(*3)} + 40 \leqq t$	85
Initiation Pressure	p (MPa)	$1.86 \geqq p$	$1.86 \geqq p$
Coolant Temperature	(K)	322 (49°C)	322 (49°C)
Injection Flow Rate	(m^3/s)	1.42×10^{-3}	Fig.5.41
LPCI			
Injection Location		Top of Core Bypass	Top of Core Bypass
Initiation Time	t (s)	$L1 + 40 \leqq t$	95
Initiation Pressure	p (MPa)	$1.57 \geqq p$	$1.57 \geqq p$
Coolant Temperature	(K)	322 (49°C)	322 (49°C)
Injection Flow Rate	(m^3/s)	3.08×10^{-3}	Fig.5.41
ADS Conditions			
Initiation Time	(s)	$L1 + 105 \leqq t$	115
Flow Rate		Scaled Flow	Fig.5.40
Orifice Diameter	(mm)	21.1	21.1

(*3) L1 : Water Level in the downcomer, 3.6 m from PV bottom

Table 4.2 Characteristics of steam discharge line valves

Valve No.	Opening Time (s)	Closing Time (s)
AV 165	——	——
AV 168	——	0.1
AV 169	0.3	2.0

Orifice No.	Diameter (mm)	Area (mm^2)
OR 3	18.0	254.5
OR 4	21.1	349.7
OR 5	not used	——

Table 4.3 Control sequence for steam line valves in RUN 983

Time	before break	break (t=0)	L1 + 3s	L1 + 105s
AV 168	Open	Open	Close	Close
CV 130	Control to maintain steady state pressure	Opened fully	Close	Close
AV 165	not used	not used	not used	not used
AV 169	Close	Close	Close	Open

AV ; Air Actuation Valve (Auto)

CV ; Control Valve (Manual)

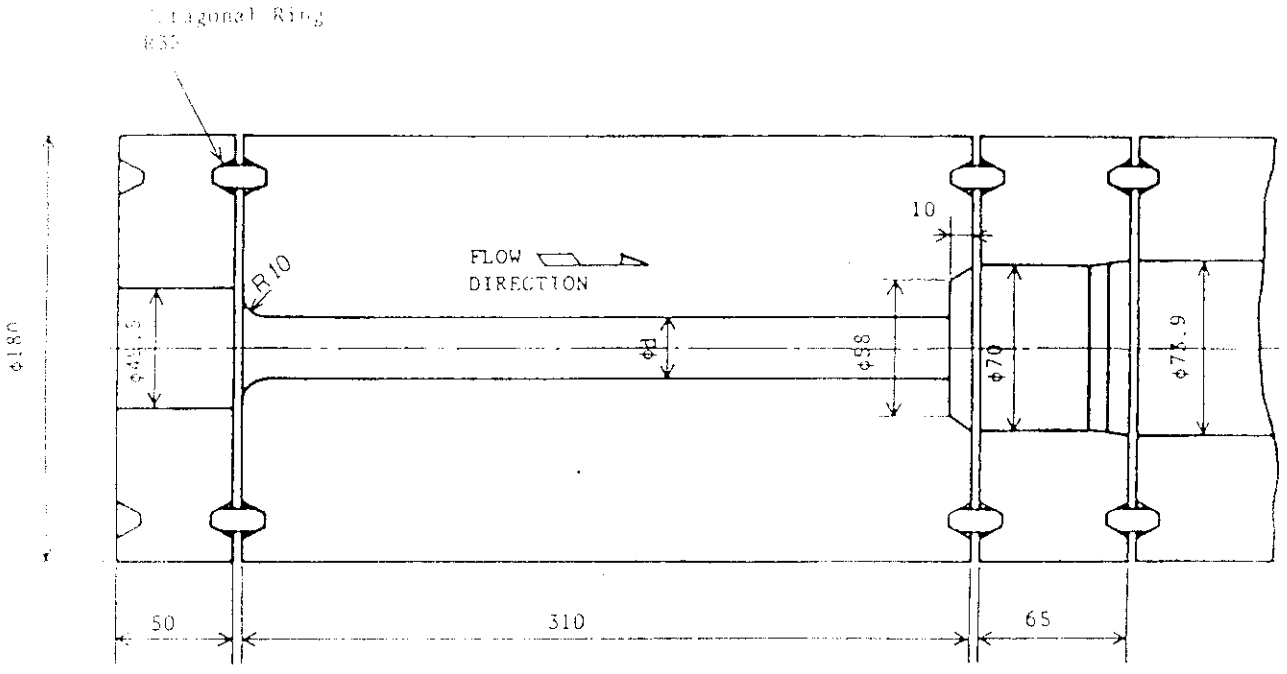

break nozzle

Break area ratio (%)	d (mm)
100	26.2

Material SUS304

Dimension in mm

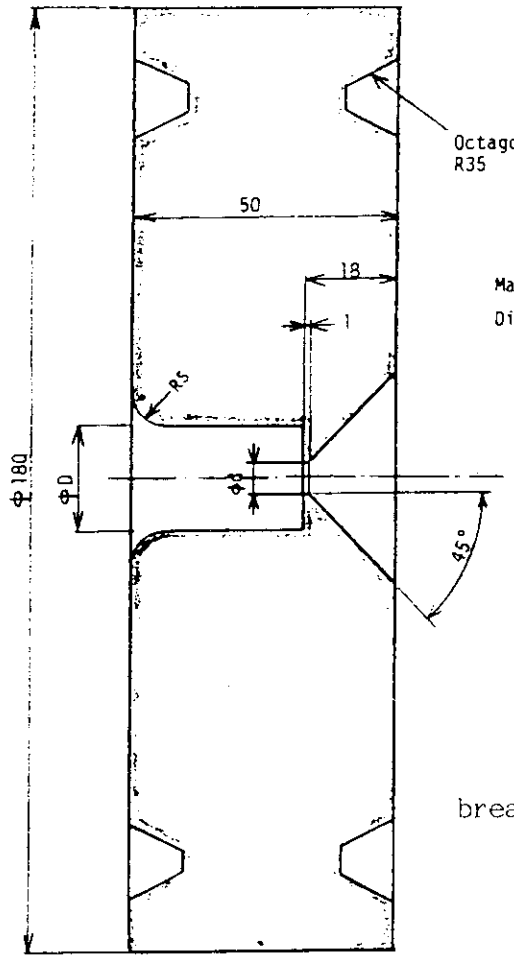

Material SUS304

Dimension in mm.

D = 30.0 mm

d = 10.1 mm

break orifice

Fig. 4.1 Details of break orifice and break nozzle in RUN 983

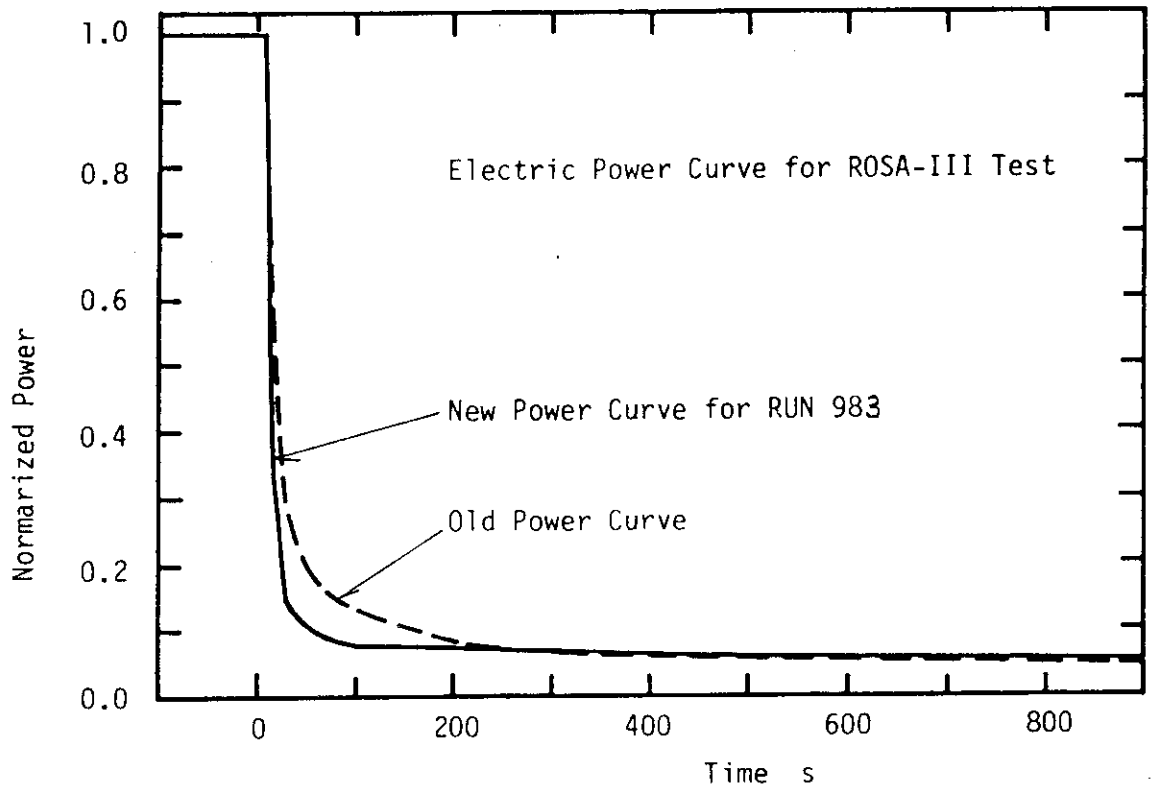

Fig. 4.2 Normalized power transient for ROSA-III test

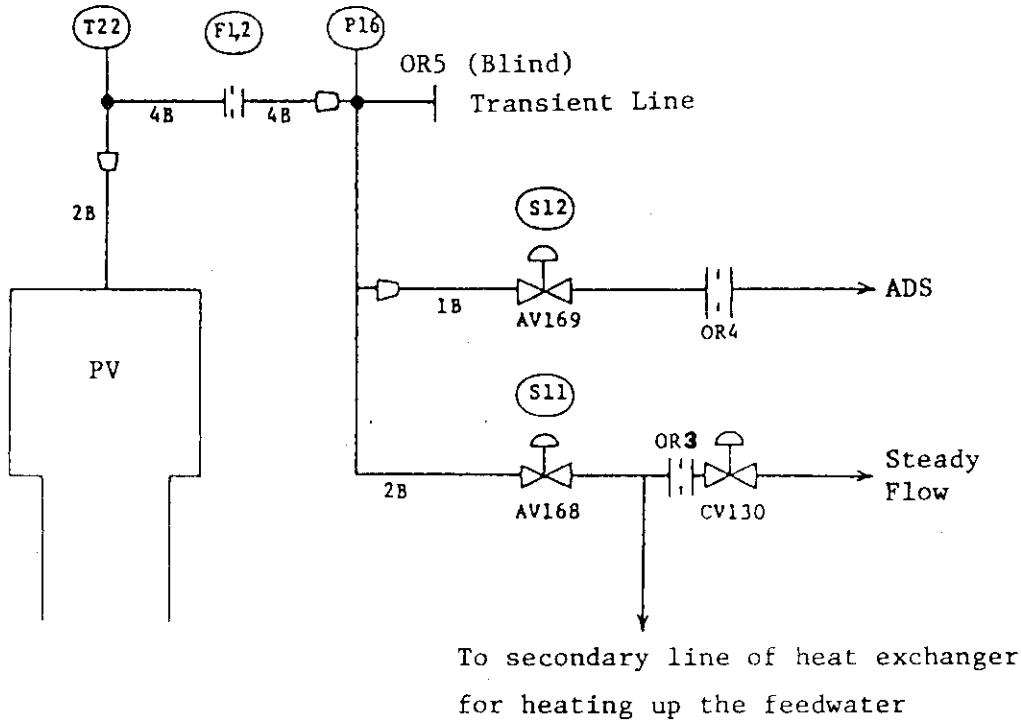

Fig. 4.3 Main steam line schematic

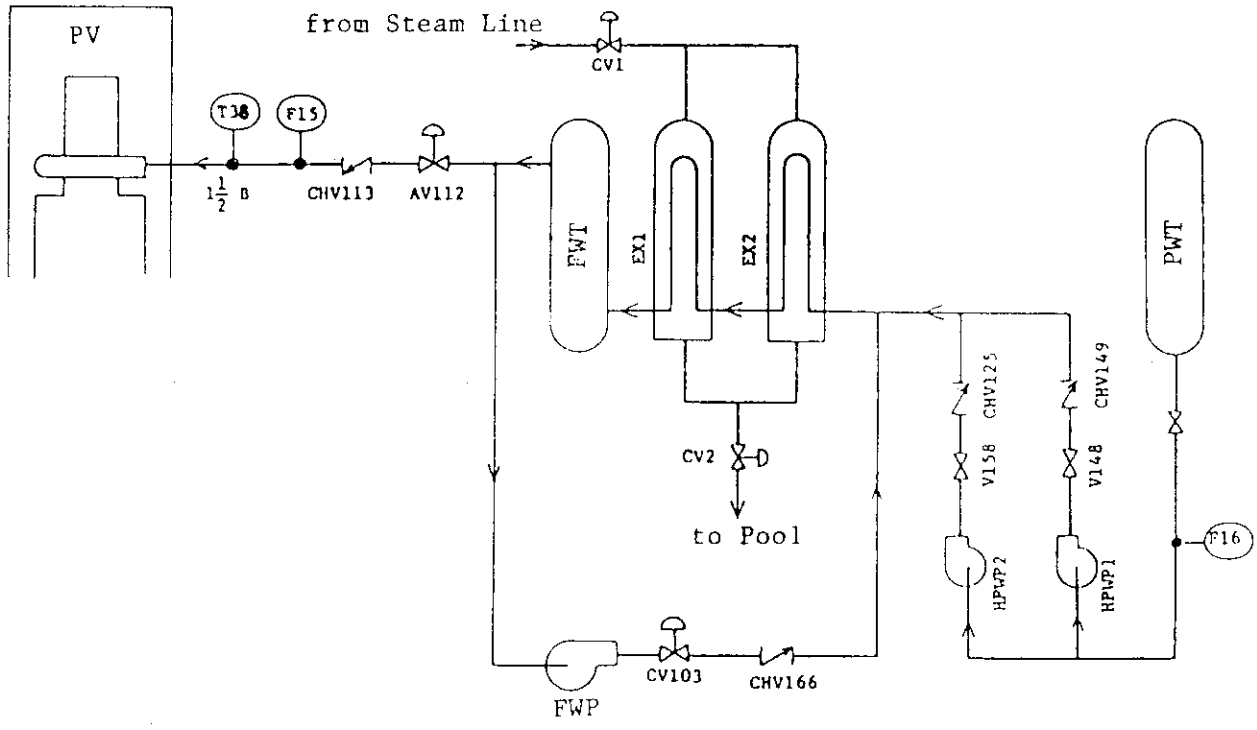

Fig. 4.4 Feedwater line schematic

5. Data Processing

In RUN 983, the data acquisition by DATAC 2000B was started 119 s before the break initiation and terminated 978 s after the break initiation. The data acquisition frequency was 10 Hz. The test data was processed and reduced to 1000 data points for computer plotting. The time span and frequency of the reduced data for plotting were 1000 s and 1 Hz, respectively.

The test data are shown in Figs. 5.1 through 5.189. In these figures, the measured quantity is identified by the channel number and the alphabetic characters (ref. Table 3.2). The major test sequences and events observed in RUN 983 are summarized in Table 5.1.

Figures 5.1 through 5.7 show the pressure data in the pressure vessel, recirculation loops and in the steam line. Figures 5.8 through 5.36 show differential pressure data between various positions in the pressure vessel and the recirculation loop. Figures 5.37 and 5.38 show the liquid levels in the ECCS tanks and downcomer. Figures 5.39 through 5.45 show the flow rates. Differential pressures across orifices and venturies shown in Figs. 5.46 through 5.55 are useful to check out the flow rate instrumentation. Figure 5.56 shows the power supplied to the core with the maximum capacities of 2100 and 3150 kW. The pump speeds of the recirculation pumps are shown in Fig. 5.57. The trip signals such as the break initiation signal and the valve positioning signals are shown in Figs. 5.58 through 5.60. Figures 5.61 through 5.67 show the fluid densities measured by the gamma densitometer. Figures 5.68 through 5.71 show momentum fluxes measured by drag disks. Figures 5.72 through 5.80 show the fluid temperatures at various positions in the system. The fuel rod cladding temperature and the surface temperatures of the water rods and the channel boxes measured at positions 1 through 7 are given in Figs. 5.81 through 5.99. Figure 5.100 shows outer surface temperatures of channel box A. Figures 5.101 through 5.132 show the fuel rod cladding temperatures in a different manner. Figures 5.133 through 5.145 show the fluid temperatures at the inlet and outlet of the channel box. The outer surface temperatures of the channel box are shown in Fig. 5.146 with the same vertical axis. The fluid temperature in the lower plenum was measured as shown in Fig. 5.147. The liquid level signals in the core, the upper and lower plena, the guide tube and the downcomer are shown in Figs. 5.148 through 5.157. The peak cladding temperature (PCT) distribution in the core is given in Table 5.2.

Quantities obtained from reduction of the test data are shown in Fig. 5.158 through 5.189.

Figures 5.158 and 5.159 show the estimated liquid levels in the core and the pressure vessel obtained by reducing the conductivity probe signals previously shown in Figs. 5.148 through 5.157. Figure 5.160 shows transients of the dryout and quenching times of the representative fuel rods in the core. Figures 5.161 through and 5.163 show the average density calculated from the data measured by two-beam gamma densitometer. The beam configurations of gamma densitometers installed in the ROSA-III facility are shown in Fig. 3.7. The average density is calculated as an arithmetic mean of the densities in multi-directions with the weight of each cord length.

For the three-beam densitometer at the jet pump outlet spool,

$$\rho_{av} = 0.3221\rho_A + 0.43\rho_B + 0.2479\rho_C \tag{5.1}$$

where,

ρ_{av}: average density obtained from the three-beam gamma densitometer,
ρ_A : density measured by beam A (bottom),
ρ_B : density measured by beam B (middle),
ρ_C : density measured by beam C (top),

For the two-beam densitometer at the break spool piece,

$$\rho_{av} = 0.5863\rho_A + 0.4137\rho_B \tag{5.1}$$

where,

ρ_{av}: average density obtained from the two-beam gamma densitometer,
ρ_A : density measured by beam A (bottom),
ρ_B : density measured by beam B (top).

Figures 5.164 through 5.167 show the flow rates at upstream sides of the break in the recirculation loop. The flow rate is computed from the drag disk data and the gamma densitometer data using the following equation,

$$G = C_D \cdot A \cdot \sqrt{\rho_{av} \cdot \rho v^2} \tag{5.2}$$

where,

G : mass flow rate,
C_D : drag coefficient (= 1.13),
A : flow area (= 1.923 × 10^{-3} m^2),
ρ_{av}: average density from gamma densitometer,
ρv^2: momentum flux from drag disk.

The total break flows are derived from the flow rates in the recirculation loop as follows (Figs. 5.168 and 5.169),

$$G_B = G_P + G_V \tag{5.3}$$

where,
G_B : break flow,
G_P : flow rate at the pump side of the break,
G_V : flow rate st the vessel side of the break,

The cummulated discharged mass from the breaks is calculated as integrated break flow rates as shown in Fig. 5.170.

Figures 5.171 through 5.181 show the fluid flow rates at the main steam line, the channel inlet orifices, the bypass hole and the jet pump outlets. The fluid flow rates are calculated from the test data which are the pressure drop across the orifices or venturi flow meters and the liquid density obtained from the temperature and the pressure condition. The equation used for the calculation is as follows :

$$G = C_D \cdot A \cdot \sqrt{2g \cdot \rho_l \cdot \Delta P} \tag{5.4}$$

where,
G : flow rate,
ΔP : pressure drop across the orifice,
C_D : discharge coefficient,
= 0.6552 (the orifice to measure the steam discharge flow rate)
= 0.4761 (the channel inlet orifice)
= 0.8032 (the bypass hole)
= 0.7383 (the orifice to measure the jet pump outlet flow rate)
= 1.1260 (the venturi tube to measure the jet pump outlet flow rate)

A : flow area (m^2)
= 2.875×10^{-3} (the orifice to measure the steam discharge flow rate)
= 1.521×10^{-3} (the channel inlet orifice)
= 1.758×10^{-4} (the bypass hole)
= 1.133×10^{-3} (the orifice to measure the jet pump outlet flow rate)
= 9.095×10^{-4} (the venturi tube to measure the jet pump outlet flow rate)

g : gravitational acceleration (= 9.807 m/s^2),

ρ_l : density of the single-phase liquid (kg/m^3),

This calculation method is not applicable for two-phase flow condition after the LPF initiation at the channel inlet orifice, the bypass hole and the jet pump outlet. The calculated value shows only a trend in two-phase flow condition. Total channel inlet flow rate presents the sum of four channel inlet flow rates.

Figures 5.182 and 5.183 show the collapsed water level outside and inside the core shroud. The collapped water level is obtained from the differential pressure in the pressure vessel. The differential pressure may include the flow resistance effect, however, the flow resistance becomes negligible after completion of the recirculation pump coastdown.

Figures 5.184 through 5.186 show the fluid mass inventories in the pressure vessel. The fluid mass inventory is determined from the density and configurational data inside and outside the core shroud,

$$M = \rho_l \cdot Q \tag{5.5}$$

where,

M : fluid inventory,

ρ_l : liquid density estimated from the satulation temperature and/or pressure,

Q : liquid volume calculated from the liquid level.

The volume Q (m^3) outside the shroud is given below as a function of collapsed water level (L),

$$
\begin{aligned}
Q &= 0.0 && (\quad L \leqq 0.494) \\
Q &= 0.0225L - 0.0111 && (0.494 < L \leqq 1.384) \\
Q &= 0.0697L - 0.0769 && (1.384 < L \leqq 1.519) \\
Q &= 0.0225L - 0.0048 && (1.519 < L \leqq 3.355) \\
Q &= 0.0801L - 0.1980 && (3.355 < L \leqq 4.250) \\
Q &= 0.2443L - 0.8959 && (4.250 < L \leqq 4.413) \\
Q &= 0.2611L - 0.9700 && (4.413 < L \leqq 4.578) \\
Q &= 0.2504L - 0.9211 && (4.578 < L \leqq 4.654) \\
Q &= 0.2375L - 0.8610 && (4.654 < L \leqq 4.815) \\
Q &= 0.2866L - 1.0974 && (4.815 < L \leqq 4.915) \\
Q &= 0.3396L - 1.3580 && (4.915 < L \leqq 5.143) \\
Q &= 0.3607L - 1.4665 && (5.143 < L \leqq 5.365) \\
Q &= 0.3848L - 1.5960 && (5.365 < L \leqq 5.955) \\
Q &= 0.7111 && (5.955 < L \quad)
\end{aligned}
\tag{5.6}
$$

The volume Q (m^3) inside the shroud is also given as a function of collapsed water level inside core shroud (L),

$$
\begin{aligned}
Q &= 0.0 && (\quad L \leqq 0.0) \\
Q &= 0.2350L && (0.0 < L \leqq 0.497) \\
Q &= 0.1245L + 0.0549 && (0.497 < L \leqq 1.354) \\
Q &= 0.0698L + 0.1290 && (1.354 < L \leqq 3.589) \\
Q &= 0.1648L - 0.2120 && (3.589 < L \leqq 3.744) \\
Q &= 0.1963L - 0.3299 && (3.744 < L \leqq 4.243) \\
Q &= 0.0196L + 0.4199 && (4.243 < L \leqq 4.578) \\
Q &= 0.0186L + 0.4244 && (4.578 < L \leqq 4.654) \\
Q &= 0.0410L + 0.3201 && (4.654 < L \leqq 5.099) \\
Q &= 0.0196L + 0.4292 && (5.099 < L \leqq 5.365) \\
Q &= 0.5344 && (5.365 < L \quad)
\end{aligned}
\tag{5.7}
$$

The total fluid mass inventory in the pressure vessel is obtained as the summation of the mass inventory outside and inside the shroud. However, it should be noted that the estimated mass inventories contain a certain amount of ambiguity due to the unknown void distribution over the wide regions with various flow areas. The initial mass inventory before the break initiation is estimated as 640 kg.

Figure 5.187 shows the mass decrease by the fluid discharge from the

break and the fluid mass recovery by the ECCS water and the feedwater injections. The variation of fluid mass inventory with time is calculated by the following equation,

$$M = \int_0^t \{ G + \rho_1 \cdot (W_H + W_L + W_I) + \rho_2 \cdot W_F \} dt \tag{5.8}$$

where,

M : mass accumulation,
G : steam discharge flow rate,
ρ_1 : density of satulated liquid at 315 K,
ρ_2 : density of satulated liquid at 489 K,
W_H : volumetric flow rate of the HPCS,
W_L : volumetric flow rate of the LPCS,
W_I : volumetric flow rate of the LPCI,
W_F : volumetric flow rate of the feedwater.

Figure 5.188 shows the fluid mass discharged from the break. The fluid mass discharge M_B is calculated as follows neglecting the change of the fluid mass inventory in the loops,

$$M_B = (M_P)_i - M_P + M_F \tag{5.9}$$

where,

M_B : fluid mass discharged from the break,
$(M_P)_i$: fluid mass inventory in the pressure vessel (= 640 kg),
M_P : fluid mass inventory in the pressure vessel,
M_F : net fluid mass increase by the ECCS, the feedwater flow and the steam discharge flow.

Figure 5.189 shows the break flow calculated from the fluid mass inventory in the pressure vessel. The break flow is estimated from the mass inventory as follows,

$$G_B = \frac{d}{dt} M_B \tag{5.10}$$

where,

G_B : break flow,
M_B : fluid mass discharged from the break.

Table 5.1 Sequence of events in RUN 983

Time (s)	Events and Procedures
-119	Initiation of data recording
- 10.4	Initiation of data plotting in figures
0.0	• Break initiation (QOBVs open)
	• QSV closure
	• MRP1 and MRP2 coast down
	• CV-130 full open, CV-1 and CV-2 closure
2	Feedwater stop (completed at 4 s)
6	Initiation of pressure control
8	Initiation of power decrease
10	L1 level (3.62 m from PV bottom)
12	JP suction uncovered
13	MSIV closure (completed at 15 s)
17	Recirculation line uncovered
18	Lower plenum flashing
27	HPCS actuation
85	LPCS actuation
95	LPCI actuation
115	ADS actuation
690	Termination of data plotting
978	Termination of data recording

Table 5.2 Maximum cladding temperatures distribution in core

	Pos.1	Pos.2	Pos.3	Pos.4	Pos.5	Pos.6	Pos.7
A-11 rod	TE 201	TE 202	TE 203	TE 204	TE 205	TE 206	TE 207
PCT (K)	562.5	559.1	564.9	567.1	567.1	566.2	565.9
Time (s)	0.0	0.0	0.0	0.0	0.0	0.0	2.8
A-12 rod	TE 208	TE 209	TE 210	TE 211	TE 212	TE 213	TE 214
PCT (K)	561.1	562.7	565.2	564.9	564.8	565.1	561.1
Time (s)	0.0	0.0	0.0	0.0	0.0	0.0	2.1
A-13 rod	TE 215	TE 216	TE 217	TE 218	TE 219	TE 220	TE 221
PCT (K)	563.8	569.5	565.7	566.3	564.7	565.9	563.5
Time (s)	0.0	0.0	0.0	0.0	0.0	0.0	1.4
A-14 rod	TE 222	TE 223	TE 224	TE 225	TE 226	TE 227	TE 228
PCT (K)	------	------	------	------	------	------	------
Time (s)	------	------	------	------	------	------	------
A-15 rod	TE 229			TE 230			
PCT (K)	------			------			
Time (s)	------			------			
A-17 rod	TE 231			TE 232			
PCT (K)	------			564.5			
Time (s)	------			0.0			
A-22 rod	TE 233	TE 234	TE 235	TE 236	TE 237	TE 238	TE 239
PCT (K)	562.2	559.9	563.5	565.4	567.2	566.2	562.6
Time (s)	0.0	0.0	0.0	0.0	0.0	0.0	1.4
A-24 rod	TE 240	TE 241	TE 242	TE 243	TE 244	TE 245	TE 246
PCT (K)	------	------	------	------	------	------	------
Time (s)	------	------	------	------	------	------	------

Table 5.2 Maximum Cladding Temperature Distribution in the Core (Continued)

	Pos.1	Pos.2	Pos.3	Pos.4	Pos.5	Pos.6	Pos.7
A-26 rod	TE 247			TE 248			
PCT (K)	------			------			
Time (s)	------			------			
A-28 rod	TE 249			TE 250			
PCT (K)	------			563.4			
Time (s)	------			0.0			
A-31 rod	TE 251			TE 252			
PCT (K)	------			562.1			
Time (s)	------			0.0			
A-33 rod	TE 253	TE 254	TE 255	TE 256	TE 257	TE 258	TE 259
PCT (K)	562.8	560.8	559.8	563.8	563.5	566.1	561.4
Time (s)	0.0	0.0	0.0	0.0	0.0	0.0	1.4
A-34 rod	TE 260	TE 261	TE 262	TE 263	TE 264	TE 265	TE 266
PCT (K)	------	------	------	------	------	------	------
Time (s)	------	------	------	------	------	------	------
A-37 rod	TE 267			TE 268			
PCT (K)	------			------			
Time (s)	------			------			
A-42 rod	TE 269			TE 270			
PCT (K)	------			------			
Time (s)	------			------			
A-44 rod	TE 271	TE 272	TE 273	TE 274	TE 275	TE 276	TE 277
PCT (K)	------	------	------	------	------	------	------
Time (s)	------	------	------	------	------	------	------

Table 5.2 Maximum Cladding Temperature Distribution in the Core (Continued)

	Pos.1	Pos.2	Pos.3	Pos.4	Pos.5	Pos.6	Pos.7
A-48 rod	TE 278			TE 279			
PCT (K)	------			------			
Time (s)	------			------			
A-51 rod	TE 280			TE 281			
PCT (K)	------			------			
Time (s)	------			------			
A-53 rod	TE 282			TE 283			
PCT (K)	------			------			
Time (s)	------			------			
A-57 rod	TE 284			TE 285			
PCT (K)	------			567.2			
Time (s)	------			0.0			
A-62 rod	TE 286			TE 287			
PCT (K)	------			------			
Time (s)	------			------			
A-66 rod	TE 288			TE 289			
PCT (K)	------			------			
Time (s)	------			------			
A-68 rod	TE 290			TE 291			
PCT (K)	------			564.2			
Time (s)	------			0.0			
A-71 rod	TE 292			TE 293			
PCT (K)	------			563.1			
Time (s)	------			0.0			

Table 5.2 Maximum Cladding Temperature Distribution in the Core (Continued)

	Pos.1	Pos.2	Pos.3	Pos.4	Pos.5	Pos.6	Pos.7
A-73 rod	TE 294			TE 295			
PCT (K)	------			564.5			
Time (s)	------			0.0			
A-75 rod	TE 296			TE 297			
PCT (K)	------			------			
Time (s)	------			------			
A-77 rod	TE 298	TE 299	TE 300	TE 301	TE 302	TE 303	TE 304
PCT (K)	562.5	565.4	566.3	561.0	564.0	563.4	------
Time (s)	0.0	0.0	0.0	0.0	0.0	0.0	------
A-82 rod	TE 305			TE 306			
PCT (K)	------			------			
Time (s)	------			------			
A-84 rod	TE 307			TE 308			
PCT (K)	562.5			565.6			
Time (s)	0.0			0.0			
A-85 rod	TE 309	TE 310	TE 311	TE 312	TE 313	TE 314	TE 315
PCT (K)	------	------	------	------	------	------	------
Time (s)	------	------	------	------	------	------	------
A-87 rod	TE 316	TE 317	TE 318	TE 319	TE 320	TE 321	TE 322
PCT (K)	563.4	565.8	564.9	563.5	566.1	565.3	563.3
Time (s)	0.0	0.0	0.0	0.0	0.0	0.0	0.7
A-88 rod	TE 323	TE 324	TE 325	TE 326	TE 327	TE 328	TE 329
PCT (K)	562.2	563.7	565.6	566.9	566.2	564.3	562.3
Time (s)	0.0	0.0	0.0	0.0	0.0	0.0	0.7

Table 5.2 Maximum Cladding Temperature Distribution in the Core (Continued)

	Pos.1	Pos.2	Pos.3	Pos.4	Pos.5	Pos.6	Pos.7
B-11 rod	TE 330	TE 331	TE 332	TE 333	TE 334	TE 335	TE 336
PCT (K)	562.4	563.3	565.4	564.3	563.5	564.3	------
Time (s)	0.0	0.0	0.0	0.0	0.0	0.0	------
B-13 rod				TE 337			
PCT (K)				564.3			
Time (s)				0.0			
B-22 rod	TE 338	TE 339	TE 340	TE 341	TE 342	TE 343	TE 344
PCT (K)	563.4	563.4	565.1	564.7	564.4	563.2	562.8
Time (s)	0.0	0.0	0.0	0.0	0.0	0.0	0.7
B-31 rod				TE 345			
PCT (K)				------			
Time (s)				------			
B-33 rod				TE 346			
PCT (K)				------			
Time (s)				------			
B-51 rod				TE 347			
PCT (K)				------			
Time (s)				------			
B-53 rod				TE 348			
PCT (K)				------			
Time (s)				------			
B-66 rod				TE 349			
PCT (K)				------			
Time (s)				------			

Table 5.2 Maximum Cladding Temperature Distribution in the Core (Continued)

	Pos.1	Pos.2	Pos.3	Pos.4	Pos.5	Pos.6	Pos.7
B-77 rod	TE 350	TE 351	TE 352	TE 353	TE 354	TE 355	TE 356
PCT (K)	561.3	568.0	568.5	562.8	564.9	564.3	562.3
Time (s)	0.0	0.0	0.0	0.0	0.0	0.0	1.4
B-86 rod				TE 357			
PCT (K)				------			
Time (s)				------			
C-11 rod	TE 358	TE 359	TE 360	TE 361	TE 362	TE 363	TE 364
PCT (K)	560.9	563.2	563.2	562.1	559.4	565.2	557.5
Time (s)	0.0	0.0	0.0	0.0	0.0	0.0	0.7
C-13 rod	TE 365	TE 366	TE 367	TE 368	TE 369	TE 370	TE 371
PCT (K)	559.3	561.2	563.0	563.2	563.8	564.6	562.3
Time (s)	0.0	0.0	0.0	0.0	0.0	0.0	0.7
C-15 rod				TE 372			
PCT (K)				------			
Time (s)				------			
C-22 rod	TE 373	TE 374	TE 375	TE 376	TE 377	TE 378	TE 379
PCT (K)	560.0	562.2	562.8	563.3	564.3	565.3	560.4
Time (s)	0.0	0.0	0.0	0.0	0.0	0.0	1.4
C-31 rod				TE 380			
PCT (K)				------			
Time (s)				------			
C-33 rod	TE 381	TE 382	TE 383	TE 384	TE 385	TE 386	TE 387
PCT (K)	560.7	564.3	560.7	562.4	562.9	562.3	557.5
Time (s)	0.0	0.7	0.0	0.0	0.0	1.4	0.7

Table 5.2 Maximum Cladding Temperature Distribution in the Core (Continued)

	Pos.1	Pos.2	Pos.3	Pos.4	Pos.5	Pos.6	Pos.7
C-35 rod				TE 388			
PCT (K)				------			
Time (s)				------			
C-66 rod				TE 389			
PCT (K)				------			
Time (s)				------			
C-68 rod				TE 390			
PCT (K)				------			
Time (s)				------			
C-77 rod	TE 391	TE 392	TE 393	TE 394	TE 395	TE 396	TE 397
PCT (K)	561.7	564.3	565.2	564.4	565.3	563.3	561.4
Time (s)	0.0	0.0	0.0	0.0	0.0	0.0	0.7
D-11 rod				TE 398			
PCT (K)				564.5			
Time (s)				0.0			
D-13 rod				TE 399			
PCT (K)				570.9			
Time (s)				0.0			
D-22 rod	TE 400	TE 401	TE 402	TE 403	TE 404	TE 405	TE 406
PCT (K)	561.2	574.9	562.5	566.3	564.0	565.3	560.4
Time (s)	0.0	81.2	0.0	0.0	0.0	0.0	0.7
D-31 rod				TE 407			
PCT (K)				------			
Time (s)				------			

Table 5.2 Maximum Cladding Temperature Distribution in the Core (Continued)

	Pos.1	Pos.2	Pos.3	Pos.4	Pos.5	Pos.6	Pos.7
D-33 rod				TE 408			
PCT (K)				------			
Time (s)				------			
D-51 rod				TE 409			
PCT (K)				------			
Time (s)				------			
D-53 rod				TE 410			
PCT (K)				------			
Time (s)				------			
D-66 rod				TE 411			
PCT (K)				------			
Time (s)				------			
D-77 rod				TE 412			
PCT (K)				565.3			
Time (s)				0.0			
D-86 rod				TE 413			
PCT (K)				565.1			
Time (s)				0.0			

Table 5.2 Maximum Cladding Temperature Distribution in the Core (Continued)

** Order of PCT **

No. 1	D-22 rod	Pos. 2	PCT = 574.9 (K)	Time = 81.2 (s)
No. 2	D-13 rod	Pos. 4	PCT = 570.9 (K)	Time = 0.0 (s)
No. 3	A-13 rod	Pos. 2	PCT = 569.5 (K)	Time = 0.0 (s)
No. 4	B-77 rod	Pos. 3	PCT = 568.5 (K)	Time = 0.0 (s)
No. 5	B-77 rod	Pos. 2	PCT = 568.0 (K)	Time = 0.0 (s)
No. 6	A-22 rod	Pos. 5	PCT = 567.2 (K)	Time = 0.0 (s)
No. 7	A-57 rod	Pos. 4	PCT = 567.2 (K)	Time = 0.0 (s)
No. 8	A-11 rod	Pos. 5	PCT = 567.1 (K)	Time = 0.0 (s)
No. 9	A-11 rod	Pos. 4	PCT = 567.1 (K)	Time = 0.0 (s)
No.10	A-88 rod	Pos. 4	PCT = 566.9 (K)	Time = 0.0 (s)

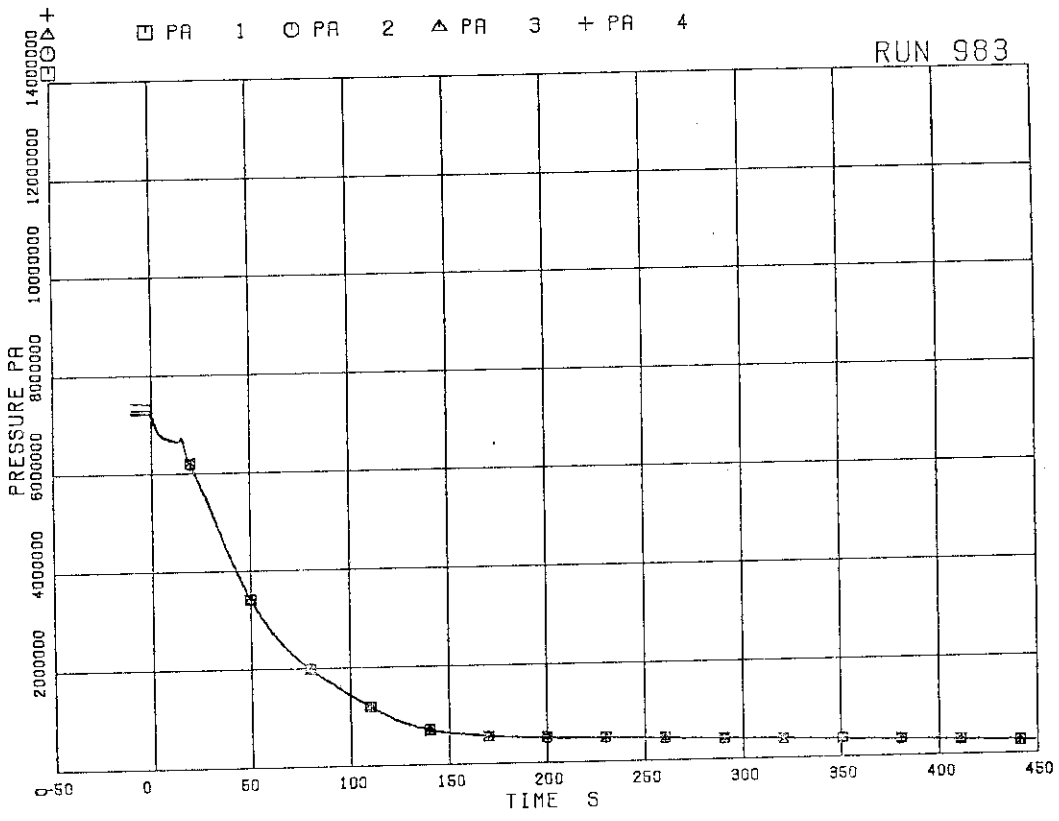

Fig. 5.1 Pressure in PV (pressure vessel)

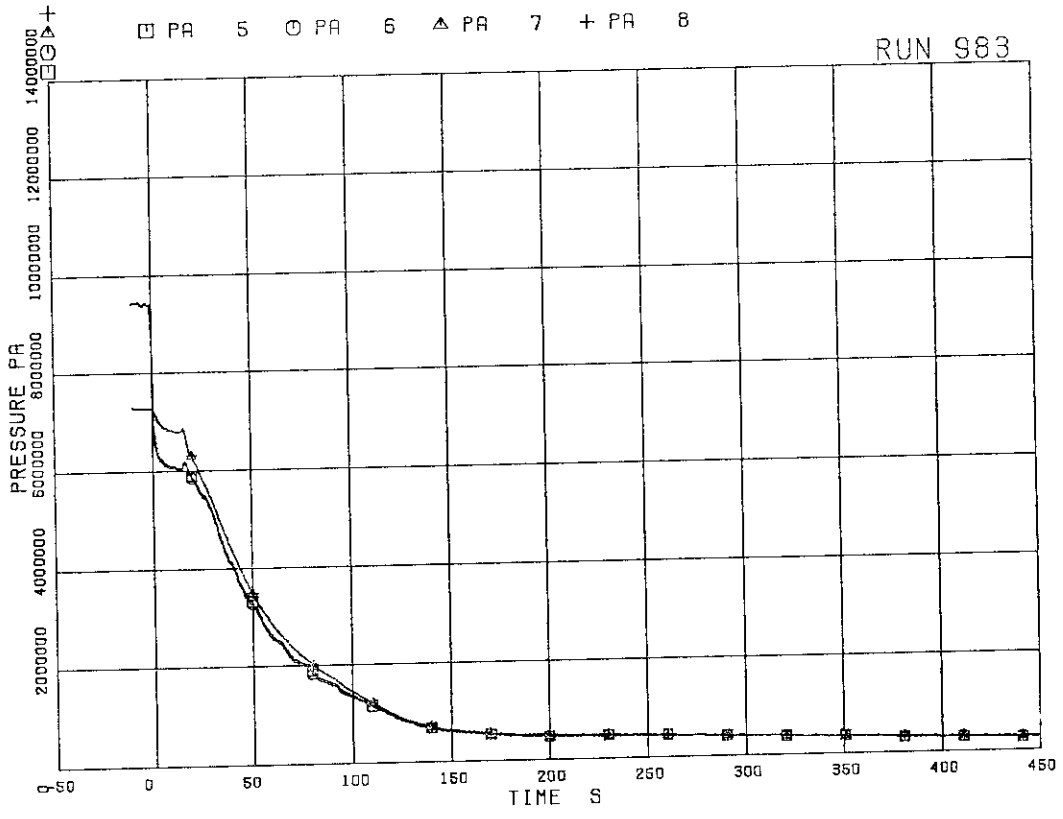

Fig. 5.2 Pressure in broken loop JP (jet pump)

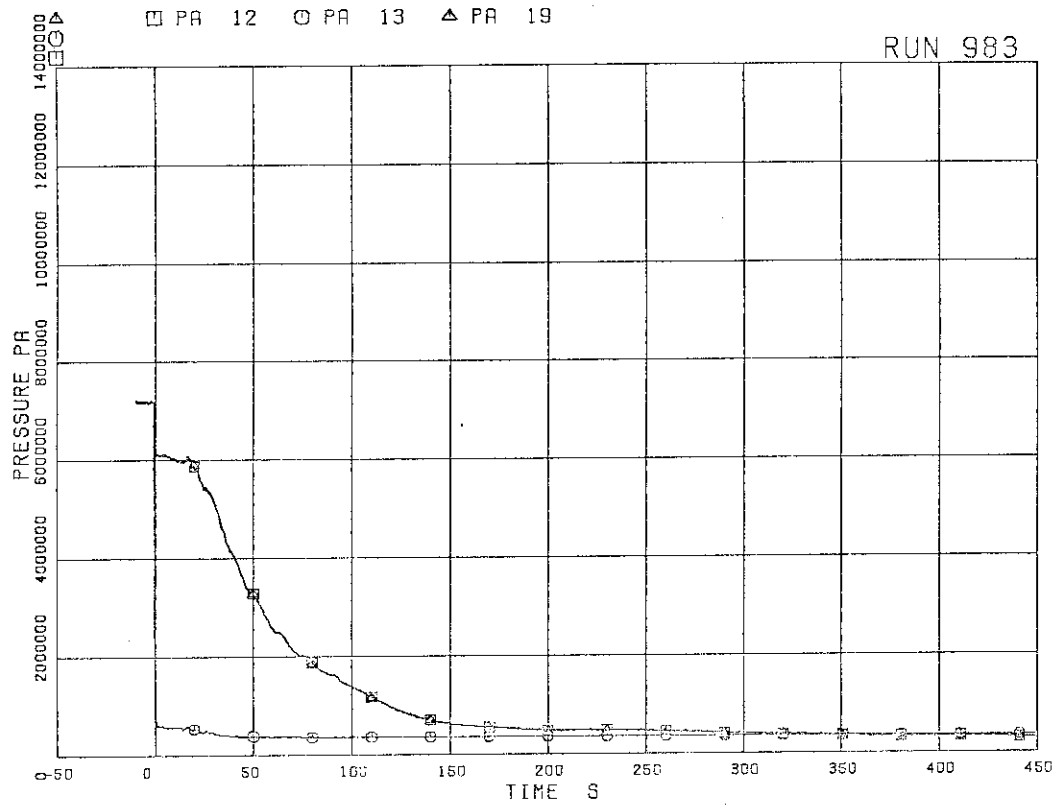

Fig. 5.4 Pressure at MRP side of break

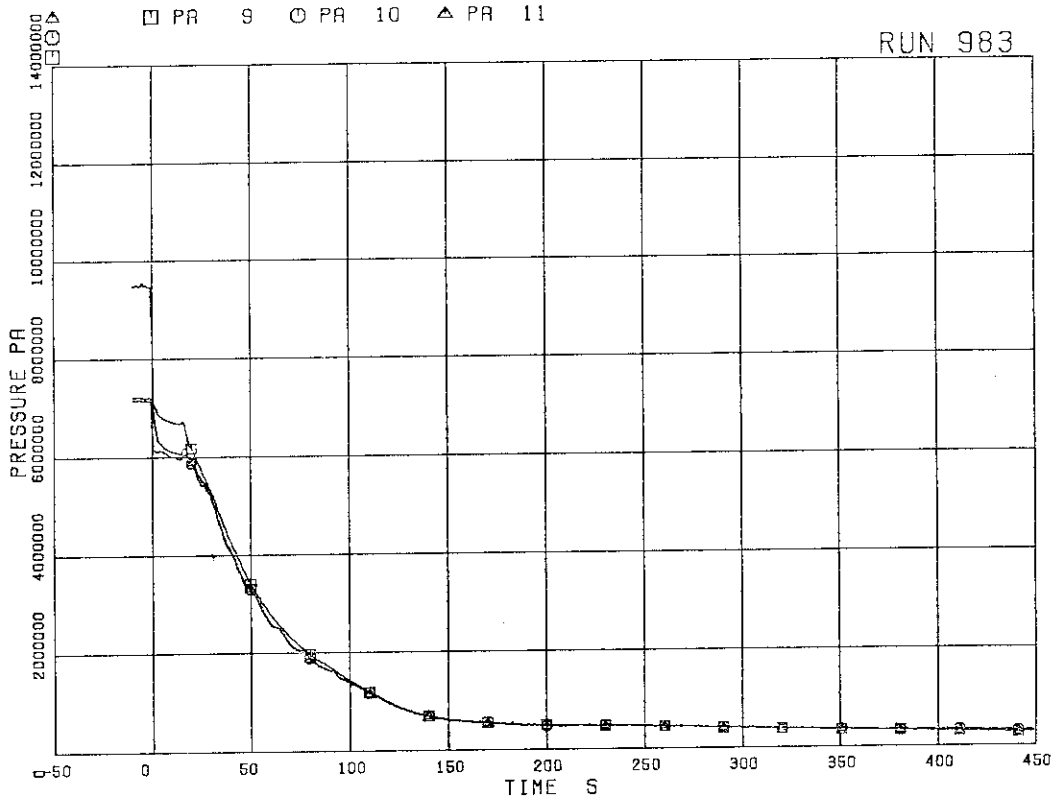

Fig. 5.3 Pressure near MRP (main recirculation pump)

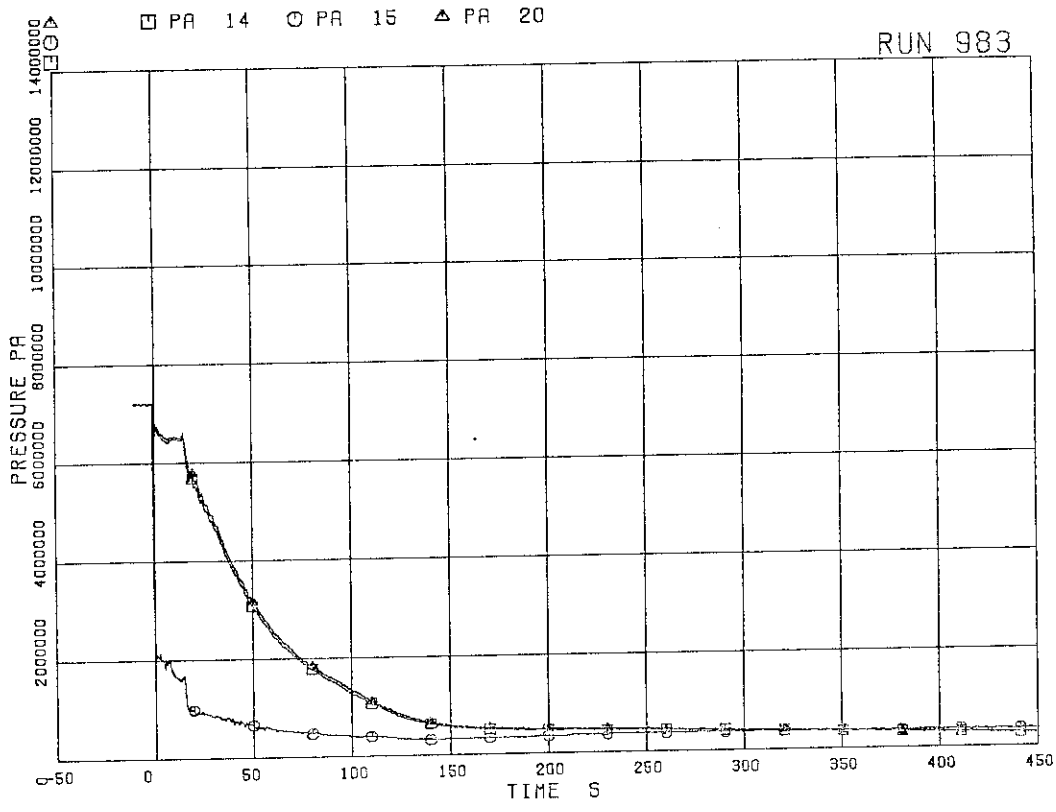

Fig. 5.5 Pressure at PV side of break

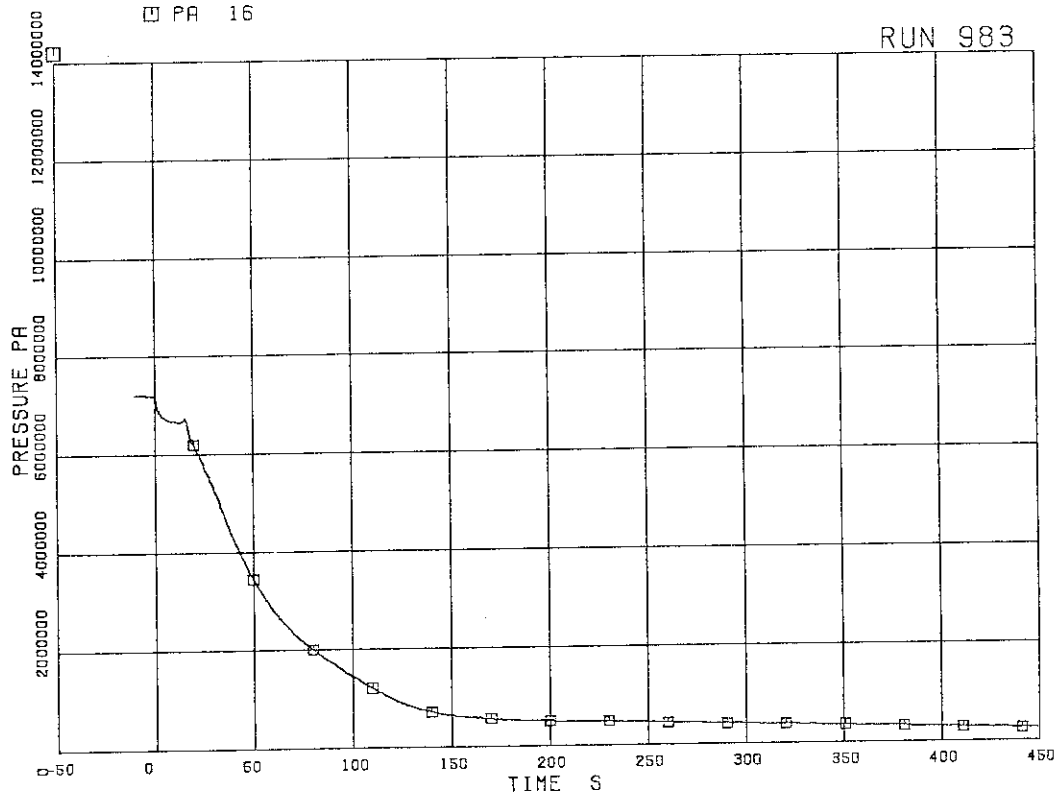

Fig. 5.6 Pressure in MSL (main steam line)

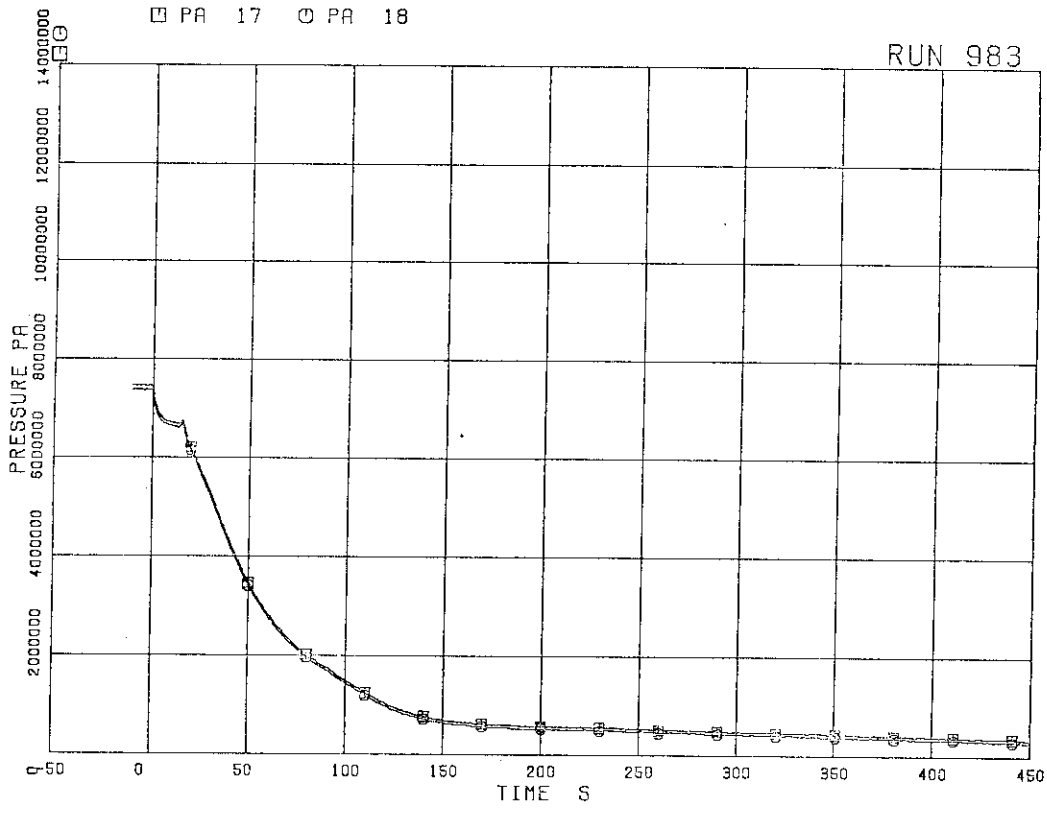

Fig. 5.7 Pressure in JP outlet spool

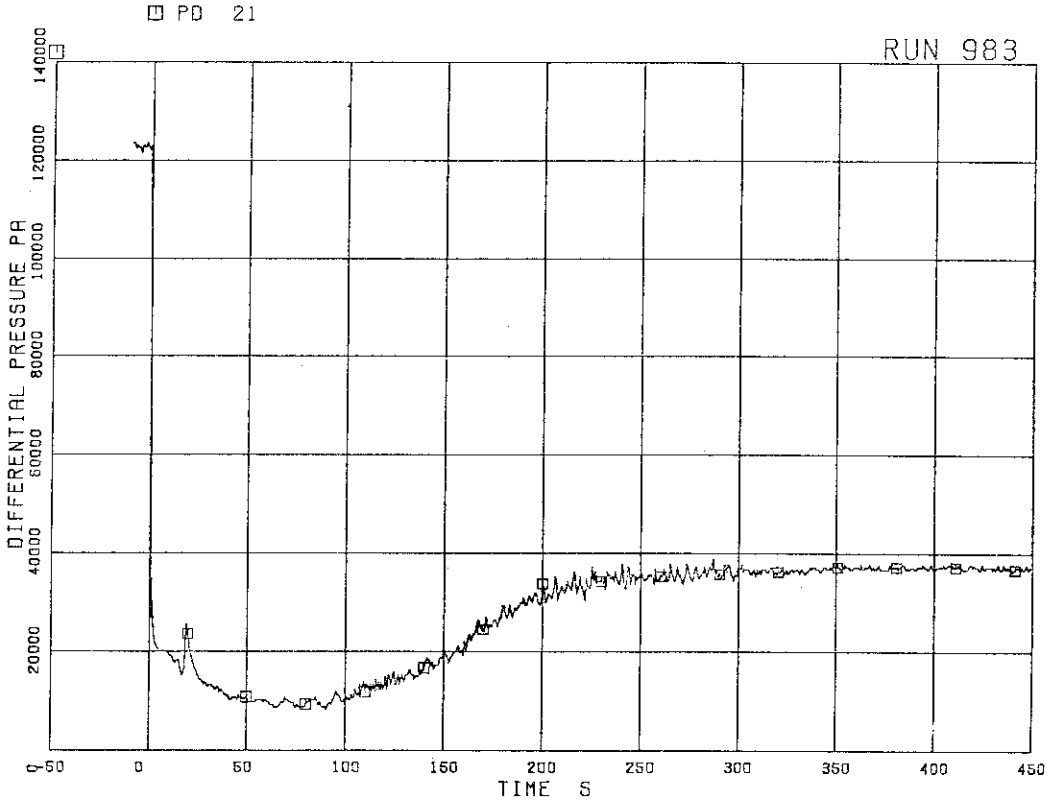

Fig. 5.8 Differential pressure between lower plenum and upper plenum

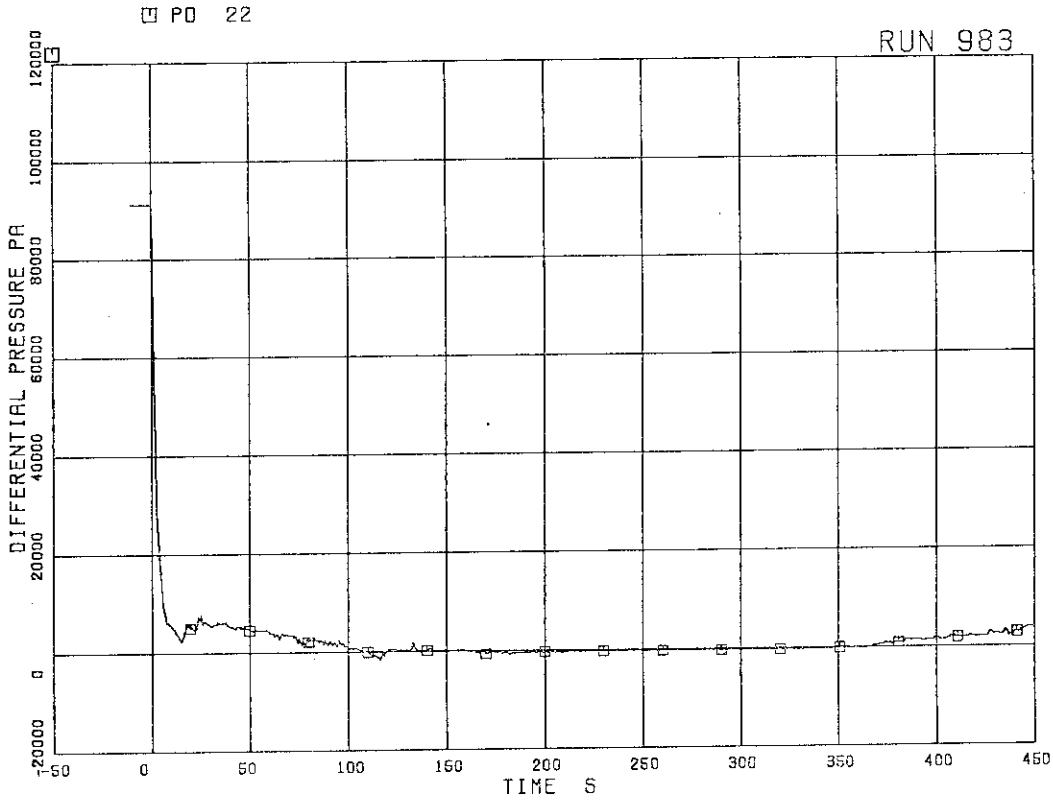

Fig. 5.9 Differential pressure between upper plenum and steam dome

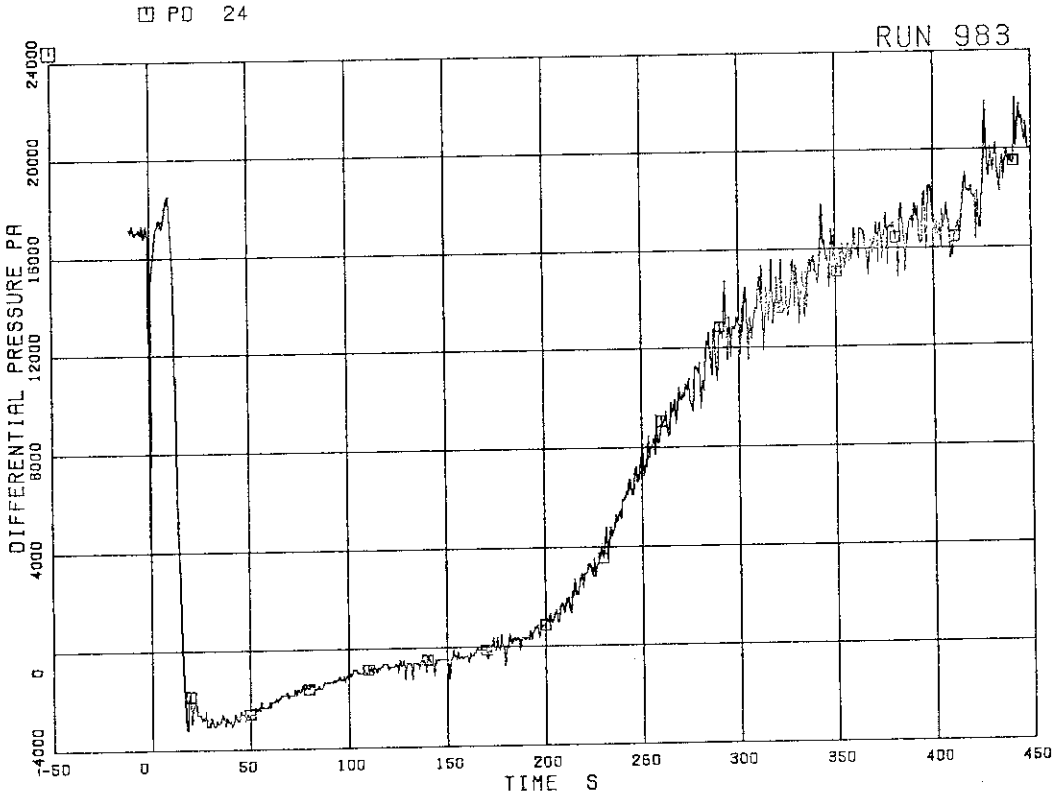

Fig. 5.10 DC (downcomer) head

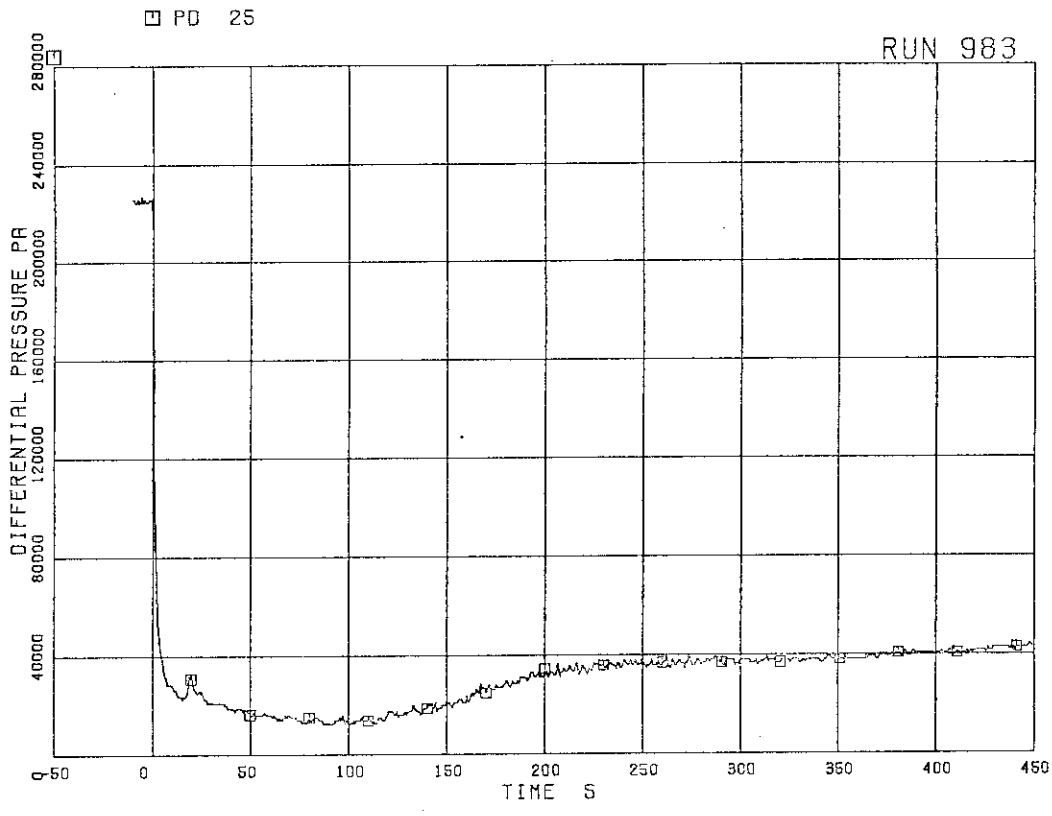

Fig. 5.11 Differential pressure between PV bottom and top

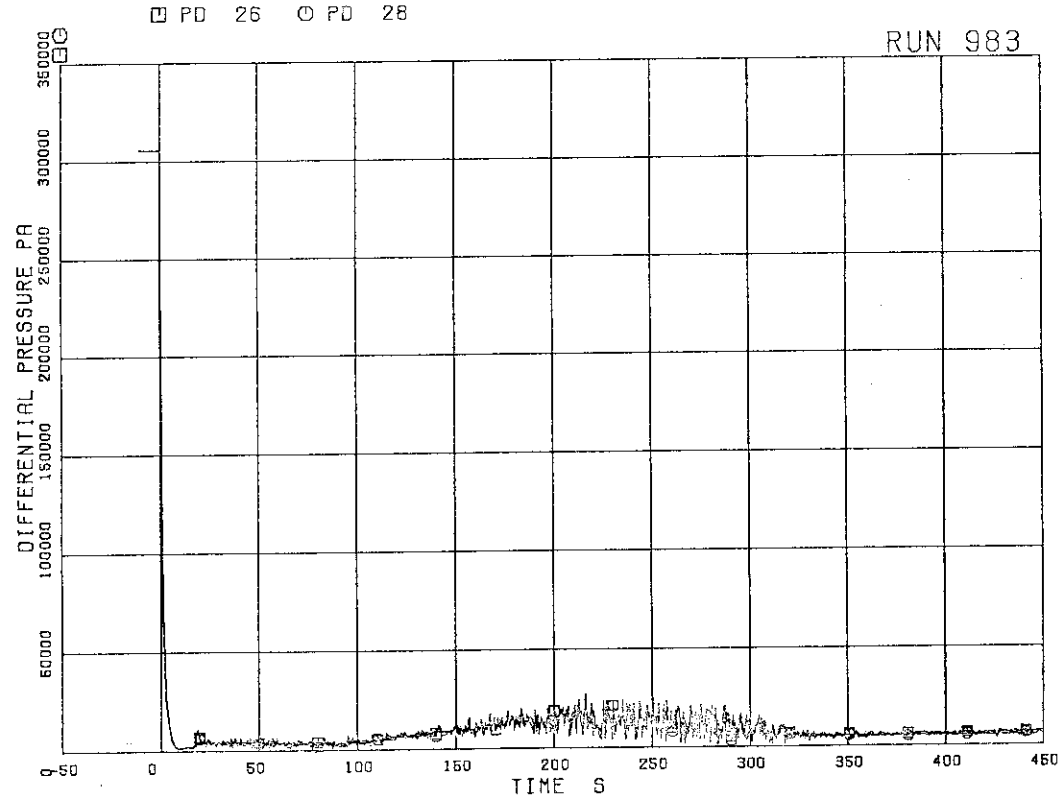

Fig. 5.12 Differential pressure between JP-1,2 discharge and suction

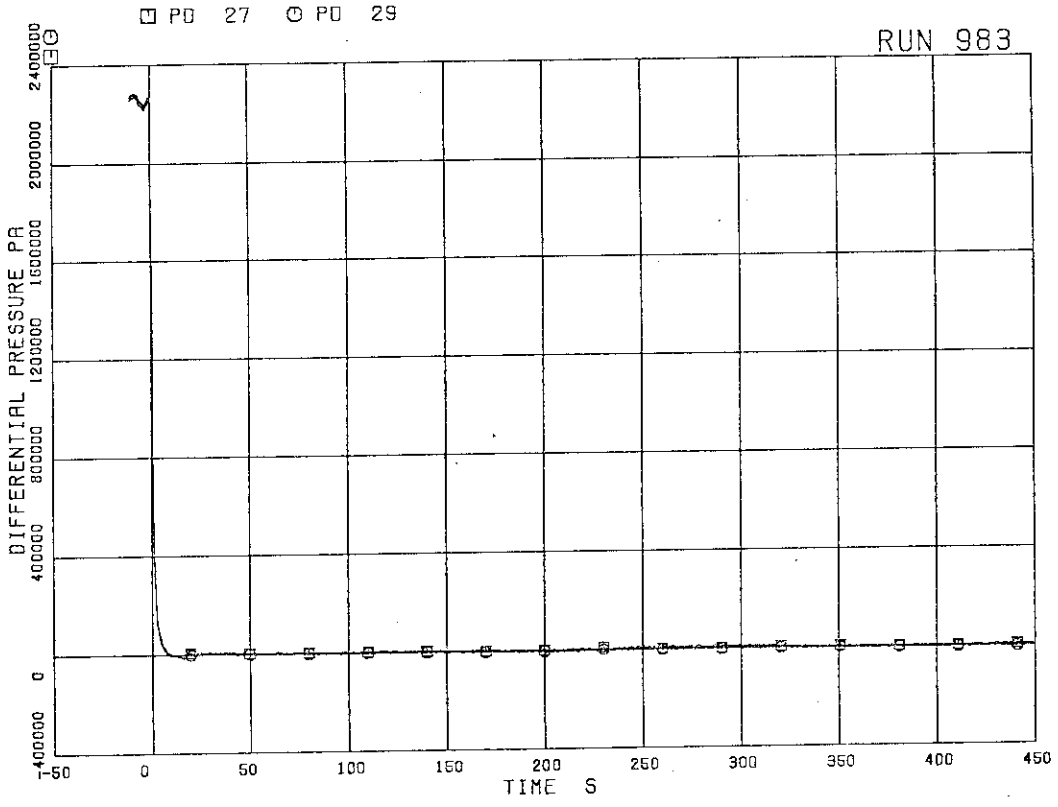

Fig. 5.13 Differential pressure between JP-1,2 drive and suction

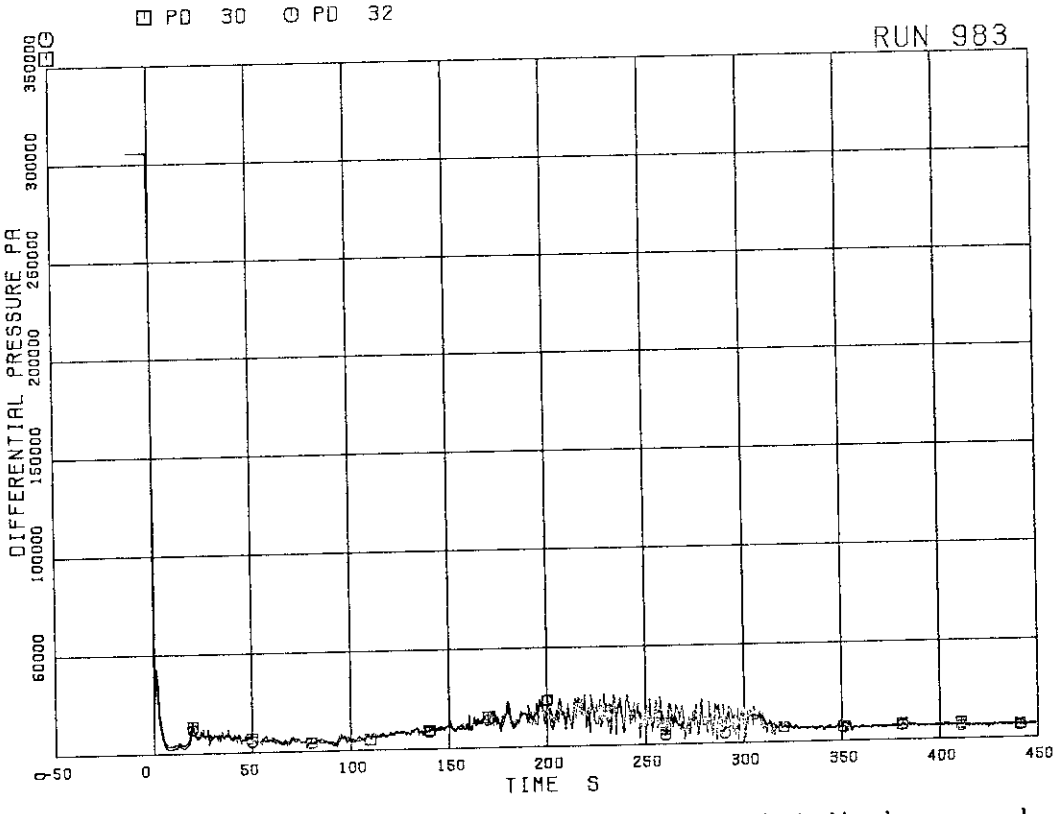

Fig. 5.14 Differential pressure between JP-3,4 discharge and suction

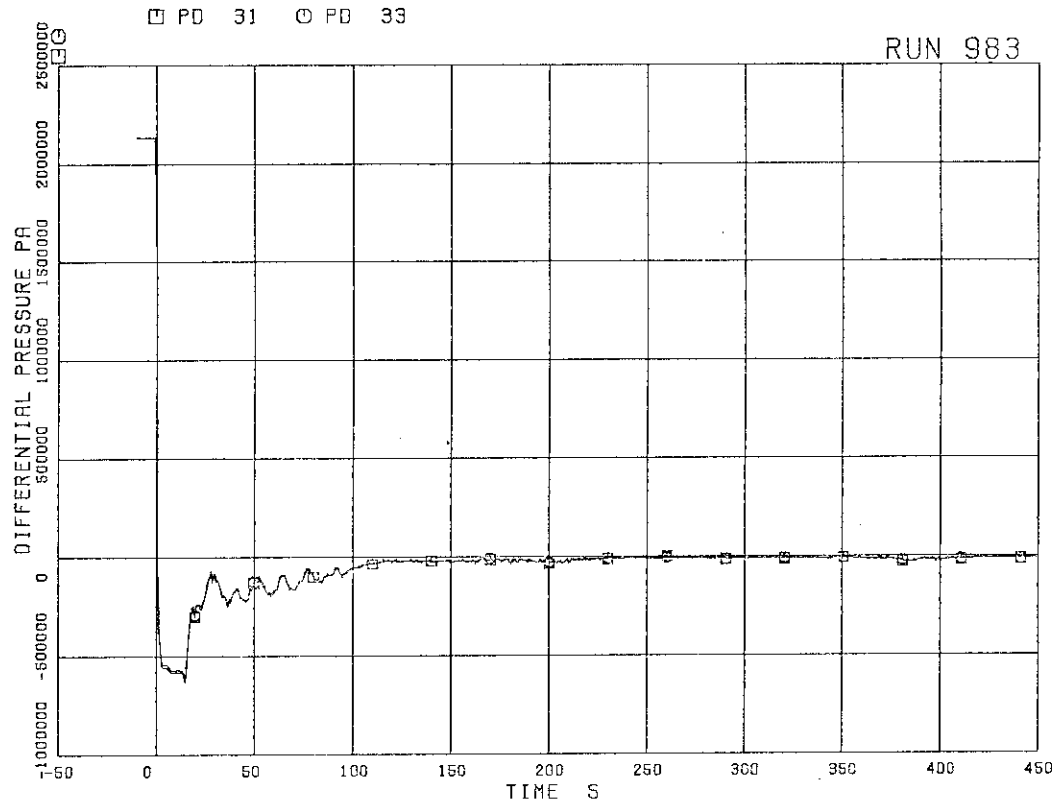

Fig. 5.15 Differential pressure between JP-3,4 drive and suction

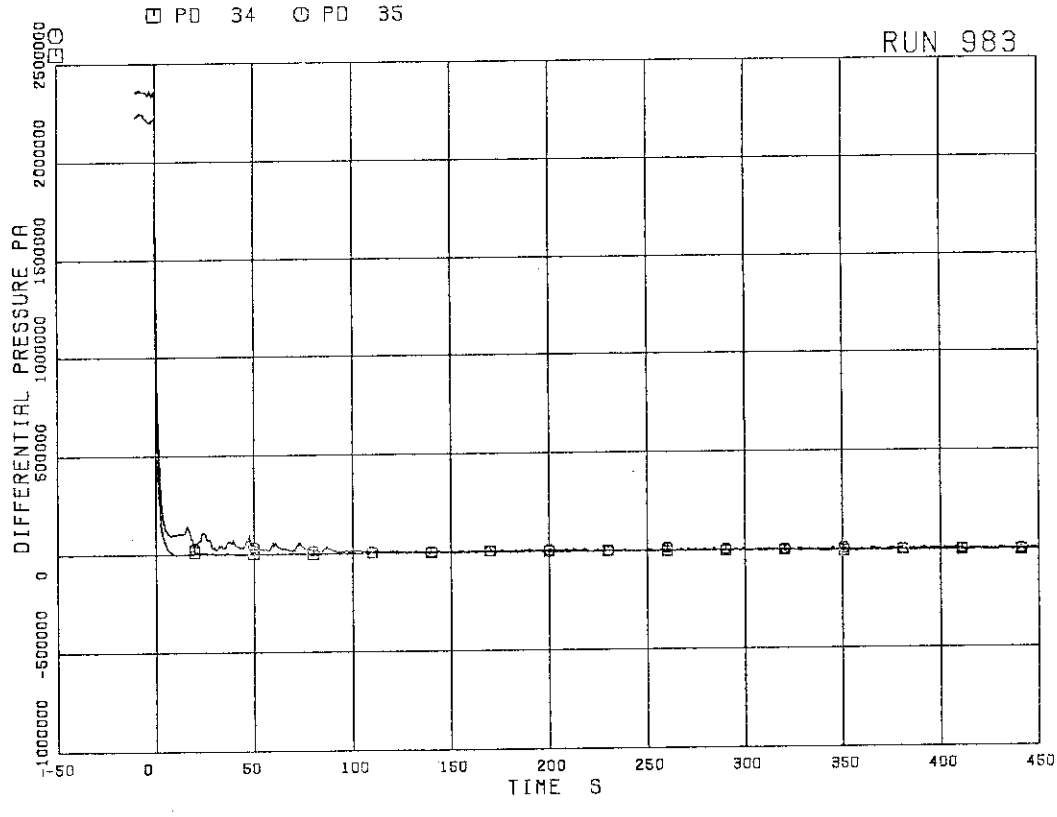

Fig. 5.16 Differential pressure between MRP delivery and suction

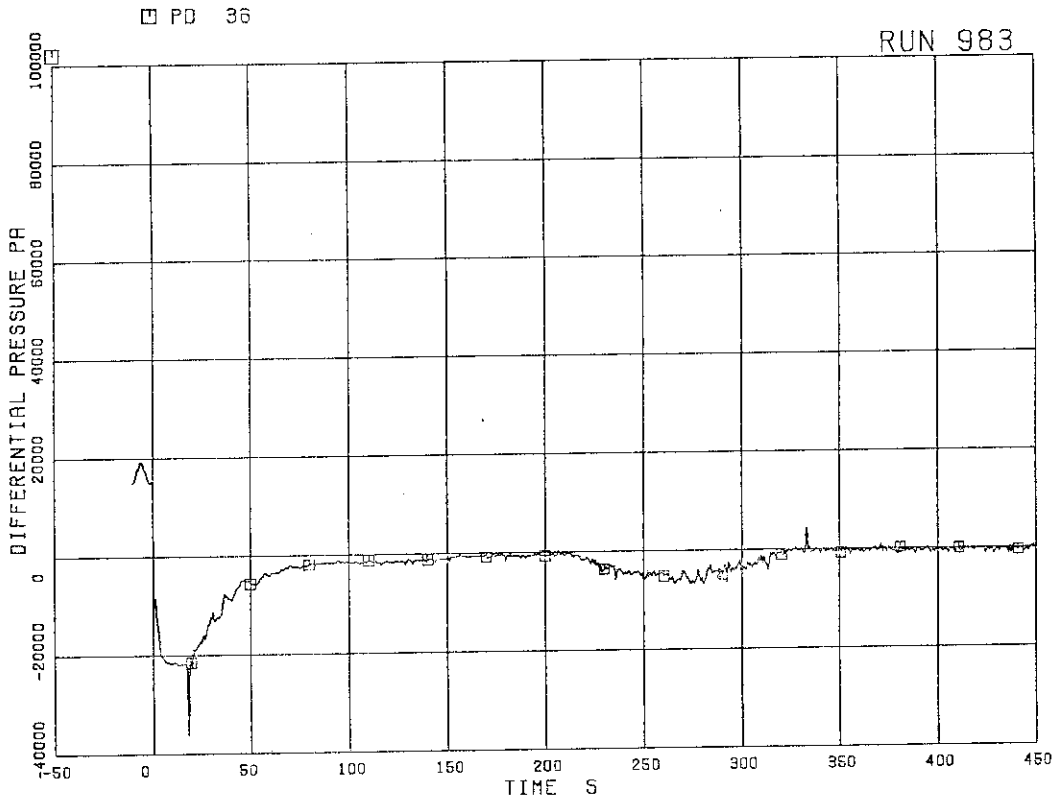

Fig. 5.17 Differential pressure between downcomer bottom and MRP1 suction

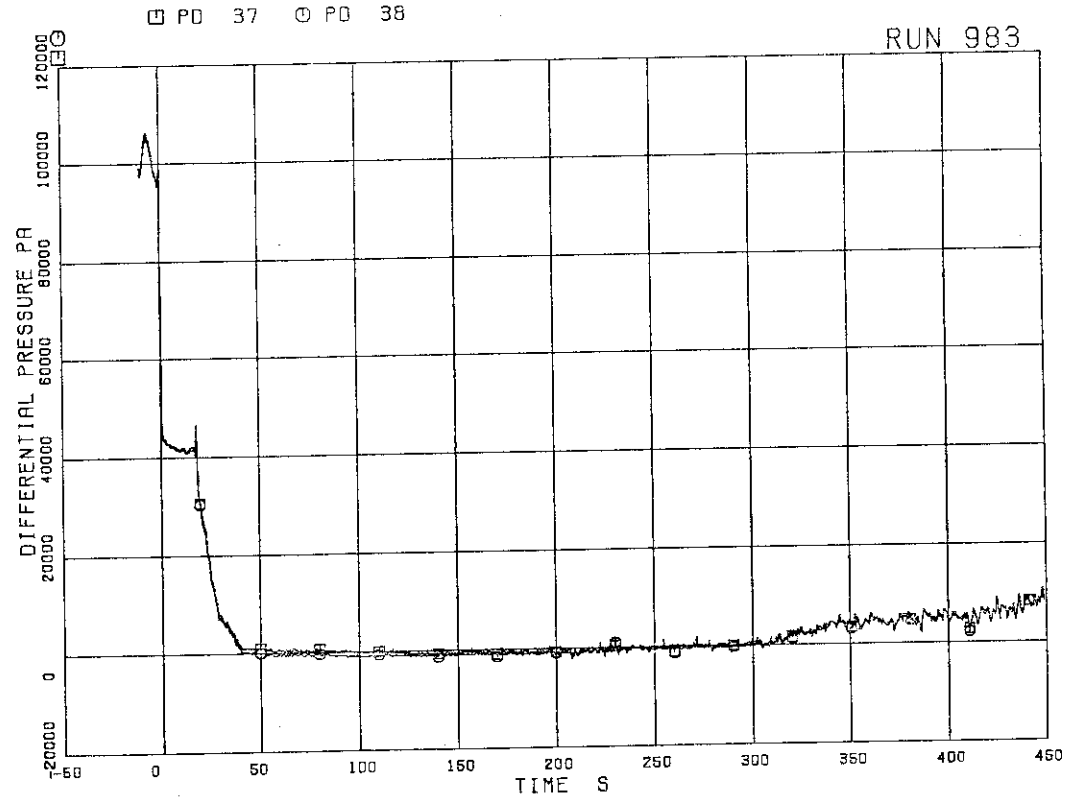

Fig. 5.18 Differential pressure between MRP1 delivery and JP-1,2 drive

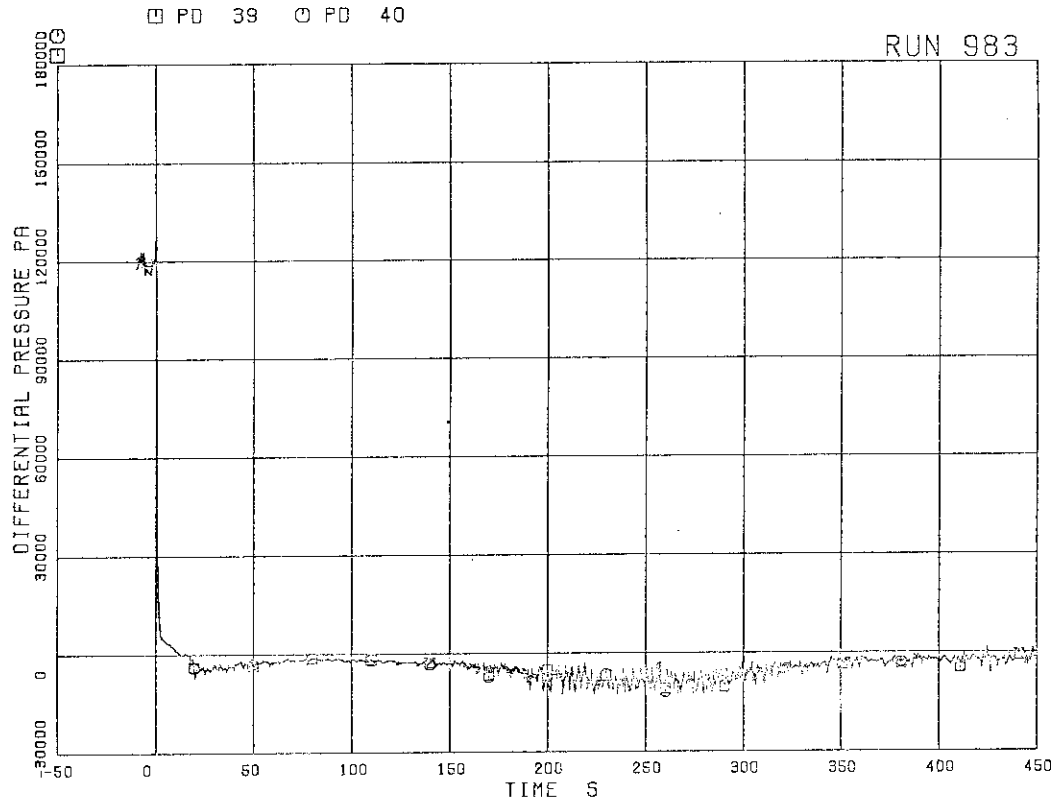

Fig. 5.19 Differential pressure between downcomer middle and JP-1,2 suction

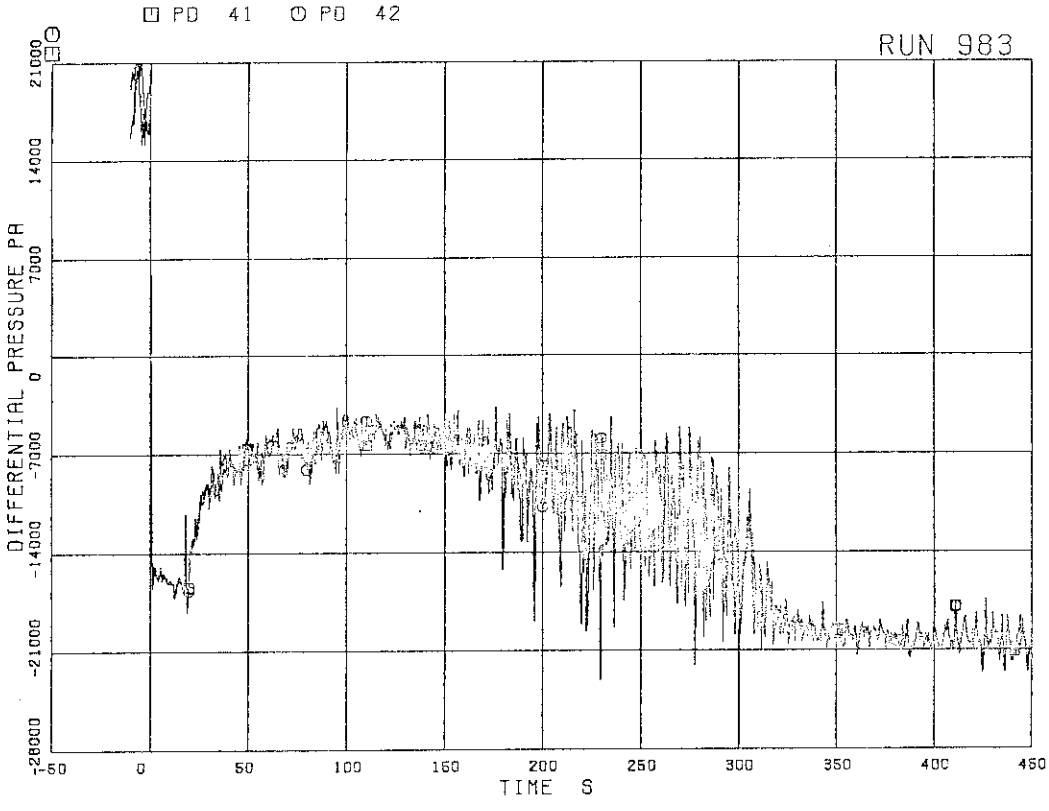

Fig. 5.20 Differential pressure between JP-1,2 discharge and lower plenum

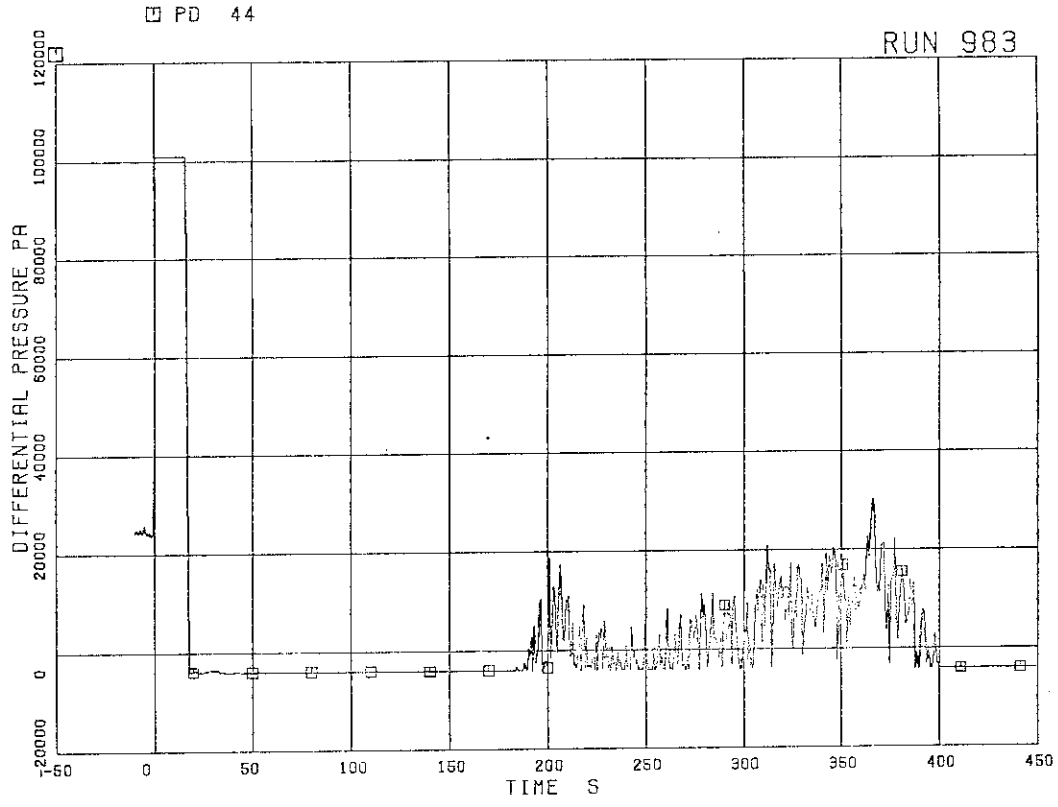

Fig. 5.21 Differential pressure between breaks A and B

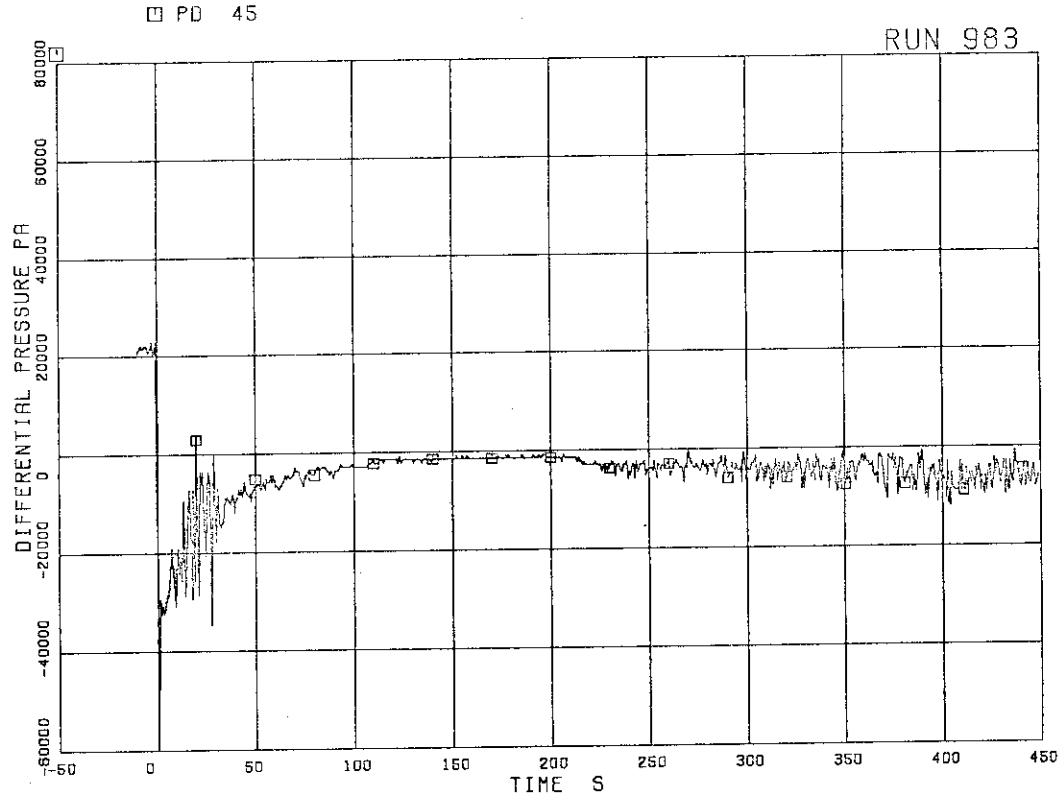

Fig. 5.22 Differential pressure between break A and MRP2 suction

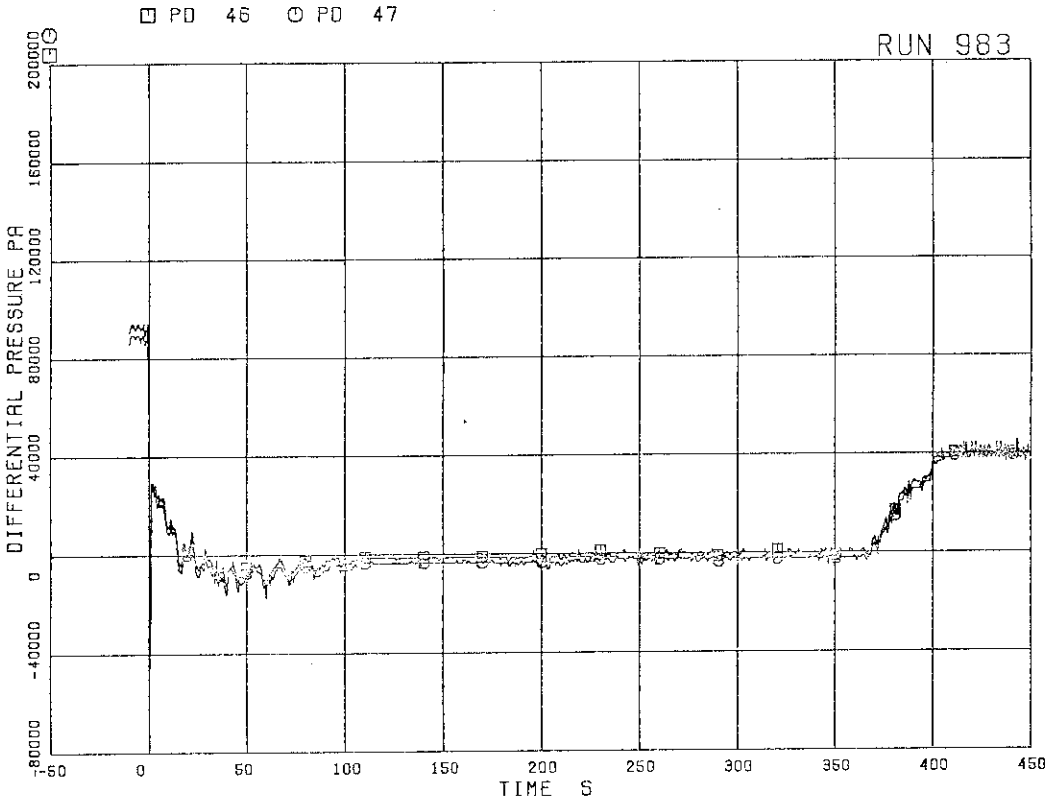

Fig. 5.23 Differential pressure between MRP2 dilivery and JP-3,4 drive

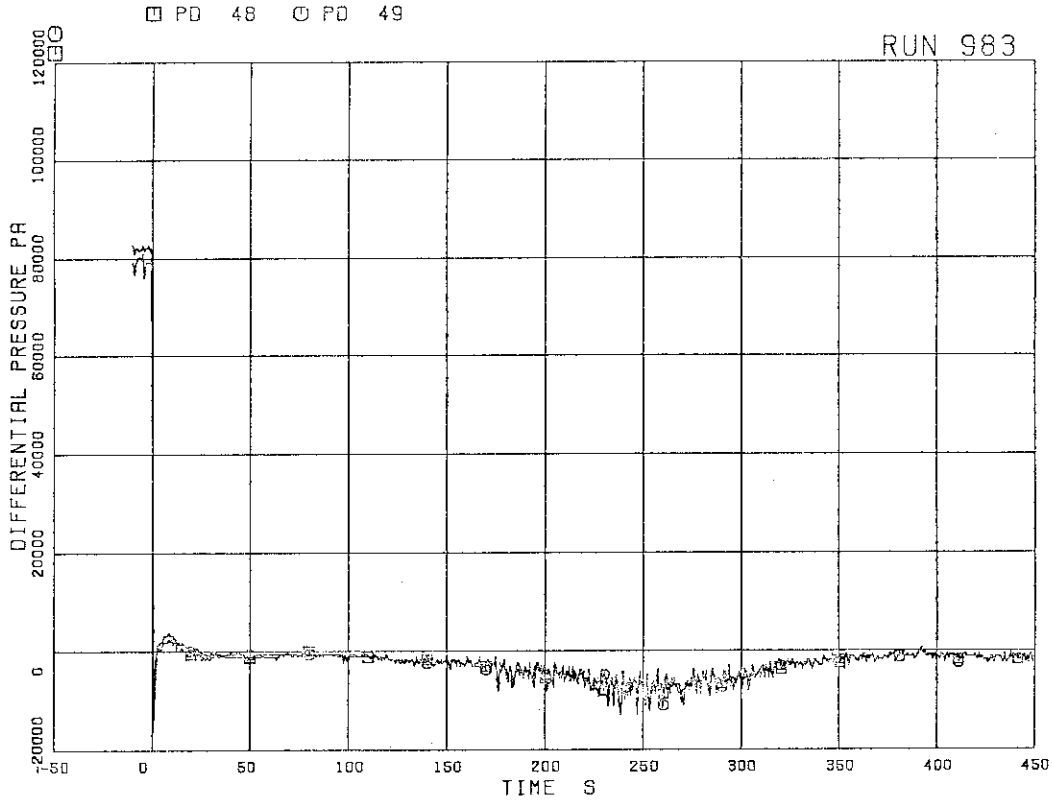

Fig. 5.24 Differential pressure between downcomer middle and JP-3,4 suction

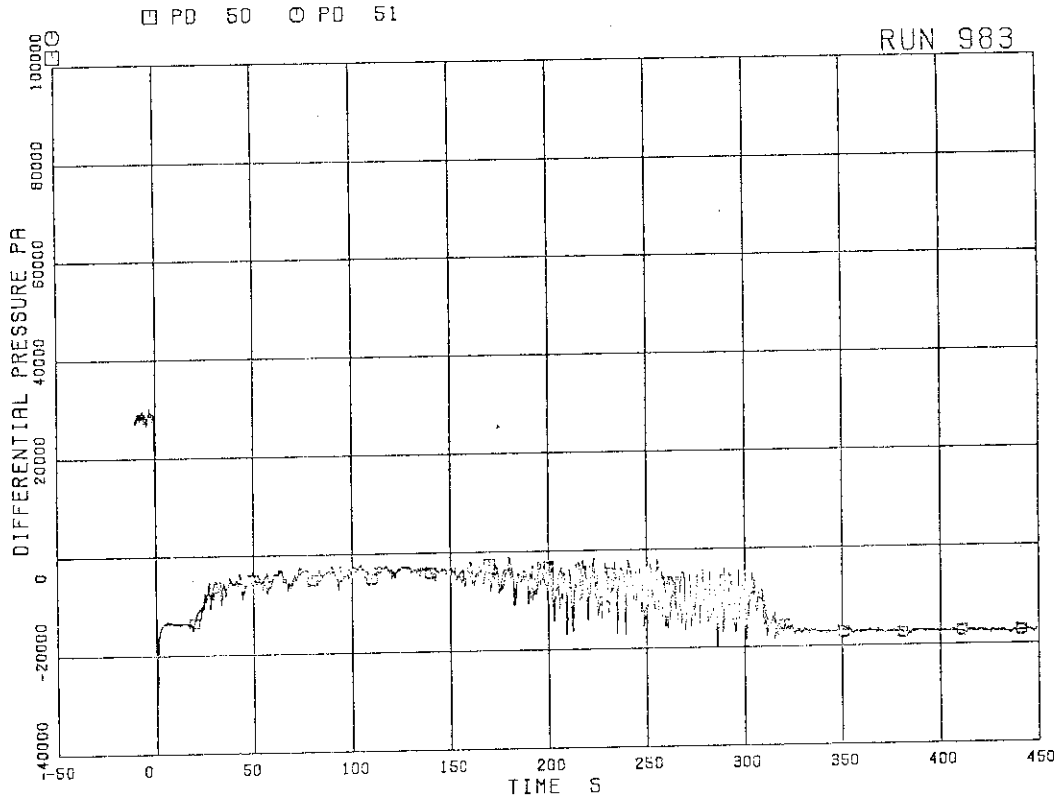

Fig. 5.25 Differential pressure between JP-3,4 discharge and confluence

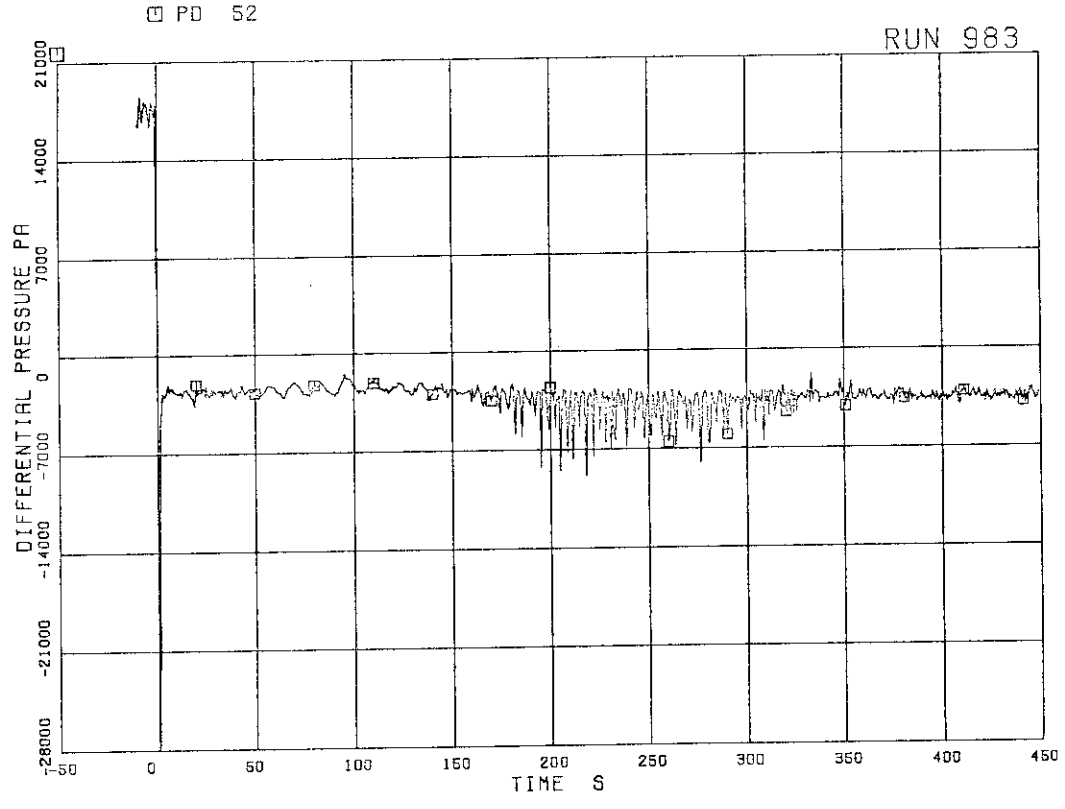

Fig. 5.26 Differential pressure between JP-3,4 confluence in broken loop and lower plenum

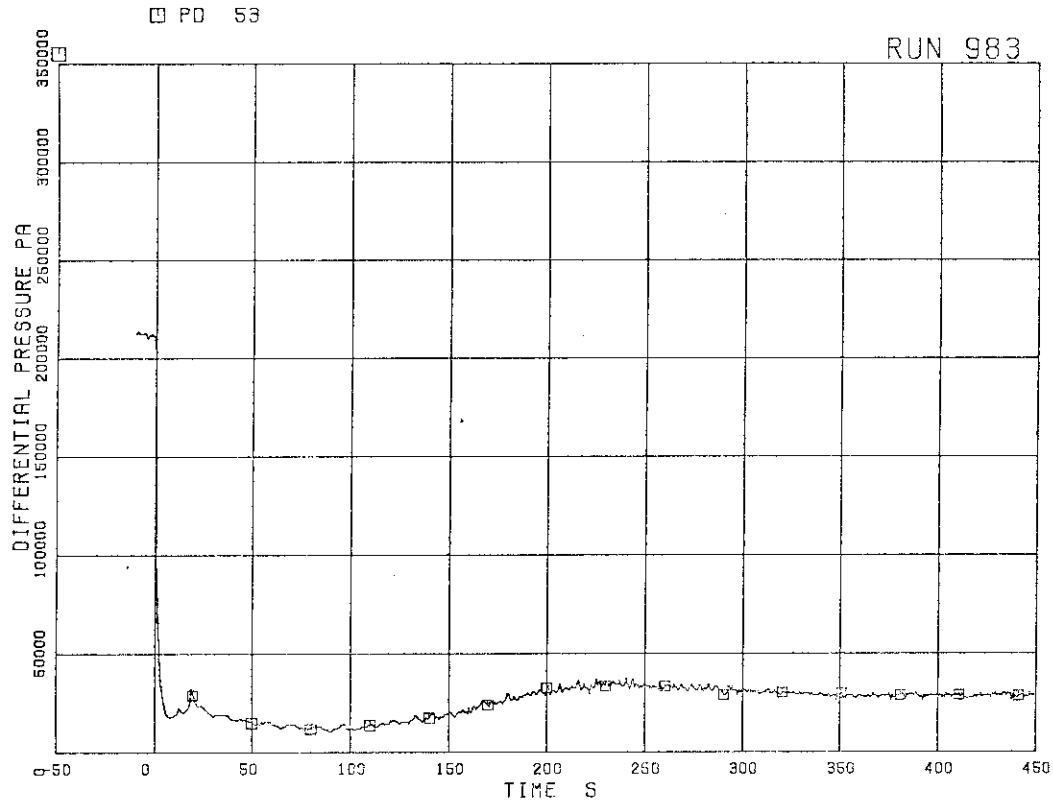

Fig. 5.27 Differential pressure between lower plenum and downcomer middle

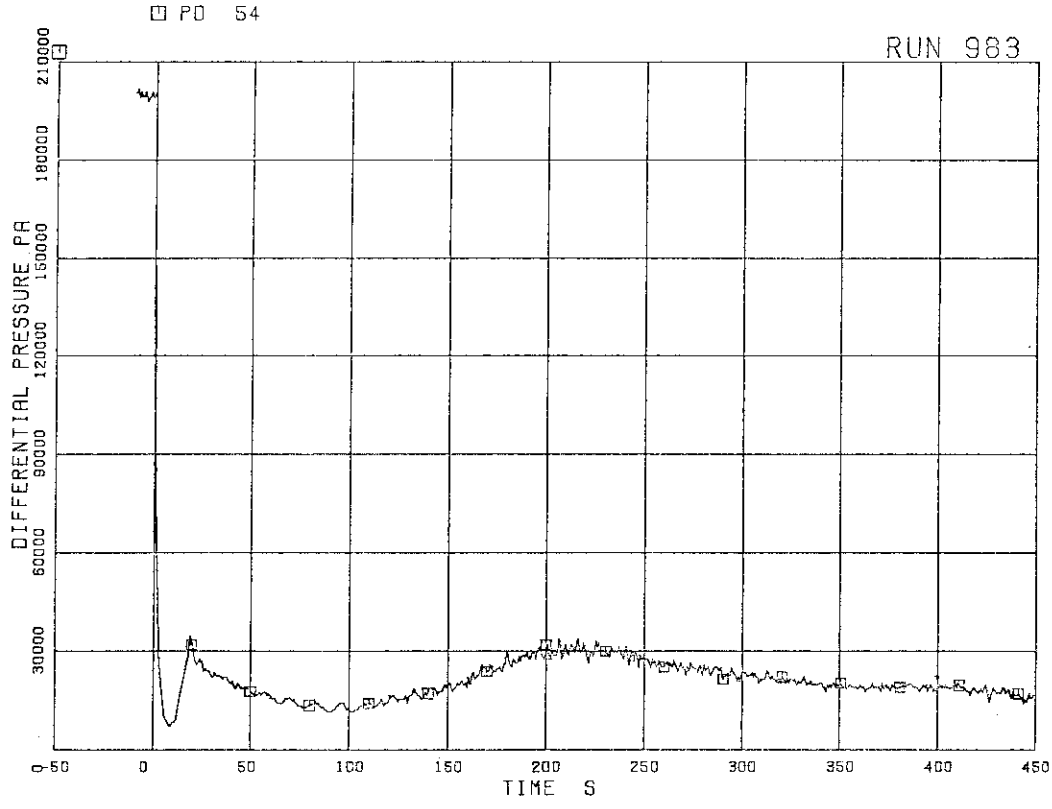

Fig. 5.28 Differential pressure between lower plenum and downcomer bottom

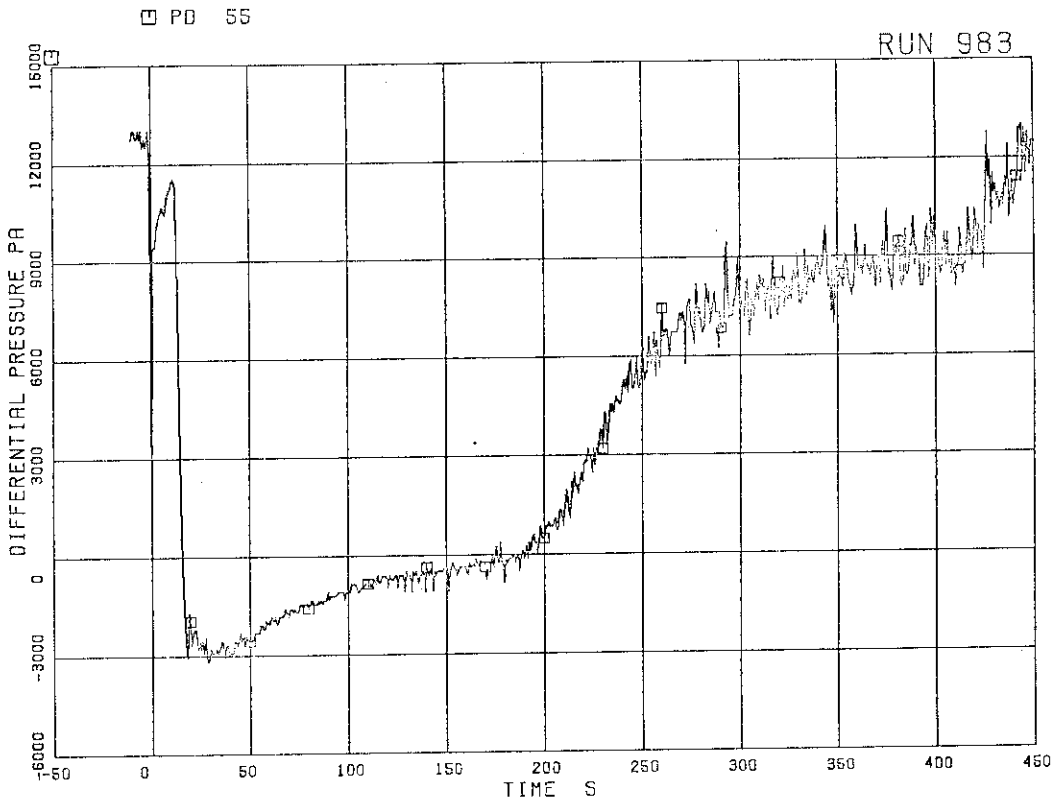

Fig. 5.29 Differential pressure between downcomer bottom and downcomer middle

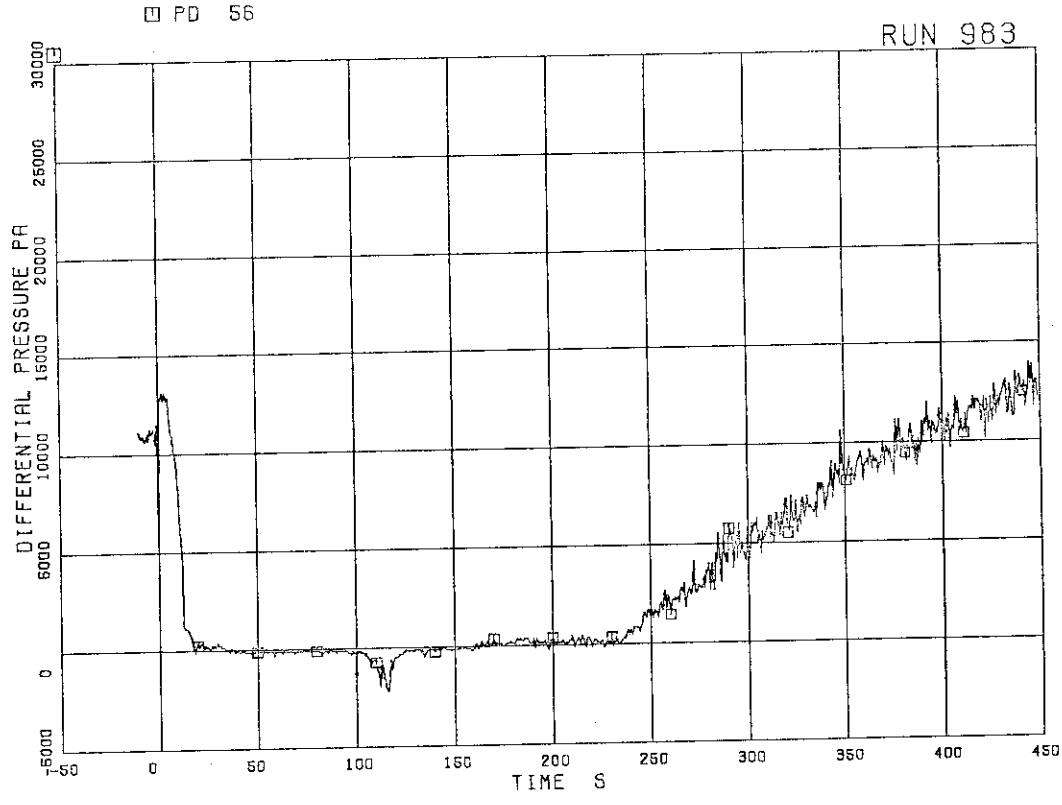

Fig. 5.30 Differential pressure between downcomer middle and steam dome

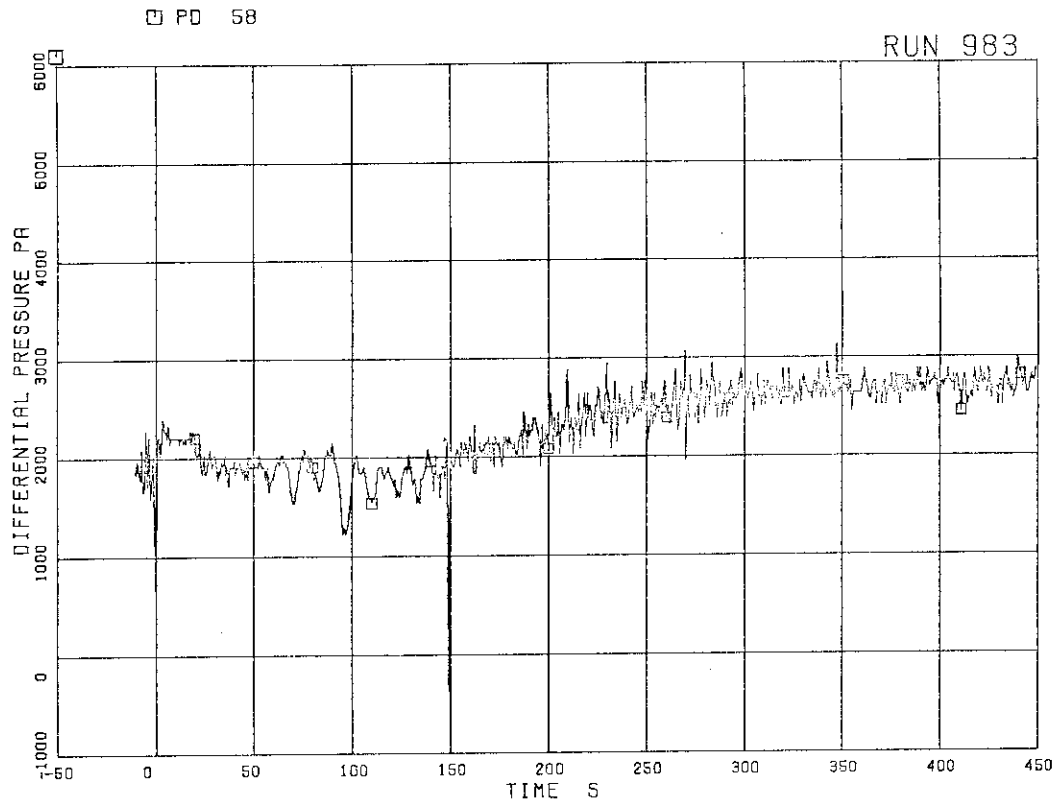

Fig. 5.31 Differential pressure between LP bottom and LP middle

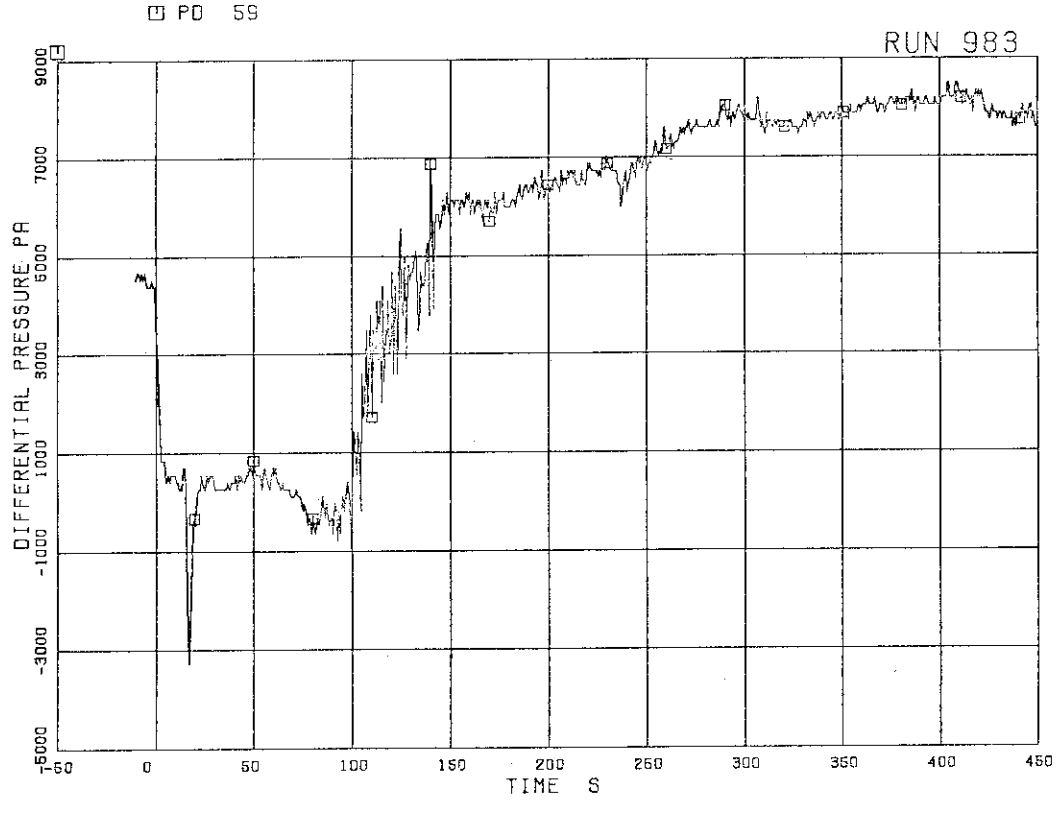

Fig. 5.32 Differential pressure between UP and DC high

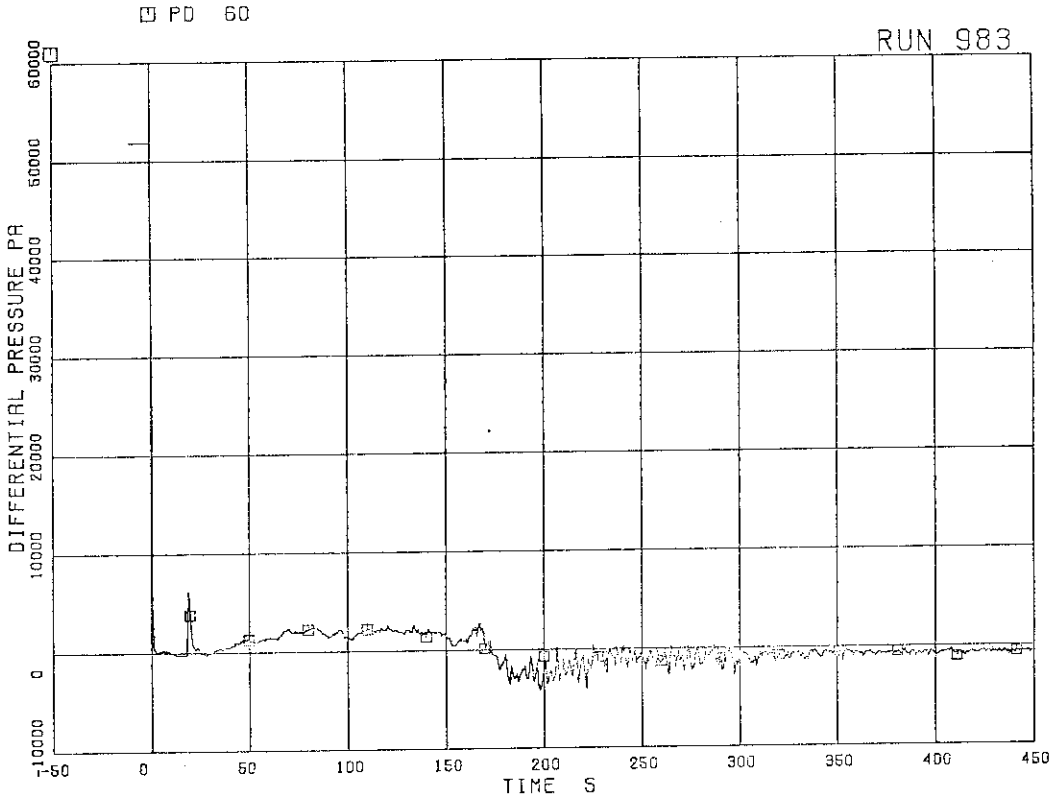

Fig. 5.33 Differential pressure across channel inlet orifice A

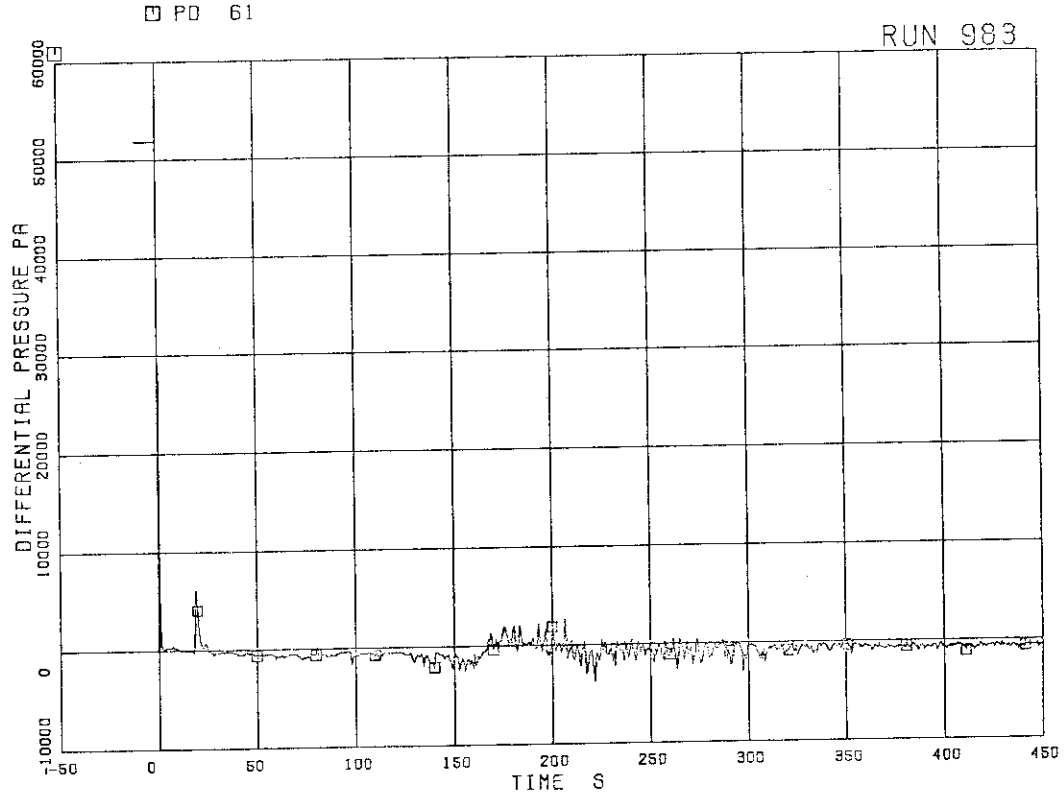

Fig. 5.34 Differential pressure across channel inlet orifice B

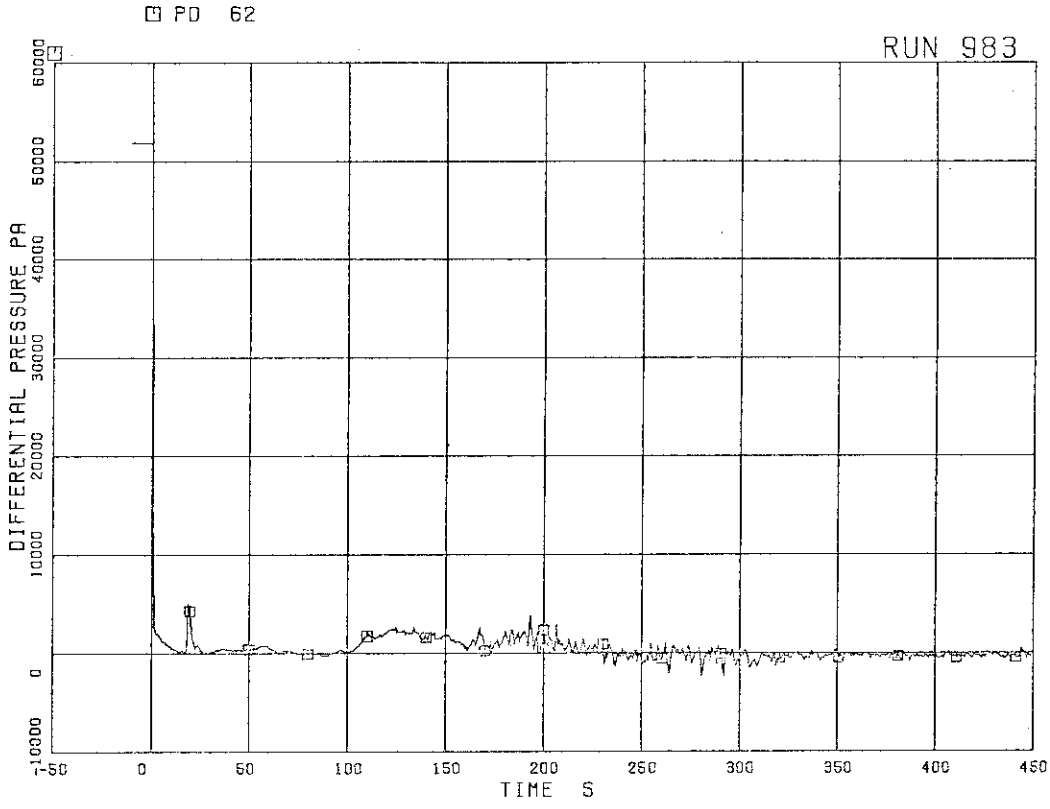

Fig. 5.35 Differential pressure across channel inlet orifice C

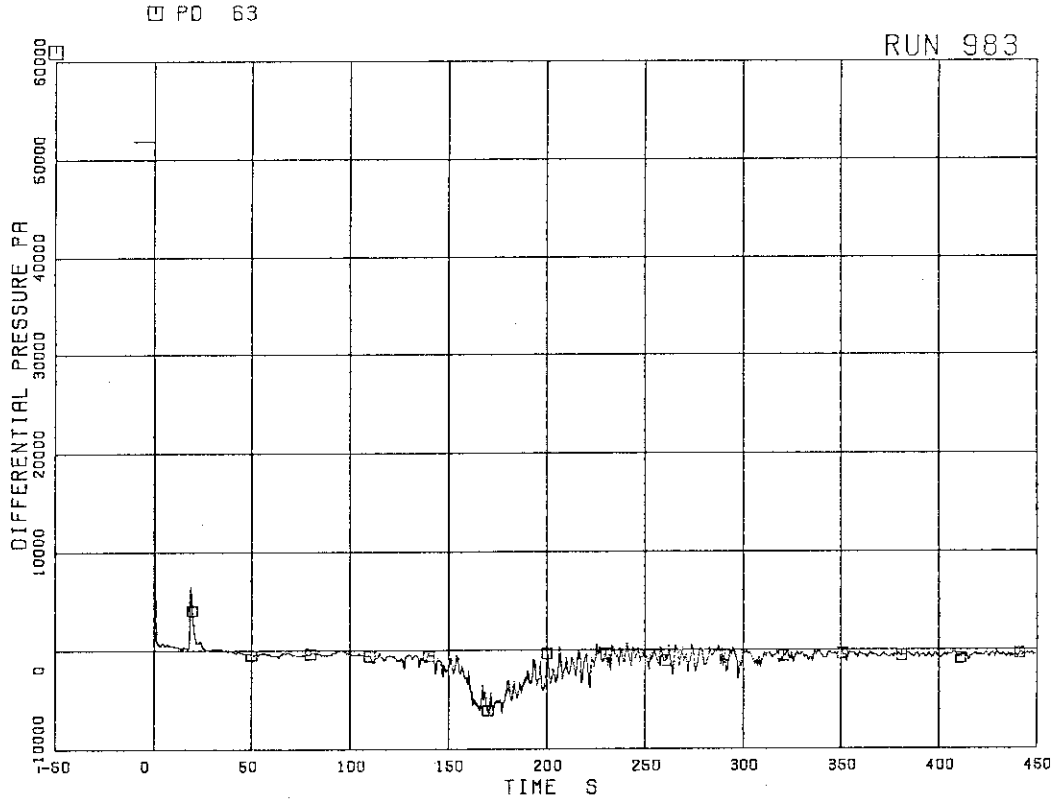

Fig. 5.36 Differential pressure across channel inlet orifice D

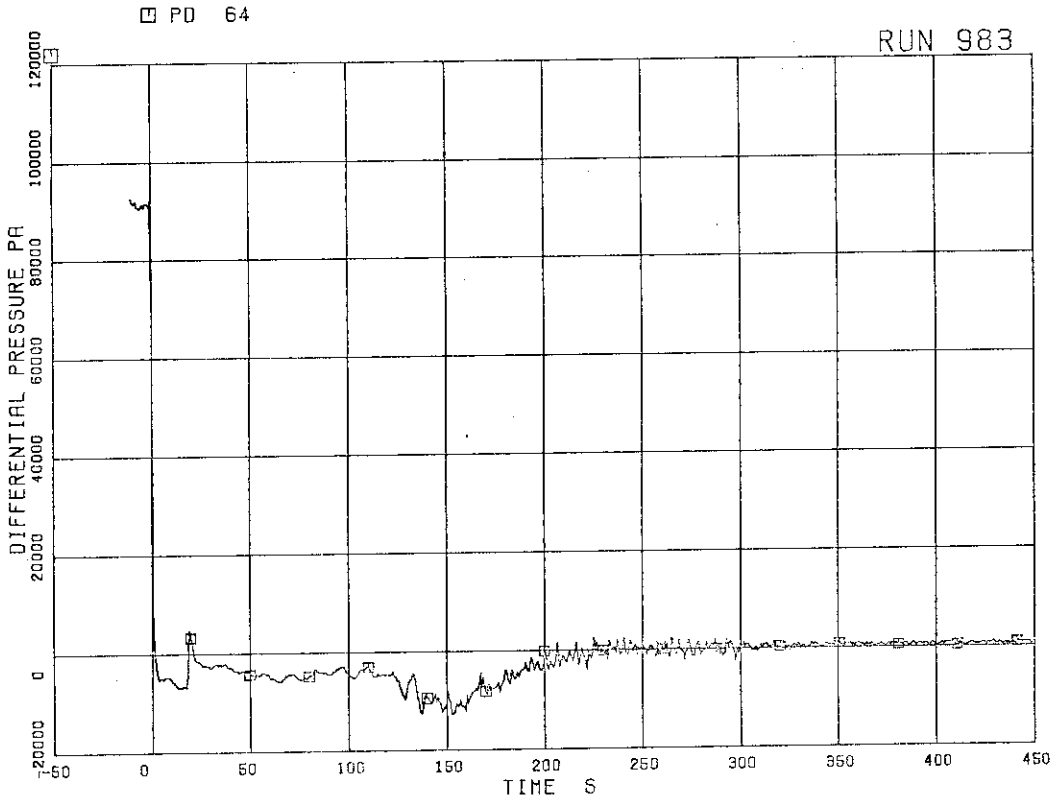

Fig. 5.37 Differential pressure across bypass hole

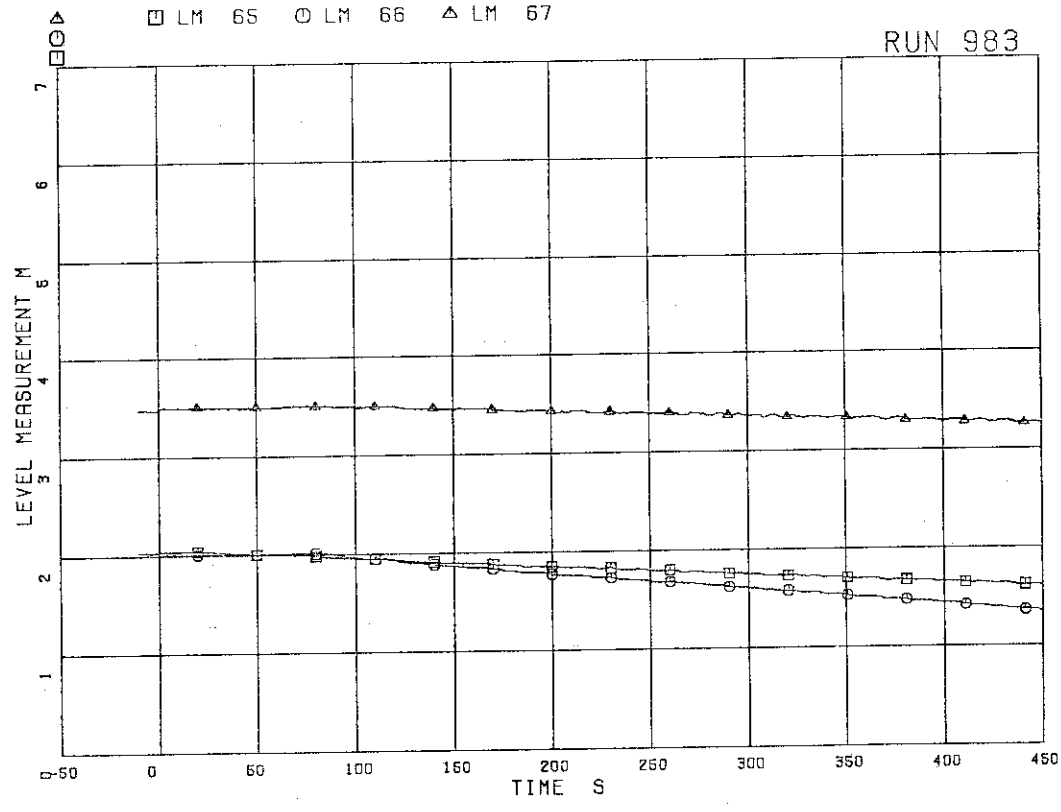

Fig. 5.38 Liquid levels in ECCS tanks

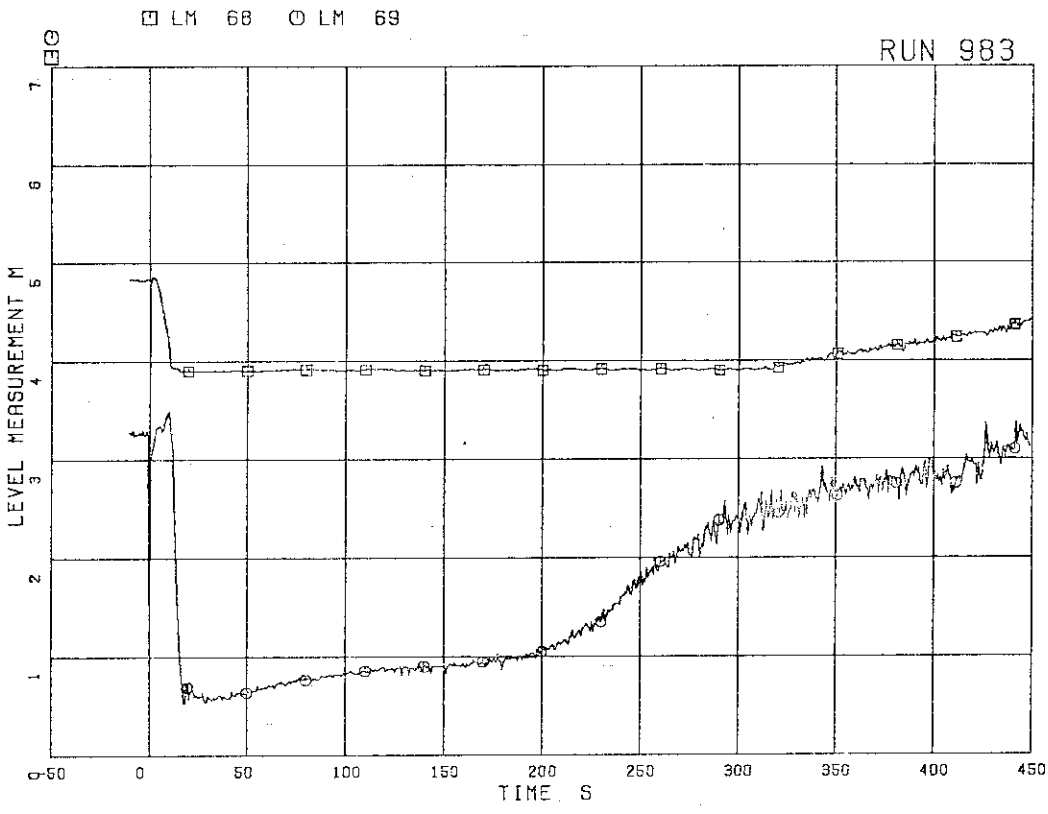

Fig. 5.39 Liquid levels in downcomer

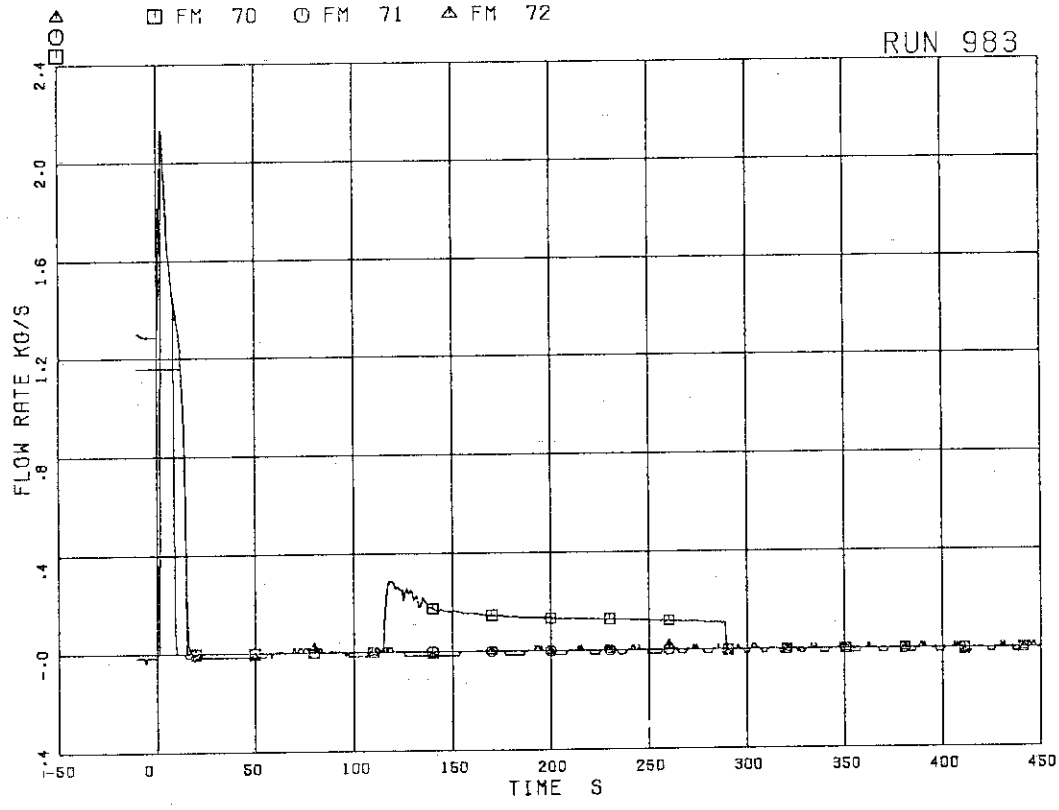

Fig. 5.40 Mass flow rate in MSL

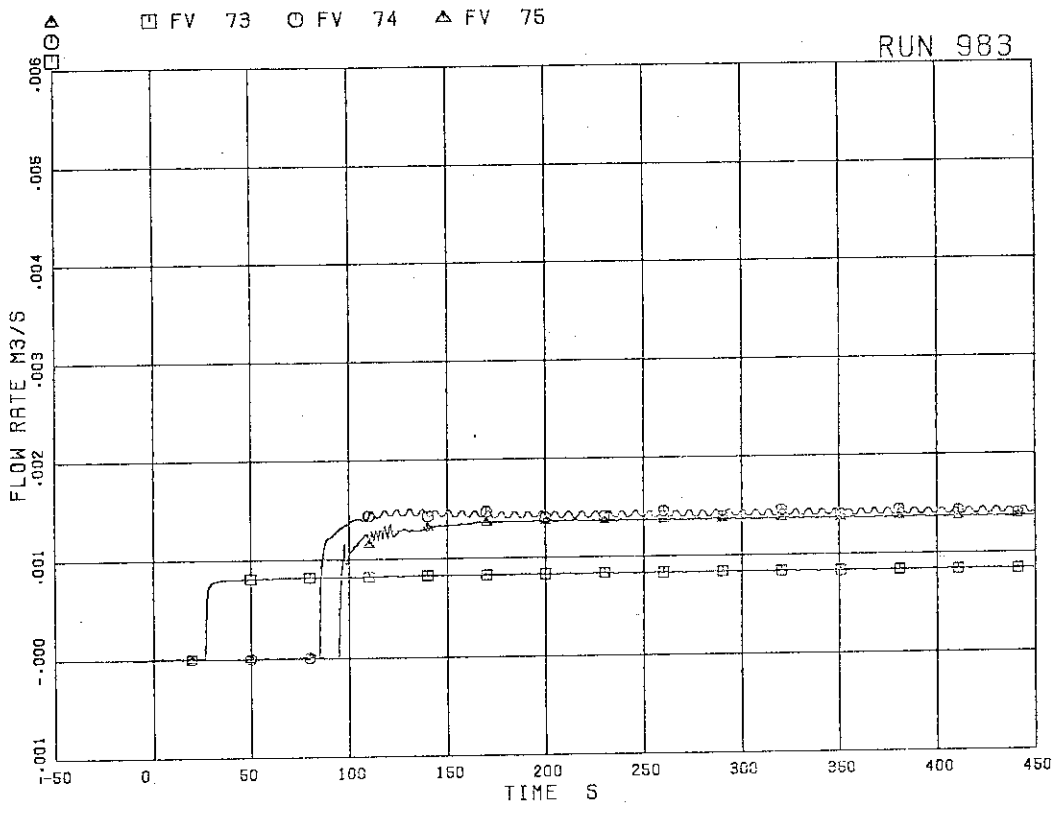

Fig. 5.41 ECC injection flow rates

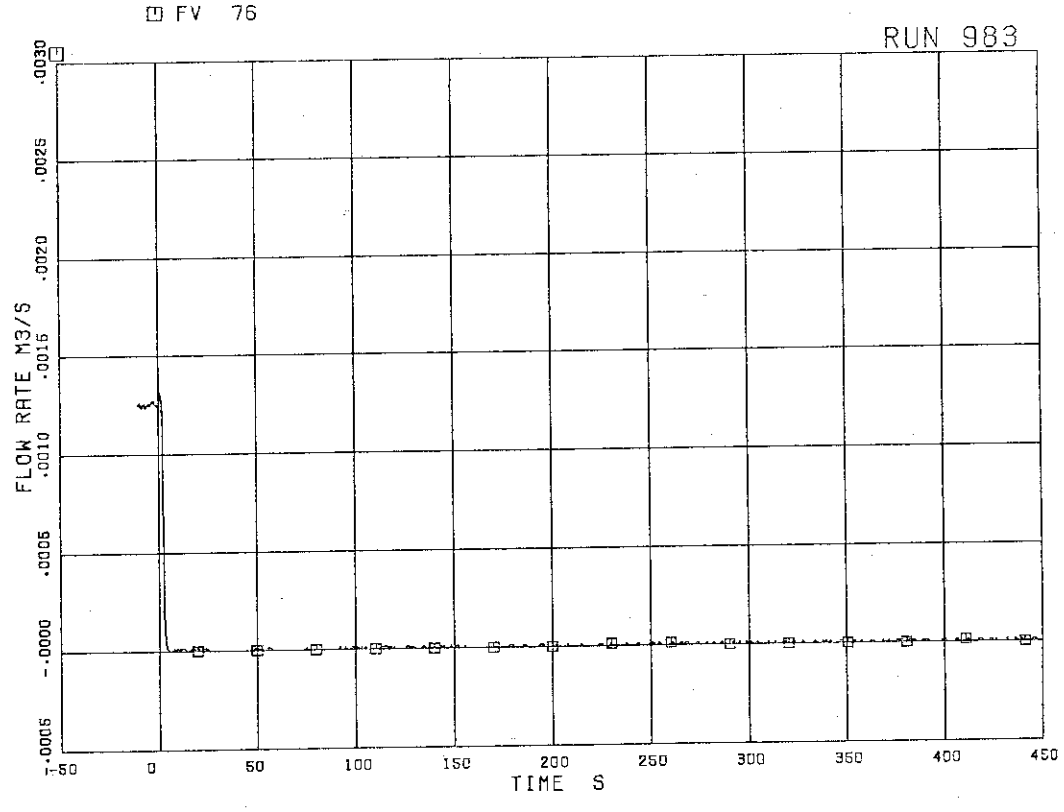

Fig. 5.42 Feedwater flow rate

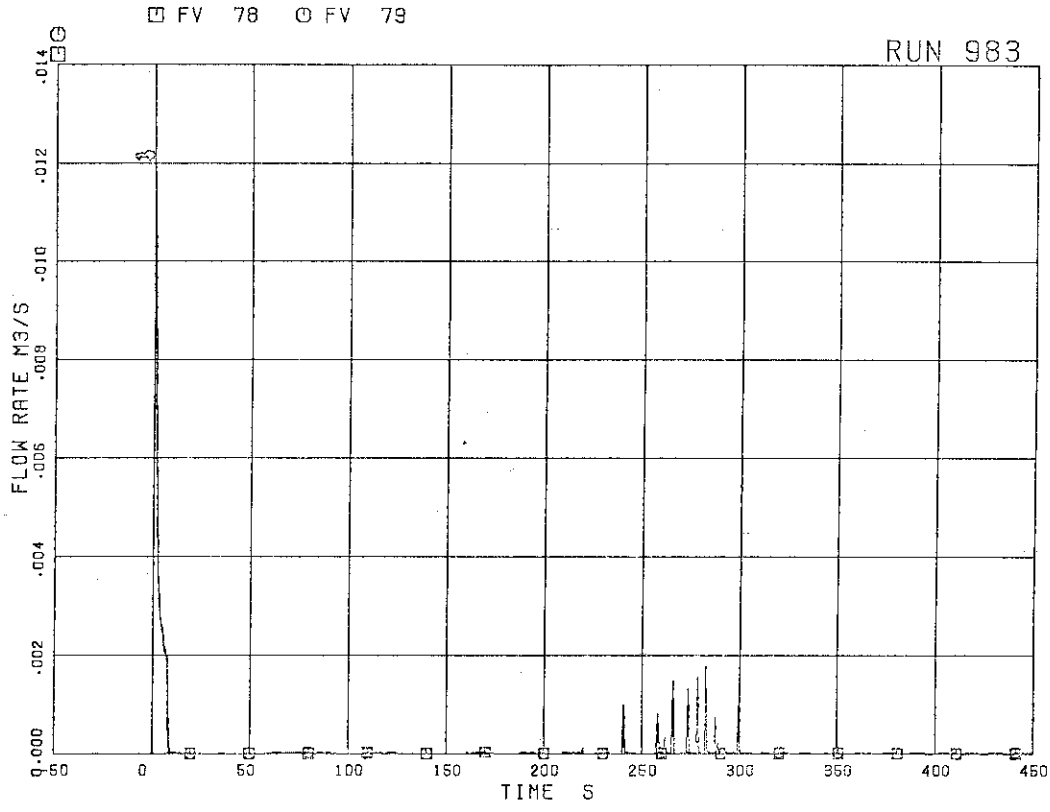

Fig. 5.43 JP-1,2 discharge flow rates (pos. flow)

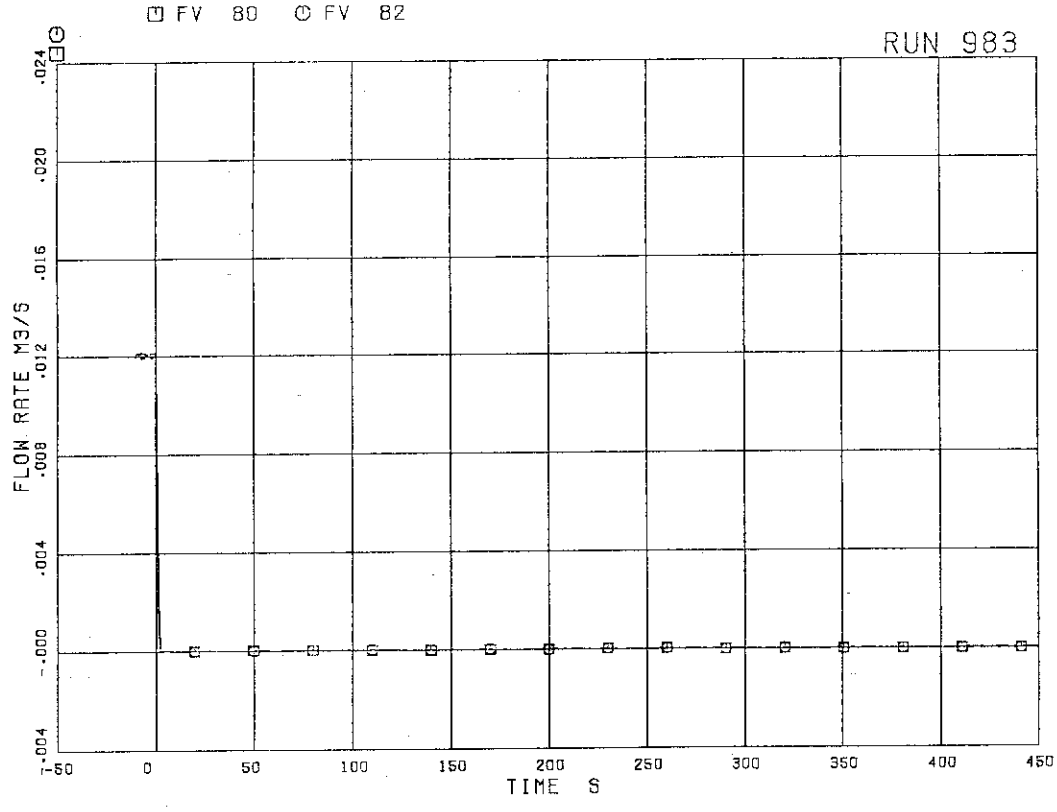

Fig. 5.44 JP-3,4 discharge flow rates (pos. flow)

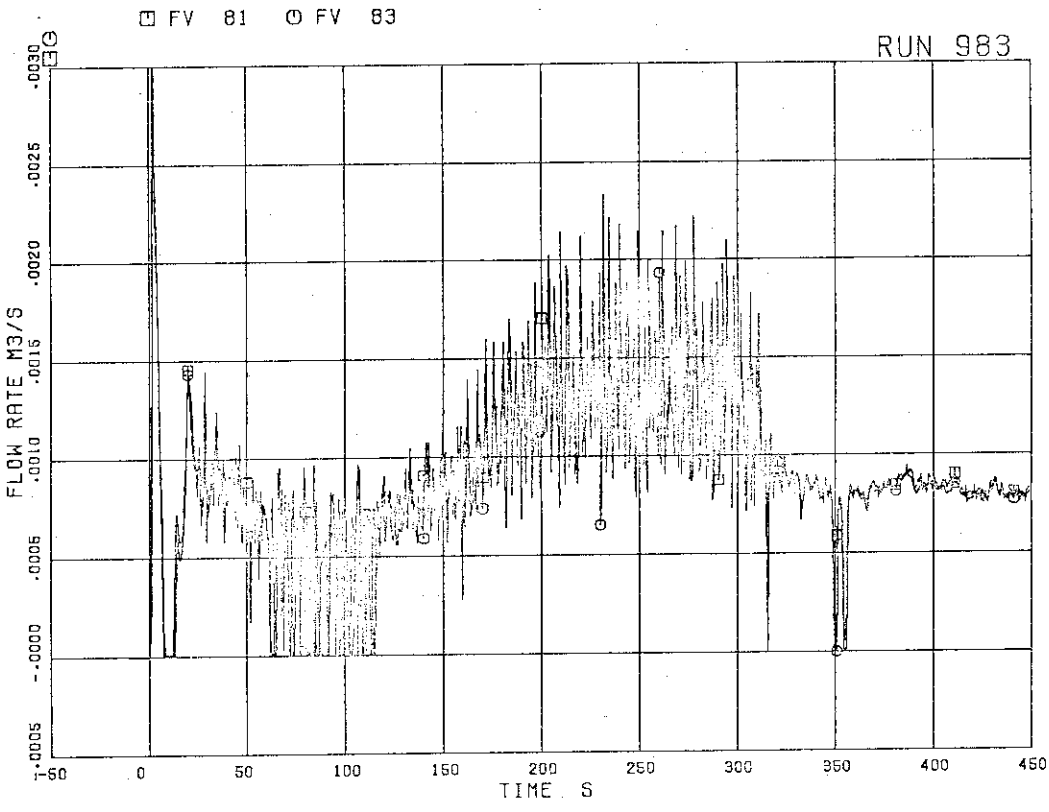

Fig. 5.45 JP-3,4 discharge flow rates (neg. flow)

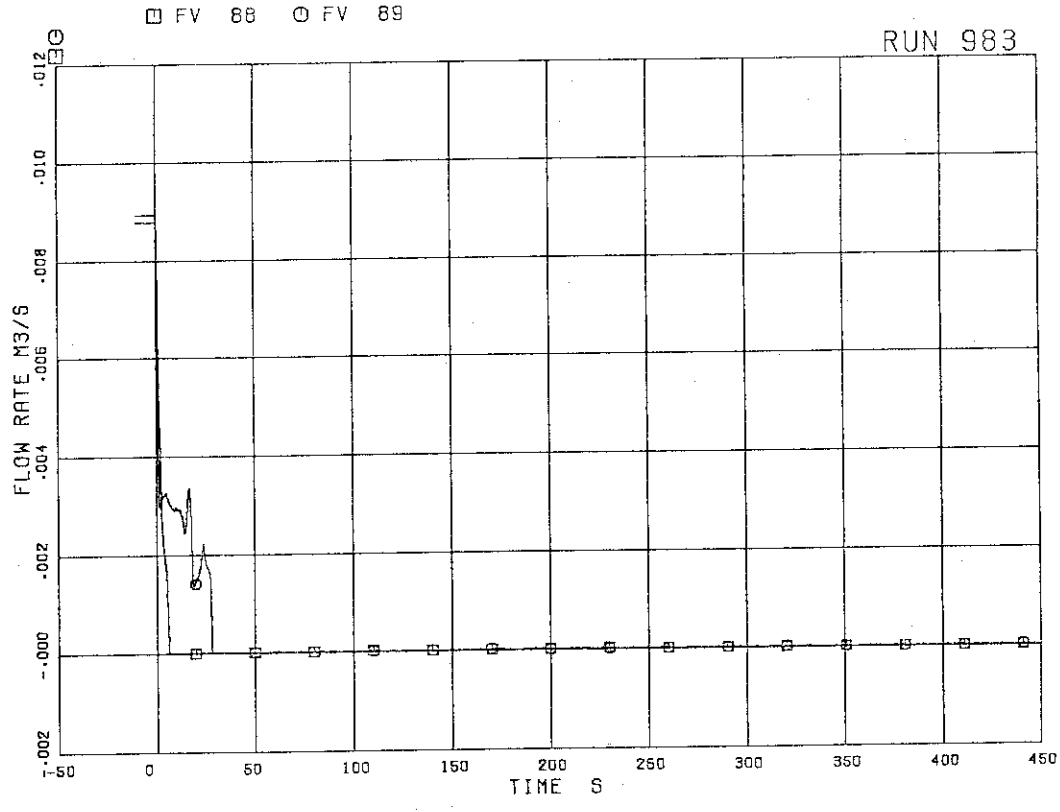

Fig. 5.46 MRP discharge flow rates

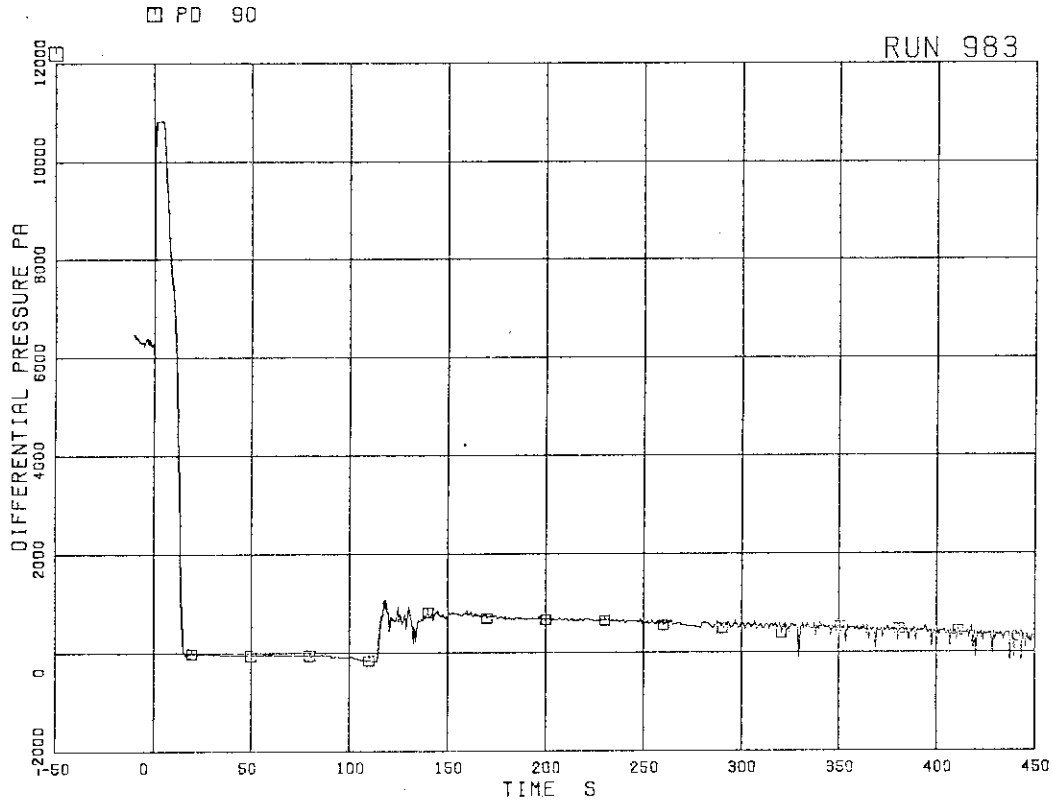

Fig. 5.47 Differential pressure across orifice flowmeter F-1

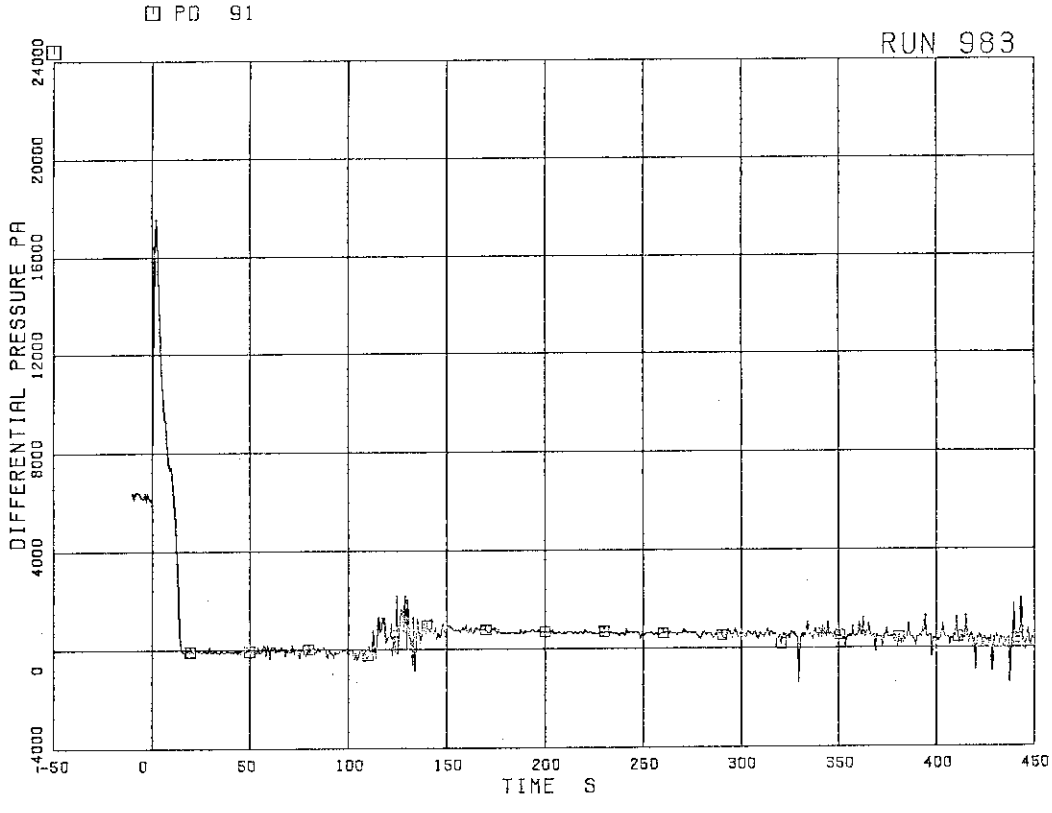

Fig. 5.48 Differential pressure across orifice flowmeter F-2

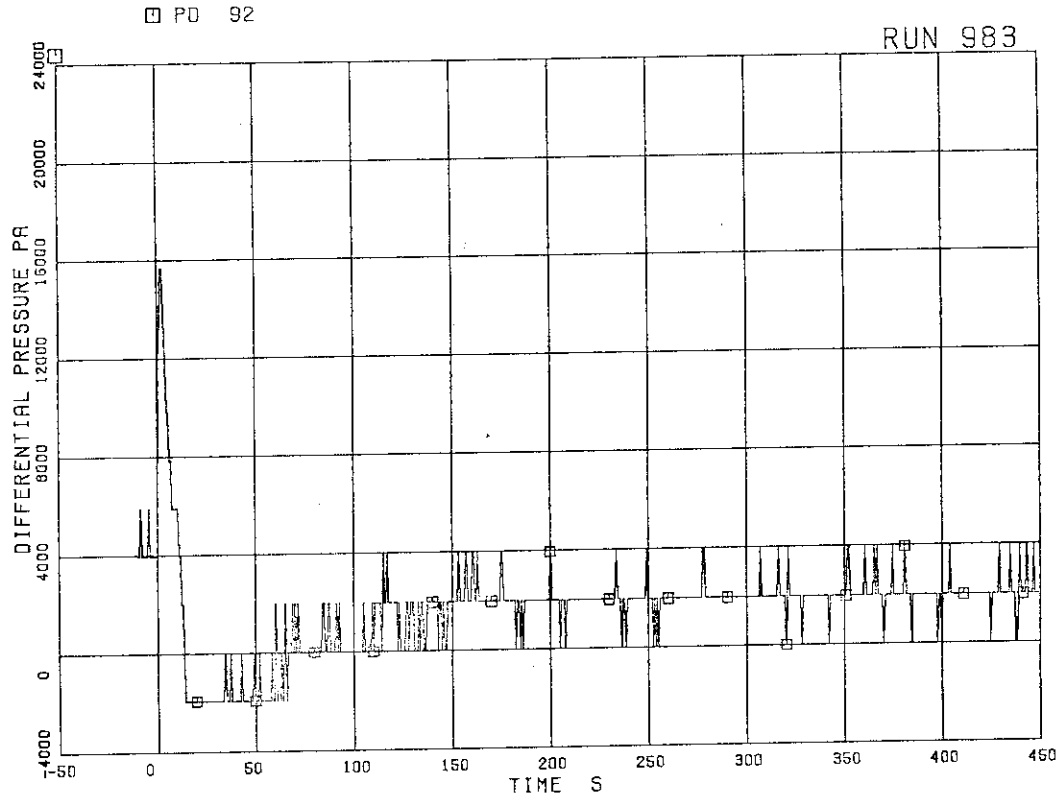

Fig. 5.49 Differential pressure across orifice flowmeter F-3

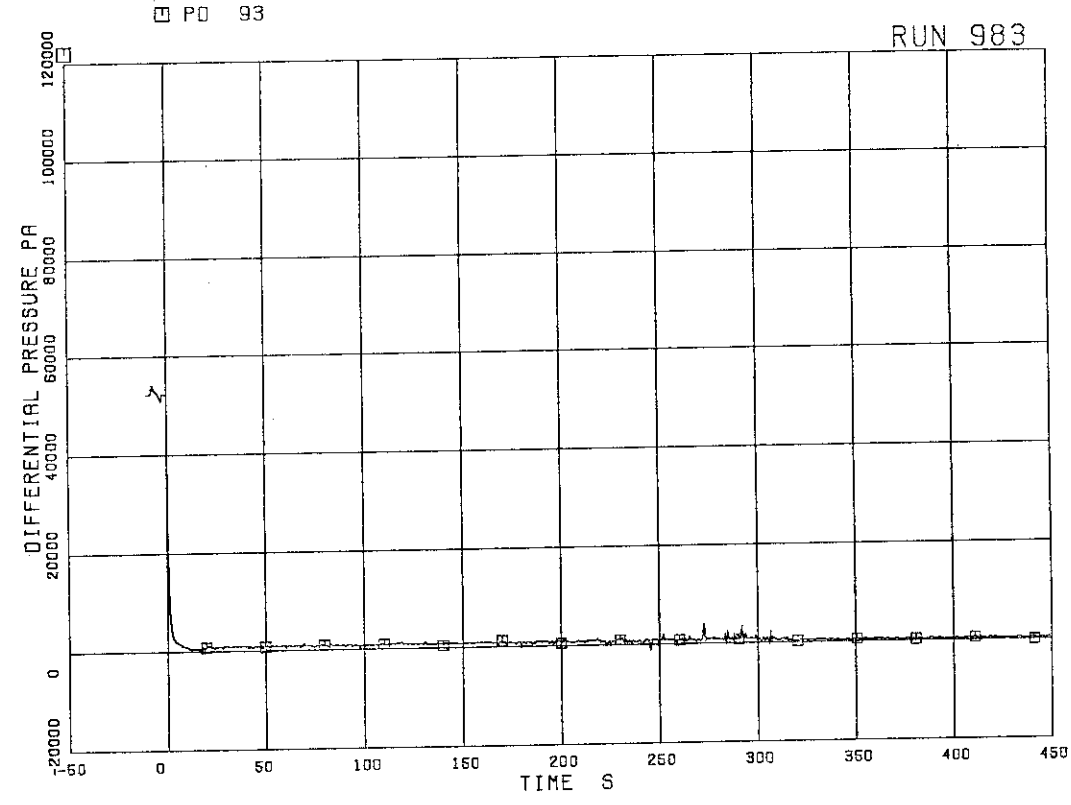

Fig. 5.50 Differential pressure across Venturi flowmeter F-17

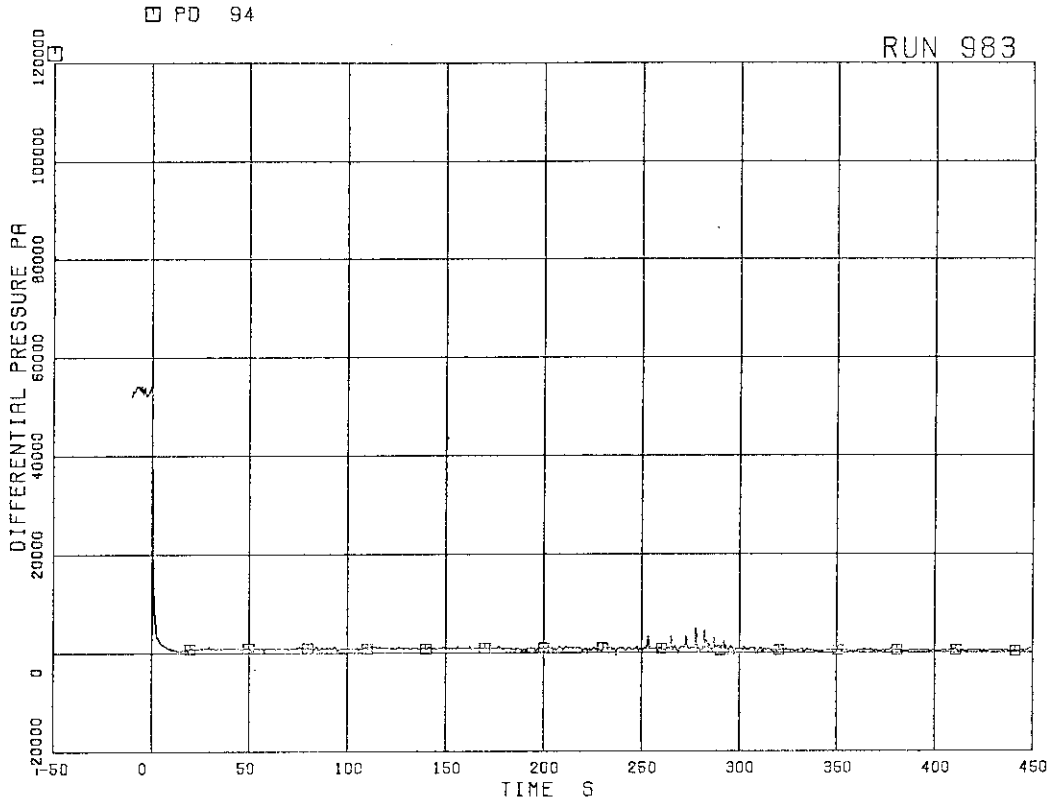

Fig. 5.51 Differential pressure across Venturi flowmeter F-18

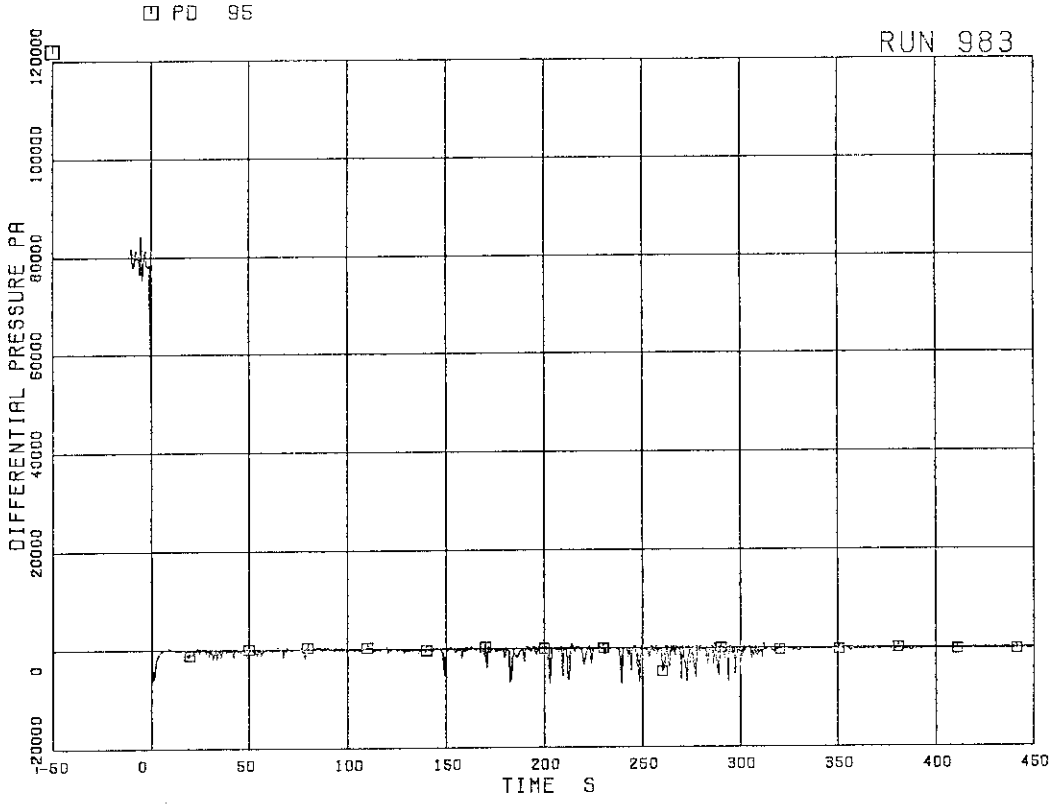

Fig. 5.52 Differential pressure across orifice flowmeter F-19

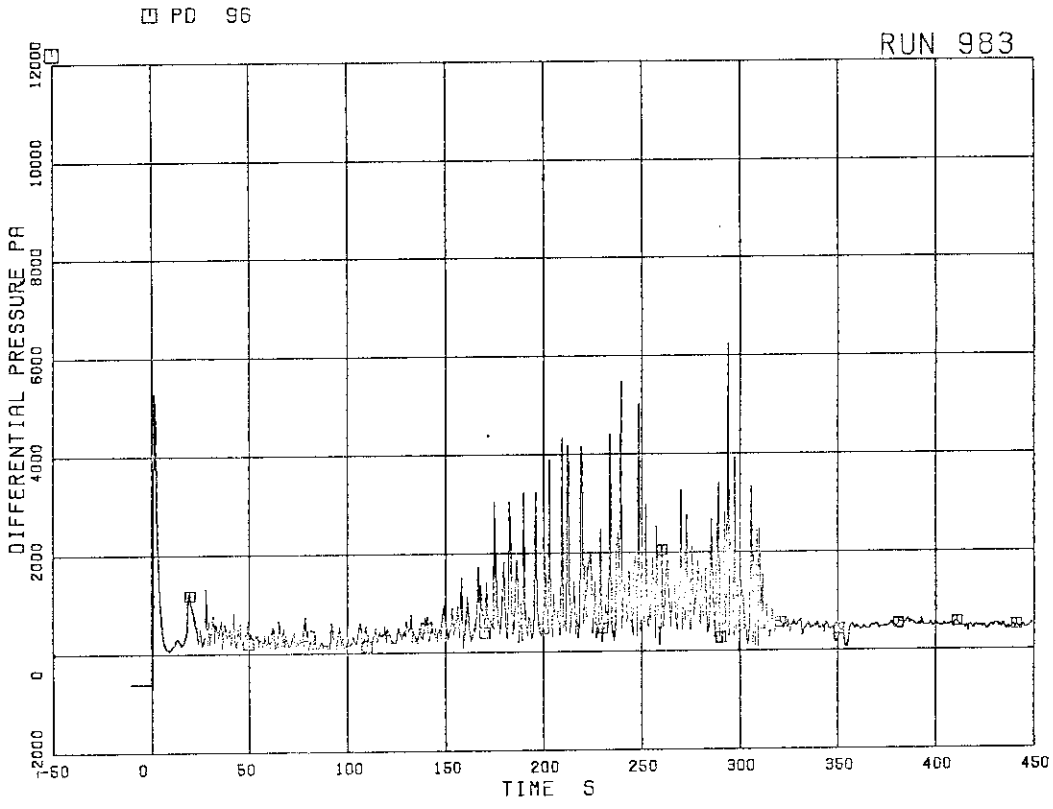

Fig. 5.53 Differential pressure across orifice flowmeter F-20

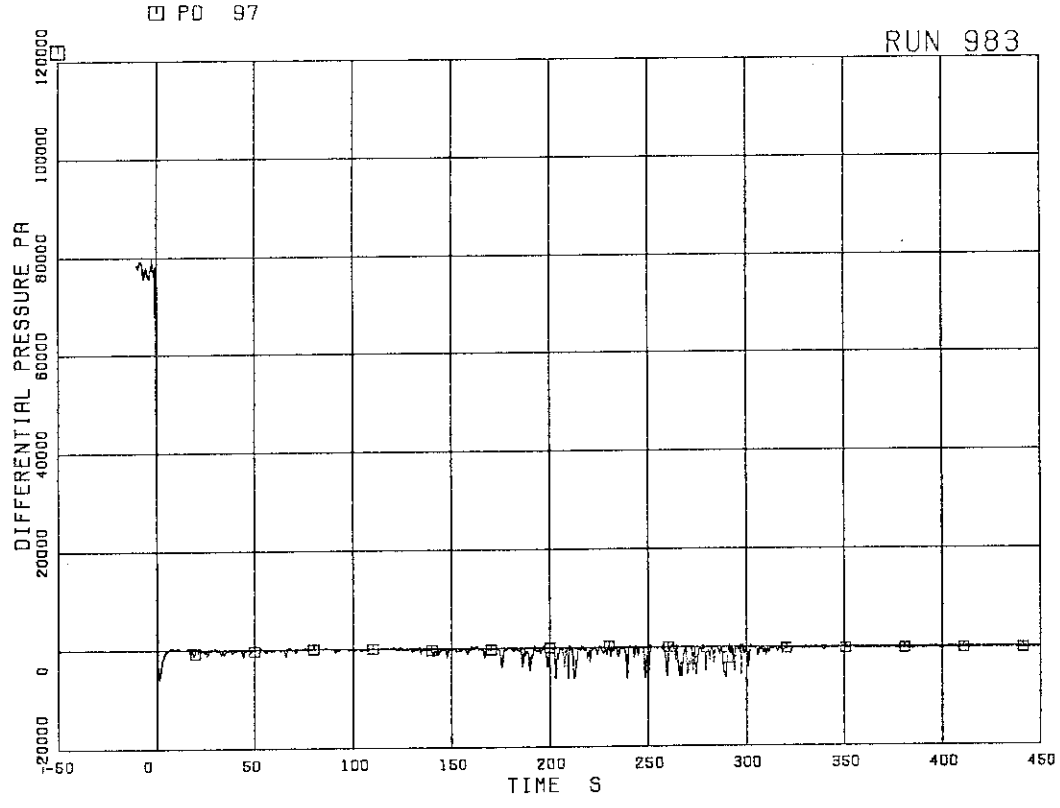

Fig. 5.54 Differential pressure across orifice flowmeter F-21

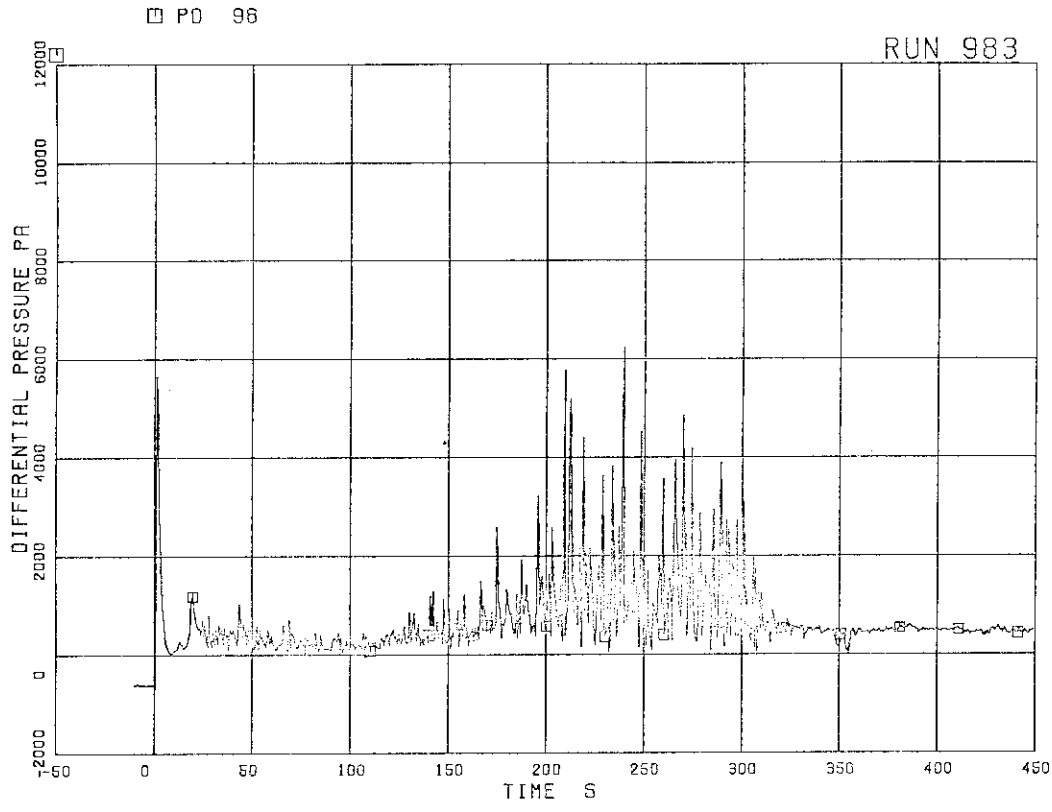

Fig. 5.55 Differential pressure across orifice flowmeter F-22

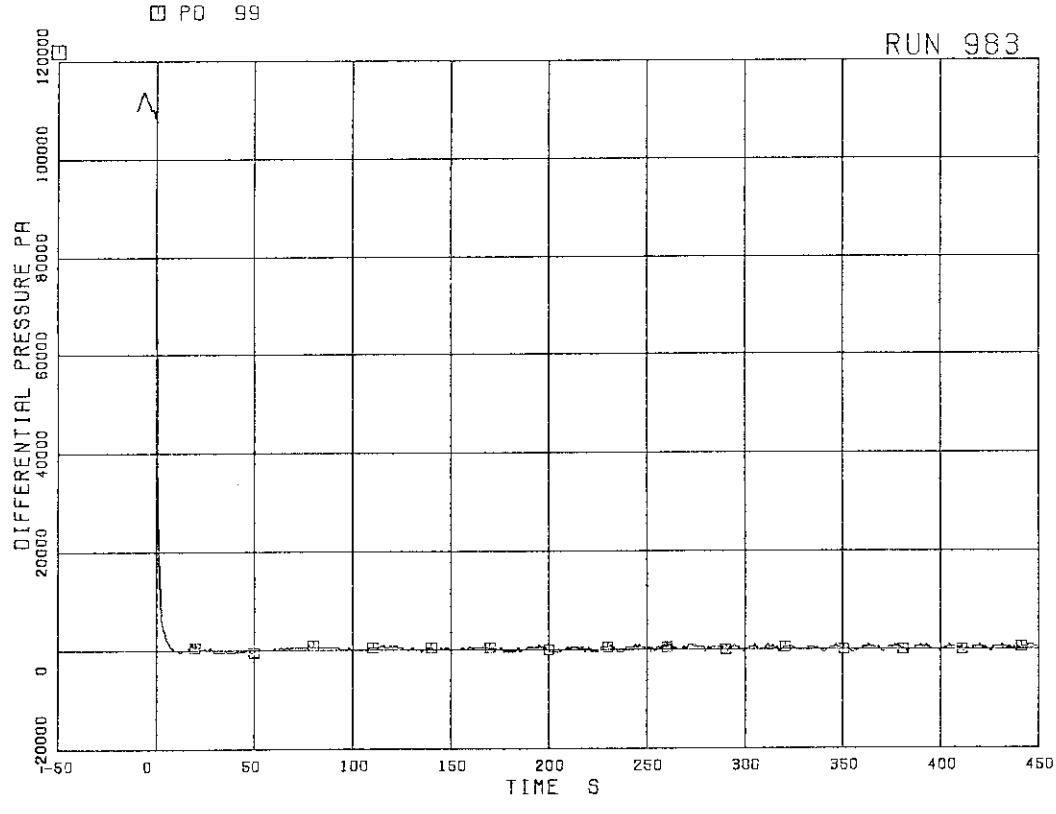

Fig. 5.56 Differential pressure across Venturi flowmeter F-27

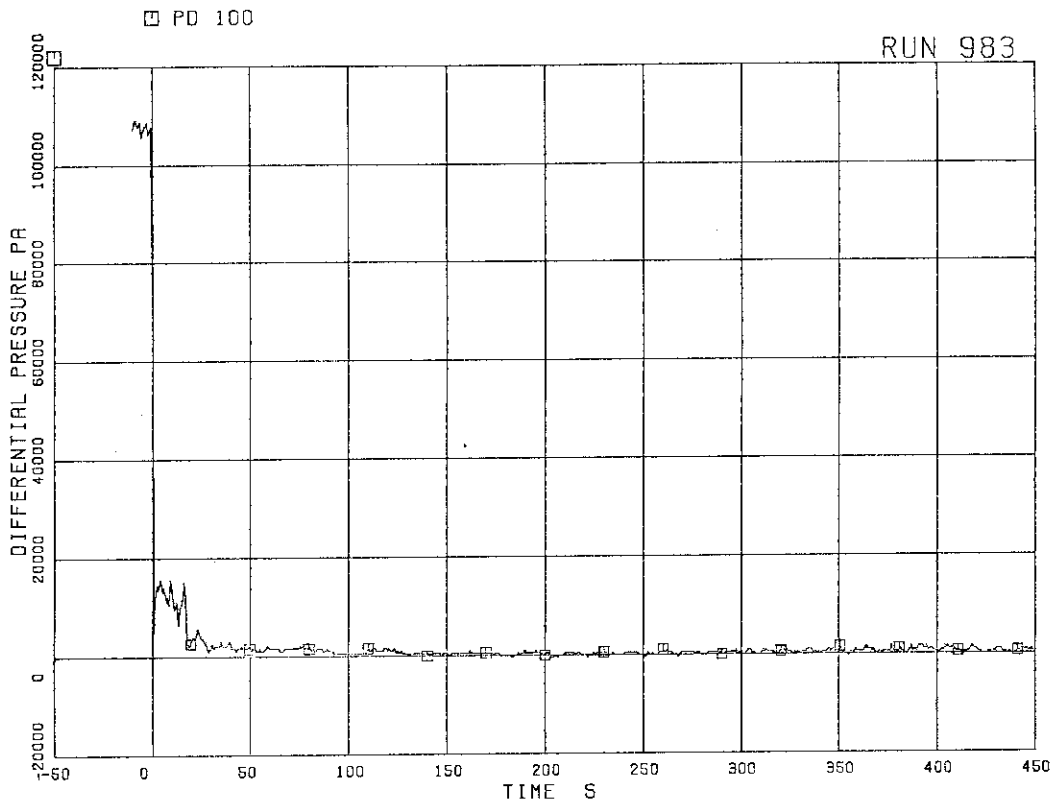

Fig. 5.57 Differential pressure across Venturi flowmeter F-28

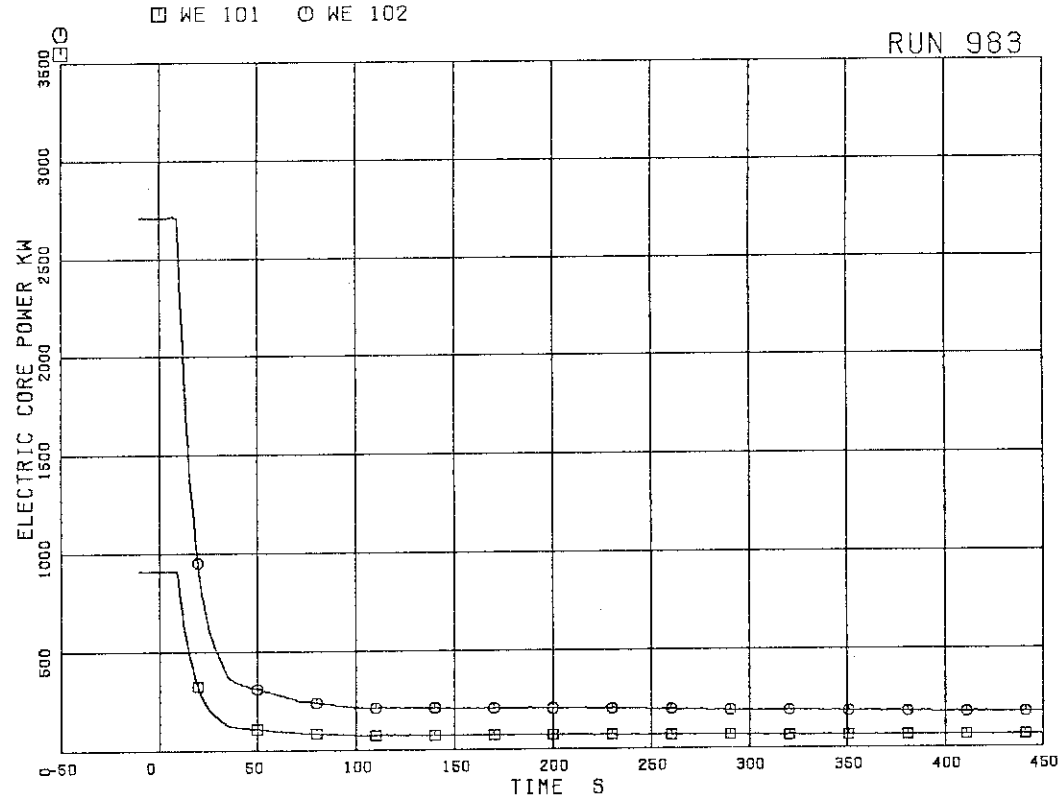

Fig. 5.58 Electric core power

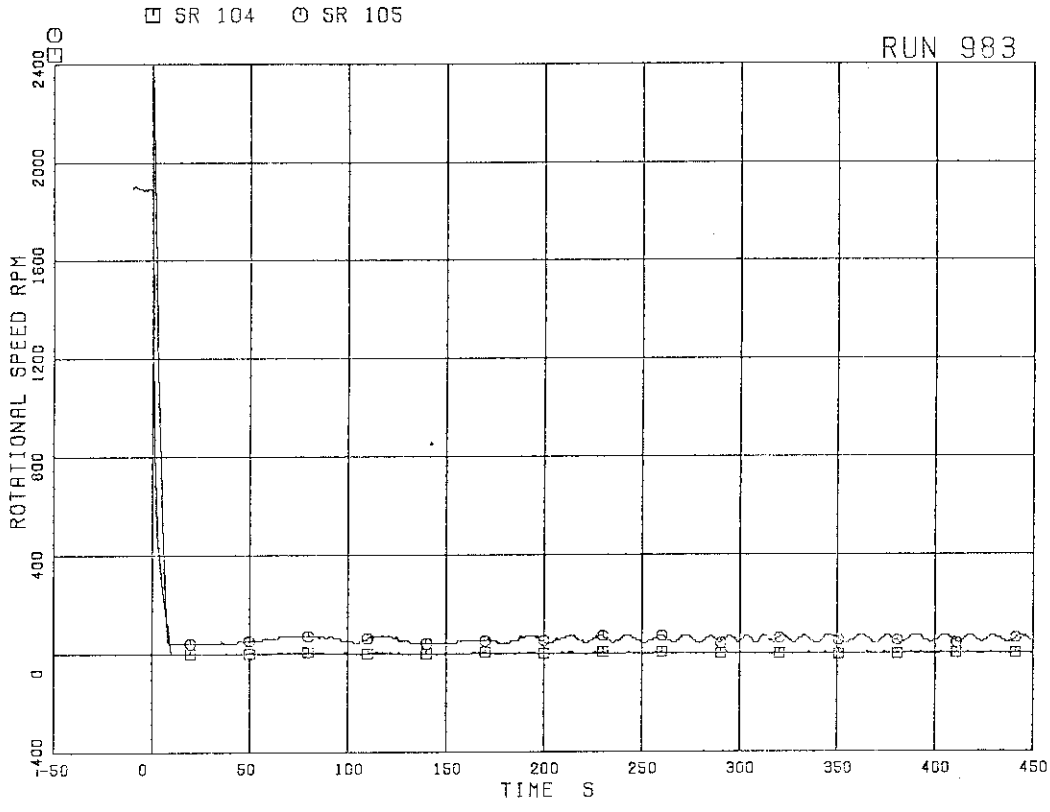

Fig. 5.59 MRP pump speeds

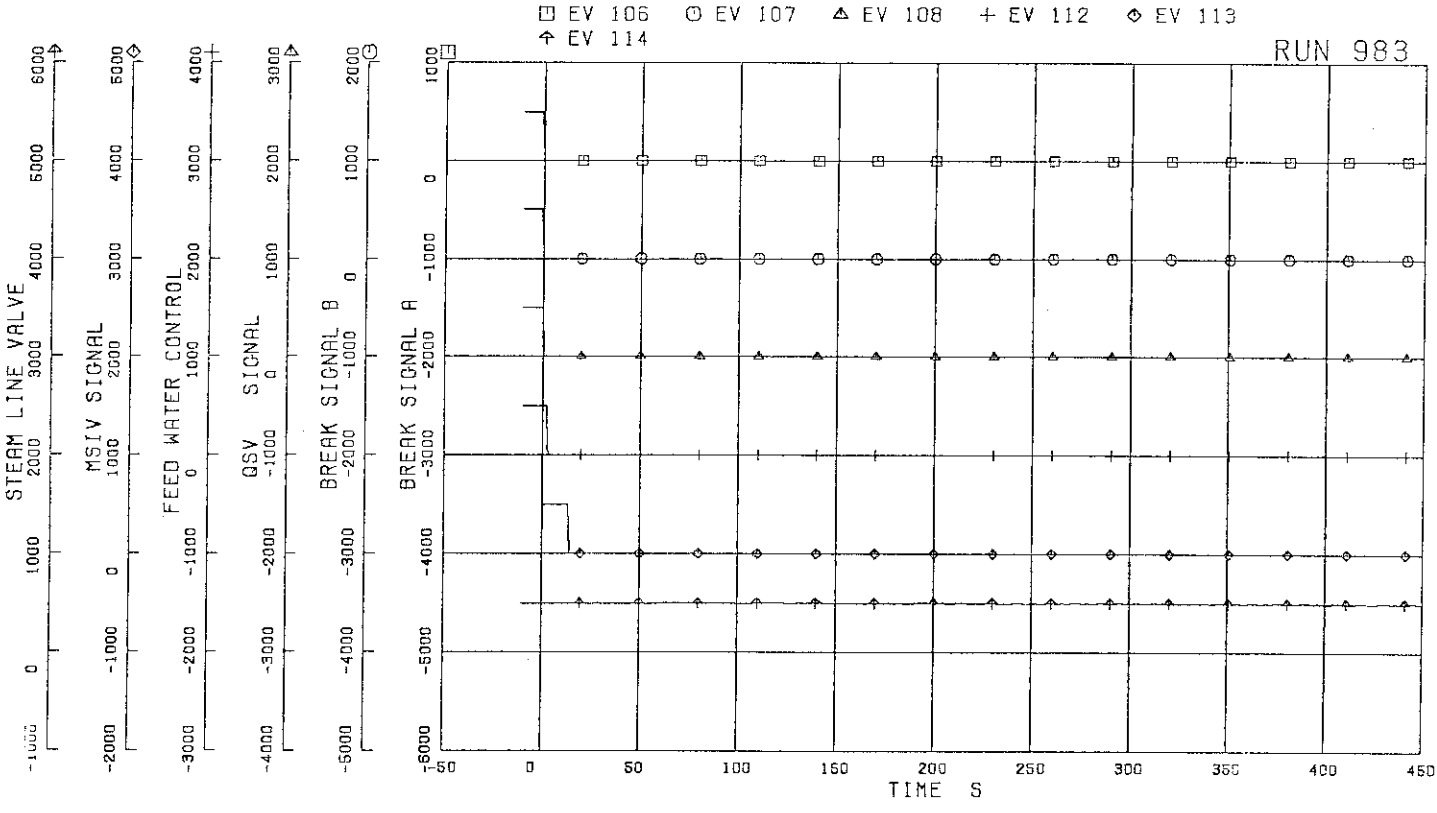

Fig. 5.60 Valve operation signals

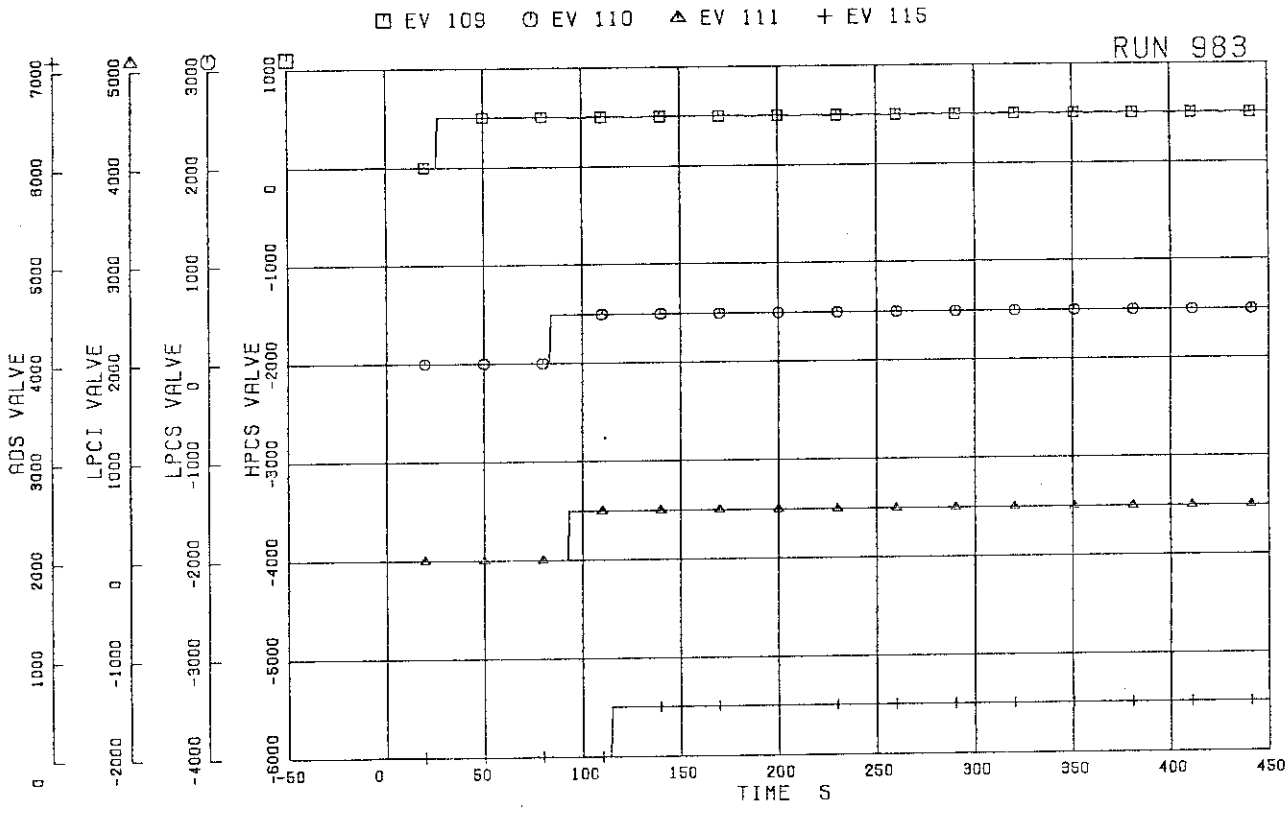

Fig. 5.61 ECCS operation signals

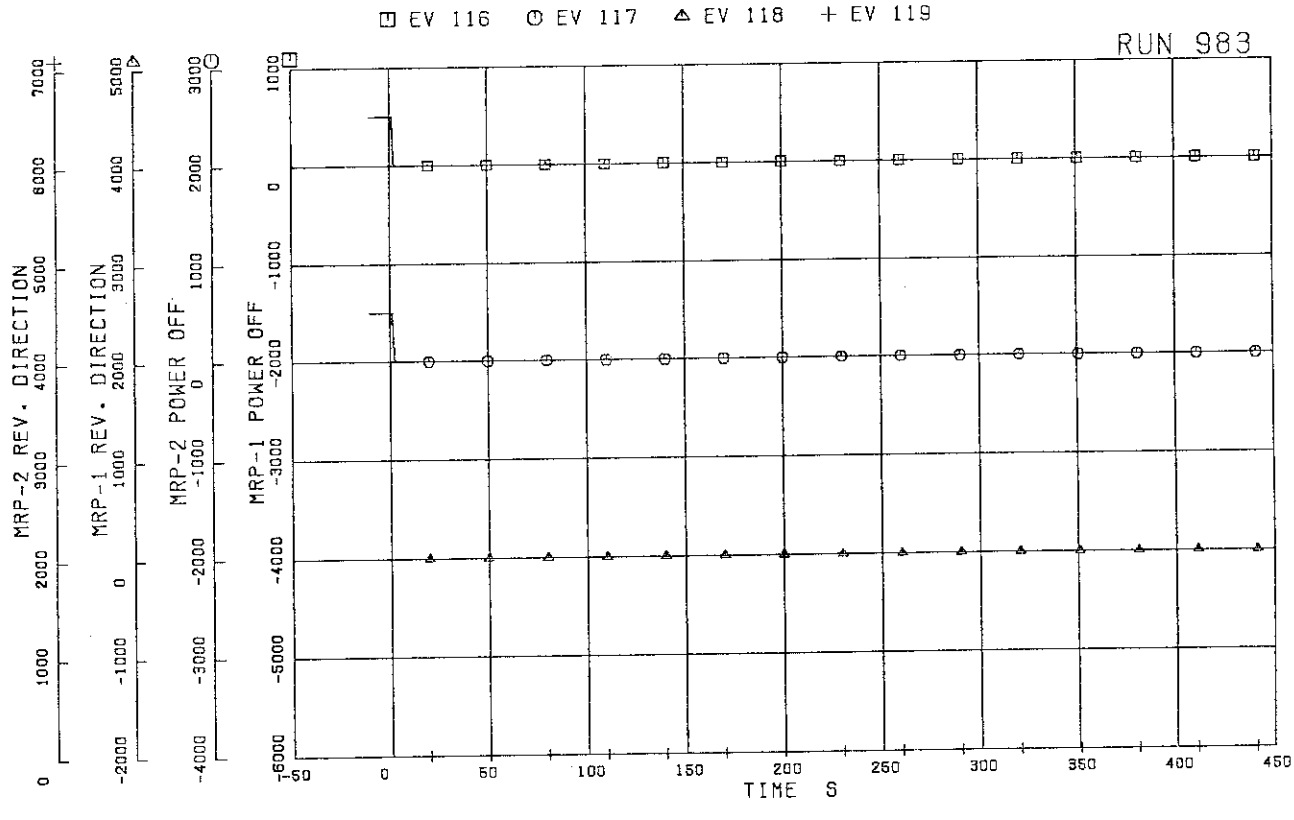

Fig. 5.62 MRP operation signals

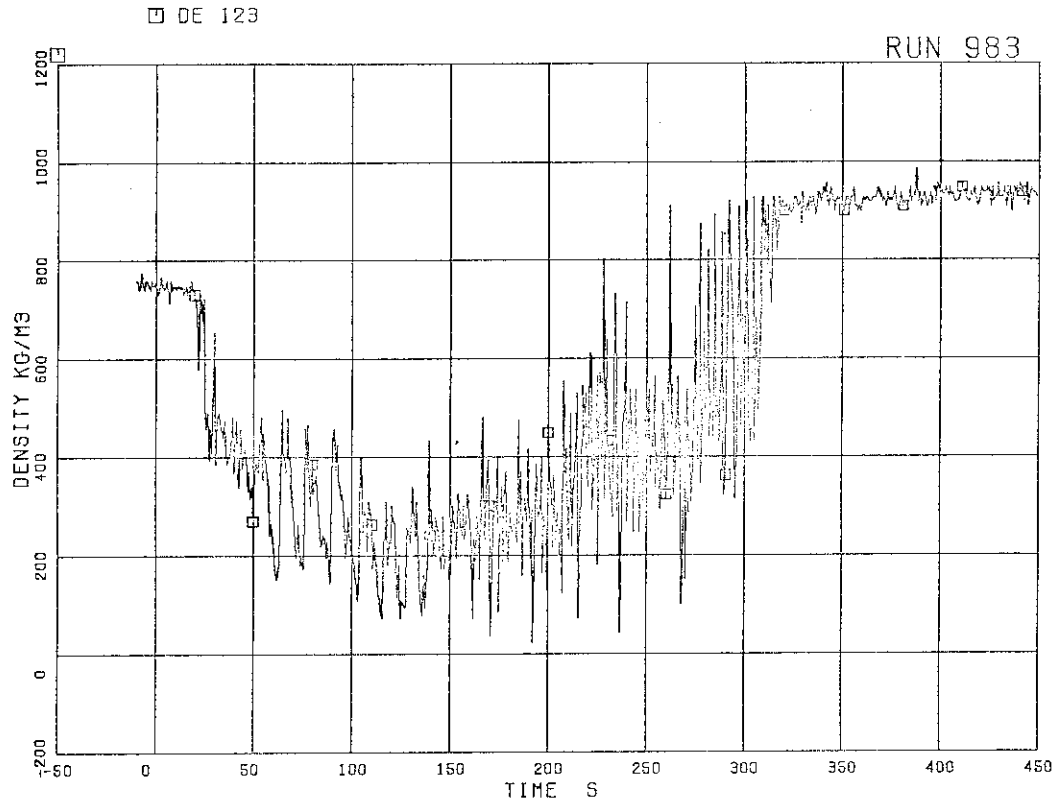

Fig. 5.63 Fluid density at JP-3,4 outlet, beam A

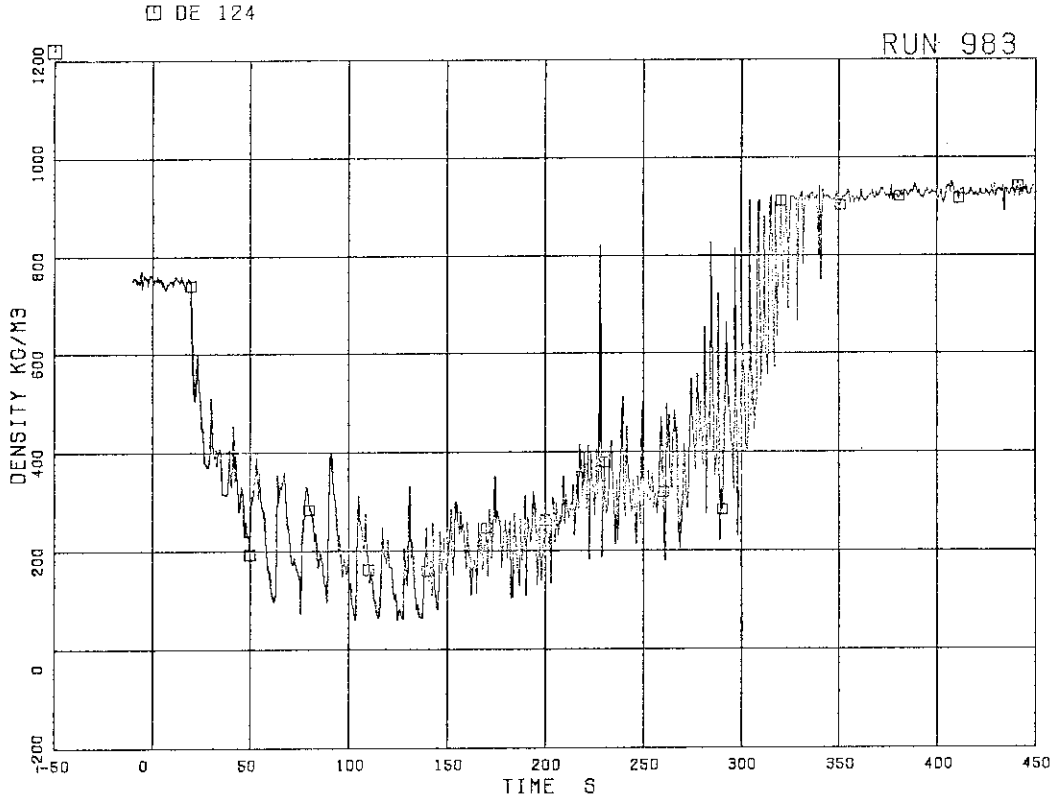

Fig. 5.64 Fluid density at JP-3,4 outlet, beam B

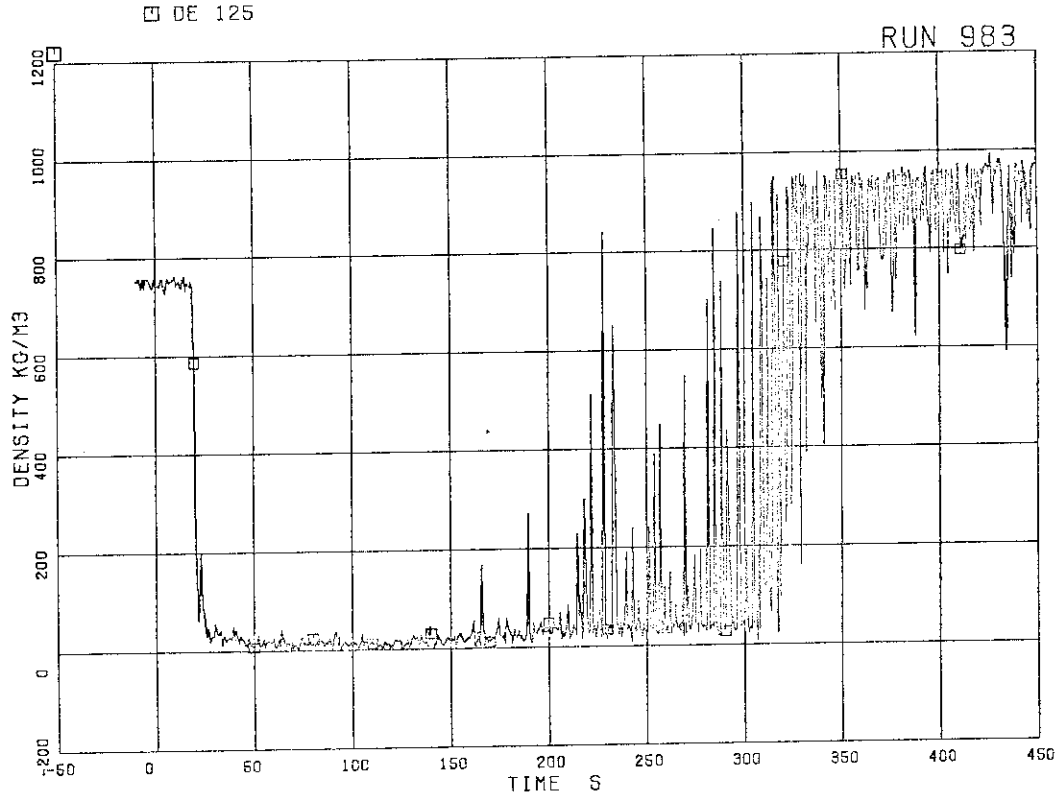

Fig. 5.65 Fluid density at JP-3,4 outlet, beam C

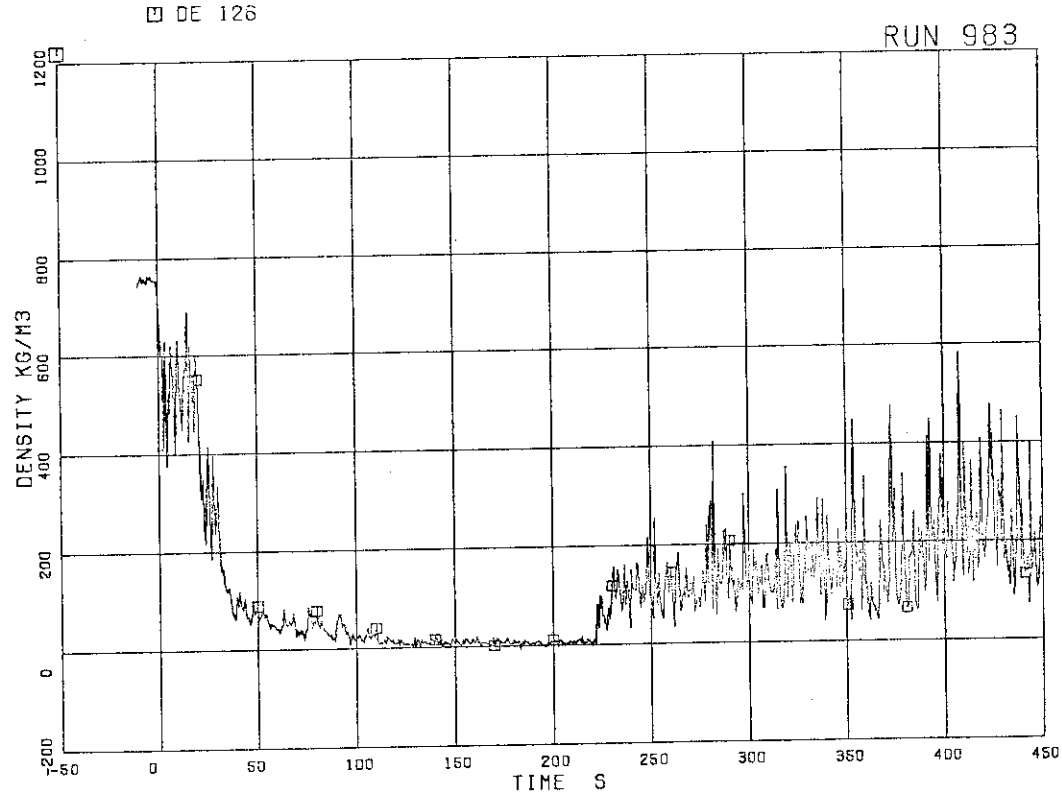

Fig. 5.66 Fluid density at JP side of break, beam A

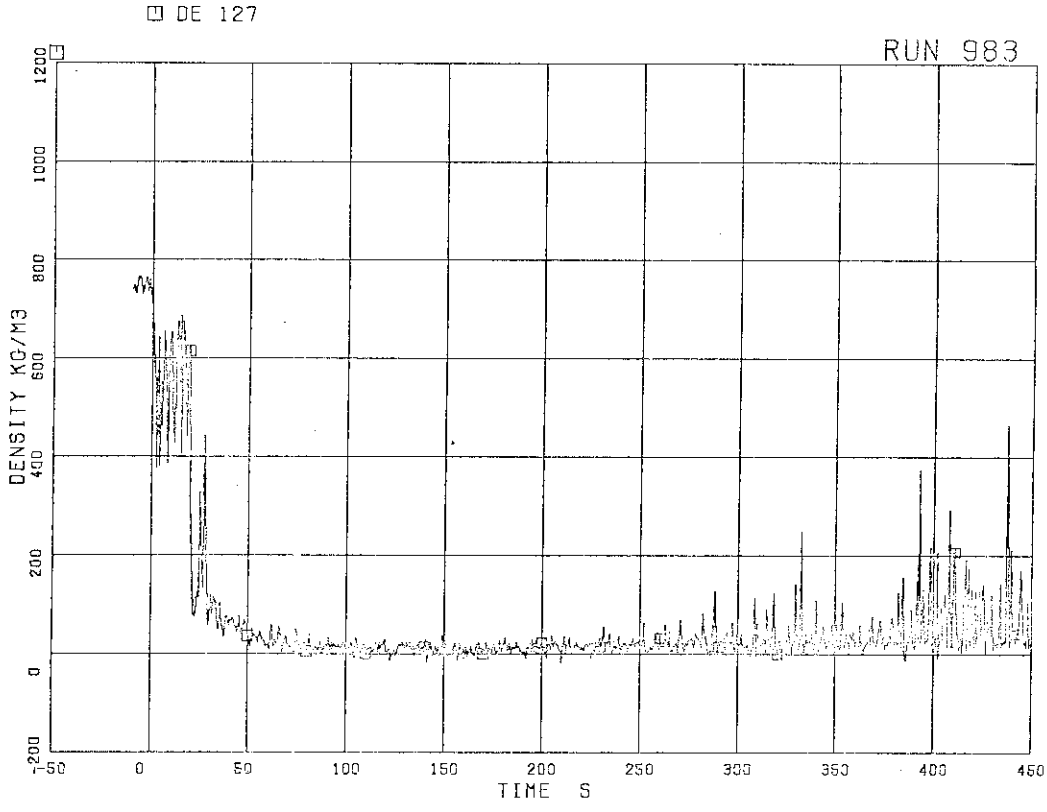

Fig. 5.67 Fluid density at JP side of break, beam B

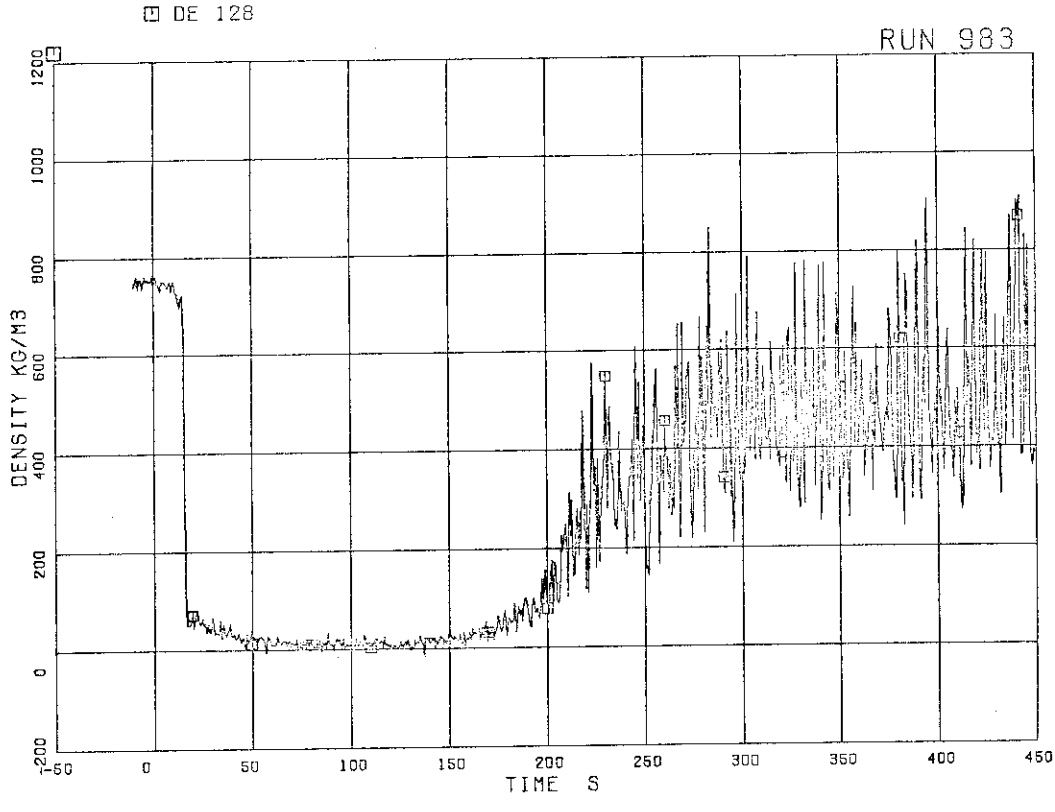

Fig. 5.68 Fluid density at MRP side of break, beam A

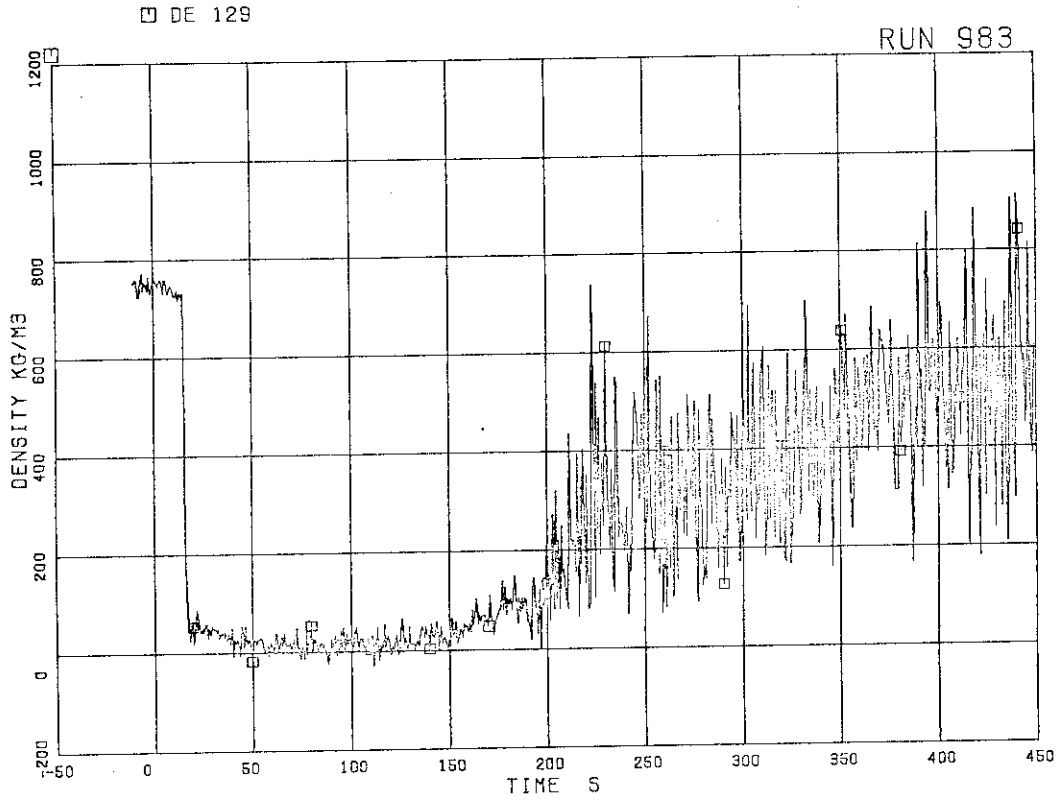

Fig. 5.69 Fluid density at MRP side of break, beam B

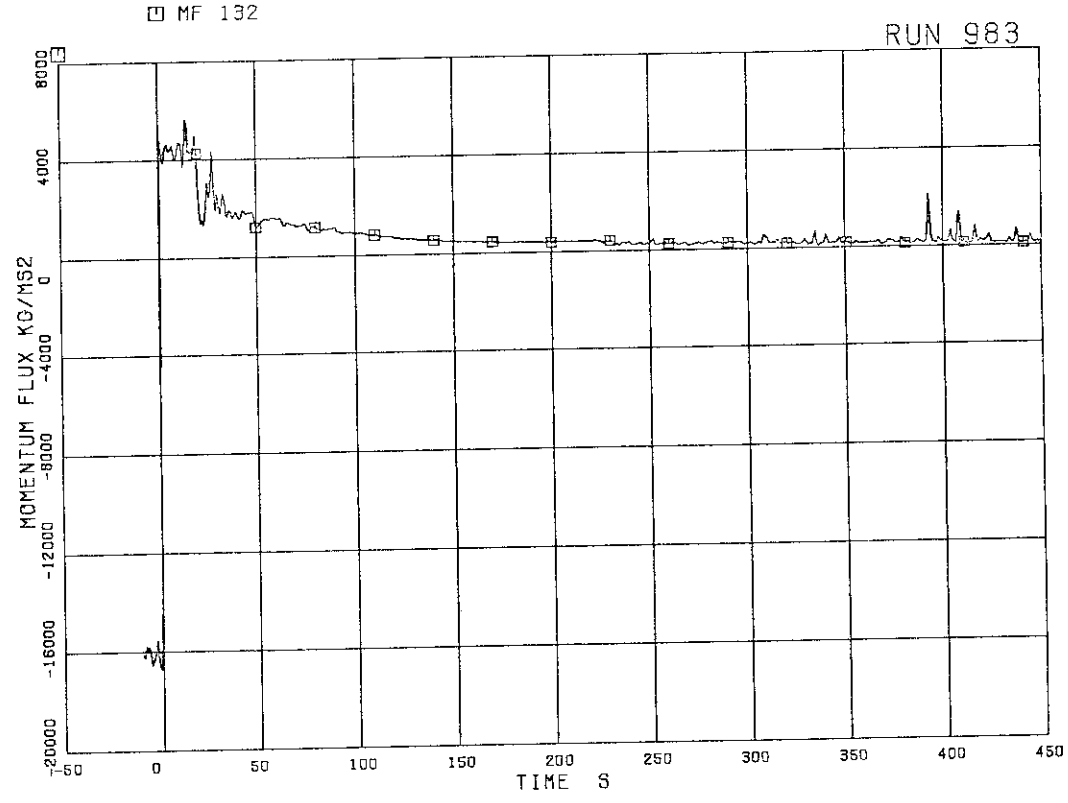

Fig. 5.70 Momentum flux at break A spool piece (low range)

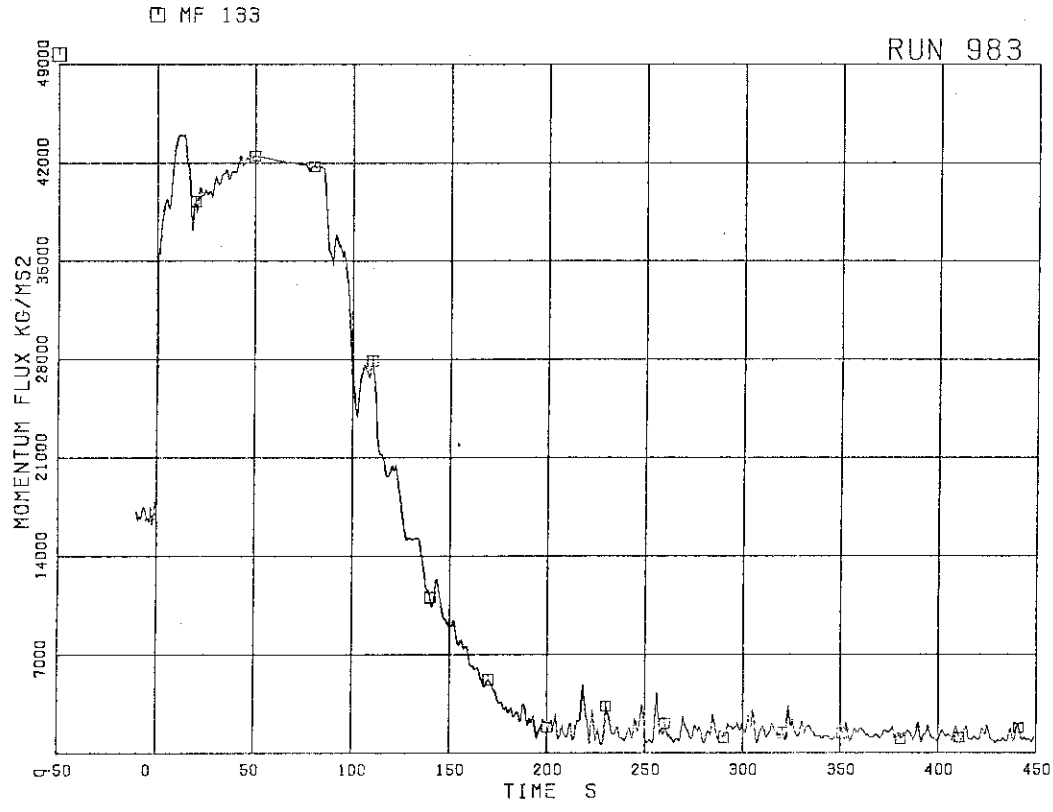

Fig. 5.71 Momentum flux at break B spool piece (low range)

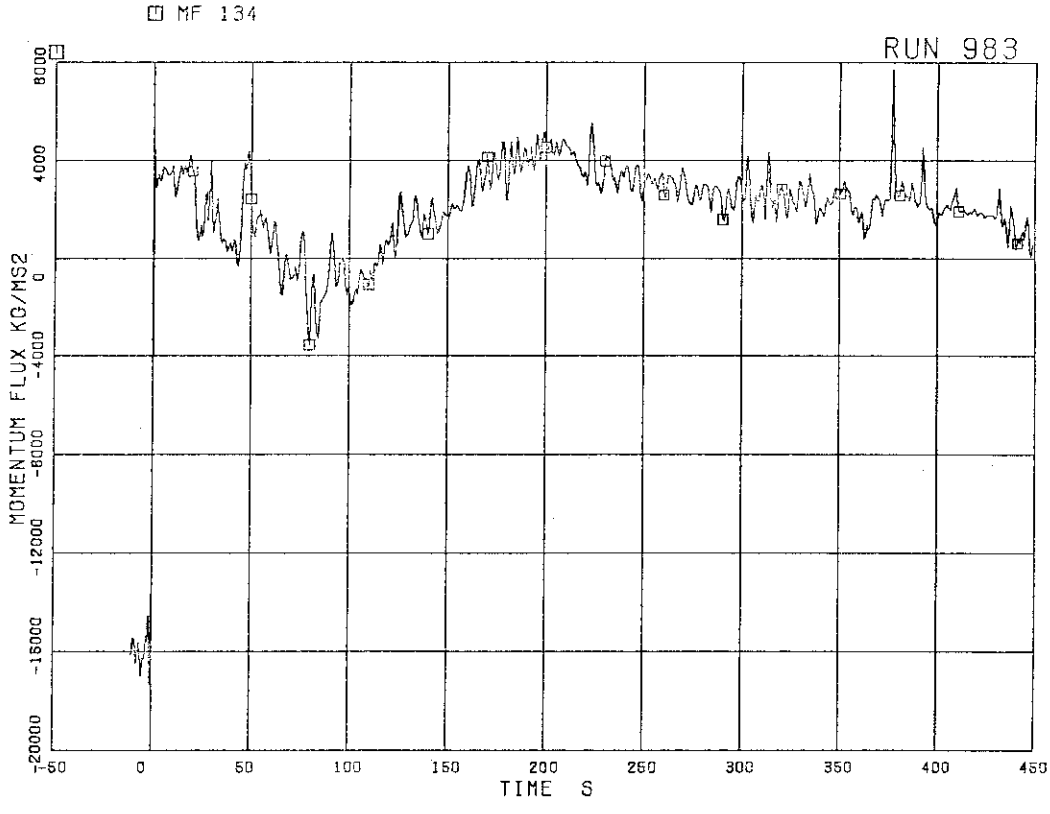

Fig. 5.72 Momentum flux at break A spool piece (high range)

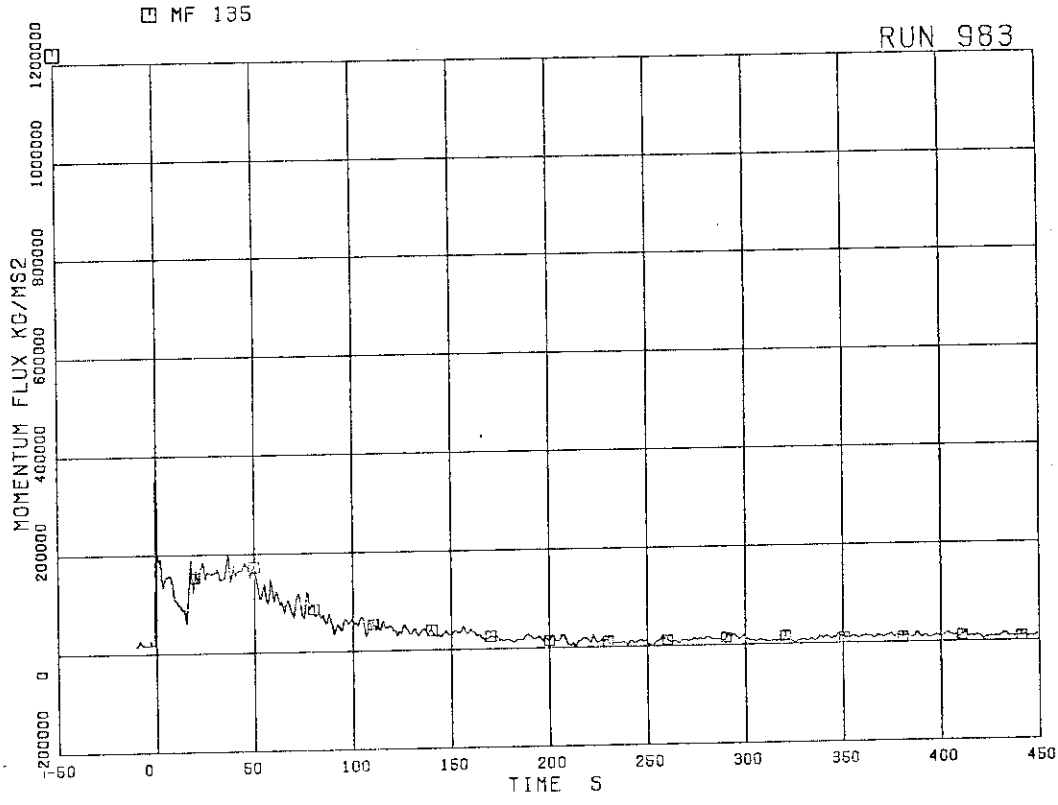

Fig. 5.73 Momentum flux at break B spool piece (high range)

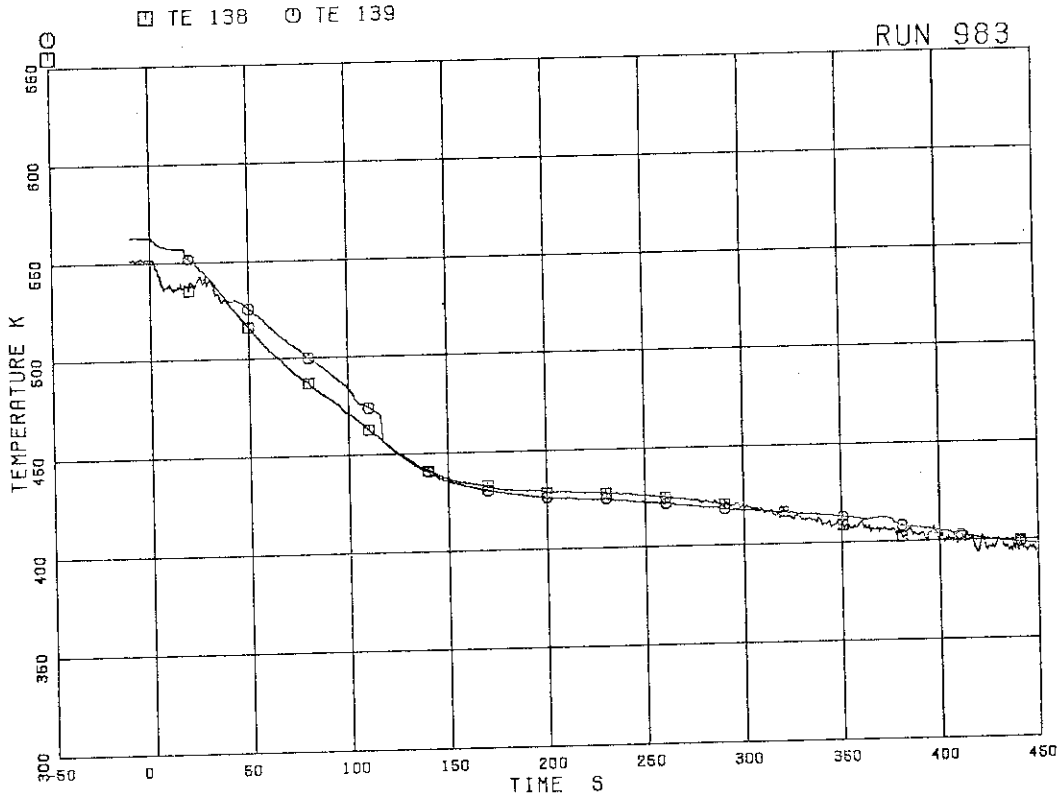

Fig. 5.74 Fluid temperatures in lower plenum and upper plenum

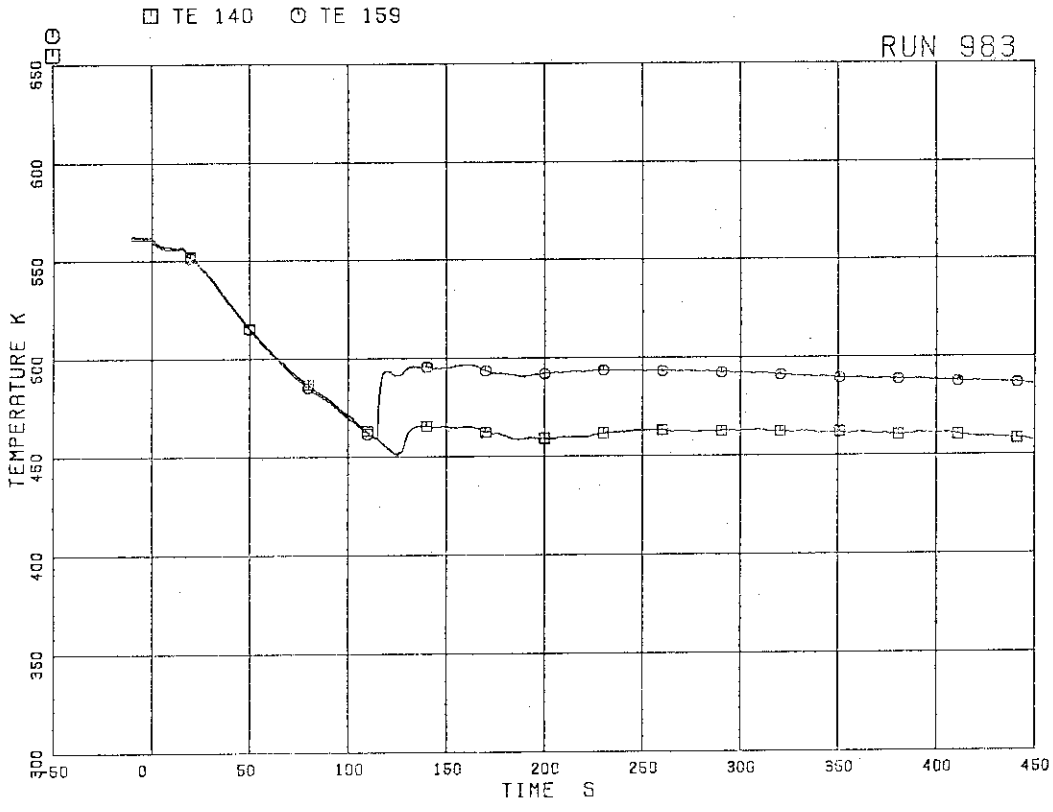

Fig. 5.75 Fluid temperatures in steam dome and MSL

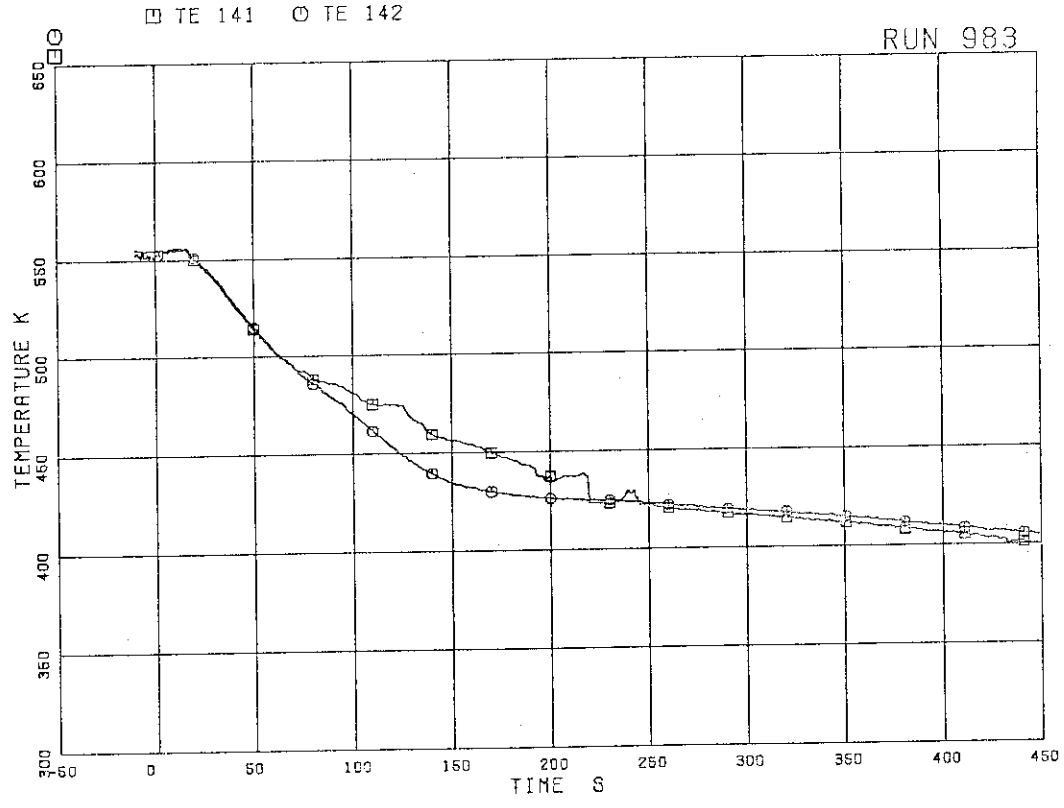

Fig. 5.76 Fluid temperatures in downcomer

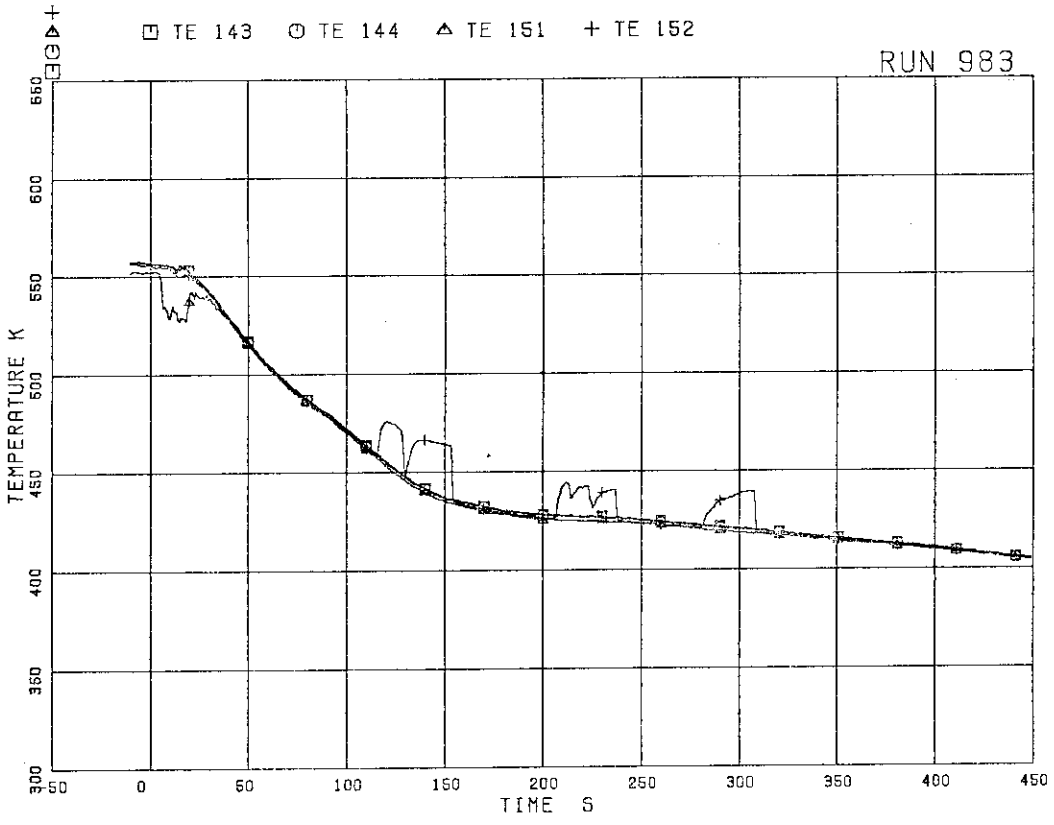

Fig. 5.77 Fluid temperatures in intact recirculation loop

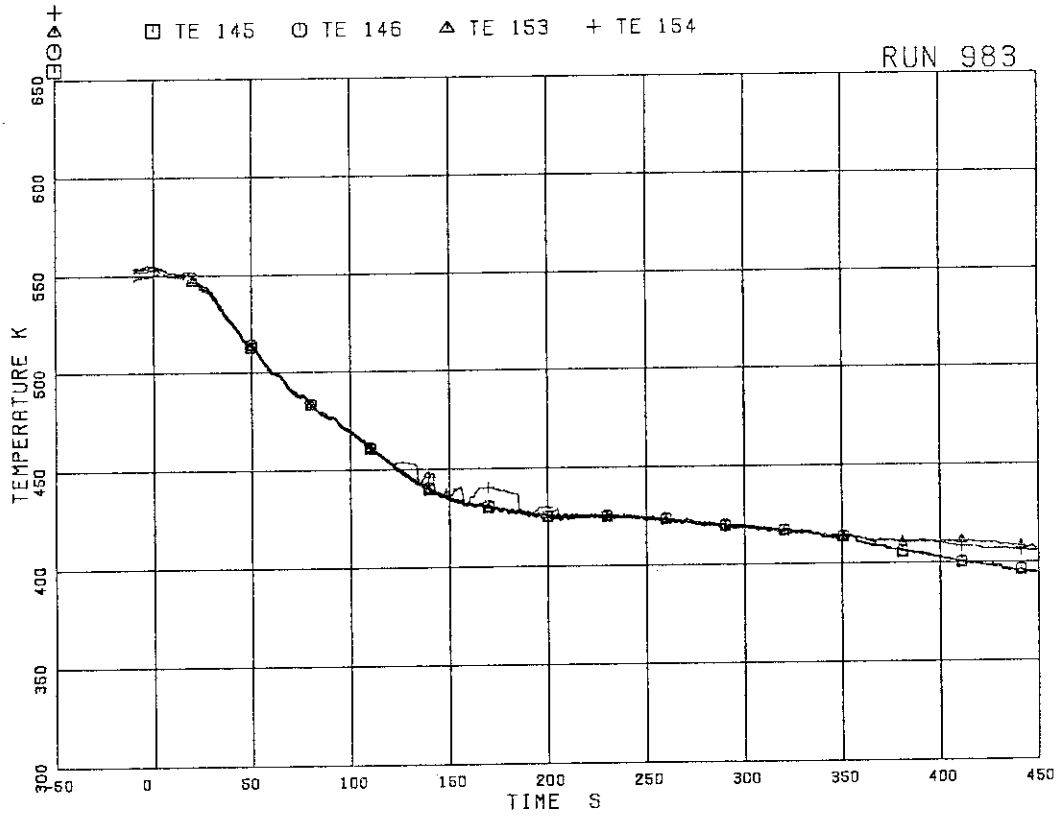

Fig. 5.78 Fluid temperatures in broken recirculation loop

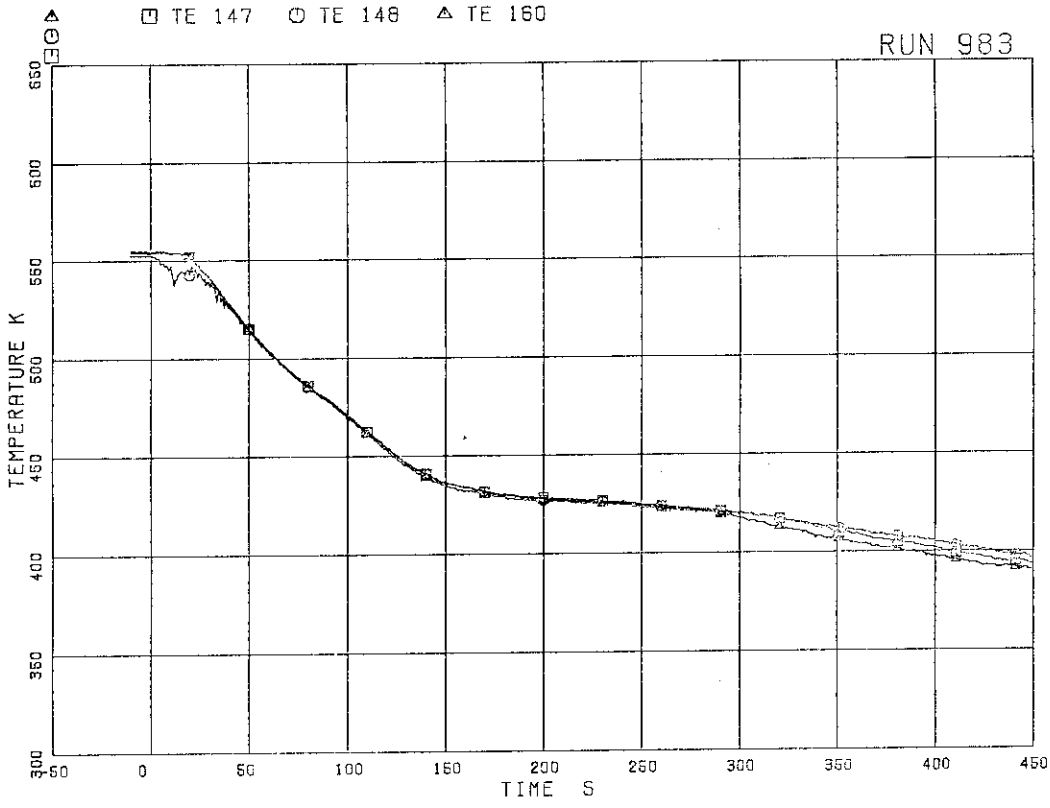

Fig. 5.79 Fluid temperatures at JP-1,2 outlet

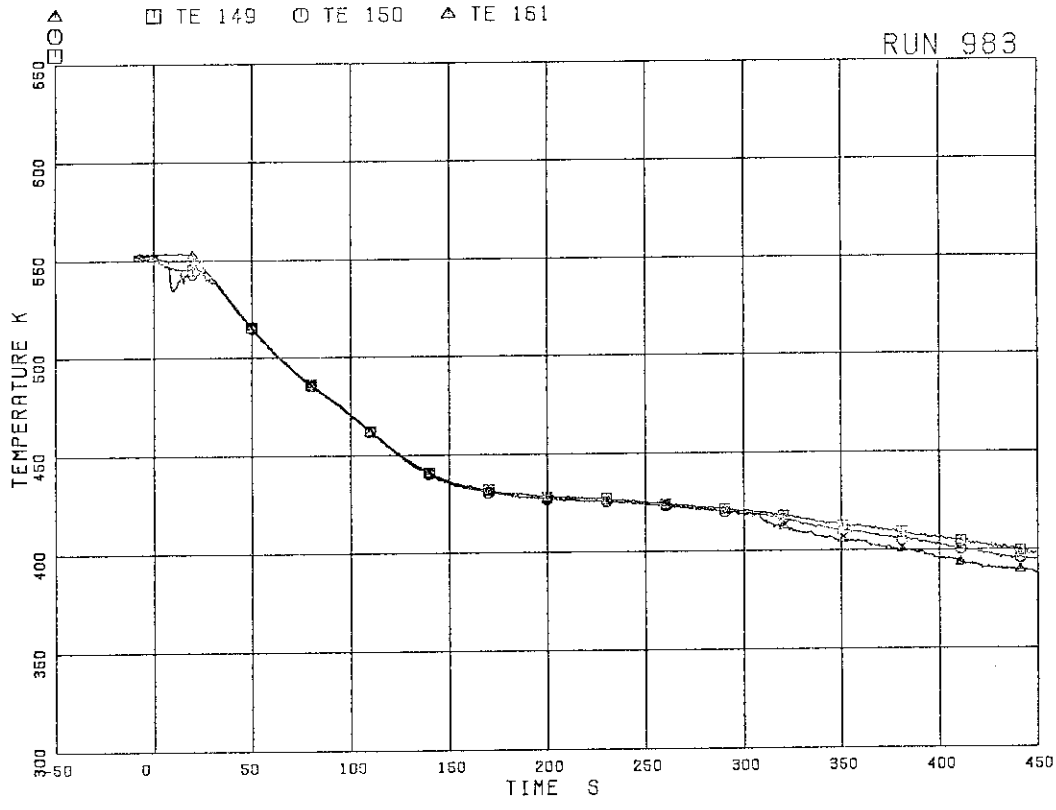

Fig. 5.80 Fluid temperatures at JP-3,4 outlet

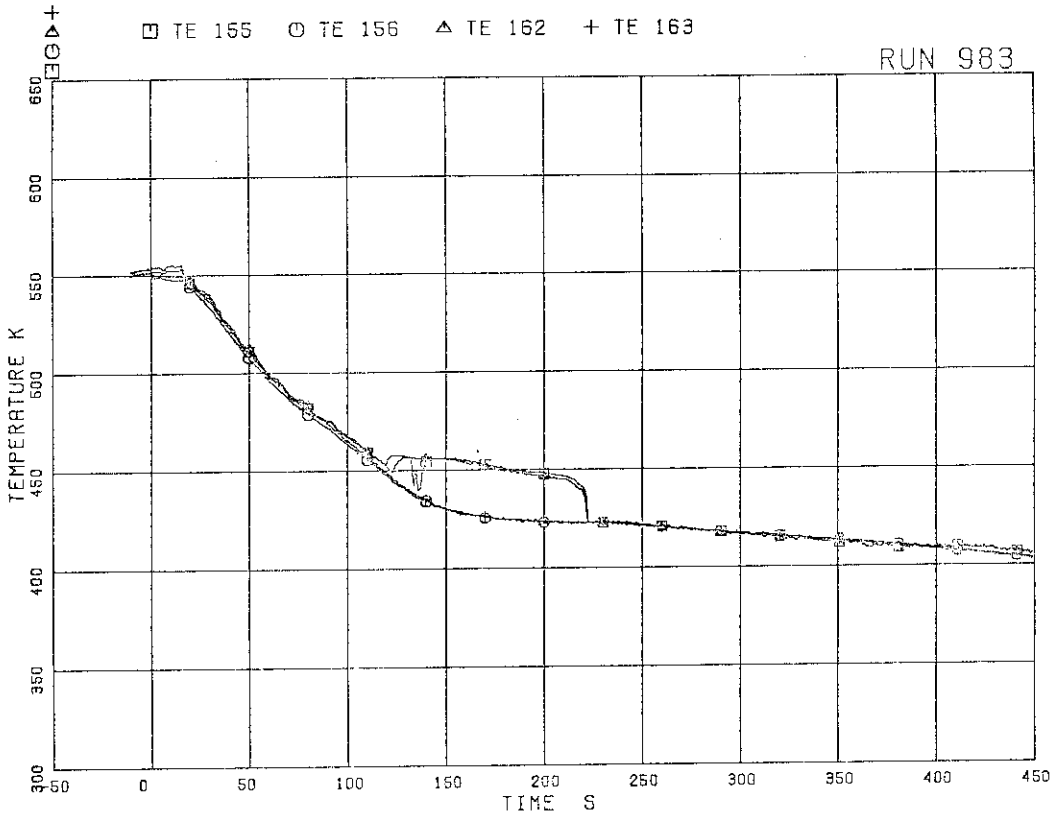

Fig. 5.81 Fluid temperatures near breaks A and B

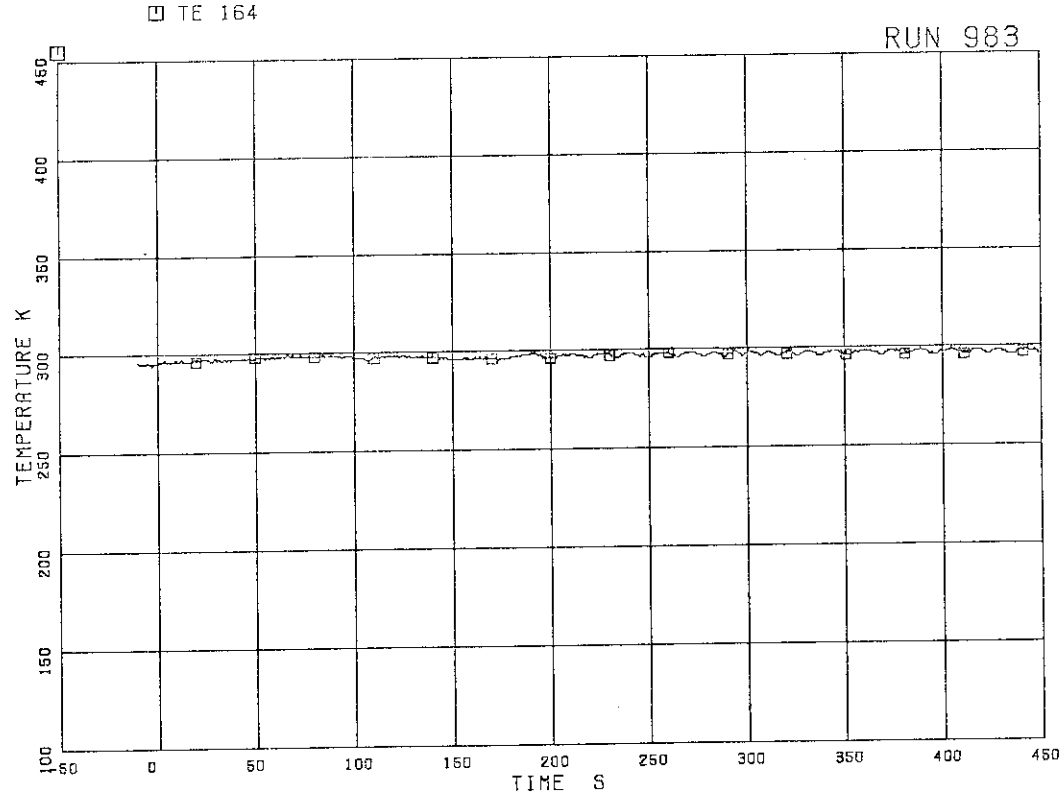

Fig. 5.82 Feedwater temperature

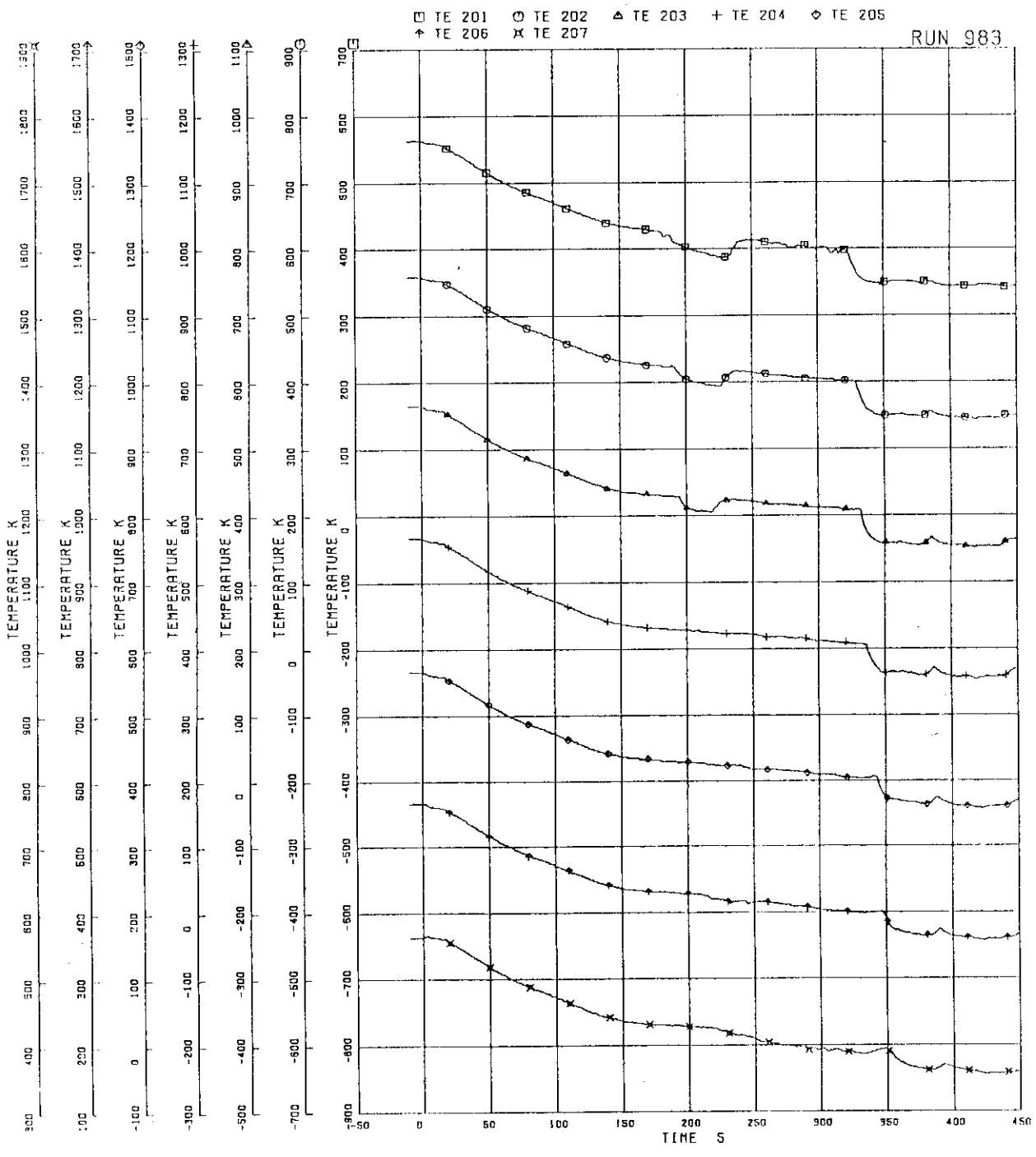

Fig. 5.83 Surface temperatures of fuel rod A11

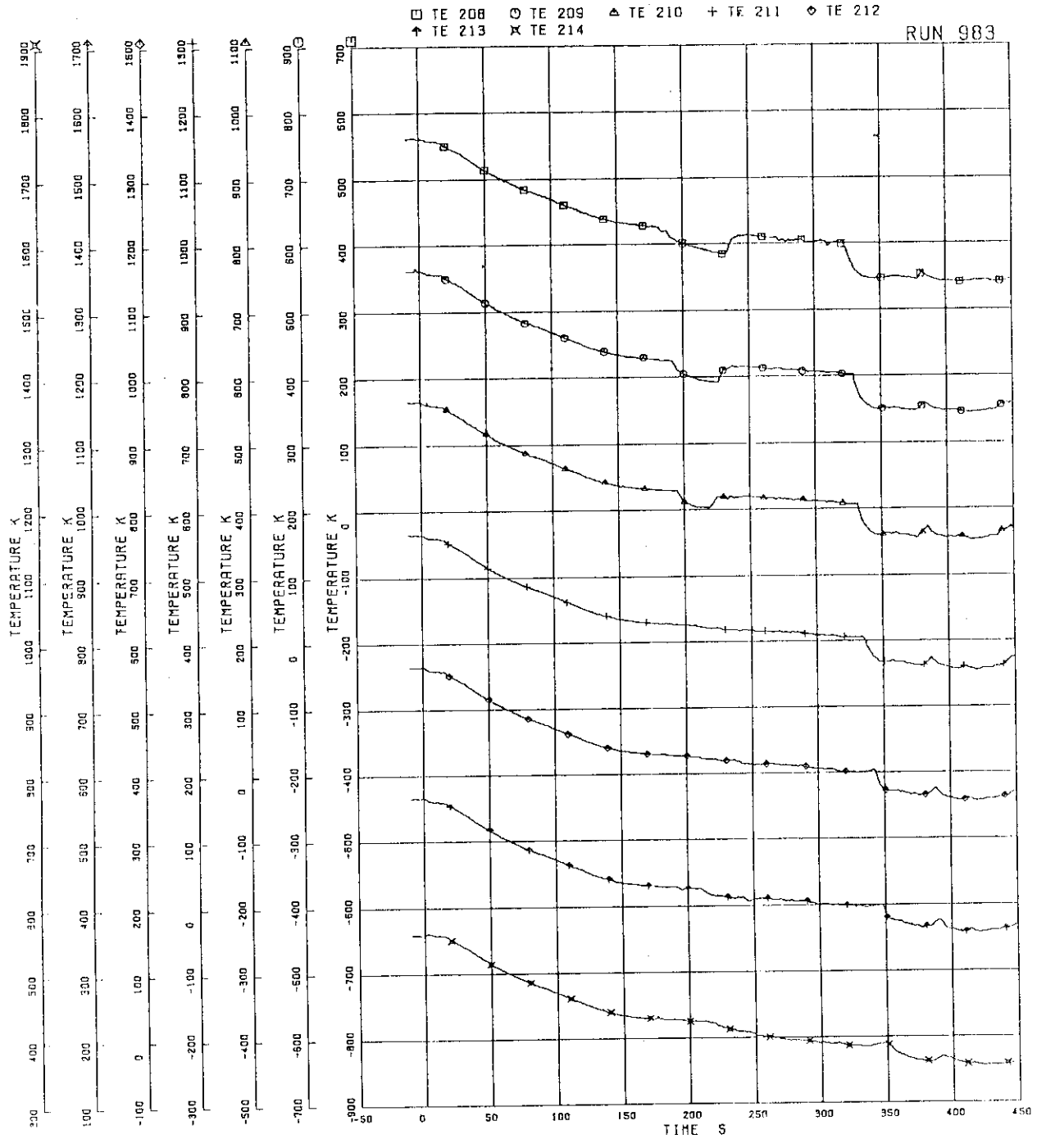

Fig. 5.84 Surface temperatures of fuel rod A12

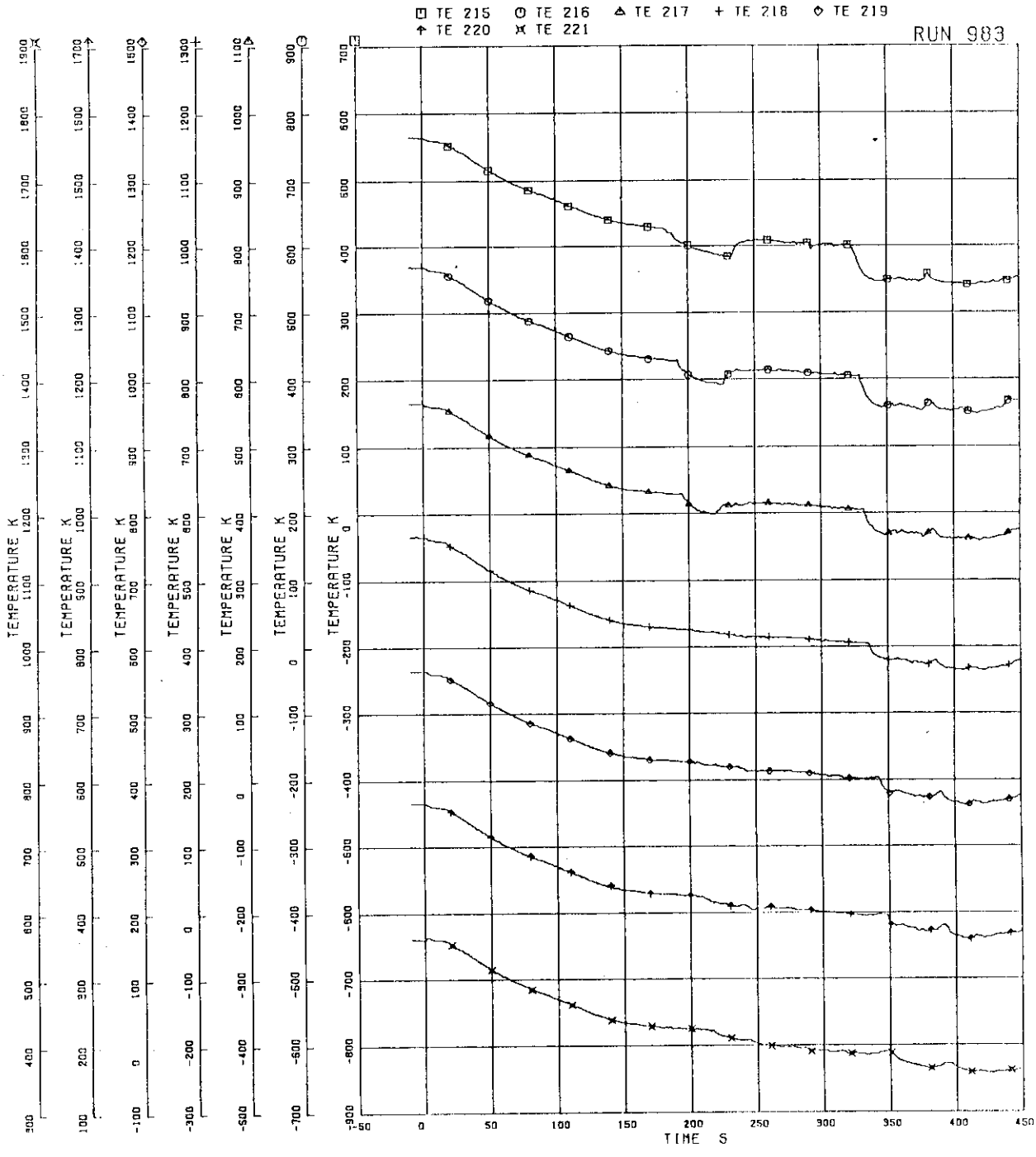

Fig. 5.85 Surface temperatures of fuel rod A13

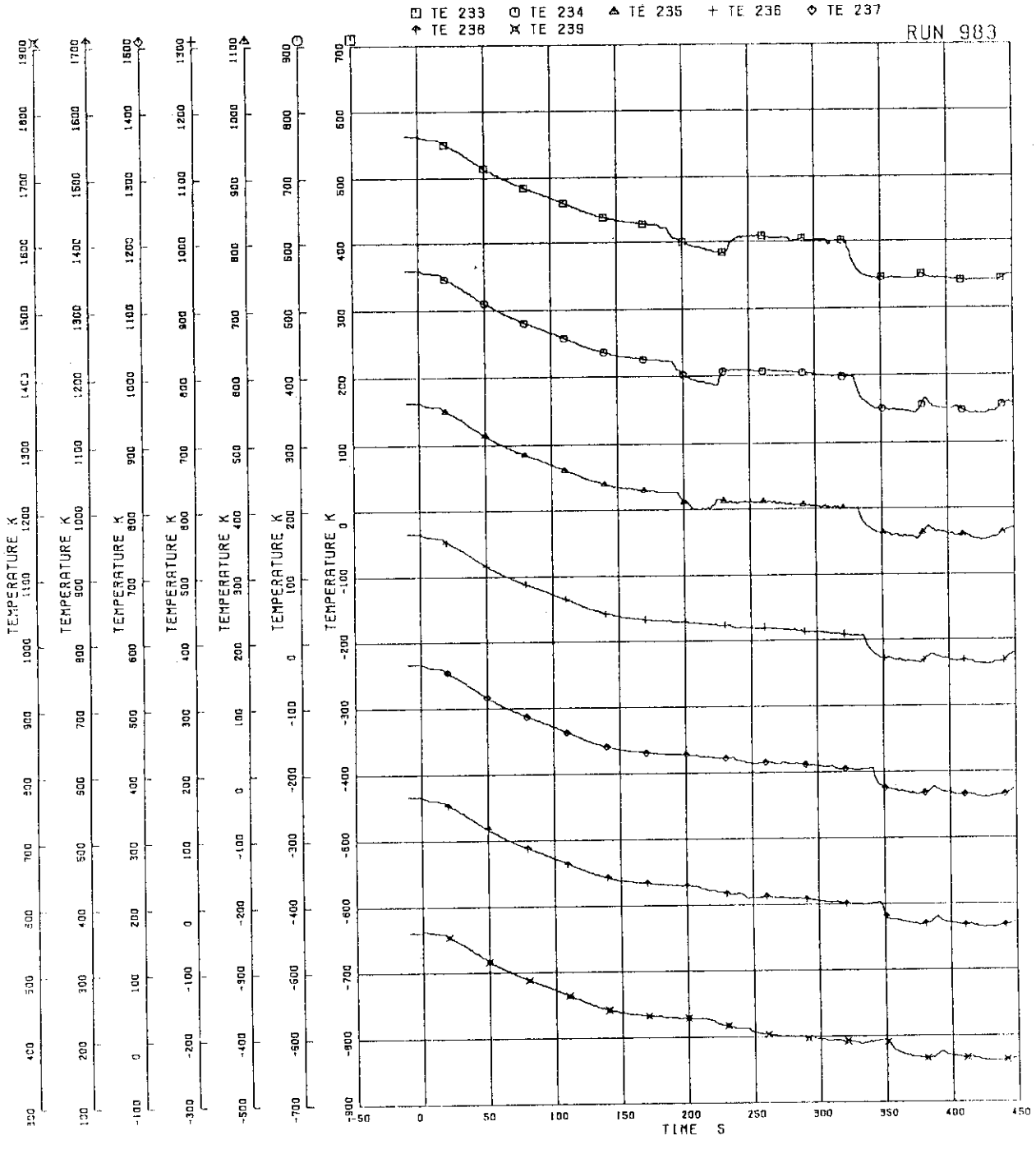

Fig. 5.86 Surface temperatures of fuel rod A22

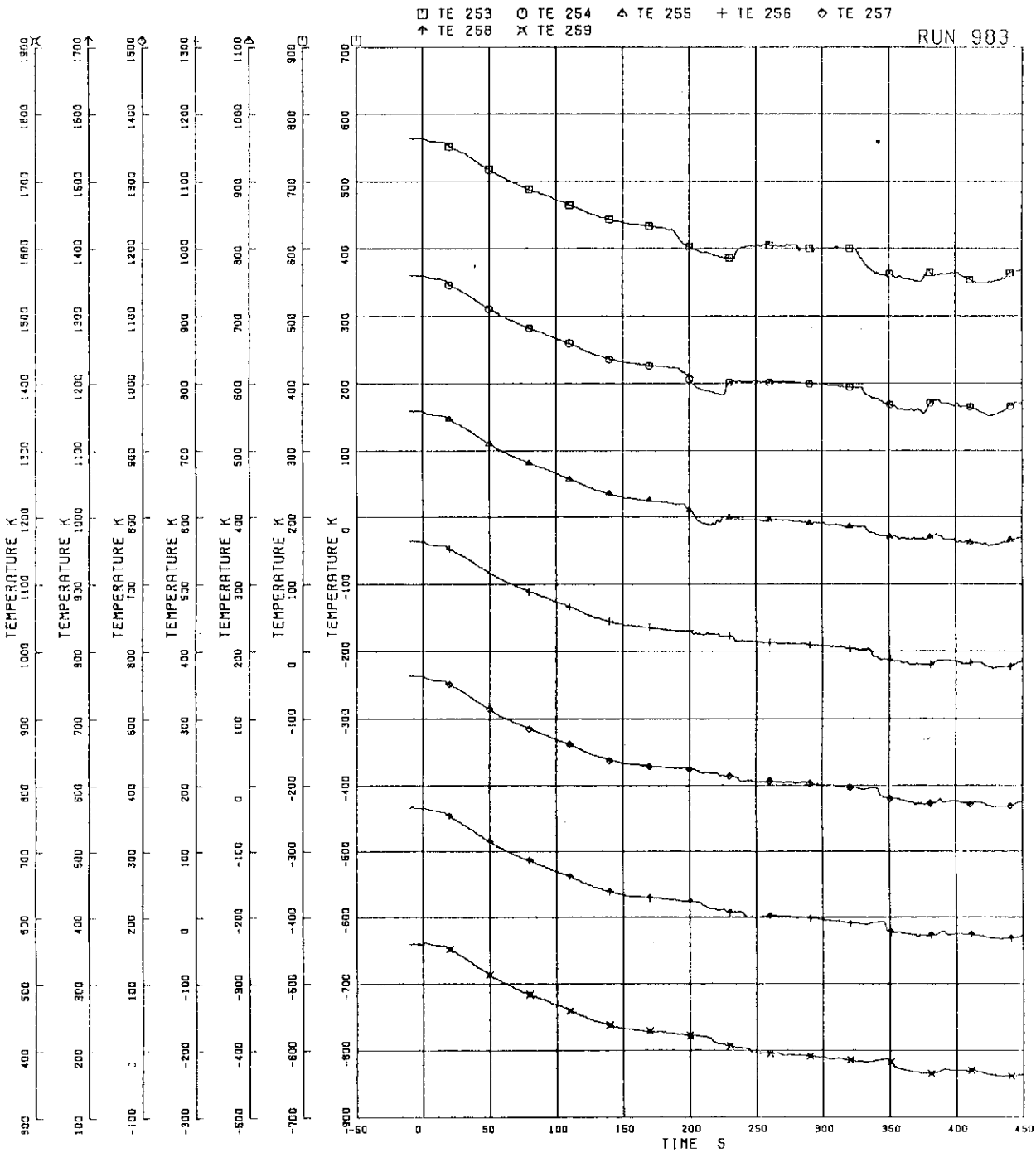

Fig. 5.87 Surface temperatures of fuel rod A33

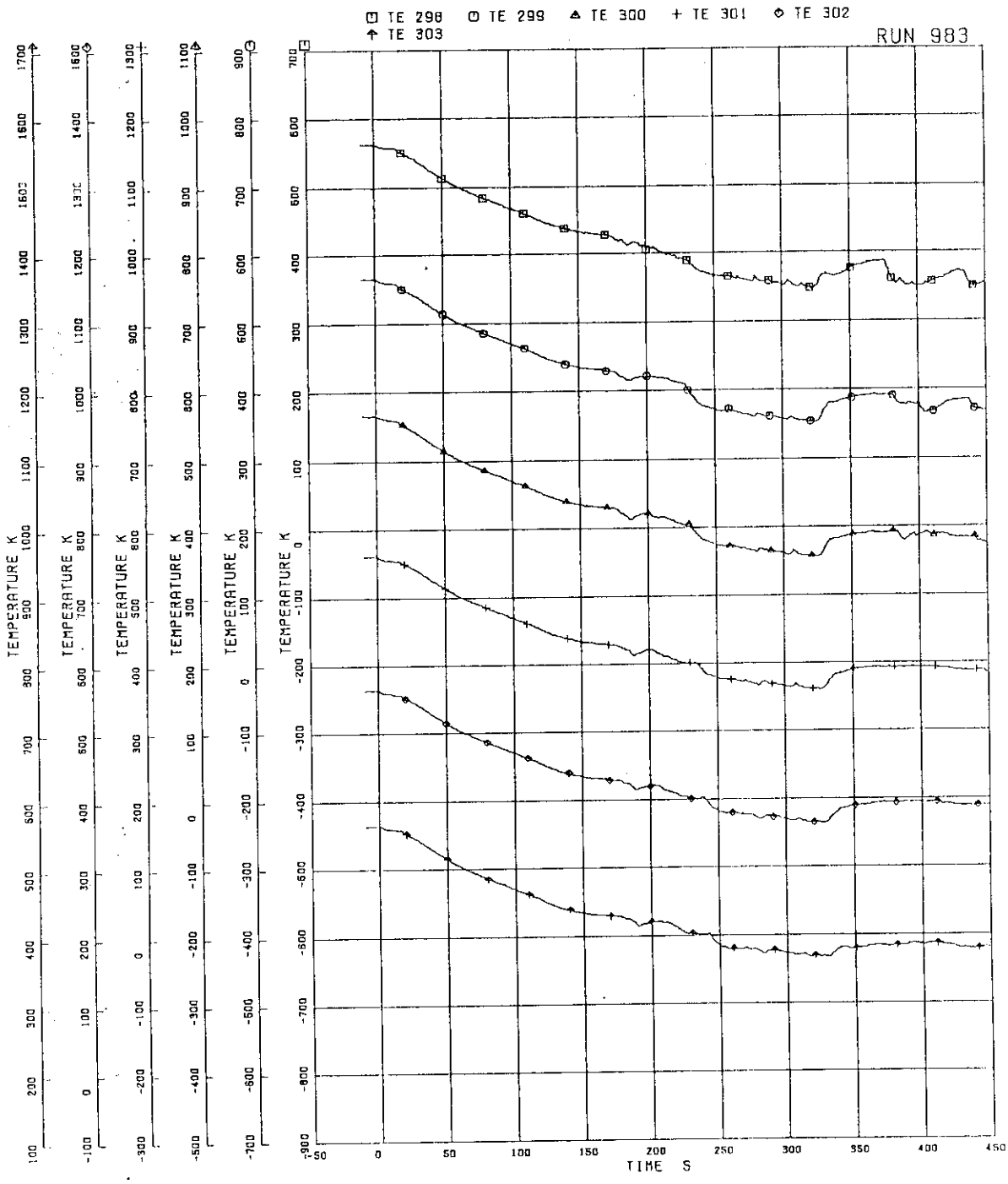

Fig. 5.88 Surface temperatures of fuel rod A77

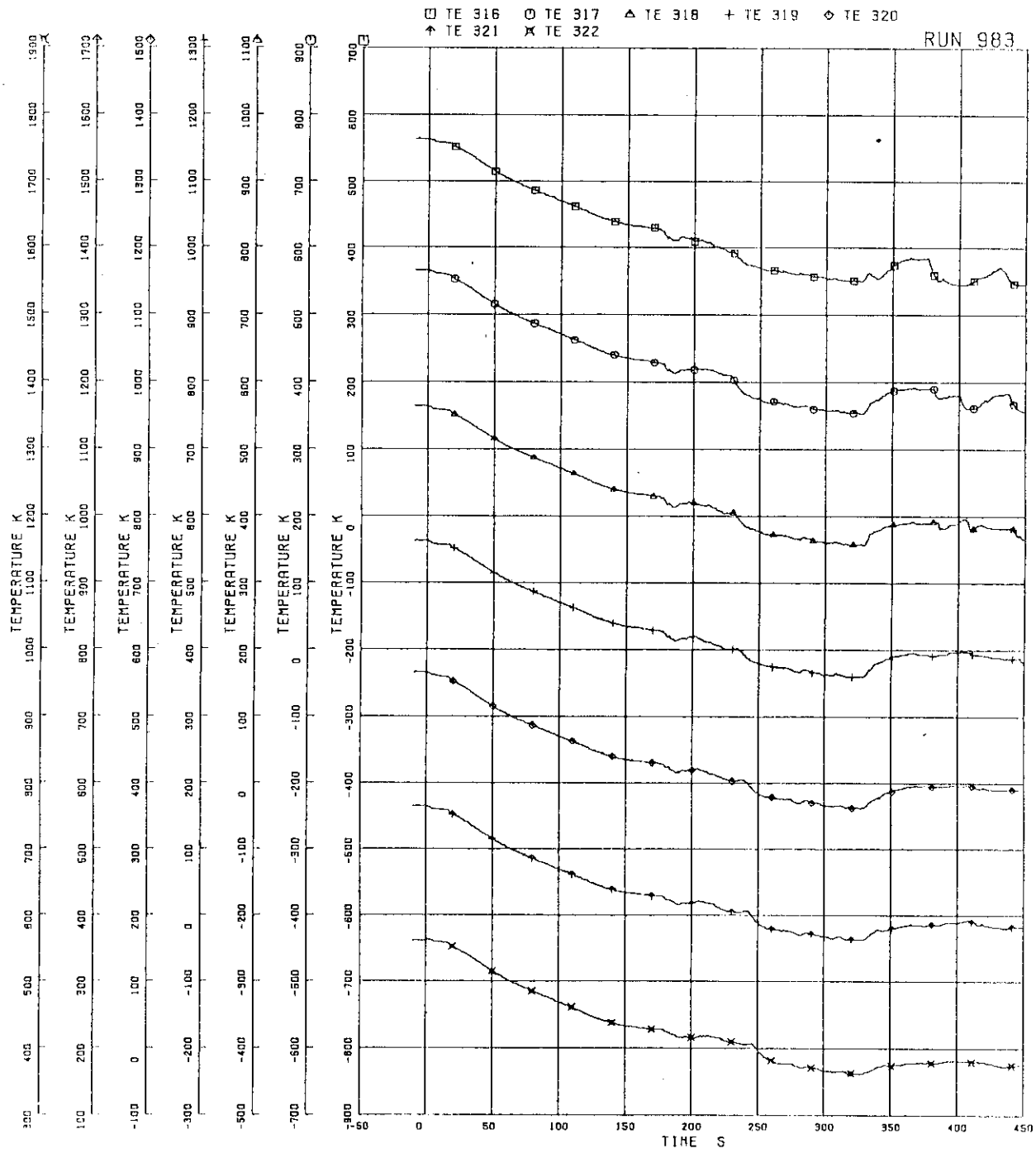

Fig. 5.89 Surface temperatures of fuel rod A87

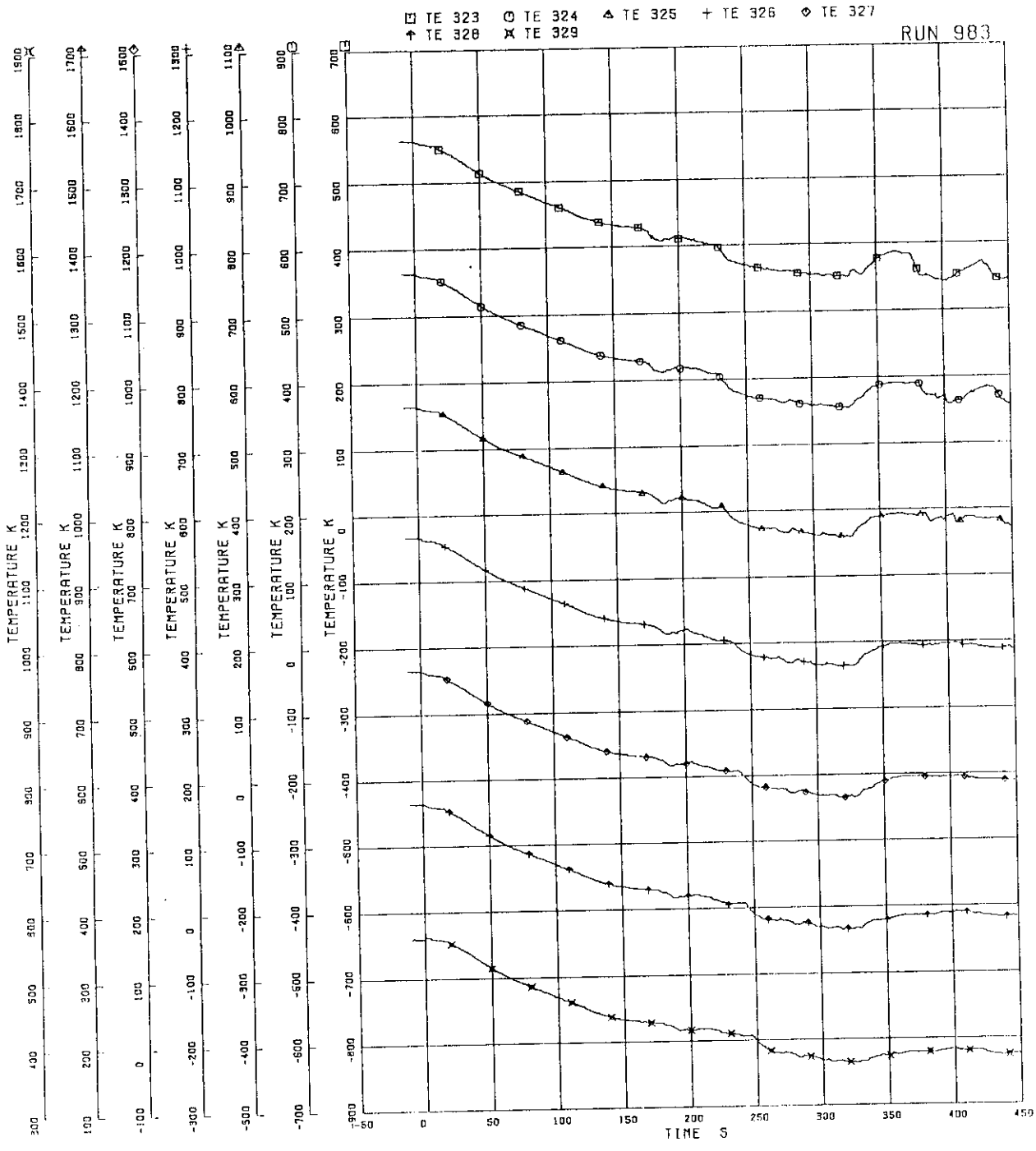

Fig. 5.90 Surface temperatures of fuel rod A88

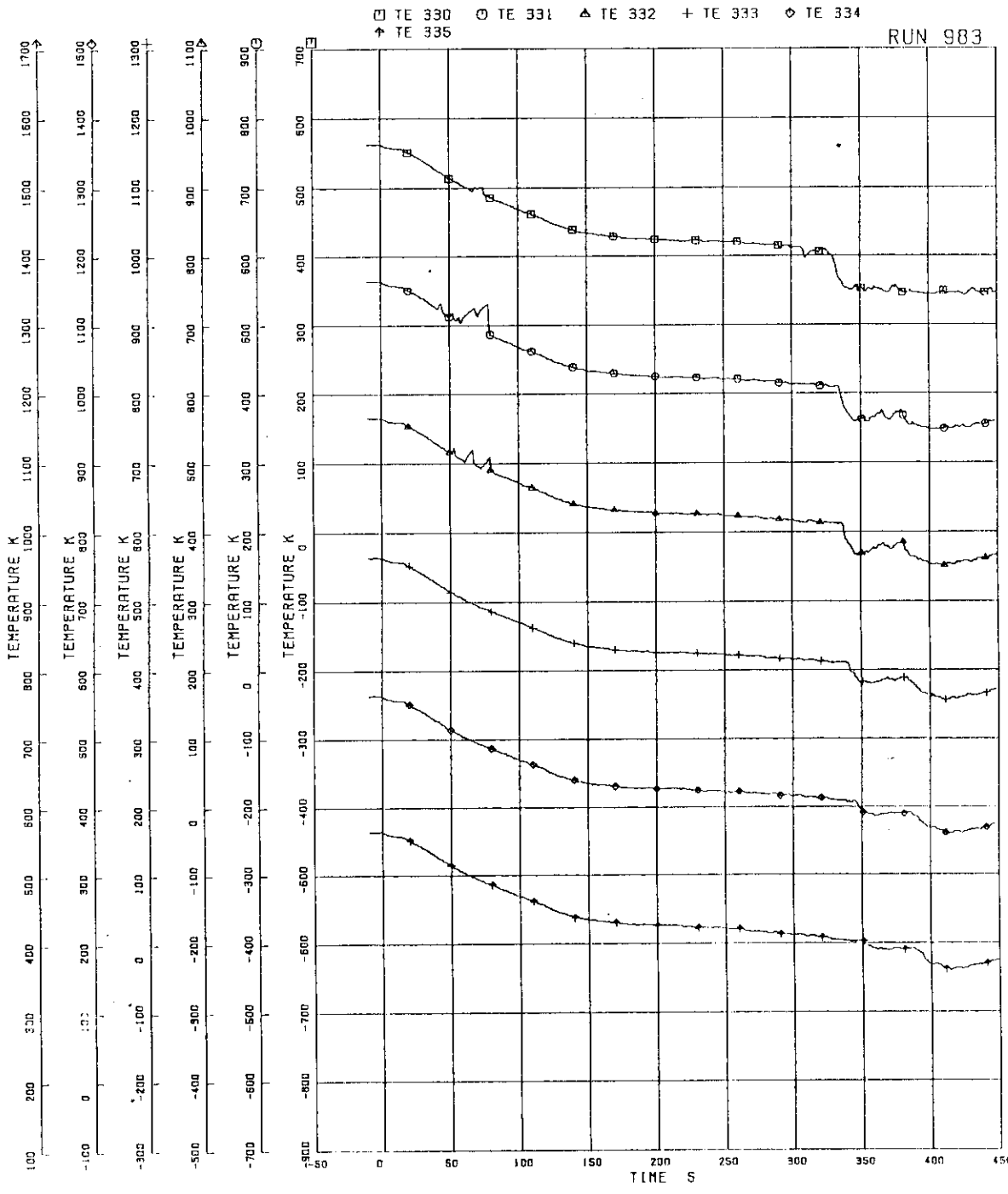

Fig. 5.91 Surface temperatures of fuel rod B11

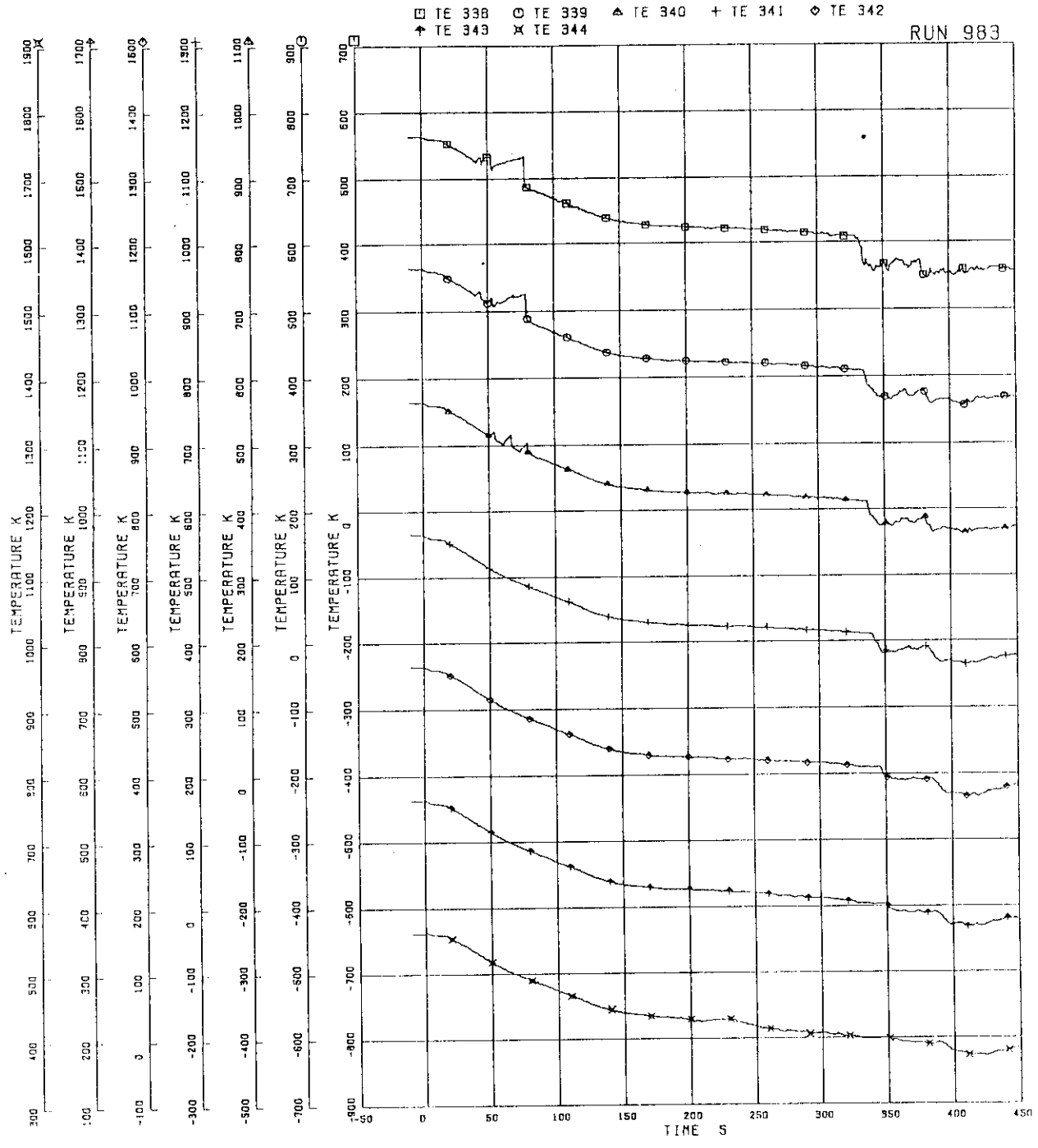

Fig. 5.92 Surface temperatures of fuel rod B22

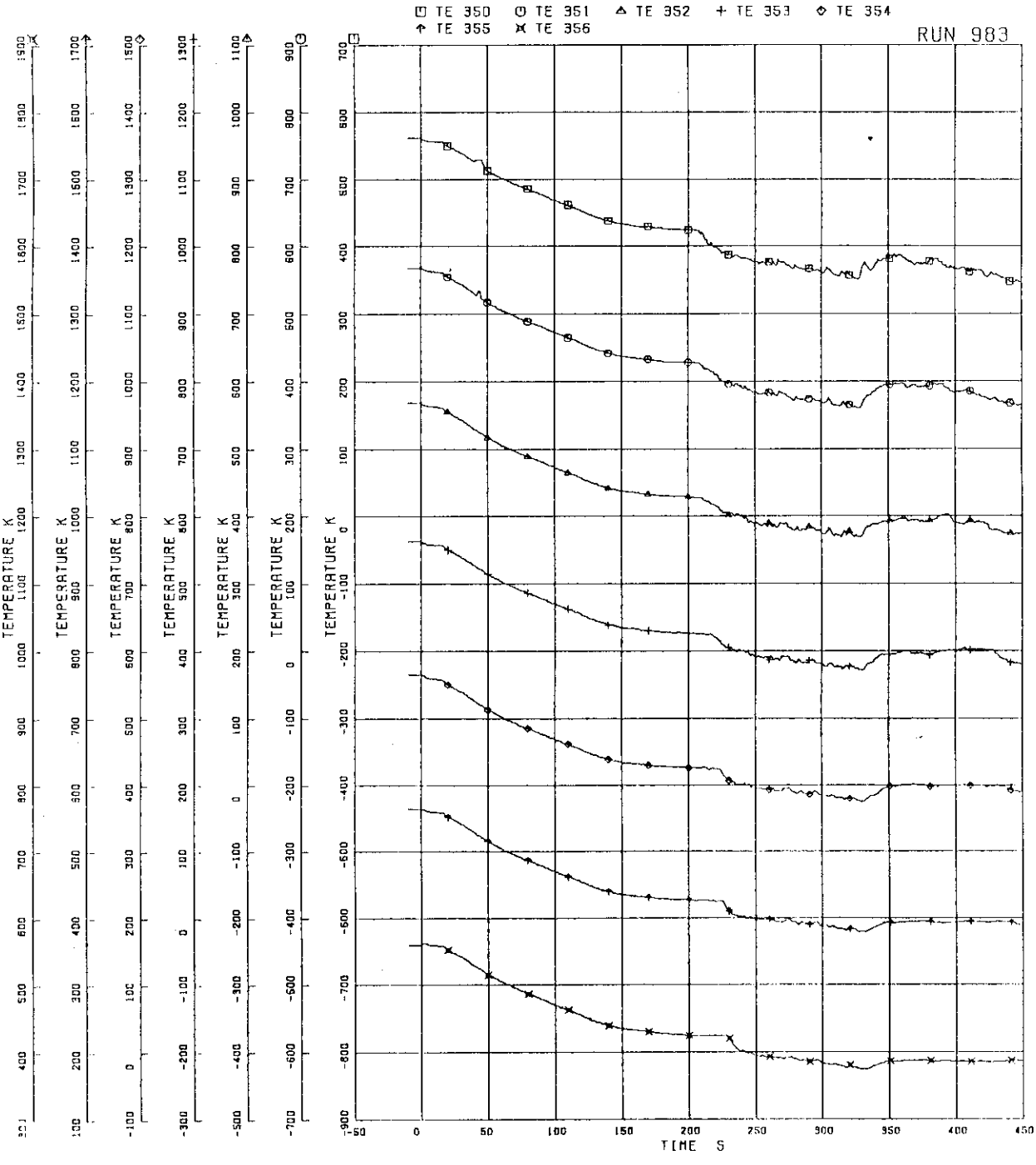

Fig. 5.93 Surface temperatures of fuel rod B77

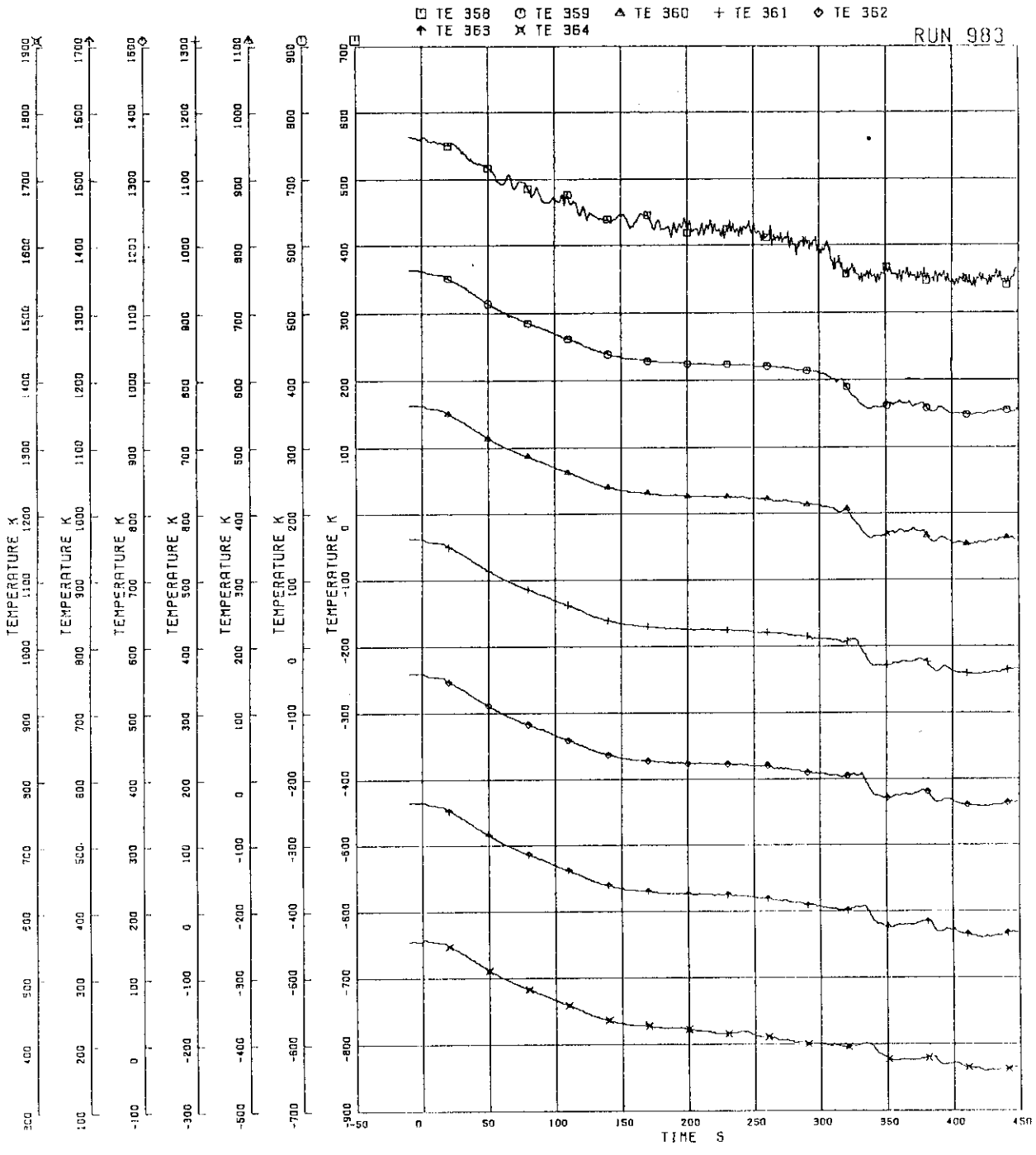

Fig. 5.94 Surface temperatures of fuel rod C11

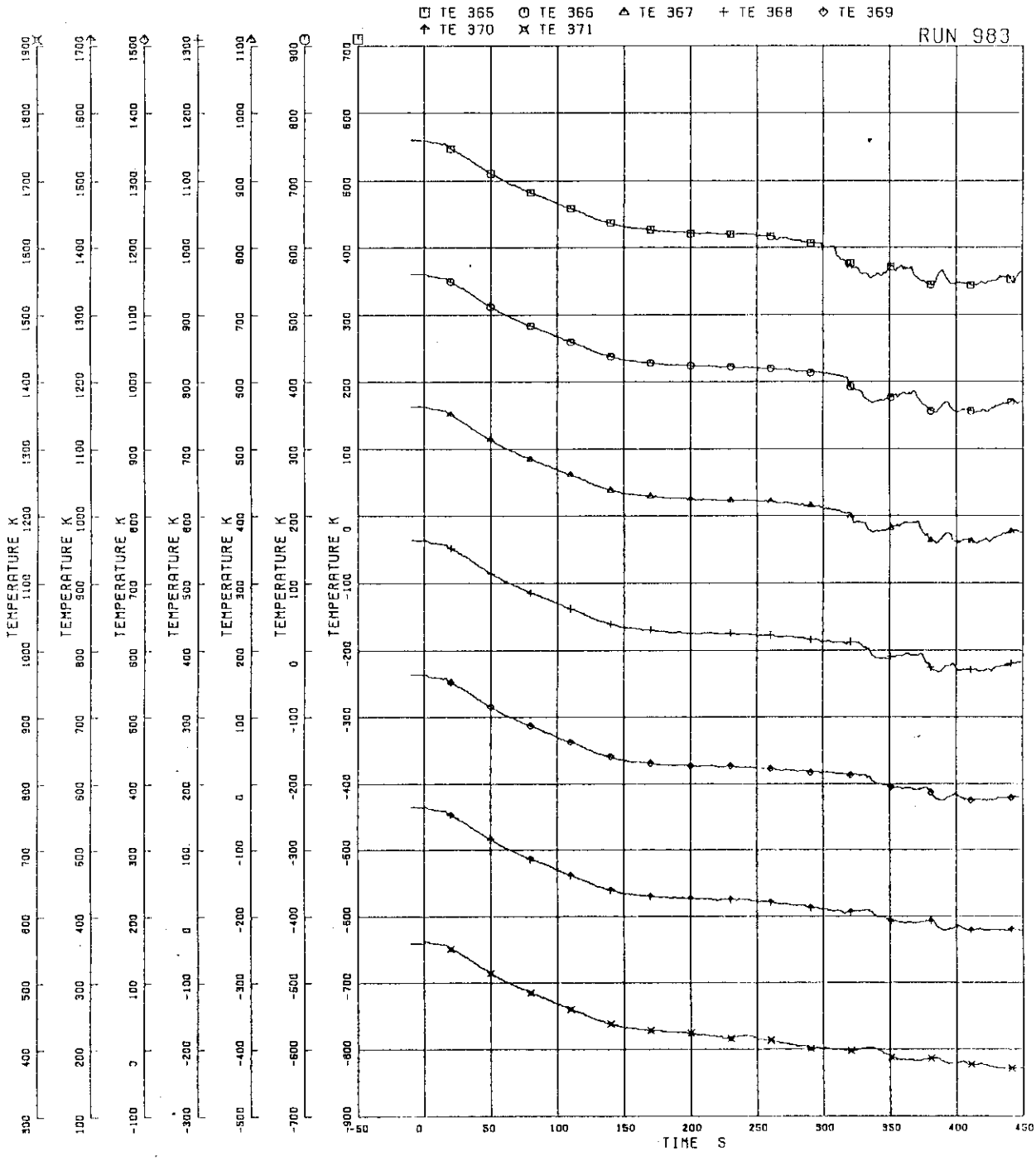

Fig. 5.95 Surface temperatures of fuel rod C13

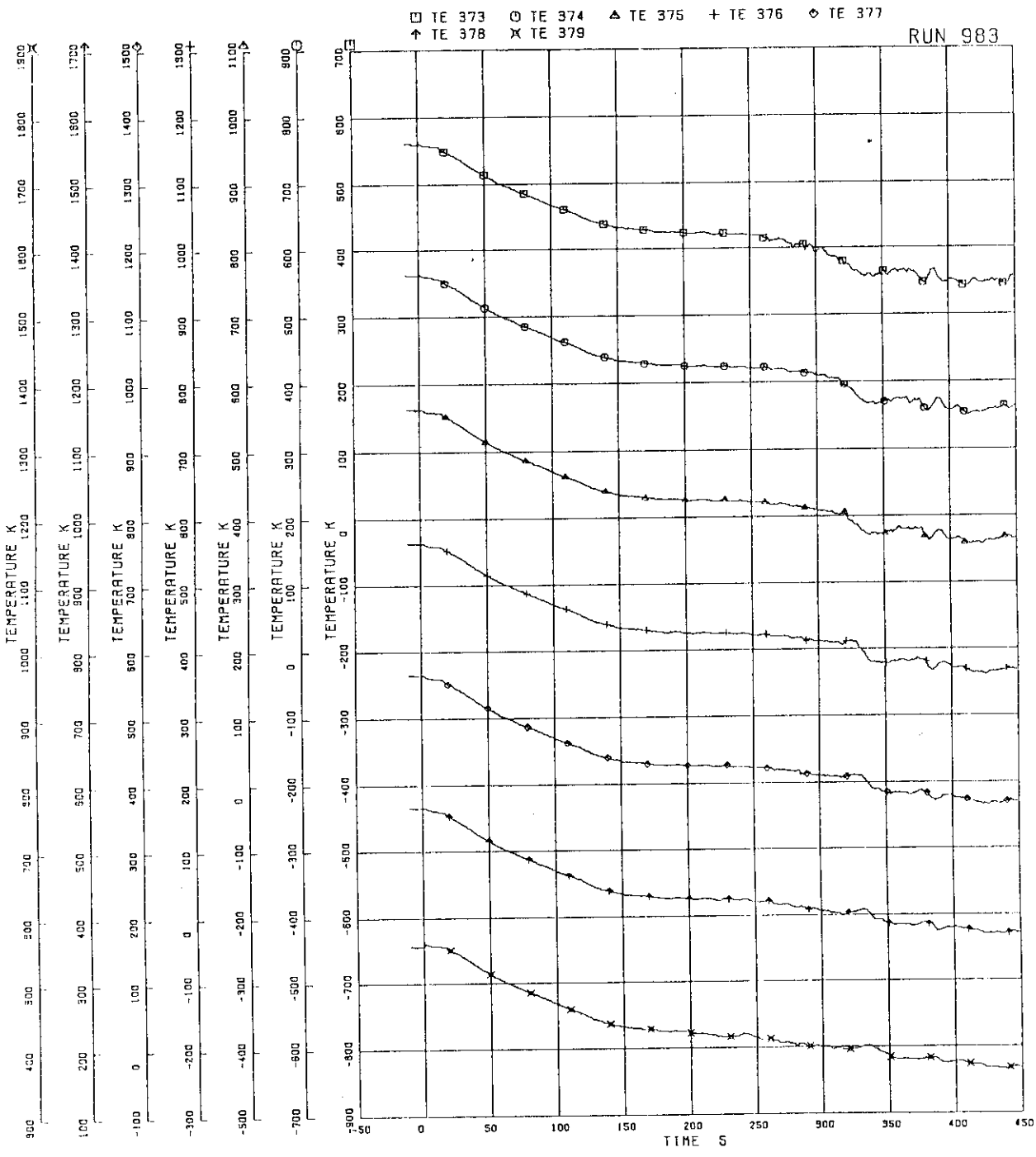

Fig. 5.96 Surface temperatures of fuel rod C22

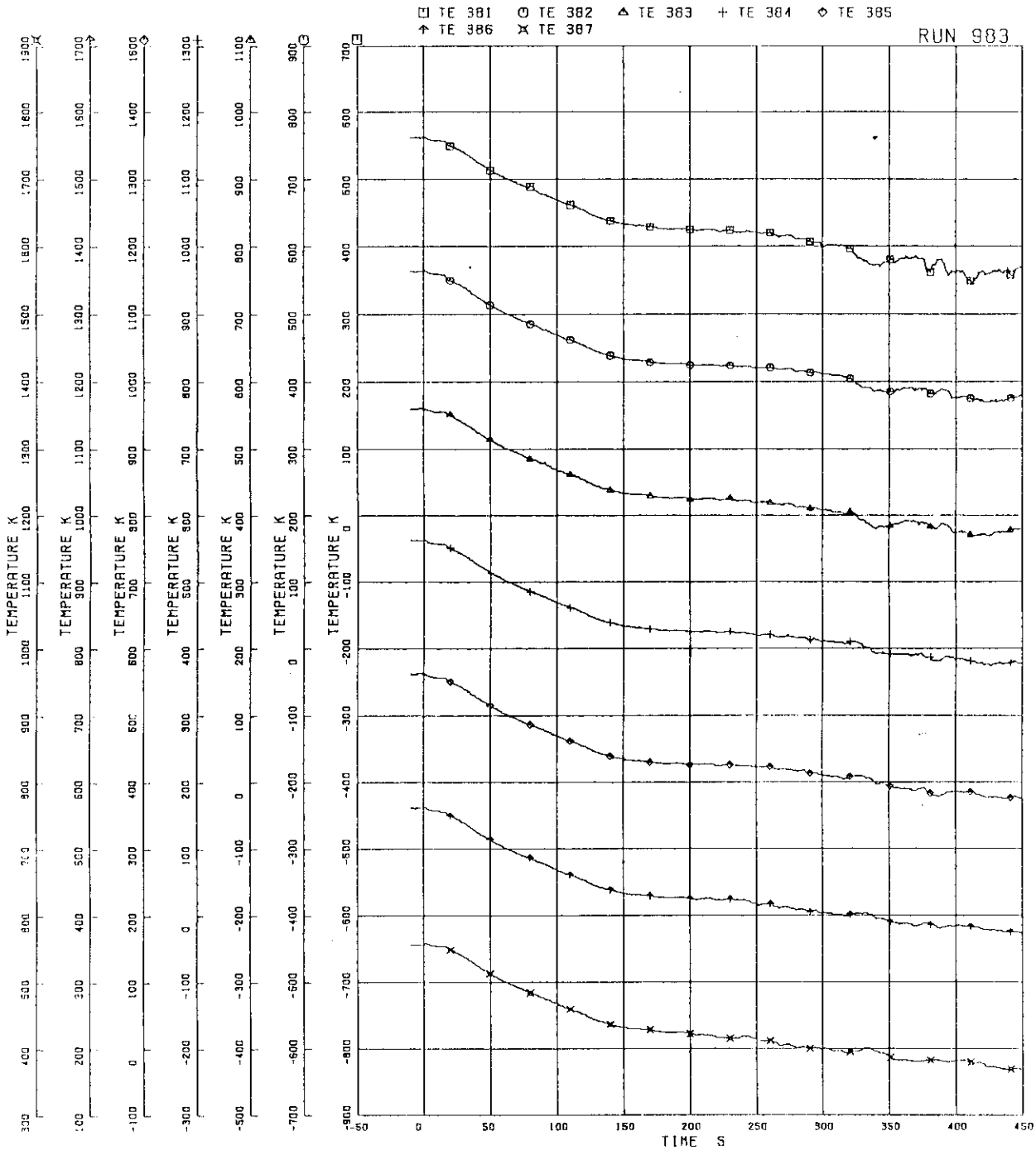

Fig. 5.97 Surface temperatures of fuel rod C33

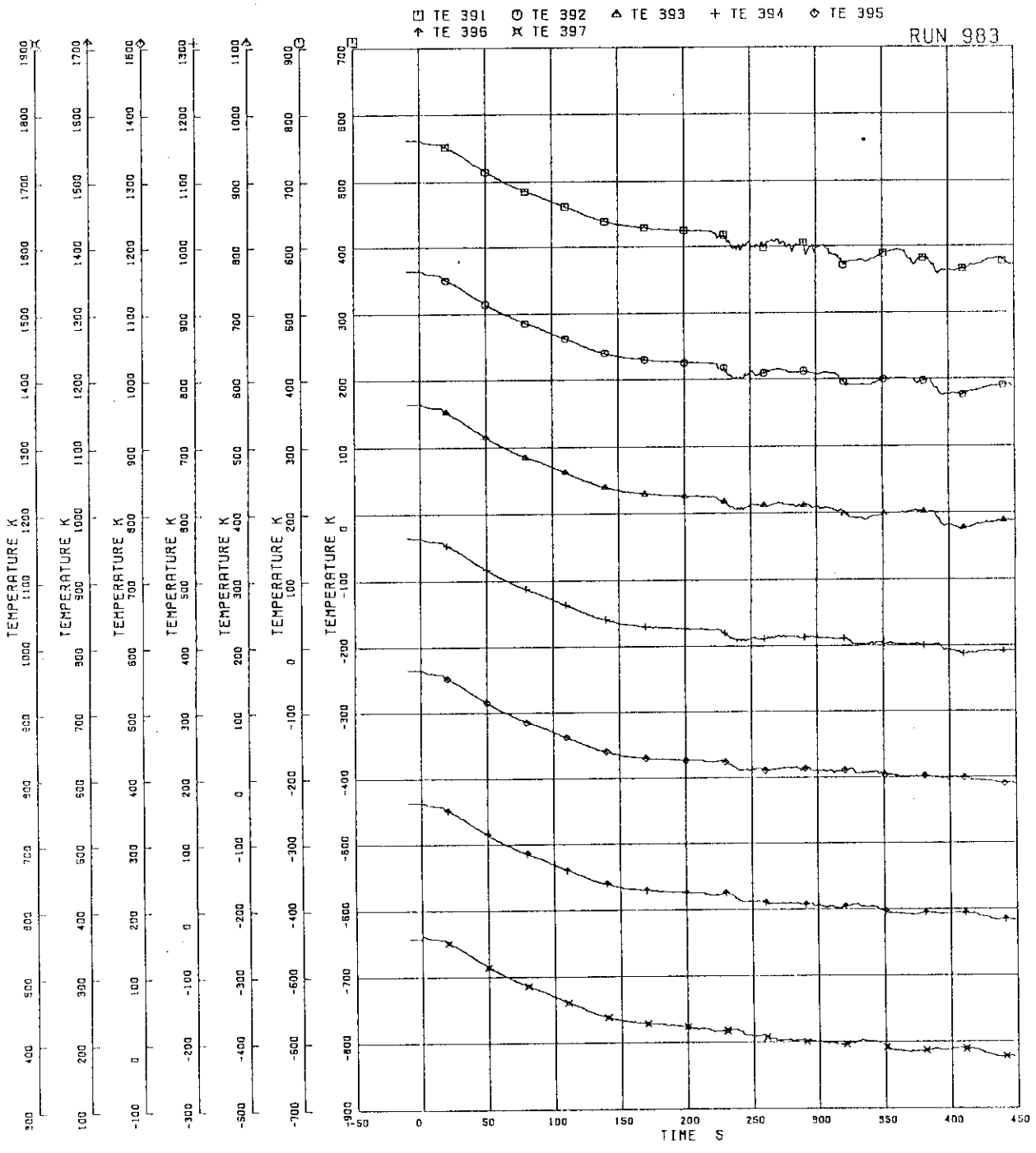

Fig. 5.98 Surface temperatures of fuel rod C77

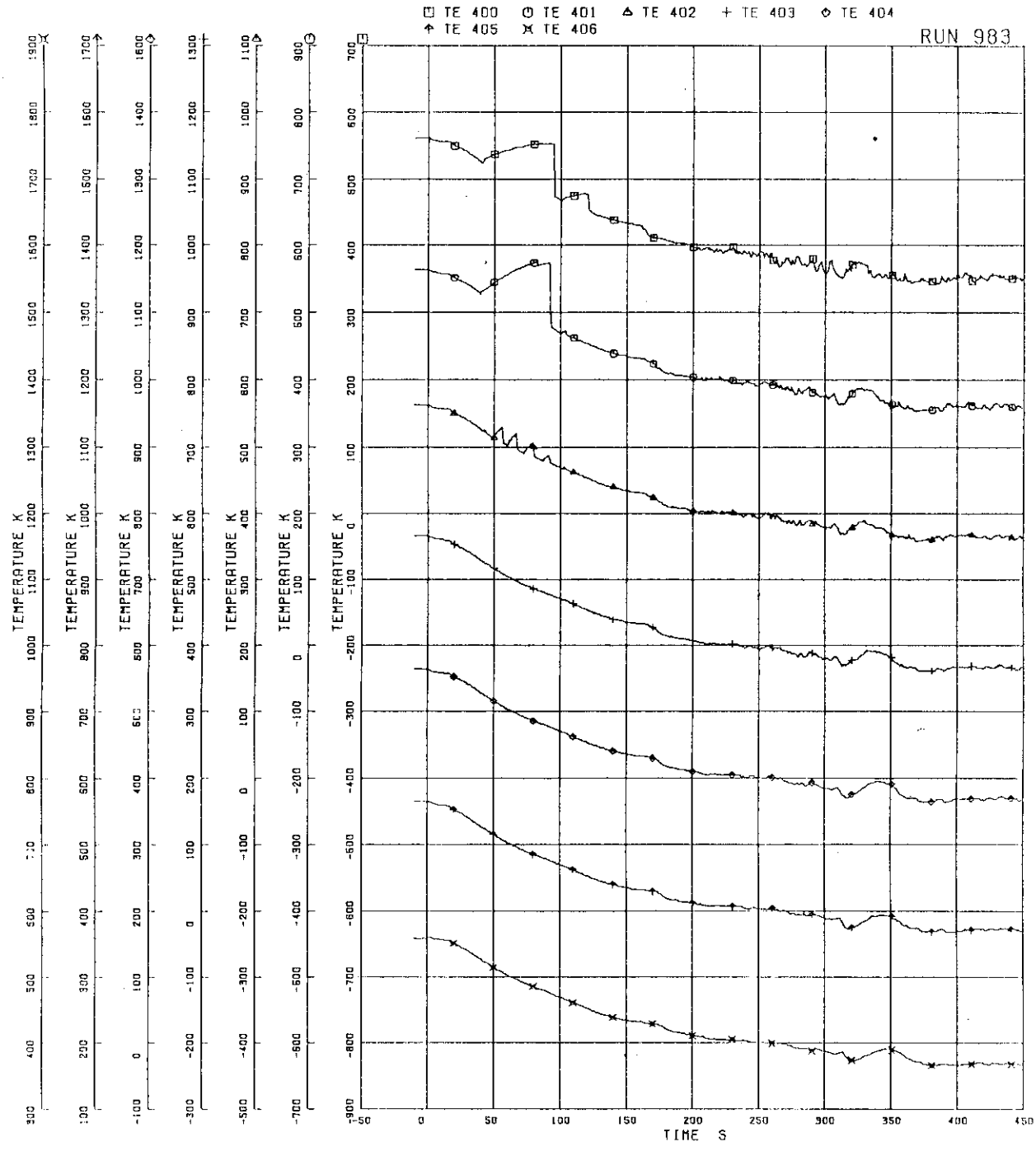

Fig. 5.99 Surface temperatures of fuel rod D22

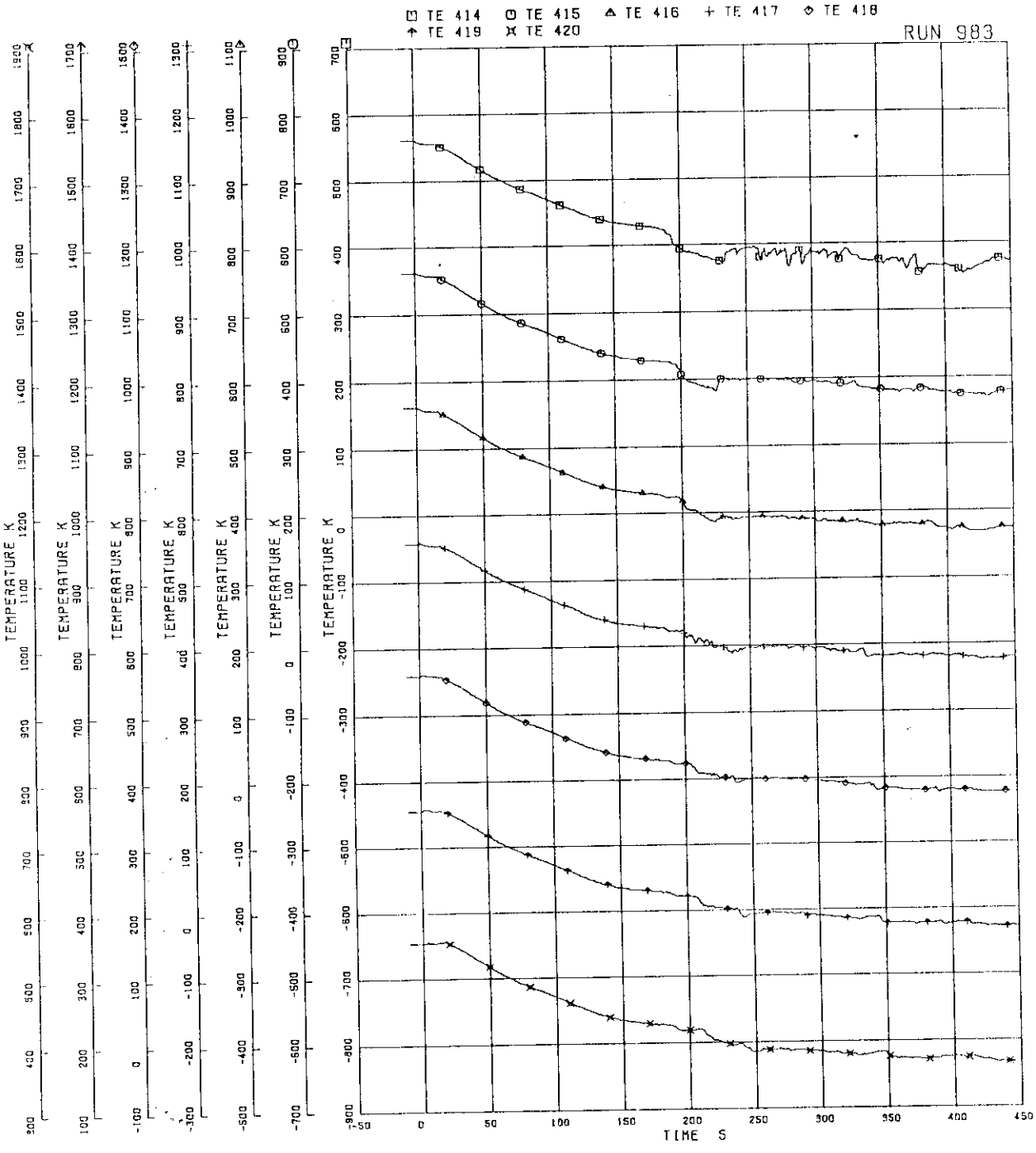

Fig. 5.100 Surface temperatures of water rod simulator A45

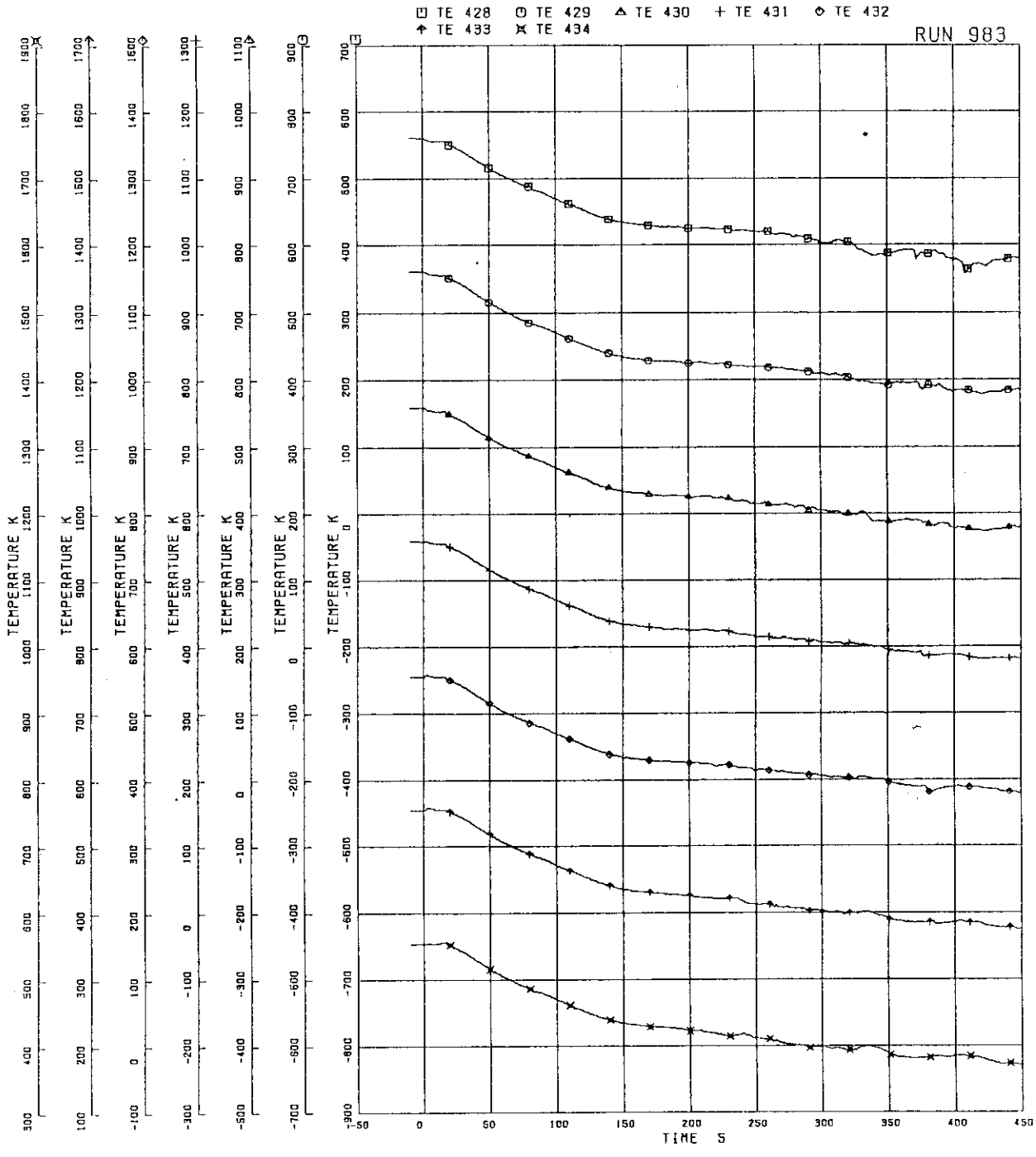

Fig. 5.101 Surface temperatures of water rod simulator C45

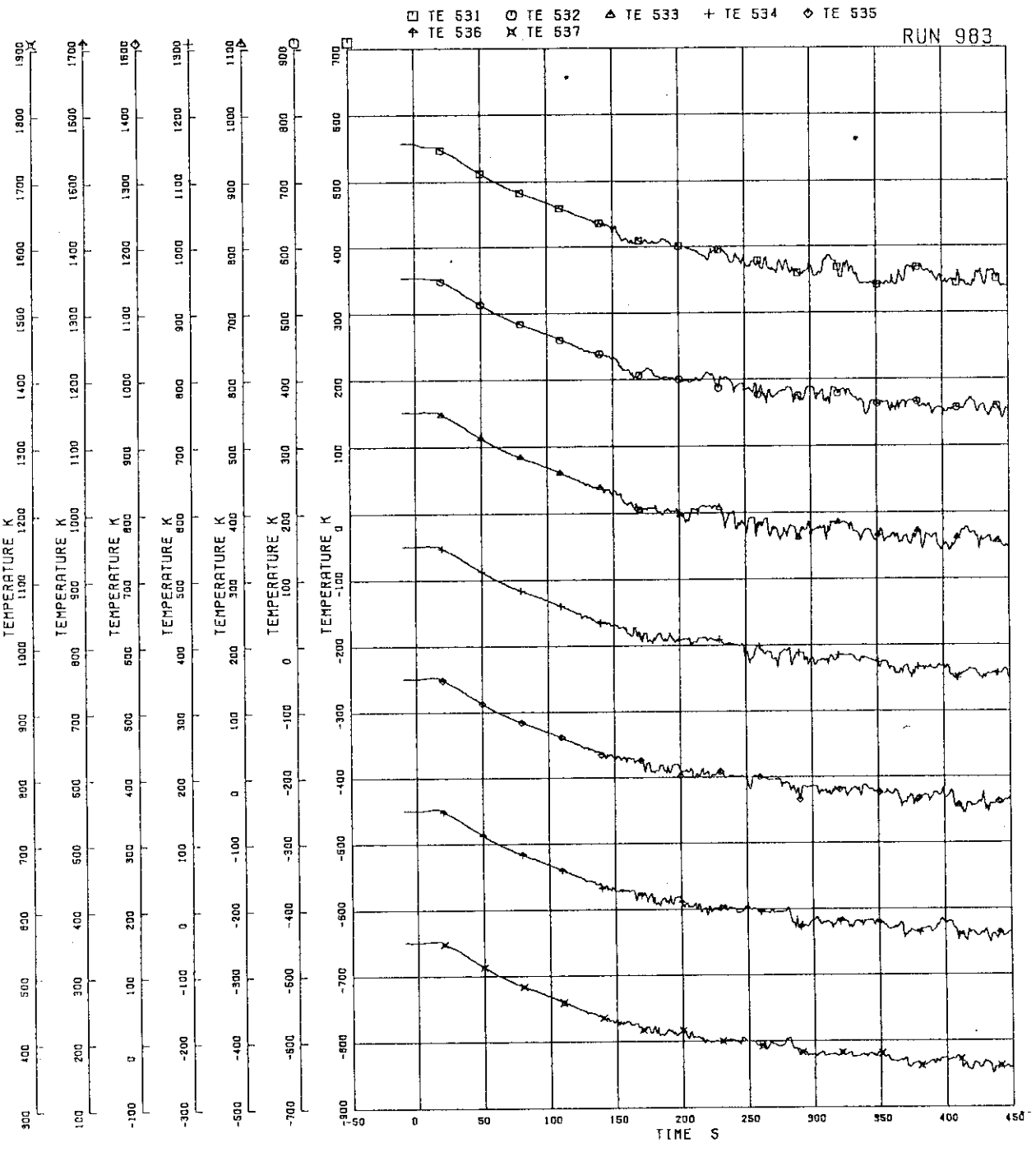

Fig. 5.102 Outer surface temperatures of channel box A

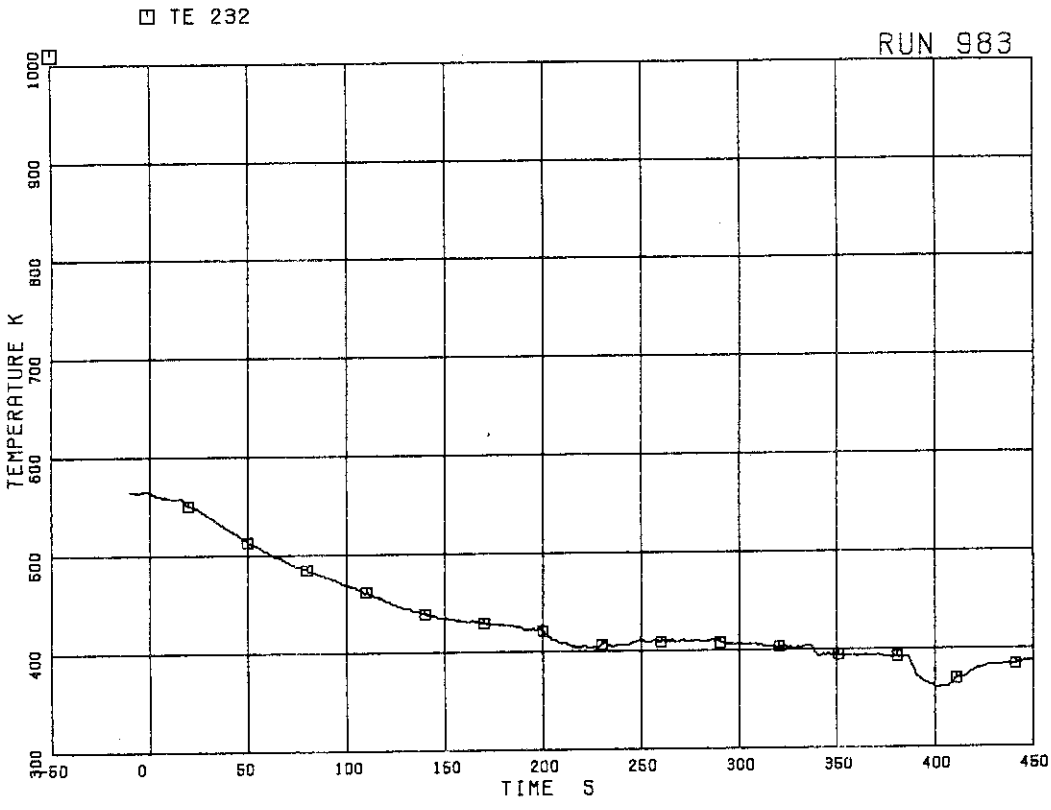

Fig. 5.103 Surface temperature of fuel rod A17 at position 4

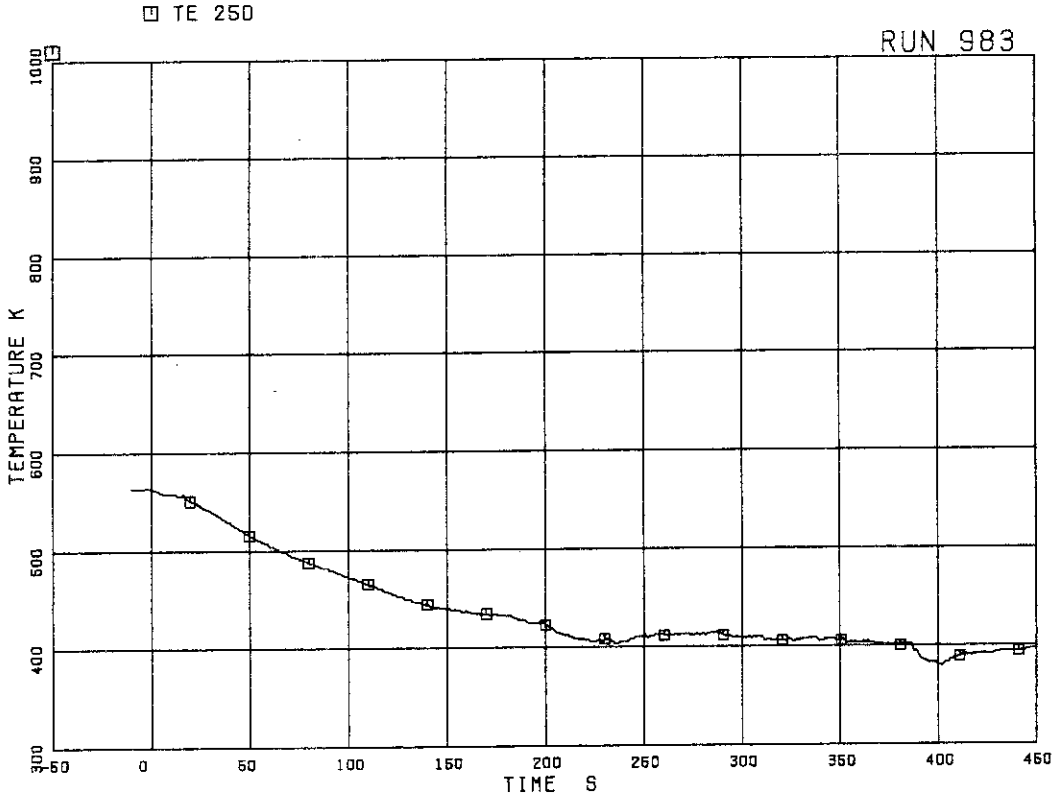

Fig. 5.104 Surface temperature of fuel rod A28 at position 4

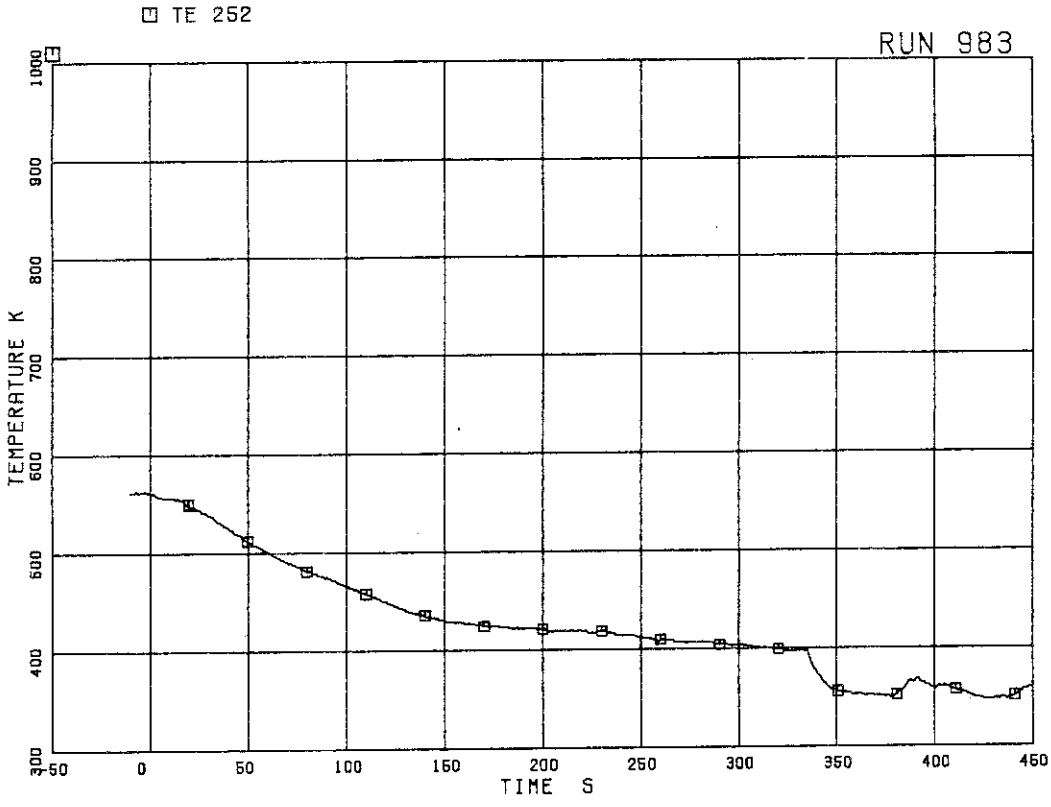

Fig. 5.105 Surface temperature of fuel rod A31 at position 4

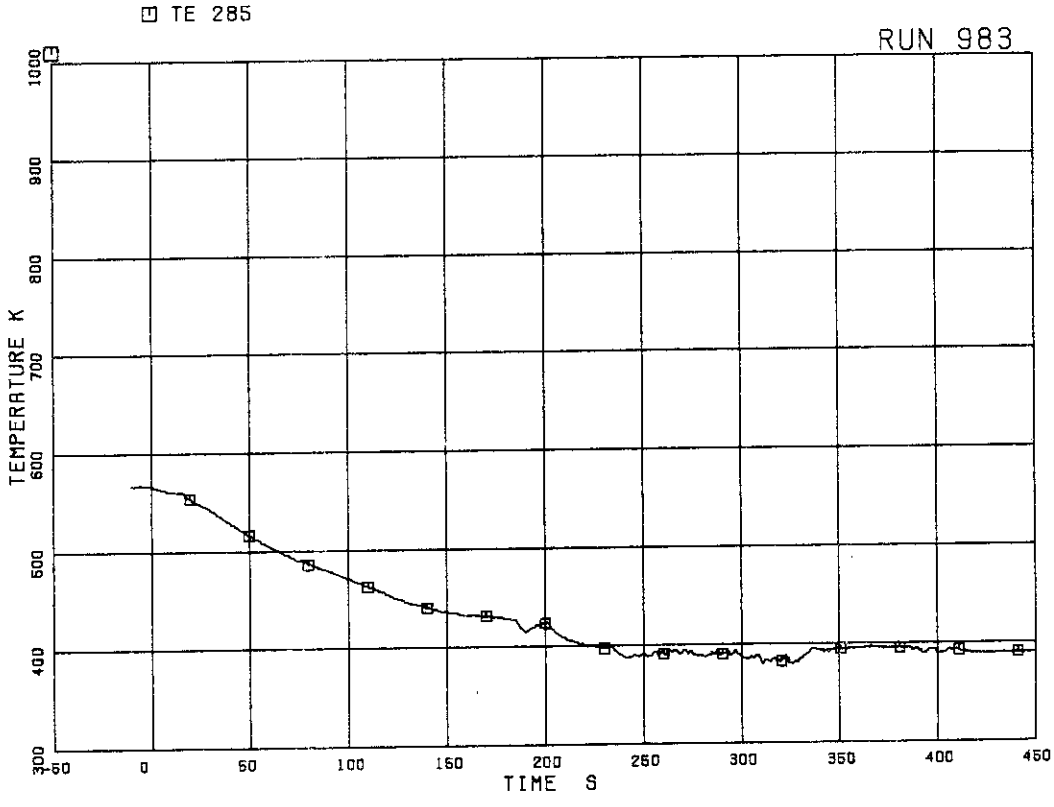

Fig. 5.106 Surface temperature of fuel rod A57 at position 4

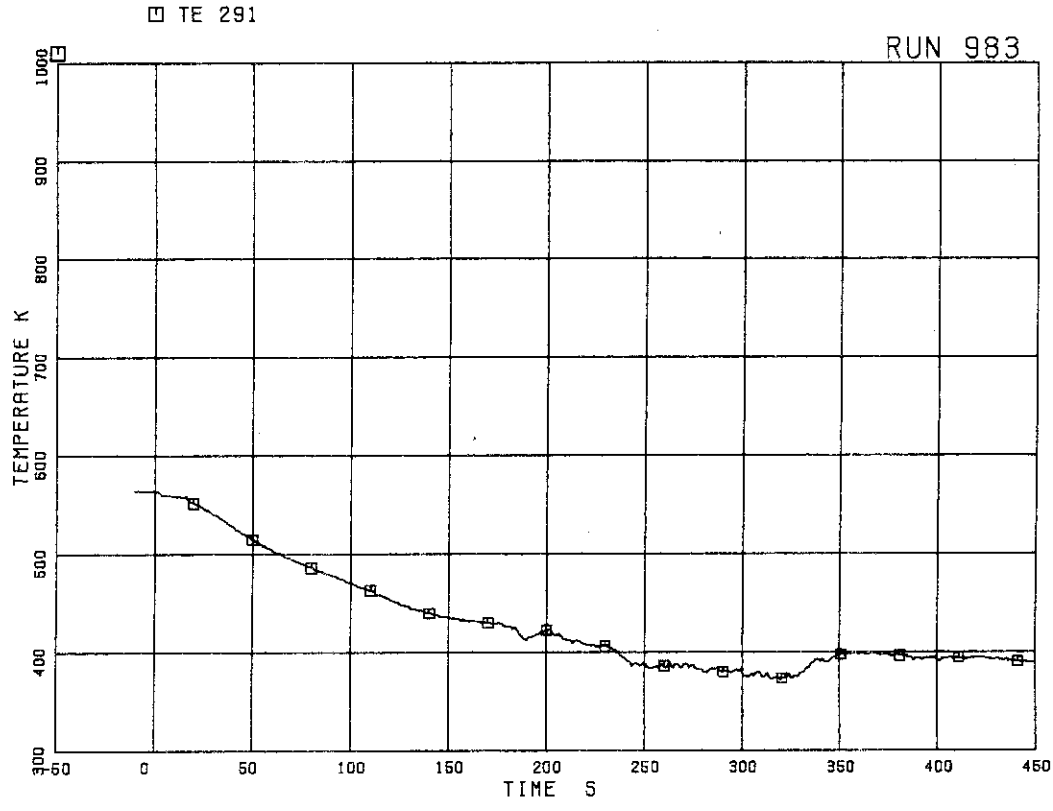

Fig. 5.107 Surface temperature of fuel rod A68 at position 4

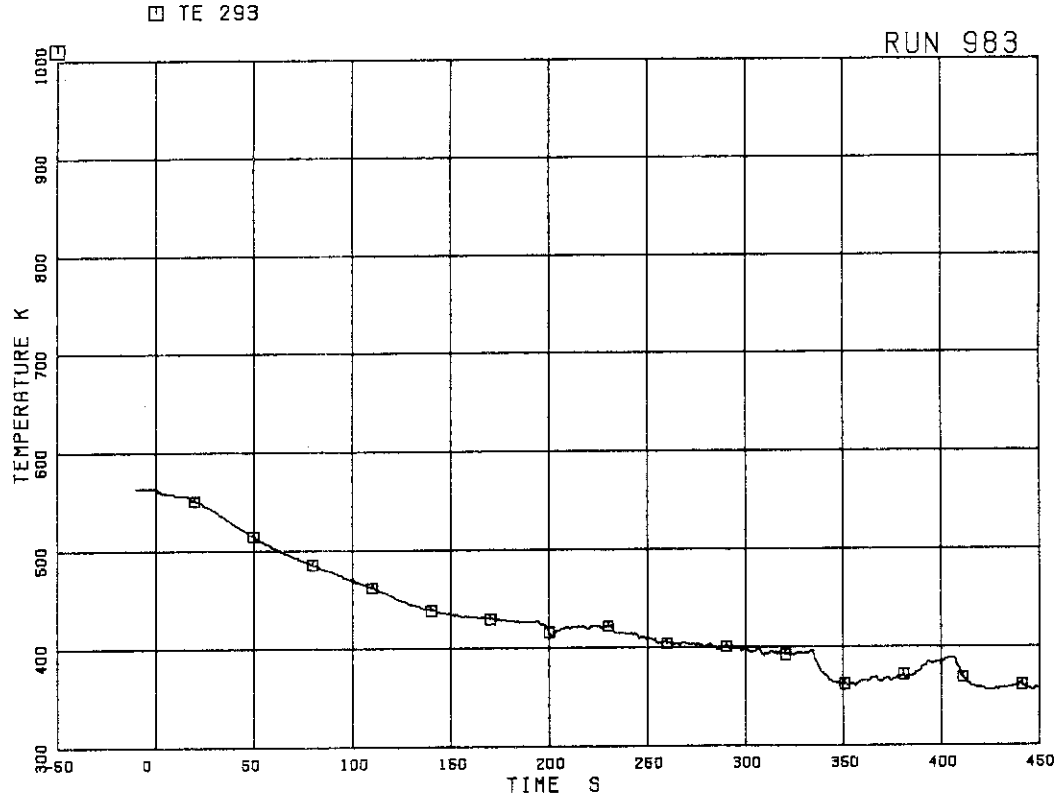

Fig. 5.108 Surface temperature of fuel rod A71 at position 4

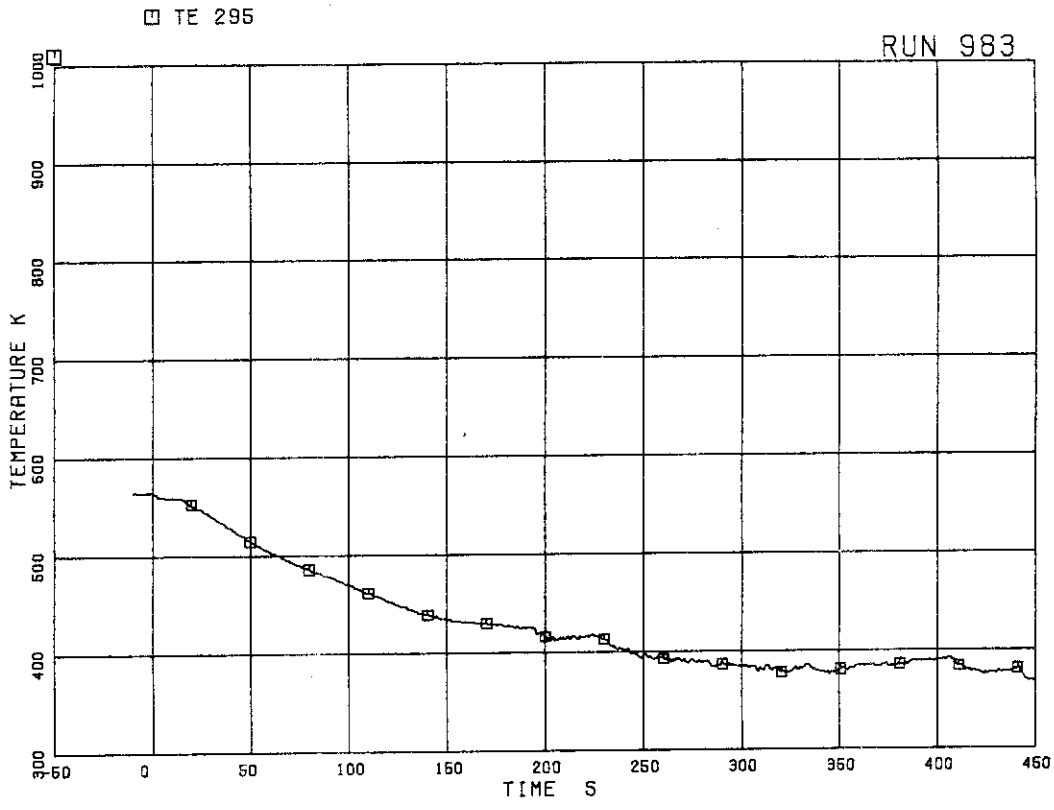

Fig. 5.109 Surface temperature of fuel rod A73 at position 4

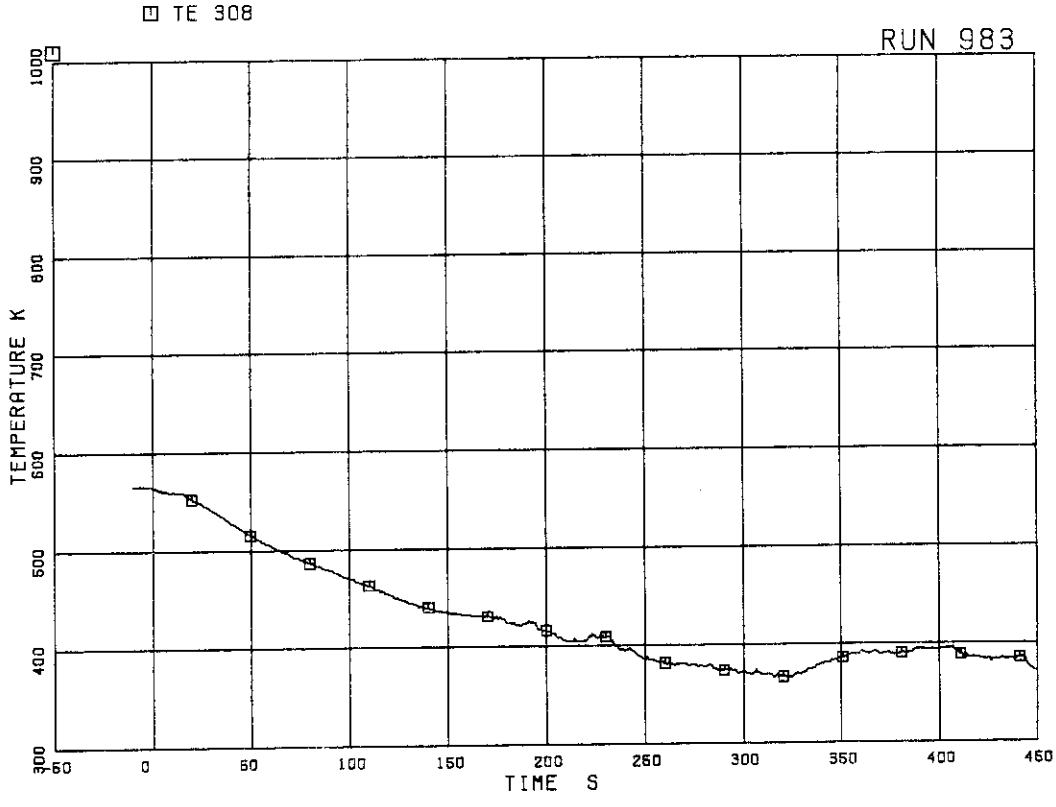

Fig. 5.110 Surface temperature of fuel rod A84 at position 4

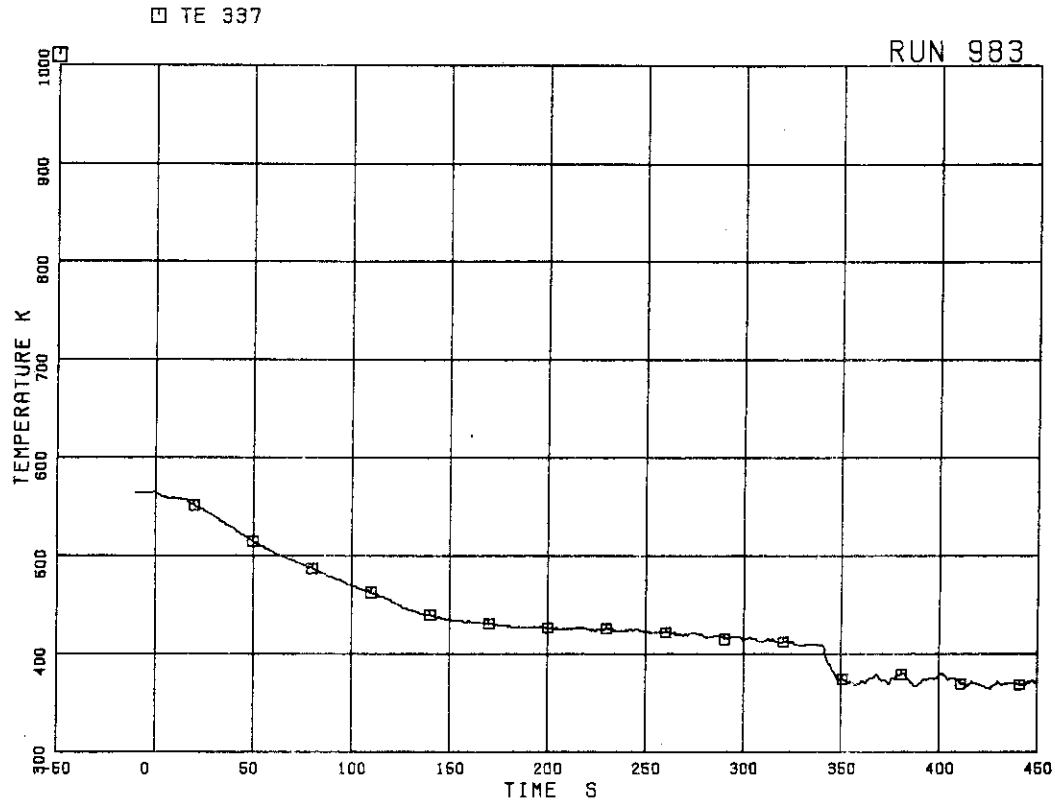

Fig. 5.111 Surface temperature of fuel rod B13 at position 4

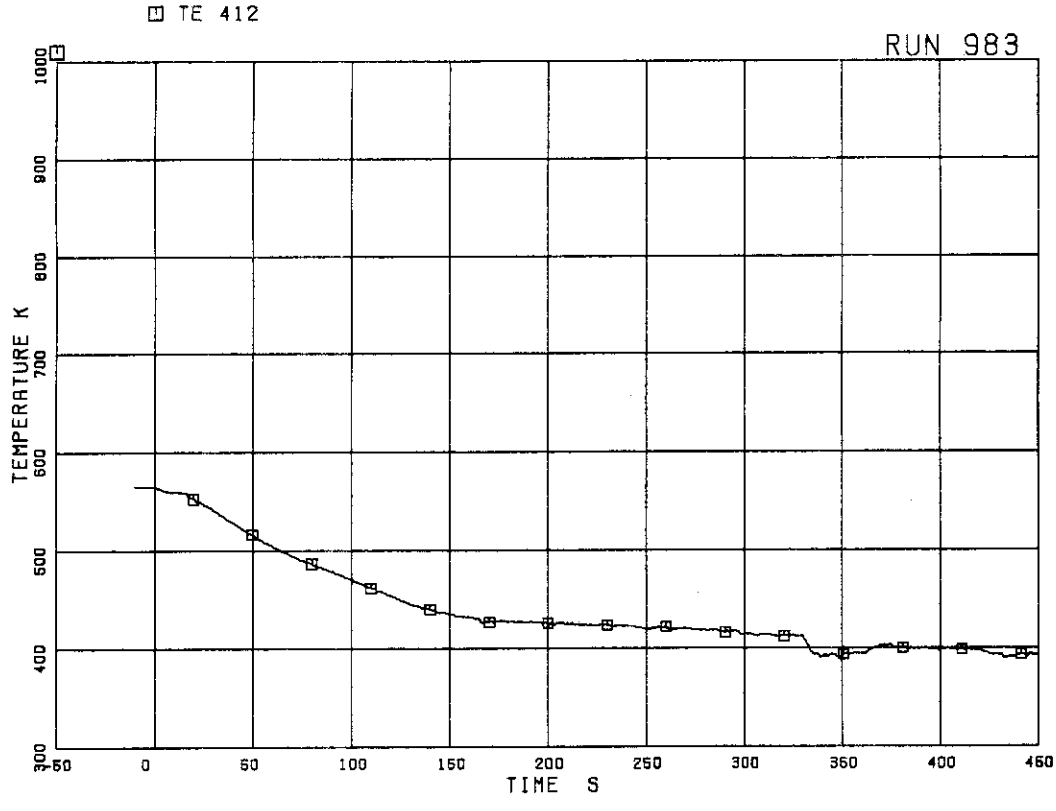

Fig. 5.112 Surface temperature of fuel rod D77 at position 4

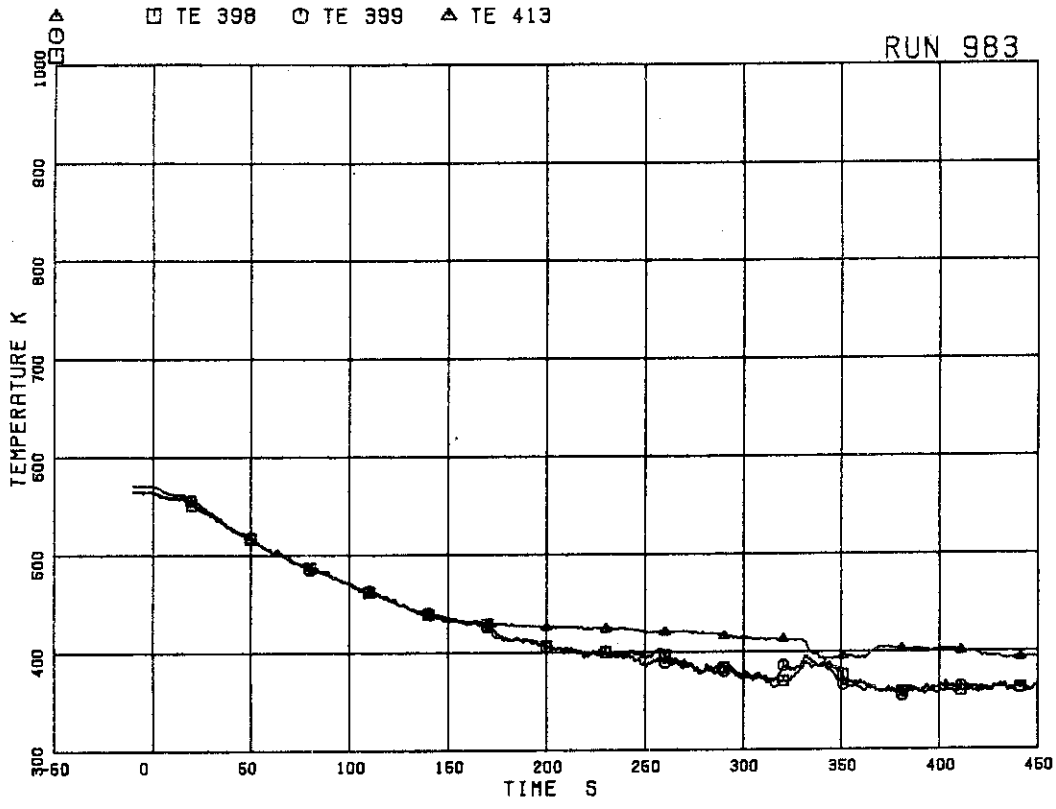

Fig. 5.113 Surface temperatures of fuel rods D11,D13 and D86 at position 4

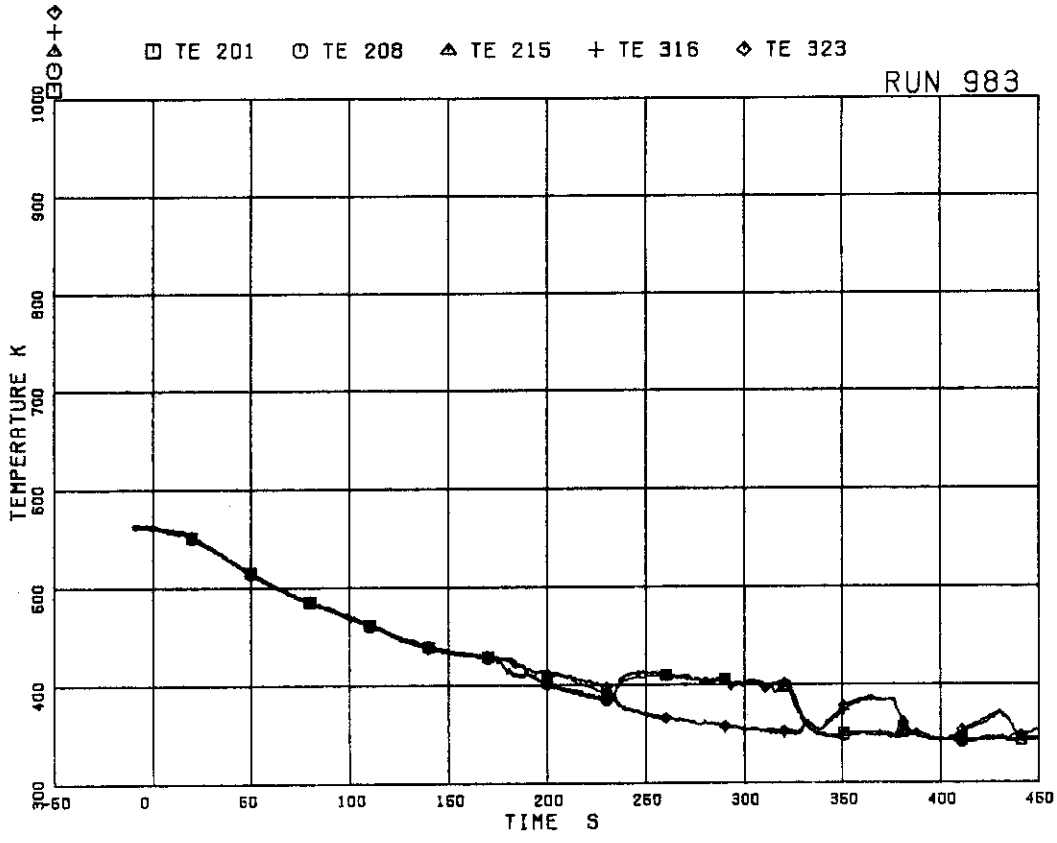

Fig. 5.114 Surface temperatures of fuel rods A11,A12,A13,A87 and A88 at position 1

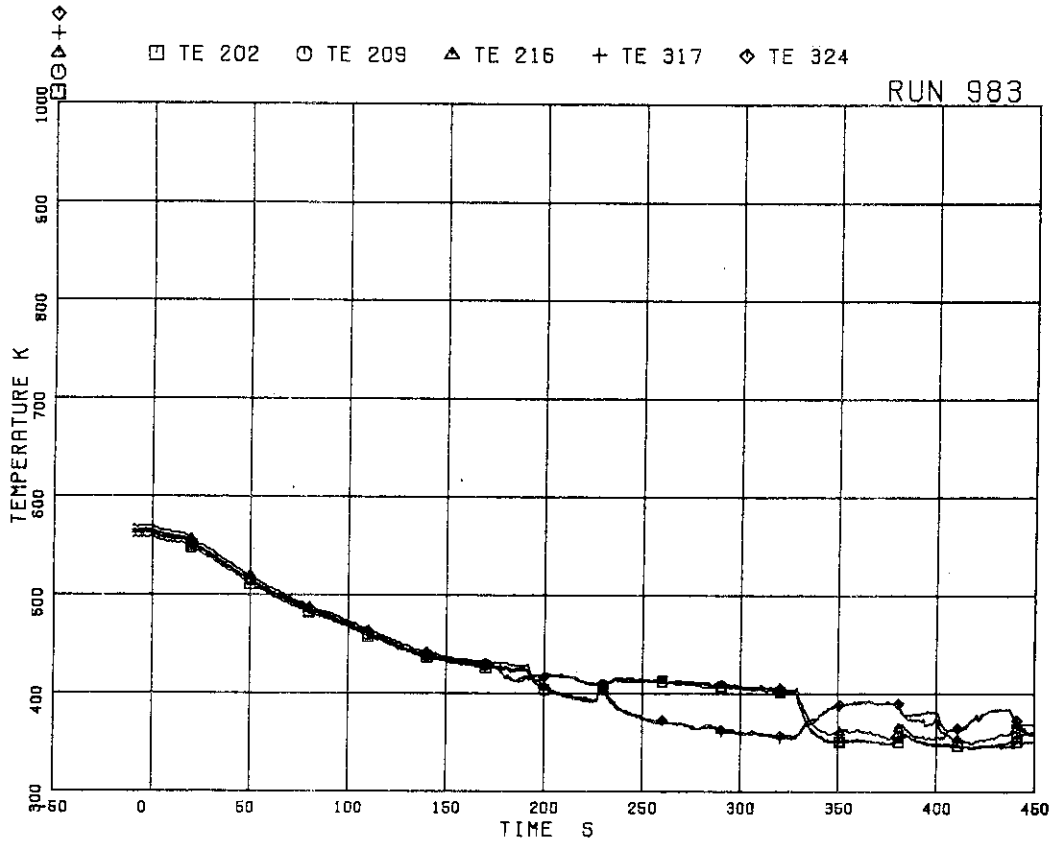

Fig. 5.115 Surface temperatures of fuel rods A11,A12,A13,A87 and A88 at position 2

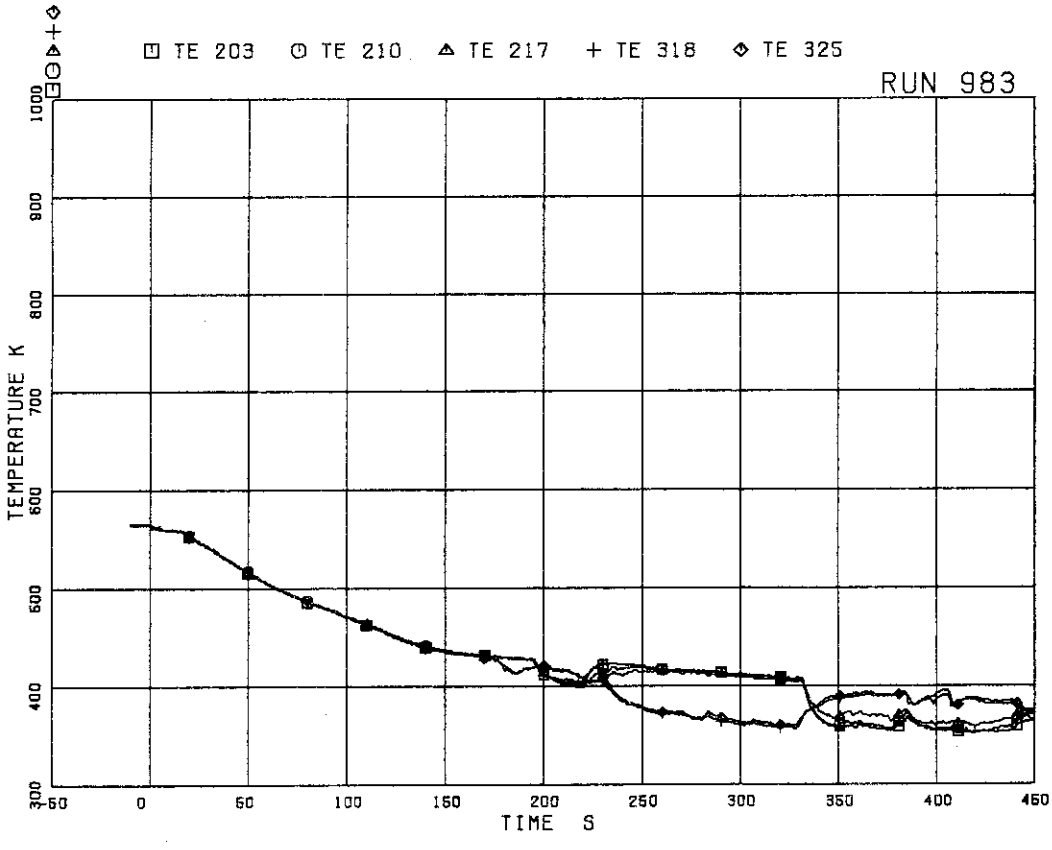

Fig. 5.116 Surface temperatures of fuel rods A11,A12,A13,A87 and A88 at position 3

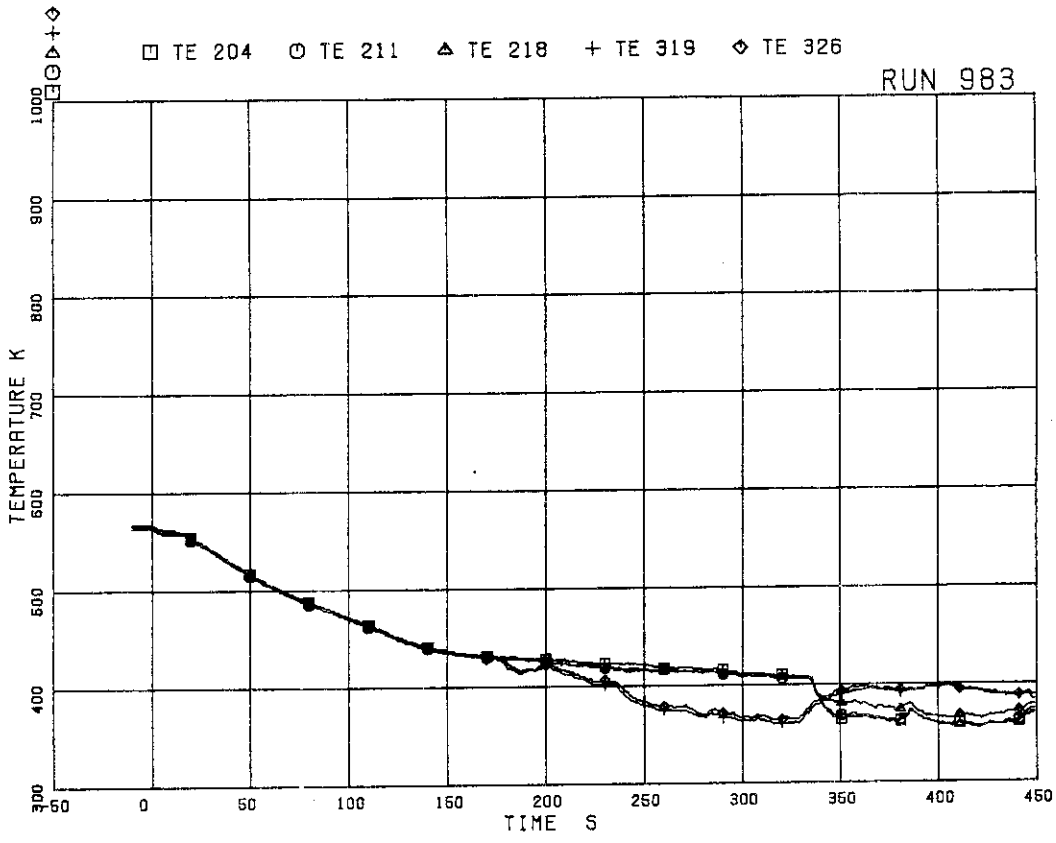

Fig. 5.117 Surface temperatures of fuel rods A11,A12,A13,A87 and A88 at position 4

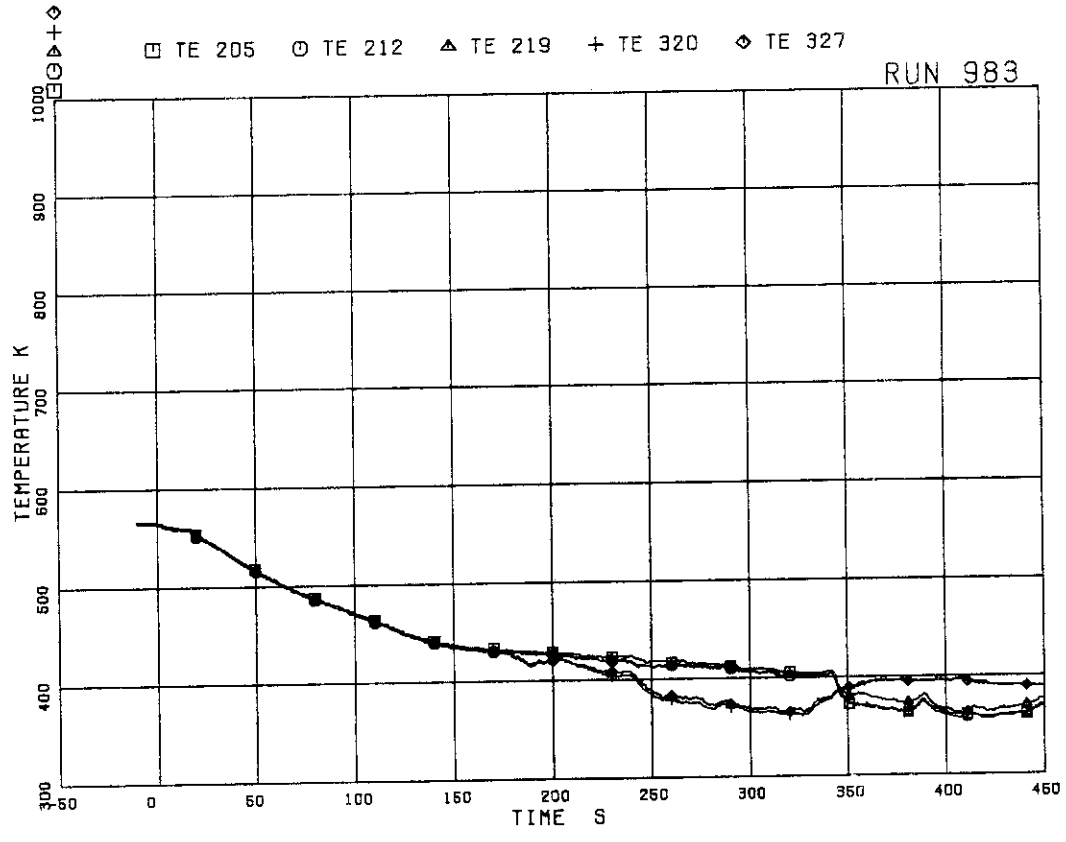

Fig. 5.118 Surface temperatures of fuel rods A11,A12,A13,A87 and A88 at position 5

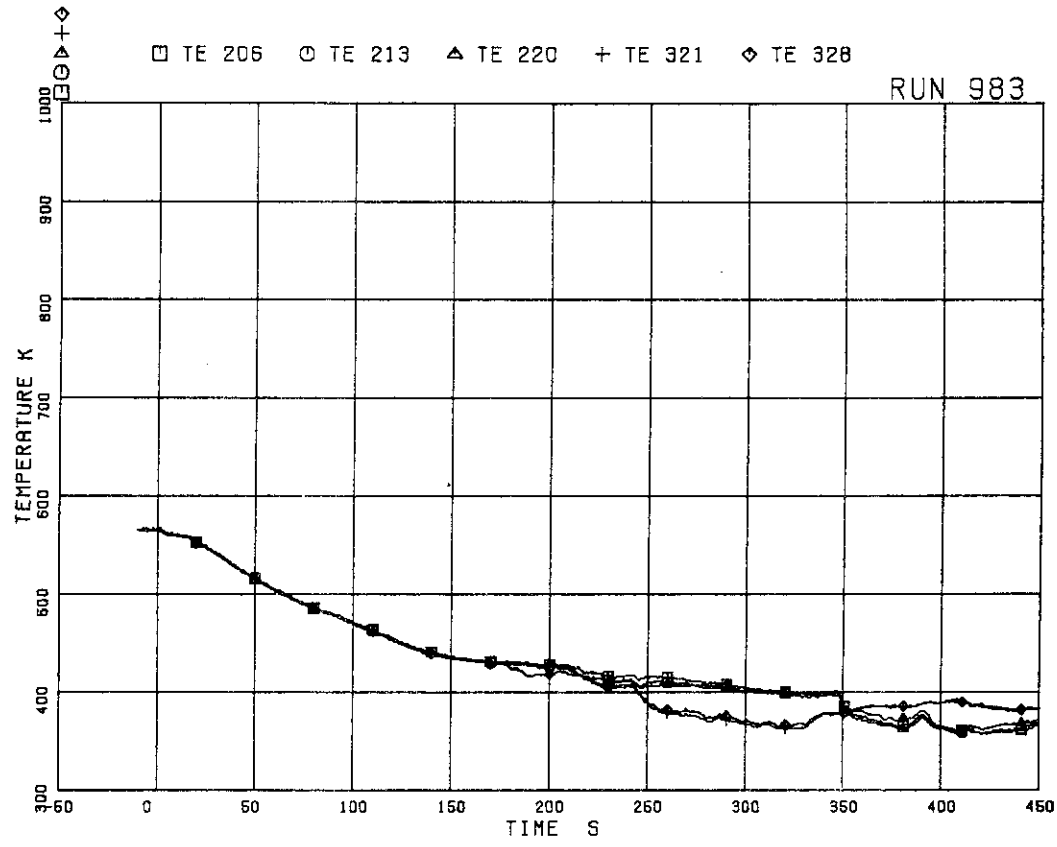

Fig. 5.119 Surface temperatures of fuel rods A11,A12,A13,A87 and A88 at position 6

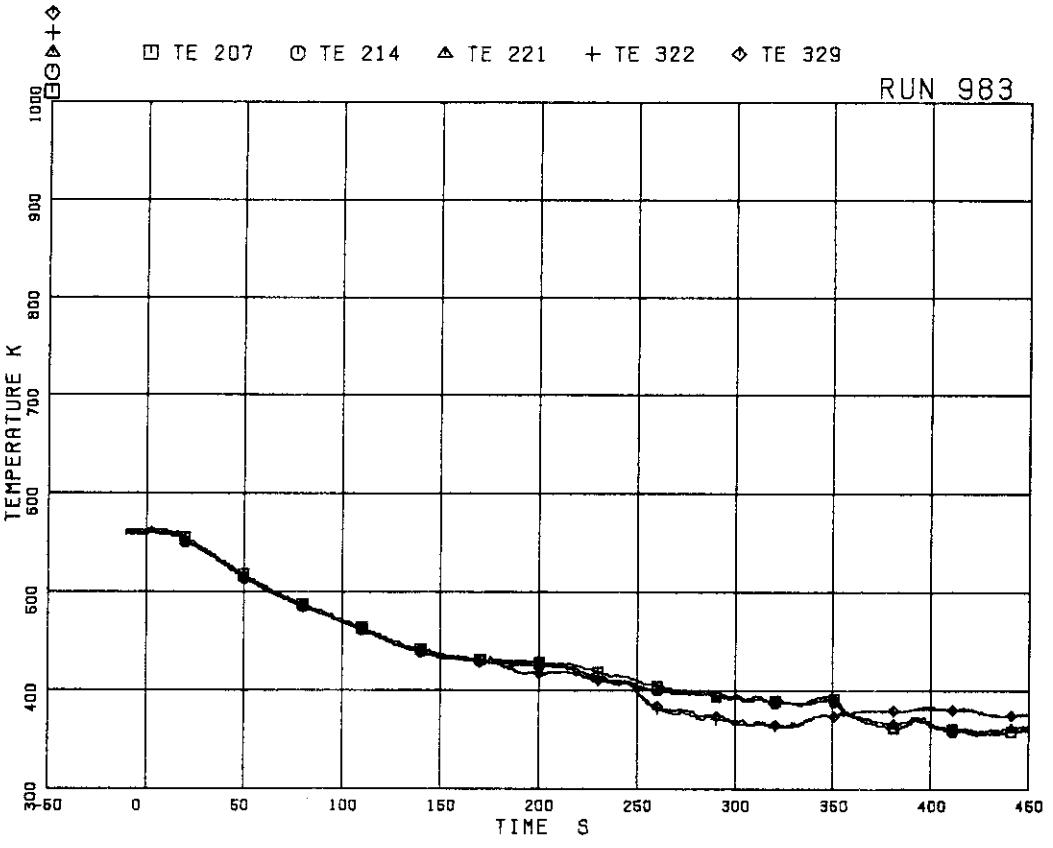

Fig. 5.120 Surface temperatures of fuel rods A11,A12,A13,A87 and A88 at position 7

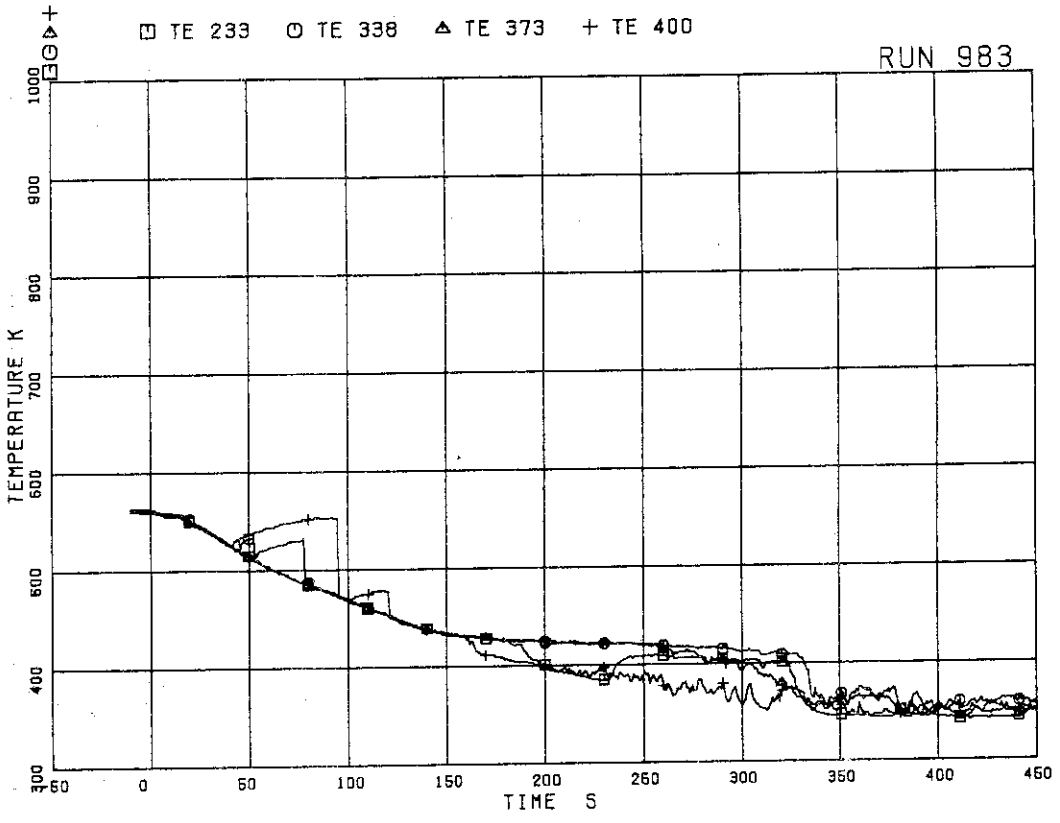

Fig. 5.121 Surface temperatures of fuel rods A22,B22,C22 and D22 at position 1

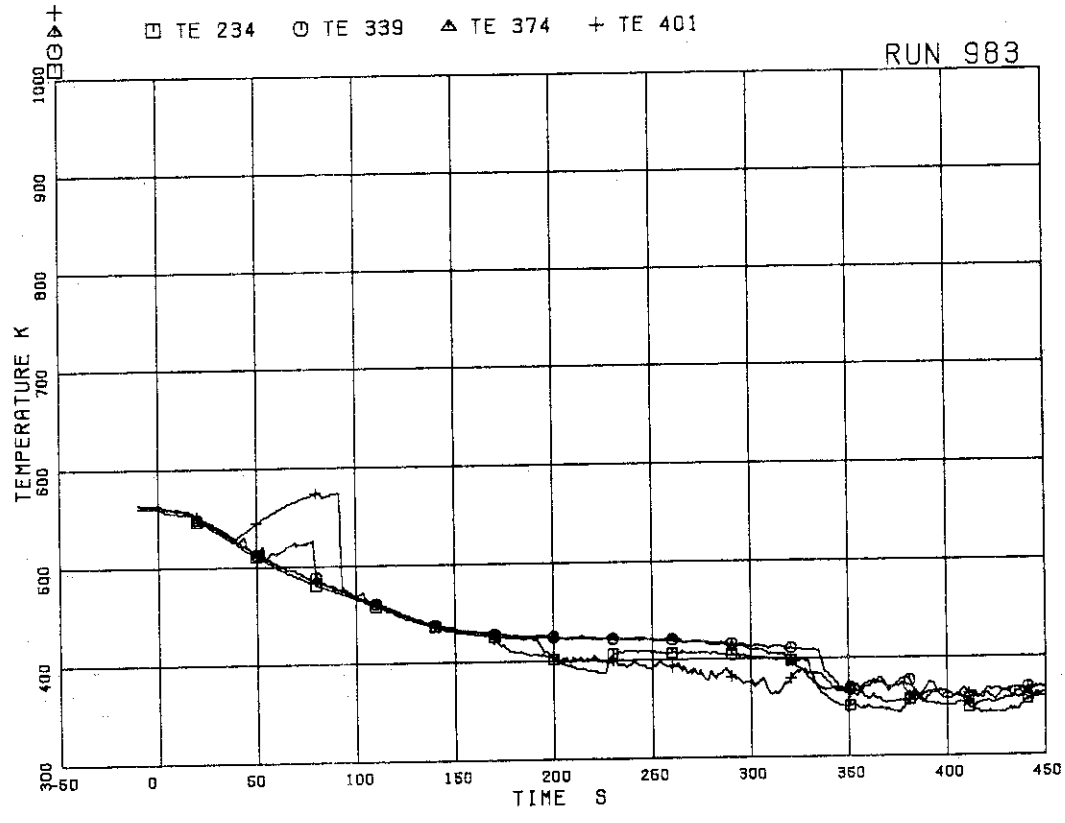

Fig. 5.122 Surface temperatures of fuel rods A22,B22,C22 and D22 at position 2

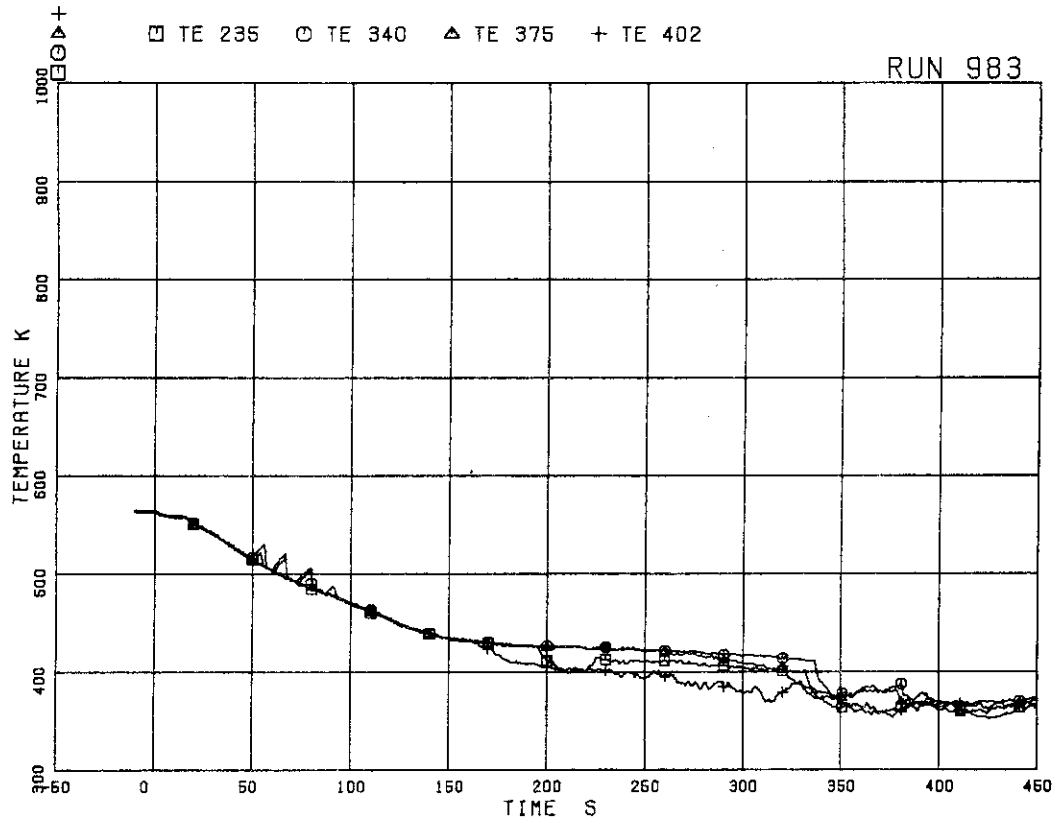

Fig. 5.123 Surface temperatures of fuel rods A22,B22,C22 and D22 at position 3

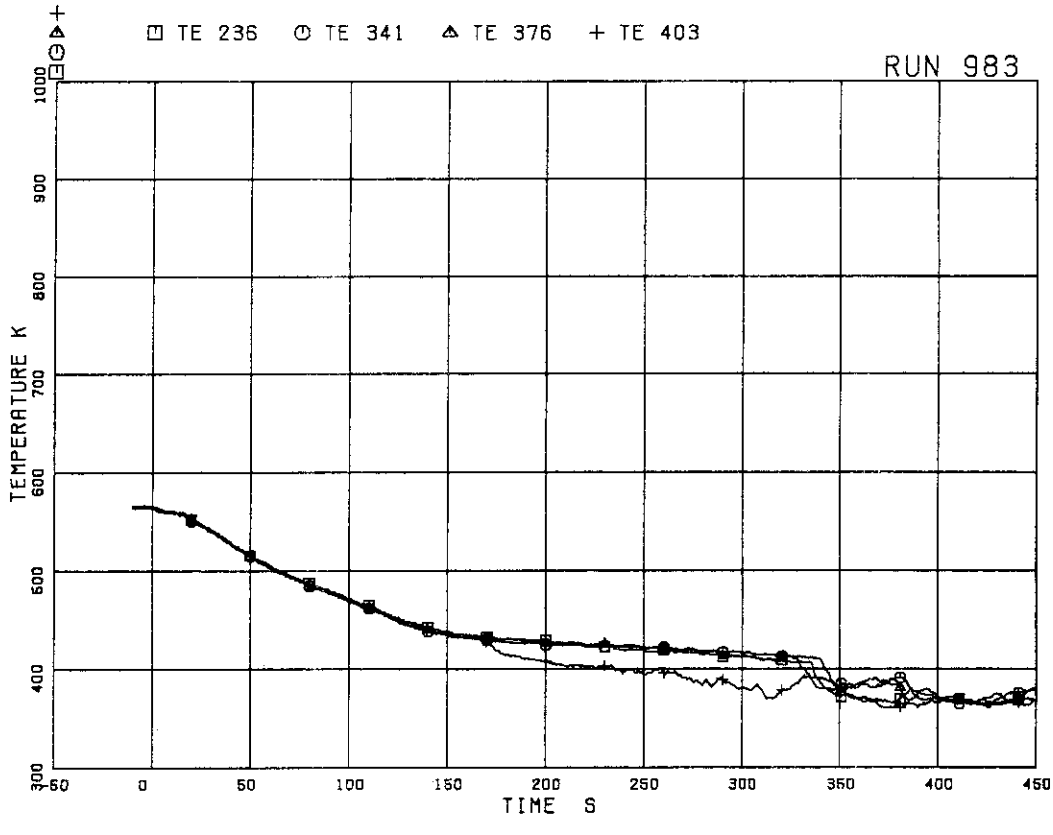

Fig. 5.124 Surface temperatures of fuel rods A22,B22,C22 and D22 at position 4

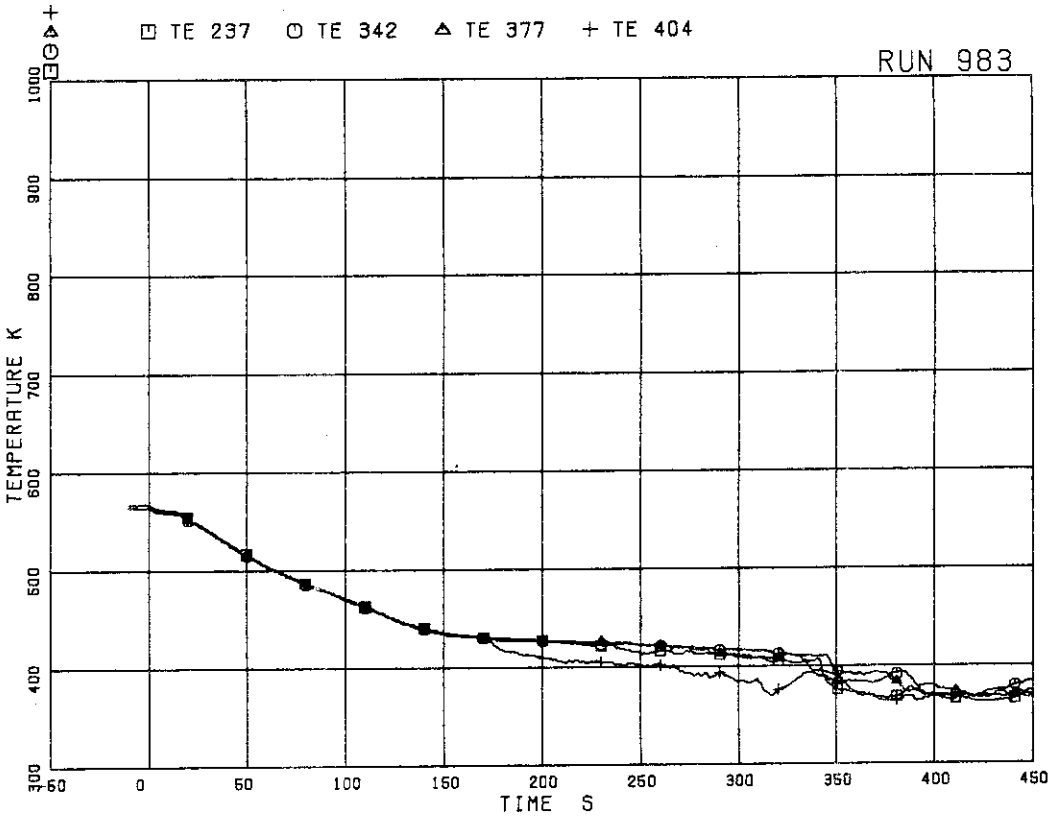

Fig. 5.125 Surface temperatures of fuel rods A22,B22,C22 and D22 at position 5

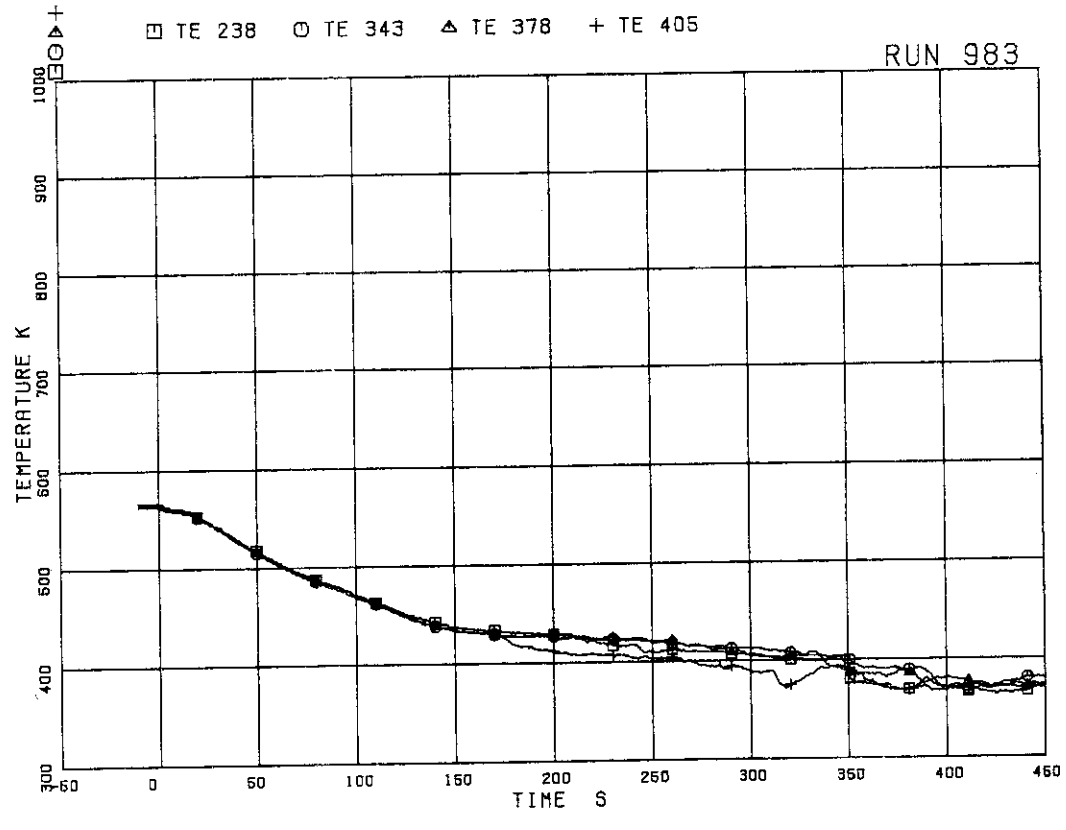

Fig. 5.126 Surface temperatures of fuel rods A22,B22,C22 and D22 at position 6

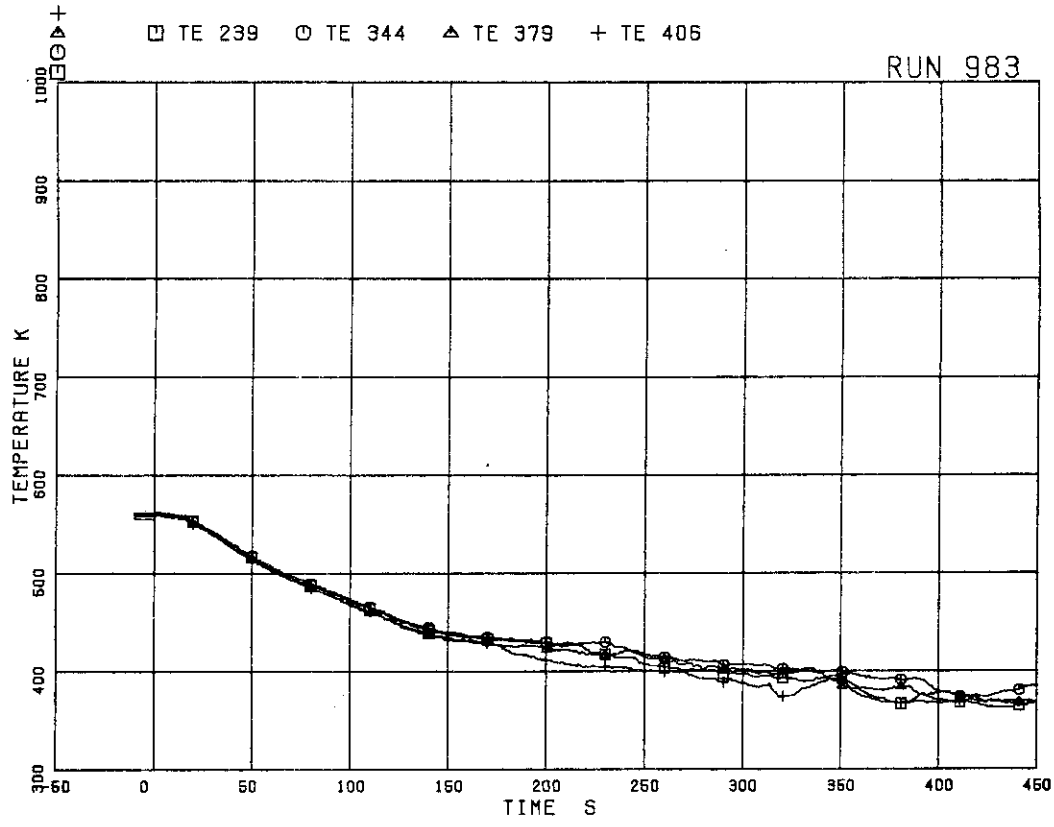

Fig. 5.127 Surface temperatures of fuel rods A22,B22,C22 and D22 at position 7

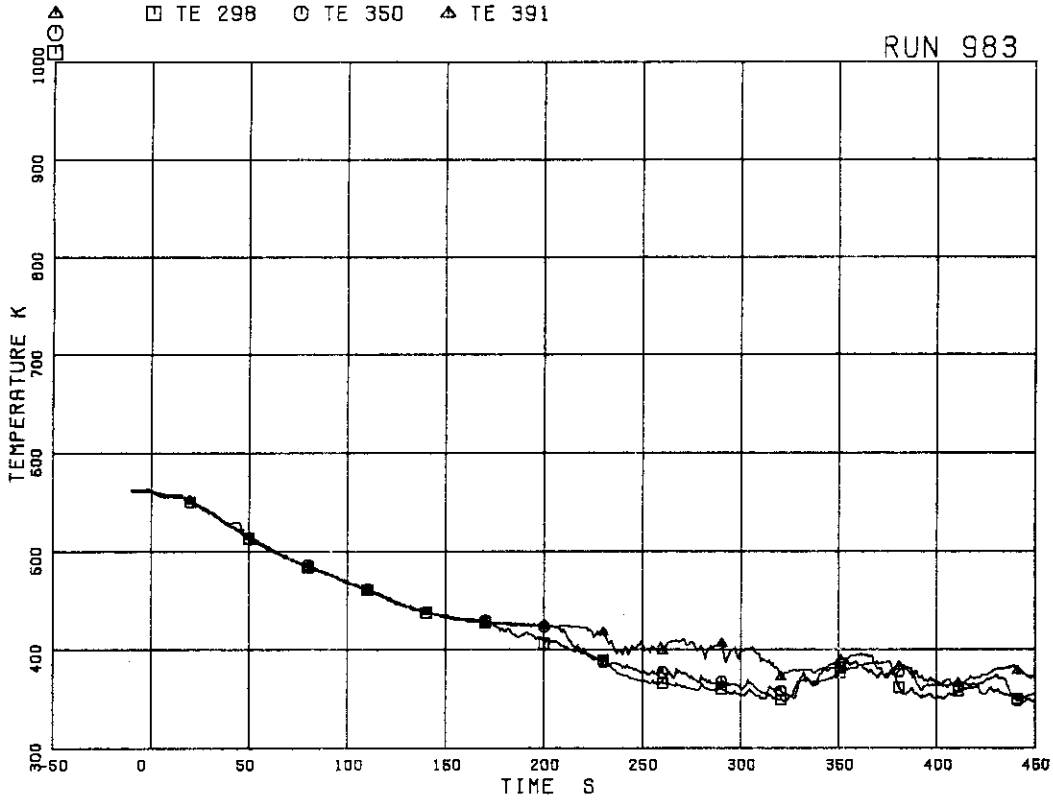

Fig. 5.128 Surface temperatures of fuel rods A77,B77 and C77 at position 1

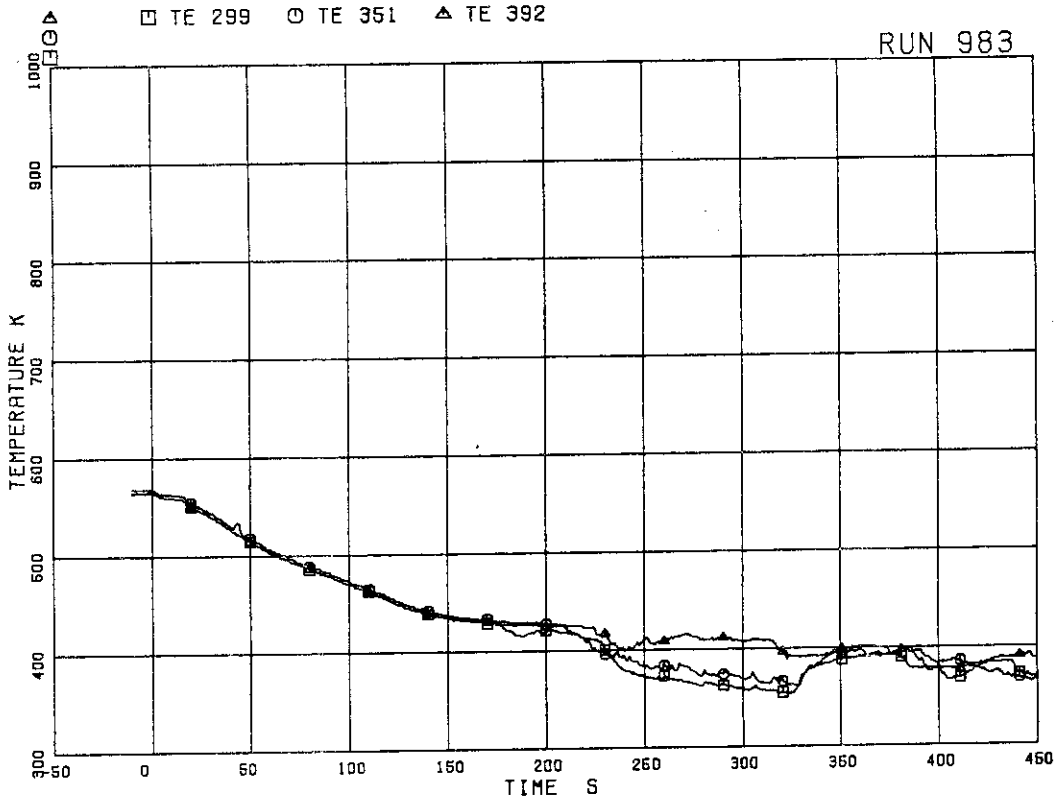

Fig. 5.129 Surface temperatures of fuel rods A77,B77 and C77 at position 2

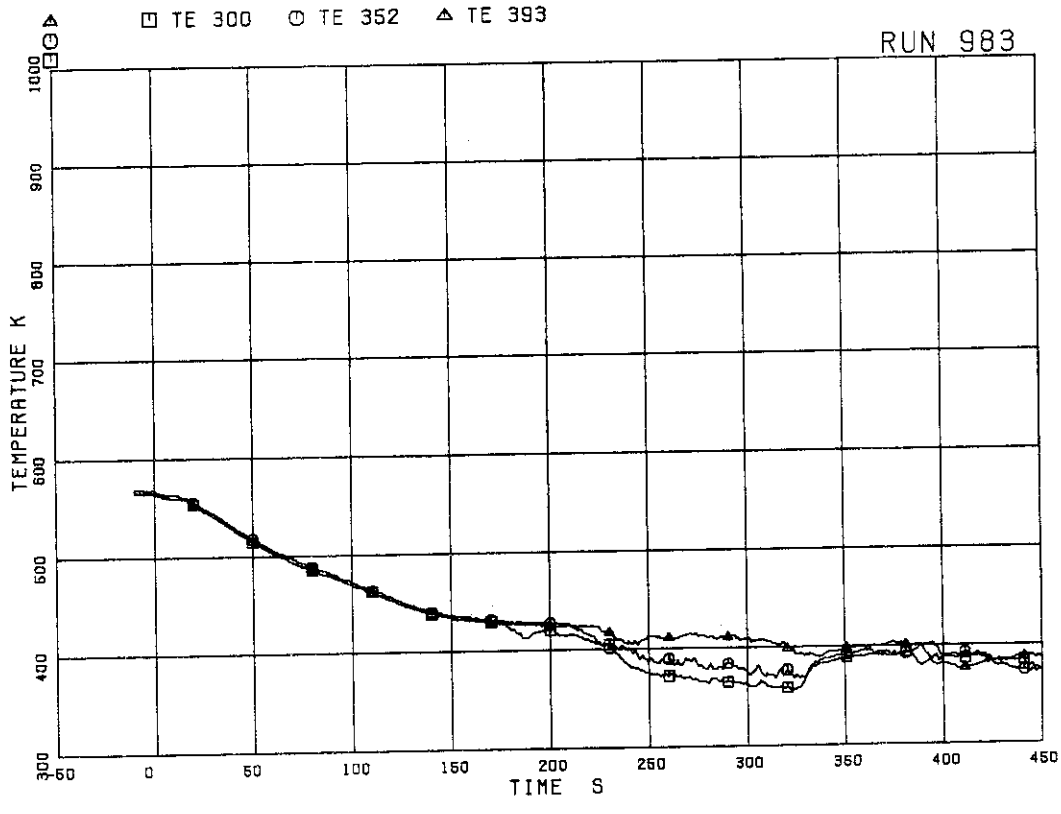

Fig. 5.130 Surface temperatures of fuel rods A77,B77 and C77 at position 3

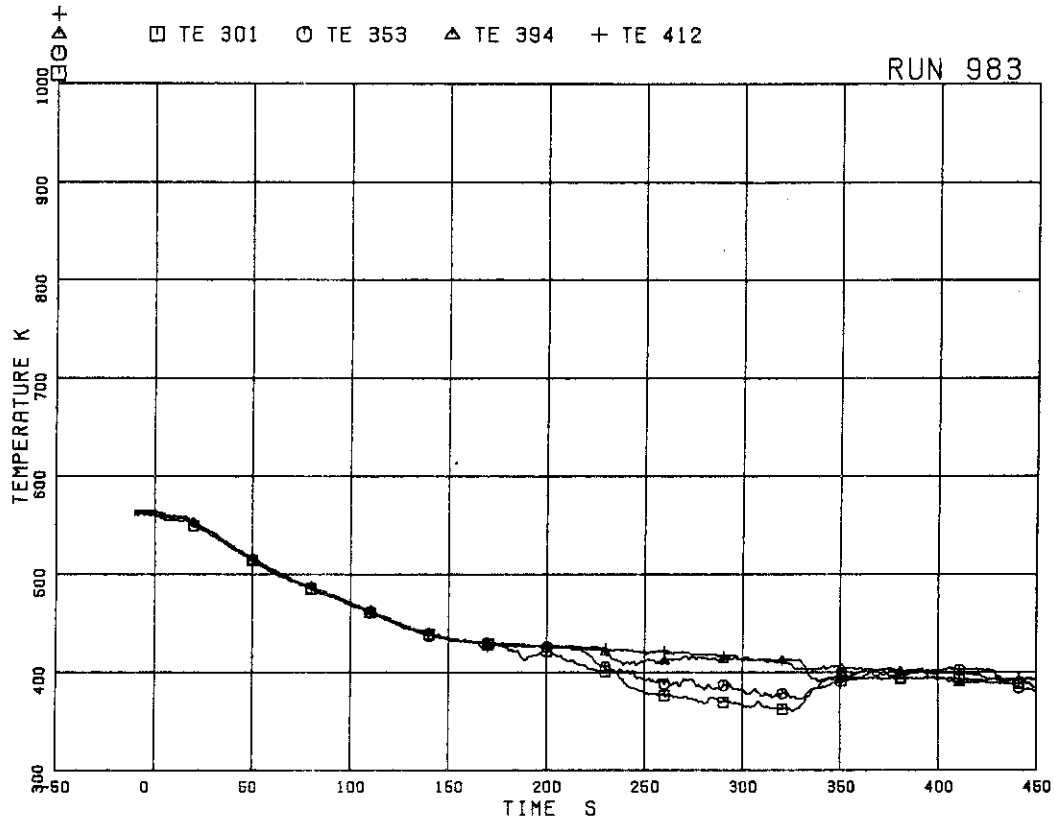

Fig. 5.131 Surface temperatures of fuel rods A77,B77 and C77 at position 4

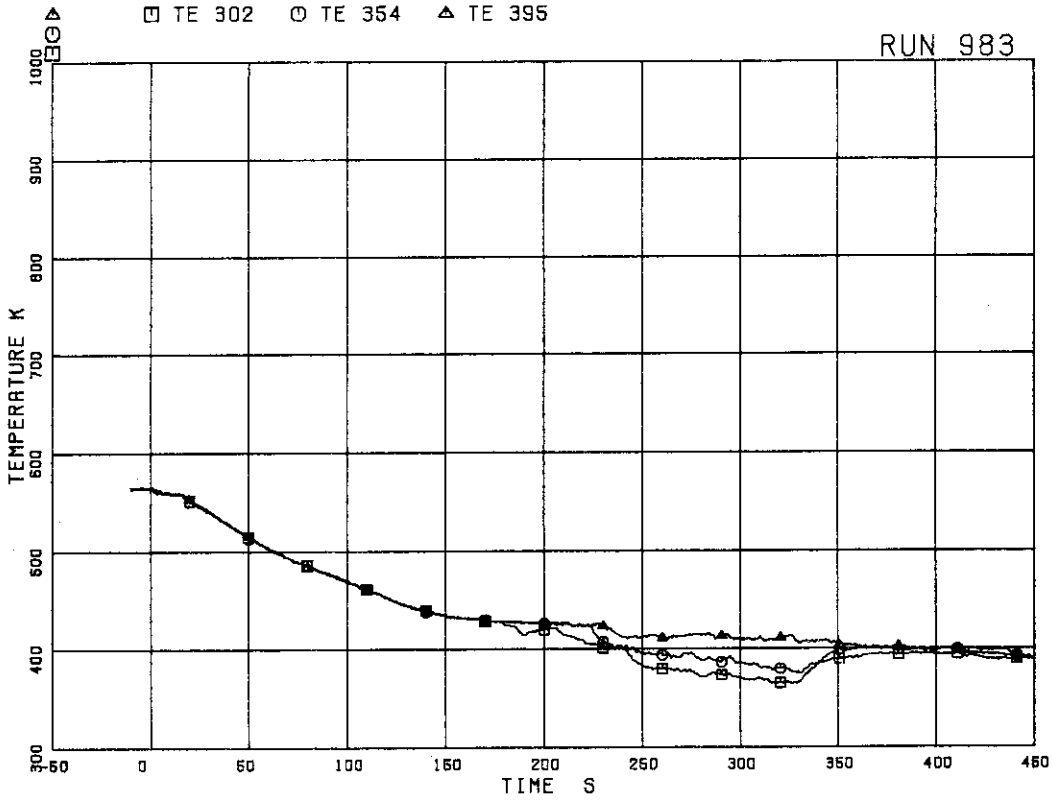

Fig. 5.132 Surface temperatures of fuel rods A77,B77 and C77 at position 5

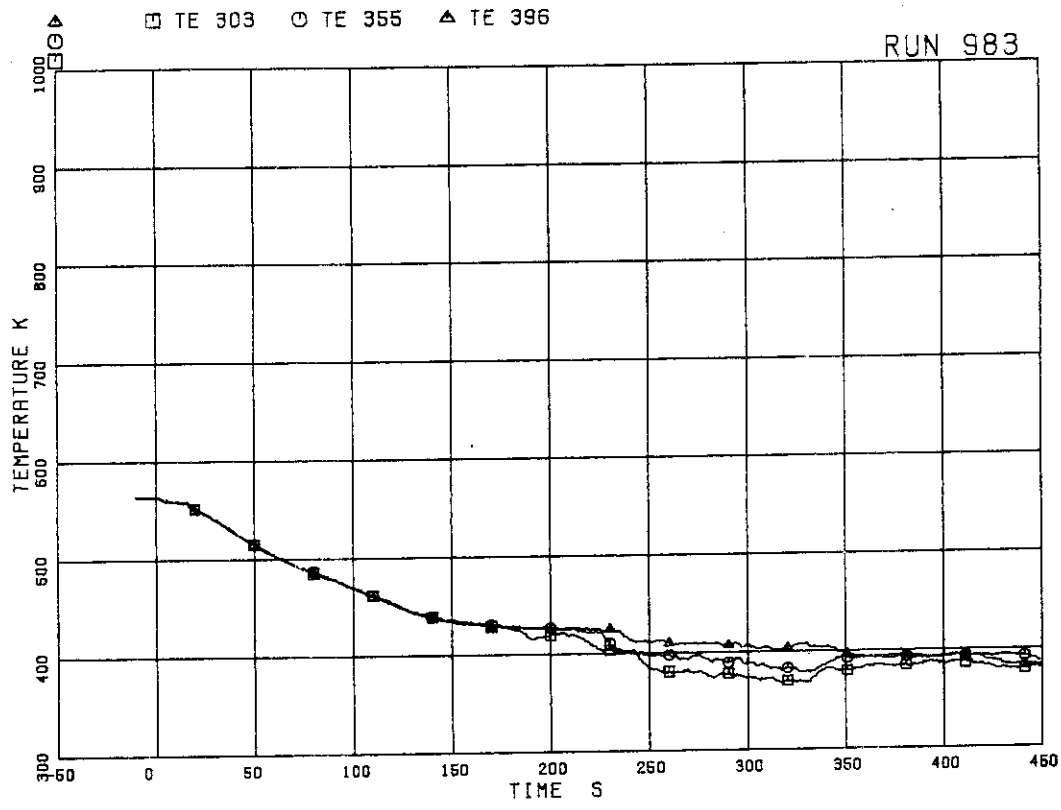

Fig. 5.133 Surface temperatures of fuel rods A77, B77 and C77 at position 6

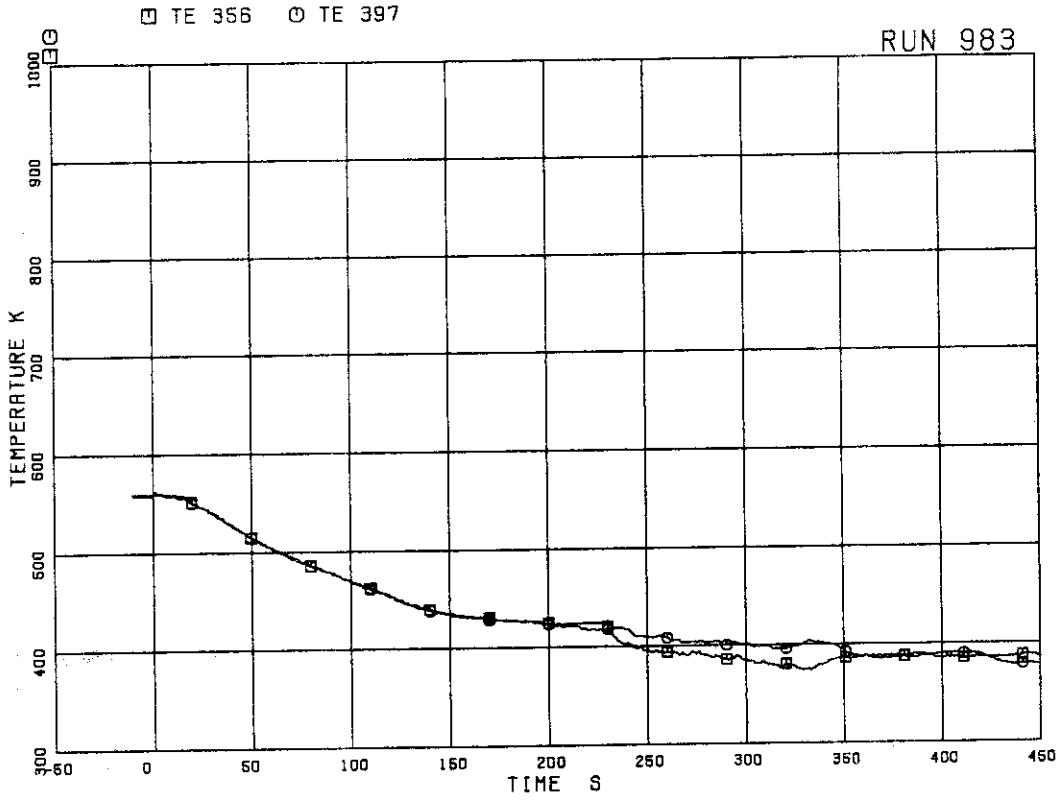

Fig. 5.134 Surface temperatures of fuel rods B77 and C77 at position 7

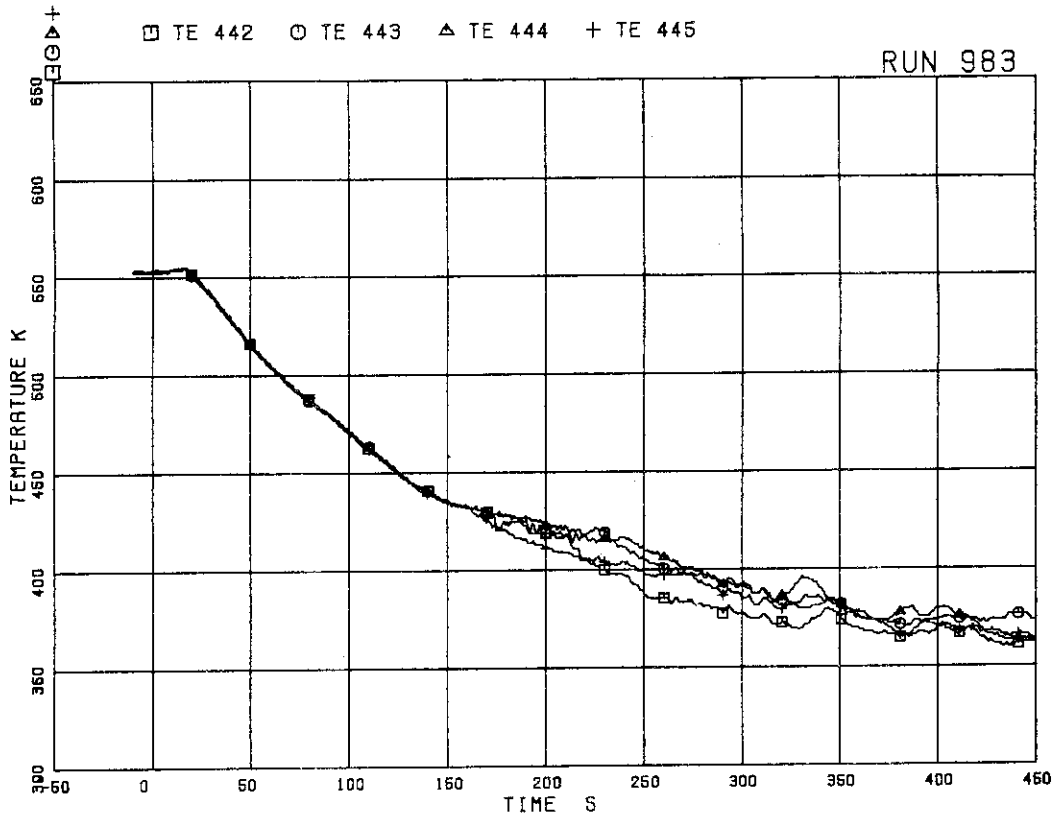

Fig. 5.135 Fluid temperatures at channel inlet

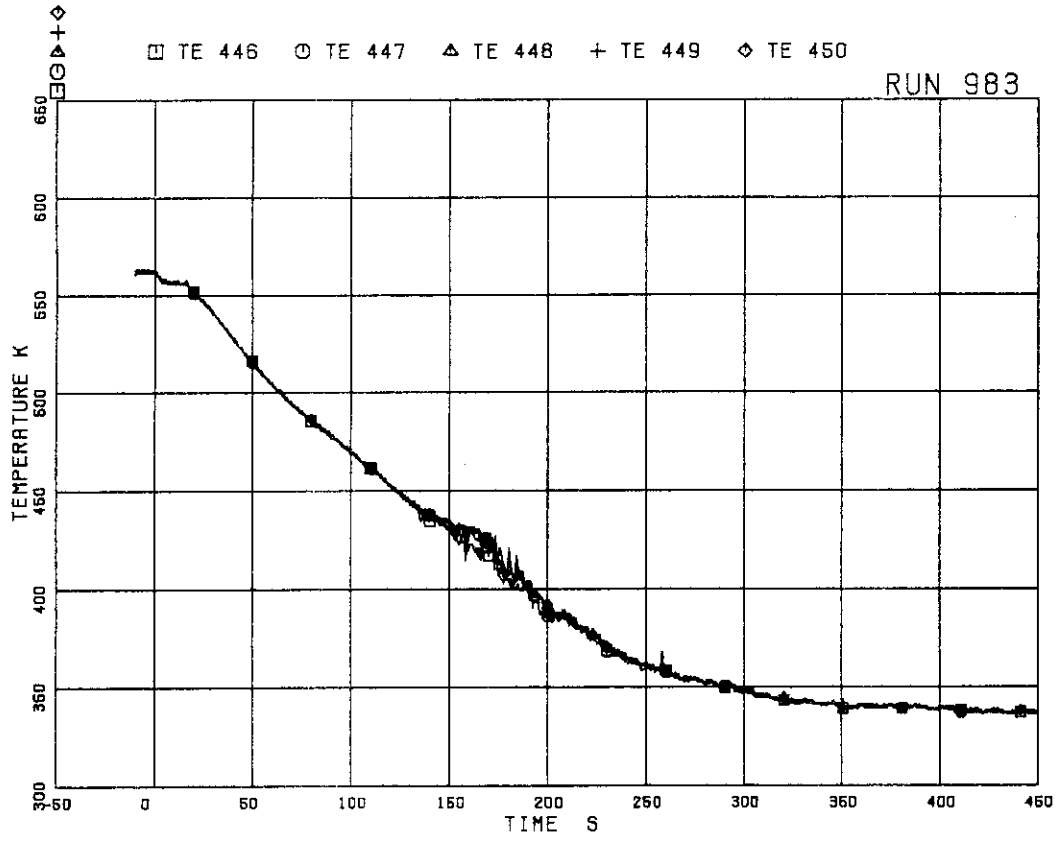

Fig. 5.136 Fluid temperatures at channel A outlet

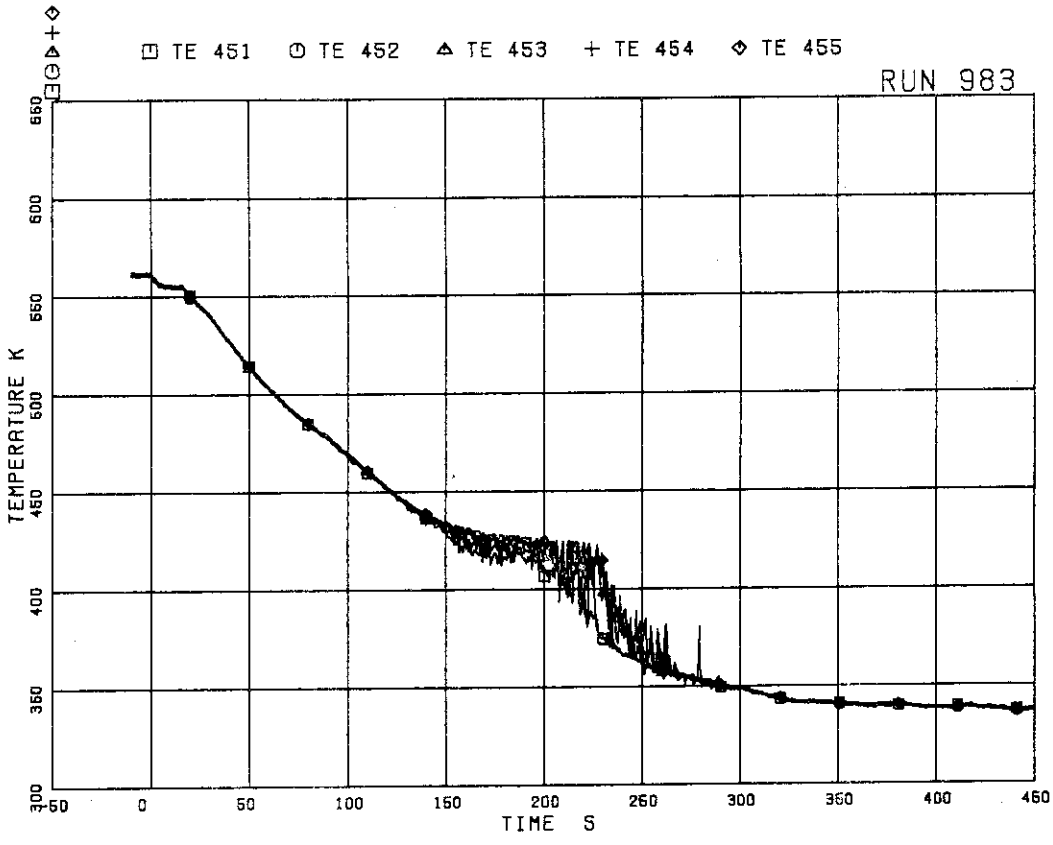

Fig. 5.137 Fluid temperatures at channel C outlet

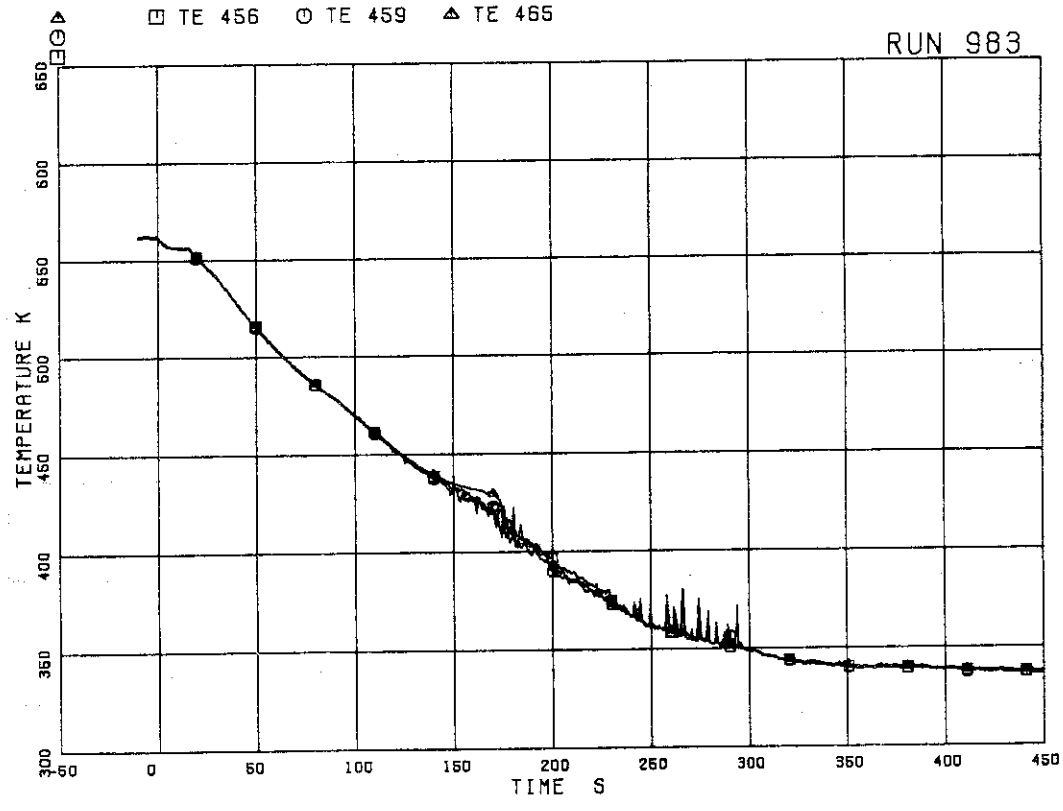

Fig. 5.138 Fluid temperatures above UTP (upper tie plate) of channel A, openings 1, 4 and 10

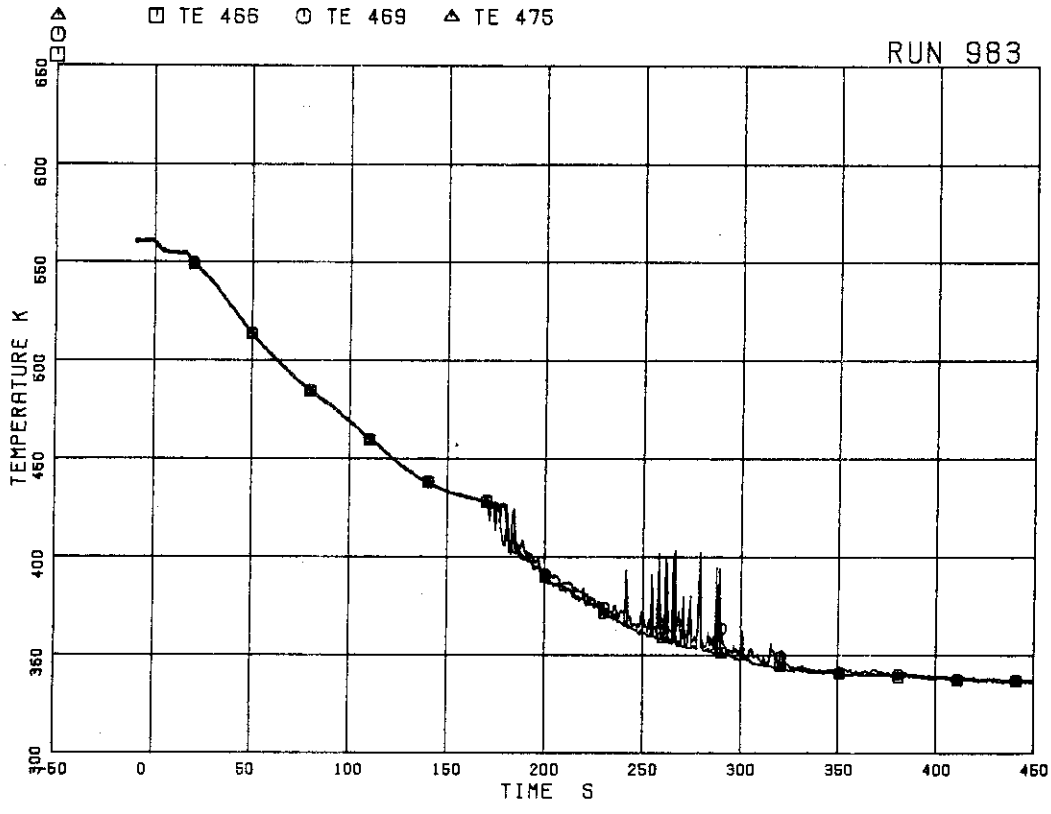

Fig. 5.139 Fluid temperatures below UTP of channel A, openings 1, 4 and 10

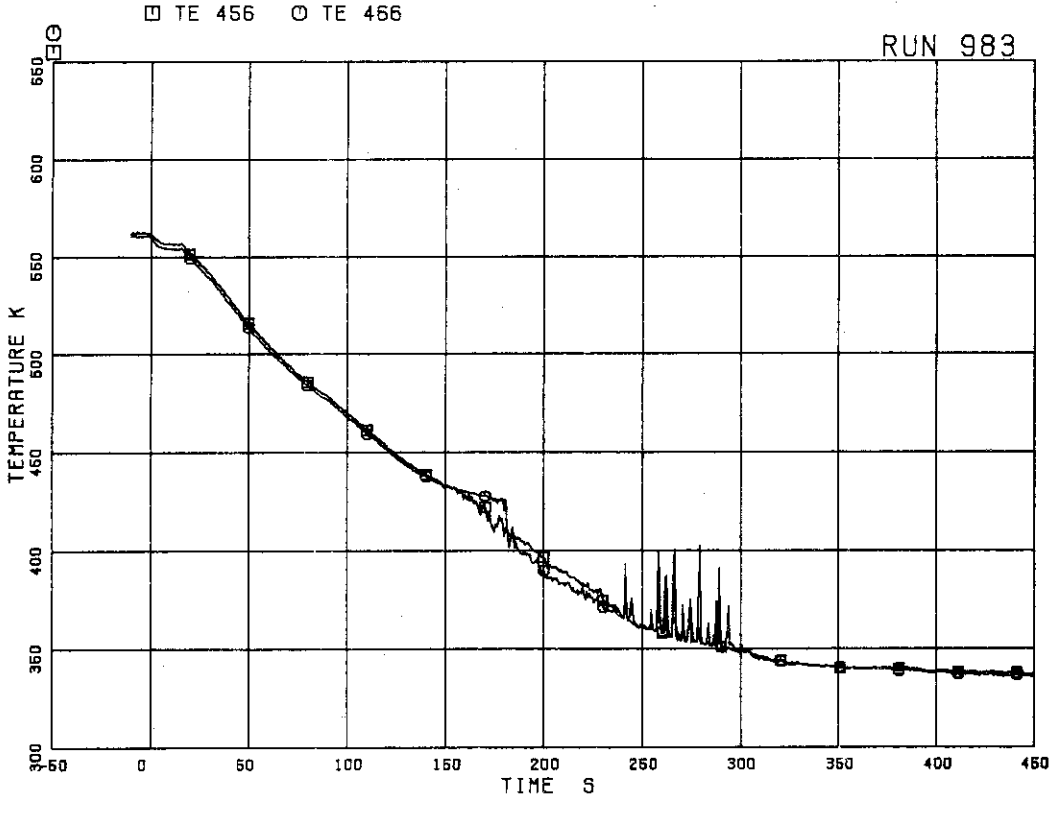

Fig. 5.140 Fluid temperatures at UTP in channel A, opening 1

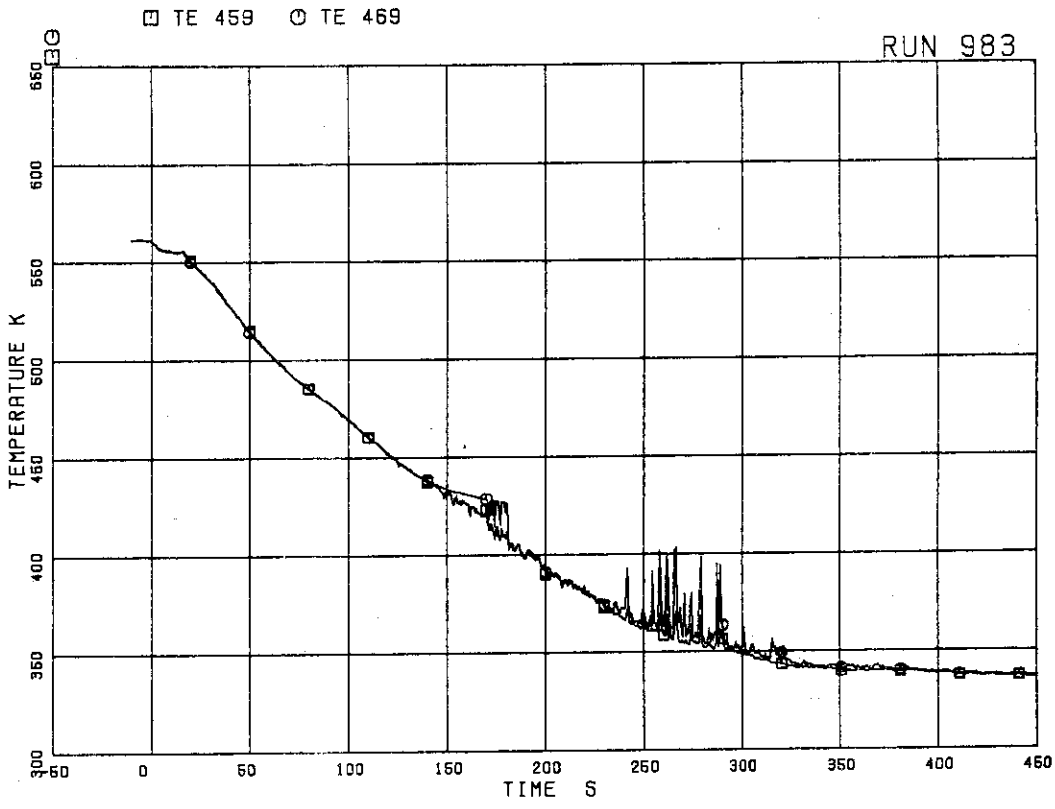

Fig. 5.141 Fluid temperatures at UTP in channel A, opening 4

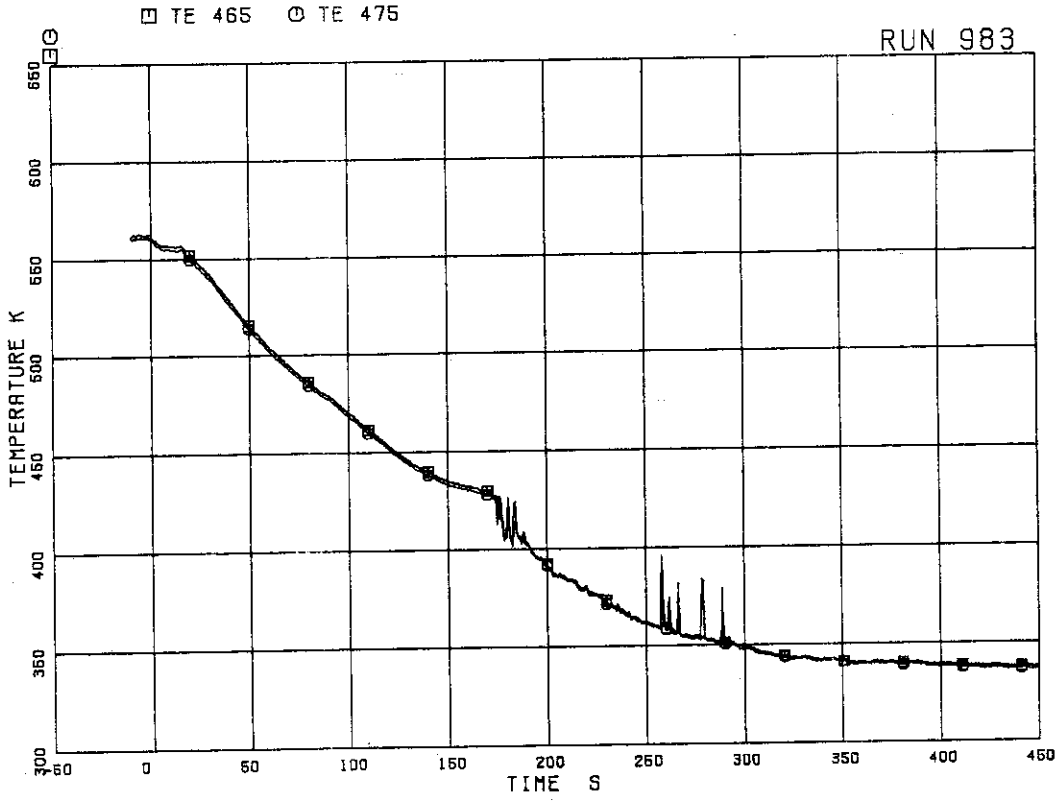

Fig. 5.142 Fluid temperatures at UTP in channel A, opening 10

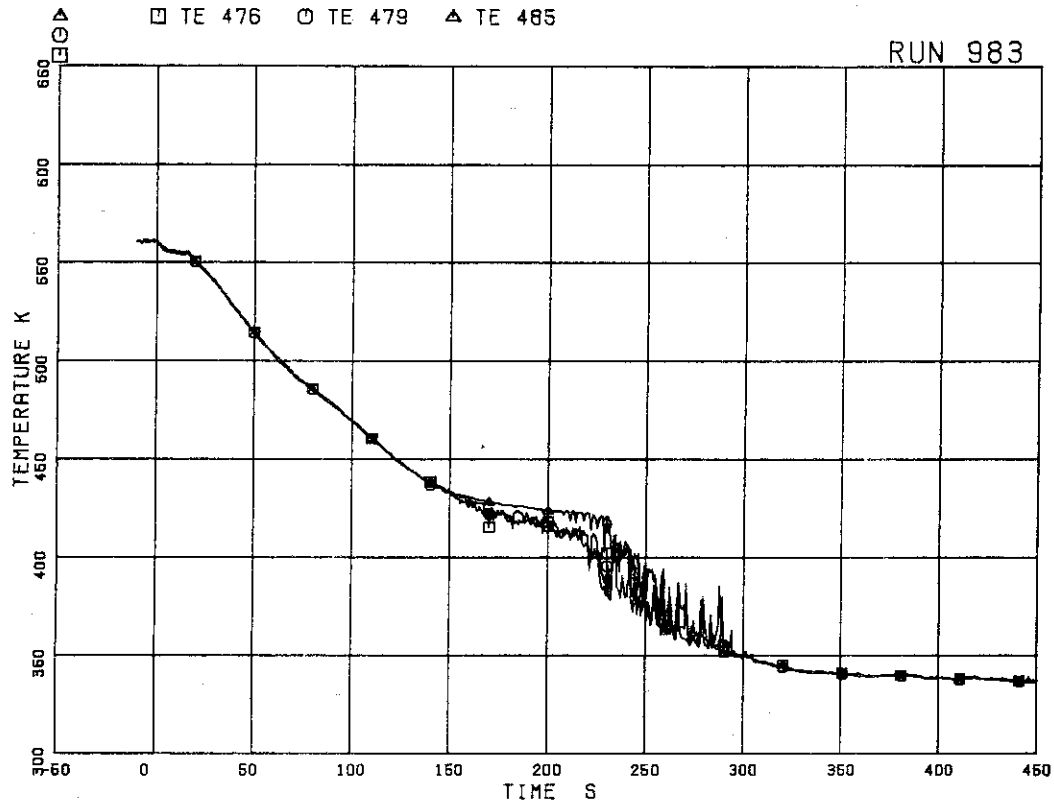

Fig. 5.143 Fluid temperatures above UTP of channel C, openings 1, 4 and 10

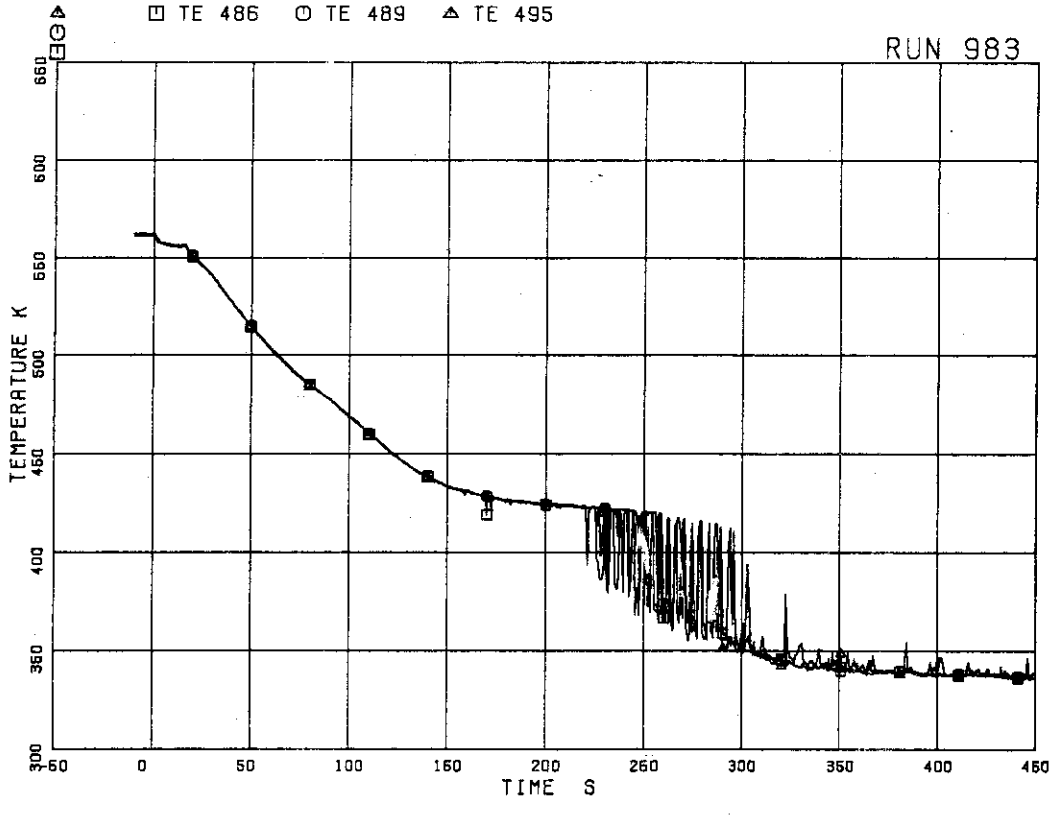

Fig. 5.144 Fluid temperatures below UTP of channel C, openings 1, 4 and 10

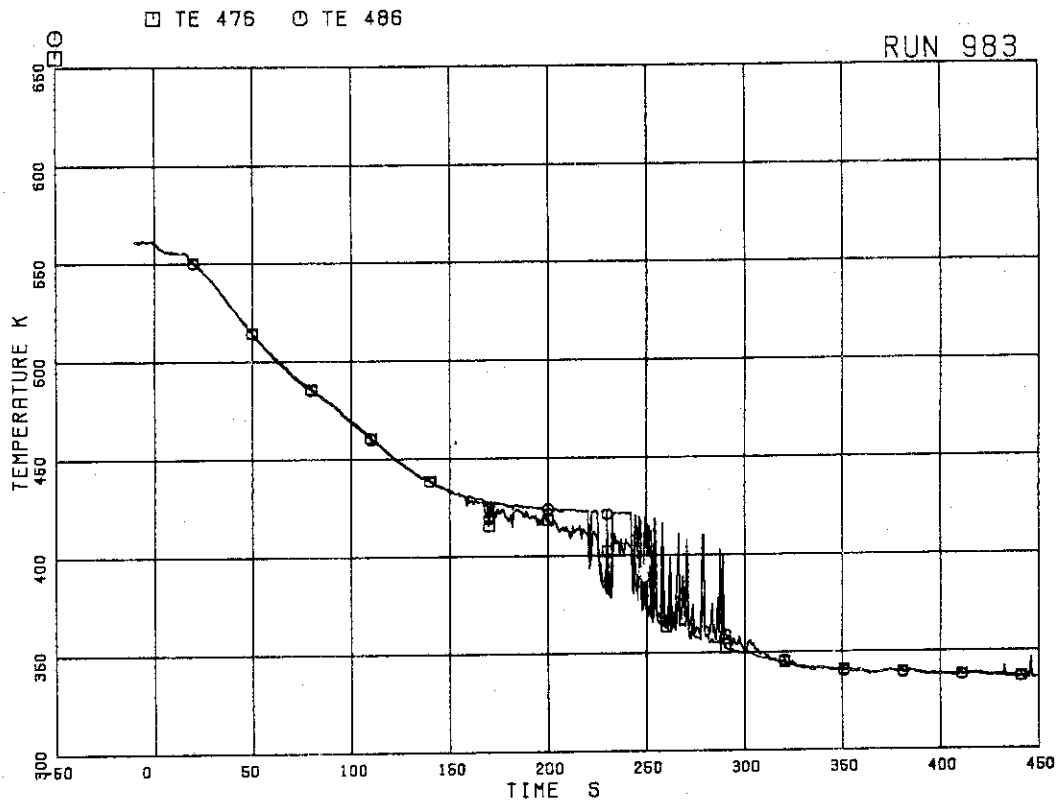

Fig. 5.145 Fluid temperatures at UTP in channel C, opening 1

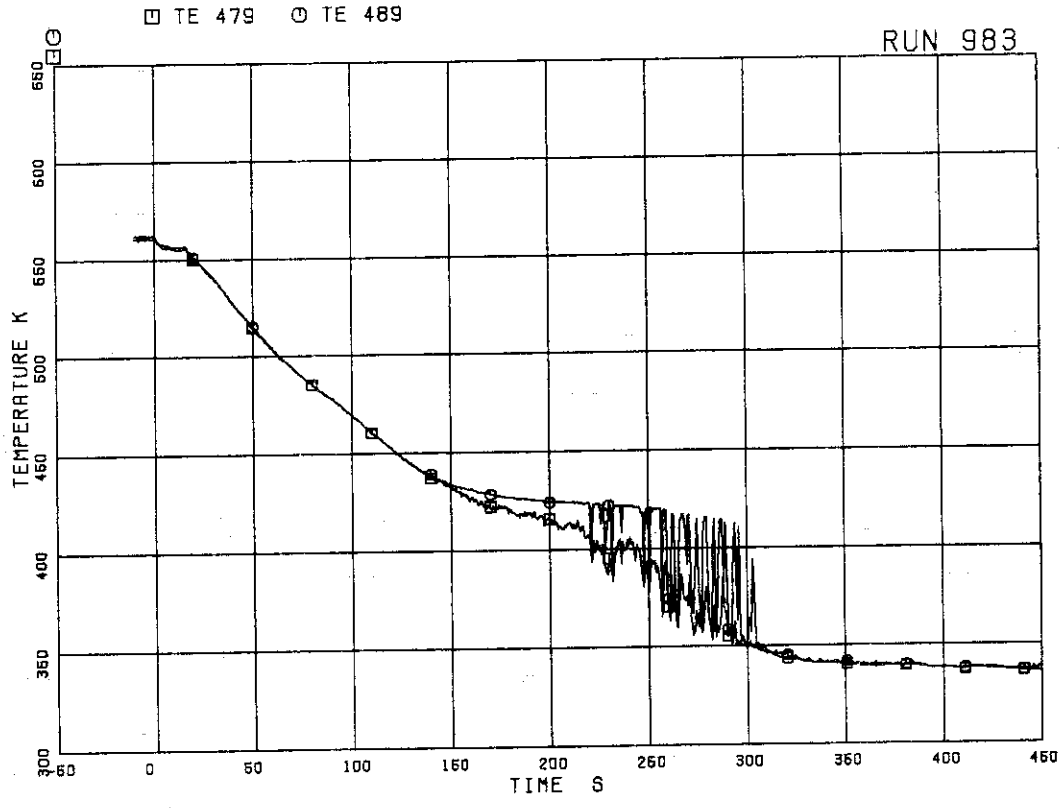

Fig. 5.146 Fluid temperatures at UTP in channel C, opening 4

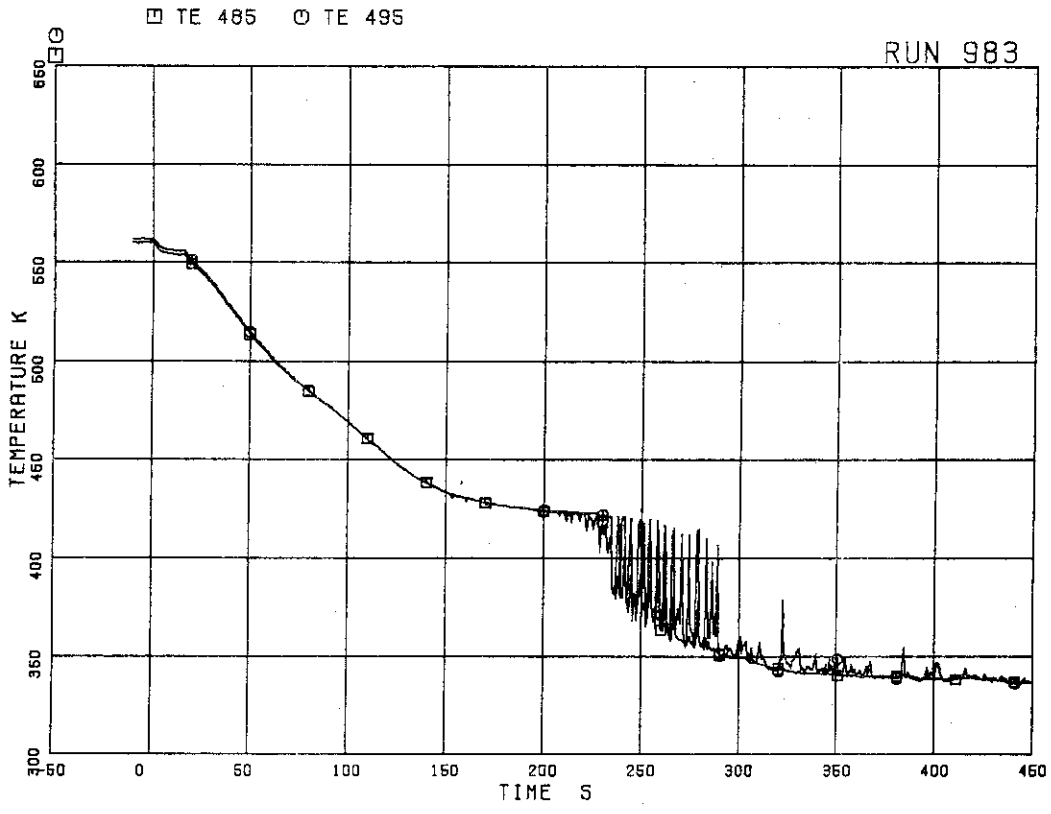

Fig. 5.147 Fluid temperatures at UTP in channel C, opening 10

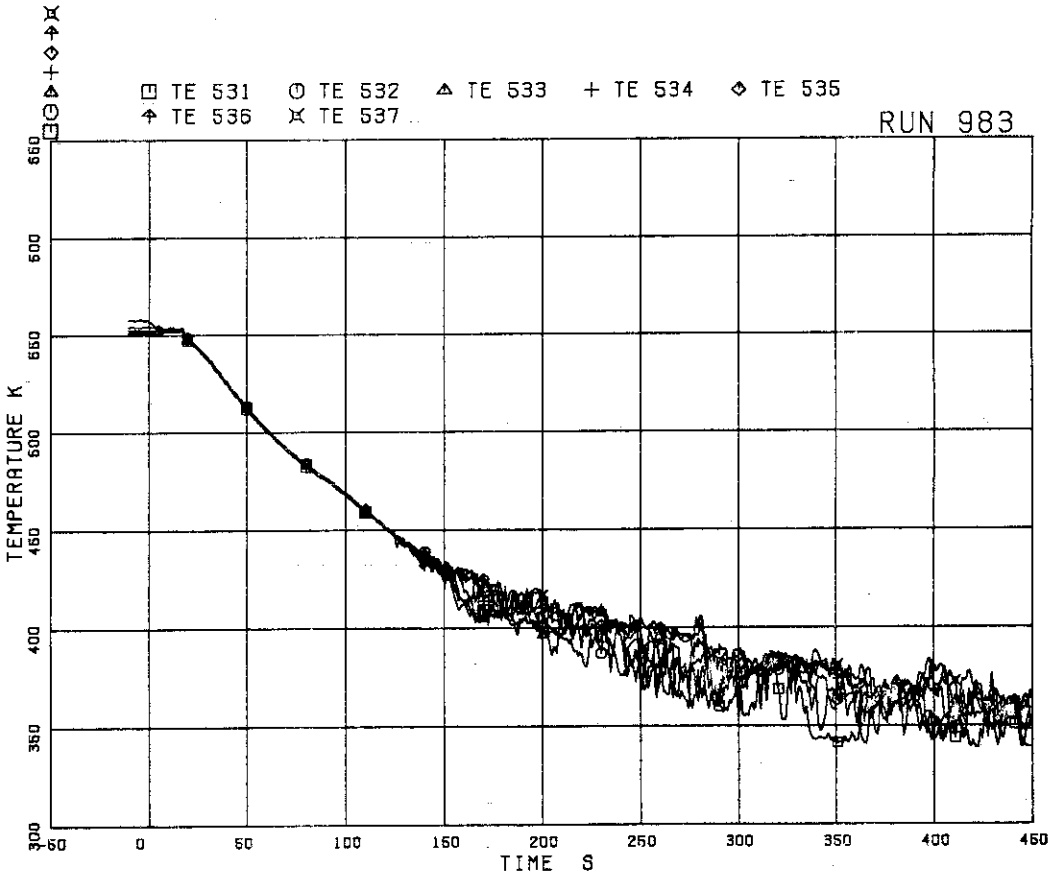

Fig. 5.148 Outer surface temperatures of channel box A at positions 1 through 7

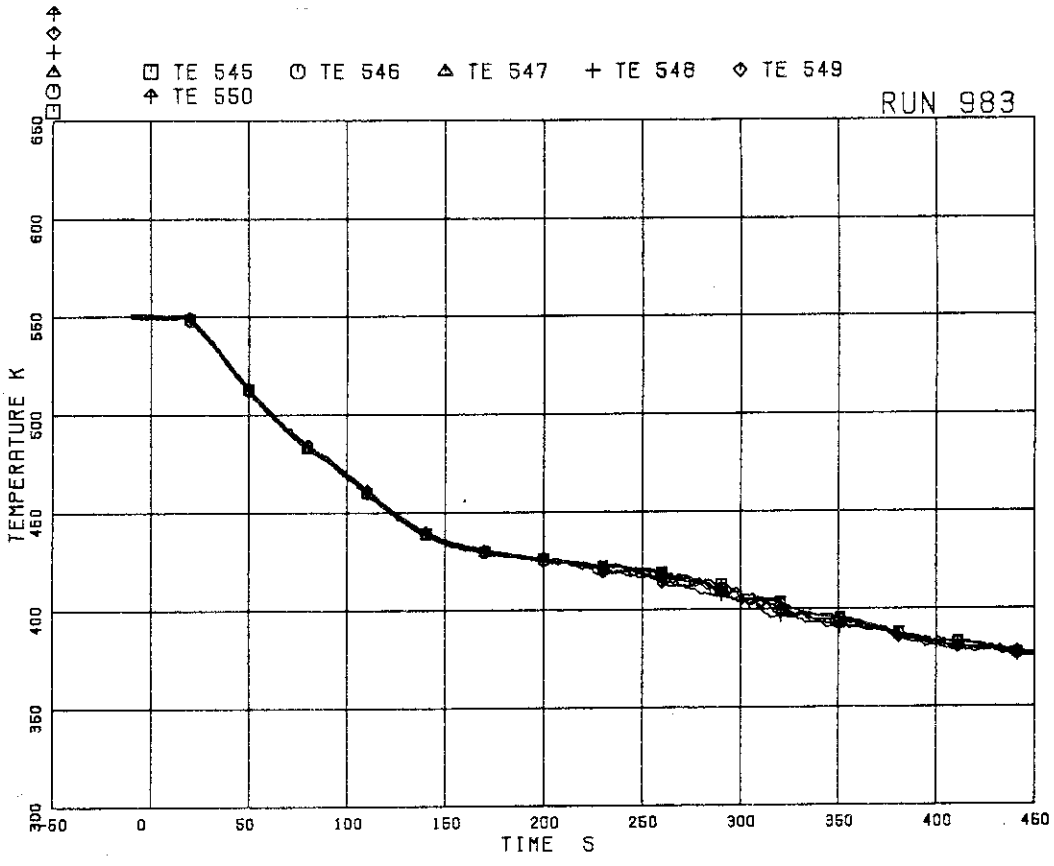

Fig. 5.149 Fluid temperatures in lower plenum, center

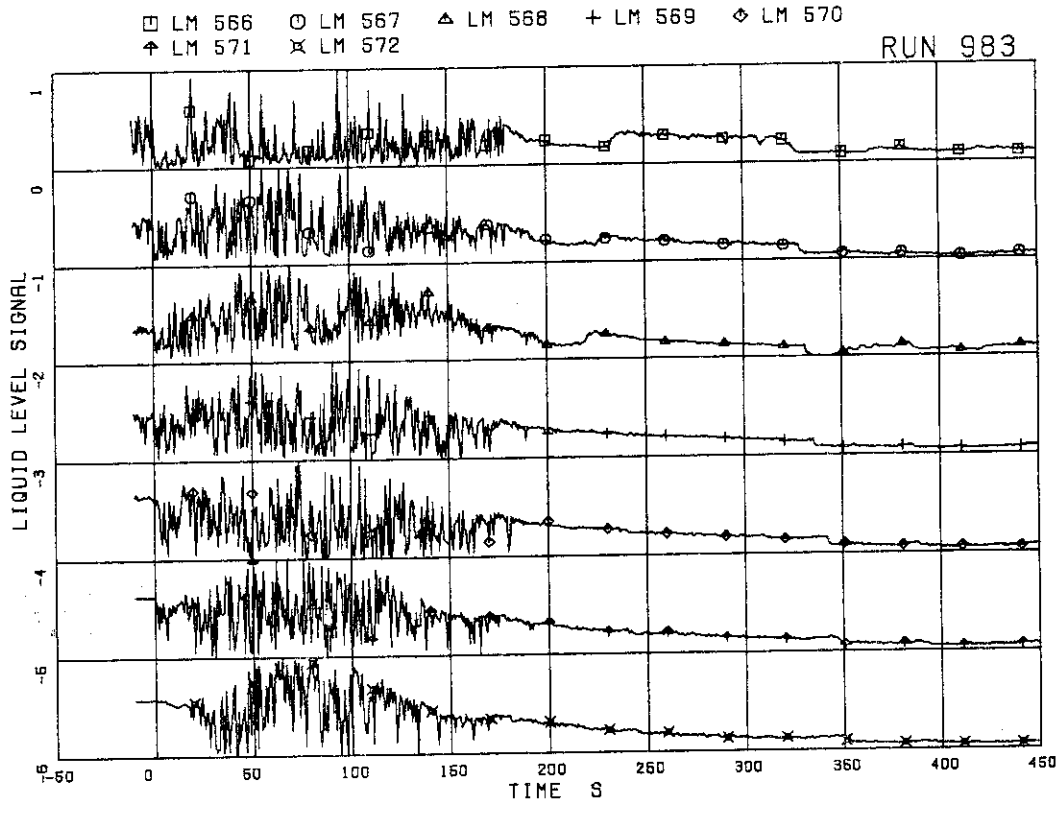

Fig. 5.150 Liquid level signals in channel box A, location A2

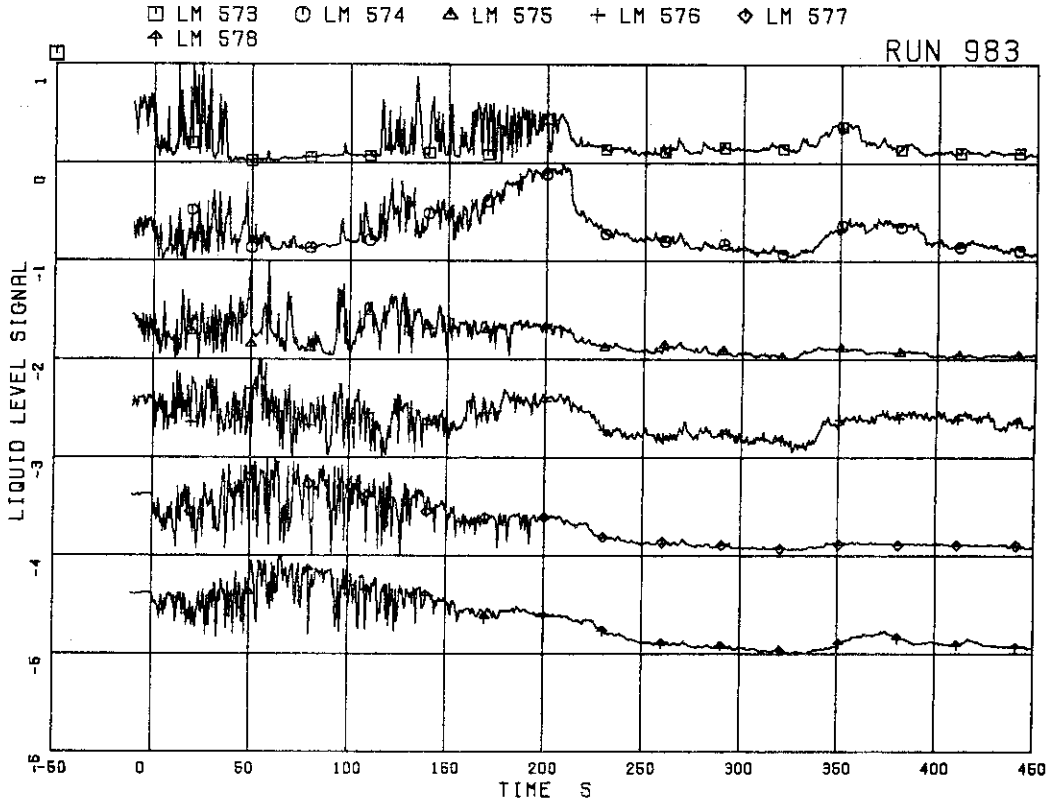

Fig. 5.151 Liquid level signals in channel box B

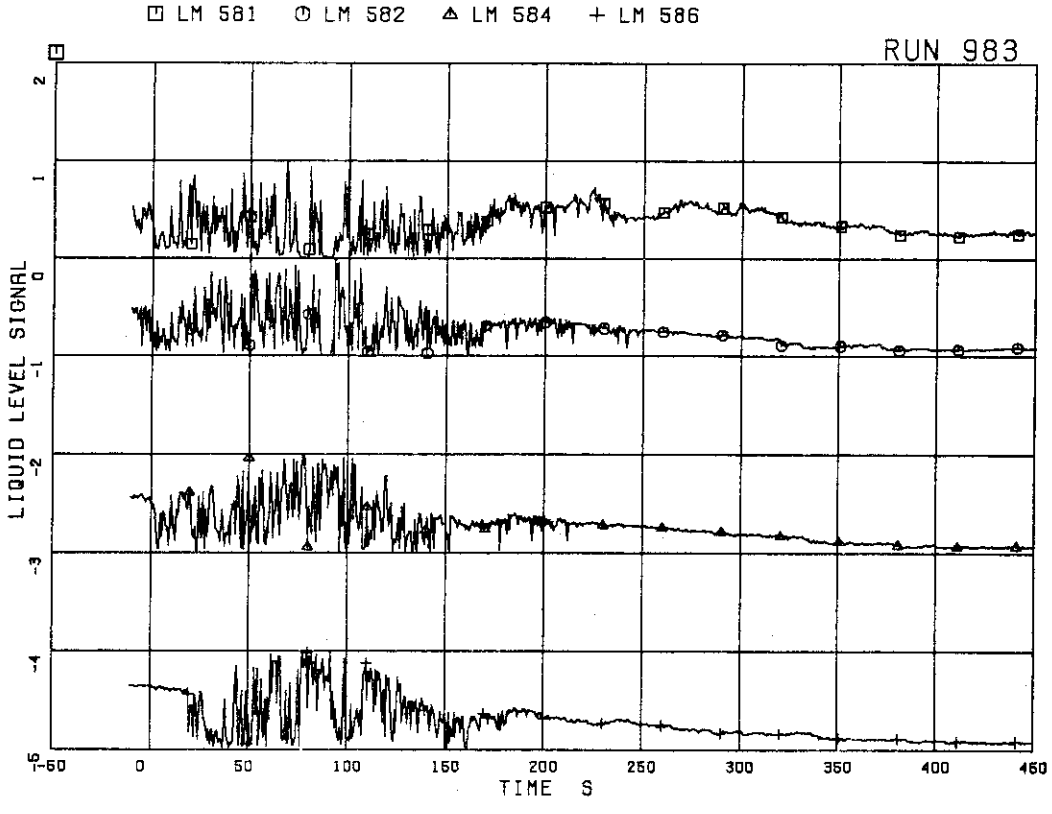

Fig. 5.152 Liquid level signals in channel box C

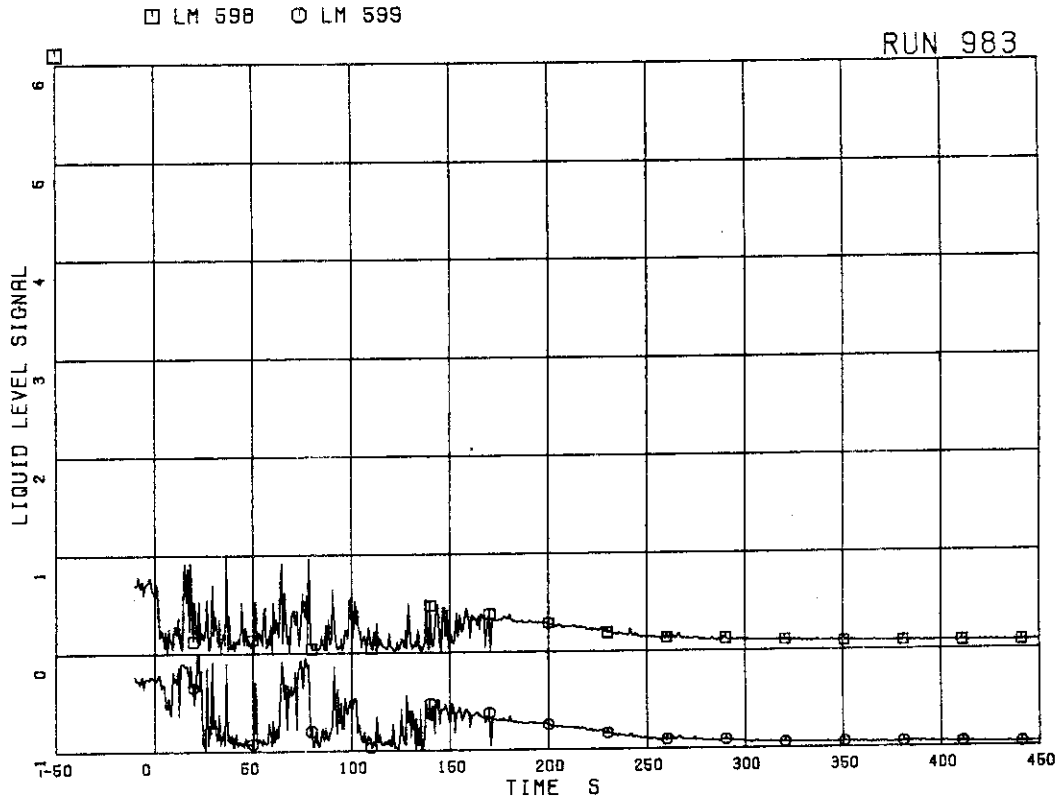

Fig. 5.153 Liquid level signals in channel A outlet, location A2

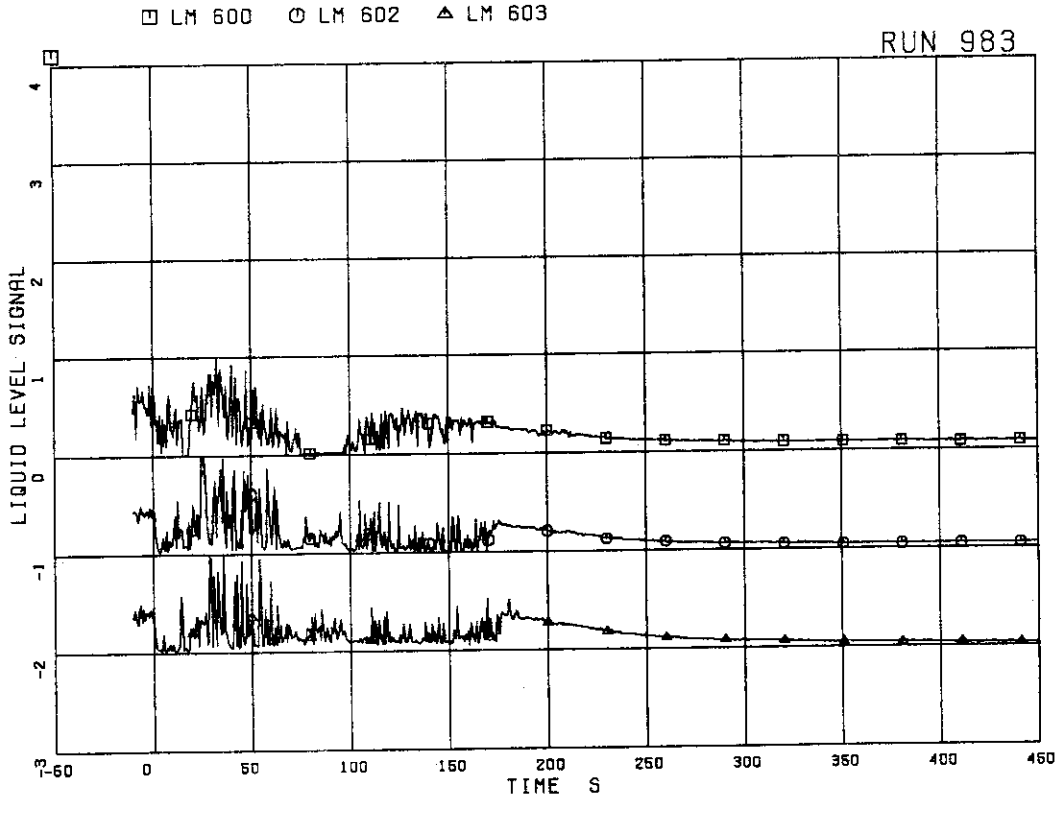

Fig. 5.154 Liquid level signals in channel A outlet, center

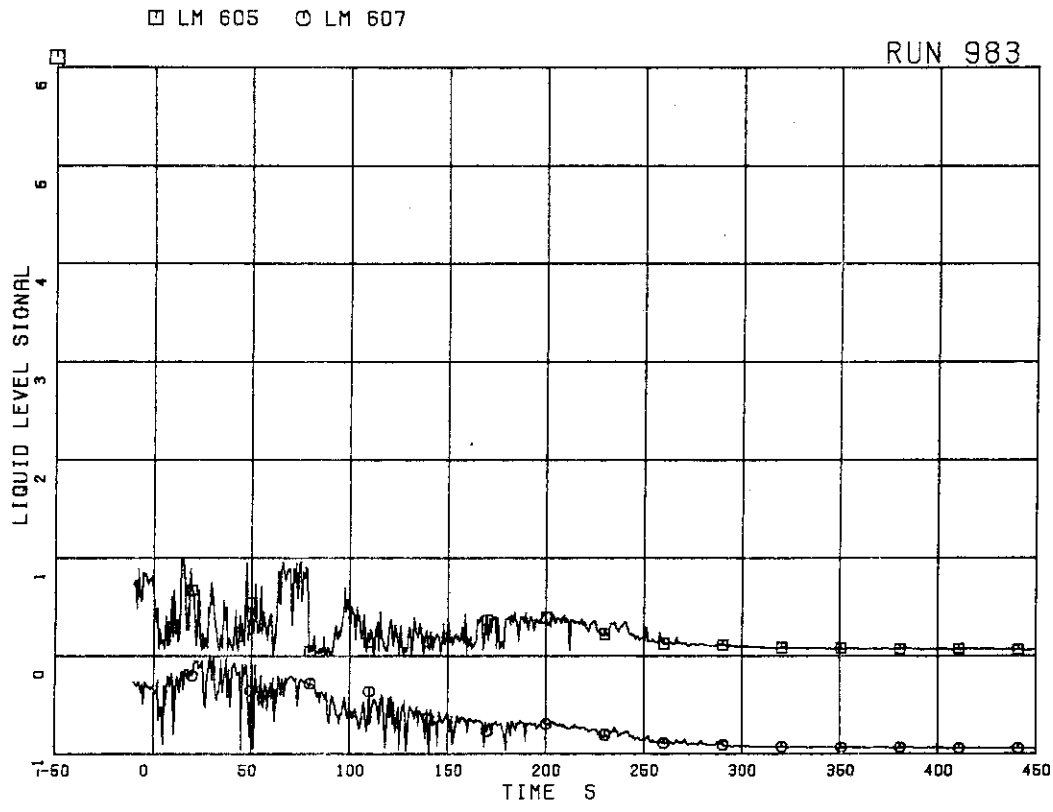

Fig. 5.155 Liquid level signals in channel C outlet, location C1

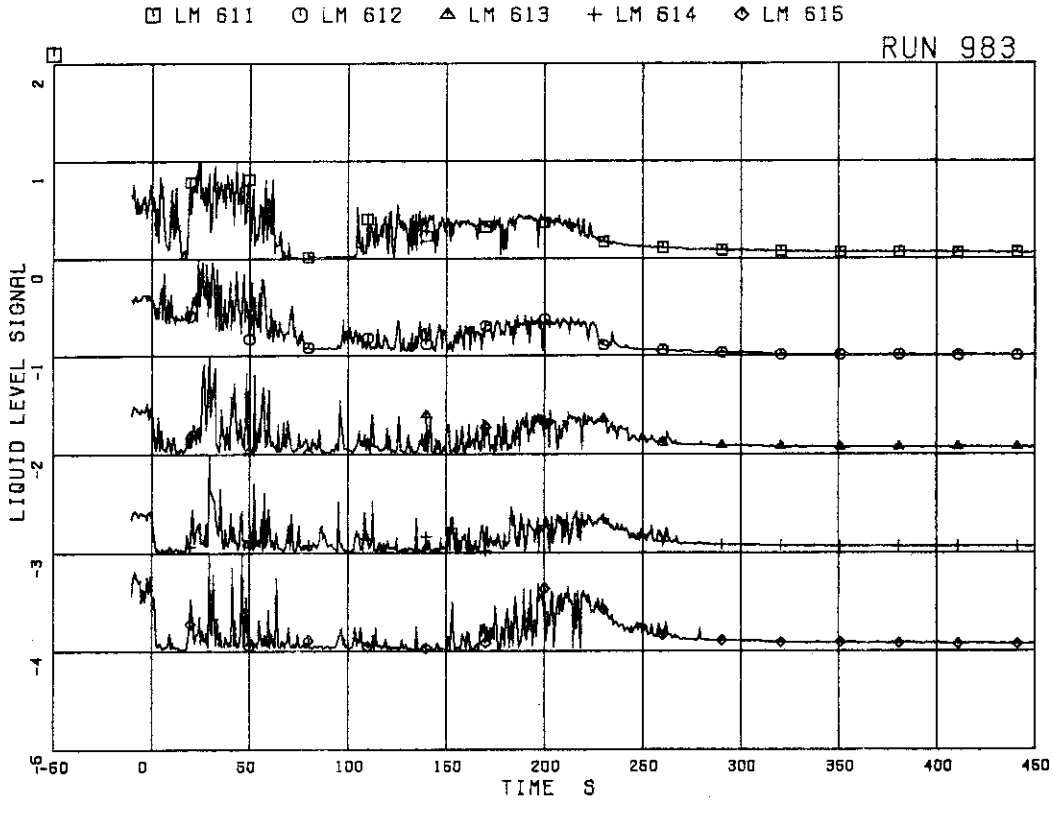

Fig. 5.156 Liquid level signals in channel C outlet, center

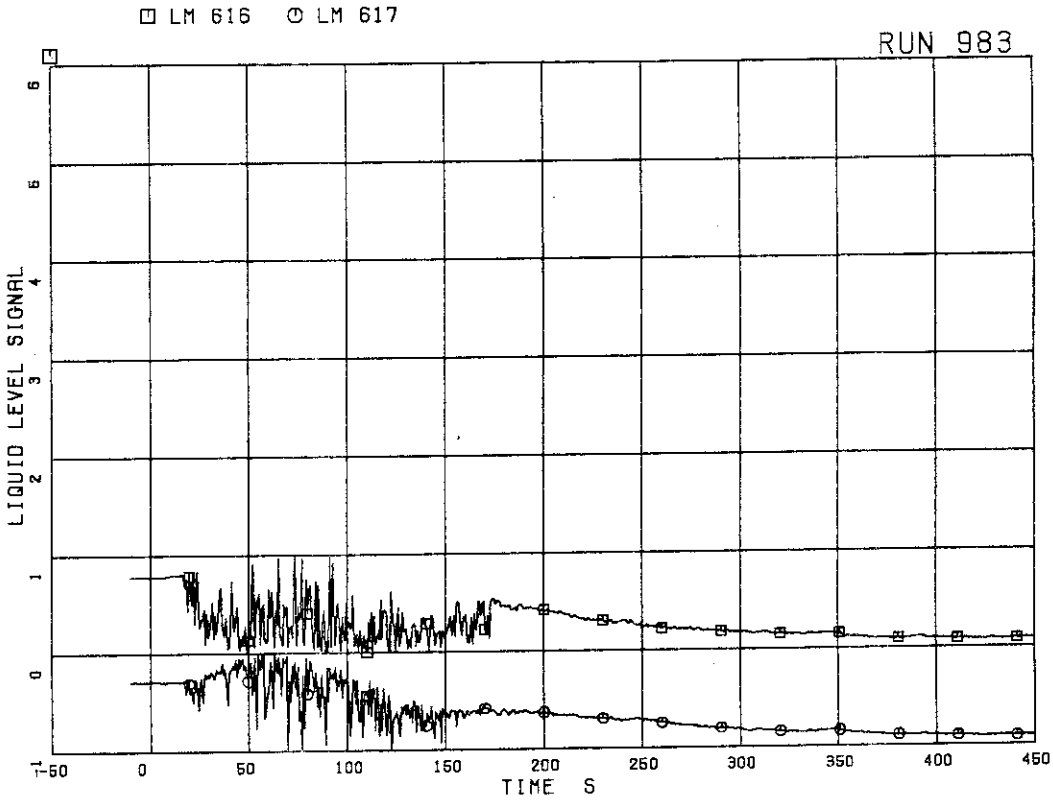

Fig. 5.157 Liquid level signals in channel A inlet

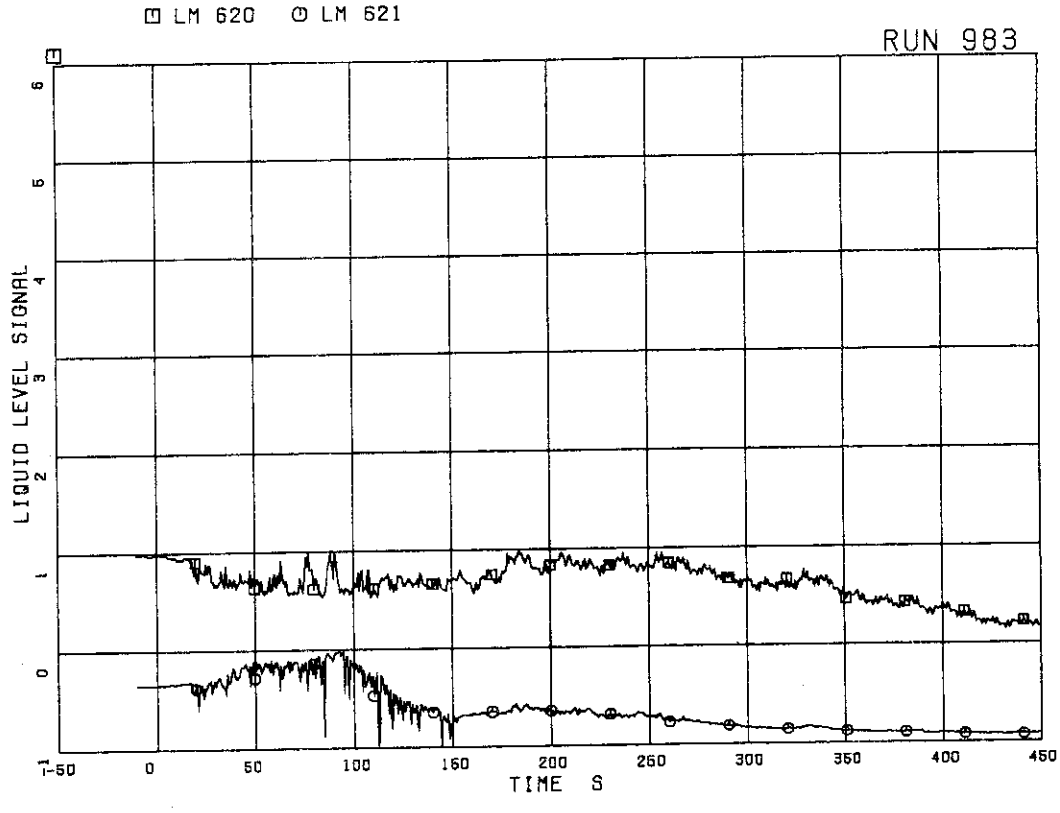

Fig. 5.158 Liquid level signals in channel C inlet

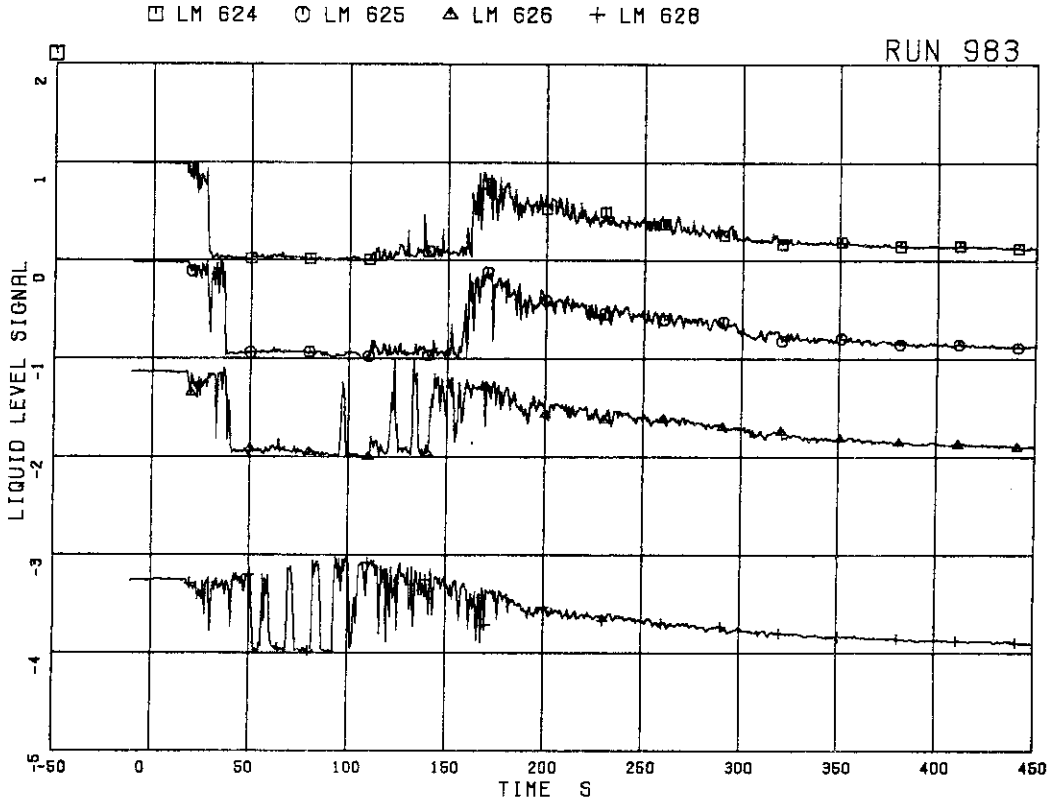

Fig. 5.159 Liquid level signals in lower plenum, north

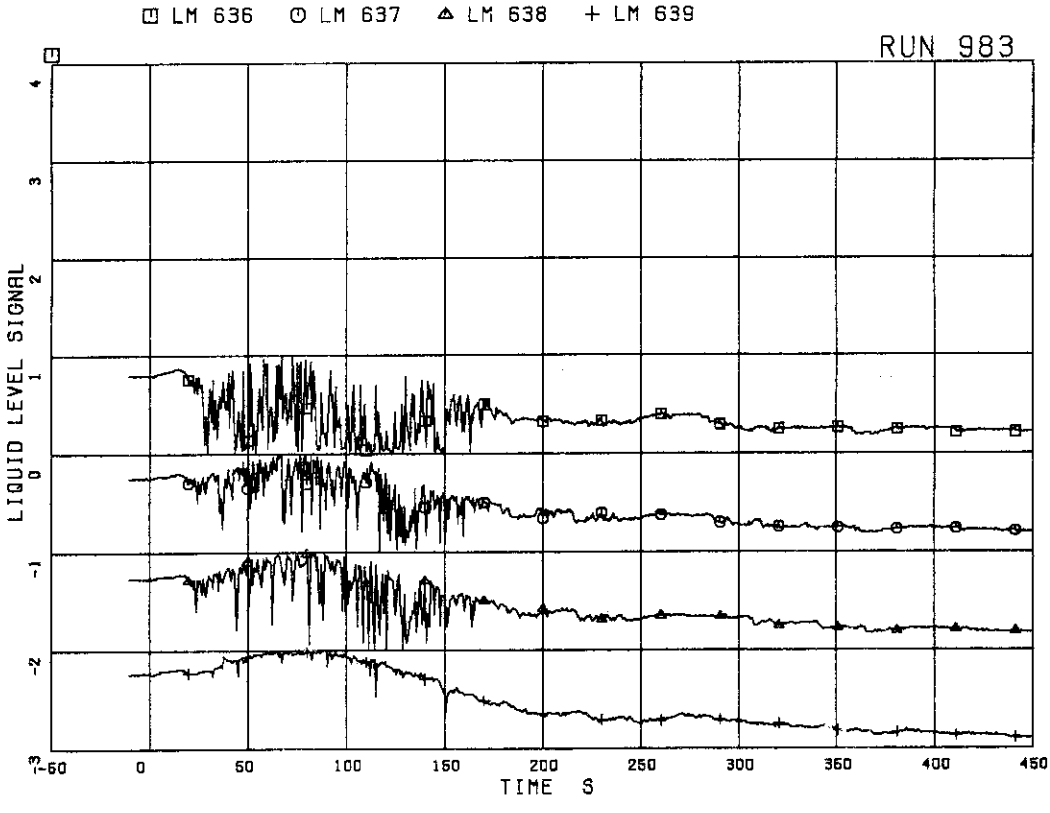

Fig. 5.160 Liquid level signals in guide tube, north side

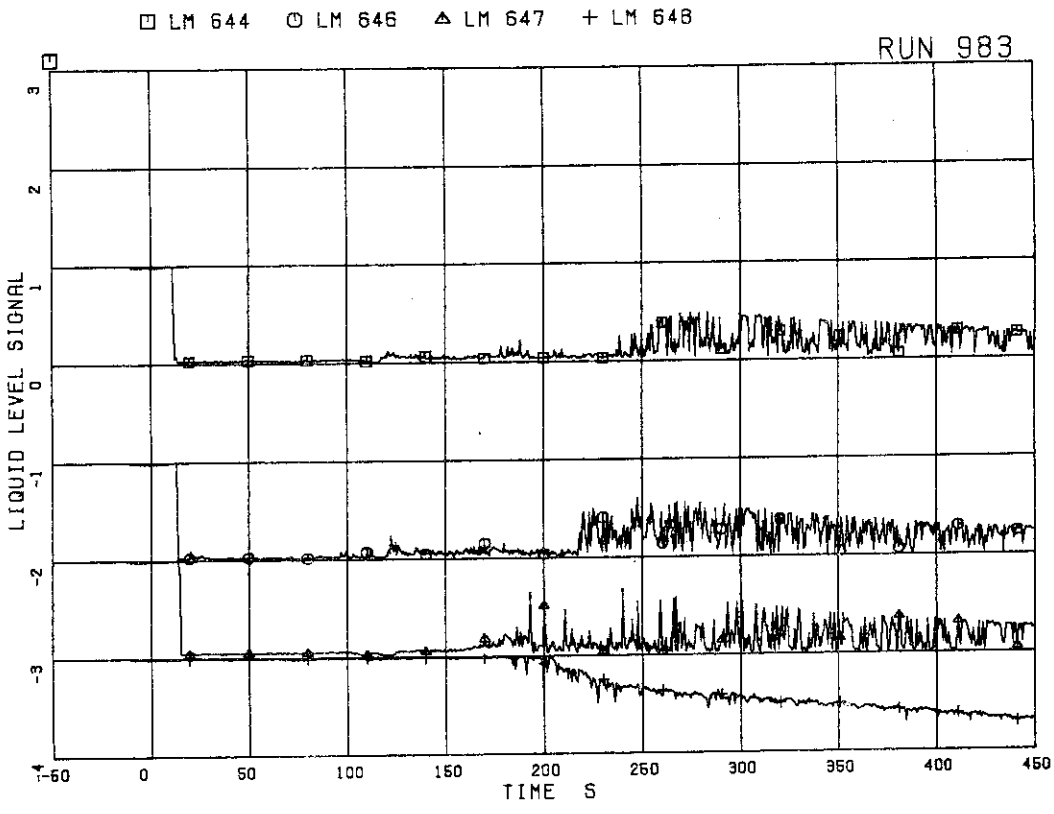

Fig. 5.161 Liquid level signals in downcomer, D side

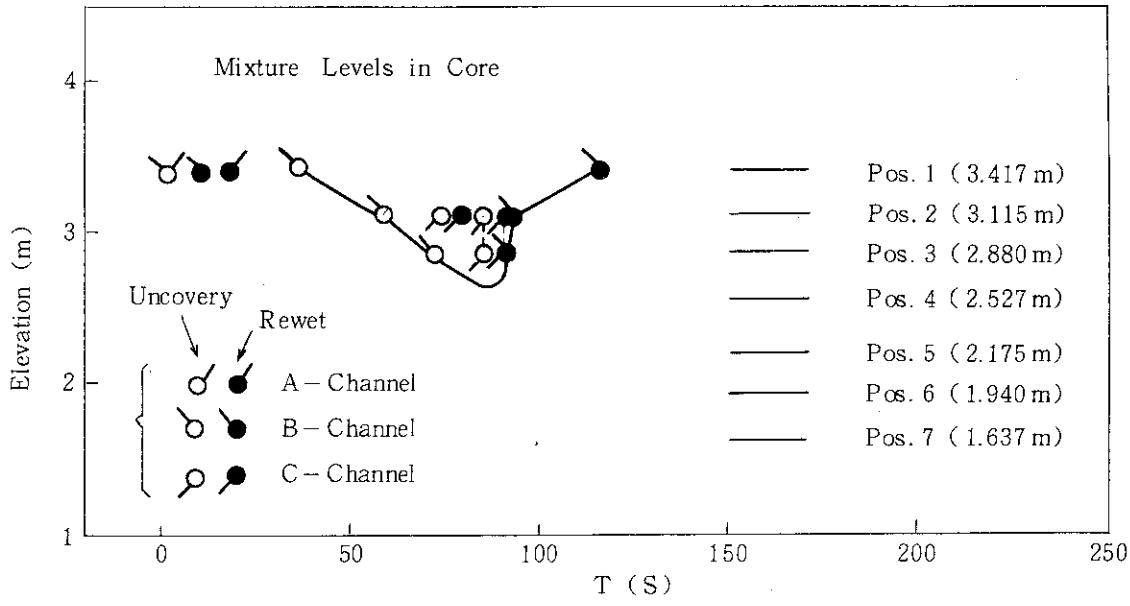

Fig. 5.162 Estimated liquid levels in core

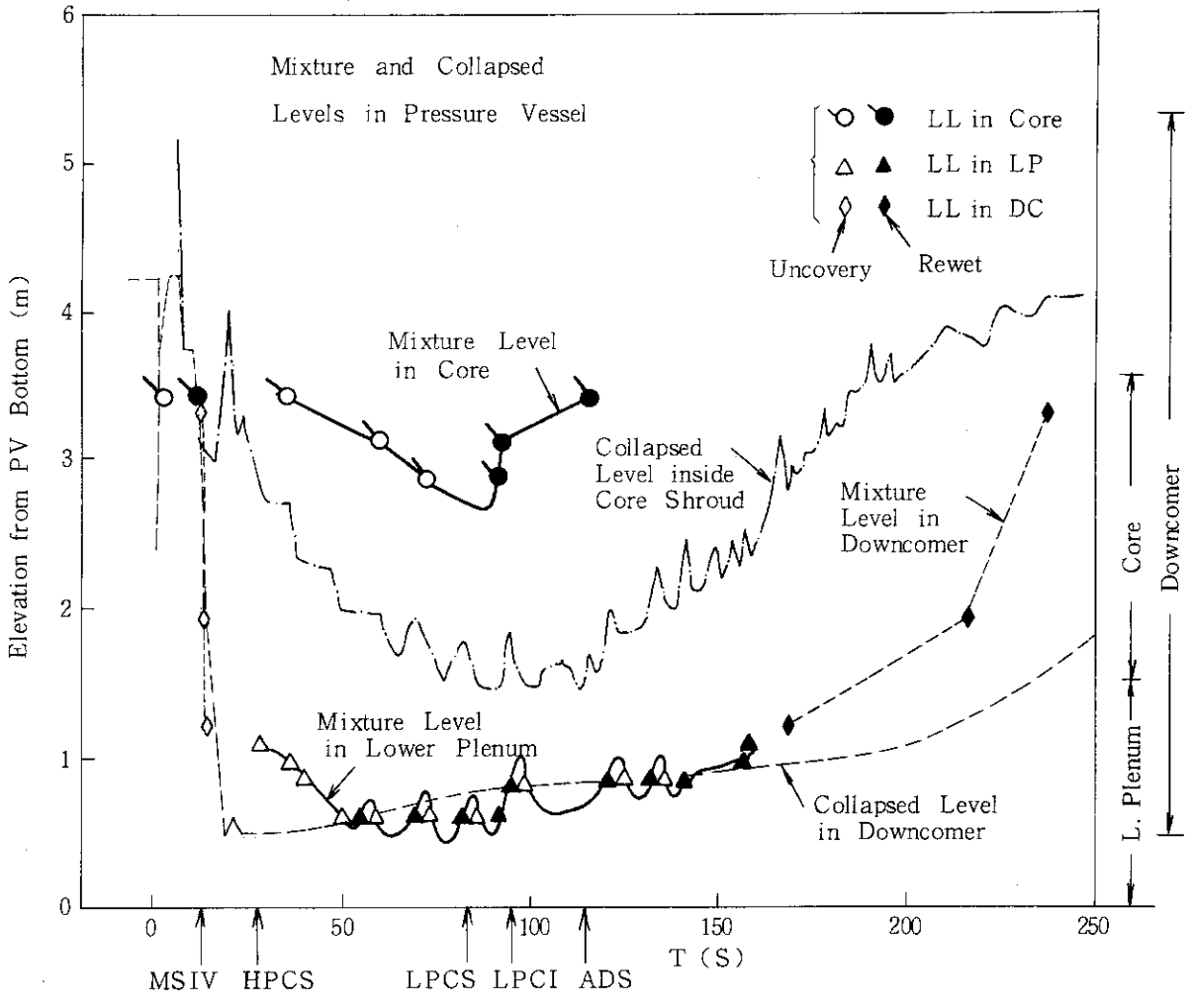

Fig. 5.163 Estimated liquid levels in pressure vessel

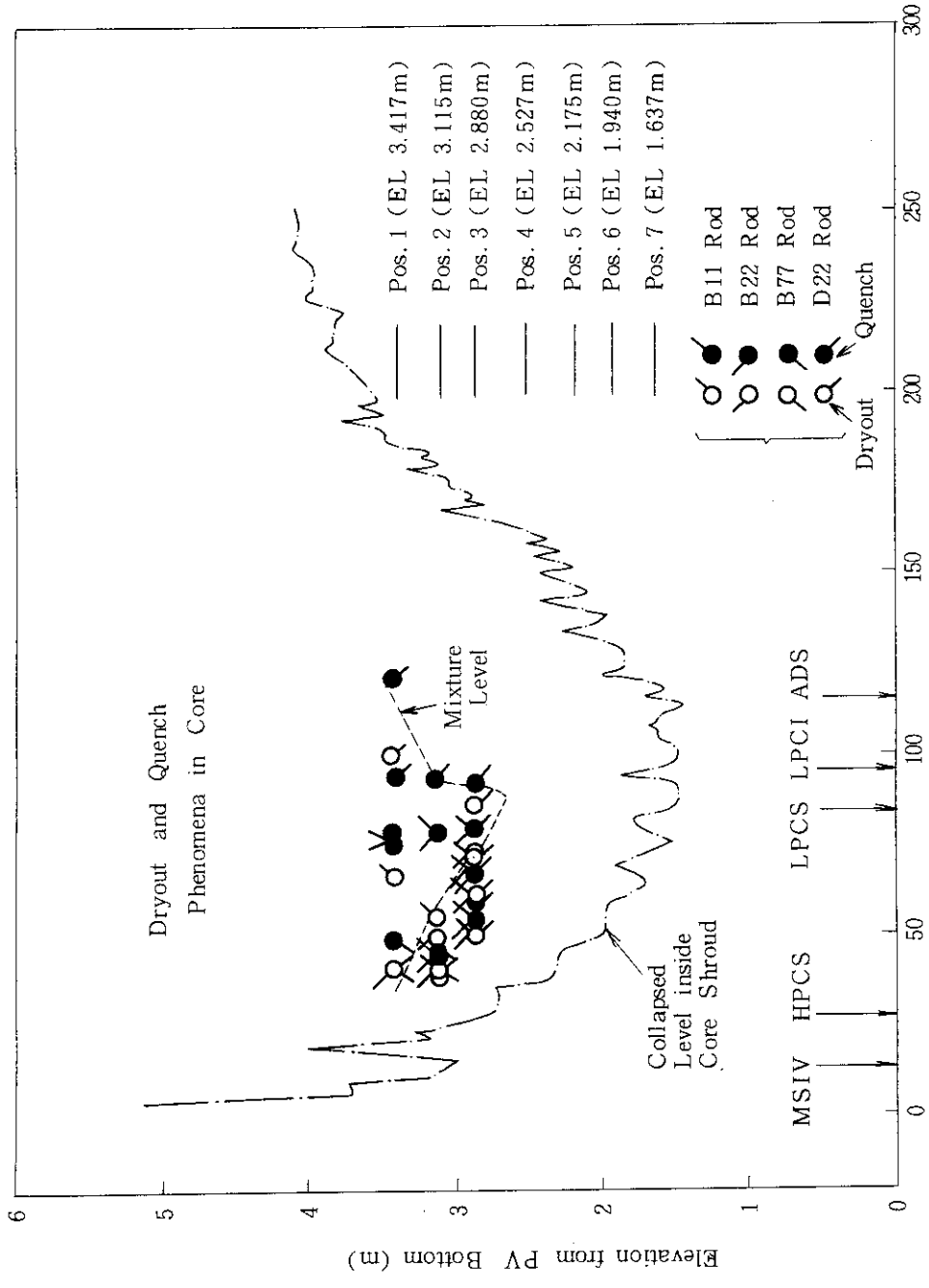

Fig. 5.164 Dryout and quench times of fuel rods in core

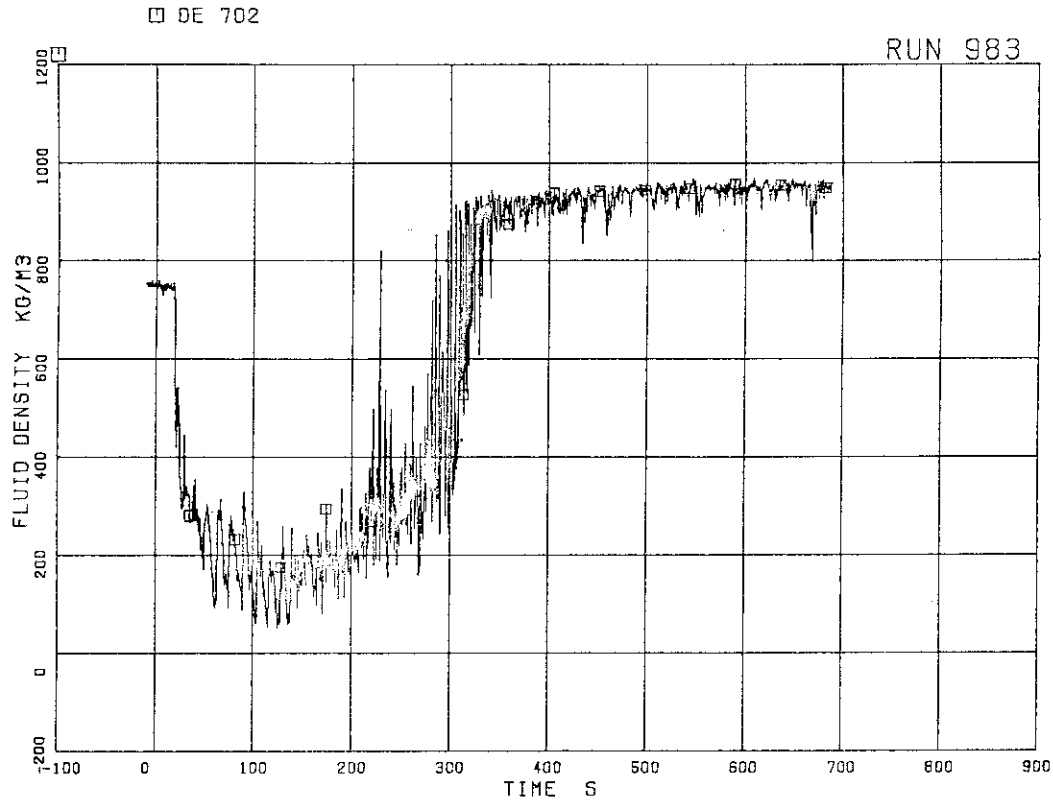

Fig. 5.165 Average density at JP3,4 outlet

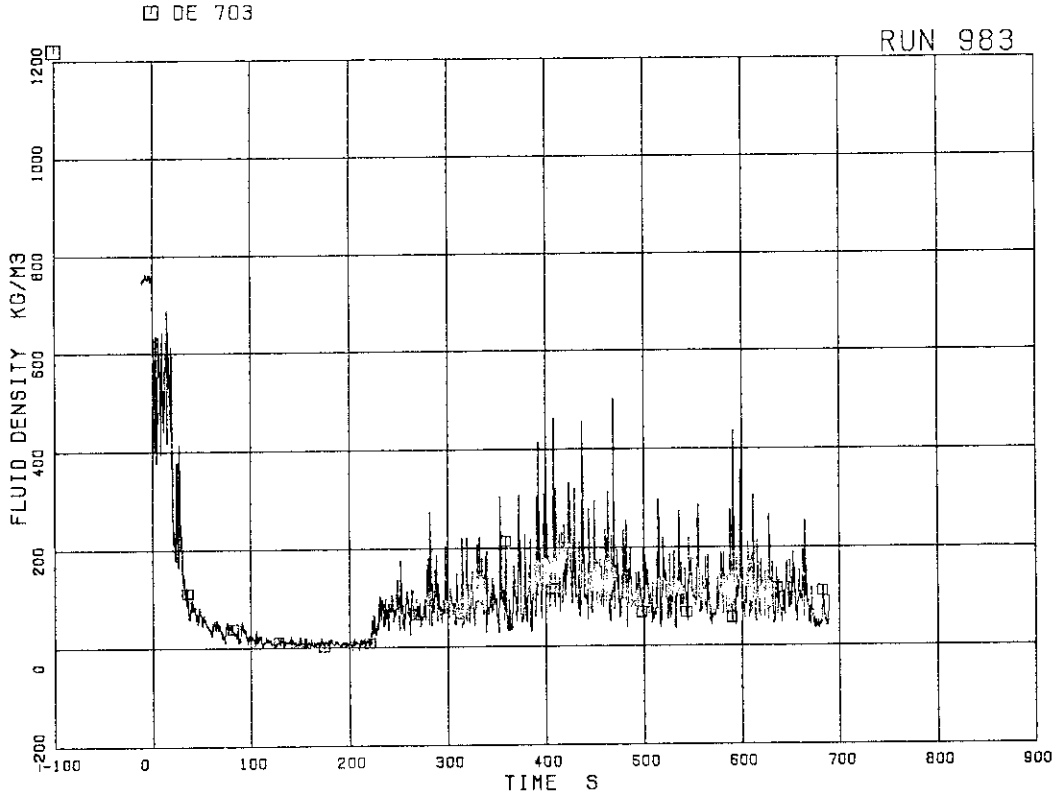

Fig. 5.166 Average density at MRP side of break (break A)

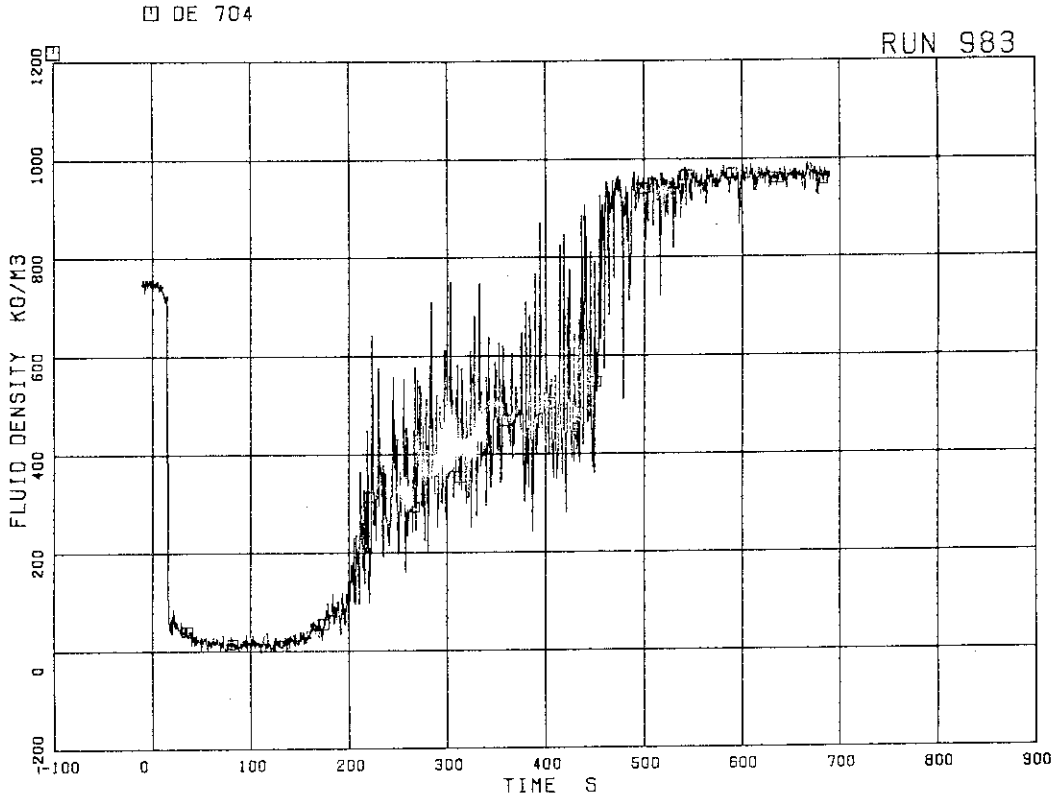

Fig. 5.167 Average density at PV side of break (break B)

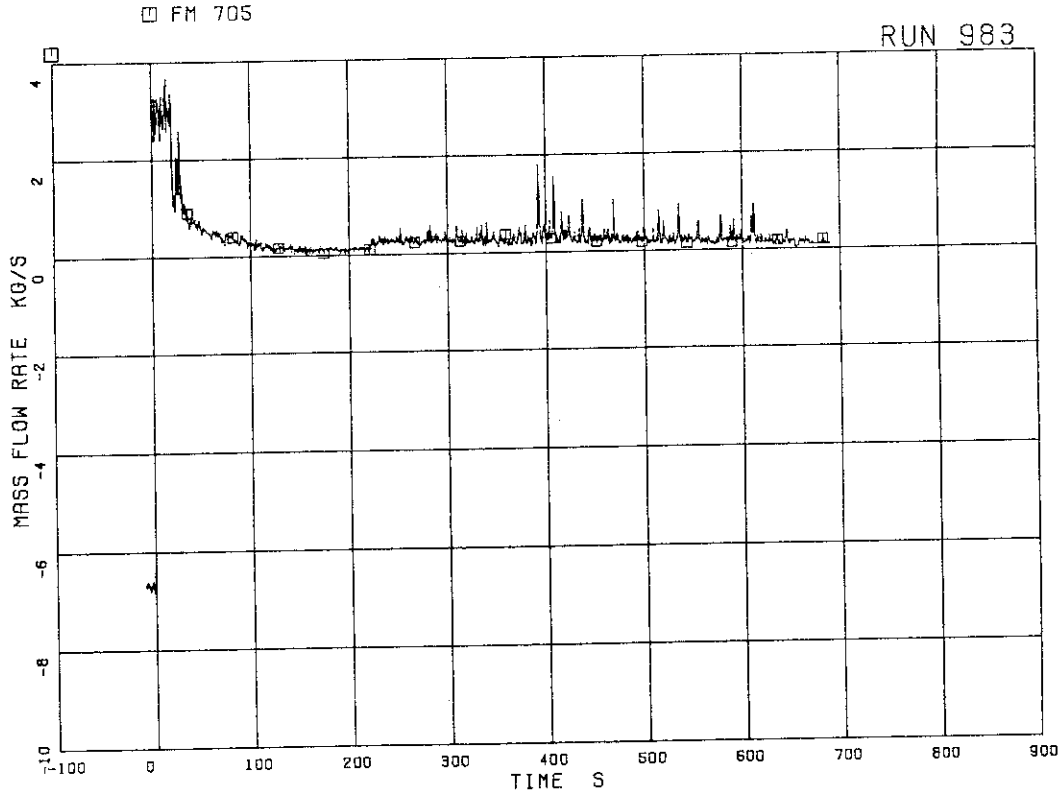

Fig. 5.168 Flow rate at MRP side of break (low range)

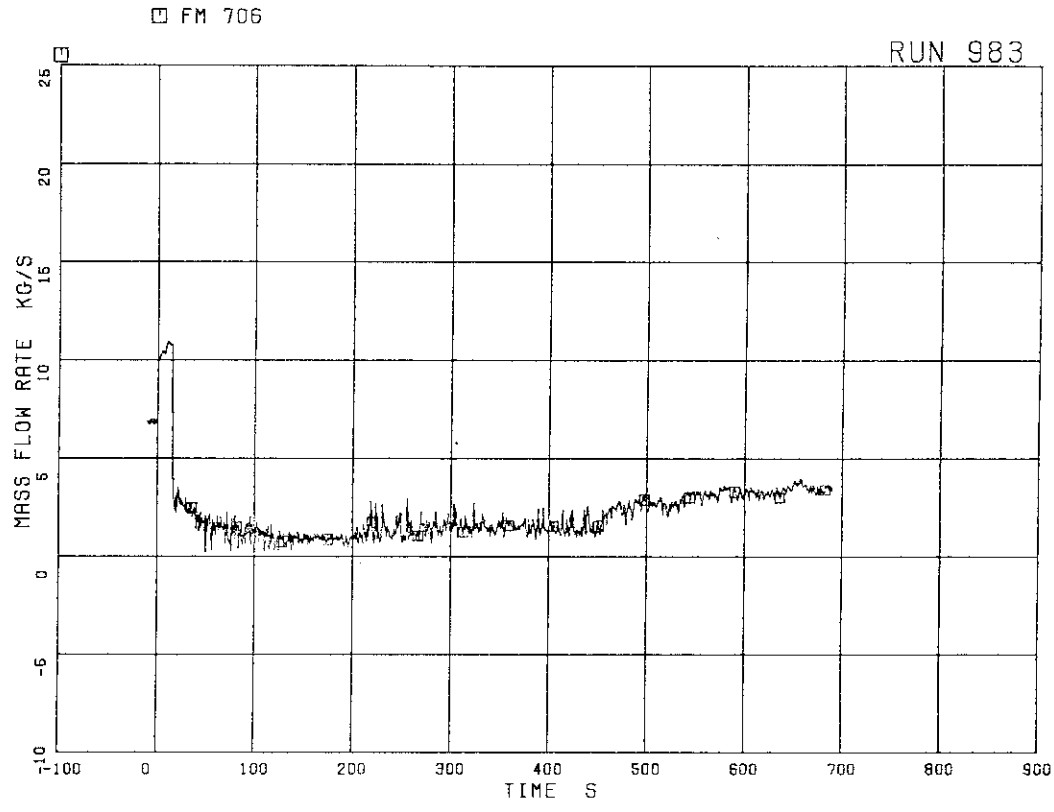

Fig. 5.169 Flow rate at PV side of break (low range)

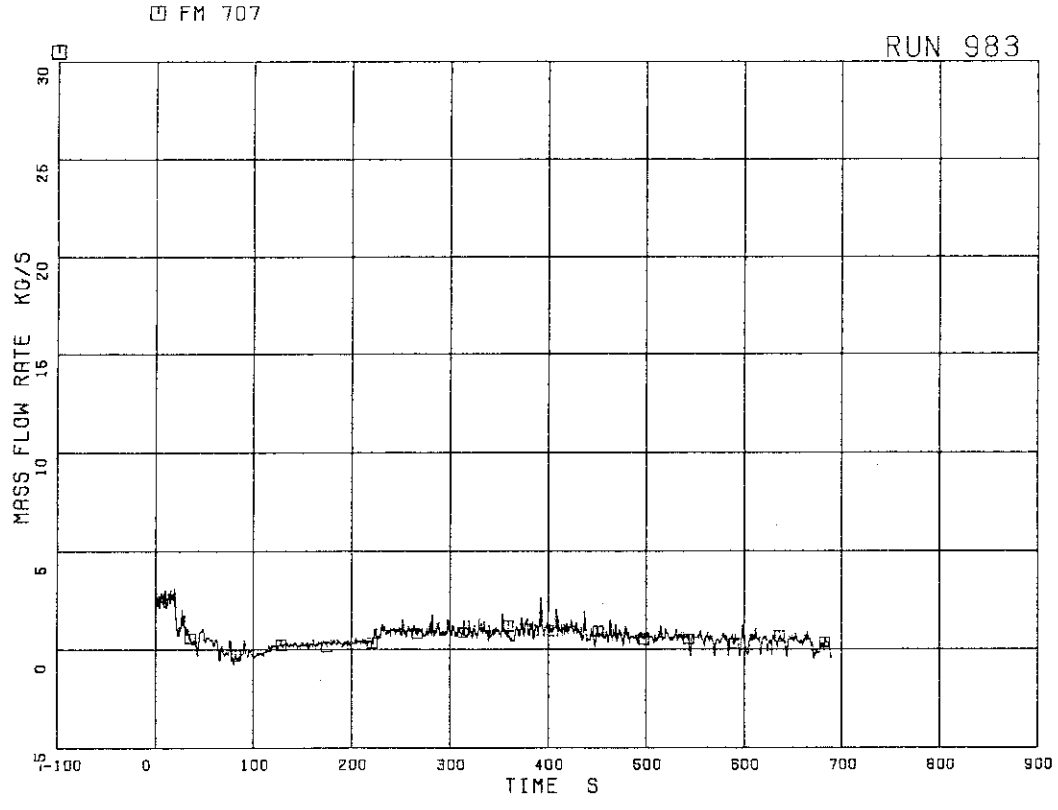

Fig. 5.170 Flow rate at MRP side of break (high range)

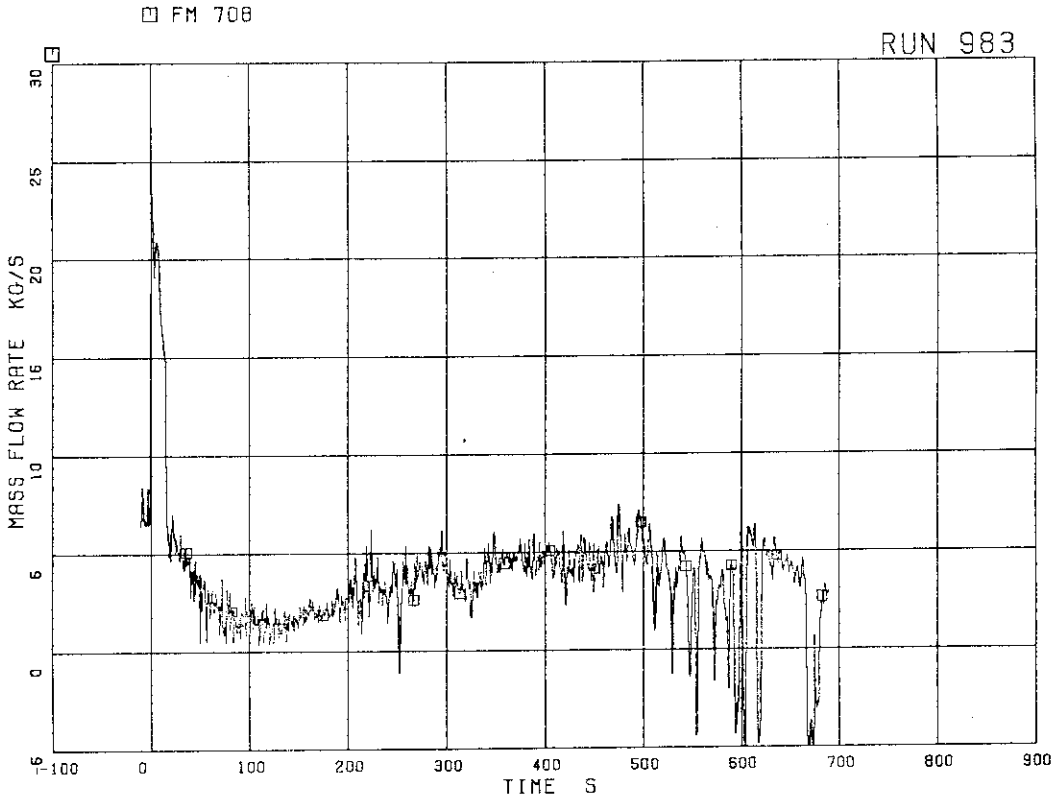

Fig. 5.171 Flow rate at PV side of break (high range)

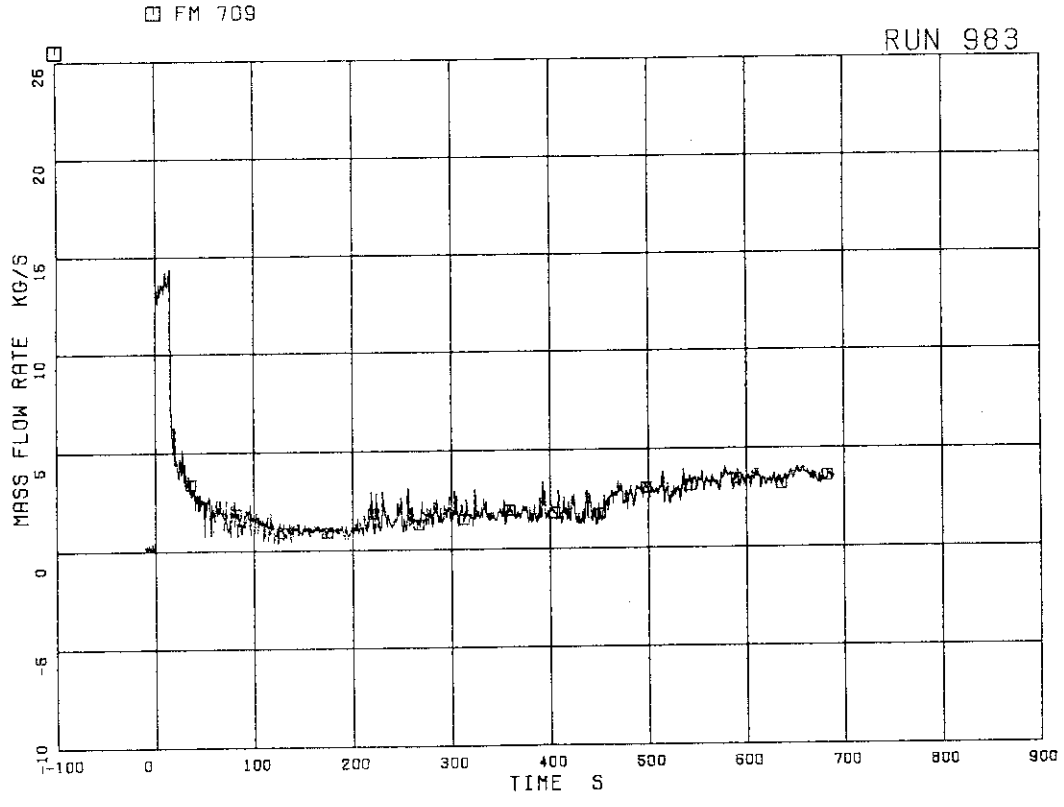

Fig. 5.172 Total discharge flow rate from break (low range)

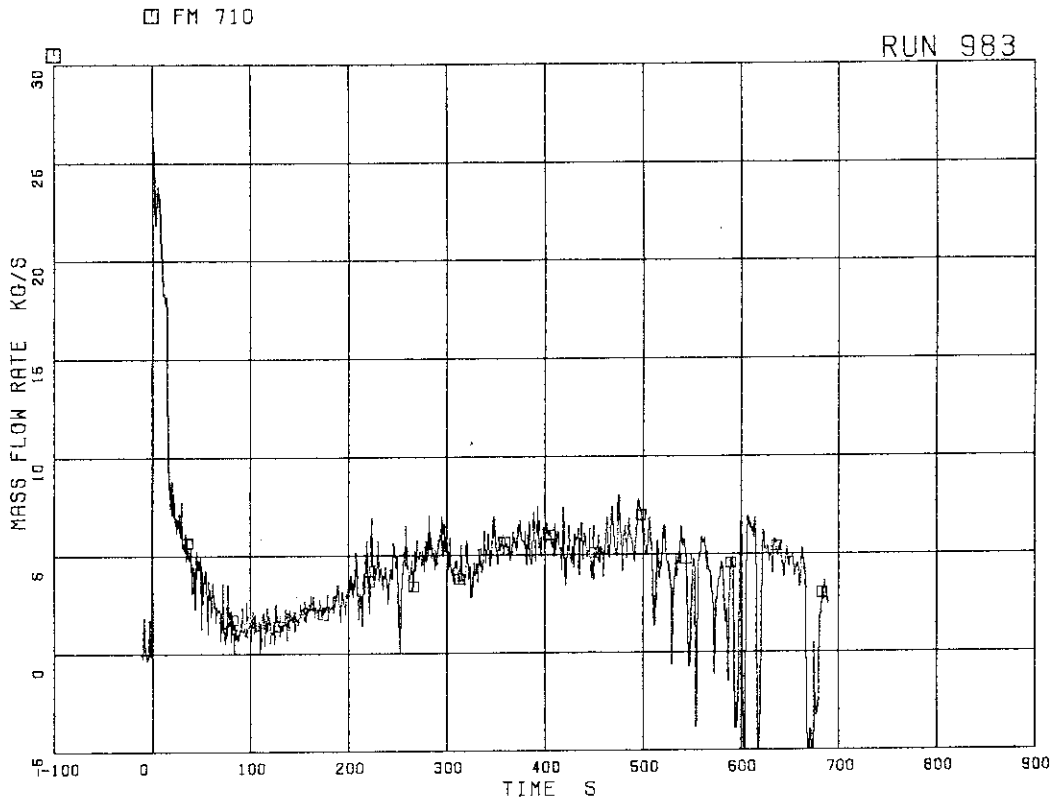

Fig. 5.173 Total discharge flow rate from break (high range)

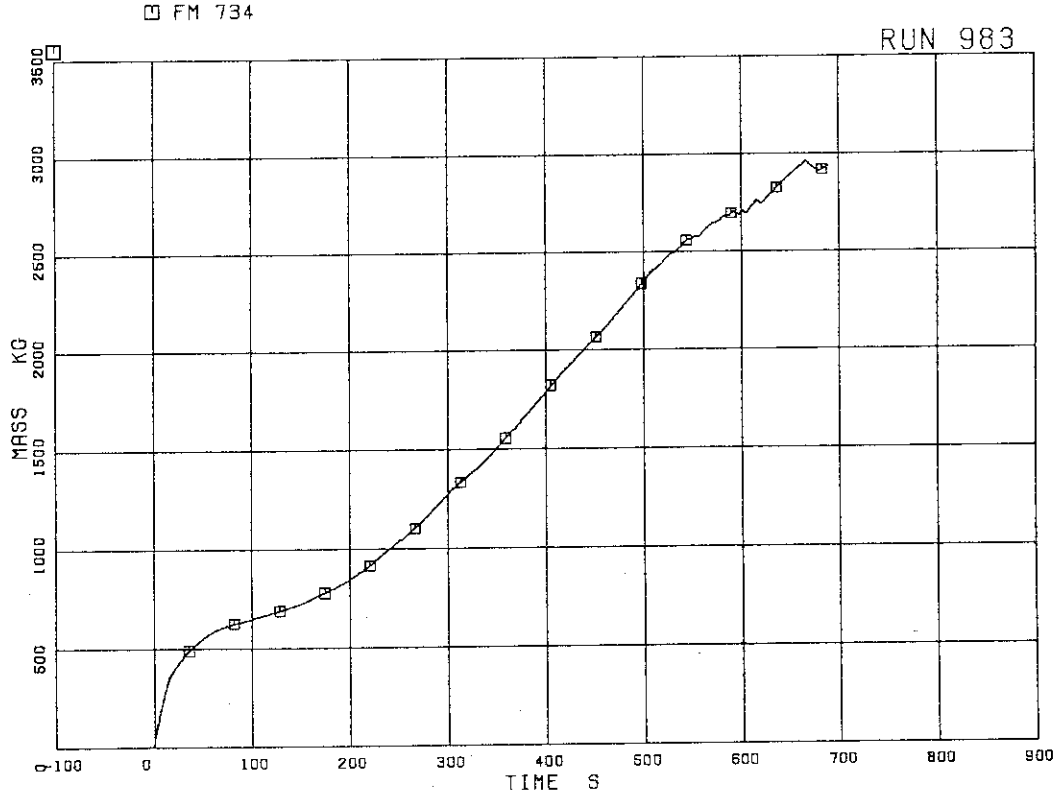

Fig. 5.174 Integrated discharged mass from breaks A and B (high range drag disk and densitometer)

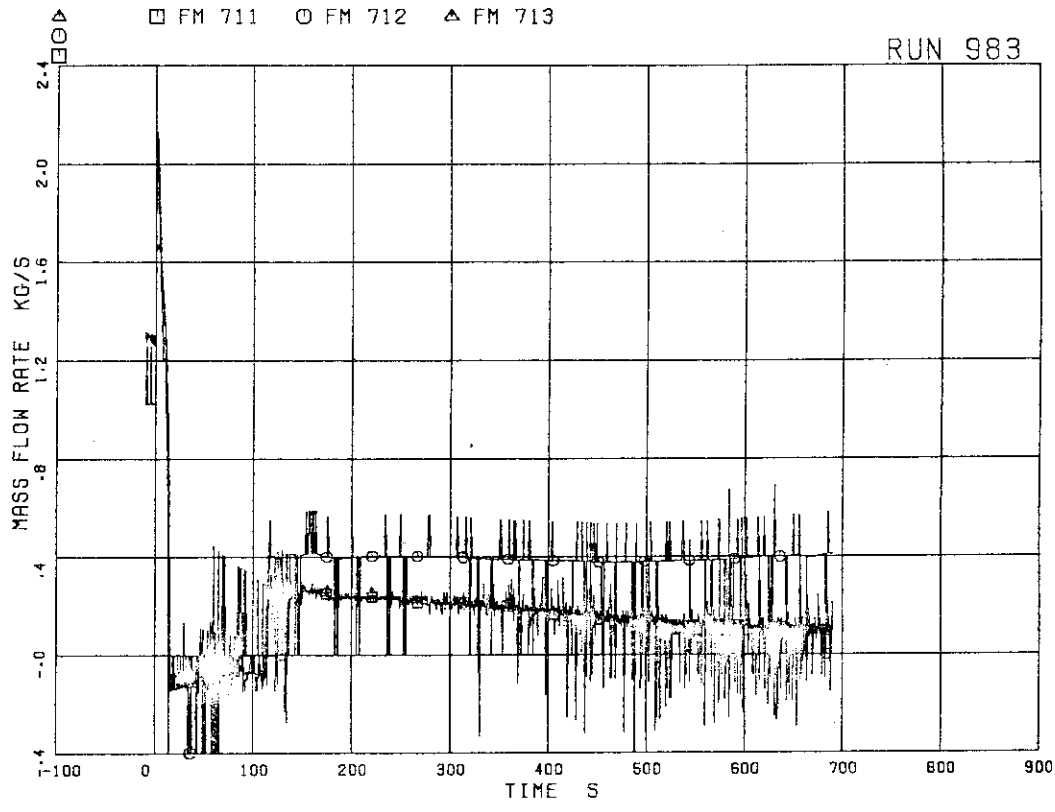

Fig. 5.175 Steam discharge flow rate through MSL

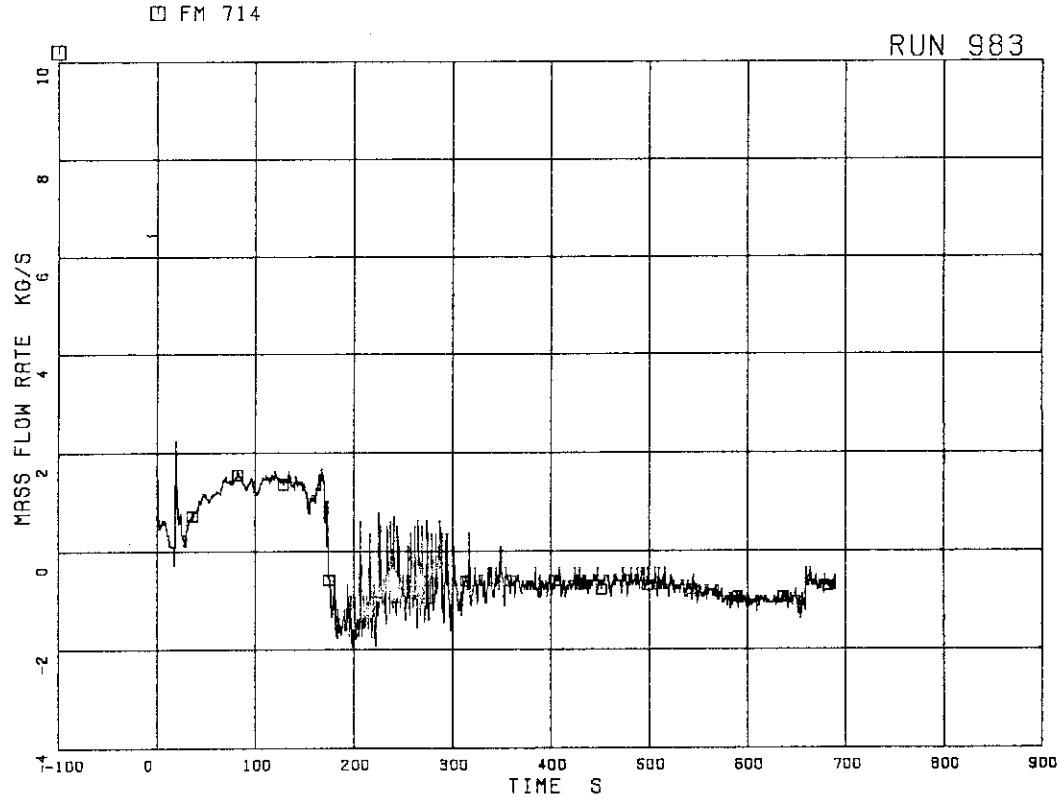

Fig. 5.176 Flow rate at channel A inlet

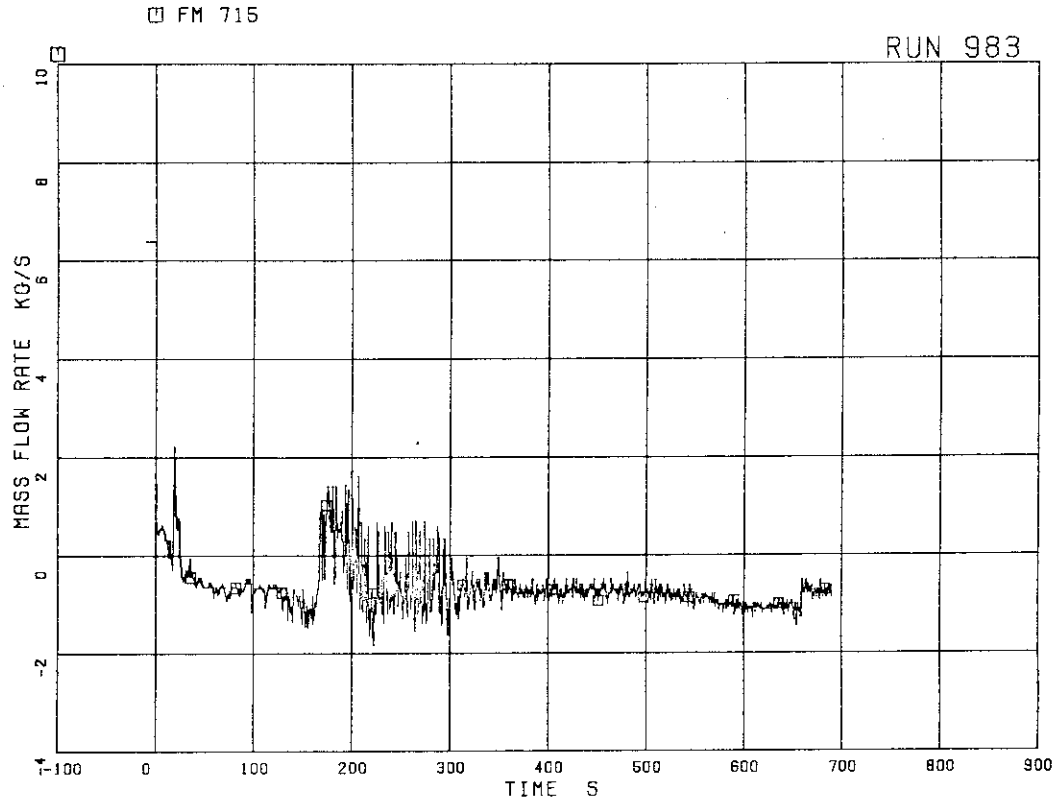

Fig. 5.177 Flow rate at channel B inlet

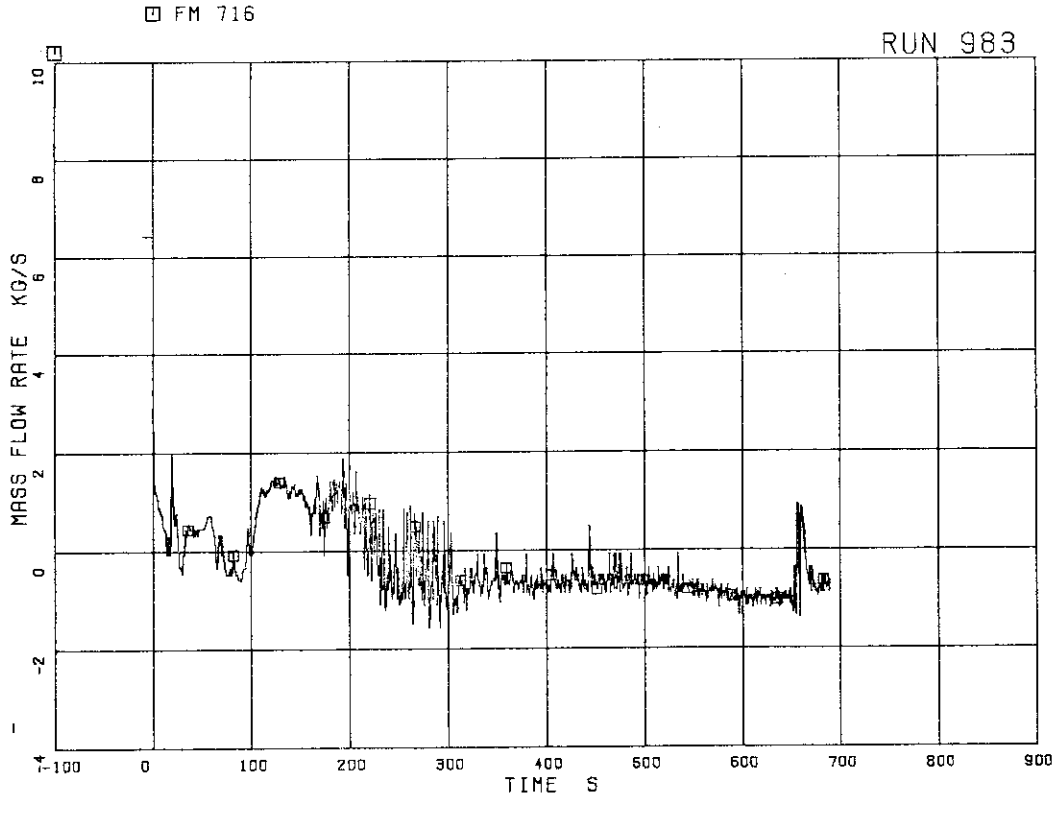

Fig. 5.178 Flow rate at channel C inlet

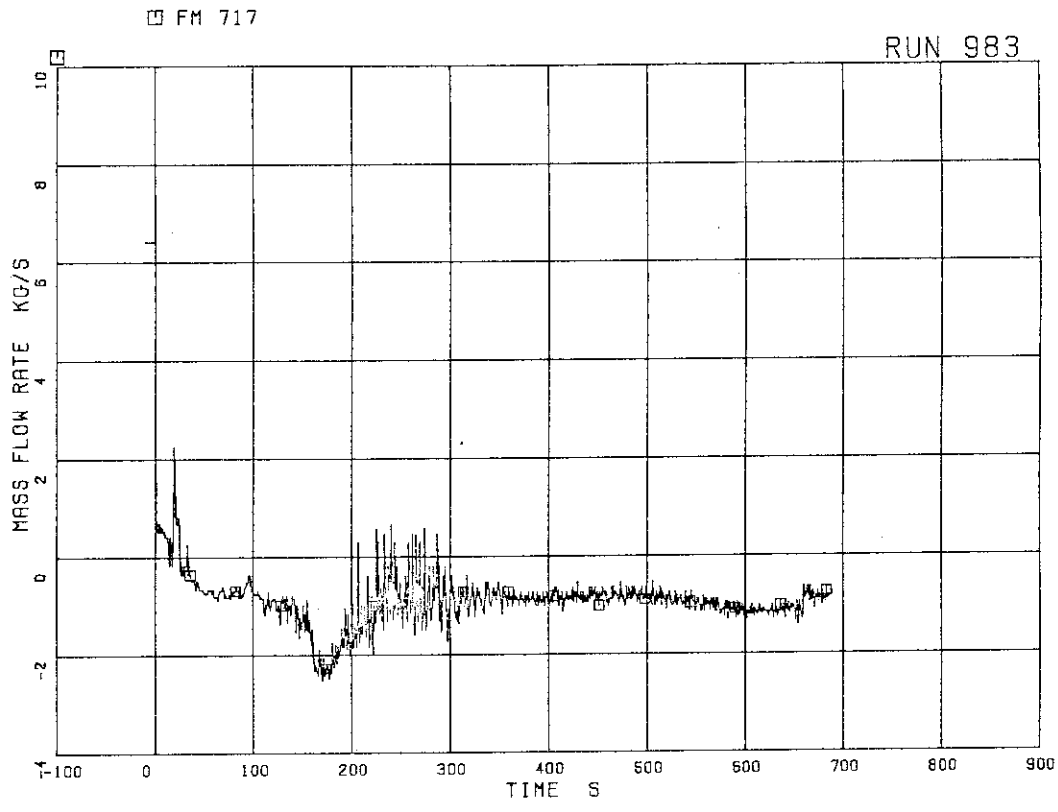

Fig. 5.179 Flow rate at channel D inlet

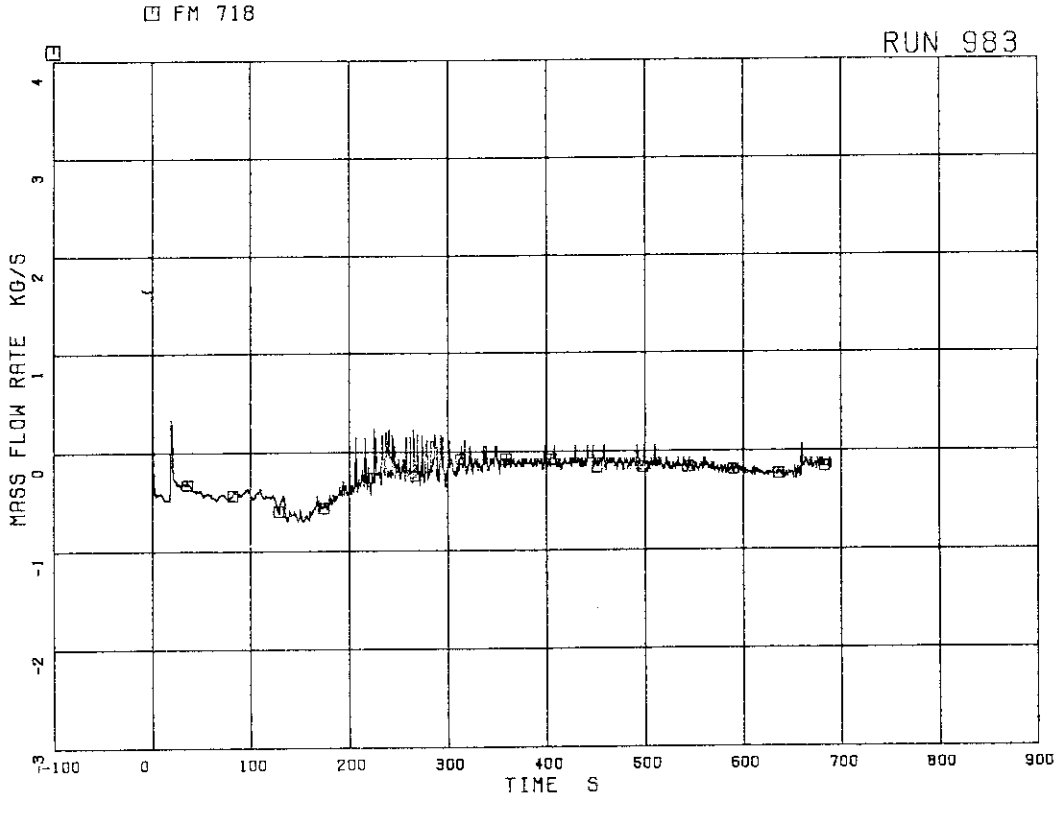

Fig. 5.180 Flow rate at bypass hole

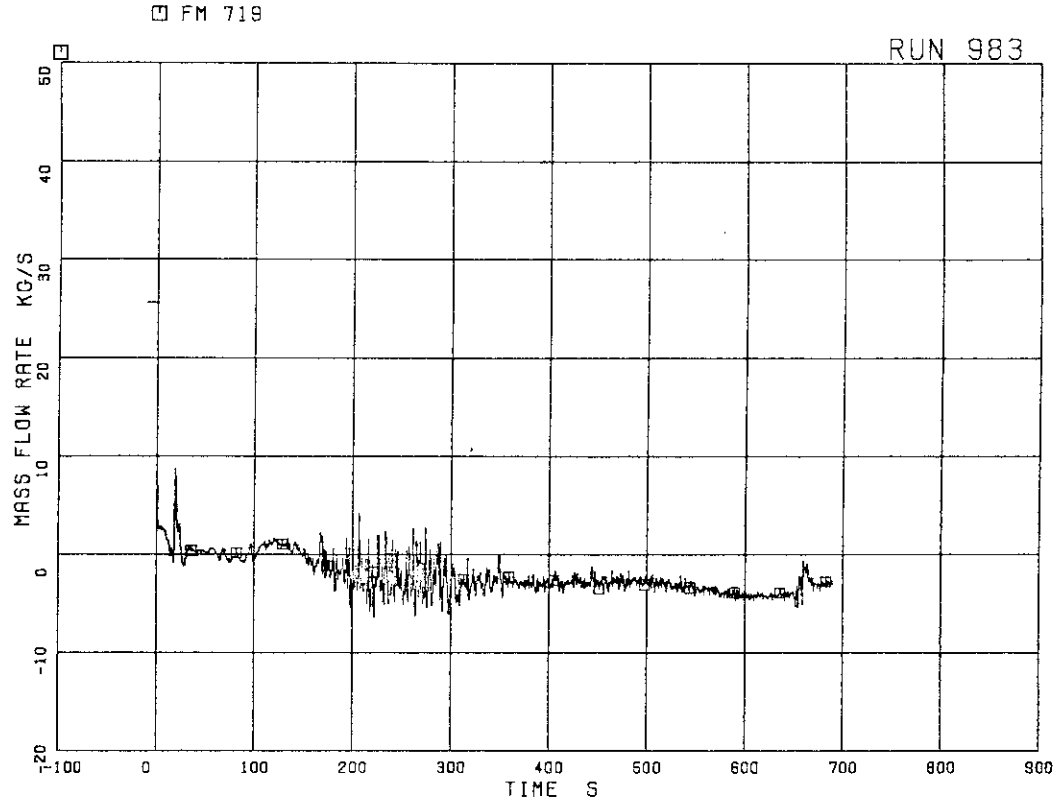

Fig. 5.181 Total channel inlet flow rate

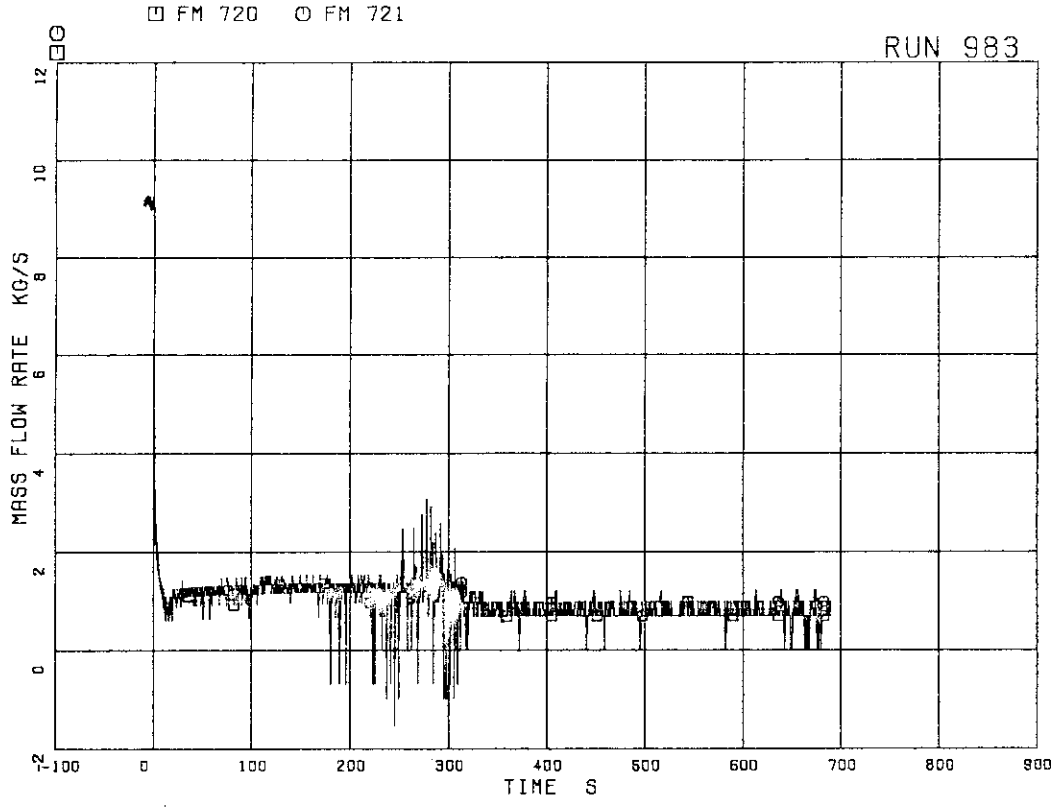

Fig. 5.182 Flow rates at JP-1,2 outlet (pos. flow)

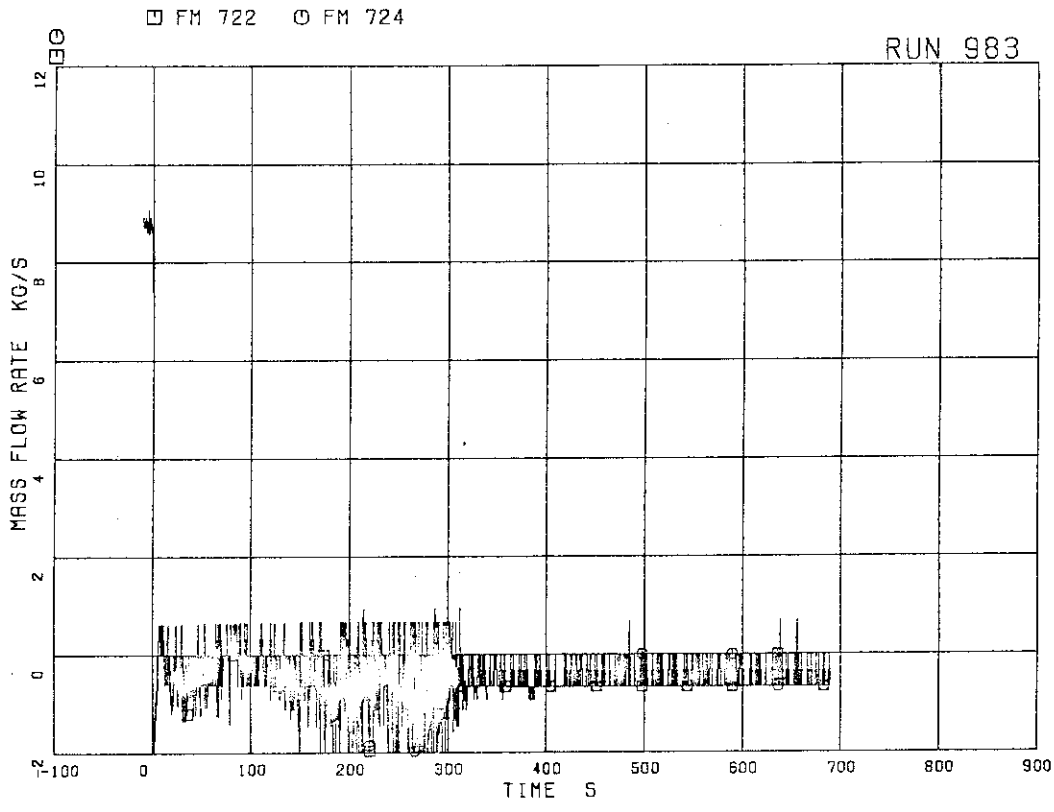

Fig. 5.183 Flow rates at JP-3,4 outlet (pos. flow)

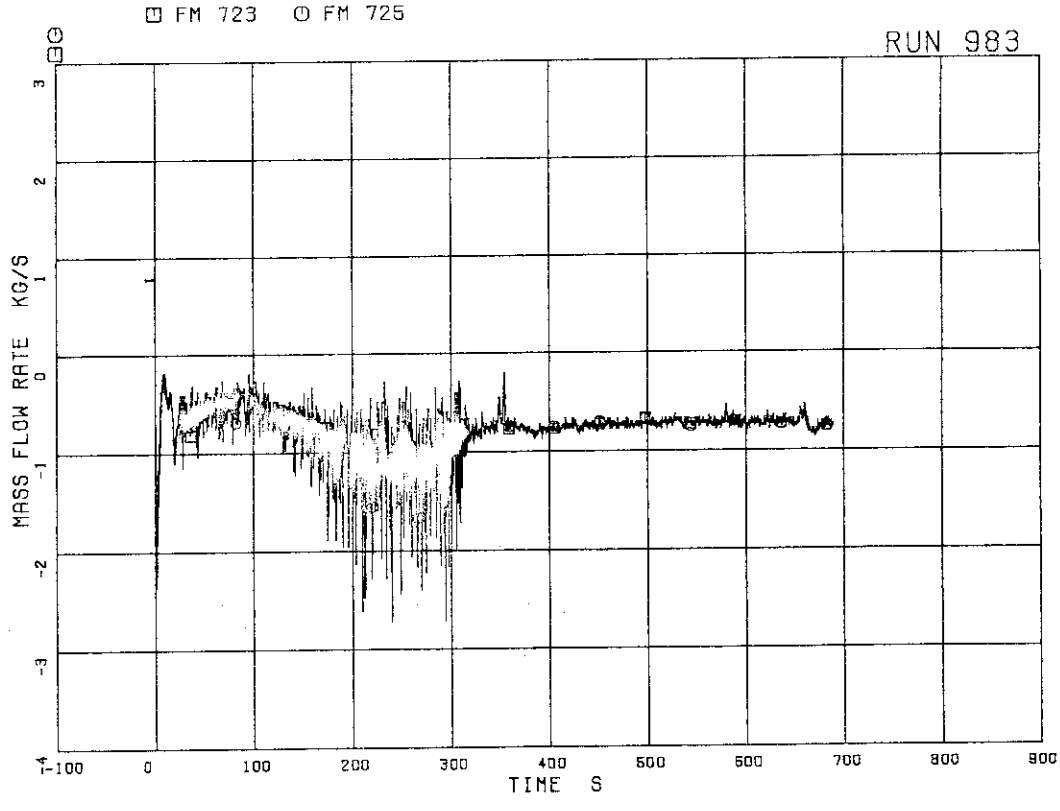

Fig. 5.184 Flow rates at JP-3,4 outlet (neg. flow)

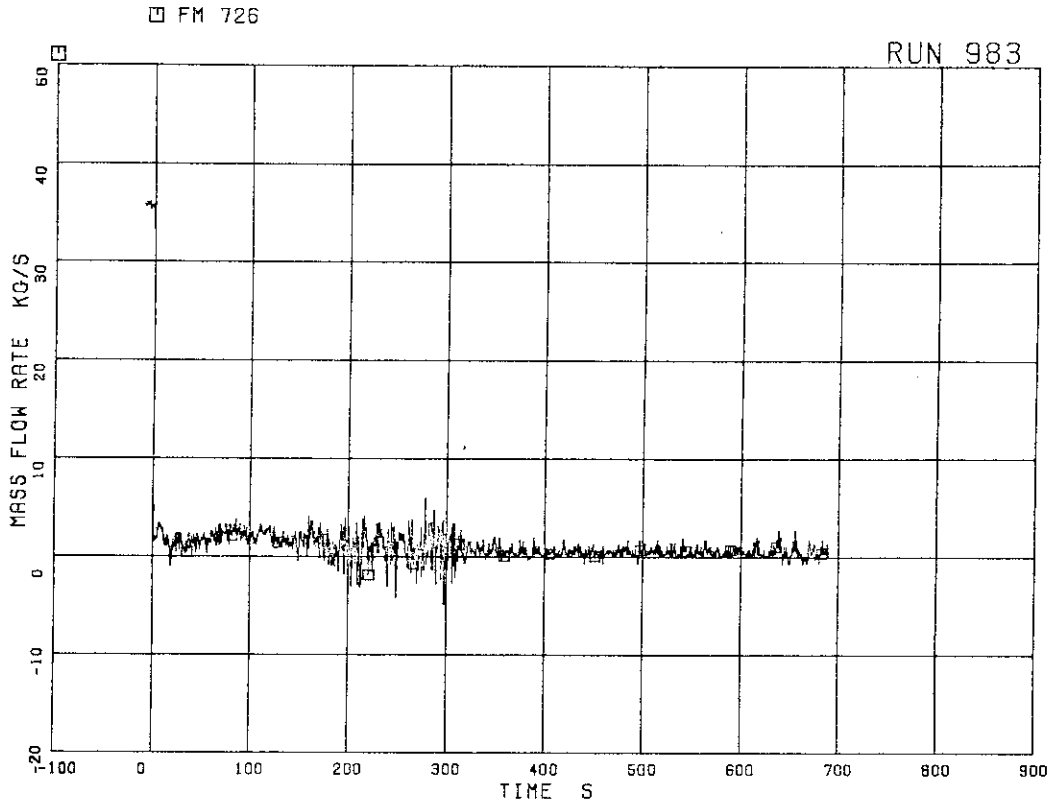

Fig. 5.185 Total JP outlet flow rate (pos. flow)

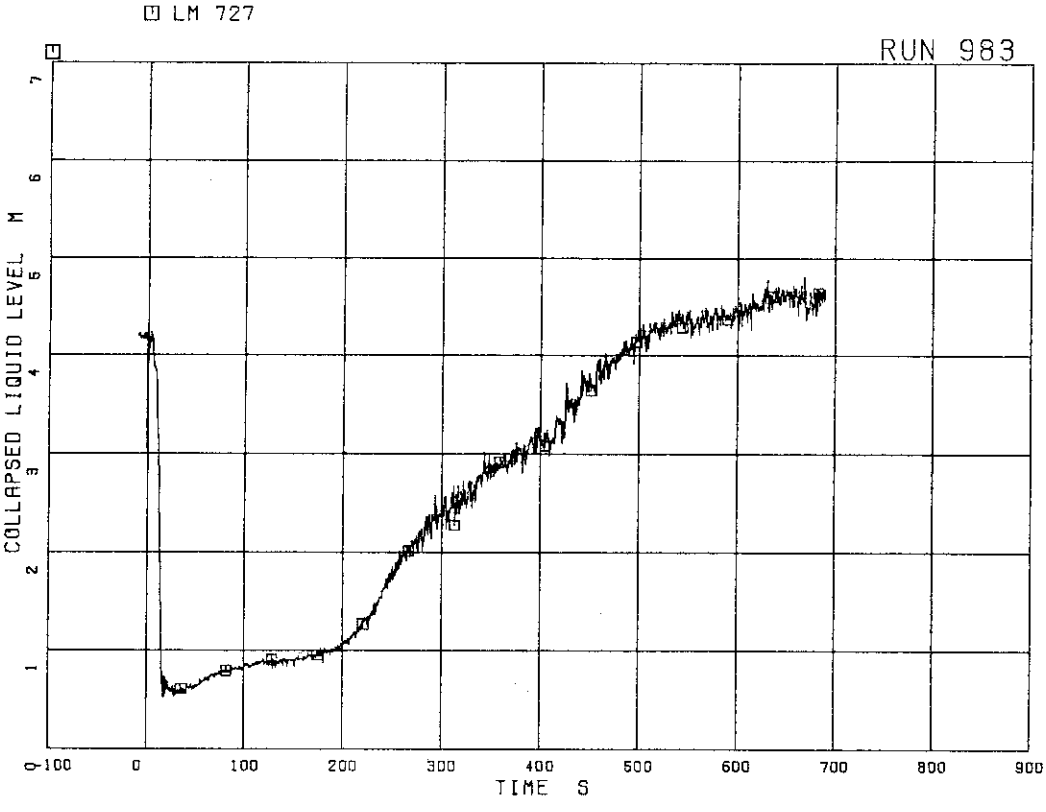

Fig. 5.186 Collapsed liquid level in downcomer

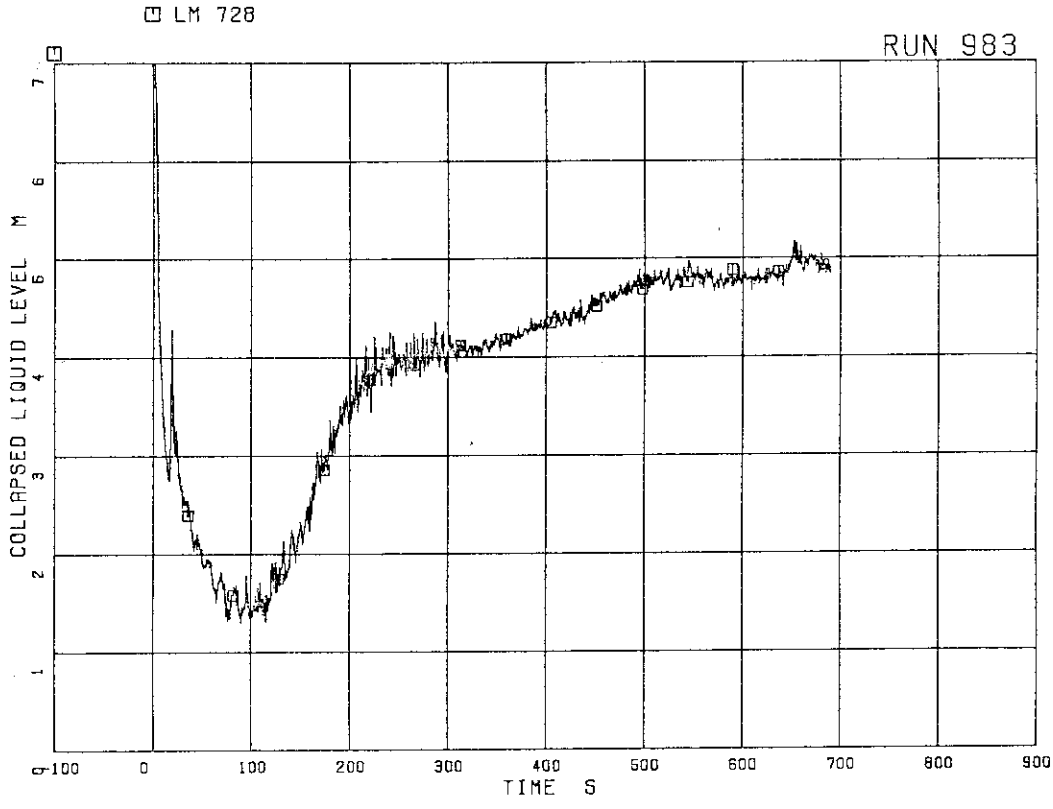

Fig. 5.187 Collapsed liquid level inside core shroud

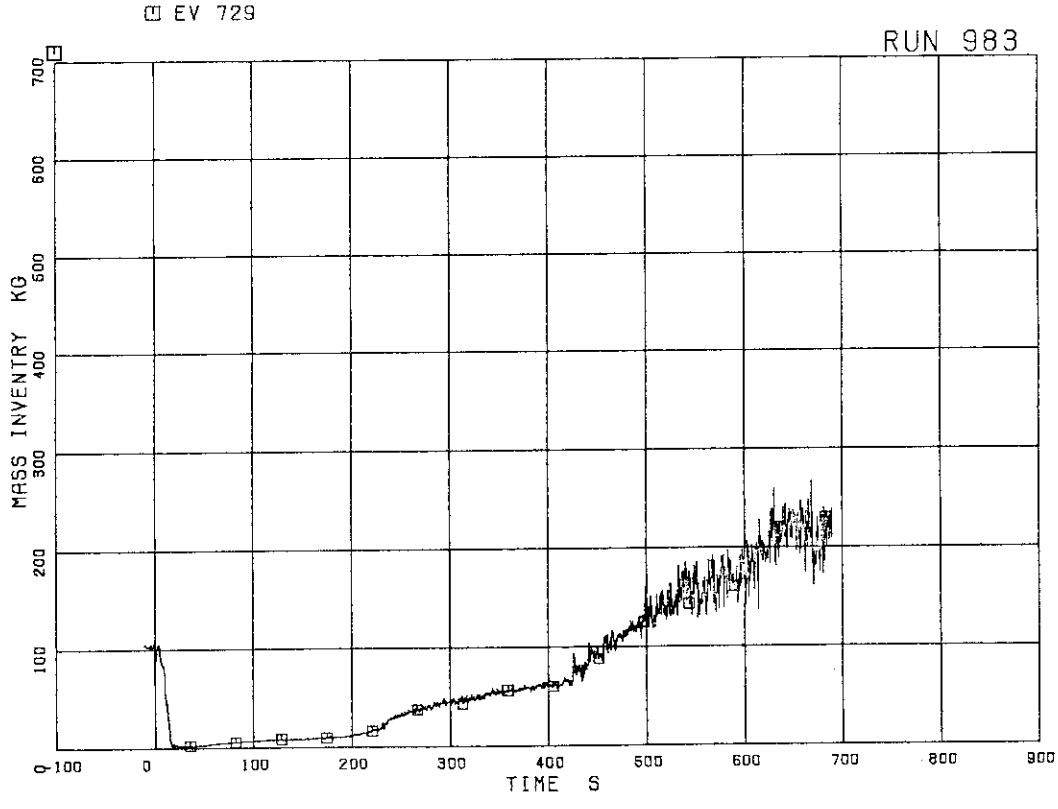

Fig. 5.188 Fluid inventory in downcomer

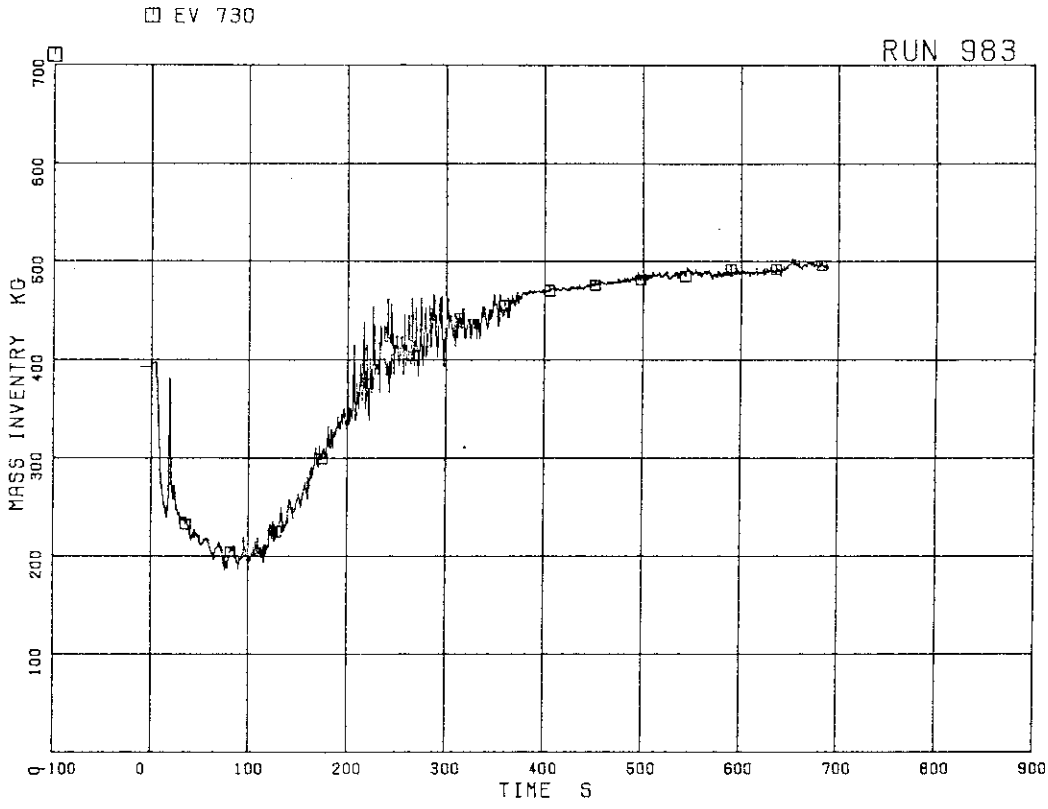

Fig. 5.189 Fluid inventory inside core shroud

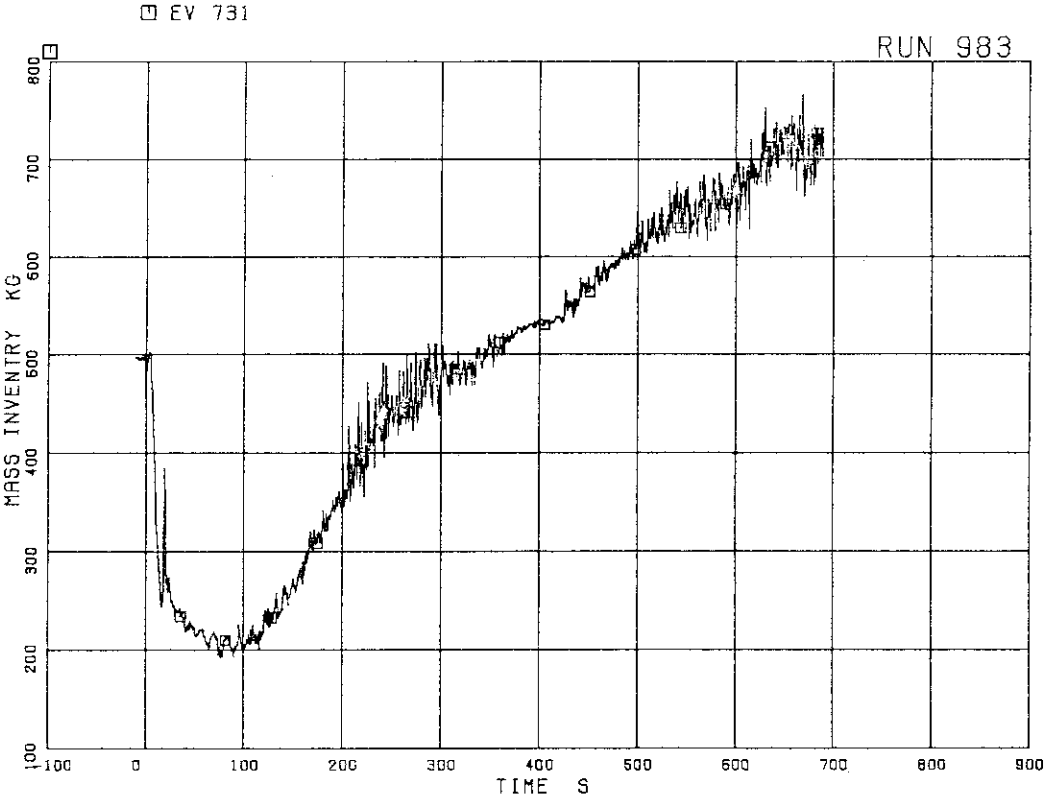

Fig. 5.190 Total fluid inventory in pressure vessel

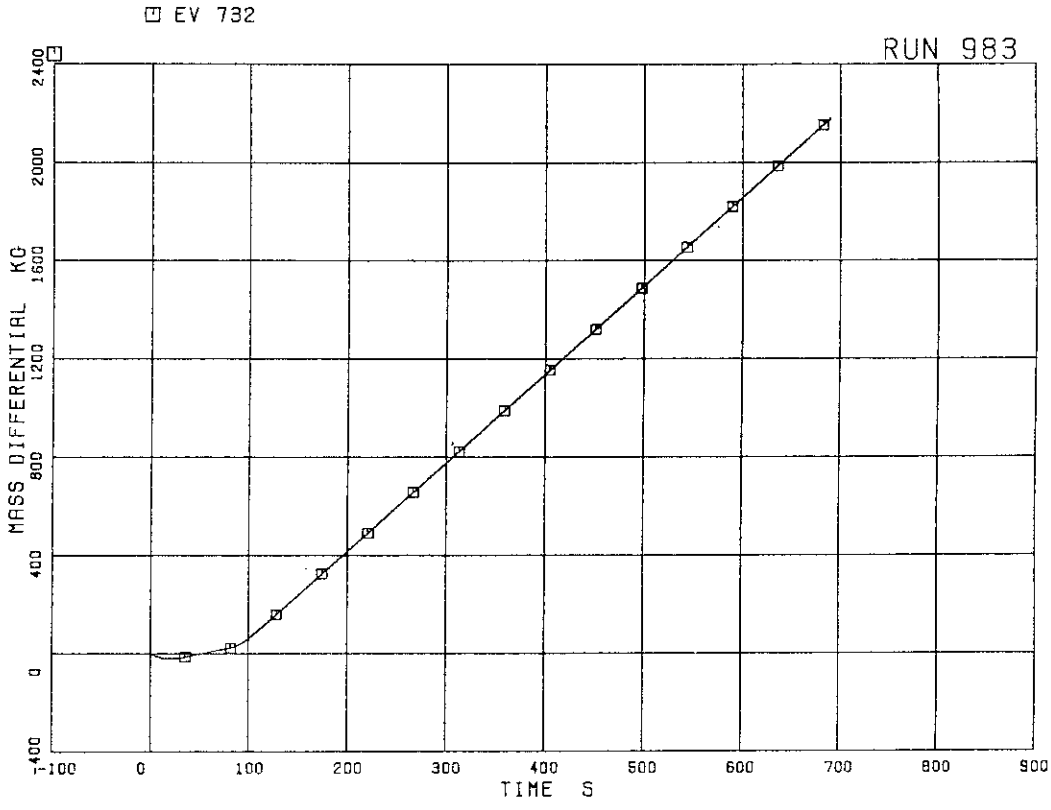

Fig. 5.191 Fluid mass increase by ECCS and FW and decrease by steam discharge flow

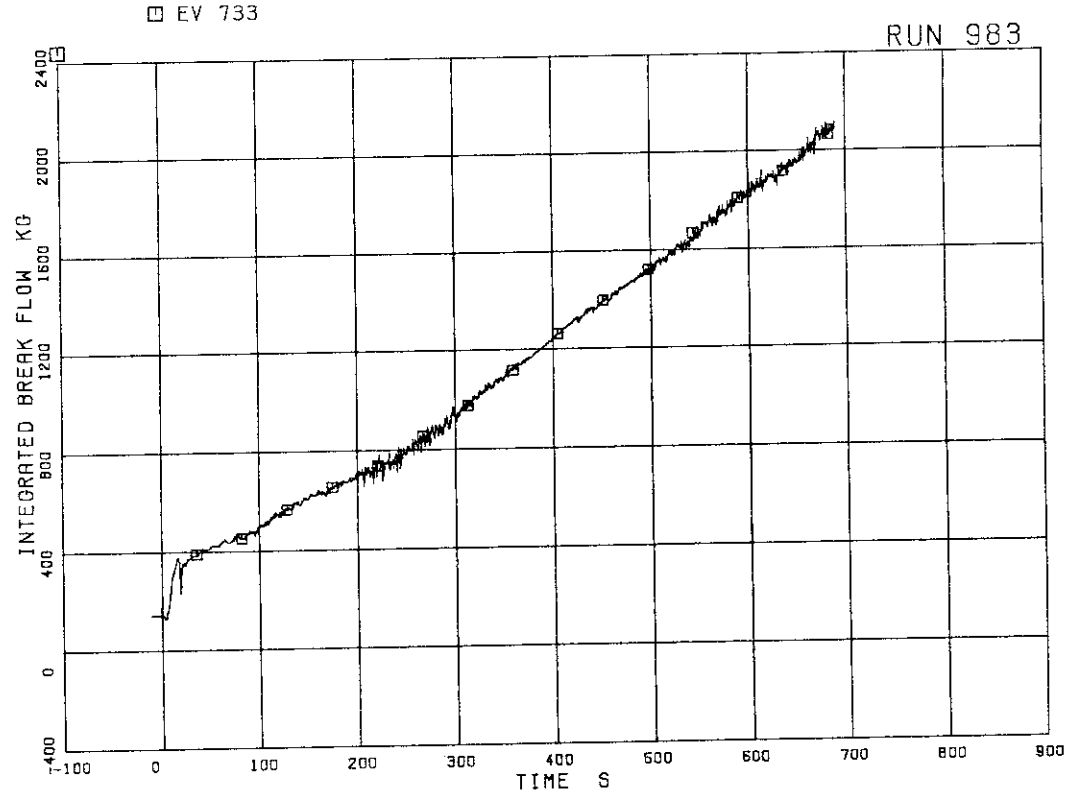

Fig. 5.192 Discharged fluid mass from break

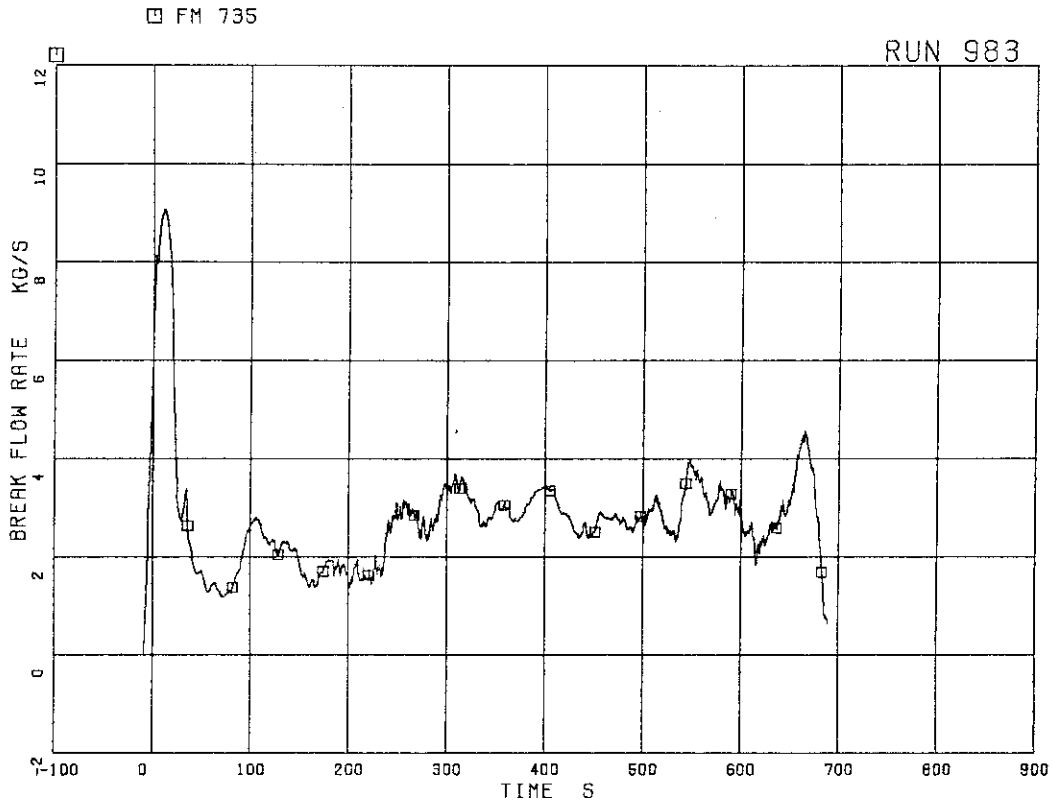

Fig. 5.193 Discharge flow rate from break

6. Test Results of ROSA-III and Discussions

Brief interpretations for the test results of a 200% suction line break test (RUN 983) in the ROSA-III facility are presentd and the foundings as to the effect of different test conditions, such as lower MSIV trip level and lower power generation rate compared with the other ROSA-III test, RUN 902 which is a 200% break test with normal test conditions are also described in this section.

6.1 Major Events of ROSA-III Test RUN 983

(1) Blowdown Phase

Major events found in the test results (see Table 5.1) of RUN 983 shown in Chapter 5 are summarized as follows.

Blowdown was initiated by quickly opening the QOBVs at breaks A and B and the QSV (quick shut valve) was closed simultaneously so that double-ended break could be simulated. Thereafter coolant in the system continued to be discharged from the breaks. There are two break flow paths i.e., one from the bottom of downcomer to break B and the other from downcomer middle part and lower plenum to break A through the jet pump drive nozzles and the recirculation pump (MRP2) in the broken loop as shown in Fig. 6.1.

The system pressure turned to decrease after break (see Fig. 5.1) and the pressure control system actuated as expected at 6.7 MPa at 6 s after break. Until initiation of the MSIV closure at 13 s after break, the system pressure was maintained constant by automatically controlling the steam flow rate. The controlled steam flow rate is shown in Fig. 5.40.

The feedwater supply was terminated between 2 s and 4 s after break. The water level in the downcomer decreased rapidly after break (see Figs. 5.39 and 5.186). The time of L1 level 10 safter break was estimated by extra-porating the data of downcomer water level fall of the other ROSA-III test. The test result showed that downcomer level fell to L1 level (3.6 m from PV bottom) actually 10 s after break. The L1 level signal caused the MSIV closure with time delay of 3 s and ADS actuation with time delay of 105 s. The recirculation line uncovery at 17 s after break caused rapid depressuri-zation and lower plenum flashing at 18 s after break.

(2) Reflooding Process

The HPCS, LPCS and LPCI were actuated at 27 s, 85 s and 95 s after break, respectively (see Fig. 5.41). Mass inventory in the downcomer increased gradually after the HPCS actuation and increased faster after the completion of reflooding inside core shroud (see Fig. 5.188), while that inside core shroud increased rapidly after the LPCI actuation (see Fig. 5.189). It is indicated in these figures that core was filled up faster than the downcomer and that voids existed in the downcomer for a little longer time than those inside core shroud because of heat release into the fluid from the vessel wall, recirculation line piping and pumps and the higher fluid temperature in the downcomer. Thus the collapsed water level inside core shroud showed higher value than that in the downcomer both in the blowdown and reflooding phases.

Mass inventory in the intact recirculation line piping can be estimated from the differential pressure data in the recirculation loops (see for example, Figs. 5.17, 5.18 and 5.20). It is found from these figures that refill of the intact recirculation loop is delayed due to larger steam generation caused by stored heat release at the recirculation pump and piping structures. Namely, initiation of refill at the jet pump discharge line, recirculation pump discharge line were observed about 30 s and 200 s after the LPCI actuation and that at the recirculation pump suction line was delayed more than 350 s after the LPCI actuation. These facts indicate that steam flooding occured at the outlet nozzle to the recirculation loop and at the jet pump nozzles for a long time after LPCI actuation.

(3) Core Cooling Behavior

Hydraulic behavior in the core is shown by the mixture level transients shown in Figs. 5.150 through 5.152 and supplemented by the surface temperatures of fuel rods shown in Figs. 5.83 through 5.134. The dryout and quench fronts of the fuel rods shown in Fig. 5.164 are similar to the water level transients shown in Fig. 5.162. The peak cladding temperatures are listed in Table 5.2.

The following observations have been obtained from these data.

(1) The peak cladding temperature (PCT) was 575 K (302 C) detected at position 2 of D22 rod at 91 s after break (6 s after LPCS actuation).

(2) Most of fuel rods were cooled well by HPCS actuation which contributed largely to supply water to the core in the early blowdown phase and by LPCS and LPCI actuations which contributed to keep the mass inventory in the core and keep the fluid temperature in the subcooled condition in the later test phase. Short dryout times were observed at the upper part of B22 and D22 rods and lessor dryout at B11 and B77 rods. These dryouts were diminished after actuations of LPCS and LPCI. No dryout of fuel rods were observed in A and C bundles.

(3) Different flow patterns were observed among the four equivallent fuel bundles during the time period after the termination of lower plenum flashing (30 s after break) until 230 s after break as shown in the core inlet flow rates (see Figs. 5.176 through 5.179). From 30 s to 170 s, downward flows were observed in B and D bundle inlets and upward flows in A and C bundle inlets. Then at 170 s, the flow pattern was changed to another flow pattern, namely large downward flows in A and D bundles and large upward flows in B and C bundles.

These are natural circulation occured among the equivallent four fuel bundles. The flow pattern change is closely related to diminishing of void fraction in the bundles, especially in the B and D bundles where dryout of fuel rods were observed.

6.2 Comparison with Related ROSA-III 200% Break Test

Major test results of RUN 983 are compared with other related ROSA-III test, RUN 902, which is a 200% suction line break test with 2 LPCI failure and normal ROSA-III test conditions. The effects of different test parameters, such as MSIV trip level, power generation rate with flat power profile and feedwater temperature on the large break LOCA phenomena are shown below.

(1) Pressure Response and Major Events

Major test conditions and events of two tests, RUNs 983 and 902, are compared in Table 6.1 and 6.2. The lower plenum pressure, collapsed water levels estimated from the differential pressure data in the upper and lower downcomer, differential pressure between top and bottom of PV, which represents mass inventory inside core shroud, steam line flow rate, feedwater

flow rate and three ECCS flow rates in the two tests are compared in Figs. 6.2 through 6.10. These test results show good coincidence of pressure response and major events, such as MSIV trip, lower plenum flashing, ECCS injection between RUNs 983 and 902 except for 17 seconds after break.

Little differences were observed between the two tests results as shown below. A faster depressurization was observed after break in RUN 983. The lower initial steam flow in RUN 983 was the results of lower core power and lower feedwater temperature compared with those of RUN 902. The steam flow rate in RUN 983 increased to the same value as that of RUN 902 after break. The lower MSIV trip level (L1: 3.6 m from PV bottom, 10 s after break) and actuation of pressure control system in RUN 983 caused also a little difference of pressure response from that of RUN 902 as shown in Fig. 6.2. The MSIV in RUN 983 tripped at 13 s , while that in RUN 902 tripped at 7 s by the L2 level (4.76 m from PV bottom) with time delay of 3 s.

A little slower level fall was observed after break in RUN 983 in spite of lower initial downcomer water level compared with those in RUN 902. The slower level fall in RUN 983 was caused by smaller discharge flow rate through the jet pump nozzles as shown below. Figures 6.11 and 6.12 show pressure distribution along the break flow path toward break A in RUNs 983 and 902, respectively. These figures show that two-phase choking occured at the break A in RUN 983, while it occured at jet pump drive nozzles and break A at least after the recirculation line uncovery at 13 s in RUN 902. Figures 6 13 and 6.14 show differential prerssures across the jet pump drive nozzles in RUNs 983 and 902, respectively. It is evident from these figures that the discharge flow rate through the jet pump nozzles in RUN 983 was much smaller than that in RUN 902. On the other hand, the break flow rate through the break B in RUN 983 was supposed to be similar to that in RUN 902 from comparison of the pressure distribution along the break path toward break B of the two teats (compare Fig. 6.15 with Fig. 6.16).

The lower feedwater temperature in RUN 983 (23 C) caused no flashing of feedwater remained in the feedwater line piping, while the feedwater flashing occured at 65 s after break in RUN 902 affected the system pressure to slow down the depressurization rate and consequently resulted in delay of LPCI injection time (see Figs. 6.2 and 6.7). In RUN 902, the flashed feedwater flowed into the upper downcomer and generated much saturated or super heated steam by receiving the stored heat of pressure vessel wall, filler blocks attached at the core shroud outer surface and other internal structures. At 65 s in RUN 902, the saturated temperature was 489 K (216

C), while the metal surface temperatures of pressure vessel wall and other thick metals were estimated as close as the initial metal temperature of 552 K (279 C) because those metals were dryed out into steam after the downcomer level fell to the bottom of the downcomer. And the remained hot feedwater in the feedwater line is 0.035 m^3, which can be compared with the remained water in the lower plenum and core estimated as 0.1 m^3 from the differential pressure data by assuming void fraction of 0.5 at the time of 65 s after break. Thus the feedwater flashing contributed to slower the depressurization rate.

A little lower power in RUN 983 compared with that in RUN 902 (see Figs. 6.23 and 6.24) contributed to the earlier depressurization. The difference of integrated powers between the two tests was estimated as 2.66 x 10^4 kJ for the bundle A and 3.24 x 10^4 kJ for the bundles B, C and D during the time period of 200 s after break, when the difference was dominant. The total value of the difference of integrated power of 5.90 x 10^4 kJ corresponded to 38% of the total power generated in the four bundles of RUN 983. This smaller power generation contributed to smaller steam generation for 200 s in RUN 983.

The HPCS was actuated at 27 s by a timer in RUN 983, while that in RUN 902 was actuated at 32 s by L2 level signal with time delay of 27 s. The LPCS injection in RUN 983 was delayed 15 s than that in RUN 902 due to lower actuation pressure compared with RUN 902. The LPCI injection flow rate of RUN 902, however, was not shown in the figure except for a short time period after actuation because of malfunction of the LPCI turbine flow meter. The average LPCI flow rate in RUN 902 was estimated as 1.343 x 10^{-3} m^3/s between 108 s and 450 s from the water level data of the LPCI tank. The ADS was actuated at 115 s in RUN 983 due to L1 level (10 s after break) with time delay of 105 s, while that in RUN 902 was actuated at 132 s by L1 level (9 s after break) with time delay of 123 s.

(2) Water Level and Mass Inventory in PV

Figures 6.17 and 6.18 show the collapsed water levels inside core shroud estimated from the gifferential pressure between top and bottom of PV (D5, see Fig. 6.4) and collapsed water level in the downcomer which are the sum of upper and lower downcomer water levels (see Fig. 6.3) built up on the bottom of downcomer (EL 0.938 m from PV bottom). The contribution of frictional pressure drop included in the estimated collapsed water levels was

negligible except for short time periods after break initiation, lower plenum flashing and ADS actuation.

These figures show the same trend of transient collapsed water levels in the pressure vessel in the two tests. Namely, the higher core shroud level than that in the downcomer was maintained in the test periods. The increase of mass inventory inside core shroud was found in common after LPCI actuation, while that in the downcomer was delayed for a long time from the LPCI actuation. The delay of downcomer level recovery was caused by steam discharge from the lower plenum, which was the results of large heat release from the lower plenum wall. The water mass flowed into the downcomer discharged from the break nozzle. Heat release from the pressure vessel wall at the downcomer and filler blocks contributed to generate steam and keep higher void fraction of the downcomer fluid.

A little later downcomer level fall was observed in RUN 983 compared with RUN 902 due to the reason mentioned previously. The excess water mass inside core shroud in the initial state of RUN 983 also contributed to the level delay. The initial fluid mass inside core shroud in RUN 983 was larger than that in RUN 902 because of the lower initial enthalpy distribution of RUN 983. The initial average fluid quality in the upper plenum was 3.4% in RUN 983, while that in RUN 902 was 13.1%. And therefore, the excess water mass inside core shroud in RUN 983 compared with RUN 902 was estimated as about 30 kg. Figures 6.19 through 6.22 show fluid densities in RUN 902 at the location of break A and break B. These density data are compared with those of RUN 983. The density data measured upstream the break B in both tests, RUNs 983 and 902 agreed well. The density data upstream the break A in RUN 983, however, was a little higher than that in RUN 902. The reason of larger amount of water mass in the break flow path between the jet pumps and break A was fairly smaller break area in RUN 983 (15%) compared with that of RUN 902 (100%). The fluid densities of RUN 983 showed earlier increase after ECCS actuation corresponding the earlier mass recovery in the pressure vessel compared with the test results of RUN 902.

(3) Fuel Rod Surface Temperature and Mixture Level in Core

Figures 6.23 and 6.24 show the electric power supplied to the bundle A and bundles B, C and D in RUNs 983 and 902. Flat power profile was given to the four bundles in RUN 983, while radial peaking factor of 1.4 was given to the high power bundle (bundle A) and 1.0 to the average power bundles

(bundles B, C and D) in RUN 902. In addition to this difference of radial peaking factor, the transient power curves of the two tests were different. The power curve used in RUN 983 (Ref. 29) was determined lately by simulating the correct rod surface heat flux of the reference BWR nuclear rods with maximum peaking factor. On the other hand, the old power curve[30] used in RUN 902 overestimated the stored heat of heater rods. Thus, the power curves of the two tests were different as shown in Figs. 6.23 and 6.24.

Figures 6.25 through 6.28 compare the surface temperatures of A11 rod Position 1 (top of core), Position 4 (center) and Position 7 (bottom of core) and C11 rod Position 4 (center) of RUNs 983 and 902. A11 rod of RUN 902 had a radial peaking factor of 1.4. These figures show that middle and upper part of A11 rod in RUN 902 dryed out into steam frequently but no dryout was observed on the A11 rod of RUN 983.

Figures 6.29 through 6.32 show the surface temperatures of A22, B22, C22 and D22 rods in RUN 902 and are compared with the corresponding surface temperatures in RUN 983 (see Figs. 5.86, 5.92, 5.96 and 5.99). Figures 6.33 and 6.34 show dryout and quench fronts in bundles A and C of RUN 902 and are compared with those of RUN 983 (see Fig. 5.164). Figure 6.35 showing the mixture level transients in the pressure vessel in RUN 902 is compared with those of RUN 983 (see Figs. 5.162 and 5.163). Figures 6.36 through 6.39 are the individual mixture level signals in RUN 902, which are compared with those of RUN 983 (Figs. 5.150 through 5.152).

It is found from the comparison of these figures between the two tests that (1) dryout points of fuel rods in RUN 983 were very few compared with RUN 902, (2) the mixture level covered most of the fuel rods in RUN 983, while those in RUN 902 fell to the lower part of the core, (3) dryout and quench fronts agreed well with the mixture level transients in both tests. On the other hand, the collapsed water level inside core shroud in RUN 983 showed similar but a little higher value than that in RUN 902 between 50 s and 250 s. The difference of collapsed level was less than 0.5 m except for a short time after initiation of feedwater flashing at 65 s after break (see Figs. 6.17 and 6.18). This little larger amount of water inside core shroud in UN 983 resulted in better core cooling shown above.

The peak cladding temperatures (PCTs) of the two tests are compared in Table 6.2. The early dryout recorded PCT in RUN 902 was not observed in RUN 983. The PCT of RUN 983, 575 K, was very low and was close to the initial rod surface temperature. The lower PCT in RUN 983 was the results of lower heat flux and higher mixture level in core compared with that of RUN 902.

Table 6.1 Test conditions of RUNs 983 and 902

Items		RUN 983	RUN 902
Objective		FIST Counter-part Test	ROSA-III Standard Test
Break Condition			
Break Area	(%)	200	200
Break Location		Suction Line	Suction Line
Initial Conditions			
Pressure in Steam Dome	(MPa)	7.19	7.35
Total Core Power	(MW)	3.614	3.962
Radial Peaking Factor		1.0	1.4
Power Curve		New	Old
Total Core Flow	(kg/s)	35.9	16.2
Core Inlet Subcooling	(K)	11.6	10.3
Upper Plenum Quality	(%)	3.4	13.1
Feedwater Temperature	(K)	296	489
Water Level	(m)	4.8	5.0
Transient Conditions			
ECCS Mode		2 LPCI Failure	2 LPCI Failure
HPCS Actuation		27	L2 + 27 s
LPCS Actuation		L1 + 40 s	L1 + 40 s
		$P \leqq 1.9$ MPa	$P \leqq 2.2$ MPa
LPCI Actuation		L1 + 40 s	L1 + 40 s
		$P \leqq 1.6$ Mpa	$P \leqq 1.6$ MPa
ADS Actuation		L1 + 105 s	L1 + 120 s
ADS Orifice Diameter	(mm)	21.1	15.5
MSIV Trip		L1 + 3 s	L2 + 3 s
L2 Level	(m)	4.60	4.76
L1 Level	(m)	3.62 (10s)	4.25

Table 6.2 Comparison of major events in RUNs 983 and 902

Events (s)	RUN983	RUN902
Break Initiation	0	0
Initiation of Pressure Control	6	-
Initiation of Power Decrease	8	9
L1 Level	10	9
MSIV Closure	13	7
Recirculation Line Uncovered	17	13
Lower Plenum Flashing	18	18
HPCS Actuation	27	32
Feedwater Line Flashing	-	65
LPCS Actuation	85	70
LPCI Actuation	95	95
ADS Actuation	115	132
PCT Time (s)	91	20
PCT (K)	575	761

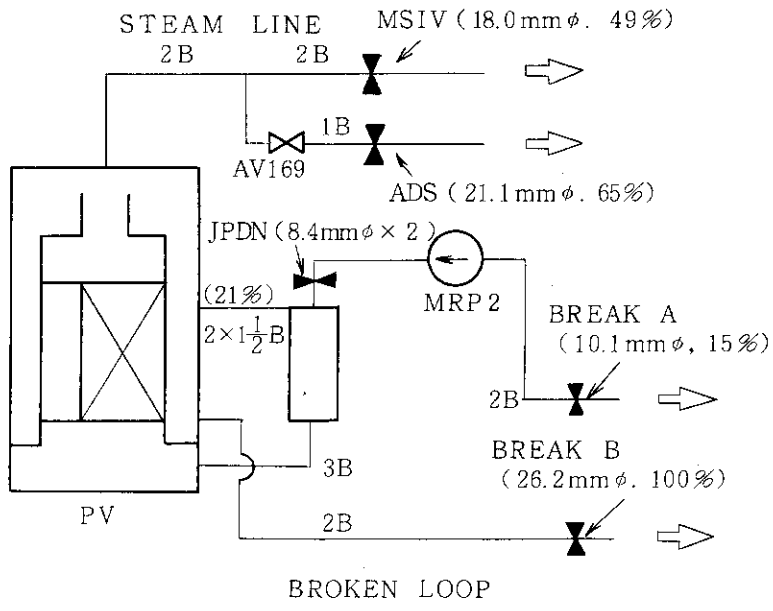

Fig. 6.1 Break flow paths in RUN 983

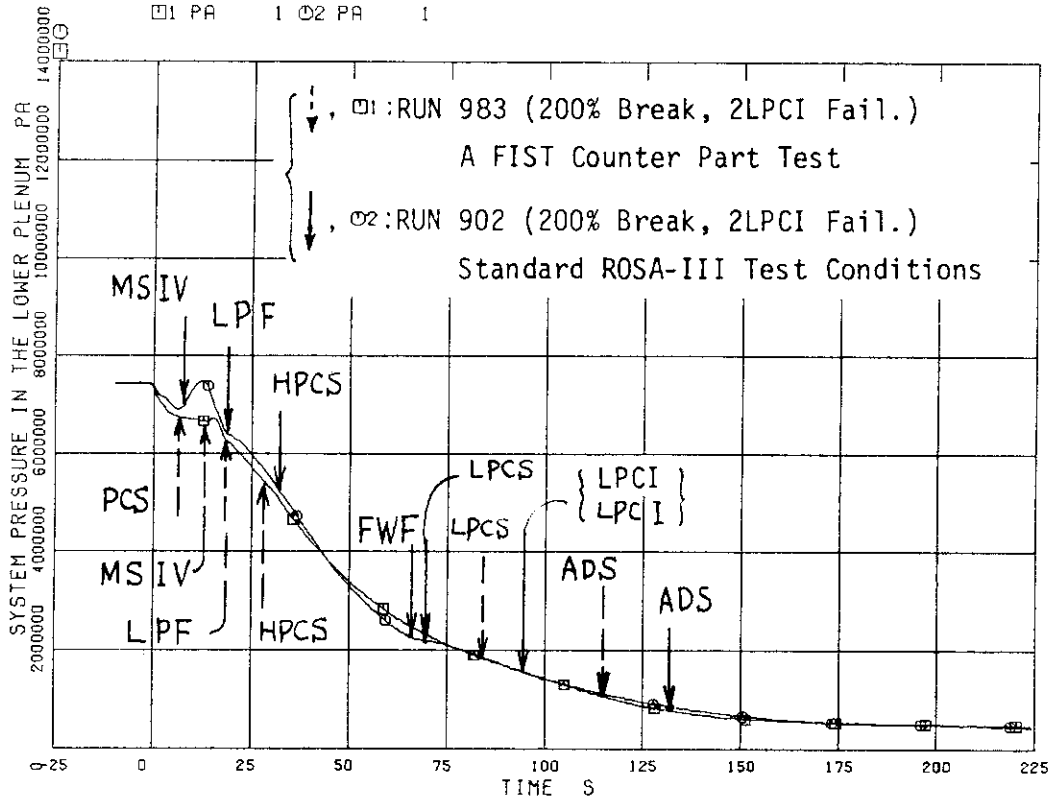

Fig. 6.2 Comparison of pressure transients of RUNs 983 and 902

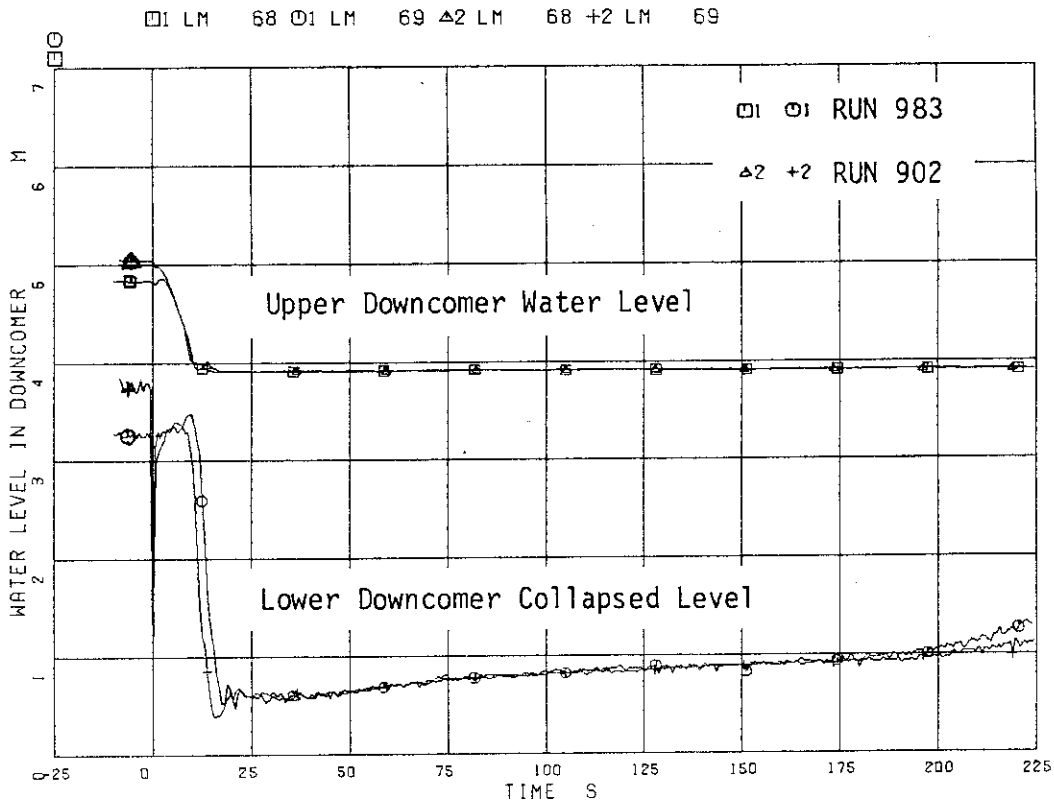

Fig. 6.3 Comparison of downcomer levels between two tests

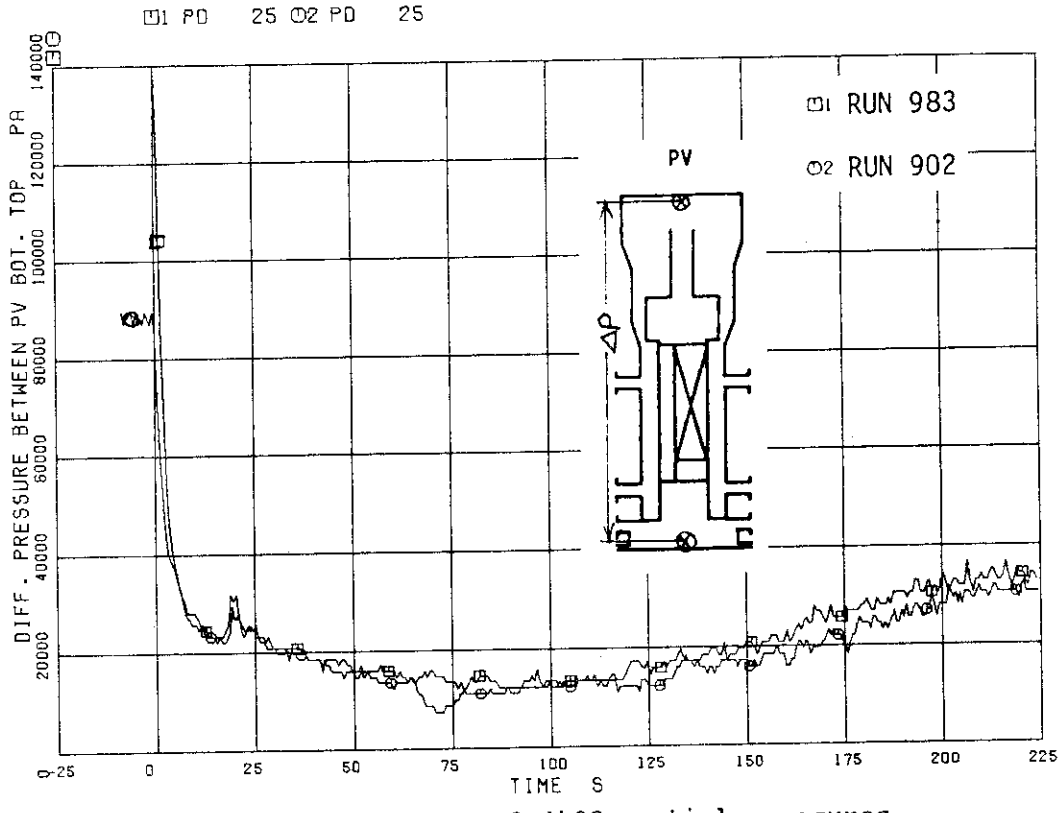

Fig. 6.4 Comparison of differential pressures inside core-shroud between two tests

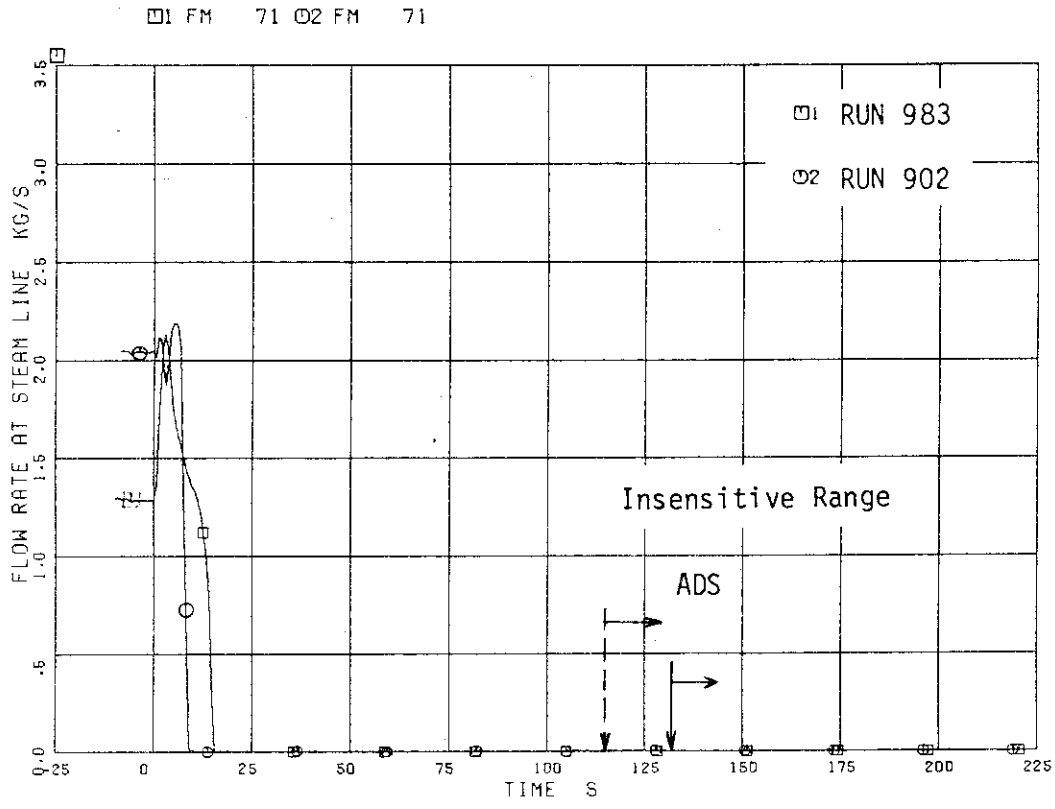

Fig. 6.5 Comparison of steam flow rates (high range)

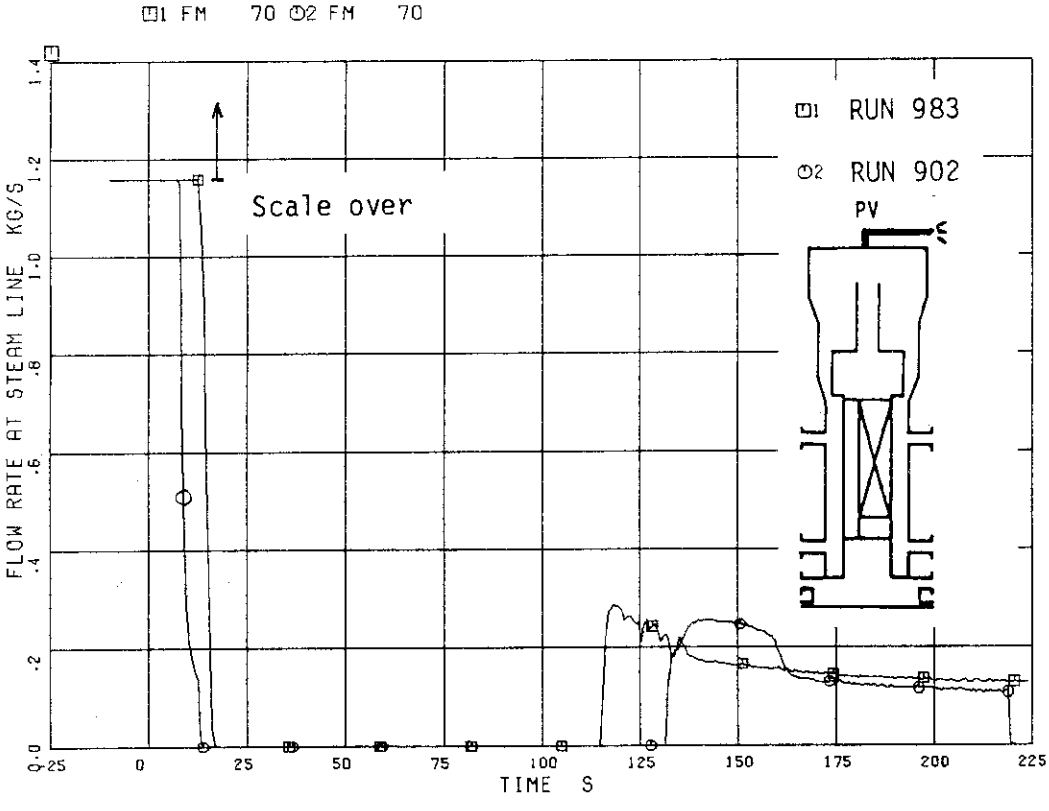

Fig. 6.6 Comparison of steam flow rates (low range)

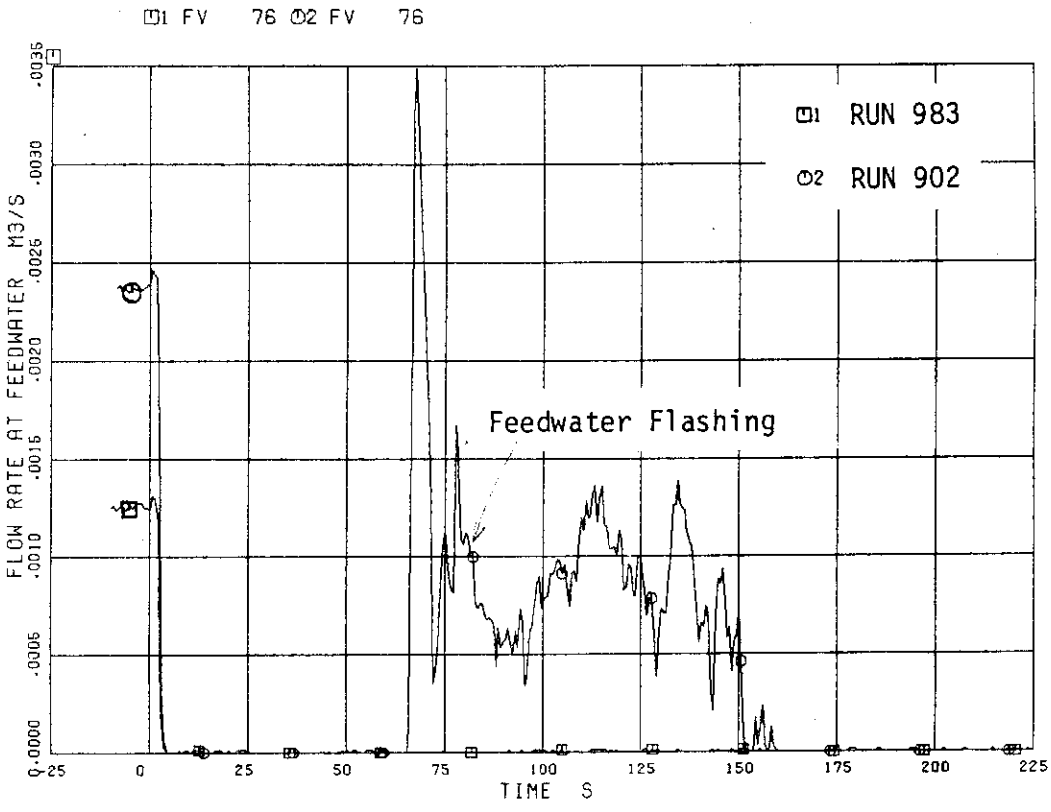

Fig. 6.7 Comparison of feedwater flow rates

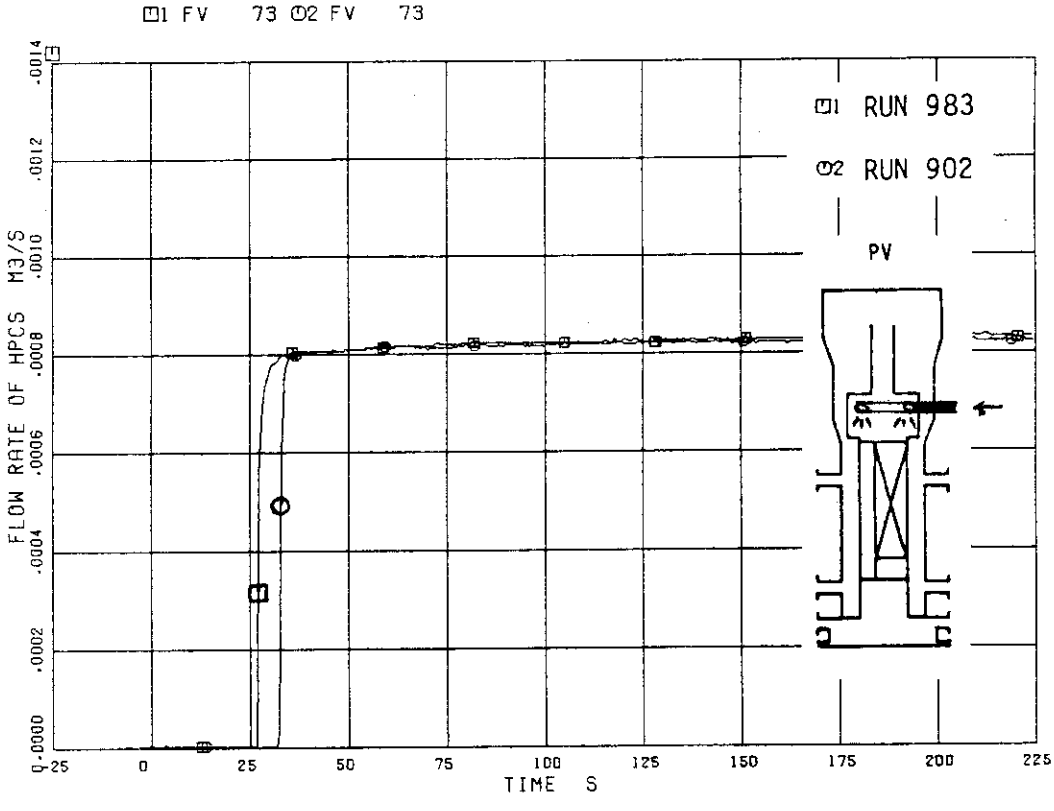

Fig. 6.8 Comparison of HPCS flow rates

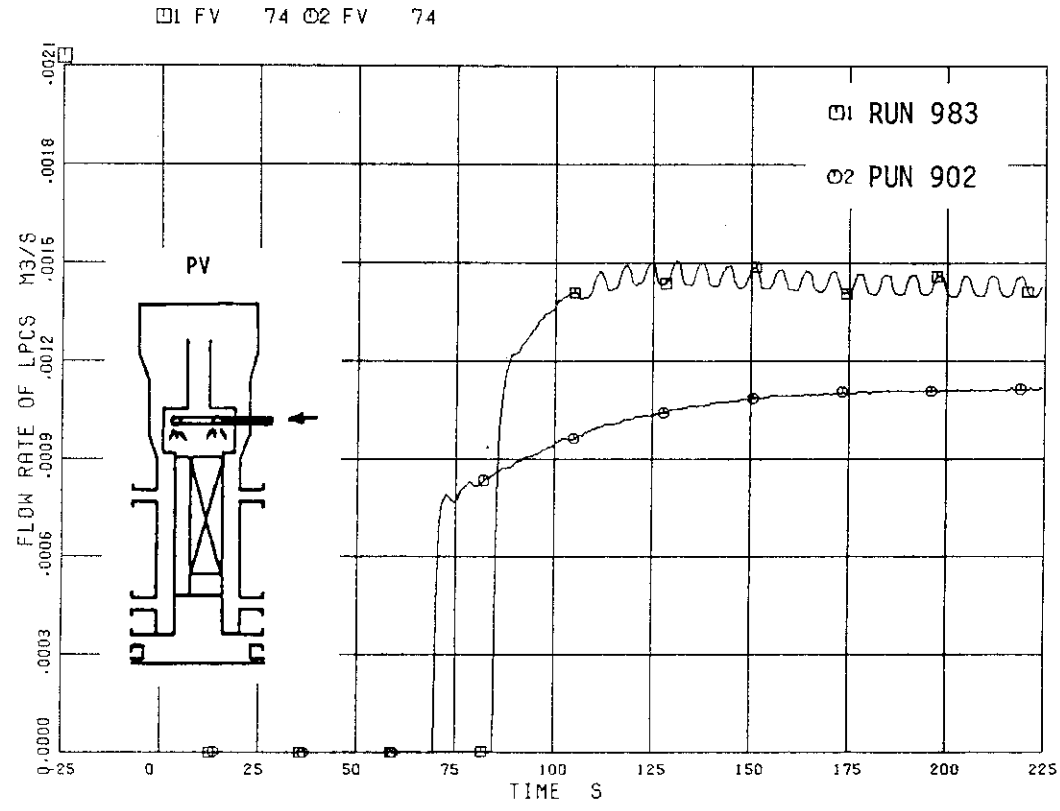

Fig. 6.9 Comparison of LPCS flow rates

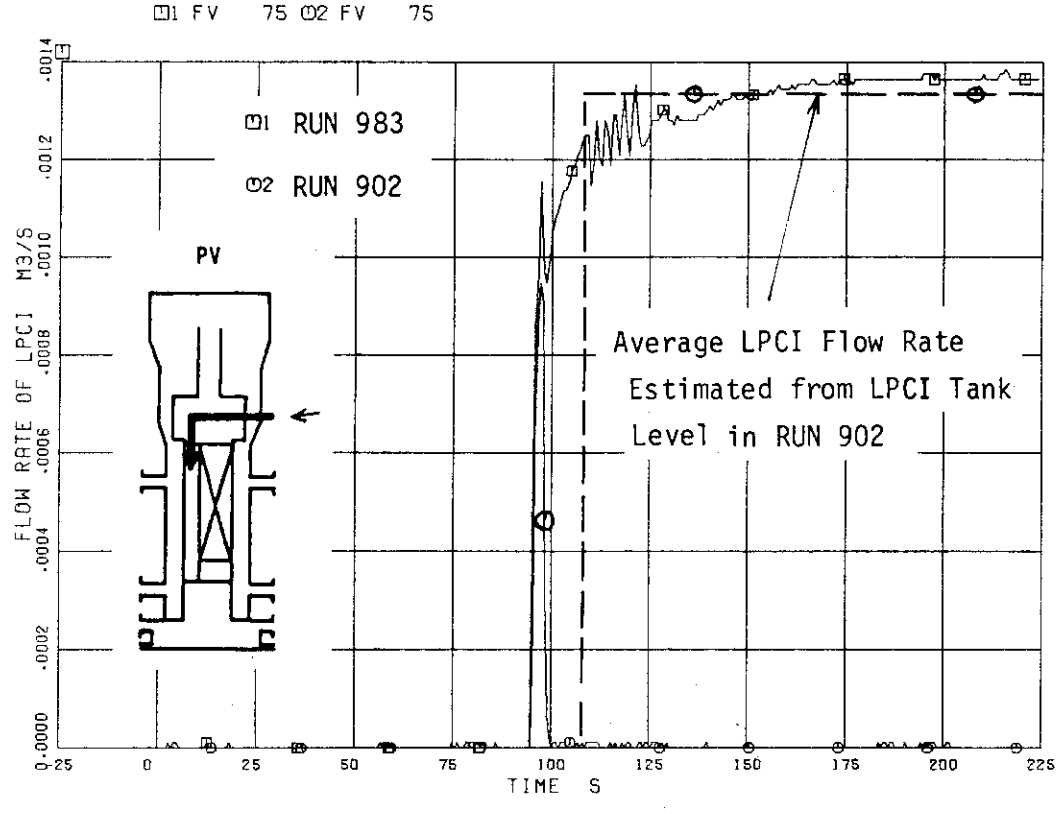

Fig. 6.10 Comparison of LPCI flow rates

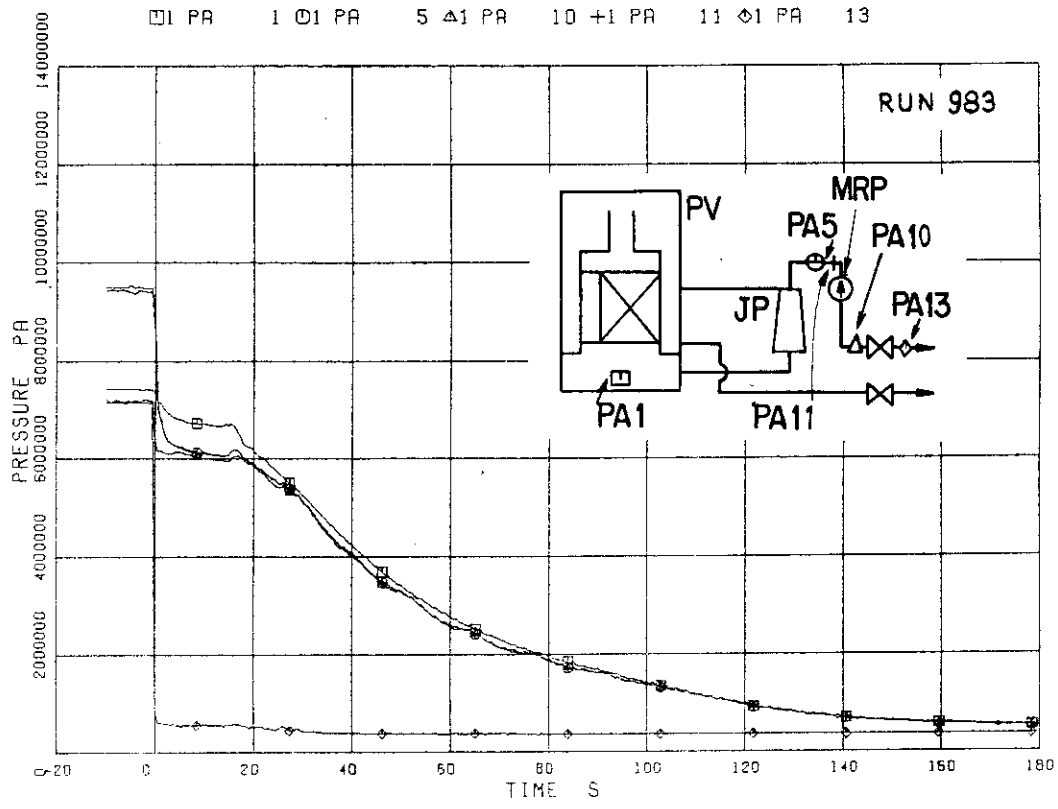

Fig. 6.11 Pressure distribution along JP side break flow path in RUN 983

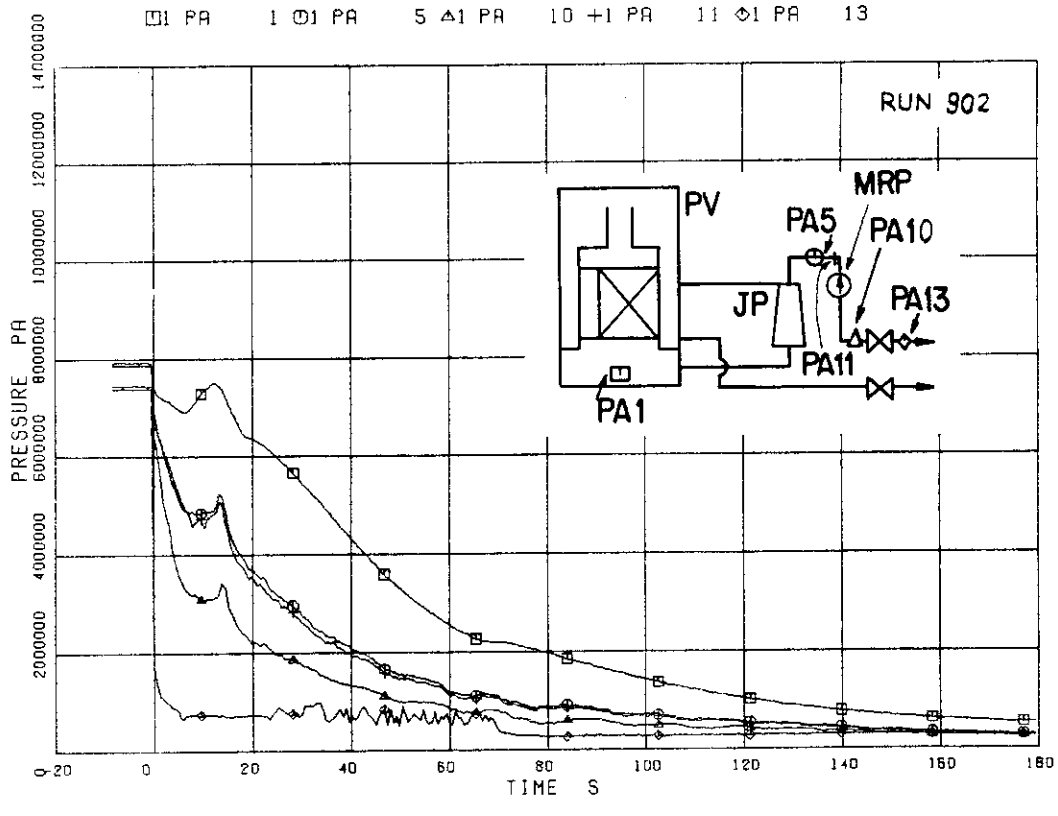

Fig. 6.12 Pressure distribution along JP side break flow path in RUN 902

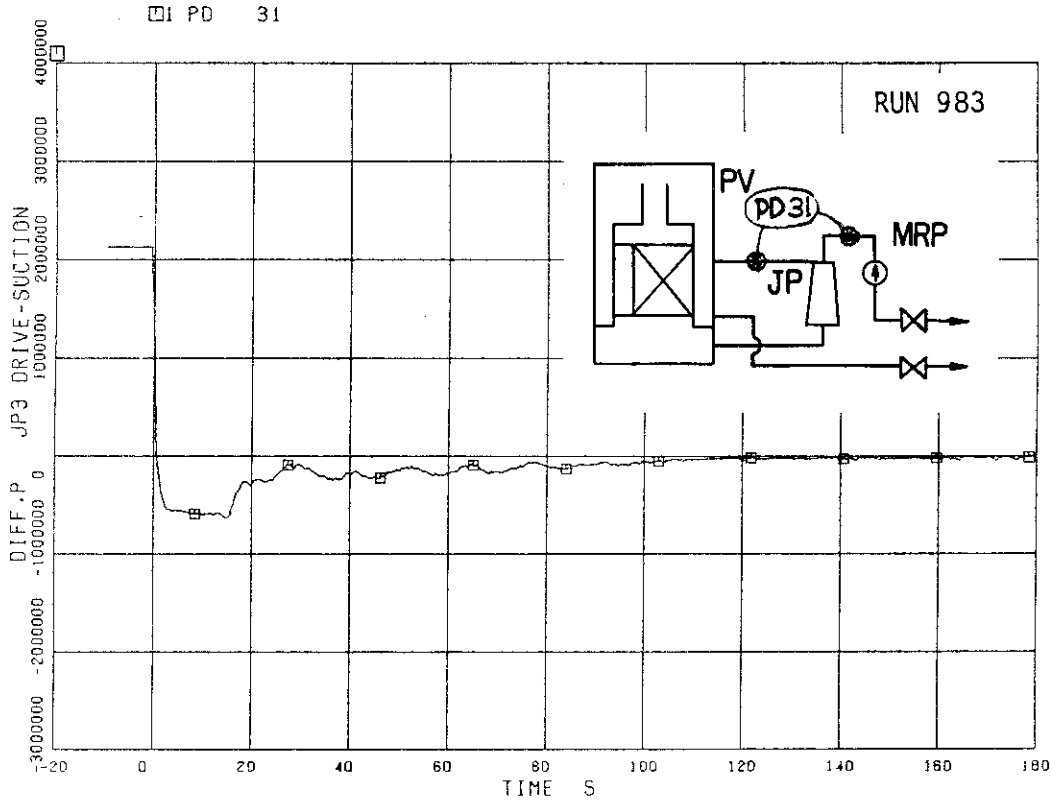

Fig. 6.13 Differential pressure across JP drive nozzles in broken loop of RUN 983

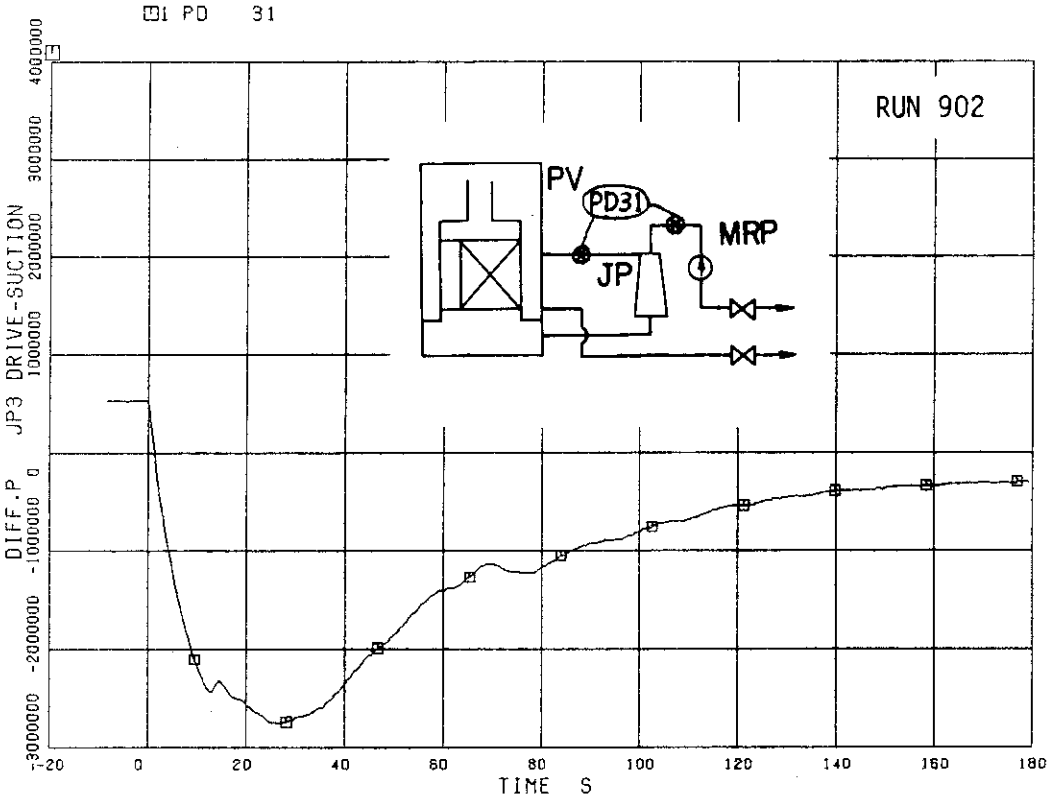

Fig. 6.14 Differential pressure across JP drive nozzles in broken loop of RUN 902

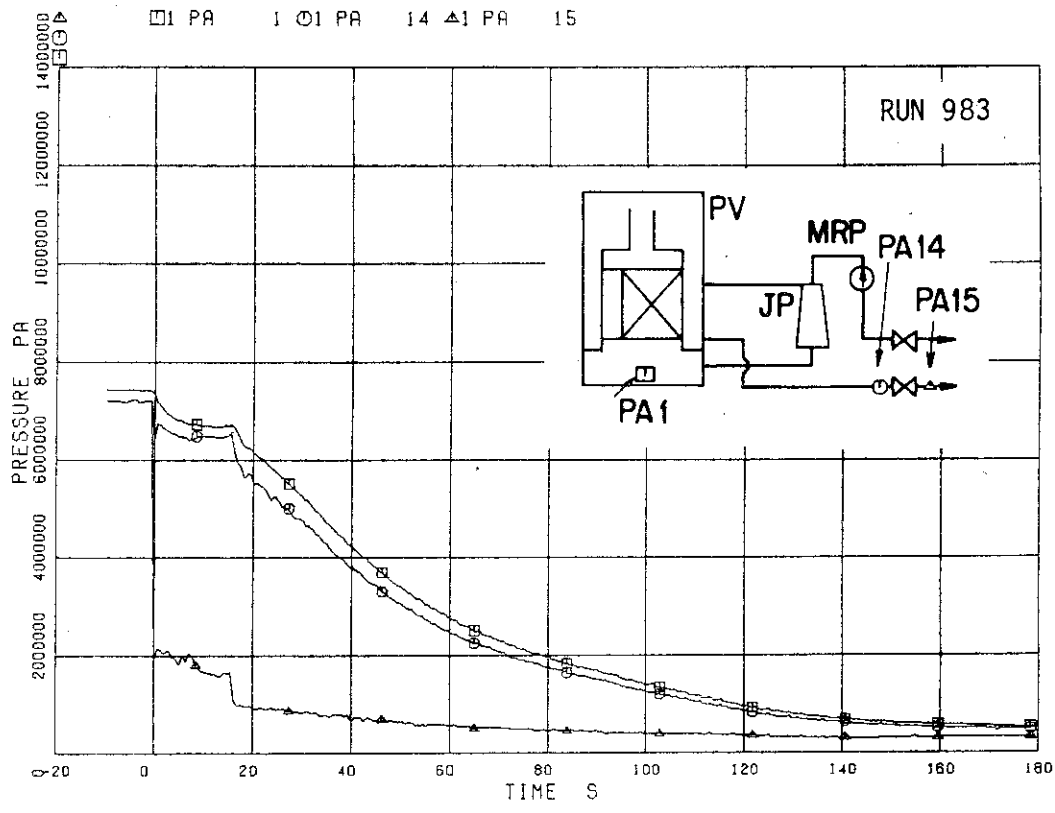

Fig. 6.15 Pressure distribution along PV side break flow path in RUN 983

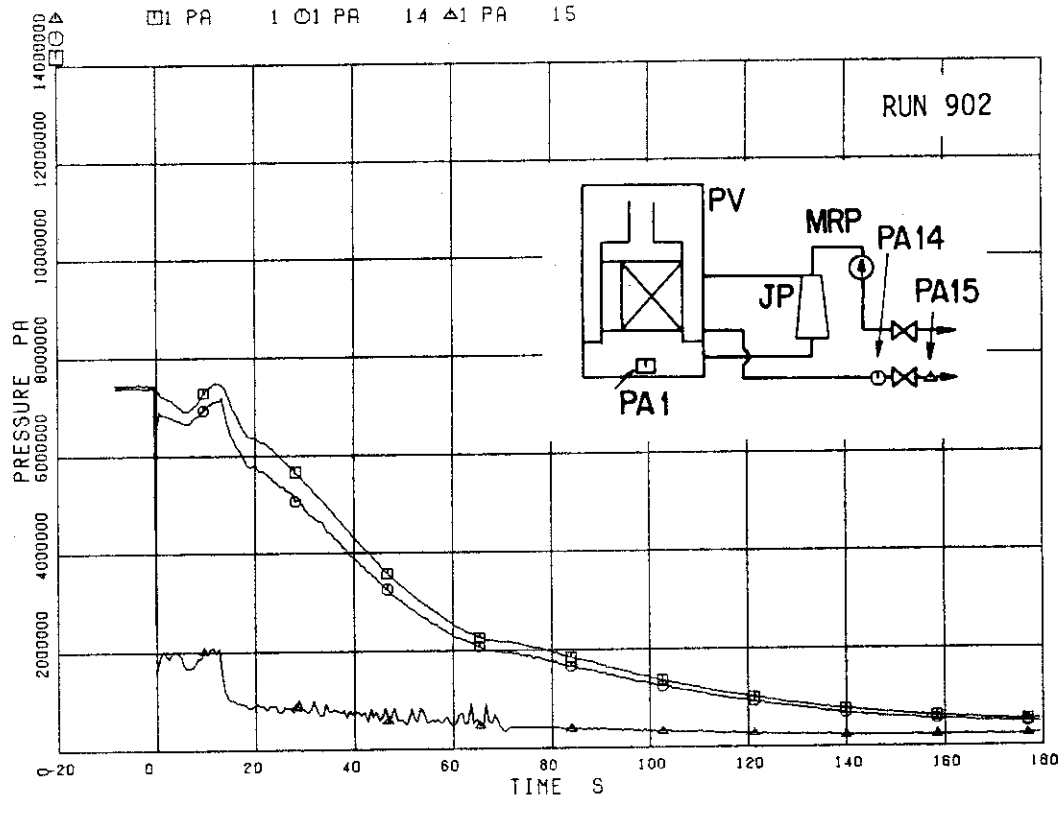

Fig. 6.16 Pressure distribution along PV side break flow path in RUN 902

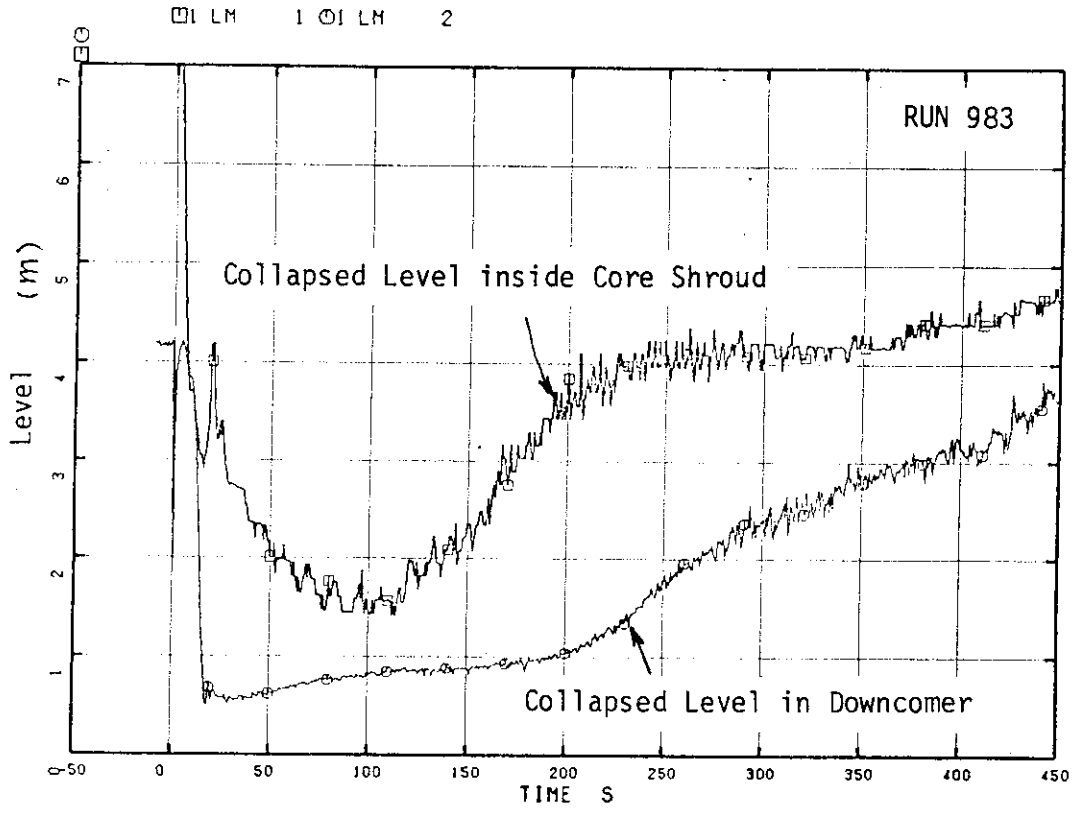

Fig. 6.17 Collapsed levels in PV in RUN 983

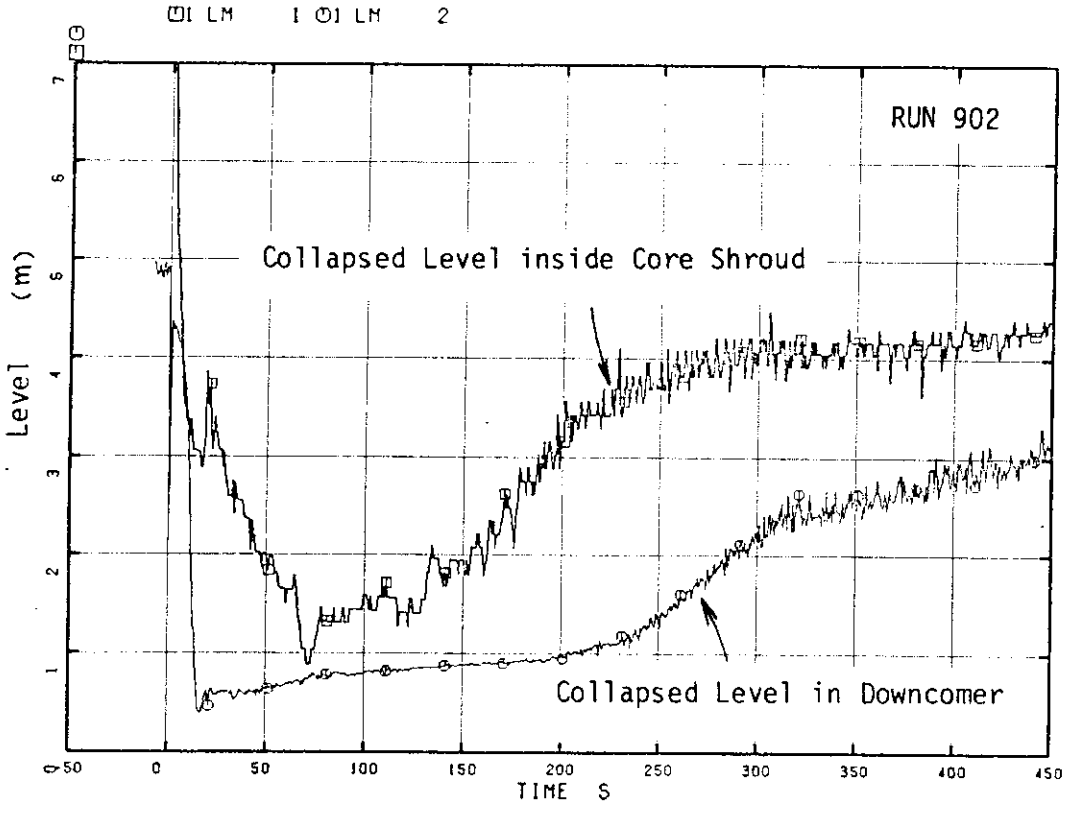

Fig. 6.18 Collapsed levels in PV in RUN 902

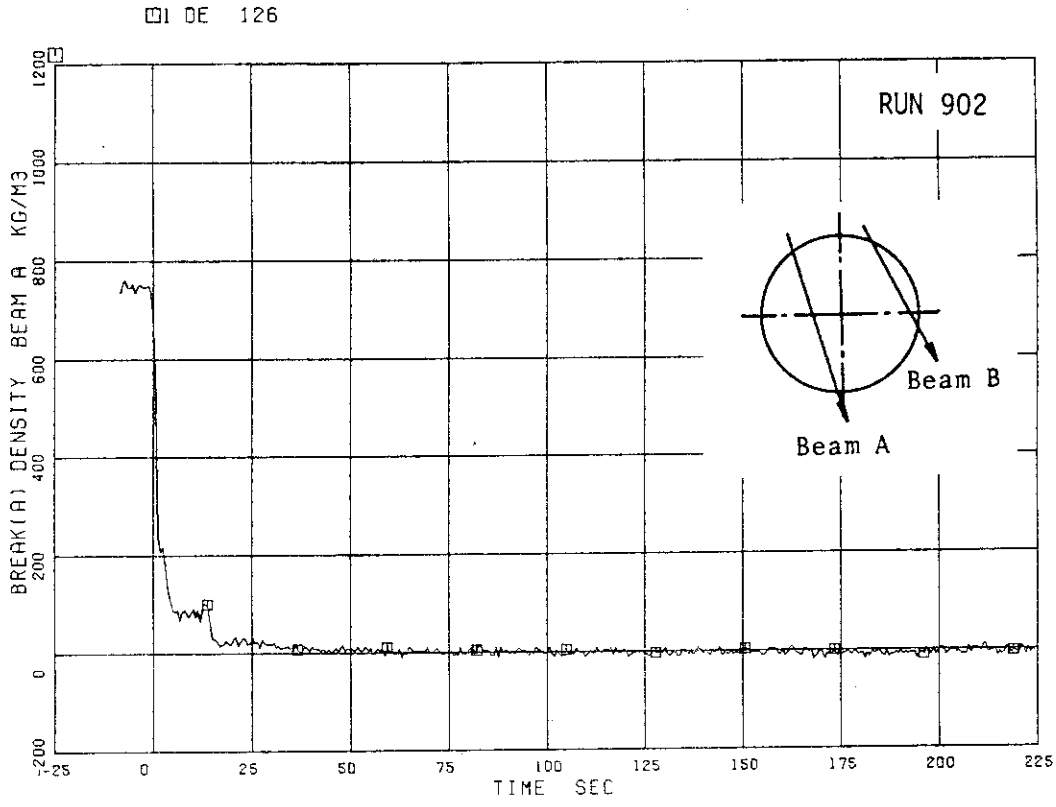

Fig. 6.19 Fluid density at break A, beam A in RUN 902

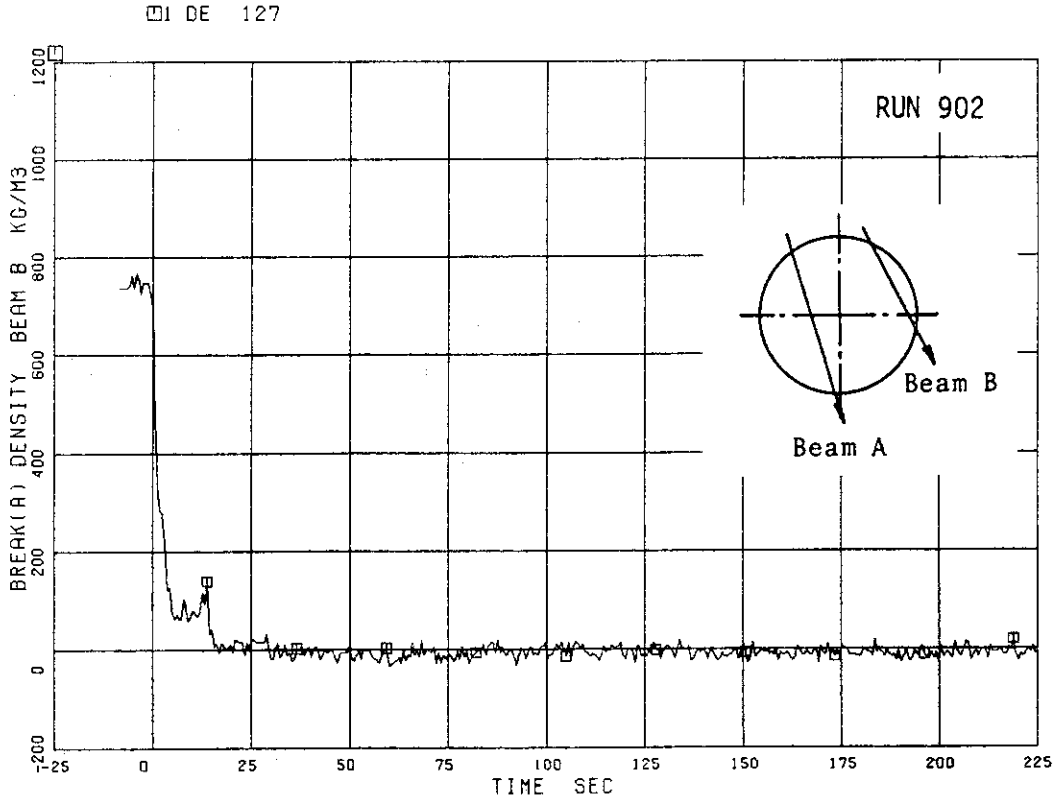

Fig. 6.20 Fluid density at break A, beam B in RUN 902

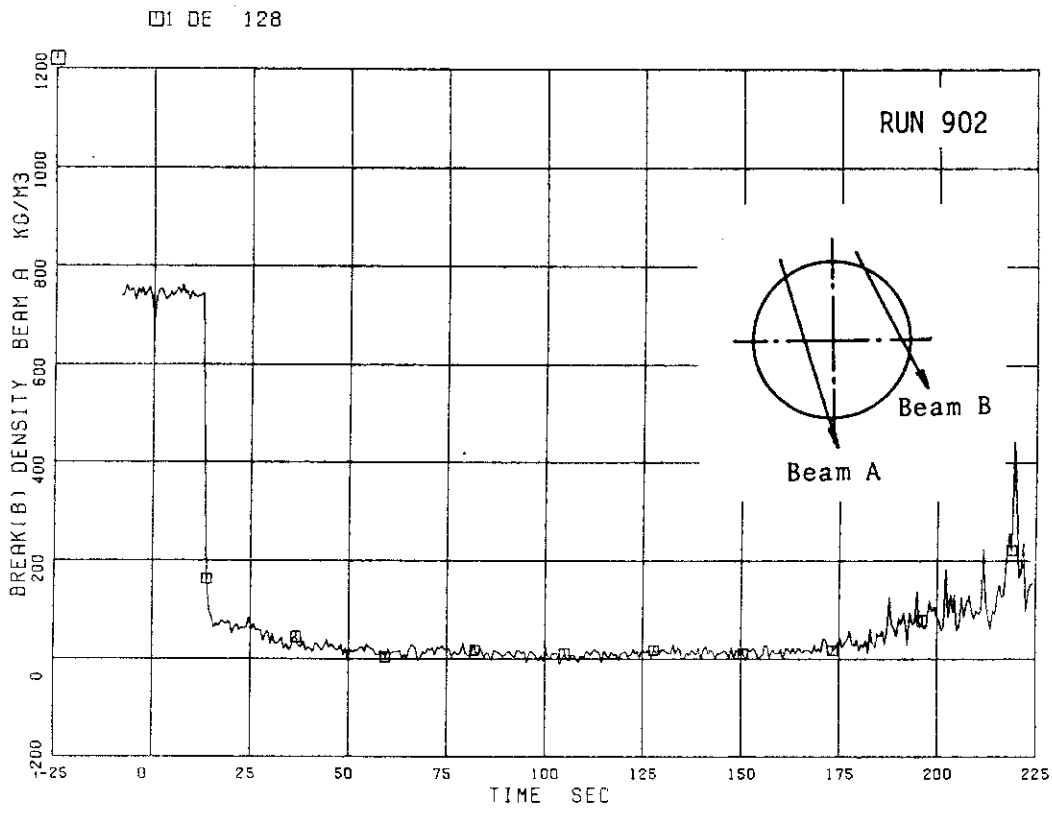

Fig. 6.21 Fluid density at break B, beam A in RUN 902

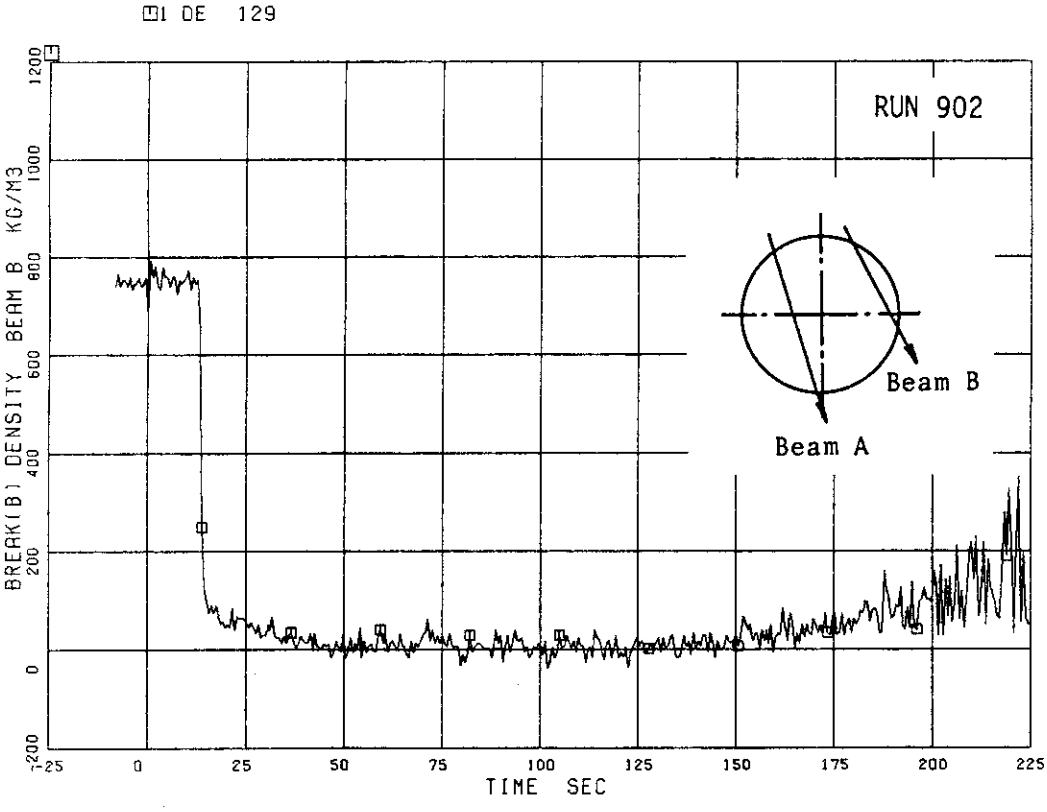

Fig. 6.22 Fluid density at break B, beam B in RUN 902

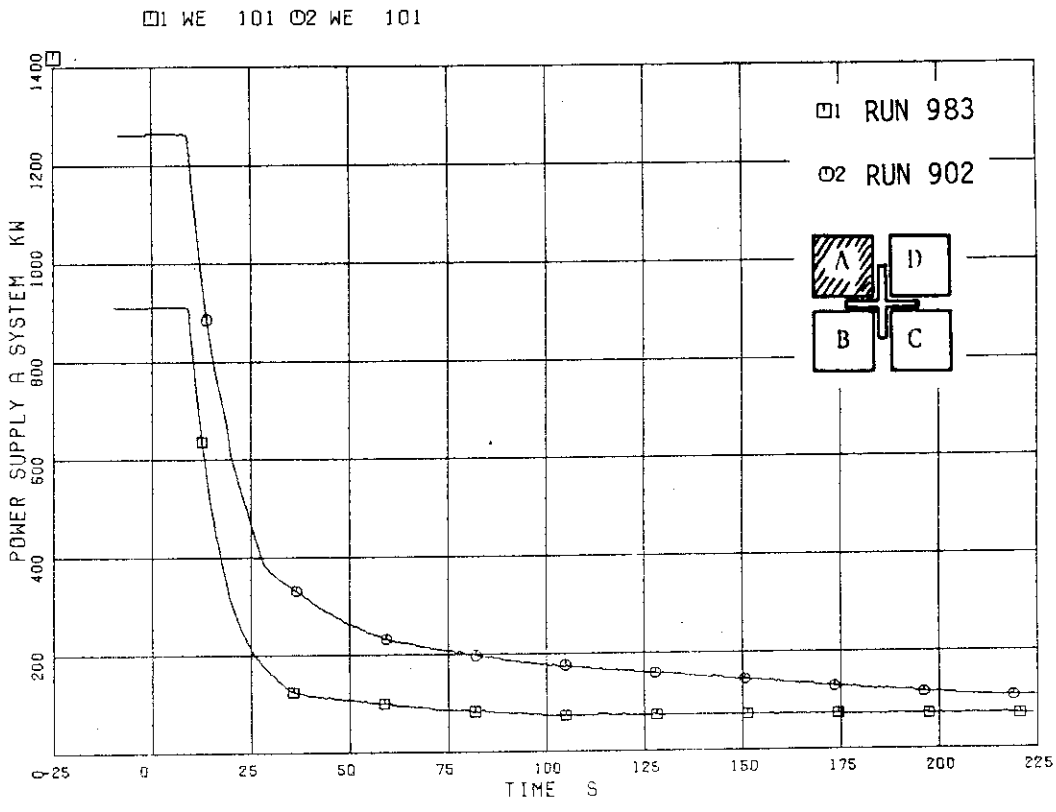

Fig. 6.23 Comparison of A-channel powers between two tests

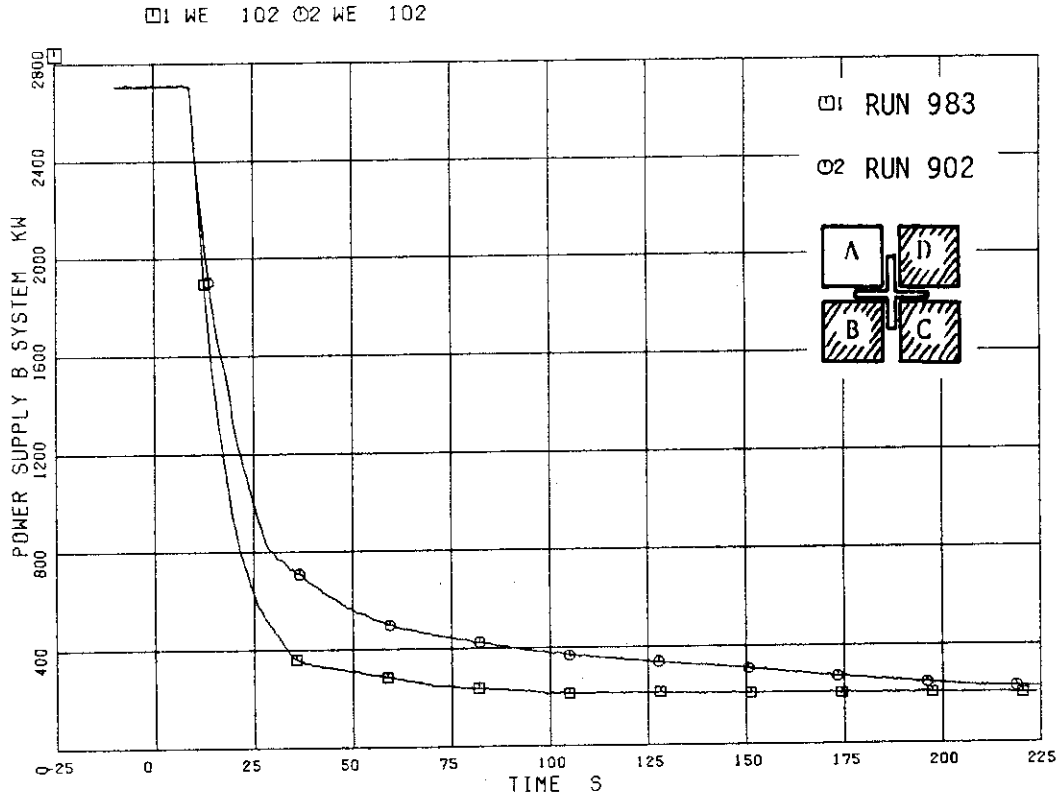

Fig. 6.24 Comparison of powers of B, C and D channels between two tests

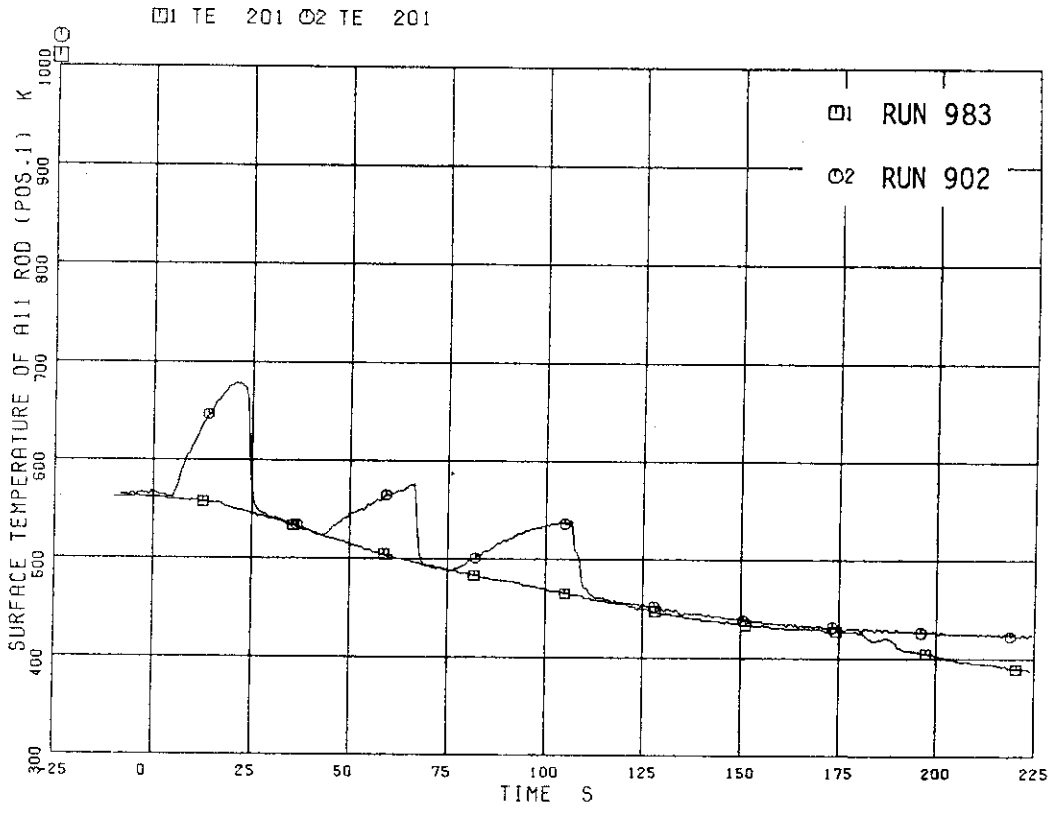

Fig. 6.25 Comparison of rod surface temperatures of A11 rod Position 1 between two tests

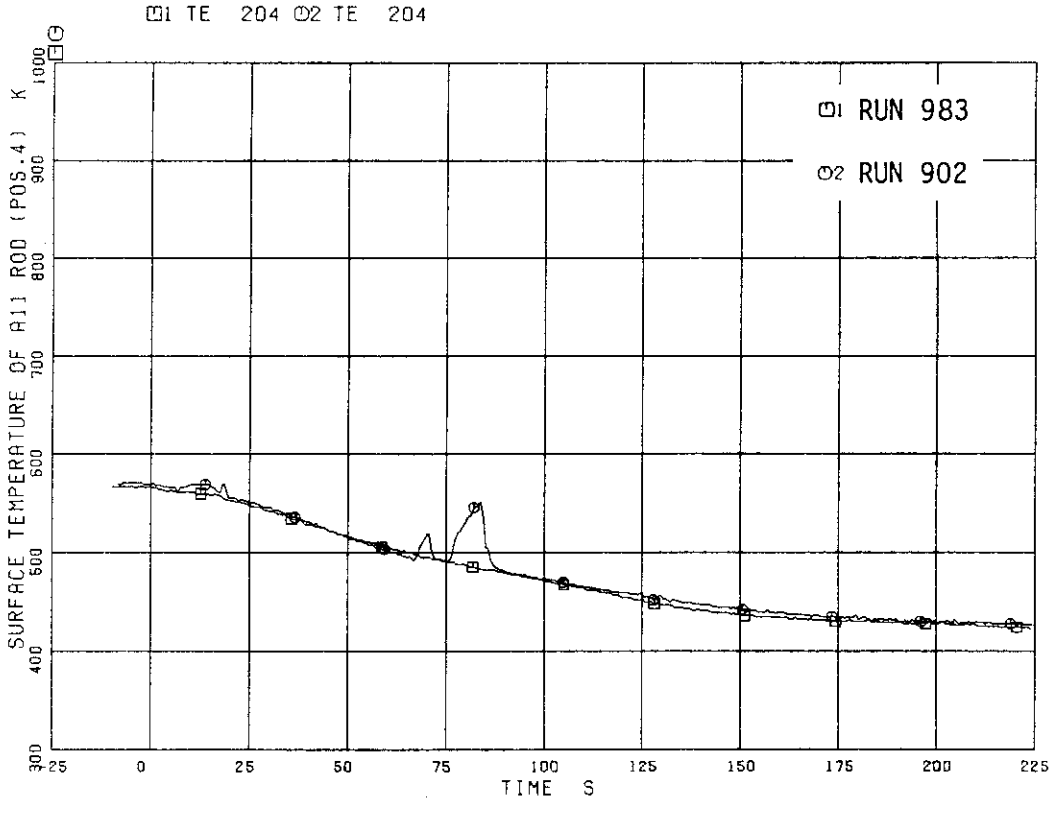

Fig. 6.26 Comparison of rod surface temperatures of A11 rod Position 4 between two tests

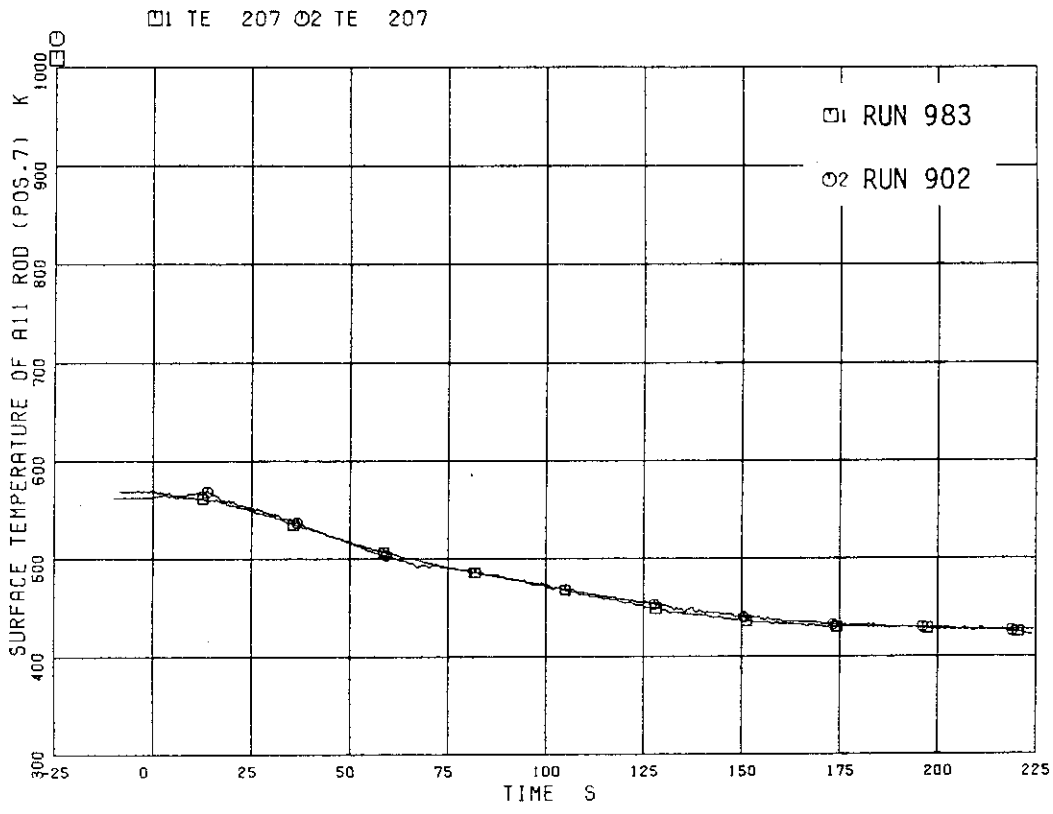

Fig. 6.27 Comparison of rod surface temperatures of A11 rod Position 7 between two tests

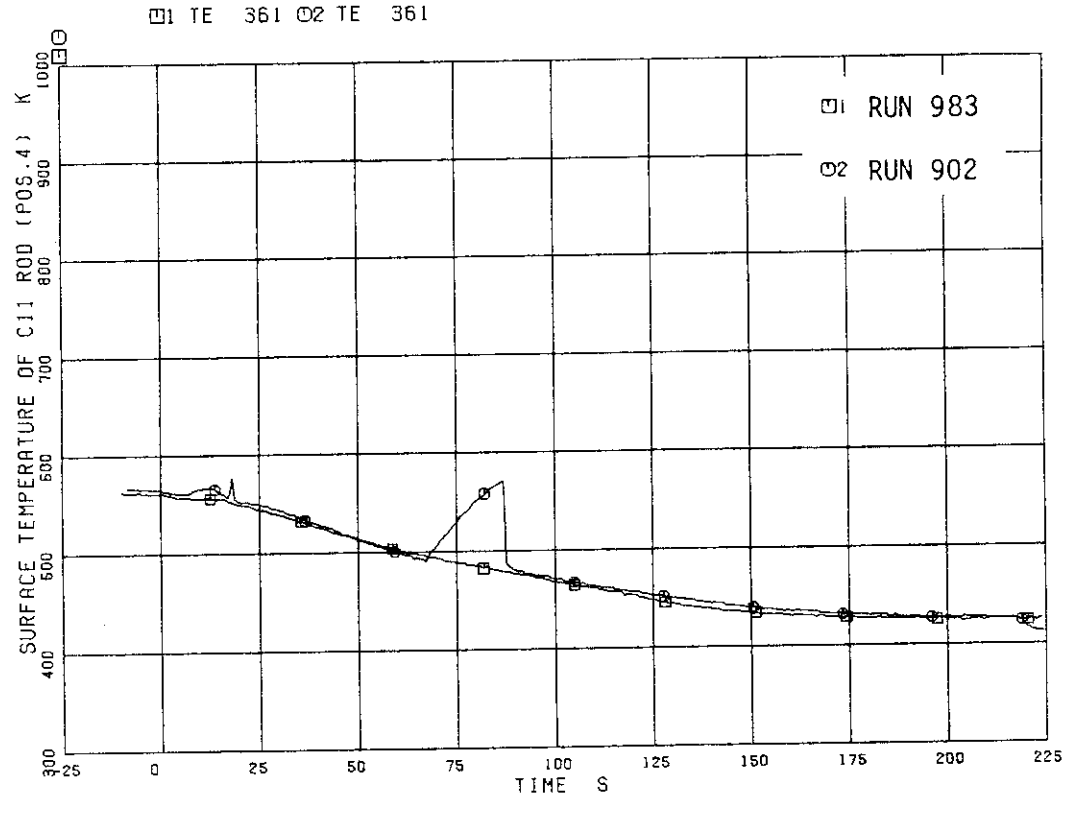

Fig. 6.28 Comparison of rod surface temperatures of C11 rod Position 4 between two tests

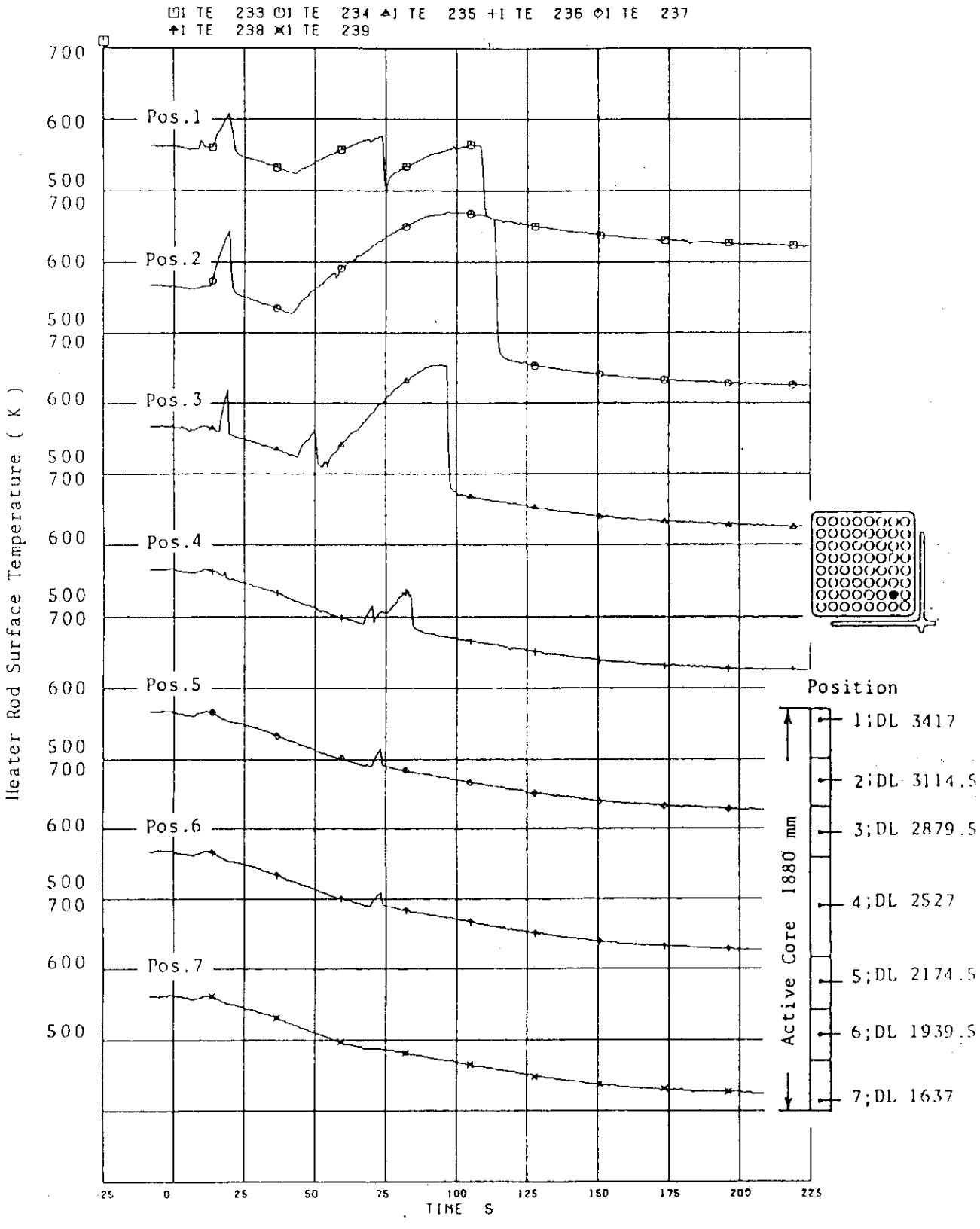

Fig. 6.29 Surface temperatures of A22 rod in RUN 902

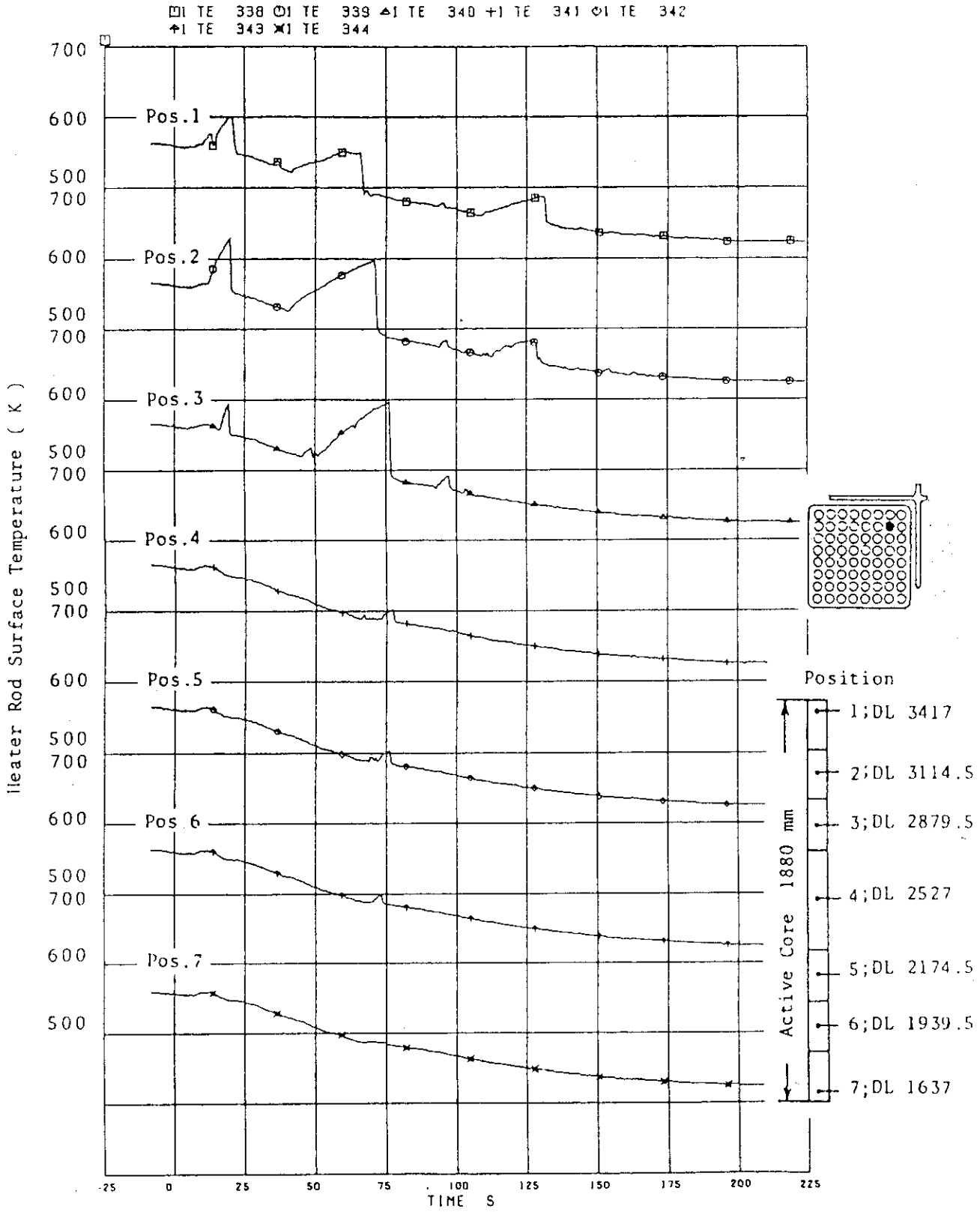

Fig. 6.30 Surface temperatures of B22 rod in RUN 902

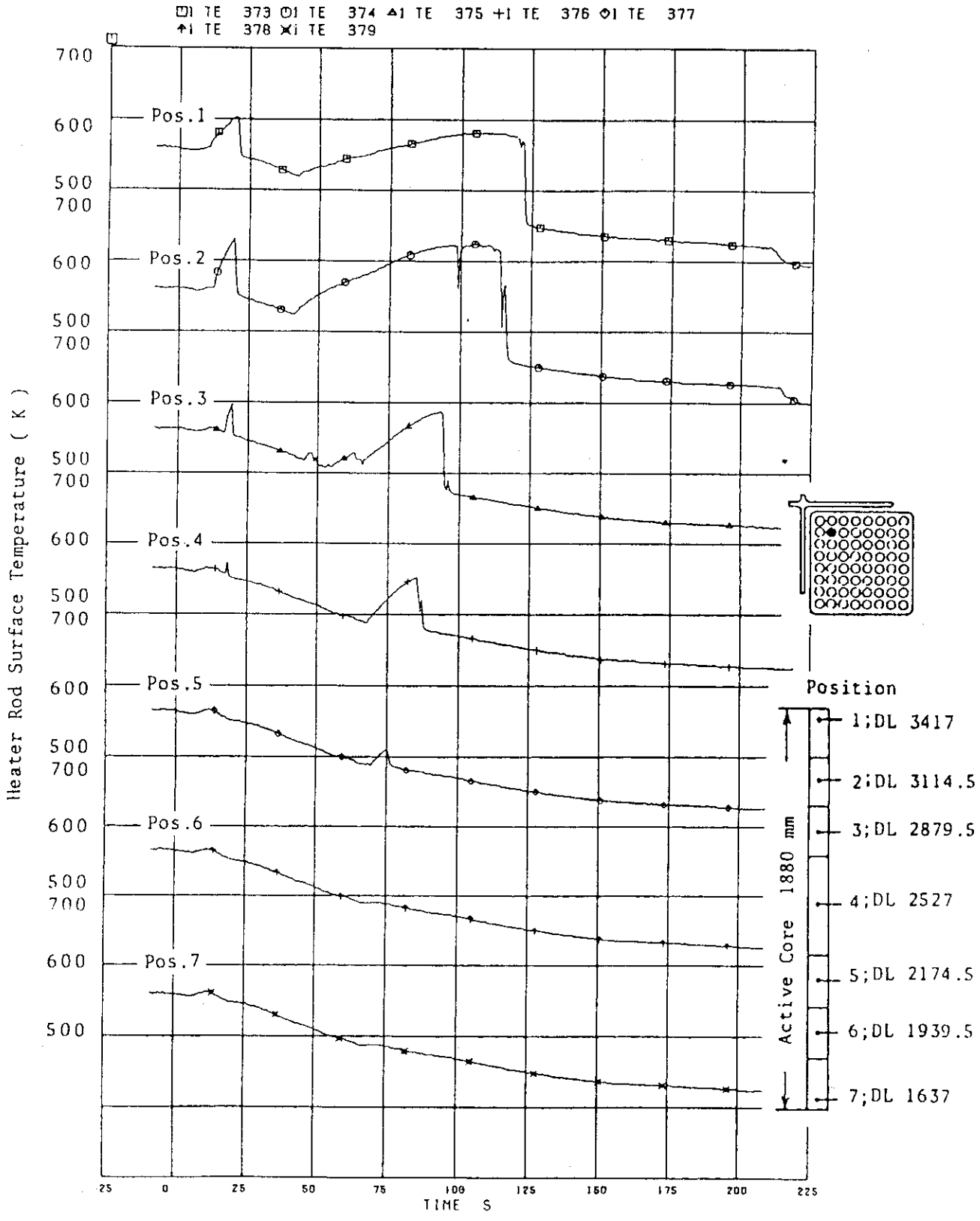

Fig. 6.31 Surface temperatures of C22 rod in RUN 902

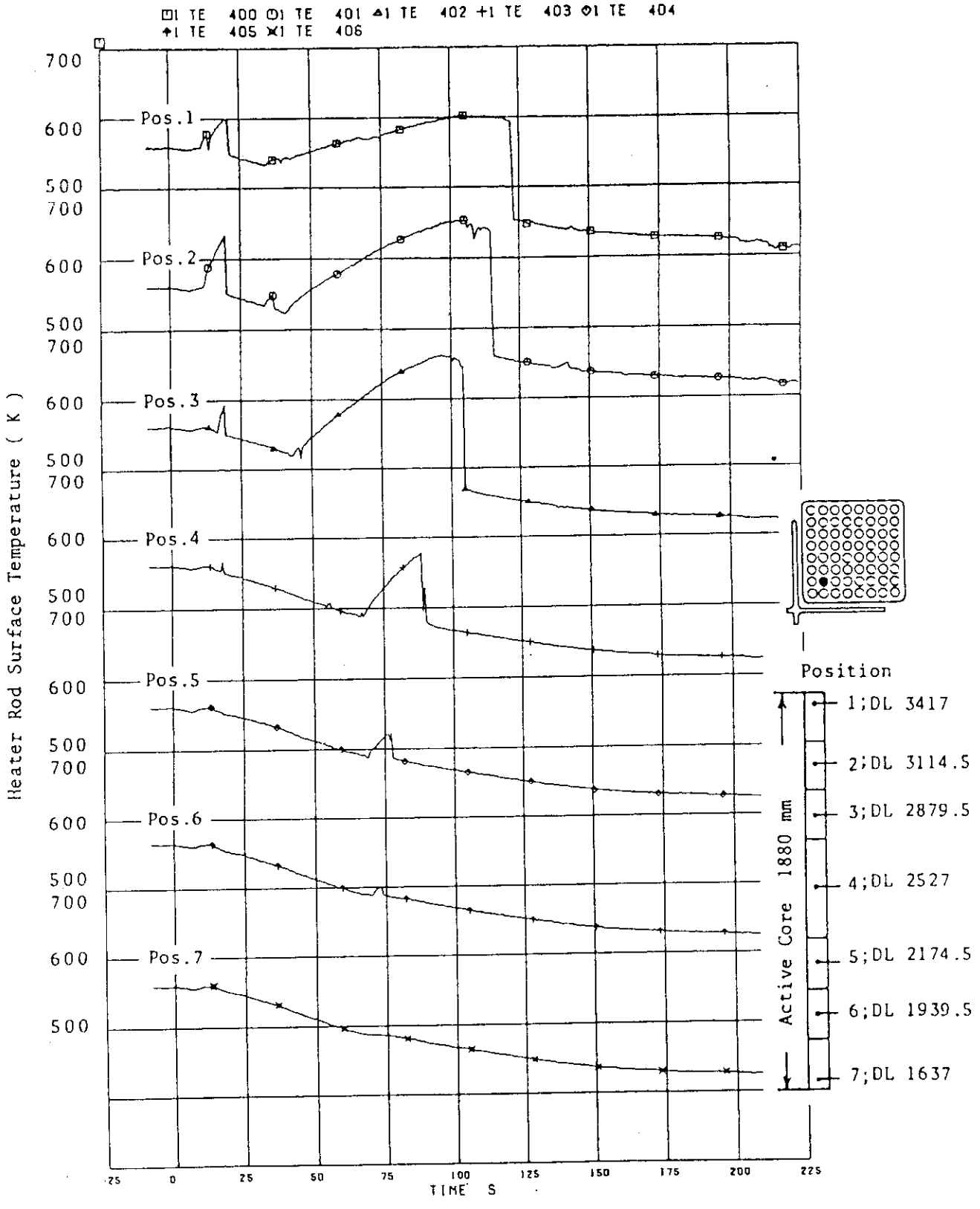

Fig. 6.32 Surface temperatures of D22 rod in RUN 902

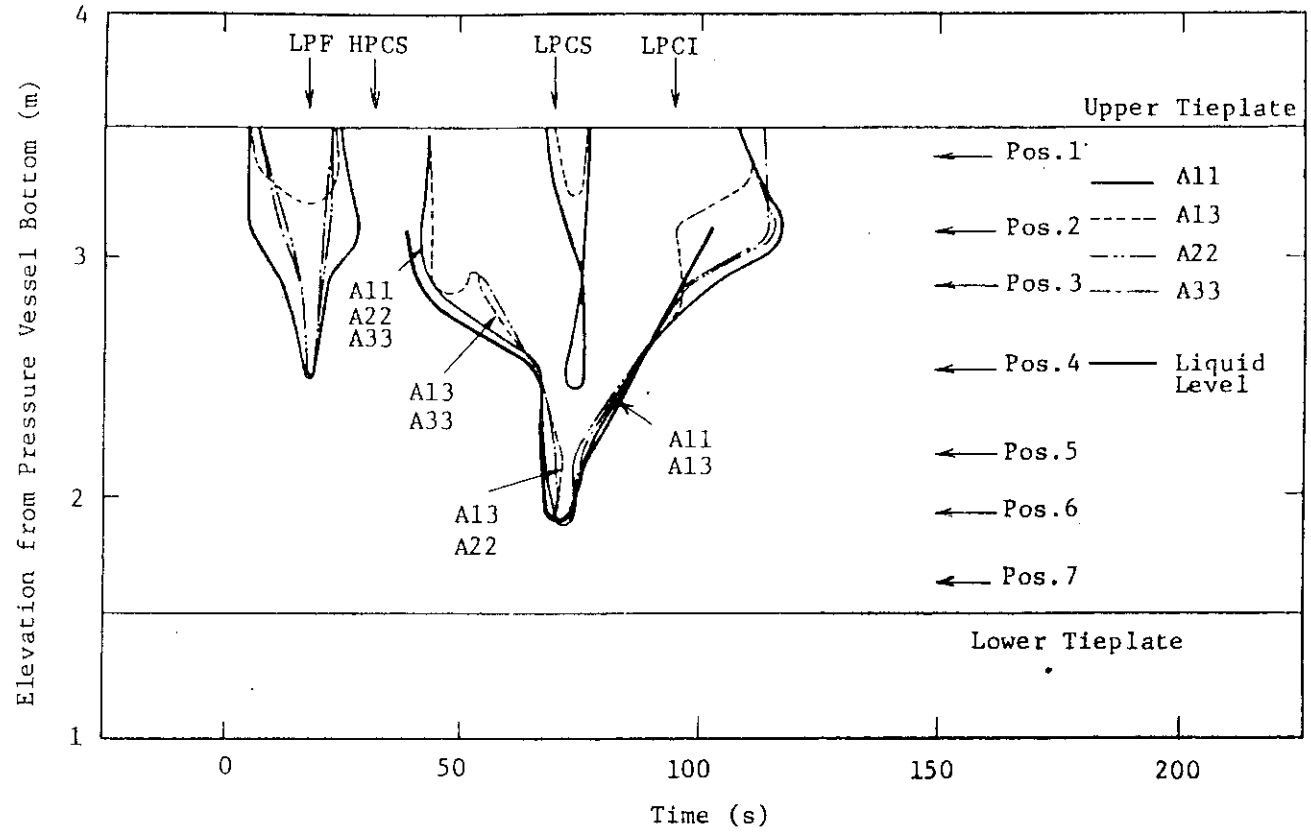

Fig. 6.33 Dryout and quench fronts in Channel A in RUN 902

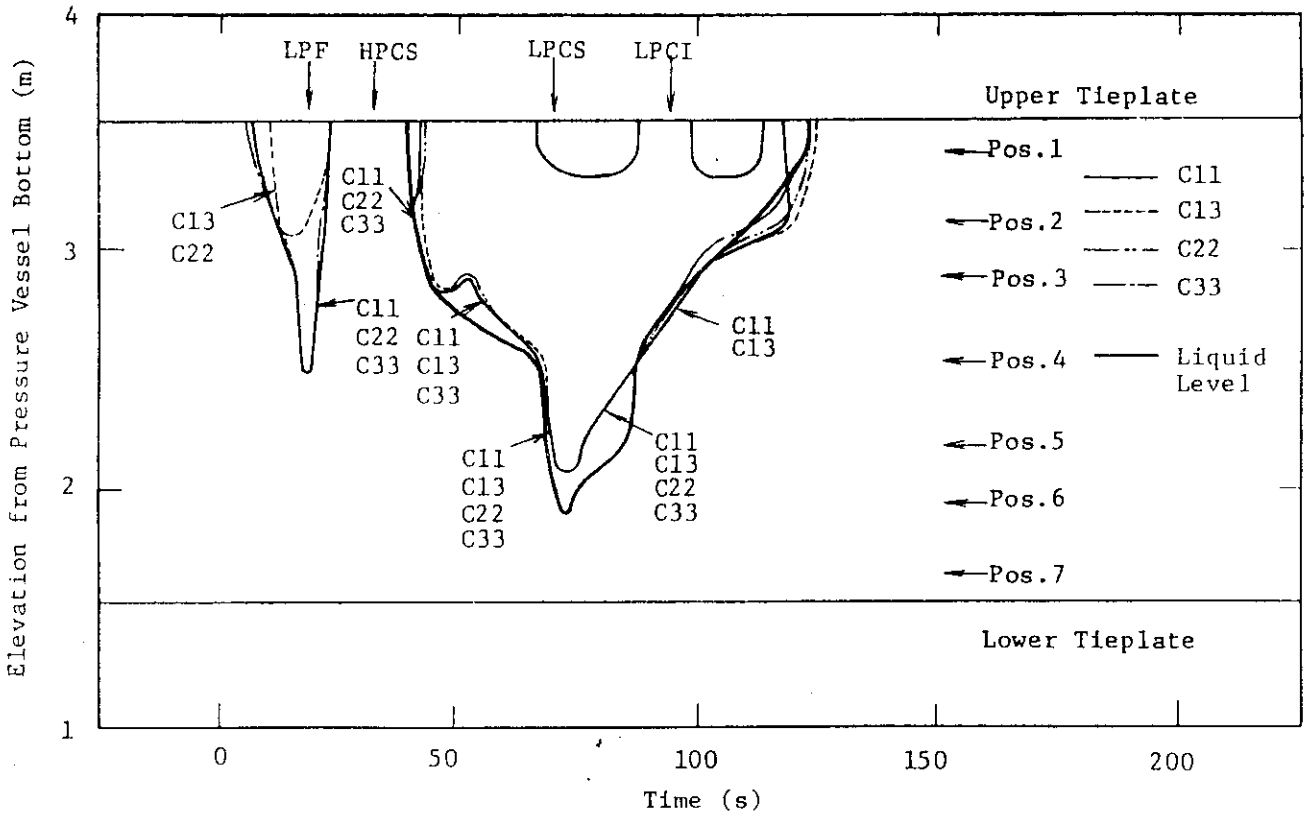

Fig. 6.34 Dryout and quench fronts in Channel C in RUN 902

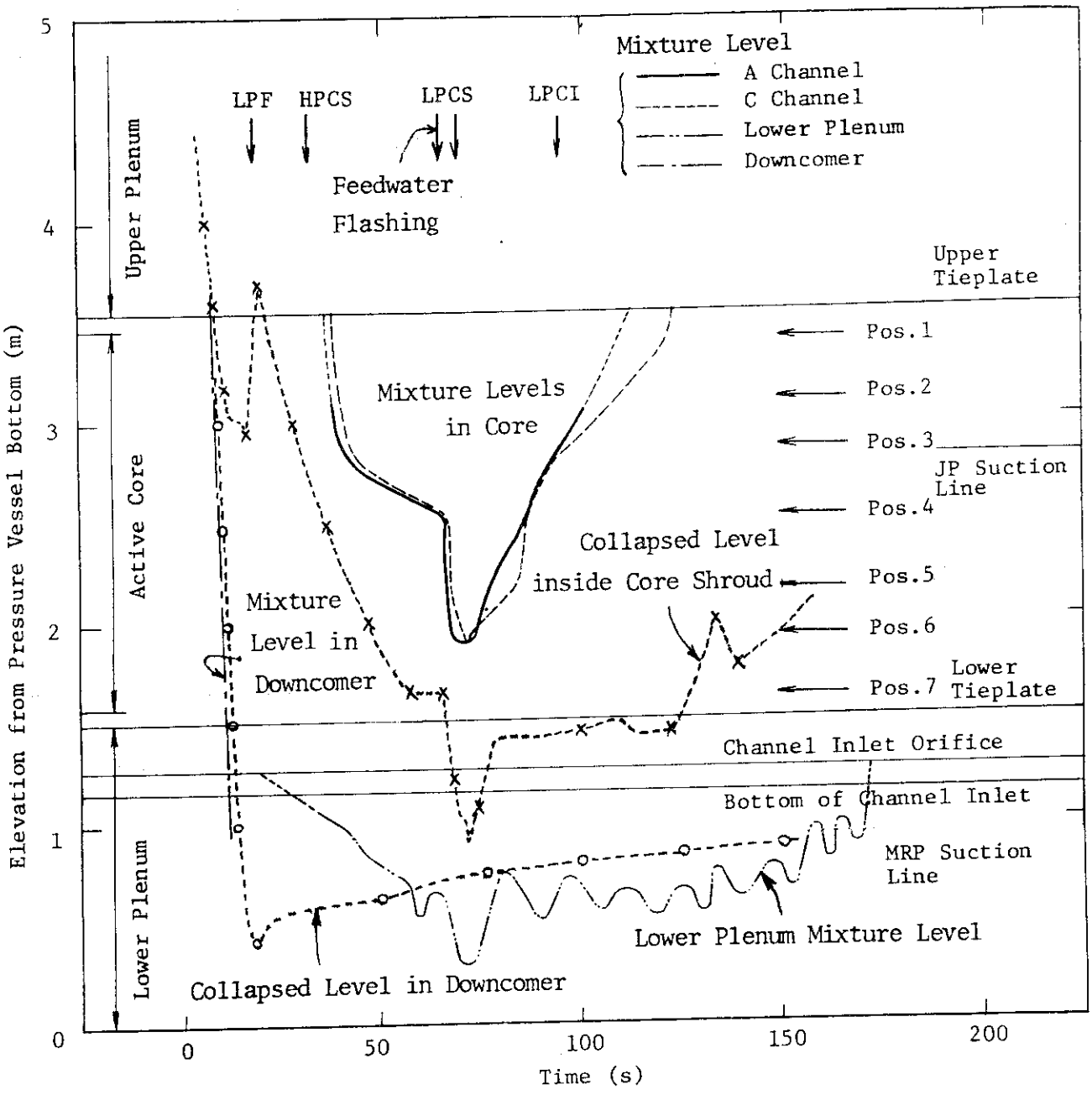

Fig. 6.35 Estimated liquid level in core, channel inlet, lower plenum and downcomer in RUN 902

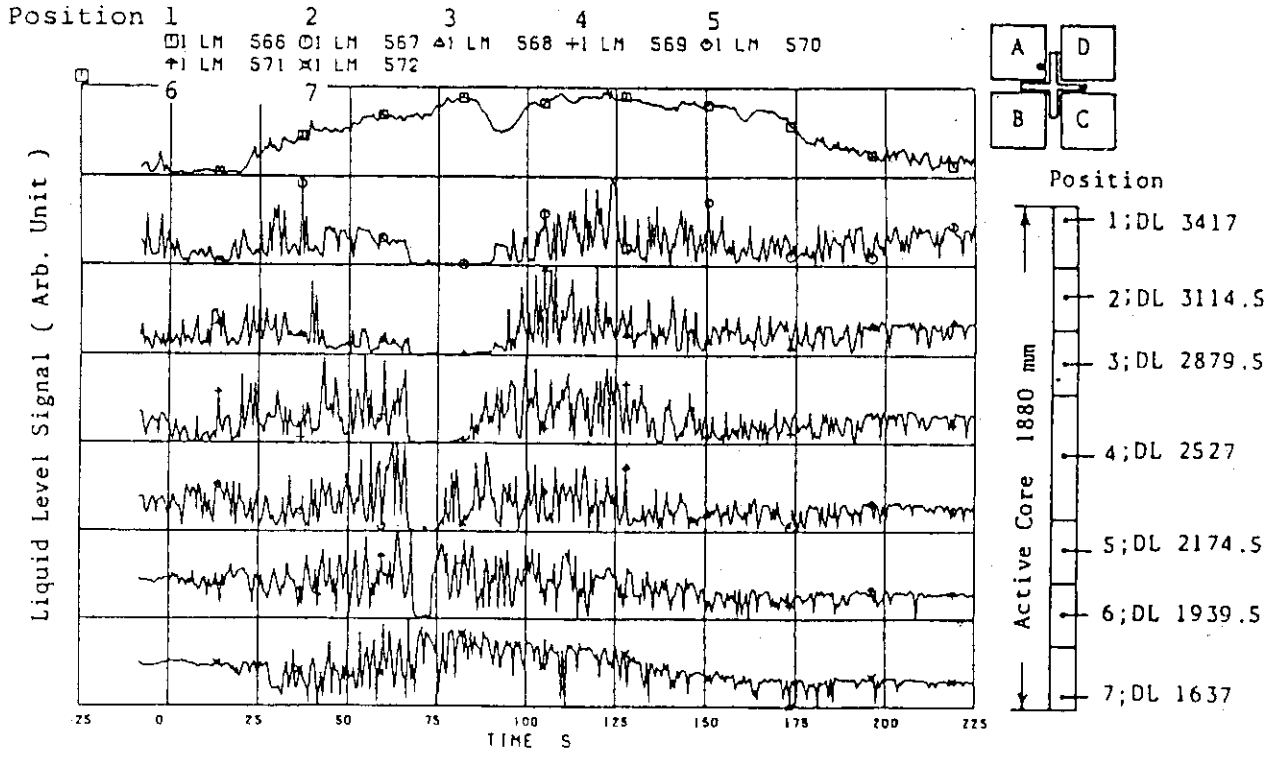

Fig. 6.36 Liquid level signals in channel A in RUN 902

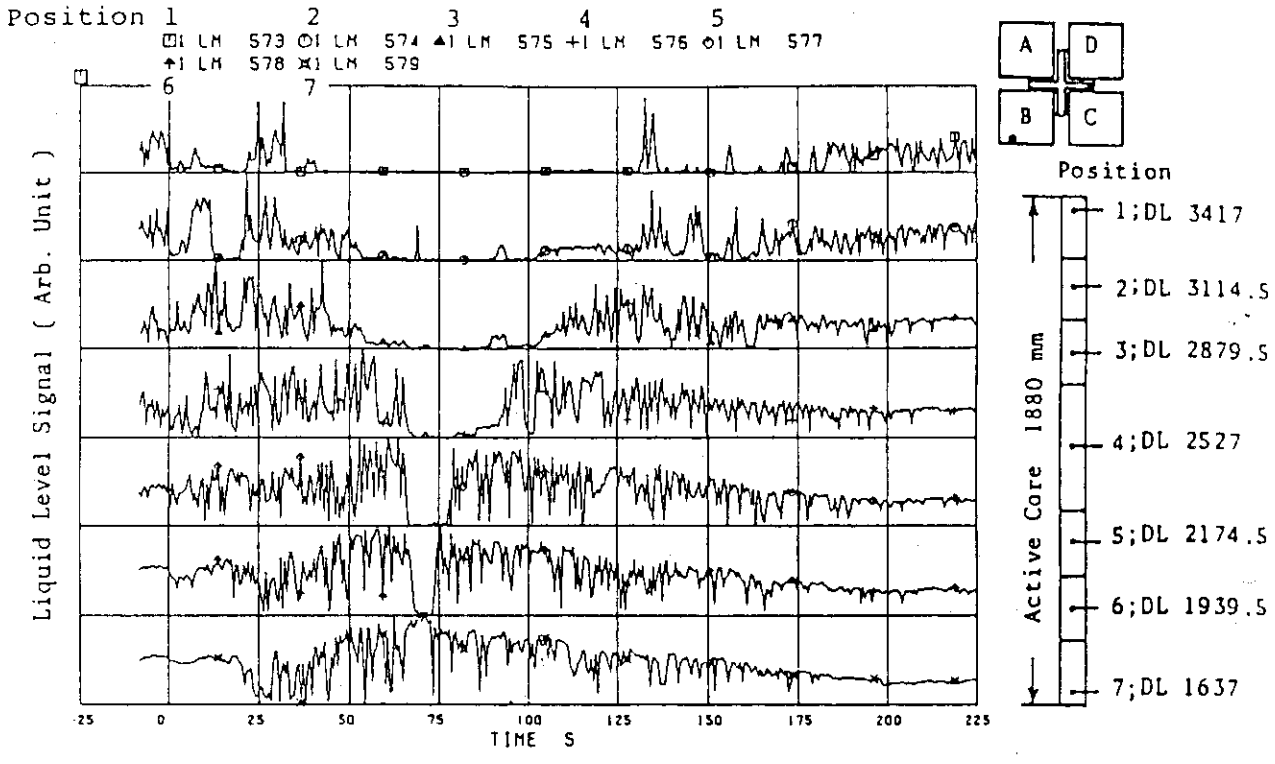

Fig. 6.37 Liquid level signals in channel B in RUN 902

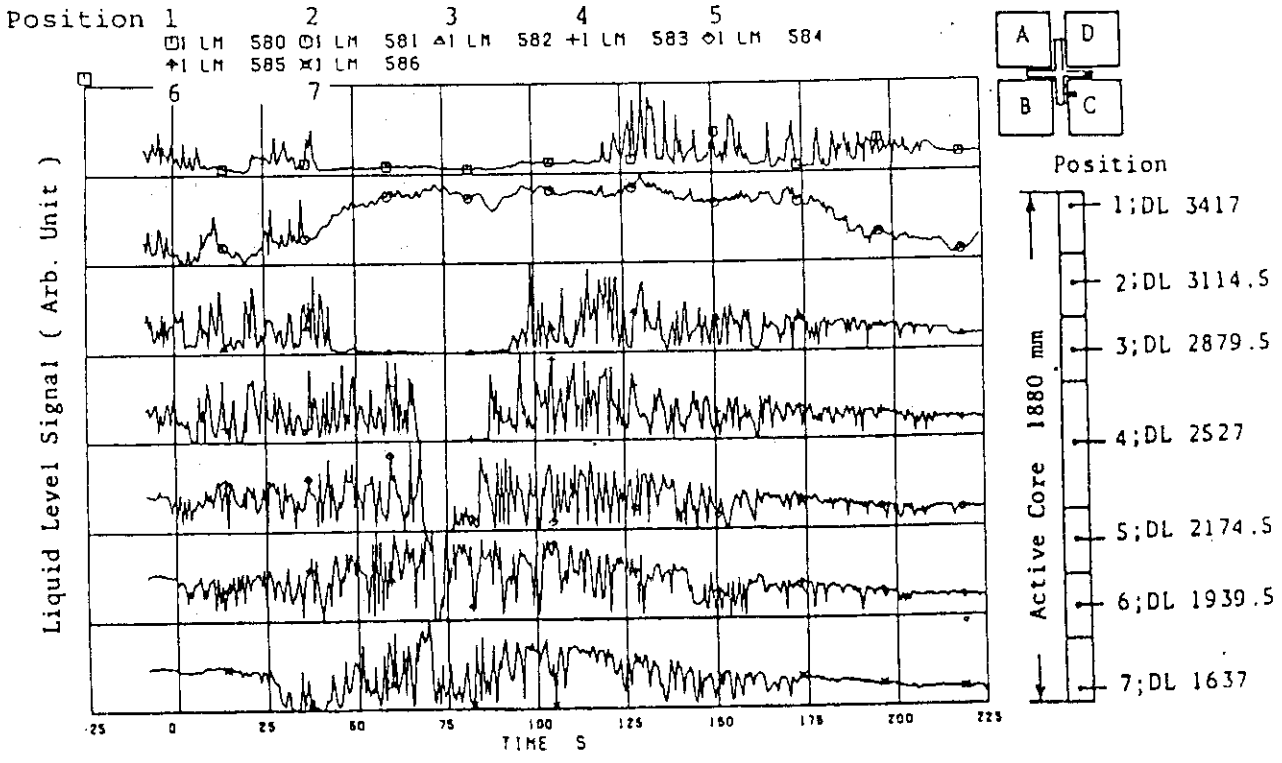

Fig. 6.38 Liquid level signals in channel C in RUN 902

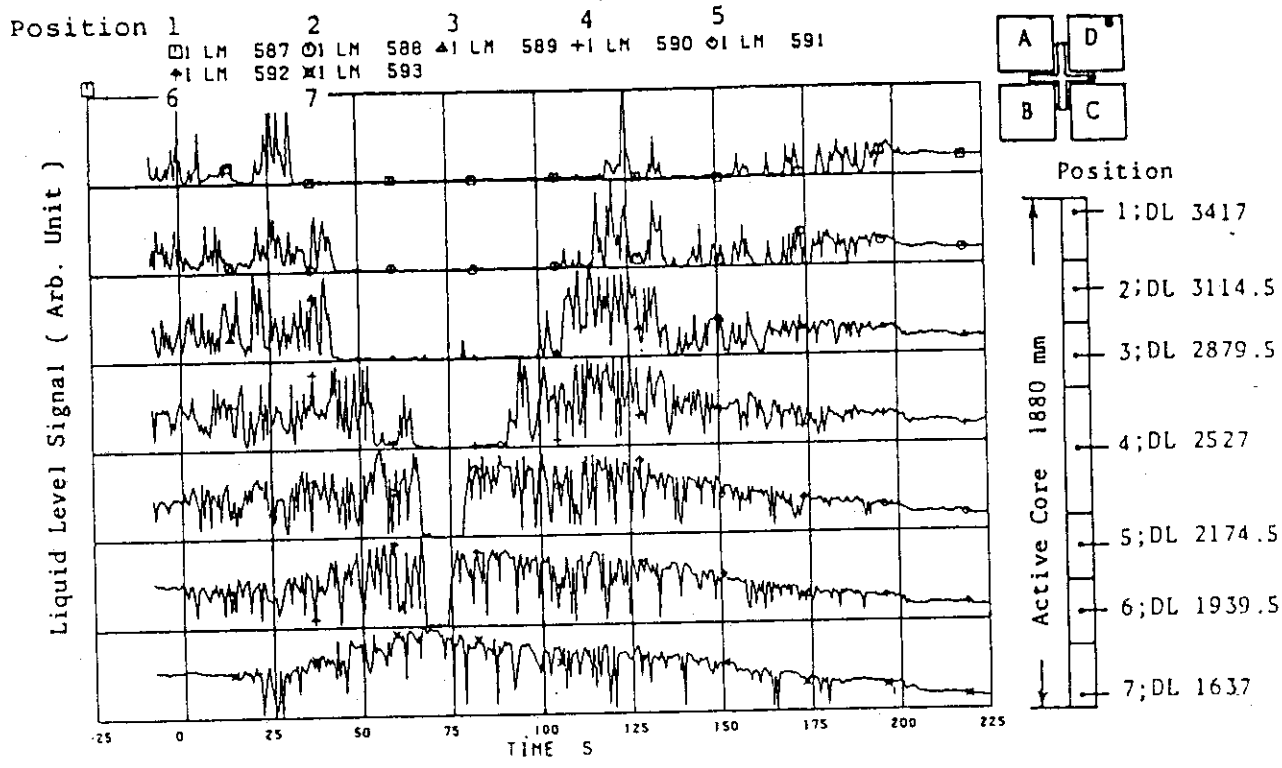

Fig. 6.39 Liquid level signals in channel D in RUN 902

7. Conclusions

A 200% recirculation loop suction line break test, RUN 983, was performed assuming 2 LPCI failures in the ROSA-III program.

Findings obtained in the test RUN 983 are ;

(1) Initial and transient test conditions were successfully achieved and most of the instrumentation functioned well. The test data are presented in Figures and Tables with time scale between -10 s and 690 s.

(2) The pressure transient shows that the system pressure was maintained at 6.7 MPa due to actuation of pressure control system and initiated to increase at 13 s after break due to MSIV closure caused by L1 trip level signal with a time delay of 3 s. The lower plenum flashing occured immediately after the uncovery of the recirculation line. The HPCS, LPCS and LPCI were injected at 27 s, 85 s and 95 s, respectively.

(3) Most of the fuel rods were cooled well. The HPCS actuation contributed primarily to the better core cooling. Short time dryout was observed at the upper region in the two bundles B and D (namely at B11, B22, B77 and D22 rods). The PCT was 575 K (302 C) observed after LPCS actuation at position 2 of D22 rod.

(4) The dryout behavior of fuel rods had a close relation to the mixture level fall in the core detected by the conduction probes at the inner surfaces of the channel boxes.

(5) Two flow patterns were observed among the four fuel bundles which had the same power generation. Namely, downward flow was observed after the lower plenum flashing at the side entry orifices (SEOs) of the bundles B and D and upward flow for bundles A and C. After completion of quench in the bundles B and D, the flow pattern was changed to downward flow at SEOs of the bundles A and D and upward flow for the bundles B and C.

The effects of following test parameters on the large break LOCA phenomena were obtained by comparing the test results of RUN 983 and RUN 902. The major differences in the test conditions between the two tests were (a) MSIV trip level, (b) feedwater temperature, (c) radial power profile and (d) power curve.

(1) The lower MSIV trip level in the downcomer water level resulted in a delay of MSIV closure and resulted in the actuation of the pressure control system. In a large break LOCA, alteration of MSIV trip level from L2 to L1 affected little the pressure response and the mass inventory.

(2) The lower feedwater temperature (296 K) resulted in no flashing and faster depressurization which caused the earlier actuations of LPCS and LPCI and therefore the lower PCT.

(3) The effect of core power profile on the transient core cooling phenomena was not so evident as the difference of transient heat fluxes between the two tests.

(4) The lower PCT was resulted in RUN 983 by lower heat generation rate and higher mixture level in the core compared with those of RUN 902. The larger mass inventory due to lower initial core outlet quality in RUN 983 contributed to the higher transient mixture level in core.

Acknowledgment

The authors are grateful to M. OKAZAKI of Institute of Nuclear Safety, Japan and Y. KOIZUMI of Reactor Safety Lab.1 in JAERI for their contributions in planning and conducting the ROSA-III test, H. ASAHI, T. ODAIRA, T. TAKAYASU, Y. KITANO and T. NUMATA of Nuclear Engineering Corporation for their assistance in conducting the experiment and H.GOTOH and K. HIYAMA of Information System Laboratory Corporation for preparing the data plots.

(1) The lower MSIV trip level in the downcomer water level resulted in a delay of MSIV closure and resulted in the actuation of the pressure control system. In a large break LOCA, alteration of MSIV trip level from L2 to L1 affected little the pressure response and the mass inventory.

(2) The lower feedwater temperature (296 K) resulted in no flashing and faster depressurization which caused the earlier actuations of LPCS and LPCI and therefore the lower PCT.

(3) The effect of core power profile on the transient core cooling phenomena was not so evident as the difference of transient heat fluxes between the two tests.

(4) The lower PCT was resulted in RUN 983 by lower heat generation rate and higher mixture level in the core compared with those of RUN 902. The larger mass inventory due to lower initial core outlet quality in RUN 983 contributed to the higher transient mixture level in core.

Acknowledgment

The authors are grateful to M. OKAZAKI of Institute of Nuclear Safety, Japan and Y. KOIZUMI of Reactor Safety Lab.1 in JAERI for their contributions in planning and conducting the ROSA-III test, H. ASAHI, T. ODAIRA, T. TAKAYASU, Y. KITANO and T. NUMATA of Nuclear Engineering Corporation for their assistance in conducting the experiment and H.GOTOH and K. HIYAMA of Information System Laboratory Corporation for preparing the data plots.

References

(1) K.TASAKA, et al., "Study on the Similarity between ROSA-III Experi- ment and BWR LOCA", JAERI-M 6703 (1976).

(2) Y.ANODA, et. al.,"ROSA-III System Description for Fuel Assembly No. 4", JAERI-M 9363 (1981).

(3) General Electric Company, "General Electric Standard Safety Analysis Report, BWR/6", DOCKET-STN-50477 (1978).

(4) M.SHIBA, et. al.,"Small Break LOCA Experiment in ROSA-III", IAEA-CN-39/69 (1981).

(5) M.SHIBA, et. al.,"Break Area Test Series of ROSA-III for BWR LOCA/ECCS Test", 9th Water Reactor Safety Research Information Meeting (1981).

(6) K.TASAKA, et. al.,"BWR LOCA/ECCS Integral Test at ROSA-III, (Recirculation Pump Discharge Line and Steam Line Breaks)", 10th Water Reactor Safety Research Information Meeting (1982).

(7) K.TASAKA, et. al.,"The LOCA/ECCS System Effect Tests at ROSA-III Changing the Break Area as Test Parameter", Int. Meeting on Ther. Nucl. Reactor Safety (Chicago, 1982).

(8) K.SODA et al.,"Boiling Water Reactor Loss of Coolant Tests (Single Failure Tests with ROSA-III)", J. Nucl. Sci. Tech. (20) (1983).

(9) K.TASAKA, et. al.,"Simulation Experiment of Five Percent Small Break LOCA of BWR", J. Nucl. Sci. Tech. (20) (1983).

(10) K.TASAKA et. al.,"ROSA-III Base Test Series for a Large Break Loss of Coolant Accident in a Boiling Water Reactor", Nucl. Techn. (57)(1982)

(11) K.TASAKA et. al.,"Steam Line Break, Jet Pump Drive Line Break and Natural Circulation Tests in ROSA-III Program for BWR LOCA/ECCS Integral Tests", 11th Water Reactor Safety Research Inform. Meeting (1983).

(12) M.SOBAJIMA, et. al.,"Experiment Test Data of ROSA-III Test RUN 701 (Decay Heat Simulation Test with ECCS Actuation)", JAERI-M 8604 (1979).

(13) Y.ANODA et. al.,"Experiment Data of ROSA-III Test RUN 703 (Split Break Simulation Test with ECCS Actuation)", JAERI-M 8967 (1980).

(14) Y.ANODA et. al.,"Experiment Data of ROSA-III Test RUN 704 (Standard Test with ECCS Actuation)", JAERI-M 8968 (1980).

(15) M.OKAZAKI et. al.,"Experimet Test Data of ROSA-III Integral Test RUN 705 (Isothermal Blowdown Test without ECCS Actuation)", JAERI-M 8723 (1980).

(16) M.SUZUKI et. al.,"Experiment Data of ROSA-III Integral Test, RUN 706", JAERI-M 8737 (1980).

(17) M.OKAZAKI et. al.,"Experiment Data of ROSA-III Integral Test RUN 708 (Standard Test without ECCS Actuation)", JAERI-M 8738 (1980).

(18) Y.KOIZUMI et. al.,"Experiment Data of ROSA-III Integral Test, RUN 710", JAERI-M 9249 (1981).

(19) Y.ANODA et. al.,"Experimet Data of ROSA-III Integral Test RUN912 (5% Split Break Test without HPCS Actuation)", JAERI-M 82-010.

(20) H.NAKAMURA et. al.,"Experiment Data of ROSA-III Integral Test RUN 901 (200% Double-Ended Break with Full ECCS Actuation)", JAERI-M 84-007.

(21) H.NAKAMURA et. al.,"Experiment Data of ROSA-III Integral Test RUN 926 (200% Double-Ended Break with HPCS Failure)", JAERI-M 84-008.

(22) M.SUZUKI et. al.,"Chracteristics of the ROSA-III Test Facility (Chracteristics Test of the Jet Pumps in Normal and Reverse Flow)", JAERI-M 8670 (1980).

(23) M.SUZUKI et. al.,"Heat Loss and Fluid Leakage Tests of the ROSA-III Facility", JAERI-M 9834 (1981).

(24) M.SUZUKI et. al.,"Experiment Data of 200% Recirculation Pump Discharge Line Break Integral Test RUN 961 with HPCS Failure at ROSA-III and Comparison with Results of Suction Line Break Tests", JAERI-M 84-045 (1984).

(25) M.SUZUKI et. al.,"Recirculation Pump Suction Line 2.8% Break Integral Test at ROSA-III with HPCS Failure, RUN 984", JAERI-M 84-100, (1984).

(26) W. J. Letzring, et. al.,"BWR Blowdown/ECC Program Preliminary Facility Description Report for the BD/ECC1a Test Phase", GEAP-23592.

(27) GE, EPRI and NRC,"Full Integral Simulation Test (FIST) Program Test Plan", EPRI NP-2313, GEAP 22053, (1981).

(28) M.SOBAJIMA et. al.,"Instrumentation and Data Processing Method of the ROSA-III Test", JAERI-M 8499 (1979).

(29) M.IRIKO et. al.,"Updated Core Power Curves for ROSA-III Facility", JAERI-M 84-029 (1984).

(30) N.ABE et. al.,"Electric Power Tansient Curve for ROSA-III Tests", JAERI-M 8728 (1980).